Methods in Molecular Biology 1524

Springer Protocols

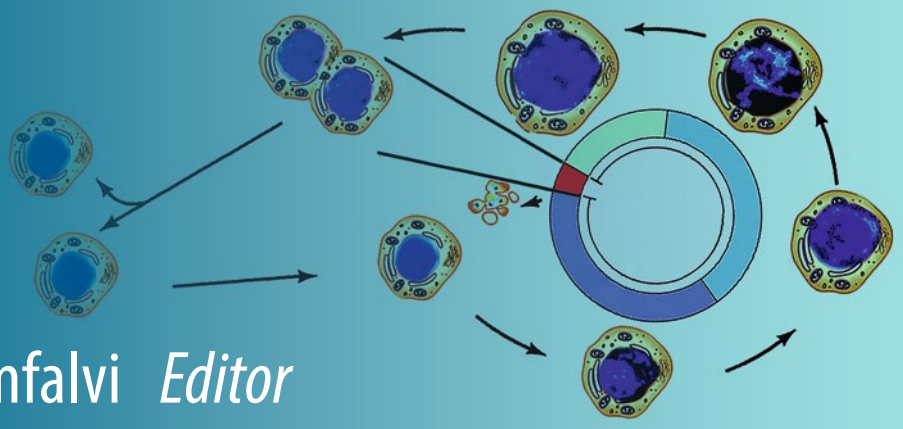

Gaspar Banfalvi *Editor*

Cell Cycle Synchronization

Methods and Protocols

Second Edition

Humana Press

METHODS IN MOLECULAR BIOLOGY

Series Editor
John M. Walker
School of Life and Medical Sciences
University of Hertfordshire
Hatfield, Hertfordshire, AL10 9AB, UK

For further volumes:
http://www.springer.com/series/7651

Cell Cycle Synchronization

Methods and Protocols

Second Edition

Edited by

Gaspar Banfalvi

Department of Biotechnology and Microbiology, University of Debrecen, Debrecen, Hungary

Humana Press

Editor
Gaspar Banfalvi
Department of Biotechnology and Microbiology
University of Debrecen
Debrecen, Hungary

ISSN 1064-3745 ISSN 1940-6029 (electronic)
Methods in Molecular Biology
ISBN 978-1-4939-6602-8 ISBN 978-1-4939-6603-5 (eBook)
DOI 10.1007/978-1-4939-6603-5

Library of Congress Control Number: 2016955331

Printed on acid-free paper

This Humana Press imprint is published by Springer Nature
The registered company is Springer Science+Business Media LLC
The registered company address is: 233 Spring Street, New York, NY 10013, U.S.A

Preface

What Kind of Cells Can Be Synchronized?

To study how cells progress through the cell cycle, cell cultures have to be brought to the same phase. The unique feature of this book is exactly this: to prepare synchronized cells representing different stages of the cell cycle. The book also shows the latest techniques for the enhanced study of regulatory mechanisms to understand cell cycle events. The synchronization methods presented in the book are based principally on two major strategies. The "arrest-and-release" approach involves different chemical treatments to block cells at certain stages of the cell cycle. The physical strategy contains physical methods to collect cells belonging to subpopulations of the cell cycle. The collection of synchronized cells from asynchronous bacterial, plant, protozoan, yeast, fish, and mammalian cell cultures consisting of individual cells is described by professionals of their respective field. Additional chapters include synchronization of transfected and embryonic cells.

What Motivated the Second Edition of *Cell Cycle Synchronization*?

The interest in the first edition of *Cell Cycle Synchronization* is indicated by the 49,074 chapter downloads between 2012 and February 2016. There are always scientists who are desperately looking for synchronization protocols. Researchers are interested in synchronizing mammalian, plant, yeast, fungal, and even bacterial cells, but often do not know how to do it. Enthusiastic students try synchronization without experience and then recognize that it does not work. In such cases the easiest way is to ask someone known for his/her expertise to send a protocol. As some of the synchronizing techniques are tricky, brief instructions usually would not help either. Alternatively, one can trace research papers that contain descriptions without extensive practical details, but describe only rarely how problems encountered could be solved. This book aims to address such deficiencies. But the most important feature of this updated book is to give detailed protocols providing first the theoretical background of the procedure then step-by-step instructions on how to implement synchronization and finally how to avoid pitfalls referred to in the Notes. Chapters of the book are written for those competent scientists who would like to do, but are not familiar with, synchronization. They should be able to carry out successfully the technique at the first attempt by following closely the detailed practical instructions of the protocols. If your attempt would fail, you can still contact and ask preferentially the first or last author about the technical details of the chapter you are interested in.

Major Sections of Chapters

Each protocol starts with an Abstract and consists of four major sections: Introduction, Materials, Methods, and Notes. Exceptions are only the first and last review chapters that do not follow this format. The "Abstract" gives an overview of the synchronization

technique(s). The "Introduction" contains a summary, a brief theoretical view of the procedure referring to the work of other authors, and outlines the major procedures of the protocol. The "Materials" section is the major part of the chapter listing the buffers, reagents, solutions, disposables, and equipment necessary to carry out the synchronization. Attention is called to special requirements such as storage conditions, stability, purity, toxicity of reagents, special treatment, or protection. The "Materials" section contains all relevant practical details and explains individual steps to be carried out normally by listing these steps in numerical order. The "Notes" section is the hallmark of the series of Methods in Molecular Biology as it is meant to indicate the sources of problems and how to identify and overcome them.

Brief Content of Chapters

The introductory chapter overviews synchronization methods. Chapters of physical fractionations include centrifugal elutriation of healthy and apoptotic cells, and nuclei of mammalian cells (Chapter 2), image cytofluorometry for the quantification of ploidy and stress of cancer cells (Chapter 3), and large-scale mitotic cell synchronization (Chapter 4). Chemical blockades imply intervention on the spindle assembly checkpoint (Chapter 5), synchronization by serum deprivation (Chapters 6 and 10), DNA replication stress inhibitors (Chapters 7), chromosome formation during fertilization in eggs (Chapter 8), synchronization with butyrate (Chapters 8 and 10), nocodazole to arrest cells at the G_2/M border, and aphidicolin to synchronize cells at the G_1/S border and to monitor progression through S phase by pulse-labeling individual cultures with [^{3}H]-thymidine (Chapter 11). Different ways have been used to synchronize HeLa cells in Chapter 12. The synchronization of unicellular organisms (*Bacillus subtilis*, yeast, protozoans) is described in Chapters 13–15. The synchronization of maturation of porcine oocytes is described in Chapter 16. Plant cell synchronization is dealt with in Chapter 17. A protocol for the synchronization for the purposes of nuclear transfer is given in Chapter 18. Hematopoietic stem cells improve the engraftment in transplantation (Chapter 19). Flow cytometry developments and perspectives in clinical studies are described in Chapter 20. Finally, cell cycle control is discussed in Chapter 21.

Which Is the Best Synchronization Protocol?

It was neither the intention of the first edition nor the second edition of this book to make judgement as to which synchronizing procedure would be the best or to set a "gold standard" against which other methods should be measured. Debates on cell-cell synchronization methodologies can be found in opinion papers referred to in Chapter 1 [14-18]. A simple method for obtaining synchrony in all types of cells, which would last through several cycles and with minimal overall metabolic perturbations, does not exist. Thus scientists interested in synchronization after reading the chapters of interest can decide by themselves which technique would be appropriate for adaptation.

The Potential Audience of This Book

Primarily those students and scientists were interested in the first edition who were looking for synchronization protocols. The main target audience includes the following:

- libraries of universities and biological research institutions,
- researchers interested in general science, pharmacy, medicine and public health, computer science, and the life sciences;
- specialist and professionals in cell biology, genetics, molecular biology, biochemistry, pharmacology;
- biologists, molecular biologists, biotechnologists, geneticists, immunologists, medical students, PhD students, and postdoctoral fellows who are expected to be the primary users of the synchronizing techniques and protocols;
- pharma companies and factories.

Debrecen, Hungary *Gaspar Banfalvi*

Contents

Contributors

Edit Ábrahám • *Laboratory of Plant Genomics, Biological Research Center, Hungarian Academy of Sciences, Szeged, Hungary*

Ferhan Ayaydin • *Laboratory of Cellular Imaging, Biological Research Center, Hungarian Academy of Sciences, Szeged, Hungary*

Gaspar Banfalvi • *Department of Biotechnology and Microbiology, University of Debrecen, Debrecen, Hungary*

Norma Bloy • *Centre de Recherche des Cordeliers, Equipe 11 labellisée Ligue contre le Cancer, INSERM, France*

Salvatore J. Caradonna • *Department of Molecular Biology, Rowan School of Osteopathic Medicine, University of Medicine and Dentistry of New Jersey, Stratford, NJ, USA*

Richard C. Chou • *Dartmouth School of Medicine, Lebanon, NH, USA*

Attila Csikász-Nagy • *Randall Division of Cell and Molecular Biophysics, Institute for Mathematical and Molecular Biomedicine, King's College London, London, UK; Faculty of Information Technology and Bionics, Pázmány Péter Catholic University, Budapest, Hungary*

Zbigniew Darzynkiewicz • *Department of Pathology, Brander Cancer Research Institute, New York Medical College, Valhalla, NY, USA*

Julie Demaret • *Immunology Laboratory, Hospices Civils de Lyon, E. Herriot Hospital, Lyon, Cedex, France; EA Pathophysiology of Injury-induced Immunosuppression (PI3—University Claude Bernard Lyon 1—Hospices Civils de Lyon— bioMérieux), Lyon, France*

Yohann Demont • *Centre de Recherche des Cordeliers, Equipe 11 labellisée Ligue contre le Cancer, INSERM, France*

Alla Dolnikov • *Sydney Cord and Marrow Transplant Facility, Sydney Children's Hospital, Graduate School of Biomedical Engineering, University of New South Wales, Randwick, NSW, Australia; Faculty of Medicine, University of New South Wales, Sydney, NSW, Australia*

Kalyan Dulla • *Department of Cell Biology, Max Planck Institute of Biochemistry, Martinsried, Germany; Department of Molecular Diagnostics, Philips Corporate Technologies, AE Eindhoven, The Netherlands*

Huzefa Dungrawala • *Department of Biochemistry, Vanderbilt University School of Medicine, Nashville, TN, USA*

Eszter Fidrus • *Department of Biotechnology and Microbiology, University of Debrecen, Debrecen, Hungary*

Jennifer A. Fischer • *Department of Molecular Biology, University of Medicine and Dentistry of New Jersey, Stratford, NJ, USA*

Jorge Garcia • *Department of Pathology, Brander Cancer Research Institute, New York Medical College, Valhalla, NY, USA*

Morgane Gossez • *Immunology Laboratory, Hospices Civils de Lyon, E. Herriot Hospital, Lyon, Cedex, France; EA Pathophysiology of Injury-induced Immunosuppression (PI3—University Claude Bernard Lyon 1—Hospices Civils de Lyon— bioMérieux), Lyon, France*

Dorota Halicka • *Department of Pathology, Brander Cancer Research Institute, New York Medical College, Valhalla, NY, USA*
Yuji Hirao • *National Agriculture and Food Research Organization (NARO), Institute of Livestock and Grassland Science, Ibaraki, Japan*
Gábor V. Horváth • *Laboratory of Molecular Regulators of Plant Growth, Biological Research Center, Hungarian Academy of Sciences, Szeged, Hungary*
Hui Hua • *Department of Biochemistry, Vanderbilt University School of Medicine, Nashville, TN, USA*
Juliette Humeau • *Centre de Recherche des Cordeliers, Equipe 11 labellisée Ligue contre le Cancer, INSERM, France*
Takashi Iwamatsu • *Aichi University of Education, Ichigaya, Karia, Japan*
Mohamed Jemaà • *Department of Cardiology, Vascular Medicine and Physiology, University of Tuebingen, Tuebingen, Germany*
Kap-Hyoun Ko • *Sydney Cord & Marrow Transplant Facility, Sydney Children's Hospital, Graduate School of Biomedical Engineering, University of New South Wales, Sydney, NSW, Australia*
Edit Kotogány • *Flow Cytometer and Cell Sorter Laboratory, Biological Research Center, Hungarian Academy of Sciences, Szeged, Hungary*
Guido Kroemer • *Centre de Recherche des Cordeliers, Equipe 11 labellisée Ligue contre le Cancer, INSERM, France*
Thomas J. Langan • *Department of Neurology, Jacobs School of Medicine and Biomedical Sciences, Children's Hospital of Buffalo, State University of New York at Buffalo, Buffalo, NY, USA; Department of Pediatrics, Jacobs School of Medicine and Biomedical Sciences, Children's Hospital of Buffalo, State University of New York at Buffalo, Buffalo, NY, USA; Department of Physiology, Jacobs School of Medicine and Biomedical Sciences, Children's Hospital of Buffalo, State University of New York at Buffalo, Buffalo, NY, USA; Department of Biophysics, Jacobs School of Medicine and Biomedical Sciences, Children's Hospital of Buffalo, State University of New York at Buffalo, Buffalo, NY, USA*
Cong-Jun Li • *Animal Genomics and Improvement Laboratory, Beltsville Agricultural Research Center, ARS, USDA, Beltsville, MD, USA*
Jiangwei Li • *Department of Pathology, Brander Cancer Research Institute, New York Medical College, Valhalla, NY, USA*
Hoi Tang Ma • *Division of Life Science, Center for Cancer Research and State Key Laboratory of Molecular Neuroscience, The Hong Kong University of Science and Technology, Hong Kong, China*
Gwenola Manic • *Regina Elena National Cancer Institute, Rome, Italy*
Arkadi Manukyan • *Department of Biochemistry and Molecular Genetics, University of Virginia, School of Medicine, Charlottesville, VA, USA*
Guillaume Monneret • *Immunology Laboratory, Hospices Civils de Lyon, E. Herriot Hospital, Lyon, Cedex, France; EA Pathophysiology of Injury-induced Immunosuppression (PI3—University Claude Bernard Lyon 1—Hospices Civils de Lyon— bioMérieux), Lyon, France*
Gabor Nagy • *Department of Biotechnology and Microbiology, University of Debrecen, Debrecen, Hungary*
Robert Nordon • *Graduate School of Biomedical Engineering, University of New South Wales, Kensington, NSW, Australia*
Tracey A. O'Brien • *Sydney Cord & Marrow Transplant Facility, Sydney Children's Hospital, Centre for Children's Cancer & Blood Disorders, Sydney Children's Hospital, Randwick, NSW, Australia*

Cihan Oguz • *Department of Biological Sciences, Virginia Tech, Blacksburg, VA, USA*
Alida Palmisano • *Biometric Research Program, Division of Cancer Treatment and Diagnosis, National Cancer Institute (NIH/NCI), Bethesda, MD, USA; Department of Biological Sciences, Virginia Tech, Blacksburg, VA, USA; Department of Computer Science, Virginia Tech, Blacksburg, VA, USA*
Monika Podhorecka • *Department of Hemato-Oncology and Bone Marrow Transplantation, Medical University, Lublin, Poland*
Randy Y.C. Poon • *Division of Life Science, Center for Cancer Research and State Key Laboratory of Molecular Neuroscience, The Hong Kong University of Science and Technology, Hong Kong, China*
Benjamin E. Reubinoff • *Department of Obstetrics and Gynecology, and the Hadassah Human Embryonic Stem Cells Research Center, The Goldyne-Savad Institute of Gene Therapy, Hadassah-Hebrew University Hospital, Jerusalem, Israel*
Kyla R. Rodgers • *Department of Medicine, Geisel School of Medicine at Dartmouth, Hanover, NH, USA*
Anna Santamaria Margalef • *Cell Cycle and Cancer, Biomedical Research Group in Gynecology, Vall Hebron Research Institute (VHIR) – UAB, Barcelona, Spain*
Brandt L. Schneider • *Department of Medical Education, Texas Tech University Health Sciences Center, Lubbock, TX, USA*
Laura Senovilla • *Centre de Recherche des Cordeliers, Equipe 11 labellisée Ligue contre le Cancer, INSERM, France*
Yoel Shufaro • *Infertility and IVF Unit, Beilinson Women's Hospital, Rabin Medical Center, Petach-Tikva, Israel; The Sackler Faculty of Medicine, Tel Aviv University, Tel Aviv, Israel*
Jessica Smith • *Department of Cell Biology and Biochemistry, Texas Tech University Health Sciences Center, Lubbock, TX, USA*
Tamás Somfai • *National Agriculture and Food Research Organization (NARO), Institute of Livestock and Grassland Science, Ibaraki, Japan*
Staffan Svärd • *Department of Cell and Molecular Biology, Uppsala University, Uppsala, Sweden*
Geoff Symonds • *Faculty of Medicine, University of New South Wales, Sydney, NSW, Australia*
Laszlo Talas • *Department of Biotechnology and Microbiology, University of Debrecen, Debrecen, Hungary*
Bence Tanczos • *Department of Biotechnology and Microbiology, University of Debrecen, Debrecen, Hungary*
Karin Troell • *Department of Microbiology, National Veterinary Institute, Uppsala, Sweden*
Fabienne Venet • *Immunology Laboratory, Hospices Civils de Lyon, E. Herriot Hospital, Lyon, Cedex, France; EA Pathophysiology of Injury-induced Immunosuppression (PI3—University Claude Bernard Lyon 1—Hospices Civils de Lyon— bioMérieux), Lyon, France*
Ilio Vitale • *Regina Elena National Cancer Institute, Rome, Italy; Department of Biology, University of Rome "Tor Vergata", Rome, Italy*
Judit Zámborszky • *Hungarian Academy of Sciences, Research Centre for Natural Sciences, Institute of Enzymology, Budapest, Hungary*
Hong Zhao • *Department of Pathology, Brander Cancer Research Institute, New York Medical College, Valhalla, NY, USA*

Part I

Cell Cycle Synchronization

Chapter 1

Overview of Cell Synchronization

Gaspar Banfalvi

Abstract

The widespread interest in cell synchronization is maintained by the studies of control mechanism involved in cell cycle regulation. During the synchronization distinct subpopulations of cells are obtained representing different stages of the cell cycle. These subpopulations are then used to study regulatory mechanisms of the cycle at the level of macromolecular biosynthesis (DNA synthesis, gene expression, protein synthesis), protein phosphorylation, development of new drugs, etc. Although several synchronization methods have been described, it is of general interest that scientists get a compilation and an updated view of these synchronization techniques. This introductory chapter summarizes: (1) the basic concepts and principal criteria of cell cycle synchronizations, (2) the most frequently used synchronization methods, such as physical fractionation (flow cytometry, dielectrophoresis, cytofluorometric purification), chemical blockade, (3) synchronization of embryonic cells, (4) synchronization at low temperature, (5) comparison of cell synchrony techniques, (6) synchronization of unicellular organisms, and (7) the effect of synchronization on transfection.

Key words Basic concepts of synchronization, Criteria of synchronization, DNA staining, DNA analysis, C-value

1 Introduction

The description of the double helical structure of DNA was and has remained the most famous research paper in biology [1]. In 1953, another important paper was published that established the model of the cell cycle as we know it today [2]. The famous statement of the reduplication of DNA recognized by Watson and Crick: "It has not escaped our notice that the specific pairing we have postulated immediately suggests a possible copying mechanism for the genetic material" initiated studies on DNA replication. Howard and Pelc used ^{32}P label and after the incorporation of the biological tracer in the root cells of *Vicia faba* (broad bean) they removed all of the non-DNA phosphorus labeled compounds with hydrochloric acid at 60 °C which allowed them to trace the cellular levels of DNA. Their autoradiographic analysis showed that DNA synthesis occurs only at one discrete period during the

Gaspar Banfalvi (ed.), *Cell Cycle Synchronization: Methods and Protocols*, Methods in Molecular Biology, vol. 1524,
DOI 10.1007/978-1-4939-6603-5_1,

interphase between two mitoses. Microspectrometric methods confirmed that DNA replication is limited to a well-defined segment of the interphase preceded and succeeded by other periods where the DNA content was constant [3, 4]. Better spatial resolution was obtained when the highly localized tritiated thymidine was introduced as a radioactive probe and increased the precision of autoradiographic procedures [5]. The incorporation of tritiated thymidine was restricted specifically to DNA, not to RNA and only one of the double strands was labeled. This result was consistent with semiconservative model proposed by Watson and Crick. The principle of semiconservative replication was then proved by the classical experiments of Meselson and Stahl in 1958 [6].

The importance of the experiments of Howard and Pelc is that they led to the recognition that the cell cycle consists of phases known as G1, S, G2, and M. Although the examination of the kinetics of cell proliferation with labeled compounds and autoradiography remained an important technique especially when the duration of the cell cycle phases matters, flow cytometry has become a more popular way to study the cell cycle. Laser scanning cytometry (LSC) technology of flow cytometry heritage is not limited to cell cycle analysis. LSC also allows to inspect and interrogate specific cells of defined genetic, biochemical, or morphological properties.

1.1 Basic Concepts of Cell Cycle Synchronization

Synchronization of cell populations offers a unique strategy to study the molecular and structural events taking place as cells travel through the cell cycle. It allows the exact study of individual phases of the cell cycle, the regulatory mechanisms which determine cell cycle regulation at the level of gene expression and posttranscriptional protein modifications, and contributes to drug discovery. Before going into details first of all we define the basic concepts of cell cycle synchronization. In the process of synchronization cells representing different stages of the cell cycle are selected and brought to the same phase. The cell cycle is composed of the replication of genetic materials (S phase) and the successive distribution of genetic materials as well as the other components of the cell onto two daughter cells (M phase). The progression of these two processes is intermitted by two gap phases (G1 and G2) and defined as the cell cycle (Fig. 1).

Originally the cell cycle was recognized in plant cells [7], but soon it turned out that the principal mechanism of the cell cycle is common in all eukaryotic organisms. The study of molecular events of the cell cycle was taken over by animal and yeast cells [8] simply because there were no suitable cell synchronization systems in plant cells.

1.2 Principal Criteria and Shortcomings of Synchronization Methods

There are several principal criteria for synchronization that should be met: (a) both normal and tumor cells should be arrested at the same specific phase of the cell cycle, (b) synchronization must be noncytotoxic and reversible, (c) the metabolic block should be targeted to

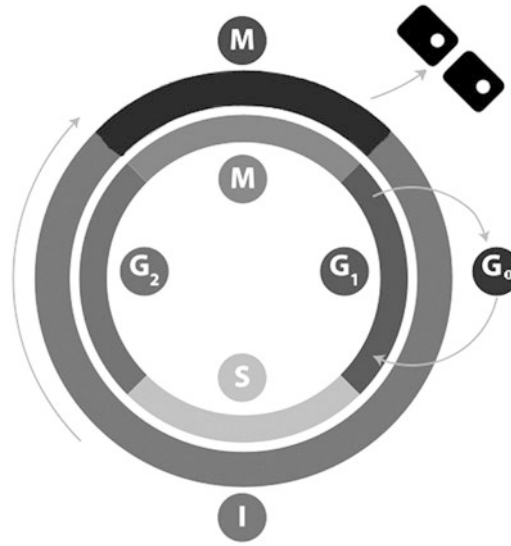

Fig. 1 Cell cycle phases of eukaryotic cells. Cells start to increase in size in Gap 1 (G1) phase. In the resting phase (G_0, Gap 0) cells have left the cycle and stopped dividing. DNA replication occurs during the synthetic (S) phase. During the Gap 2 (G2) between DNA synthesis and mitosis cells continue to grow. In mitosis (M) cell growth stops and the orderly division into two daughter cells takes place. Interphase (I) consists of three stages: G1, S, G2

a specific reaction and must be reversible, (d) large quantities of synchronous cell populations should be obtained, (e) the synchronization must be medium independent, (f) synchrony should be maintained for more than one cell cycle to study biochemical processes taking place in cycling cells, (g) synchronized cells should exhibit uniform size, (h) DNA content in the initial cell culture and during their growth should be the same. These criteria turned out to be quite stringent and resulted in heated debates that still exist among scientists. The major problem is that although many methods have been developed, none of them seems to be perfect for more reasons: (a) the proportion of synchronized cells is not sufficiently high, (b) manipulations during synchronization perturb cell physiology to an unacceptable extent, (c) most of the synchronizing methods are toxic and not applicable in vivo. For example agents that prevent DNA synthesis (excess thymidine, hydroxyurea, aphidicolin) or inhibit the formation of mitotic spindles (nocodazole) not only arrest the cell cycle at certain points [9, 10], but their toxic effect may kill important fractions of the cells [11]. The low cost and simplicity of DNA replication inhibitors is contrasted by their major disadvantage of inducing growth imbalance. Another example is nocodazole treatment. Cells subjected to this agent do not enter mitosis and cannot form metaphase spindles due to the inhibition of polymerization of microtubules. Moreover, when nocodazole was

used as a whole-culture synchronization agent, it worked poorly on bovine kidney (MDBK) cells. After 0.5 ng/ml nocodazole treatment for 4 h there was no accumulation of M phase cells, rather a massive cell death (>80%) was induced [12]. Other observations also demonstrated that populations of synchronized cells obtained by different drug treatments supposedly blocked at biochemically distinct cell cycle points were not apparent by cytometric measurement of DNA content. These results indicate that induced synchrony methods may differ with respect to their impact on cell cycle organization and from the pattern seen with nonperturbing cell selection methods [13]. It is neither the intension of this book to make strict distinctions nor to decide which method should be used. Debates on cell-synchronization methodologies are found in opinion papers [14–18].

2 Methods of Cell Cycle Synchronization

The most widely used methods of cell cycle synchronization are based on two distinct strategies:

1. Physical fractionation.
2. Chemical approach.

2.1 Physical Fractionation

The separation of cells by physical means is based on cell density, cell size, antibody binding to cell surface epitopes, fluorescent emission of labeled cells and light scatter analysis. The two most often used methods of biophysical fractionation are the centrifugal elutriation and fluorescent activated cell sorting.

2.1.1 Velocity Sedimentation

Several techniques that separate cells take advantage of their differences in sedimentation velocity. These methods belong to three classes:

1. Sedimentation at unit gravity [19–21].
2. Density gradient centrifugation [22–25].
3. Velocity sedimentation by counterstreaming centrifugation [26–32].

Major objections against the velocity sedimentation techniques are that they are relatively slow and the size of the nearby fractions may overlap substantially increasing the heterogeneity of the samples. Other major problems with the sedimentation at unit gravity and density gradient centrifugation are the reproducibility, owing to artifacts associated with sedimentation in swinging bucket rotors [33]. These two techniques are not used anymore and therefore not discussed here.

2.1.2 Centrifugal Elutriation

The sedimentation velocity that is based on cell size is operative in the technique of centrifugal elutriation also referred to as counterstreaming centrifugation [26–32]. Lindahl was the first to describe the separation of cells by velocity sedimentation utilizing counterstreaming centrifugation. His method was later modified and renamed centrifugal elutriation. The Beckman elutriation system is an advanced centrifugation device that uses an increasing sedimentation rate to yield a better separation of cells in a specially designed centrifuge and a rotor containing the elutriation chamber. The advantages of centrifugal elutriation are as follows:

1. Differences in sedimentation velocity are exploited to isolate various types of cells from various inhomogeneous cell suspensions,
2. Different subpopulations representing different stages of the cell cycle of the same cell type can be separated.
3. The isolated cells or subpopulations of cells can be used in clinical experiments.
4. Centrifugal elutriation fulfills the three principal criteria for synchronization.

Autoradiographic data indicated that fractions containing ≥ 97% G1 cells, > 80% S cells, and 70–75% G2 cells could be routinely recovered with centrifugal elutriation [34]. This distribution indicates that the resolution of the G1 and S phases belonging to the interphase could be increased while the heterogeneity of the G2 and M phases would not allow a higher resolution. In exponentially growing cultures ≥ 20% of the cells are in G1, about ≥60% in S phase and only 16–18% in G2/M phase. This distribution makes it clear that in animal cells the resolution of the interphase G1 and S phases would be possible. As a result of the improved resolution of the centrifugal elutriation the two known replicative phases (early and late S phase) could be resolved to many subphases the number of which corresponded to the number of chromosomes [35, 36].

In the budding yeast G1-phase cells are unbudded and often smaller than one would expect from the cell cycle status. The budding profile serves as a basis of estimating cell synchrony. In the fission yeast there are no such distinctive features that would allow the morphological determination of the cell cycle position. The cell cycle progression of the yeast cells is size dependent similarly to the cells of budding yeasts and higher eukaryotes [37].

With centrifugal elutriation, several different cell populations synchronized throughout the cell cycle could be rapidly obtained with a purity comparable to mitotic selection and cell sorting [38]. Centrifugal elutriation will be described in Chapter 2. Chapter 14 compares the results from the elutriation protocols with other synchronization protocols.

2.1.3 Flow Cytometry and Cell Sorting

The original name of this technology was pulse cytophotometry, but flow cytometry became the most popular among others such as cytofluorometry, flow microfluorometry. To understand this technique that uses a system for the measurement on individual cells obtained from cell suspension the analogy with a conveyor belt is taken. Conveyor belts have been originally used as rubber belts in factories [39], but they are also running in supermarkets, where they carry to selected goods to the interrogation point, where the cashier picks them individually and identifies them with a laser that reads the barcode. At the interrogation point the items can then be packed without selection into shopping bags or similar items can be grouped and then packed in separate bags. A similar process takes place during flow cytometry without the separation of cells or combined with their separation named cell sorting (Fig. 2).

Flow cytometry is a technique that allows the counting and examination of small (0.2–150 μm) particles (cells, nuclei, chromosomes) suspended in a stream of fluid passed through an electronic detection apparatus. In cell biology individual cells contained in a thin stream of fluid intercept the light source. These cells scatter light and fluorochrome dyes are excited. There are several

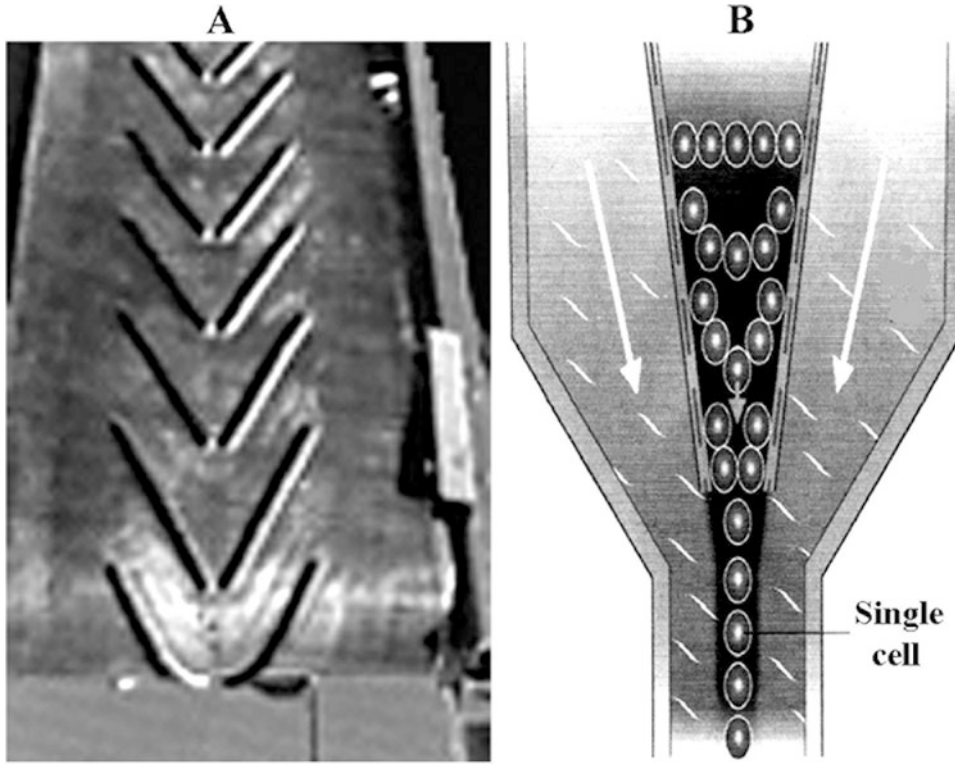

Fig. 2 Analogy between a conveyor belt and flow cytometry. (**a**) Industrial belt [39], (**b**) Hydrodynamic focusing during flow cytometry to produce a single stream of cells [40]

fluorochrome dyes that can be used for DNA staining. For quantitative DNA analysis, cells are normally fixed in ethanol. followed by staining with DNA-binding dyes, such as:

1. Propidium iodide (Phenanthridinium compound).
2. Hoeschst 33342 (Bisbenzimidazole).
3. DAPI (4′-6-diamidino-2-phenylindole).
4. 7 Aminoactinomycin D (Actinomycin).
5. Mithramicin (Chromomycinone).
6. DRAQ5 (Anthraquinone).
7. TO-PRO-3 (comprising a single cyanine dye and a cationic side chain, with only two positive charges).

Some of the dyes are used to quantitatively stain DNA and to separate live from dead cells in unfixed samples. Fluorochromes excited from a lower (300–650 nm) to a higher energy state emit this energy as a photon of light at various frequencies (450–700 nm) with spectral properties unique to different fluorochromes. Photomultipliers convert the light to electrical signals and cell data is collected. High purity (100%) cell sub-populations can be identified and sorted when flow cytometry is combined with cell sorting.

Flow cytometers and analyzers are capable to collect multiparameter cytometry data but do not separate or purify cells. Sorting is an additional process requiring sophisticated electronic components not incorporated into most benchtop instruments. In flow cytometry and fluorescent activated cell sorting (FACS analysis) the light beam (regularly laser) is directed to the stream of fluid containing the particles. Most often used light sources in flow cytometry are argon-, krypton-, helium-neon-, helium cadmium lasers and mercury lamp. Detectors are focused to the interrogation point where the light beam (regularly laser beam) passes through the fluid stream. In forward scatter analysis (FSC) detectors are in line with the light beam, while in side scatter analysis (SSC) several detectors, among them fluorescent detectors, are directed perpendicularly to the beam. Forward and side scatter are used for the preliminary identification of cells. Forward scatter depends on the cell volume and cell size, while side scatter analysis is correlated with the inner complexity of the particle (i.e., shape of the cell or nucleus, amount and type of granules or roughness of cellular membranes). Forward and side scatter were used earlier to exclude debris and dead cells. Recently it has been adapted for the detection of apoptotic cell death.

Advantages and disadvantages of flow cytometry:

1. Flow cytometry measures fluorescence per cell or particle and contrasts with spectrophotometry where the percent absorption and transmission at a certain wavelength is measured for a bulk volume. One of the fundamentals of flow cytometry is its ability to measure the properties of individual particles.

2. The sorting of particles based on their physical properties, to purify populations of interest.
3. The simultaneous physical and/or chemical analysis of thousands of particles per second.
4. Routinely used diagnostic tool in health disorders (especially cancers) and has many applications in both research and clinical practice.
5. Data of samples can be stored in computer as listmode and/or histogram files.
6. The disadvantage of cell sorting is that it exhibits limitations in sample size and time required for synchronization [40].

Listmode files contain the complete list of all events corresponding to all the parameters collected and written in the file. Listmode files contain raw cytometer data. Listmode describes flow cytometry values of the scatter and fluorescence parameters for each event, in the order it passed through the cytometer's interrogation point. Listmode files can be replayed by the computer and appropriate software. Different signals can be amplified and processed by an Analog to Digital Converter (ADC) allowing the events to be plotted on a graphical scale. These histogram files can be either single-parameter

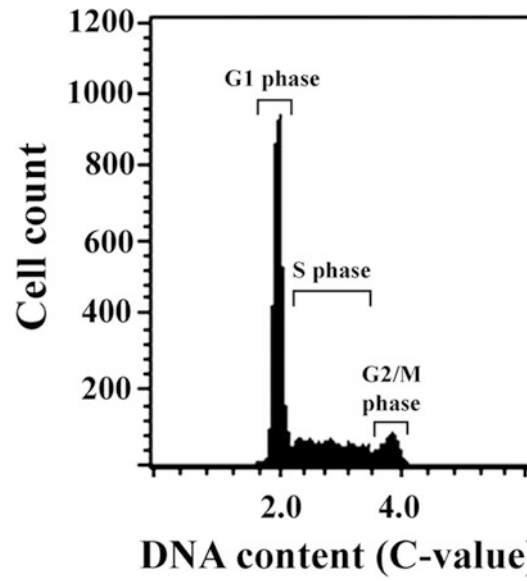

Fig. 3 Flow cytometry: single-parameter histogram. Flow cytometry measures the properties of individual particles. After injecting the sample solution into to flow cytometer, the particles are randomly distributed in three-dimensional space. Upon hydrodynamic focusing, each particle passes through one or more beams of light. Single particles can be interrogated by the machine's detection system. Histograms can be given as density plots, contour diagrams, single parameter (*see* DNA profile above) or two-parameter (dual-color fluorescence) histograms (next figure)

or two-parameter files. The single-parameter histograms have 1024 channels and consist of graphs plotting the cell count on the y-axis and the measurement parameter (e.g., C-value) on x-axis (Fig. 3). When measuring fluorescence from a DNA-binding fluorochrome we regard this to be the same as the DNA content expressed in C-value (C value of 1 corresponds to haploid DNA content per cell). A graph of a two parameter histogram represents two parameters of measurements: the DNA content on the x- and the cell count height on the y-axis similarly to a topographical map (Fig. 4).

DNA histograms yield the relative number of cells in G1/G0, S, and G2/M phases of the cell cycle. The percentage of cells being in each of these phase can be estimated. However, the static information of histograms does not provide information how many cells are progressing through these phases and what percentage of cells is trapped in these phases.

2.1.4 Cytofluorometric Purification of Cells

A novel procedure for the purification of cells in distinct phases of the cell cycle was developed based on the stable transfection of cells with a chimeric protein made up by histone H2B and green fluorescent protein (GFP) [11]. Cytofluorometric purification of cells by their size and their H2B-GFP-dependent fluorescence allowed the efficient separation of diploid and tetraploid cells in a fluorescence-activated cell sorter (FACS). DNA content analysis after staining with fluorochromes (propidium iodide, Hoechst 33342) serves as a basis for fluorescence-activated cell sorting (FACS) to obtain synchronous cell populations. A more detailed description and protocol for cytofluorometry for the quantification of ploidy is given in Chapter 3.

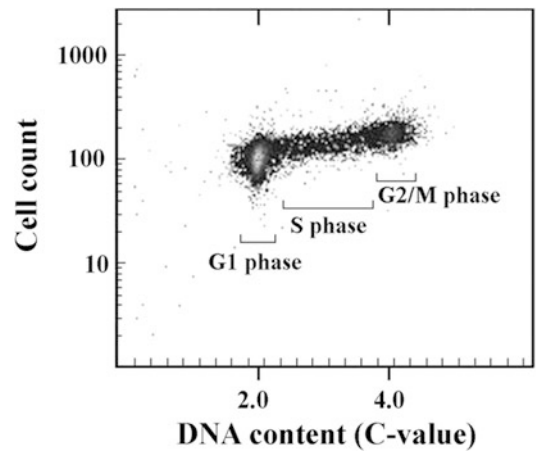

Fig. 4 Flow cytometry: two-parameter histogram. The graph displays two measurement parameters, one on the *y*- and one on the *x*-axis and the cell count as a density plot. Parameters may come from side scatter channel (SSC), forward scatter channel (FSC), or fluorescence

2.1.5 Microchip-Based Flow Cytometers

Flow cytometry is carried out for various medical purposes including the counting of blood cells, detection of pathogenic microbes etc. However, the running of commercial flow cytometers is expensive and requires skilled operators. Miniaturized microchip-based flow cytometers have been developed with built in chambers and tunnels which require much lower volumes of reagents. These devices reduce substantially the cost of diagnosis especially when the chips are disposable. In microchip-based flow cytometers the detected and sort particles are focussed hydrodynamically to pass them through a small detection region [41–46]. Particles are pressed through the device under an external hydrostatic pressure gradient, or under electro-osmotic flow by controlling the movement of the fluid.

2.1.6 Flow Cytometry to Monitor Nucleocytoplasmic Protein Expression

This new flow cytometry assay avoids cell synchronization and applies a stepwise biochemical fractionation procedure to whole cells and isolated nuclei. DNA and immunostaining techniques for the dual labeling of cells and nuclei for DNA and nuclear proteins have been combined with refined flow cytometric data processing and calculation. The combination of flow cytometry with cell size analysis established a resolution map of cell cycle progression to which protein expression in cells or nuclei was correlated [47].

2.1.7 Dielectrophoresis

This method uses laminar flow and electrokinetic forces for the efficient, noninvasive separation of living cells. The alternative current moves particles forward and backward from microelectrodes by periodically reversing the direction of the electric charge [48, 49]. A dielectrophoresis activated cell synchronizer device has been constructed that accepts an asynchronous mixture of cells, fractionates the cell populations according to the cell-cycle phase, and elutes them through different outlets. The device utilizes electric fields that are 1–2 orders of magnitude below those used in electroporation and enriches asynchronous tumor cells in the G1 phase to 96% in one round of sorting, in a continuous flow manner [50].

2.2 Cell Separation with Chemical Blockade ("Arrest and Release" Strategy)

2.2.1 Mitotic Selection

An alternative to overcome the objections of the mitosis-inhibiting (stathmokinetic) approaches involves mitotic selection [51]. Stathmokinetic approaches are discussed later. In monolayer cultures cells are spread over a relatively large area. During mitosis cell become spherical and only a small area of cell membrane remains in contact with the containing vessel. The nuclear material is divided during mitosis (Fig. 5).

The mitotic cells can be completely detached by gently shaking and isolated from the supernatant medium by centrifugation. In actively dividing cells the percentage of mitotic cells known as the mitotic index is relatively low. The mitosis is relatively short compared to the duration of the cell cycle. It can be judged by multiplying the mitotic index by the cell cycle which is normally between 1.0 and 2.5 h. Assuming that the average durations of G1, S, and

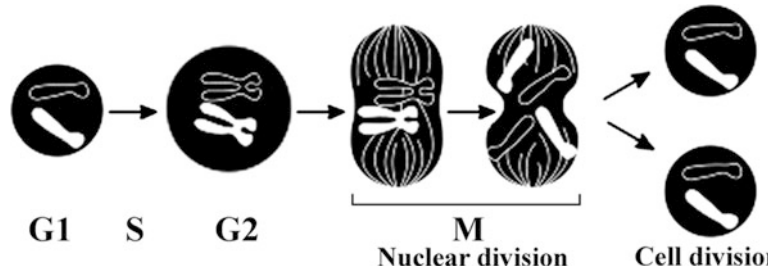

Fig. 5 Nuclear and cell division. The scheme does not show the duration of these processes which represent only a short period of time (1.5–2.5 h) of the cell cycle

G2+M are 8, 10, and 2 h, respectively, then the mitosis takes less than 10% of the cell cycle. To collect sufficient number of mitotic cells for synchronization purpose, the mitotic shake-off should be repeated after 2 h. However, the use of this method is limited to only those cell lines that are grown in a single layer on a flask or Petri dish containing the culture medium and detach during mitosis. Consequently, this method is applicable only to anchorage-dependent, monolayer cell cultures (e.g., HeLa, HaCaT, CHO). Nevertheless, either alone or in combination with blocking agents such as hydroxyurea, the mitotic shake-off turned out to be an excellent method for synchronizing cells [38]. Large scale isolation of mitotic mammalian cells is described in Chapter 4.

2.2.2 Membrane-Elution for Synchronization ("Baby Machine")

This method is analogous to the mitotic shake-off in the sense that one can harvest synchronized cells without any chemical treatment. In this method for batch synchronization of membrane-elution growing cells are bound to a membrane. Baby machines incubate "mother cells" under normal conditions and collect their "babies" similar in cell cycle phase and in age. At division, one cell remains attached to the membrane, the other small daughter cell ("baby") is released into the medium [52, 53]. These newborn cells have a G1 phase DNA content that reflects a normal cell cycle [11]. Among the several macroscale and microfluidic baby machines applied to synchronization, a new baby machine has been presented for rod-shaped cells like fission yeast (*Schizosaccharomyces pombe*). This microfluidic device fixes one end of the cell and releases the free-end daughter cell every time the cell finishes cytokinesis [54].

2.2.3 Types of Chemical Blockade

The idea behind in vitro chemical synchronization is the exposure of a random population of cells to agents that interfere with specific biosynthetic processes, such as DNA replication. The cells blocked in a specific stage of the cell cycle are then released by washing in control media or buffer, followed by the addition of exogenous substrates (e.g., nucleosides, nucleotides) to follow the wavelike rhythm of the cell cycle.

Cells separation by blocking metabolic reactions has been reviewed by Merrill in 1998 [55]. The steady state of cell growth can be altered by the addition of drugs that block or delay the progression of the cell cycle in a specific phase. Methods may be grouped depending on which cell cycle phase has been arrested. Classes of batch synchronization methods arrests cells at:

1. Mitosis by mitotic spindle poisons such as colchicine, vinca alkaloids (vincristine), and nocodazole. Razoxane specifically inhibits the enzyme topoisomerase II resulting in the inhibition of cell division in the premitotic and early mitotic phases of the cell cycle.
2. Other synchronization methods affect DNA synthesis and are proposed to block the cell cycle in S phase (double thymidine block, hydroxyurea, aphidicolin),
3. The third class of chemical synchronization arrests cells at a specific point in the G1 phase, often at the "restriction point" (serum starvation).
4. Combined administration of blocking agents.

Chemical Blockade of Mitosis

Roscovitine. This is an olomoucine-related purine flavopiridol, and is a highly potent inhibitor for the kinase activity of cyclin-dependent kinases (CDK1, CDK2, CDK5, and CDK7, but not for CDK4 and CDK6) by competing with ATP at the ATP binding site of the kinase [56]. Roscovitine is a potent inhibitor acting in G0/G1. However, roscovitine has been reported to prevent cell cycle progression of mammalian cells not only at the G_1–S but also in G_2–M checkpoints [57, 58].

Mimosine. The plant amino acid mimosine may inhibit initiation at origins of replication [59]. Theoretical considerations argue against the use of batch synchronization methods as they are likely to disturb cell growth and prevent the understanding the normal cell cycle [11].

Colchicine. One of the best known examples of chemical synchronization is the addition of colchicine (colcemid) which causes cell cycle arrest in metaphase by depolymerizing tubulin in microtubules. After treating cells with colcemid (or rasoxane, ICRF 159) cells accumulate in M phase and cannot proceed to anaphase. Sampling of cell populations at intervals after colcemid treatment showed a progressive shift of the flow cytometric profile from left to the right. Colchicine has been used to increase proportions of G2/M cells from 13 to 27–32% in pig mammary cells, and up to 37% in fibroblasts [60].

Vincristine (*Oncovin*, *leurocristine*). This vinca alkaloid from the Madagascar periwinkle *Catharanthus roseus* (*Vinca rosea*) is also a mitotic inhibitor, and is used in cancer chemotherapy. The mitodepressive effect and stathmokinetic action of cathinone from

Catha edulis [61] and pantopon, a preparation of opiates [62], were reported on the meristematic region in the root tips of *Allium cepa* (garden onion).

Major objections against these and other stathmokinetic (mitosis-inhibiting) approaches are that cell cycle blockades are likely to perturb and alter the behavior of the cell population in an unpredictable manner. Such a known example is the colcemid block of mitogenically stimulated B lymphocytes that resulted not only in G2 block but also in a G1 arrest. Moreover, tumorigenic lymphoblastoid cell lines have lost their sensitivity to growth inhibition by colcemid during early G1 [63].

Cell Separation by the Inhibition of DNA Synthesis

One method that is generally used is the exposure of randomly proliferating cells to agents that interfere with specific biosynthetic activities, e.g., DNA replication. The cells blocked in the S phase are subsequently released by washing in control media, followed in some cases by the addition of exogenous tracers such as nucleotides. The removal of the blocking agent permits cells to move into succeeding segments of the cell cycle.

Metabolic reactions of cells are most often blocked by the inhibition of DNA synthesis and by nutritional deprivation. DNA synthesis can be inhibited during S phase by inhibitors of DNA replication such as excess thymidine [64], aminopterin (4-amino folic acid) [65–67], hydroxyurea [68, 69], methotrexate [70], fluorodeoxyuridine [71], butyrate [12, 72, 73], cytosine arabinoside [74], and low temperature [75]. The cell cycle is blocked by these inhibitors primarily in S phase resulting in viable cells. Their effects are variable and often debated.

Nutrient modification or stability. Best known nutrient deprivation methods are serum starvation and statin (e.g., lovastatin) treatment. By optimizing nutrient modulation periods using a microfluidic device a relatively high level (80%) of synchronization could be achieved [76]. In this nutrient modification system the microfluidic cell culture chip was fixed on the motorized stage of an inverted microscope, which made the multipoint data acquisition possible. Two kinds of culture media were perfused with the help of two syringe pumps [76]. Alternatively, the stability of nutrient can be maintained by giving fresh medium and removing the old one from the cell culture. The addition of synchronizing agents can also be performed in such a perfusion system adapted for the synchronization of cells based on time-lapse microscopy and using syringe pumps (Chapter 10).

Double thymidine block (*early S-phase block*). A typical procedure for a double-thymidine block was described by Whitfield in 2002 [77]. Cells (e.g., HeLa) at ~30% confluency are washed with buffer (PBS) growth medium and cells are grown in the presence of 2 mM thymidine for 18 h. After the first block thymidine is removed, cells are washed and grown in fresh medium for 9 h to

release cells from the block. The release is followed by the second block by the addition of 2 mM thymidine and cultivation for 17 h. As a result of this synchronization cells progress synchronously through G2- and mitotic phase and will be arrested at the beginning of S phase. Synchrony can be monitored by flow cytometry of propidium iodide-stained cells. After release from the thymidine block, >95% of the cells entered S phase (in 0–4 h), progressed into G2 phase (5–6 h), underwent a synchronous mitosis at 7–8 h, and reentered S phase after completing one full cell cycle at 14–16 h. Typically two to three additional synchronous cell cycles were obtained [77]. Thymidine synchronization showed a constant rate of synthesis of DNA throughout S-phase, but cells synchronized with aminopterin show a slower initial rate of DNA synthesis [67].

Hydroxyurea. Hydroxyurea is used to treat certain types of cancer or blood disorders. This medication may also be useful for chronic urinary tract infections or certain cases of psoriasis. In cell biology hydroxyurea synchronization increases mitotic yield of cell lines. Large quantities of synchronized cells have been isolated in late G1 by growth in isoleucine-deficient medium followed by resuspension in fresh, complete medium containing either hydroxyurea (to 10^{-3} M) or cytosine arabinoside (to 5 μg/ml) [78].

The inhibitors that have been used most frequently for synchronization are hydroxyurea, which inhibits ribonucleotide reductase [79], and aphidicolin, an inhibitor of DNA polymerases [80]. However, none of these agents has been regarded as truly satisfactory since both are chain elongation inhibitors that would not inhibit initiation of replication at the replication forks. Thus, most of the events of interest (i.e., initiation at early-firing origins) would have already occurred prior to release from the blocking agent. Unfortunately, drugs that specifically prevent either entry into the S period or initiation at origins have not yet been identified.

Aphidicolin. This tetracyclic diterpenoid produced by the fungus *Cephalosporium aphidicola* [81] selectively inhibits DNA polymerase α [82]. This enzyme is essential for nuclear replicative DNA synthesis, without affecting nuclear DNA repair synthesis and mitochondrial DNA replication [83, 84]. Rodent and porcine fibroblasts can be reversibly synchronized at the S phase with aphidicolin treatment [85, 86]. Aphidicolin turned out to be an effective agent in the synchronization of human HeLA [87] blocking the cell cycle at the transition from G1 to S phase [80]. Cell synchronization is achieved by inhibition of DNA replication in Chapter 7.

Butyrate. A specific cell cycle synchronization was developed for a bovine kidney (MDBK) cell line. Exposure of MDBK cells to 10 mM butyrate caused inhibition of cell growth and cell cycle arrest in a reversible manner. Flow cytometric evidence was presented that butyrate affected the cell cycle at a specific point immediately after

mitosis at the early stage of G1 phase. In comparison with other inhibitors, such as serum deprivation and aphidicolin, butyrate induced similar synchrony of cell populations [12]. A protocol for cell cycle synchronization with butyrate and cell cycle analysis by flow cytometry will be given in Chapters 9 and 10.

Nutrient Deprivation

Serum starvation (*G0/G1 block*). Removal of serum from a rapidly growing cell culture for about 24 h results in the accumulation of cells in G1 phase. Synchronized cells can then be released into S phase by the addition of serum. Nutritional serum starvation has been widely used for synchronizing cells by arresting them in the G0/G1 phase of the cell cycle, but it often reduced cell survival and increased DNA fragmentation [86] which caused high-embryonic losses after NT [88]. Regularly only non-tumor cells can be synchronized in G_0/G_1 by removal of growth factors ("serum starvation", amino-acid depletion). In transformed cells proliferation is relatively independent of serum and growth factors, thus neoplastic cells may not cease proliferation upon serum deprivation, nor do they cease stringent G_0 arrest [89]. A generally applicable procedure to synchronize mammalian cells by serum deprivation is given in Chapter 6.

Treatment with statins. The mechanism by which lovastatin synchronizes cells is unknown. Lovastatin suppresses the synthesis of mevalonate by inhibiting 3-hydroxy-3-methylglutaryl-coenzyme A (HMG-CoA) reductase, the rate-limiting enzyme in the sterol-biosynthetic pathway. In addition to the deprivation of mevalonate by lovastatin, compactin (mevastatin), a related fungal toxin [90] and mevinolin [91], these statins also inhibit DNA replication [92–97]. Lovastatin was successfully introduced as an early G1 synchronization agent with cell lines including normal and tumor cells of mouse, hamster and human origin [98]. Statins as G_1 inhibitors prevent farnesylation and geranylation of proteins [99] and are effective CDK2 protein kinase inhibitors [100–102]. Synchronization was achieved by the use of compactin [90, 103] presumably by blocking DNA replication and mevalonate production

Other inhibitors. It has been reported that roscovitine, a specific cyclin-dependent kinase (CDK) 2 inhibitor more efficiently synchronized cells in the G0/G1 phase of the cell cycle than serum starvation, and resulted in an increase in cloning efficiency as defined in terms of survival of fetuses and calves following embryo transfer [104].

Combined Administration of Blocking Agents

Blocking agents have been often applied for synchronization due to the simple procedure consisting of cell growth in the presence of the inhibitor. Cells blocked in one of the cell cycle phases (regularly in S phase) were then subsequently released by washing away the inhibitor and thereby permitting their simultaneous movement into succeeding segments of the cell cycle. Partial synchronization

of cell division in vitro has been obtained with considerable success through the implementation of these techniques. The utilization of more than one antimetabolite was expected to improve the efficiency of synchronization.

Thymidine–nocodazole. Cells can be arrested in mitosis by blocking first in thymidine followed by release and then blocking in nocodazole. After release from the nocodazole block, most of the cells (>75%) divided synchronously within 2 h of release from the arrest, entered S phase by 10–12 h after release, and completed the next synchronous mitosis by 18–20 h, ultimately completing two full cell cycles [77].

Thymidine–colcemid. When Successive treatment with excess thymidine and colcemid was applied all in one generation a high degree of synchrony was achieved by this method [105]. The mitosis index of blastomeres increased from 9% metaphases (colchicine synchronization) to 18% (thymidine + colchicine synchronization) per embryo. The in vitro development of embryos was not affected by treatment [106].

Cytosine arabinoside–colcemid. A number of studies have demonstrated that cytosine arabinoside (ara-C) inhibits mitotic activity in mammalian cells both in vitro [107] and in vivo [108, 109]. The mitotic activity of Lieberkuhn's crypt epithelial components increased from 3 to 5% levels to peak values of 15% in rats treated with a single injection of either ara-C or colcemid. In animals treated with ara-C followed by colcemid the efficiency of synchronization was significantly improved, at least two-thirds of the epithelial cells were identified as dividing cells [110].

Methotrexate versus *serum deprivation and colcemid treatment*. Methotrexate or aphidicolin treatment induces a reversible blockade at the beginning of S phase which can be reversed upon drug removal with a consequent wave of synchronization [111]. The combination of serum deprivation and aphidicolin was compared with low nontoxic concentrations (0.04–0.08 μM) of methotrexate under standard culture conditions in cancer cell lines. Synchronization with methotrexate alone turned out to be a better choice for obtaining highly synchronous human cancer cell population than those induced by aphidicolin alone or by a combination of serum deprivation and aphidicolin [112]. These experiments indicate that the combination of synchronization techniques and/or repeated perturbation of cell physiology do not necessarily contribute to a more homogeneous pool of synchronized cells. It is thus better to use the combination of methods that have less or no effect on the cell cycle. Such a combination is centrifugal elutriation with a nutrient starvation protocol. Nutrient starvation contributes to a better size selection and improves synchrony. Moreover, less cells will be needed for elutriation.

2.3 Synchronization of Embryonic Cells

Serum deprivation of embryonic stem cells before cell transplantation was adapted to decrease the rate of cell death after transplantation [113]. To decide whether G0 or G1 cells function better as donor cells has been analyzed during the cell cycle of goat transfected fibroblasts and determined the timing of transition from G0 to G1. Northern blot analysis showed that after 4 days 4-day serum-starved quiescent cells started entering G1 and a few hours after addition of 10% serum to the medium cells were at the mid-G1 stage [114].

2.4 Synchronization at Low Temperature

Human fibroblasts which are in S phase at the time of switching to low temperature (30 °C) complete their DNA synthesis and become arrested in the G1 phase of the cell cycle. The arrested cells can continue proliferation by restoration of the optimal growth temperature (37 °C). At 30 °C DNA replication was inhibited while the excision-repair process was operative but at a slightly reduced rate in comparison. This method was recommended for the study of S-phase-dependent processes, as well as for repair studies in the absence of cell division [115]. The effect of low incubation temperature on synchronization was also studied in cultures of *Plasmodium falciparum*. Growth seemed to be arrested when parasites reached maturation, but reestablished their growth normally when returned to 37 °C [116].

2.5 Comparison of Cell Synchrony Techniques

Different methods–same cell culture. This was done by taking aliquots from the same culture of exponentially growing CHO cells, which were then synchronized using mitotic selection, mitotic selection and hydroxyurea block, centrifugal elutriation, or an EPICS V cell sorter. It was concluded that, either alone or in combination with blocking agents such as hydroxyurea, elutriation and mitotic selection were both excellent methods for synchronizing cells [38]. The use of aphidicolin or hydroxyurea resulted in highly synchronized CHO cell populations, but methotrexate yielded inadequate synchronization [117]. It was demonstrated that both aphidicolin and hydroxyurea were useful drugs for obtaining highly synchronized cell populations after an initial synchrony in mitosis. Aphidicolin was regarded as the best choice because of less toxicity to S phase cells when used in low concentrations.

Selecting inhibitors for bone marrow cultures. Methods for synchronization of bone marrow cells with fluorodeoxyuridine (FdU) and methotrexate (MTX) were compared. Fluorodeoxyuridine did not require cell washing for release of the DNA synthesis block and was found to be more beneficial for bone marrow cultures because it generally produced a higher mitotic yield and was less damaging to chromosomes than methotrexate [71]. However, after FdU treatment flow cytometric analysis showed not only the accumulation of cells in early S phase over time, but also the increased radiation sensitivity of the entire population. Early S turned out to be the most

radiosensitive phase of the cell cycle [118]. Synchrony was tested in vivo in acute leukemic patients after a single injection of l-asparaginase, hydrocortisone, cyclophosphamide, cytosine arabinoside, methotrexate, and an exchange transfusion (62% of the total blood volume). l-asparaginase and hydrocortisone were found to arrest the entry of cells into the S period. Cyclophosphamide appeared to inhibit DNA synthesis, arrested cells in mitosis, and inhibited the entry of cells into the S period. Cytosine arabinoside and methotrexate inhibited DNA synthesis. During the period of time the cells were inhibited in the S phase by these two drugs, cells continued to enter the S period. Thus partial synchronization was achieved after Cytosine arabinoside, and methotrexate treatment [74].

Selection among G1/S blocking agents. For cytogenetic replication studies the timing of cell synchronization is restricted to G1 or early S phase. To get more precise information with regard to the point of G1–S transition different blocking systems have been investigated. Human amniotic fluid cells and fibroblast were temporarily blocked by replication inhibitors: thymidine (dT) surplus, fluorodeoxyuridine (FU), hydroxyurea (HU), and methotrexate uridine (MU). Most variation was found after HU treatment. MU synchronized cells before the unset of S phase. The arresting point of dT surplus and FdU was in early S phase [119].

2.6 Synchronization of Unicellular Organisms

Synchronization of E. coli. To synchronize E. coli cells in culture, two major approaches have been routinely used. One involves temperature-sensitive alleles of the DNA replication protein DnaC [120] that interacts with DNA helicase, DnaB [121] required for the initiation of DNA replication. When the culture is shifted to nonpermissive temperature this will allow all replication forks to be completed without the initiation of new ones. Subsequent shift to permissive temperature allows initiation of the synchronized culture [122]. The other method is based on the attachment of cells to a membrane, while newborn cells are released to the medium. This technique is the adaptation of the "baby machine" [123, 124]. Although cells are hardly perturbed, large quantities of cells cannot be collected by this method. Moreover, there are significant variations in stickiness among different *E. coli* strains [124]. A new method of *E. coli* synchronization applies DL-serine hydroxamate, an amino acid analog, which arrests DNA replication at initiation [125]. Sporulation of bacteria and outgrowth of spores can be utilized for the synchronization of *B. subtilis* (Chapter 13).

The stationary phase was selected for the synchronization of *Escherichia coli* and *Proteus vulgaris.* This method utilized the early stationary phase, by harvesting bacteria quickly under minimal conditions of stress, and inoculating them into fresh medium at a dilution of about sevenfold. Repeated partial synchronization up to four-generation, cycles of high percentage of phasing were obtained [126]. Other earlier methods used filtration to synchronize bacteria

[127–129], by binding bacteria to various surfaces and elute unbound sister cells from the surface [123, 130], by means of temperature shift [131], or by amino acid starvation [132].

Synchronization of yeast. Budding yeast can utilize a wide range of carbon sources (glucose, galactose, ethanol, and glycerol. These carbon sources may serve as a means to control cell cycle times, growth rates, and cell size can be useful in the development of synchronization methods, which in turn may contribute to exploit yeasts in biotechnology.

The synchronization of yeast cells include: feeding and starving, magnesium exhaustion, repetitive heat shock, DNA division cycle block and release, α-factor mating pheromone block, cdc mutants arresting at specific cell cycle stages at a restrictive temperature, continuous synchrony by periodic feeding or dilution. These methods have been summarized by Walker in 1999 [133]. An overview of the most commonly used methods to generate synchronized yeast cultures is presented in Chapter 14.

2.7 Effect of Synchronization on Transfection

Aphidicolin cell synchronization in G2/M phase led to a slight increase in plasma membrane permeabilization, to a three-fold increase in percentage of transfected Chinese hamster cells and to an eight-fold increase in gene expression. This increase in cell transfection was specifically due to the G2/M synchronization process. Cell synchronization in G1 phase by sodium butyrate had no effect on cell permeabilization and transfection [134]. S-phase synchronized CHO cells also showed elevated transfection efficiency [135]. The hypothesis that cell cycle synchronization increases transfection was efficiency was confirmed in human trabecular meshwork cells. While efficiency of transfection increased about three–fold in synchronized cells compared to controls, it still remained low (~3%) [136].

2.8 Assessment of Synchronization

Validation protocols. Several protocols including flow cytometry with propidium iodide or BrdU labeling, immunoblotting, detecting the levels of cyclins, fluorescent ubiquitin-based cell cycle indicators and time-lapse microscopy, for validation of synchrony of the cells and monitoring the progression of the cell cycle are provided in Chapter 12.

Chapters related to cell cycle. Fertilized eggs shift their cell cycle from mitotic to meiotic pattern for embryogenesis. The formation of chromosomes during fertilization in eggs is described in Chapter 8. Enzymes play a key role in maintaining genomic integrity during the cell cycle. The turnover of these nuclear uracil-DNA glycosylase enzymes during the cell cycle is presented in Chapter 11. Cytofluorometric and time-lapse videomicroscopy methods to detect cell cycle progression, including the assessment of cell cycle distribution, mitotic cell fraction, and single cell fate profile of living cells, can be found in Chapter 5. Time-lapse videomicroscopy

perfusion system is used to visualize individual cells synchronized by butyrate and serum starvation in Chapter 10. Protocols for the synchronization of unicellular organisms are given for bacteria (Chapter 13), yeast (Chapter 14), and protozoans (Chapter15). The synchronization of nuclear progression of porcine oocytes has been achieved by the transient inhibition of meiotic resumption (Chapter 16). Synchronization of cell division can be achieved using different plant tissues. Chapter 17 describes the methodology of the establishment, propagation and analysis of a *Medicago sativa* suspension culture.

Stem cells. Cloning of organisms by mammalian somatic cell nuclear transfer (SCNT) was successfully accomplished in farm animals initially in sheep (Dolly the Sheep), then in rodents, and more recently in primates for reproductive and therapeutic purposes. Somatic cell nuclear transplantation has become the focus in stem cell research. Chapter 18 describes how mouse somatic cell transfer is performed after the treatment and synchronization of donor cells. The next chapter deals with the generation of large numbers of hematopoietic stem cells (Chapter 19).

Clinical aspects and applications of flow cytometry are represented by novel intracellular protocols in Chapter 20.

Cell cycle control. The last chapter reviews the aspects of physiological and molecular transitions that occur in the cell cycle and discusses the role of mathematical modeling in elucidating these transitions and understanding of cell cycle synchronization (Chapter 21).

References

1. Watson JD, Crick FH (1953) Molecular structure of nucleic acids: a structure for deoxyribonucleic acid. Nature 171:737–738
2. Howard A, Pelc S (1953) Synthesis of deoxyribonucleic acid in normal and irradiated cells and its relation to chromosome breakage. Heredity 6:261–273
3. Walker PM, Yates HB (1952) Nuclear components of dividing cells. Proc R Soc Lond B Biol Sci 140:274–299
4. Swift H (1953) Nucleoproteins in the mitotic cycle. Tex Rep Biol Med 11:755–774
5. Taylor JH, Woods PS, Hughes WL (1957) The organization and duplication of chromosomes as revealed by autoradiographic studies using tritium-labeled thymidine. Proc Natl Acad Sci U S A 43:122–128
6. Meselson M, Stahl FW (1958) The replication of DNA in Escherichia coli. Proc Natl Acad Sci U S A 44:671–682
7. Howard A, Pelc SR (1951) Nuclear incorporation of P^{32} as demonstrated by autoradiographs. Exp Cell Res 2:178–187
8. Baserga R (1985) The biology of cell reproduction. Harvard University Press, Cambridge, MA
9. Amon A (2002) Synchronization procedures. Methods Enzymol 351:457–467
10. Cooper S (2003) Rethinking synchronization of mammalian cells for cell cycle analysis. Cell Mol Life Sci 60:1099–1106
11. Coquelle A, Mouhamad S, Pequignot MO, Braun T, Carvalho G, Vivet S et al (2006) Enrichment of non-synchronized cells in the G1, S and G2 phases of the cell cycle for the study of apoptosis. Biochem Pharmacol 72:1396–1404
12. Li CJ, Elasser TH (2006) Specific cell cycle synchronization with butyrate and cell cycle analysis by flow cytometry for Madin Darby Bovine Kidney (MDBK) cell line. J Anim Vet Adv 5:916–923
13. Urbani L, Sherwood SW, Schimke RT (1995) Dissociation of nuclear and cytoplasmic cell cycle progression by drugs employed in cell synchronization. Exp Cell Res 219:159–168

14. Cooper S (2004) Is whole-culture synchronization biology's 'perpetual-motion machine'? Trends Biotechnol 22:266–269
15. Cooper S (2004) Rejoinder: whole-culture synchronization cannot, and does not, synchronize cells. Trends Biotechnol 22:274–276
16. Spellman PT, Sherlock G (2004) Reply: whole-culture synchronization - effective tools for cell cycle studies. Trends Biotechnol 22:270–273
17. Spellman PT, Sherlock G (2004) Final words: cell age and cell cycle are unlinked. Trends Biotechnol 22:277–278
18. Liu SV (2005) Debating cell-synchronization methodologies: further points and alternative answers. Trends Biotechnol 23:9–10
19. Macdonald HR, Miller RG (1970) Synchronization of mouse L-cells by a velocity sedimentation technique. Biophys J 10:834–842
20. Durand RE (1975) Isolation of cell subpopulations from in vitro tumor models according to sedimentation velocity. Cancer Res 35:1295–1300
21. Tulp A, Welagen JJ (1976) Fractionation of ascites tumour cells at 1 g: separation of cells in specific stages of the life cycle. Europ J Cancer 12:519–526
22. Mitchison JM, Vincent WS (1965) Preparation of synchronous cell cultures by sedimentation. Nature 205:987–989
23. Schindler R, Ramseier L, Schaer JC, Grieder A (1970) Studies on the division cycle of mammalian cells. 3. Preparation of synchronously dividing cell populations by isotonic sucrose gradient centrifugation. Exp Cell Res 59:90–96
24. Wolff DA, Pertoft H (1972) Separation of HeLa cells by colloidal silica density gradient centrifugation. I. Separation and partial synchrony of mitotic cells. J Cell Biol 55:579–585
25. Probst H, Maisenbacher J (1973) Use of zonal centrifugation for preparing synchronous cultures from Ehrlich ascites cells grown in vivo. Exp Cell Res 78:335–344
26. Lindahl PE (1956) On counter streaming centrifugation in the separation of cells and cell fragments. Biochim Biophys Acta 21:411–415
27. Sörenby L, Lindahl PE (1964) On the concentrating of ascites tumour cells in stages of pre-mitosis and mitosis by counter-streaming centrifugation. Exp Cell Res 35:214–217
28. Grabske RJ, Lake S, Gledhill BL, Meistrich ML (1975) Centrifugal elutriation: separation of spermatogenic cells on the basis of sedimentation velocity. J Cell Physiol 86:177–189
29. Meistrich ML, Meyn RE, Barlogie B (1977) Synchronization of mouse L-P59 cells by centrifugal elutriation separation. Exp Cell Res 105:169–177
30. Grdina DJ, Peters LJ, Jones S, Chan E (1978) Separation of cells from a murine fibrosarcoma on the basis of size. I. Relationship between cell size and age as modified by growth in vivo or in vitro. J Natl Cancer Inst 61:209–214
31. Gohde W, Meistrich ML, Meyn RE, Schumann J, Johnston D, Barlogie B (1979) Cell-cycle phase-dependence of drug-induced cycle progression delay. J Histochem Cytochem 27:470–473
32. Shumaker VN (1967) Zone centrifugation. Adv Biol Phys 11:245–339
33. Banfalvi G (2008) Cell cycle synchronization of animal cells and nuclei by centrifugal elutriation. Nat Protoc 3:663–673
34. Keng PC, Li CKN, Wheeler KT (1980) Synchronization of 9L rat rain tumor cells by centrifugal elutriation. Cell Biophys 2:191–206
35. Banfalvi G, Mikhailova M, Poirier LA, Chou MW (1997) Multiple subphases of DNA replication in Chinese hamster ovary (CHO-K1) cells. DNA Cell Biol 16:1493–1498
36. Rehak M, Csuka I, Szepessy E, Banfalvi G (2000) Subphases of DNA replication in Drosophila cells. DNA Cell Biol 19:607–612
37. Day A, Schneider C, Schneider BL (2004) Yeast cell synchronization. Methods Mol Biol 241:55–76, Clifton NJ
38. Grdina DJ, Meistrich ML, Meyn RE, Johnson TS, White RA (1984) Cell synchrony techniques. I. A comparison of methods. Cell Tissue Kinet 17:223–236
39. Continental conveyors Ltd http://www.ccpl.in/?gclid=CL2u7qbjxp8CFVmHzAodFzb4ew
40. Rahman M http://www.abdserotec.com/uploads./Flow-Cytometry.pdf
41. Lee G-W, Hung C-I, Ke B-J, Huang G-R, Hwei G-R, Hwei B-H et al (2001) Hydrodynamic focussing for a micromachined flow cytometer. Trans ASME 123:62–679
42. Fiedler S, Shirley SG, Schnelle T, Fuhr G (1998) Dielectrophoretic sorting of particles and cells in a microsystem. Anal Chem 70:1909–1915
43. Fu AY, Spence C, Scherer A, Arnold FH, Quake SR (1999) A microfabricated fluorescence-activated cell sorter. Nat Biotech 17:1109–1111

44. Gawad S, Schild L, Renaud P (2001) Micromachined impedance spectroscopy flow cytometer for cell analysis and particle sizing. Lab Chip 1:76–82
45. Kruger J, Singh K, O'Neill A, Jackson C, Morrison A, O'Brien P (2002) Development of a microfluidic device for fluorescence activated cell sorting. J Micromech Microeng 12:486–494
46. Schrum DP, Culbertson CT, Jacobson SC, Ramsey JM (1999) Microchip flow cytometry using electrokinetic focusing. Anal Chem 71:4173–4177
47. Rosner M, Schipany K, Hengstschläger M (2013) Merging high-quality biochemical fractionation with a refined flow cytometry approach to monitor nucleocytoplasmic protein expression throughout the unperturbed mammalian cell cycle. Nat Protoc 8:602–623
48. Morgan H, Holmes D, Green NG (2003) 3D focusing of nanoparticles in microfluidic channels. IEE Proc Nanobiotechnol 150:76–81
49. Holmes D, Sandison ME, Green NG, Morgan H (2005) On-chip high-speed sorting of micron-sized particles for high-throughput analysis. IEE Proc Nanobiotechnol 152:129–135
50. Kim U, Shu CW, Dane KY, Daugherty PS, Wang JY, Soh HT (2007) Selection of mammalian cells based on their cell-cycle phase using dielectrophoresis. Proc Natl Acad Sci U S A 104:20708–20712
51. Teresima T, Tolmach LJ (1963) Growth and nucleic acid synthesis in synchronously dividing populations of HeLa cells. Exp Cell Res 30:344–362
52. Thornton M, Eward KL, Helmstetter CE (2002) Production of minimally disturbed synchronous cultures of hematopoietic cells. Biotechniques 32:1098–1100
53. Cooper S (2002) Minimally disturbed, multicycle, and reproducible synchrony using a eukaryotic "baby machine". Bioessays 24:499–501
54. Wang S, Luo C (2016) Cell cycle synchronization using a microfluidic synchronizer for fission yeast cells. Methods Mol Biol 1342:259–268
55. Merrill GF (1998) Cell synchronization. Methods Cell Biol 57:229–249
56. Mgbonyebi OP, Russo J, Russo IH (1999) Roscovitine induces cell death and morphological changes indicative of apoptosis in MDA-MB-231 breast cancer cells. Cancer Res 59:1903–1910
57. Rudolph B, Saffric JZ, Henglein B, Muller R, Ansorge W, Eilers M (1996) Activation of cyclin-dependent kinases by Myc mediates induction of cyclin A but not apoptosis. EMBO J 15:3065–3076
58. Azevedo WF, Leclerc S, Meijer L, Havlicek I, Strnad M, Kim SH (1997) Inhibition of cyclin-dependent kinases by a purine analogs: crystal structure of human cdk2 complexed with roscovitine. Eur J Biochem 243:518–526
59. Mosca PJ, Dijkwel PA, Hamlin JL (1992) The plant amino acid mimosine may inhibit initiation at origins of replication in Chinese hamster cells. Mol Cell Biol 12:4375–1483
60. Boquest AC, Day BN, Prather RS (1999) Flow cytometric cell cycle analysis of cultured porcine fetal fibroblast cells. Biol Reprod 60:1013–1019
61. Al-Meshal IA (1987) Mitodepressive effect of (–)-cathinone, from Catha edulis (khat), on the meristematic region of Allium cepa root tips. Toxicon 4:451–454
62. Kabarity A, El-Bayoumi A, Habib AA (1979) Mitodepressive effect and stathmokinetic action of pantopon hydrochloride. Mutat Res-Gen Tox En 2:143–148
63. Kenter AL, Watson JV, Azim T, Rabbitts TH (1986) Colcemid inhibits growth during early G1 in normal but not in tumorigenic lymphocytes. Exp Cell Res 167:241–251
64. Viegas-Pequiqnot E, Dutrillaux B (1970) Une methode: simple pour obtenis des prophases et des prometaphases. Ann Genet 21:122–125
65. Rueckert RR, Mueller GC (1960) Studies on unbalanced growth in tissue culture. I. Induction and consequences of thymidine deficiency. Cancer Res 20:1584–1591
66. Kishimoto S, Lieberman I (1965) Nuclear membranes of cultured mammalian cells. J Biol Chem 25:103–107
67. Adams RLP (1969) The effect of endogenous pools of thymidylate on the apparent rate of DNA synthesis. Exp Cell Res 56:55–58
68. Gallo JH, Ordomez JV, Brown GE, Testa JR (1984) Synchronization of human leukemic cells: relevance for high resolution chromosome banding. Hum Genet 66:220–224
69. Biegel JA, Leslie DS, Bigner DD, Bigner SH (1987) Hydroxyurea synchronization increases mitotic yield in human glioma cell lines. Acta Neuropathol 73:309–312
70. Yunis JJ, Bloomfield GD, Ensrud K (1981) All patients with acute nonlymphocytic leukemia may have a chromosomal defect. N Engl J Med 305:135–139
71. Webber LM, Garson OM (1983) Fluorodeoxyuridine synchronization of bone

marrow cultures. Cancer Genet Cytogenet 8:123–132

72. Wright JA (1973) Morphology and growth rate changes in Chinese hamster cells cultured in presence of sodium butyrate. Exp Cell Res 78:456–460
73. Kruh J, Defer N, Tichonicky L (1992) Molecular and cellular action of butyrate. C R Seances Soc Biol Fil 186:12–25
74. Lampkin BC, Nagao T, Mauer AM (1971) Synchronization and recruitment in acute leukemia. J Clin Invest 50:2204–2214
75. Boucher B, Norman CS (1980) Cold synchronization for the study of peripheral blood and bone marrow chromosomes in leukemia and other hematologic disease states. Hum Genet 54:207–211
76. Tian Y, Luo C, Lu Y, Tang C, Ouyang Q (2012) Cell cycle synchronization by nutrient modulation. Integr Biol (Camb) 4:328–334
77. Whitfield ML, Sherlock G, Saldanha AJ, Murray JI, Ball CA, Alexander KE et al (2002) Identification of genes periodically expressed in the human cell cycle and their expression in tumors. Mol Biol Cell 13:1977–2000
78. Tobey RA, Crissman HA (1972) Preparation of large quantities of synchronized mammalian cells in late G1 in the pre-DNA replicative phase of the cell cycle. Exp Cell Res 75:460–464
79. Skoog L, Nordenskjold B (1971) Effect of hydroxyurea and 1-0-D-arabinofuranosylcytosine on deoxyribonucleotide pools in mouse embryo cells. Eur J Biochem 19:81–89
80. Wang TF (1991) Eukaryotic DNA polymerases. Annu Rev Biochem 60:513–552
81. Brundret KM, Dalziel W, Hesp B, Jarvis JAJ, Neidle S (1972) X-ray crystallographic determination of the structure of the antibiotic aphidicolin: a tetracyclic diterpenoid containing a new ring system. J Chem Soc Chem Commun 18:1027–1028
82. Nagano H, Ikegami S (1980) Aphidicolin: a specific inhibitor of eukaryotic DNA polymerase alpha. Seikagaku 52:1208–1216
83. Sala F, Parisi B, Burroni D, Amileni AR, Pedrali-Noy G, Spadari S (1980) Specific and reversible inhibition by aphidicolin in the alpha-like DNA polymerase of plant cells. FEBS Lett 117:93–98
84. Sala F, Galli MG, Levi M, Burroni D, Parisi B, Pedrali-Noy G, Spadari S (1981) Functional roles of the plant alpha-like and gamma-like DNA polymerases. FEBS Lett 124:112–118
85. Levenson V, Hamlin J (1993) A general protocol for evaluation the specific effects of DNA replication inhibitors. Nucleic Acids Res 21:3997–4004
86. Kues WA, Anger M, Carnwarth JW, Motlik J, Nieman H (2000) Cell cycle synchronization of porcine fibroblasts: effects of serum deprivation and reversible cell cycle inhibitors. Biol Reprod 62:412–419
87. Pedrali-Noy G, Spadari S, Miller-Faurès A, Miller AO, Kruppa J, Koch G (1980) Synchronization of HeLa cell cultures by inhibition of DNA polymerase alpha with aphidicolin. Nucleic Acids Res 8:377–387
88. Lawrence JL, Schrick FN, Hopkins FM, Welborn MG, McCracken MD, Sonstegard T et al (2005) Fetal losses and pathologic findings of clones derived from serum-starved versus serum-fed bovine ovarian granulosa cells. Reprod Biol 5:171–184
89. Scher CD, Stone ME, Stiles CD (1979) Platelet-derived growth factor prevents Go growth arrest. Nature 281:390–392
90. Endo A, Kuroda M, Tansawa K (2004) Competitive inhibition of 3-hydroxy-3-methylglutaryl coenzyme A reductase by ML-236A and ML-236B fungal metabolites having hypocholesterolemic activity. Atheroscler Suppl 5:39–42
91. Langan TJ, Slater MC (2005) Isoprenoids and astroglial cell cycling: diminished mevalonate availability and inhibition of dolichol-linked glycoprotein synthesis arrest cycling through distinct mechanisms. J Cell Physiol 149:284–292
92. Larson RA, Chung J, Scanu AM, Vachnin S (1982) Neutrophils are required for the DNA synthetic response of human lymphocytes to mevalonic acid: evidence suggesting that a nonsterol product of mevalonate is involved. Proc Natl Acad Sci U S A 79:3028–3032
93. Habenicht AJ, Glomset JA, Ross R (1980) Relation of cholesterol and mevalonic acid to the cell cycle in smooth muscle and swiss 3T3 cells stimulated to divide by platelet-derived growth factor. J Biol Chem 255:5134–5140
94. Maltese WA, Sheridan KM (1987) Isoprenylated proteins in cultured cells: subcellular distribution and changes related to altered morphology and growth arrest induced by mevalonate deprivation. J Cell Physiol 133:471–481
95. Langan TJ, Volpe JJ (1987) Cell cycle-specific requirement for mevalonate, but not for cholesterol, for DNA synthesis in glial primary cultures. J Neurochem 49:513–521
96. Doyle JW, Kandutsch AA (1988) Requirement for mevalonate in cycling cells: quantitative and temporal aspects. J Cell Physiol 137:133–140

97. Sinensky M, Logel J (1985) Defective macromolecule biosynthesis and cell cycle progression in a mammalian cell starved for mevalonate. Proc Natl Acad Sci U S A 82:3257–3261
98. Keyomarsi K, Sandoval L, Band V, Pardee AB (1991) Synchronization of tumor and normal cells from G1 to multiple cell cycles by lovastatin. Cancer Res 51:3602–3609
99. Jakóbisiak M, Bruno S, Skierski J, Darzynkiewicz Z (1991) The cell cycle specific effects of lovastatin. Proc Natl Acad Sci U S A 88:3628–3632
100. Crissman HA, Gadbois DM, Tobey RA, Bradbury EM (1991) Transformed mammalian cells are deficient in kinase-mediated progression through the G_1 phase of the cell cycle. Proc Natl Acad Sci U S A 88:7580–7585
101. Bruno S, Ardelt B, Skierski JS, Traganos F, Darzynkiewicz Z (1992) Different effects of staurosporine, an inhibitor of protein kinases, on the cell cycle and chromatin structure of normal and leukemic lymphocytes. Cancer Res 52:470–476
102. Bruno S, Traganos F, Darzynkiewicz Z (1996) Cell cycle synchronizing properties of staurosporine. Methods Cell Sci 18:99–107
103. Nagel WW, Vallee BL (1995) Cell cycle regulation of metallothionein in human colonic cancer cells. Proc Natl Acad Sci U S A 92:579–583
104. Gibbons J, Arat S, Rzucidlo J, Miyoshi K, Waltenburg RD, Respess DS et al (2002) Enhanced survivability of cloned calves derived from roscovitine-treated adult somatic cells. Biol Reprod 66:895–900
105. Doida Y, Okada S (1967) Synchronization of L5178Y cells by successive treatment with excess thymidine and colcemid. Exp Cell Res 48:540–548
106. Rottmann OJ, Arnold S (1983) Enhancing the mitotic index of blastomeres by thymidine synchronization. Anim Reprod Sci 6:239–242
107. Kim JH, Eidinoff ML (1965) Action of 1-(3-D-arabinofuranosylcytosine on the nucleic acid metabolism and viability of HeLa cells. Cancer Res 25:698–702
108. Lenaz L, Sternberg SS, Philips FS (1969) Cytotoxic effects of 1-beta-D-arabinofuranosyl-5-fluorocytosine and of 1-beta-D-arabinofuranosylcytosine in proliferating tissues in mice. Cancer Res 29:1790–1798
109. Bertalanffy FD, Gibson MHL (1971) The in vivo effects of arabinosylcytosine on the proliferation of murine B16 melanoma and Ehrlich ascites tumor. Cancer Res 31:66–71
110. Verbin RS, Diluiso G, Liang H, Farber E (1972) Synchronization of cell division in vivo through the combined use of cytosine arabinoside and colcemid. Cancer Res 32:1489–1495
111. Erba E, Sen S, Lorico A, D'Incalci M (1992) Potentiation of etoposide cytotoxicity against a human ovarian cancer cell line by pretreatment with non-toxic concentrations of methotrexate or aphidicolin. Eur J Cancer 28:66–71
112. Erba E, Sen S (1996) Synchronization of cancer cell lines with methotrexate in vitro. Meth Cell Sci 18:149–163
113. Zhang E, Li X, Zhang S, Chen L, Zheng X (2005) Cell cycle synchronization of embryonic stem cells: effect of serum deprivation on the differentiation of embryonic bodies in vitro. Biochem Biophys Res Commun 333:1171–1177
114. Memili E, Behboodi E, Overton SA, Kenney AM, O'Coin M, Zahedi A et al (2004) Synchronization of goat fibroblast cells at quiescent stage and determination of their transition from G0 to G1 by detection of cyclin D1 mRNA. Cloning Stem Cells 6:58–66
115. Enninga IC, Groenendijk RT, van Zeeland AA, Simons JW (1984) Use of low temperature for growth arrest and synchronization of human diploid fibroblasts. Mutat Res 130:343–352
116. Rojas MO, Wasserman M (2007) Effect of low temperature on the in vitro growth of plasmodium falciparum. J Eukaryot Microbiol 40:149–152
117. Fox MH, Read RA, Bedford JS (1987) Comparison of synchronized Chinese hamster ovary cells obtained by mitotic shake-off, hydroxyurea, aphidicolin, or methotrexate. Cytometry 8:315–320
118. Miller EM, Kinsella TJ (1992) Radiosensitization by fluorodeoxyuridine: effects of thymidylate synthase inhibition and cell synchronization. Cancer Res 52:1687–1694
119. Vogel W, Schempp W, Sigwarth I (1978) Comparison of thymidine, fluorodeoxyuridine, hydroxyurea, and methotrexate blocking at the G_1/S phase transition of the cell cycle, studied by replication patterns. Hum Genet 45:193–198
120. Carl PL (1970) Escherichia coli mutants with temperature-sensitive synthesis of DNA. Mol Gen Genet 109:107–122
121. Wickner S, Hurwitz J (1975) Interaction of *Escherichia coli* dnaB and dnaC(D) gene products *in vitro*. Proc Natl Acad Sci U S A 72:921–925
122. Withers HL, Bernander R (1998) Characterization of dnaC2 and dnaC28

mutants by flow cytometry. J Bacteriol 180:1624–1631

123. Helmstetter CE, Cummings DJ (1963) Bacterial synchronization by selection of cells at division. Proc Natl Acad Sci U S A 50:767–774
124. Helmstetter CE, Eenhuis C, Theisen P, Grimwade J, Leonard AC (1992) Improved bacterial baby machine: application to *Escherichia coli* K-12. J Bacteriol 174:3445–3449
125. Ferullo DJ, Cooper DL, Moore HR, Lovett ST (2009) Cell cycle synchronization of Escherichia coli using the stringent response, with fluorescence labeling assays for DNA content and replication. Methods 48:8–13
126. Cutler RG, Evans JE (1966) Synchronization of bacteria by a stationary-phase method. J Bacteriol 91:469–476
127. Maruyama Y, Yanagita T (1956) Physical methods for obtaining synchronous culture of *Escherichia coli*. J Bacteriol 71:542–546
128. Abbo FE, Pardee AB (1960) Synthesis of macromolecules in synchronously dividing bacteria. Biochim Biophys Acta 39:473–48
129. Lark KG, Lark C (1960) Changes during the division cycle in bacterial cell wall synthesis, volume, and ability to concentrate free amino acids. Biochim Biophys Acta 43:520–530
130. Helmstetter CE, Uretz RB (1963) X-ray and ultraviolet sensitivity of synchronously dividing *Escherichia coli*. Biophys J 3:35–47
131. Lark KG, Maaloe O (1954) The induction of cellular and nuclear division in *Salmonella typhimurium* by means of temperature shift. Biochem Biophys Acta 15:345–356
132. Ron EZ, Rozenhak S, Grossman N (1975) Synchronization of cell division in *Escherichia coli* by amino acid starvation: strain specificity. J Bacteriol 123:374–376
133. Walker GM (1999) Synchronization of yeast cell populations. Methods Cell Sci 21:87–93
134. Golzio M, Teissié J, Rols M-P (2002) Cell synchronization effect on mammalian cell permeabilization and gene delivery by electric field. Biochim Biophys Acta 1563:23–28
135. Grosjean F, Batard P, Jordan M, Wurm FM (2002) S-phase synchronized CHO cells show elevated transfection efficiency and expression using CaPi. Cytotechnology 38:57–62
136. Hoffman EA, Poncius A, McKay BS, Stamer WD (2004) Cell cycle synchronization and transfection efficiency of human trabecular meshwork cells. Invest Ophthalmol Vis Sci 45:4432

Part II

Physical Fractionation

Chapter 2

Synchronization of Mammalian Cells and Nuclei by Centrifugal Elutriation

Gaspar Banfalvi

Abstract

Synchronized populations of large numbers of cells can be obtained by centrifugal elutriation on the basis of sedimentation properties of small round particles, with minimal perturbation of cellular functions. The physical characteristics of cell size and sedimentation velocity are operative in the technique of centrifugal elutriation also known as counterstreaming centrifugation. The elutriator is an advanced device for increasing the sedimentation rate to yield enhanced resolution of cell separation. A random population of cells is introduced into the elutriation chamber of an elutriator rotor running in a specially designed centrifuge. By increasing step-by-step the flow rate of the elutriation fluid, successive populations of relatively homogeneous cell size can be removed from the elutriation chamber and used as synchronized subpopulations. For cell synchronization by centrifugal elutriation, early log S phase cell populations are most suitable where most of the cells are in G1 and S phase (>80%). Apoptotic cells can be found in the early elutriation fractions belonging to the sub-Go window. Protocols for the synchronization of nuclei of murine pre-B cells and high-resolution centrifugal elutriation of CHO cells are given. The verification of purity and cell cycle positions of cells in elutriated fractions includes the measurement of DNA synthesis by [^{3}H]-thymidine incorporation and DNA content by propidium iodide flow cytometry.

Key words Counterstreaming centrifugation, Cell separation, Velocity sedimentation, Elutriator, Resolution power

1 Introduction

1.1 Definition of Terms: Elution, Elutriation, Centrifugal Elutriation

Elution is an analytical process by which chemicals are emerging from a chromatography column and normally flow into a detector. The material obtained with the carrier (eluent) is the mobile phase and known as the eluate. In liquid column chromatography, the eluent is a solvent (Fig. 1a). Elutriation is a technique to separate small particles suspended in a fluidized bed into different size groups by passing an increasing flow rate through the elutriation chamber. In elutriation, particles are suspended in a moving fluid which can be liquid or gas. In vertical elutriation, smaller particles move upward with the fluid. Large particles will not be driven out of the elutriation chamber and tend to settle out on the walls or at

Gaspar Banfalvi (ed.), *Cell Cycle Synchronization: Methods and Protocols*, Methods in Molecular Biology, vol. 1524,
DOI 10.1007/978-1-4939-6603-5_2,

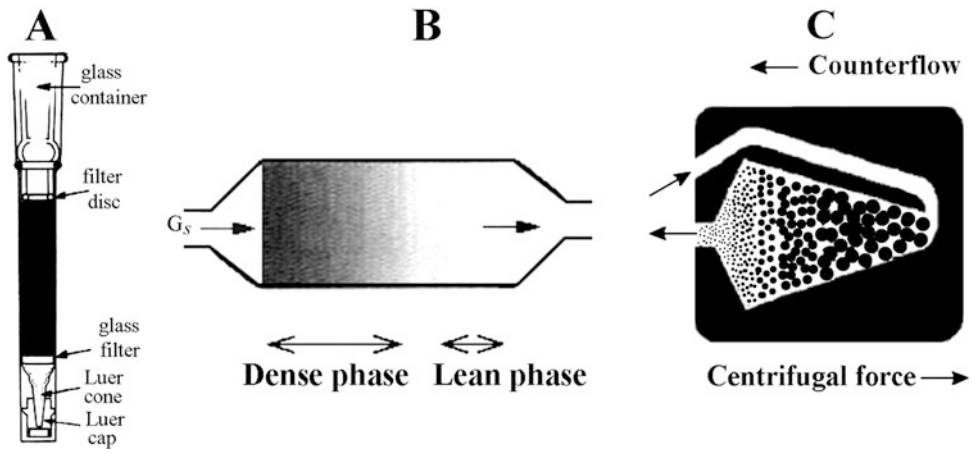

Fig. 1 Schematic views of elution, elutriation, and centrifugal elutriation. (**a**) For elution in column chromatography, a liquid eluent is used. (**b**) Horizontal elutriation in a fluidized bed of particles with flux G_s. (**c**) Fractionation of cells by centrifugal elutriation. Cells are introduced with an initial lower flow rate which is opposed be the centrifugal force. By increasing the flow rate, the floating cells in the elutriation chamber can be driven out and separated into 10–30 distinct size fractions

the bottom of the elutriator due to the higher gravity exerted on their larger size. In horizontal position, the suspended particles are passed through the elutriation chamber. By increasing stepwise the fluid velocity, the particles can be separated into fractions (Fig. 1b). The principle of centrifugal elutriation is similar to elutriation except that the fluid is pumped into a rotating separation chamber that converges into an outlet tube (Fig. 1c).

1.2 Development and Application of Centrifugal Elutriation

The first apparatus that exploited differences in velocity sedimentation for the separation of cells by counterstreaming centrifugation was described by Lindahl in 1948 [1]. The Beckman Instrument Company modified this instrument and named it elutriator and termed the process centrifugal elutriation [2]. Further refinement and a second chamber style know as the Sanderson chamber was introduced giving a better resolution especially with small cells [3]. Centrifugal elutriation has been applied to separate hemopoietic cells, mouse tumor cells, testicular cells, and a variety of other specialized cells from other cells and cells in particular phases of the cell cycle reviewed first by Pretlow in 1979 [4]. Several further applications have been described [5–9]. The construction of the commercially available centrifugal elutriator resulted in a rapid purchase of these instruments especially in the United States in the second half of the 1970s, with high expectations and significantly lower outcome than originally expected. The major reason of insufficient or lacking data is the missing technical skill necessary for the assembling and operation of these instruments and the use of such heterogeneous batch cultures that made the separation irreproducible. It is thus important to discuss first the

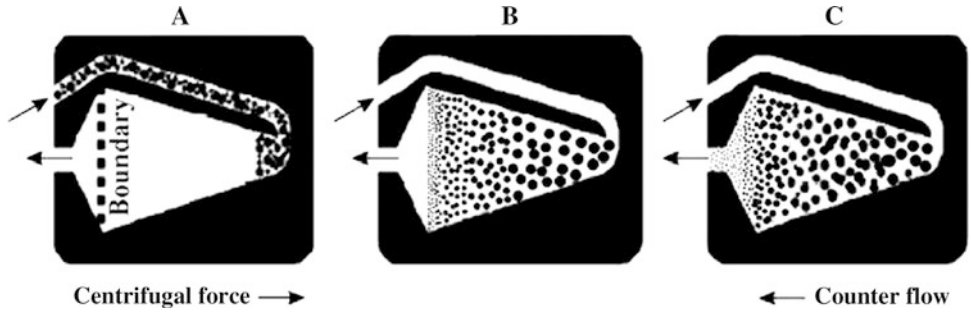

Fig. 2 Cell synchronization by centrifugal elutriation based on different cell size. The centrifugal force and the counter stream act in opposite directions in the elutriation chamber. (**a**) Early S phase cells enter the elutriation chamber. (**b**) Size gradient is balanced by centrifugal force and counterflow of elutriation keeping cells floating inside the chamber. (**c**) Increasing flow rate elutes smaller cells first followed by larger ones. Reproduced with permission of Banfalvi [11]

circumstances that may cause experimental failures during the centrifugal elutriation.

1.3 Principles of Centrifugal Elutriation

Among the methods used to monitor cell cycle changes, two distinct strategies prevailed [10]. One is the chemical "arrest-and-release" approach that arrests cells at a certain stage of the cell cycle and then by the removal of the blocking agent synchronized cells are released to the next phase. In the alternative approach, cells are separated by physical means such as mitotic shake-up, gradient centrifugation, cell sorting, and centrifugal elutriation. These methods have been overviewed in Chapter 1.

Counterflow centrifugal elutriation separates subpopulations of cells on the basis of cell volume and density. As there is only a slight change in cell density during the cell cycle, the principle of cell separation during elutriation is based on cell size (Fig. 2).

Before going to the point-by-point elutriation protocol, the following precautions are advised to avoid unnecessary mistakes and problems during the execution of this cell synchronization technique:

Culture medium. For test run and pilot experiments, saline can be used to find out the right conditions (centrifugal force, flow rate) for cell fractionation. Although any medium can be used for elutriation, it is advised that the elutriation fluid should be the physiological culture medium. To limit the cost of elutriation, the fetal calf serum concentration can be reduced to 1%. Some investigators use cost-efficient 1% bovine serum albumin. The protein content prevents cells from clumping and the cellular debris from adhering to the chamber wall. Cell aggregates normally accumulate at the entrance of the elutriation chamber and may clog it. In such case, the chamber has to be disassembled, whipped out with a soft paper towel, cleaned with a mild detergent, and reassembled

taking care of the right position of the plastic insolation. High protein concentration may cause foaming and cell lysis. The culture medium should contain only soluble materials, any particle left in the medium may contribute to aggregation or will appear in one of the elutriated fractions obscuring the cell cycle profile.

Cells. Most significant cell growth takes place in S phase; it is thus not surprising that nearly 100% of G1 cells and more than 80% of S cells could be recovered by centrifugal elutriation [12]. Best separation can be achieved by using cell populations maintained in early S phase of growth for several generations. This will reduce the number of aging and dying cells due to anoxia, the formation of artifacts, cell debris, and will prevent clumpiness. Early S phase cells contribute to the reproduction of the results causing only small shift in the elutriation profile that can be attributed to minor differences in cell distribution.

Any suspension cell line can be used for centrifugal elutriation. Cells that tend to stick together or attach to the culture substrate (e.g., Chinese hamster ovary cells) need more attention. These cells should be kept in suspension before synchronization by growing them in spinner flasks continuously stirred with a magnetic stirrer at speed high enough to prevent sedimentation and low enough to avoid cell breakage (Fig. 3). The resuspension of the cell suspension is also recommended by passing it several times through an 18-gauge needle right before loading in the elutriation chamber to ensure monodispersion. Once cells are in the chamber, the flotation of cells keeps them separated.

1.4 Components of the Centrifugal Elutriation System

The counterflow elutriation system (earlier Beckman, now Beckman-Coulter Inc.) consists of a centrifuge, elutriation rotor containing the elutriation chamber, stroboscop, peristaltic pump, manometer, sample mixing tube, and the flow system (gauge for monitoring back pressure, injection and bypass valves, T-connector, rubber stoppers, and silanistic tubing) (Fig. 4). Additionally, the pump may be interfaced with a fraction collector. The cell separation is carried out in a specially designed centrifuge hosting either the standard JE-6B rotor or the larger JE-5.0 rotor. The standard elutriation chamber is available in two sizes. The small elutriation chamber has a capacity of approximately 4.5 ml and is suitable for the fractionation of 10^7–10^9 cells. The large chamber is able to separate ten times more volume and cells. The geometry of the Sanderson chamber gives a better resolution for the separation of small cells in the range between 10^6–10^8 cells. The peristaltic pump is providing a gradually changing flow through the chamber with flow rates between 2 and 400 ml/ml depending on the size of the chamber and the cells. The elutriation system uses either a constant centrifugal force and gradually increasing counterflow rate or constant flow rate and reducing rotor speed to yield high resolution of synchronization. As the fine control of rotor speed reduction is not

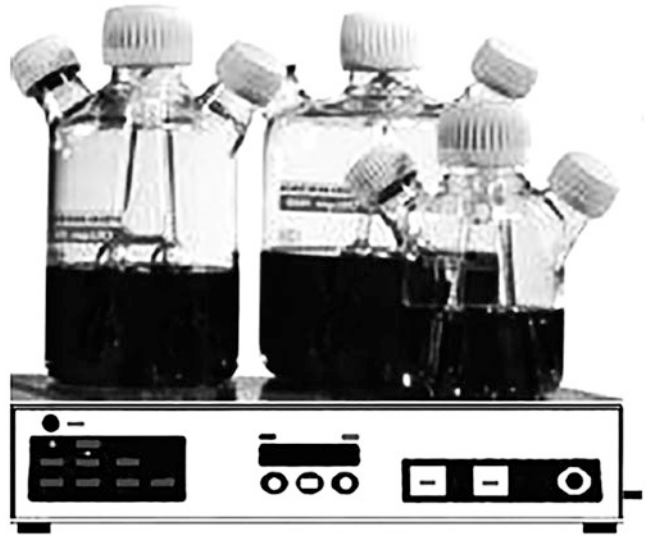

Fig. 3 Spinner flasks for suspension cultures. Cell cultures (suspension or monolayer) are started in T-flasks containing 25 ml medium. After reaching confluency, the cells of two flasks are combined in a smaller (200 ml) spinner flask that is sitting in the CO_2 incubator. Cells in suspension are grown under constant stirring in 100 ml medium starting at ~10^5 ml/ml density. Logarithmic growth is maintained by scaling up daily from 100 to 200 ml medium, then switching to a larger spinner flask (2 L) and doubling the volume of the medium to 400, 800 and if necessary 1600 ml. Up to 3–4 × 10^8 cells can be grown in one week before starting elutriation

possible, constant speed and increasing flow rate are preferred. The rotor speed may vary between 1800 and 3500 rpm (~550–1700 g relative centrifugal force) depending on cell size. Although higher speed gives a better resolution, the pump speed will also go up increasing the shearing force and the amount of cell debris. The relationship between cell size and centrifugal force is demonstrated in Table 1.

1.5 Monitoring the Efficiency of Centrifugal Elutriation

Due to the close correlation between cell size and DNA content, the effectiveness of the separation can be tested by monitoring the results by cell number, cell size, and DNA content. The most simple method is to count the cells and estimate their size in a hemocytometer. This indispensible method visualizes cells and distinguishes among small and large cells as well as cell aggregates. Particle counters generally monitor changes in conductivity and help to automatize the counting procedure. Most of these devices provide information with respect to particle size and volume distribution. However, size distributions do not exclude errors generated by aggregation, coincidence, and by nonspherical particles. Coincidence can be taken into consideration by counting the same cell population several times in a Bürker chamber and by the

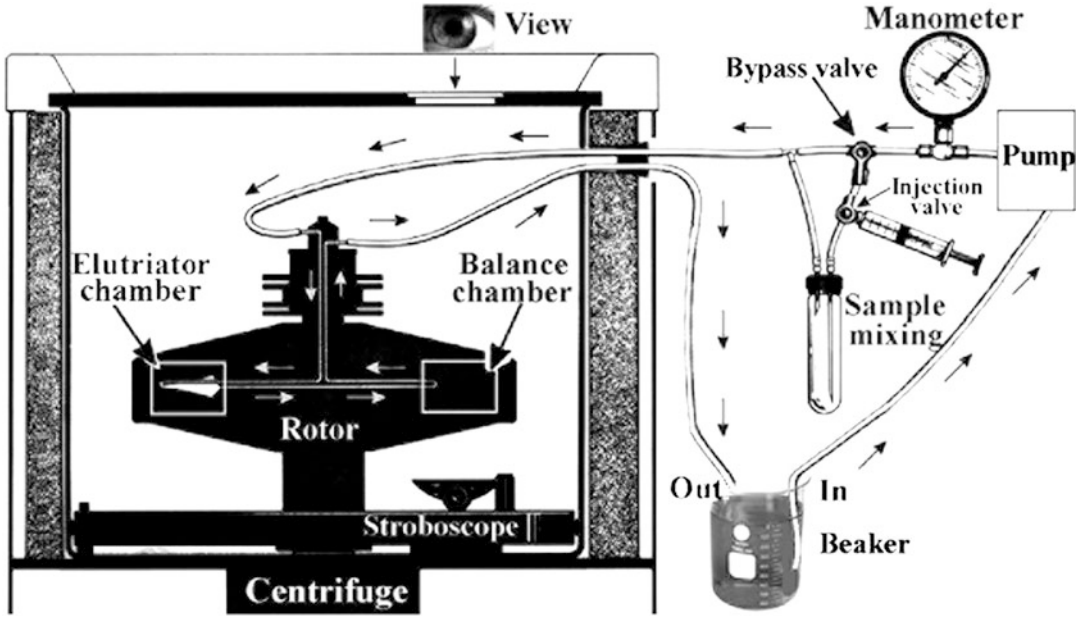

Fig. 4 Counterflow centrifugal elutriation system. The stroboscope is placed and fixed at the bottom of the centrifuge. The centrifuge is hosting the rotor that is running with constant speed. The pump is turned on and sterilization takes place by running 70 % ethanol through the system followed by physiological buffer to remove traces of ethanol. The physiological buffer is then replaced by the elutriation fluid at an initial flow rate. The preliminary run also serves to remove bubbles from the system. The loading chamber serves as a sample mixer and in its bypass position traps small remaining bubbles and compensates pump pulsation. The bypass valve helps to remove residual bubbles from the sample mixer chamber. Reproduced with permission of Banfalvi [11]

Table 1
Elutriation conditions for *Drosophila* and mammalian cells and murine preB nuclei

			Centrifugal force of elutriation		
Cell type	**Cell diameter (μm)**	**Flow rate (ml/min)**	**Rpm**	**Rcf average (g)**	**Rcf maximum (g)**
CHO	11.9	12–49	2000	569	753
CHO	11.9	19–52	2200	575	683
Indian muntjac	11.4	12–50	2200	575	683
Murine preB	10.2	11–73	2200	688	911
Drosophila S2	8.1	13–53	2500	889	1176
PreB nuclei	5.0	14–77	3500	1742	2305

Temperature was 20 °C for each elutriation
Cell diameter refers to an average value of exponentially growing cells and average size of nuclei before synchronization, measured by multiparametric particle size counting
Rotational speed is given as revolution per minute (Rpm), relative centrifugal force (Rcf) in *g*. Reproduced with permission of Banfalvi [11]

particle counter. The ratio of cell count obtained by the cell number counted by the Bürker chamber over the cell number obtained by the particle counter serves then as a factor which is used to multiply the counter number to get the real cell number.

Flow cytometry is used to asses the quality of synchronization by monitoring size distribution with forward scatter analysis and concomitantly the DNA content of each elutriated fraction after staining with propidium iodide. Flow cytometry is also generally accepted for the evaluation of cellular processes [13, 14] for calculating proliferative parameters [15] to identify apoptotic cells by nuclear staining [16–18] or by the appearance of phosphatidylserine on cell surface [19] and monitor other cellular changes [20–22].

2 Materials

2.1 Disposables

1. 1.5 ml microcentrifuge tubes.
2. 15 and 50 ml centrifuge tubes.
3. 15 and 50 ml conical centrifuge tubes.
4. Polystyrene test tubes.
5. 25 and 75 cm^2 flasks for cell culture.
6. 5 ml, 12 × 75 mm FACS tubes.

2.2 Media and Solutions

1. RPMI 1640 growth medium.
2. Fetal bovine serum (FBS).
3. *Ham's medium*: Measure 10.64 g l-glutamine containing F12 powder for 1 L of 1× solution. Add 1.176 g/L of $NaHCO_3$ powder. Adjust pH to 7.1–7.2, as it will rise to 0.2–0.3 pH units during filtration. Filter-sterilize it immediately using a membrane with a porosity of 0.22 μm. Aseptically dispense into 100-ml sterile bottles. Store them in a cold room or in a refrigerator under 5 °C until use. Before use, add 11 ml FBS albumin to each 100-ml F12 medium. F12 can be ordered as 1-, 5-, 10-, and 50-L liquid medium containing l-glutamine, without sodium hydrogen carbonate. Sterilized medium can be stored at 5 °C for several weeks if unopened.
4. *Elutriation medium* (for 30 elutriation fractions): Prepare fresh 3.5 L of F12 culture medium in a 4-L flask containing 1% FBS. Omit filter sterilization, as fractionated cells are processed immediately after elutriation. Larger particles originating from F12 medium or from cell aggregates can be removed by passing the medium and cell suspension through a 100-mesh stainless steel sieve.

5. *Phosphate-buffered saline (PBS)*: Instead of culture medium plus 1% FBS, Ca^{2+}- and Mg^{2+}-free PBS with 0.01% EDTA or without EDTA is successfully used as elutriation buffer. PBS contains 2.7 mM KCl, 4.3 mM sodium phosphate dibasic (Na_2HPO4), 1.8 mM potassium phosphate monobasic (KH_2PO4), 137 mM NaCl, pH 7.2. Sterilize in an autoclave.
6. *Saline*: Dissolve 9 g of NaCl in 1 L of distilled water and sterilize in an autoclave.
7. *Trypsin/EDTA solution*: Make up from 0.25% (wt/vol) trypsin, 1 mM EDTA in phosphate-buffered saline (PBS). Filter-sterilize. Stored at –20 °C.
8. *PI solution for flow cytometry*: Dissolve 50 mg/ml of PI in 0.1 M ammonium citrate solution (not sterile).

3 Methods

3.1 Cell Growth

1. Keep the epithelial-like CHO-K1 cells (ATCC, CCL61) in suspension culture in spinner flasks using F12 Ham's medium supplemented with 10% heat-inactivated FBS at 37 °C and 5% CO_2. Grow the murine pre-B cell line 70Z/3-M8 [23] in suspension culture at 37 °C in RPMI 1640 medium supplemented with 10% FBS, 2 mg/ml mycophenolic acid, 150 mg/ml xanthine and 15 mg/ml hypoxanthine and 2×10^{-5} M β-mercaptoethanol.
2. Maintain CHO cells as either monolayers in 75 cm^2 tissue culture flasks when smaller quantities of cells (10^6–10^7) are needed or in suspension in 250 ml and in 1-L spinner flasks if many cells are required, such as in elutriation ($2–3 \times 10^8$).
3. Maintain cells in logarithmic growth and high viability by culturing at densities between 1×10^5 and 4×10^5.
4. Replace media by splitting cells in the ratio of 1:2 daily. Grow CHO cells in suspension culture in 1 L spinner flasks containing a final volume of 800 ml F12 Ham's medium supplemented with 10% FBS. The suspension culture should initially contain $1–2 \times 10^5$ cells/ml[1] at 37 °C in 5% CO_2.
5. Grow cells for 24 h to a final concentration of $2–4 \times 10^5$ cells/ml for fractionation by centrifugal elutriation. Harvest cells by centrifugation at $600 \times g$ for 5 min at 5 °C and resuspend in 10 ml of F12 medium containing 1% FBS. To avoid the presence of dead and fragmented cells in elutriated fractions, *see* **Note 1**. Remove cell aggregates by passing the cell suspension through a 100-mesh stainless steel sieve.

3.2 DNA Isolation

Isolate high molecular weight DNA from 10^6 cells of elutriated fractions, determine the amount of DNA by a DyNA Quant fluorimeter (Hofer Scientific Instruments) using Hoechst 33258 dye,

which binds to the minor groove of double-stranded DNA. Excite the bound dye with long UV light at 365 nm and measure its fluorescence at 458 nm with calf thymus as DNA standard.

3.3 Determination of DNA Content

1. Isolate DNA from elutriated fractions by phenol extraction from an equal number of cells (10^6) from each elutriated fraction.
2. Stain the DNA. The amount of DNA can be determined by specific dyes (e.g., Hoechst 33258).
3. Excite the bond dye with UV light and measure DNA content. Use calf thymus DNA as DNA standard.

3.4 Measurement of Cell Number and Cell Size

Confirm the synchrony of elutriated fractions by measuring cell size in a Coulter Channelyzer or Coulter multisizer. The measurement of gradual and simultaneous increase both in cell size and cell volume as well as the correlation between cell size and DNA content confirm that synchrony is maintained not only at low, but also at increased and higher resolution.

3.5 Flow Cytometry

1. Stain cells with 50 mg/ml of PI in 0.1 M ammonium citrate for 15 min at 0 °C.
2. Add an equal volume of 70% ethanol.
3. Perform cell cycle analysis in a fluorescence-activated cell sorter. Use the flow cytometric profiles of elutriated fractions to calculate the nuclear DNA content expressed in average C-values [24]. The C-value increases from 2C to 4C as the cell progresses through the S phase, providing quantities measure of cell growth. When many fractions (>20) have to be processed within the same day, stained and fixed cells can be stored overnight in refrigerator (4 °C) and flow cytometry can be performed next day.

3.6 Conditions Used for Centrifugal Elutriation

The elutriation system (earlier Beckman, now Beckman Coulter Inc.) is an advanced device that uses either a constant centrifugal force and gradually increasing counterflow rate or constant flow rate and reducing rotor speed to yield high resolution of synchronization. The cell separation is carried out in a specially designed centrifuge and rotor. This elutriator system was designed exclusively for research, not for diagnostic or therapeutic use.

3.6.1 Hardware

The hardware of the JE-6 elutriator system (JE-6B Rotor, elutriator, 6000 rpm, 5080 × *g*, recoverable cells per run 10^9) consists of the following subassemblies: centrifuge, rotor assembly, stroboscope, flow system, modified door for the Model J-21/J-21B or J2-21 centrifuges as well as various tools and lubricants. In our elutriation system, we used a J2-21 centrifuge and a JE-6B separation chamber (Beckman Coulter Inc.), in which the elutriation

fluid was circulated at an initial flow rate of 16.5 ml/min using a MasterFlex peristaltic pump (Cole-Parmer Instrument Inc.) presterilized with 70% ethanol. Elutriation was performed at a rotor speed of 2200 rpm ($683 \times g$) and temperature of 20 °C for 4–5 h. Subpopulations of cells were eluted in F12 medium containing 1% FBS. We have also used the JE-5.0 elutriation system (JE-5.0 Rotor, Elutriator, 5000 rpm, $4704 \times g$, retrievable cells per run 10^{10}), including a Sanderson elutriation chamber (5 ml) and a J-6 M1 centrifuge (Beckman Instruments Inc.) [23]. When the JE-5.0 elutriation chamber is used with the Avanti J-25 and Avanti J-26 XP series and with J6-MI centrifuges equipped with viewport door and strobe assembly, accelerated throughput, shorter run times can be achieved. The JE-6B low-volume elutriator rotor is excluded from the JE-5.0 elutriation system.

The protocol presented here has been developed to enable cell cycle studies in a variety of cell lines [25–27]. The elutriation of $1–2 \times 10^8$ cells in a JE-6B rotor and a J2-21 centrifuge was used most frequently in our experiments [28]. The small JE-6B elutriation system was assembled according to the manufacturer's instructions. Only the flow system (gauge for monitoring back pressure, two three-way valves, T-connector, rubber stoppers, and several feet of Silanistic tubing) was regularly disassembled after elutriation and reassembled before the next elutriation, as the centrifuge was normally used in several other experiments. For shaft, rotor, chamber, pressure ring, stroboscope, and flow system assembly and disassembly, see the instruction manual of the Beckman JE-6 or JE-5.0 elutriator rotor. The rotor speed and flow rate monogram in the manual give the necessary preliminary information on rotor speed (rpm), sedimentation rate, particle diameter (mm), and flow rate (ml/min).

3.6.2 Calibration of Peristaltic Pump

Among the preliminary experiments, the relationship between pump speed and flow rate has to be established. The calibration of the peristaltic pump is done by measuring the flow rates at different pump setting using elutriation buffer. It is recommended to do the calibration before the day of elutriation to lighten the burden of elutriation. The pump can be used within the linear range. In our case, linearity was maintained up to 80 ml/min.

3.6.3 Particle Size Counting

Particle size counters are recommended that produce a particulate size profile and average particle diameter for a given culture. The size limit is set for cells to count them above the limit and cell debris below the limit. The unit is cleaned and first a sample of solution (used for dilution) is analyzed, then the sample of the culture is profiled. The solution profile is subtracted from the culture profile to eliminate solution debris. This yields a debris count and a cell count. More sophisticated units include measurement of the mean particle diameter, which, for cell cultures above the size limit, equates to the average cell diameter.

We have used different counters to determine the sizes of the cells in each fraction. The counter is based on the principle of electronic particle counting, where the amplitude of a voltage pulse, caused by a change in impedance when a particle suspended in an electrolyte is drawn through an electrical field, is proportional to the volumetric size of the particle [29]. From the change in impedance, the diameter and surface area of the particle are calculated, assuming that the particles are spherical.

3.7 Installation of Elutriation System

To operate the elutriation system, install the stroboscope first, as its chamber unit has to be placed at the bottom of the centrifuge. Turn the stroboscope unit in such a way that the flashlight will be under the observation port when the door of the centrifuge is closed. Rotate the wheels on the casting to tighten the chamber of the stroboscope. Run the cables of the stroboscope through the ports of the centrifuge inside the chamber and secure them with split rubber stoppers installed from outside. Connect the cables to the control unit of the stroboscope outside the centrifuge. Turn on the power switch and verify that the lamp of the photocell is lit (*see* **Note 2**).

3.7.1 Installation of Stroboscope

3.7.2 Installation of Elutriator Rotor

Open the door of the centrifuge and install the assembled rotor containing the installed chambers (elutriator and bypass chambers). Place the rotor in the centrifuge (*see* **Note 3**).

3.7.3 Installation of Flow Harness

In addition to the port for the strobe control unit, there are two more ports in the centrifuge chamber, one for the tubing coming from the pump and the other for the outlet tubing. One can use only centrifuges that have these ports. Make sure that the tubing running from the pump to the rotor is placed in the upper (inlet) fitting and the outlet tubing in the lower fitting of the elutriator rotor (*see* **Note 4**). Connect the liquid lines. Secure tubings firmly with split rubber stoppers outside the centrifuge.

3.7.4 Installation of Control Units

The preliminary run serves to test whether the control units are functioning properly and the centrifuge is running smoothly. For the test run, check the control units of the centrifuge and set the elutriation speed of the centrifuge. When the rotor is at speed, reset the counter and push START button (*see* **Notes 5** and **6**). The rotor speed will be displayed in tens of rpm on the counter. Put the timer at "Hold" position to avoid untimely interruption of elutriation, the brake at "Maximum" and set the temperature at 20 °C, and limit its change within ±1–2 °C. On the stroboscope control, turn the FLASH DELAY potentiometer counterclockwise to 0 position and slowly turn it clockwise to bring the image of the elutriation chamber into view, seen through the viewport door of the centrifuge. If you have an old JE-6 rotor, the bypass chamber will come into view first. Keep turning the potentiometer till the

separation chamber is seen. The separation chamber has two screws in it that make it distinguishable from the bypass chamber. Watch the pressure gauge in the flow harness (*see* **Notes 7** and **8**). Rise in pressure indicates the presence of air in the system (*see* **Note 9**). Stop the pump and/or decelerate the rotor. Note that not all the cables and ports are visualized in the scheme (Fig. 4). When the pressure is zero, the rotor speed is set at elutriation speed.

3.8 Synchronization of CHO Cells

1. Prepare 3500 ml of fresh F12 elutriation medium in a 4000-ml flask.
2. Fill up a 3000-ml flask with elutriation medium to the rim. Use this as the permanent medium reservoir. Cover it with aluminum foil until further use.
3. Pour 400 ml of elutriation medium into a 500 ml beaker and use it as a temporary medium reservoir.
4. Set up your centrifugal system (Fig. 4). Pump 100 ml of 70% ethanol through the system. Then pump through PBS solution (200 ml) to remove the 70% ethanol used to provide sterilization. Start the centrifugation to remove bubbles. Remove PBS and the bubbles by pumping 100 ml of elutriation medium through the elutriation system and discard this fraction (*see* **Note 9**).
5. Replace the temporary medium reservoir with the permanent medium reservoir. Fill the cell reservoir (sample mixer) with medium using a large (30 ml) syringe. To flush all the air from the sample-mixing chamber, retract the short needle so that the end is flushed with the inside of the rubber stopper. When the sample chamber is full and no more air is seen leaving the exit flow line, close the bypass valve to make sure that the liquid does not enter the sample chamber. Set the initial flow rate of the peristaltic pump at 16.5 ml/min. Keep the elutriation fluid circulating until the cells are introduced into the sample reservoir. Make sure once more that the bypass valve is closed, the speed of the centrifuge is correct (2200 rpm, $683 \times g$), the refrigeration of the centrifuge is on and set at 20 °C and the timer of the centrifuge is set at HOLD (endless) position. Turn the flash delay potentiometer of the stroboscope clockwise slowly from 0 position to bring the image of the separation chamber into view. Number empty culture bottles (or tubes) for collecting elutriation fractions (100 ml each) and stand in ice. Use the scale on the culture bottle as the volume measure.
6. Load the sample reservoir by passing the concentrated cell suspension ($1–2 \times 10^8$ cells in 10 ml of Ham's medium containing 1% FBS in a 50-ml screw cap tube) through an 18-gauge needle three times just before loading to ensure monodispersion. Use a 10-ml Luer-lock syringe for injecting cells into the loading chamber. This also keeps the needle from jumping off the

hypodermic syringe. The needle attaches to the body of the syringe via a screw-type twist. Remove the needle from the syringe. Close the bypass valve, as elution liquid is not allowed to enter the sample reservoir during loading. Attach the syringe directly to the Luer fitting on the injector valve for sample injection. Open the injector valve and inject resuspended cells into the sample reservoir. After injecting cells slowly into the sample reservoir, close the injection valve. Air is not allowed to enter the system. As cells cannot be completely removed from the 50-ml tube and filled in the sample reservoir, those suspended cells that are left in the tube (~0.5 ml) serve as nonelutriated control.

7. Load cells into the elutriation chamber. To load cells from the sample reservoir to the elutriation chamber, turn the sample chamber upside down and open the bypass valve. Start to collect the first 100 ml fraction flushed from the centrifuge. About 100 ml of liquid is required to remove one subpopulation of cells from the 4.5-ml separation chamber. View the loading of cells through the observation window of the door of the centrifuge. The appearance of a darkening cloud indicates the introduction of cells into the elutriation chamber. After loading, no more cells are allowed to enter the elutriation chamber. Close the bypass valve and turn back the loading chamber to its original position (*see* **Note 10**). The fraction collected during loading is discarded. This fraction contains cell debris and dead cells (*see* **Notes 11** and **12**).
8. To obtain the first elutriation fraction, increase the pump speed from 16.5 ml/min to 19 ml/ml slowly by ~1 ml/min increments and collect the next 100 ml media. Gradually increase the flow rate (or decrease rotor speed) to permit the elutriation of further fractions. Collect consecutively 100 ml effluent volumes from the centrifuge. Immediately after a fraction is collected, take 2 × 1-ml samples and add 9 ml of saline to each sample for Coulter counting and cell-size measurement. Keep elutriated fractions in ice until further use and shake them gently from time to time to avoid cohesive sedimentation and loss of cells (*see* **Note 13**). We have obtained reproducible experiments by performing centrifugal elutriation at low, increased and high resolution of elutriation and collecting 9, 16, and 30 elutriation fractions, respectively (Fig. 5). Only as many samples should be collected as the small team (2–3 persons) carrying out the elutriation can process on the same day (*see* **Note 14**).
9. To finish elutriation, turn off rotor speed and let the high flow rate drive out residual particles from the elutriation chamber. Let the system run and collect 100 ml more liquid to remove all the remaining particles. Remove the medium at high flow rate and rinse the system with 200 ml of distilled water to lyse

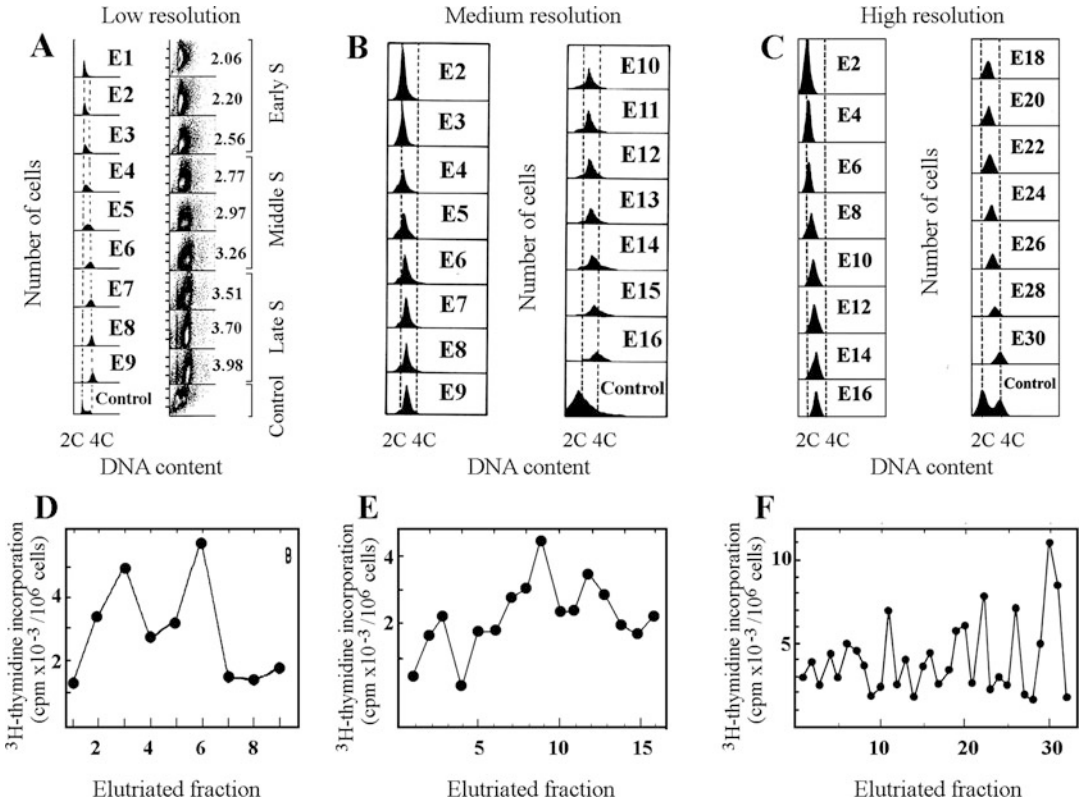

Fig. 5 Centrifugal elutriation at low, medium, and high resolution. Exponentially growing CHO cells were synchronized by counterflow centrifugal elutriation. (**a**) Flow cytometric profiles of DNA content at low (**a**), medium (**b**), and high resolution of elutriation. The cell number is indicated in the ordinate and the DNA content on the abscissa. The average C value (haploid genome content) of elutriated fractions at low resolution (9 fractions, E1–E9) was calculated. For medium resolution 16 fractions (E2–E16) and at high resolution 30 elutriation fractions (E2–E30) were collected. (**b**) DNA synthesis in elutriated fractions at low (**d**), medium (**e**), and high resolution (**f**). ^{3}H-thymidine incorporation is shown in the ordinate and fraction number on the abscissa. 2C- and 4C-values were calculated from the flow cytometric profiles of elutriated fractions [24]. Reproduced with the permission of Banfalvi et al. [30, 31]; Szepessy et al. [32]

any cell left in the system. Cells left in the elutriator chamber may cause pellet formation (*see* **Note 11**).

10. Although almost all parts of the elutriator rotor can be autoclaved, we rinse the system with 70% ethanol to sterilize it. Remove the ethanol by pumping and dry the passages with clean compressed air and leave the rotor assembled. Disconnect the liquid lines and remove the rotor and stroboscope chamber from the chamber. In case of longer storage, remove the elutriation chamber and the bypass (balance) chamber, but store the rest of the rotor assembled.
11. Check the status of your elutriator system by a test run before doing cell separation (*see* **Note 15**).

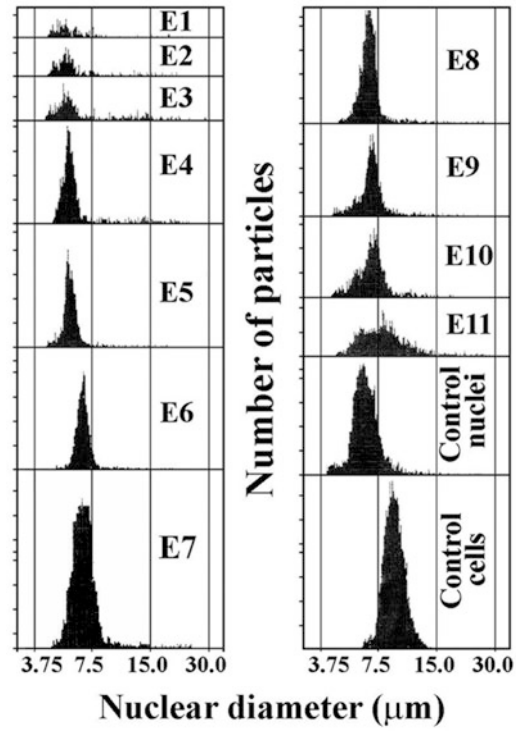

Fig. 6 Centrifugal elutriation of nuclei isolated from murine pre-B cells. Nuclear size is indicated on the abscissa, nuclear number or cell number is given on the ordinate. Cells (1.15×10^8) were subjected to the isolation of nuclei. Elutriation of 6.86×10^7 nuclei was carried out in a JE-5.0 elutriation system equipped with a 5 ml Sandetson chamber and a MasterFlex (Cole-Parmer Instruments) peristaltic pump and a J-6 M1 centrifuge (Beckman Instruments Inc.). Elutriation took place at 20 °C and 3500 rpm ($2305 \times g$). Eleven fractions (E1–E11) were collected, 100 ml each in RPMI medium 1640 supplemented with 1 % FBS. After separation, nuclei were washed with PBS and counted by Coulter multisizer, and nuclear size analysis was carried out. Control nuclei and control cells were not subjected to elutriation. Reproduced with permission of Banfalvi [11]

3.9 Synchronization of Nuclei of Murine Pre-B Cells

1. For the synchronization of isolated murine pre-B nuclei (average diameter 6.8 μm), use higher centrifugal force (3500 rpm, $2305 \times g$).
2. Use a flow rate between 14 and 77 ml/min for murine pre-B cells (average diameter 10.2 μm) and apply a similar flow rate (11–73 ml/min), but a lower centrifugal force (2200 rpm, $683 \times g$) [23, 33]. The synchronization of murine preB nuclei is demonstrated in Fig. 6.

Due to the closer correlation between nuclear size and DNA content than between cell size and DNA content, it could be of potential interest to elutriate subcellular particles to study the fine-tuning of nuclear control. The synchronization of nuclei is expected

to open new vistas for the synchronization of protoplast preparations. The synchronization is based on the nuclear size that is increasing during DNA synthesis and nuclei can be separated by centrifugal elutriation. The introduction of a density gradient during elutriation is not recommended (*see* **Note 16**). To elutriate smaller particles either the centrifugal force has to be increased, or the flow rate decreased. A lower flow rate would limit the resolution, while maximal pump speed (~500 ml/min) should also be avoided as the linearity between the pump speed and flow rate could not be maintained. Turbulence can be minimized by increasing the flow rate slowly from fraction to fraction (*see* **Note 17**).

3.10 Verification of Synchronization

1. Assay the quality of synchronization after centrifugal elutriation in each elutriated fraction. Among the methods used for the isolation and detection of homogeneous populations of cells, several flow cytometric methods are generally accepted. As its introduction, the PI flow cytometric assay has been widely used for the evaluation in different cellular processes in animal models [14] and plant cells [34].
2. Determine the DNA content by fluorometry (*see* Subheading 3.3).
3. Measure simultaneously the cell number and the increasing cell size. This option offers the fastest measurement and is recommended when many fractions are collected and several measurements have to be carried out within a short period of time. A reliable combination is to choose at least two of the three options.

3.11 Synchronized Apoptotic Cells Detected by Forward Scattering

The estimation of cellular DNA degradation during programmed cell death is closely related to the particle size that can be amplified and shows more convincingly the decrease in the cell size of apoptotic cells (Fig. 7a). The quasi 3D representation of forward light scatter analysis in Fig. 7b shows the progression of gamma irradiation-induced apoptosis during 24 h from elutriated fractions 1–9. By means of flow cytometric data, the DNA content of distinct apoptotic cell fractions was estimated and found to be increased from ~0.05 to ~1 C-value [35]. Flow cytometric forward scatter was used to determine the proportion of apoptotic cells relative to unirradiated ones after 24 h incubation. Apoptosis was low in unirradiated cells (~1%) and increased significantly in irradiated cells from 5% to 13–14% (Fig. 7c). To estimate the average value of apoptosis, non-elutriated control populations were also subjected to γ-irradiation and grown in culture medium for 2 and 24 h, respectively. Not only the increase of apoptotic cells from 4.8% to 15.6% were seen in the sub-G_1 marker window, but also the increase in G_1/G_0 and G_2/M phase and the decrease of S phase cells were observed (Fig. 7d). These changes also confirmed the

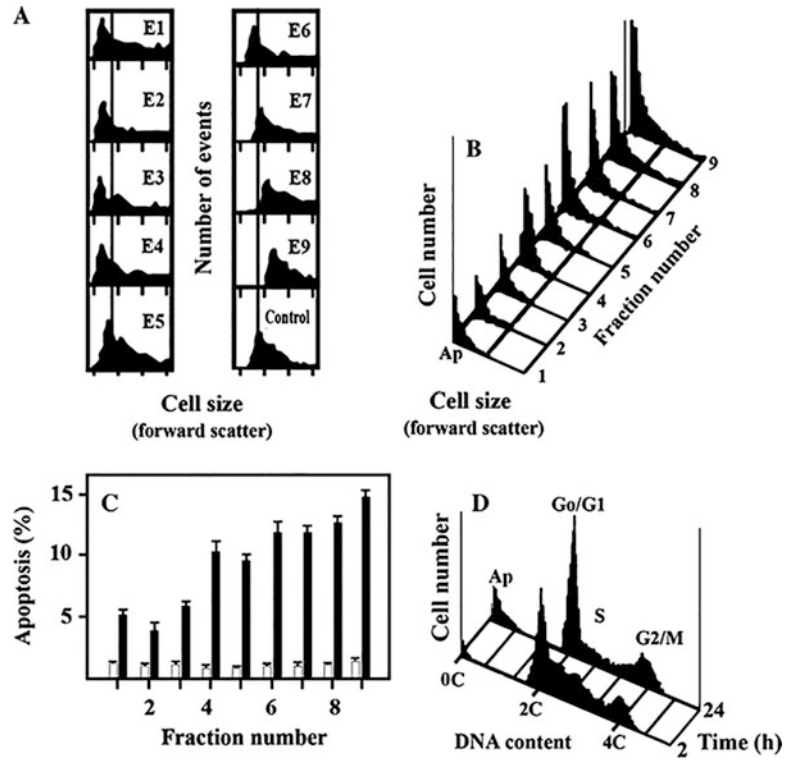

Fig. 7 Apoptotic changes detected by the forward scattering during the cell cycle. Gamma irradiated K562 human erythroleukemia cells subjected to elutriation followed by propidium iodide staining and forward light scatter analysis and found as shrinked cells in the sub-G_1 marker window. (**a**) To follow the apoptotic cell size, a vertical line was placed on the main peak of the irradiated, non-elutriated control. (**b**) After irradiation and incubation for 24 h, apoptotic cells were detected by forward scatter analysis. (**c**) Percentage of apoptotic cells of non-treated (*open square*) and of γ-irradiated (*filled square*) cell fractions. (**d**) Gamma-irradiated cells from non-elutriated populations were cultured at 37 °C. One aliquot of cells was incubated for 2 h, the other for 24 h, then stained with PI and was subjected to forward light scatter analysis. The C-values and major phases of the cell cycle are indicated. *Ap* apoptotic cells. Reproduced with permission of Banfalvi et al. [35]

radiation-induced cell cycle arrest near the G_1/G_0 and at the G_2/M checkpoints [35]. Cells representing different stages of apoptosis can be collected by choosing a somewhat lower centrifugal force for elutriation than for nuclei. By fine-scale elutriation, apoptotic cells can be separated from undamaged healthy cells (*see* **Note 18**). Cold-shock-induced apoptosis has been used without the addition of toxic compounds or antibodies, to synchronize homogeneous apoptotic cell populations [36].

4 Notes

1. *Dead cells*. Avoid the presence of dead and fragmented cells in elutriated fractions. The cell culture has to be kept constantly in logarithmic growth. Best results are obtained when cells are recultivated every day.
2. *Installation of stroboscope*. Make sure that the cables run close to the wall of the centrifuge so that the rotor cannot touch them. In case the photocell of the stroboscope does not work replace the flash lamp.
3. *Placing rotor in the centrifuge*. Be sure that the rotor is properly seated. If the pin of the rotor is improperly resting on one of the castellations, it will lift off when the drive starts. The centrifuge should be perfectly balanced and run smoothly. If you notice any vibration, the balance is imperfect. When the speed of the centrifuge is fluctuating, flow forces are not precisely balanced against centrifugal force to allow proper segregation. Check speed constancy and find the balance between centrifugal force and flow rate in preliminary test runs.
4. *Leaks*. These usually occur when (a) the chamber gasket is put backward; (b) the chamber screws are not tight; (c) tubings and connectors are not properly fitted; (d) there are nicks, scratches, irregularities on O-rings; and (e) permanently lubricated sealed bearings are washed with detergents, which can leach out the lubricant, resulting in a shortened bearing time.
   - *Seal inspection*. Clean the stained stationary seal housing (made of alumina) with soap and water or mild detergent. Abrasive materials should be used neither for cleaning nor for elutriation. Reassemble the bearing assembly (note that the seal mount has a left-handed thread). The seal should be replaced when any damage is visible.
   - *Cross leakage*. The most common problem in centrifugal elutriation is caused by defective or missing O-rings in the shaft assembly. Frequent disassembling and assembling of the elutriator system may result in defective O-rings and leaks. Make sure that all O-rings on the seal screw and transfer tube are in right place, lightly greased. Note, however, that overgreasing may clog the system. Once the subassemblies, as well as the flow system have been assembled and the system proved to be completely sealed without any leakage in the preliminary run, it is not recommended to disassemble it after each elutriation.
   - *High back pressure*. Insufficient spring pressure, which holds the rotating seal against the stationary seal, can be overcome by the back pressure, causing cross leakage. But the most common causes of high back pressure are the

opening of liquid lines in the wrong direction and inadequate de-aeration.

5. *Rotor speed*. As the flow rate relative to rotor speed can be regulated on a much broader and finer scale, it is recommended that during elutriation the rotor speed is held constant rather than using decreasing rotor speed and constant flow rate.
6. *Oscillations in rotor speed*. To avoid temporary changes in rotor speed, constant electric voltage (110 or 220 V) can be secured by plugging the centrifuge to a stabilizer.
7. *Manometer*. Keep the manometer under constant observation at the beginning of elutriation to avoid pressure formation. In the elutriation system, the presence of bubbles is indicated by the sharp increase of the pressure. In such cases, quickly turn off the speed of the centrifuge, which will drive out the bubbles. Repeatedly lower the speed of the centrifuge to remove all the bubbles before elutriation.
8. *Tightness of tubing*. Do not make the connection between the tubing and the rotor too tight; leave some movement for the tubing. As the speed of the elutriation rotors is not high (maximum 6000 rpm, 5080 × *g*), vacuum in the centrifuge is not required and could not be maintained due to the liquid lines and electric cables.
9. *Removal of bubbles*. Be sure to fill all parts of the flow harness with liquid until all the bubbles have been removed. Preworm the solutions and the centrifuge to the temperature where elutriation will be performed with the exception of the cells before their loading and the collected fractions which are kept in ice.
10. *Loading cells*. During loading cells into the elutriation chamber, one can line up cells exactly at the boundary inside the elutriation chamber (Fig. 1a): (a) a small increase of the flow rate will push forward the cell population to the boundary; (b) a small decrease of the flow rate will bring the population back to the boundary. Alternatively, the rotor speed could also be changed, but has an opposite effect as changing the flow rate. Such corrections during elutriation are recommended only for advanced users of the system. Basic principle: Do not change conditions during elutriation.
11. *Pellet formation*. Those particles that are not driven out from the separation chamber by the pumping will be pelleted at the entrance of the elutriation chamber as soon as the peristaltic pump stops. The peristaltic pump should not be turned off during elutriation. To remove the sticky pellet, the elutriation chamber has to be disassembled and cleaned.
12. *Damaged cells*. These cells release DNA and tend to stick together. Clumping of cells leads to nonhomogeneous cell populations especially at the final stage of elutriation. Solution:

Avoid rapid pipetting and fast resuspension of pelleted cells, which results in a significant loss of cell recovery, viability, release of chromosomal DNA, and stickiness of damaged cells. We have avoided DNase and EDTA treatment by the gentle treatment and loading of cells.

13. *Cell loss during elutriation*. The possible reasons are as follows: (a) cells are lysed (the system was not properly set up, check solutions for hypotony); (b) cells were left in the mixing chamber; (c) overloading the elutriation chamber results in the loss of smaller (G0/G1 and early S phase) cells; (d) the size gradient was not balanced and cells were not loaded in the elutriation chamber; (e) the centrifuge was stopped or decelerated. The particles concentrate near the increased cross-sectional area of the chamber. Flow velocity is greatest adjacent to the entrance port, the particle concentration is reduced in this area. This effect can be reduced by lowering the centrifugal force and the correspondent flow rates.
14. *High resolution of elutriation*. The danger of collecting too many elutriated fractions is that they cannot be processed. High resolution of elutriation needs the processing of many samples within the same day. Careful planning, the involvement of 2–3 persons in this highly coordinated work, some technical skill and experience are needed.
15. *Unable to judge*. This problem almost always arises when elutriation has not been done before. Consult the JE-6 or JE-5 instruction manual carefully before doing any or further installation. Carry out your first elutriation with an expert and/or discuss the details. Clarify the condition of your rotor by calling your nearest service office and ask for inspection.
16. *Application of density gradient*. Introduction of a density gradient would require a second reservoir. It is not recommended as a second reservoir would make the system too complex to handle. Growth medium with minimum FBS (1%) maintains cell viability and is dense enough to avoid contamination.
17. *Coriolis jetting effect*. Turbulence of particles inside the elutriation chamber can be minimized by increasing the flow rate slowly from fraction to fraction. The collection of many fractions (i.e., small increment in flow rate) also reduces turbulence and contributes to the increased resolution power of elutriation. A small shift (1–2 fractions) in the elutriation profile can be attributed to minor differences in cell growth. This difference can be reduced by strict cell culture conditions and corrected by calculating the C-value (haploid genome content) of each elutriated fraction from the corresponding flow cytometric profile [24].

18. The fine-scale synchronization of apoptotic cells needs specific elutriation conditions to be adapted to cell type and apoptotic treatment.

Acknowledgement

This work was supported by the OTKA grant TO42762 (G.B.).

References

1. Lindahl PE (1948) Principle of a counterstreaming centrifuge for the separation of particles of different sizes. Nature 161:648–649
2. McEwen CR, Stallard RW, Juhos ET (1968) Separation of biological particles by centrifugal elutriation. Anal Biochem 23:369–377
3. Sanderson RJ, Bird KE, Palmer NF, Brenman J (1976) Design principles for a counterflow centrifugation cell separation chamber. Appendix: a derivation of the equation of motion of a particle under combined centrifugal and hydrodynamic fields. Anal Biochem 71:615–622
4. Pretlow TG 2nd, Pretlow TP (1979) Centrifugal elutriation (counterstreaming centrifugation) of cells. Cell Biophys 1:195–210
5. Meistrich ML (1983) Experimental factors involved in separation by centrifugal elutriation. In: Pretlow TG II, Pretlow TP (eds) Cell separation, vol 2. Academic, New York, pp 33–61
6. Childs GV, Lloyd JM, Unabia G, Rougeau D (1988) Enrichment of corticotropes by counterflow centrifugation. Endocrinology 123: 2885–2895
7. Kauffman MG, Noga SJ, Kelly TJ, Donnenberg AD (1990) Isolation of cell cycle fractions by counterflow centrifugal elutriation. Anal Biochem 191:41–46
8. Bauer J (1999) Advances in cell separation: recent developments in counterflow centrifugal elutriation and continuous flow cell separation. J Chromatogr B Biomed Sci Appl 722:55–69
9. Chianea T, Assidjo NE, Cardot PJP (2000) Sedimentation field-flow-fractionation: emergence of a new cell separation methodology. Talanta 51:835–847
10. Uzbekov RE (2004) Analysis of the cell cycle and a method employing synchronized cells for study of protein expression at various stages of the cell cycle. Biochemistry 69:485–496
11. Banfalvi G (2008) Cell cycle synchronization of animal cells and nuclei by centrifugal elutriation. Nat Protoc 3:663–673
12. Keng PC, Li CK, Wheeler KT (1980) Synchronization of 9L rat brain tumor cells by centrifugal elutriation. Cell Biophys 2:191–206
13. Riccardi C, Nicoletti I (2006) Analysis of apoptosis by propidium iodide staining and flow cytometry. Nat Protoc 1:1458–1461
14. Doleel J, Greilhuber J, Suda J (2007) Estimation of nuclear DNA content in plants using flow cytometry. Nat Protoc 2:2233–2244
15. Terry NHA, White RA (2006) Flow cytometry after bromodeoxyuridine labeling to measure S and G2/M phase durations plus doubling times in vitro and in vivo. Nat Protoc 1:859–869
16. Schmid I, Uittenbogaart C, Jamieson BD (2006) Live-cell assay for detection of apoptosis by dual-laser flow cytometry using Hoechst 33342 and 7-aminoactinomycin D. Nat Protoc 1:187–190
17. Mukhopadhyay P, Rajesh M, Haskó G, Hawkins BJ, Madesh M, Pacher P (2007) Simultaneous detection of apoptosis and mitochondrial superoxide production in live cells by flow cytometry and confocal microscopy. Nat Protoc 2:2295–2301
18. Ferlini C, Scambia G (2007) Assay for apoptosis using the mitochondrial probes, Rhodamine123 and 10-N-nonyl acridine orange. Nat Protoc 2:3111–3114
19. van Genderen H, Kenis H, Lux P, Ungeth L, Maassen C, Deckers N et al (2006) In vitro measurement of cell death with the annexin A5 affinity assay. Nat Protoc 1:363–367
20. Quah BJC, Warren HS, Parish CR (2007) Monitoring lymphocyte proliferation in vitro and in vivo with the intracellular fluorescent dye carboxyfluorescein diacetate succinimidyl ester. Nat Protoc 2:2049–2056
21. Chattopadhyay PK, Yu J, Roederer M (2006) Live-cell assay to detect antigenspecific CD4+ T-cell responses by CD154 expression. Nat Protoc 1:1–6
22. Pittet MJ, Swirski FK, Reynolds F, Josephson L, Weissleder R (2006) Labeling of immune

cells for in vivo imaging using magnetofluorescent nanoparticles. Nat Protoc 1:73–79

23. Offer H, Zurer I, Banfalvi G, Rehak M, Falcovitz A, Milyavsky M et al (2001) p53 modulates base excision repair activity in a cell cycle specific manner following genotoxic stress. Cancer Res 61:88–96
24. Basnakian A, Banfalvi G, Sarkar N (1989) Contribution of DNA polymerase delta to DNA replication in permeable CHO cells synchronized in S phase. Nucleic Acids Res 17:4757–4767
25. Banfalvi G, Nagy G, Gacsi M, Roszer T, Basnakian A (2006) Common pathway of chromatin condensation in mammalian cells. DNA Cell Biol 25:295–301
26. Rehak M, Csuka I, Szepessy E, Banfalvi G (2000) Subphases of DNA replication in Drosophila cells. DNA Cell Biol 19:607–612
27. Banfalvi G (2006) Structure of interphase chromosomes in the nuclei of *Drosophila* cells. DNA Cell Biol 25:547–553
28. Banfalvi G, Littlefield N, Hass B, Mikhailova M, Csuka I, Szepessy E et al (2000) Effect of cadmium on the relationship between replicative and repair DNA synthesis in synchronized CHO cells. Eur J Biochem 267: 6580–6585
29. Coulter WH (1957) High speed automatic blood cell counter and cell size analyzer. Proc Natl Electron Conf 12:1034–1040
30. Banfalvi G, Mikhailova M, Poirier LA, Chou MW (1997) Multiple subphases of DNA replication in CHO cells. DNA Cell Biol 16:1493–1498
31. Banfalvi G, Poirier AL, Mikhailova M, Chou WM (1997) Relationship of repair and replicative DNA synthesis to cell cycle in Chinese hamster Ovary (CHO-K1) cells. DNA Cell Biol 16:1155–1160
32. Szepessy E, Nagy G, Jenei Z, Serfozo Z, Csuka I, James J et al (2003) Multiple subphases of DNA repair and poly(ADP-ribose) synthesis in Chinese hamster ovary (CHO-K1) cells. Eur J Cell Biol 82:201–207
33. Banfalvi G, Ujvarosi K, Trencsenyi G, Somogyi C, Nagy G, Basnakian AG (2007) Cell culture dependent toxicity and chromatin changes upon cadmium treatment in murine pre-B cells. Apoptosis 12:1219–1228
34. Guidozzi F (1997) Enrichment of ovarian cancer cell suspensions by centrifugal elutriation after density gradient purification. Int J Gynecol Cancer 7:100–105
35. Banfalvi G, Klaisz M, Ujvarosi K, Trencsenyi G, Rozsa D, Nagy G (2007) Gamma irradiation induced apoptotic changes in the chromatin structure of human erythroleukemia K562 cells. Apoptosis 12:2271–2283
36. Fransen JH, Dieker JW, Hilbrands LB, Berden JH, van der Vlag J (2011) Synchronized turbo apoptosis induced by cold-shock. Apoptosis 16:86–93

Chapter 3

Image Cytofluorometry for the Quantification of Ploidy and Endoplasmic Reticulum Stress in Cancer Cells

Laura Senovilla*, Yohann Demont*, Juliette Humeau, Norma Bloy, and Guido Kroemer

Abstract

One of the mechanisms of cancer-associated genomic instability involves a transient phase of polyploidization, in most cases tetraploidization, followed by asymmetric divisions and chromosome loss. Increases in ploidy are consistently accompanied by the activation of an endoplasmic reticulum (ER) stress response, resulting in the translocation of calreticulin to the outer surface of the plasma membrane where it stimulates anticancer immune responses. Conversely, immunoselection leads to a coordinated reduction in ploidy, ER stress, and calreticulin exposure. To simultaneously investigate the ER stress and ploidy, we developed an image cytofluorometric method that allows to measure DNA content, ER stress-associated phosphorylation of eIF2α, and calreticulin exposure at the cell surface. Here, we specify this methodology, which is useful for investigating the correlation between ploidy and ER stress at the single cell level.

Key words Tetraploidy, ER stress, eIF2α, Calreticulin, Image cytofluorometry

1 Introduction

One of the major biological alterations acquired during carcinogenesis is genomic instability [1]. One particular cause of genomic instability is the change in the number of chromosomes during cell divisions, leading to aneuploidy, which is a characteristic of human solid tumors [2]. Many tumors contain two cell populations, namely, near-to-diploid and near-to-tetraploid populations. This could be explained if we consider tetraploidy as an intermediate step between diploidy and aneuploidy [3, 4]. Tetraploidy has been observed in different human tumors including Barrett's esophagus, cervical, breast, and bladder cancers [2]. Tetraploidy may act as a stochastic generator of genomic instability because tetraploid cells are prone to progressively gain or lose chromosomes during aberrant rounds of asymmetric mitosis that can be multipolar [5, 6].

Both authors equally contributed for this chapter.

Gaspar Banfalvi (ed.), *Cell Cycle Synchronization: Methods and Protocols*, Methods in Molecular Biology, vol. 1524,
DOI 10.1007/978-1-4939-6603-5_3,

In normal conditions, tetraploid as well as polyploid cells die as soon as they are generated [7] probably due to the existence of a "tetraploidy checkpoint" that normally prevents the generation or propagation of tetraploid cells [8]. Nevertheless, occasionally such tetraploid cells are able to escape to this cell-intrinsic tumor-suppressive control mechanism and then are subjected to an external control by the immune system [9]. Preclinical and clinical evidence accumulating over the last few years supports the notion that malignant cells can be recognized and even eliminated by the immune system [10, 11]. In particular, increases in ploidy are consistently accompanied by the activation of the endoplasmic reticulum (ER) stress response, manifesting with the inactivating phosphorylation of the eukaryotic initiation factor 2α (eIF2α) and resulting in increased baseline levels of plasma membrane exposed of calreticulin (CALR) protein. The augmentation of CALR at the cell surface acts as an "eat-me" signal activating a complex immunogenic response that involves cross-presentation of tumor antigens by dendritic cells to cytotoxic T lymphocytes [9, 12–16].

So far, DNA content, exposure of CALR at the surface and phosphorylation of eIF2α have been measured in distinct batches of cells rather than simultaneously in the same sample. DNA content was usually analyzed by means of staining cells with fluorescent probes that interact with chromatin (such as Hoechst 33342) which can be used in live cells or DNA (such as 2-(4-Amidinophenyl)-6-indolecarbamidine dihydrochloride, DAPI, or propidium iodide, PI), which have to be used on fixed and permeabilized cells, followed by flow cytometry. Furthermore, fluorescence microscopy can be use to estimate the diameter, surface, and volume of nuclei as an indirect measurement of ploidy. CALR exposure was examined by immunofluorescence staining of live cells, while phosphorylation of eIF2α was measured by either immunofluorescence microscopy of fixed and permeabilized cells, immunohistochemical methods, or immunoblot [9, 17, 18]. The parallel use of these techniques was expensive, time–consuming, and failed to yield information on the relationship of DNA content, ER stress, and CALR exposure at the single cell level.

Driven by these considerations, we developed an image cytofluorometric method for studying DNA content, the ER stress-associated phosphorylation of eIF2α, and the translocation of CALR to the plasma membrane at single cell level. We applied these methods for comparing near-to-diploid cells compared with near-to-tetraploid cells obtained after transiently (48 h) culturing cells with nocodazole, an antimitotic agent that interferes with the polymerization of microtubules, hence arresting the cell cycle at the G_2/M phase and then causing "mitotic slippage" as a mechanism of tetraploidization.

CALR is a calcium-binding protein localized mainly in the ER lumen [19] that can translocate to the plasma membrane of

ER-stressed and dying cells. Surface CALR confers immunogenic properties to cancer cells, presumably because it facilitates their phagocytosis by dendritic cells [20]. To confirm that CALR is exposed to the cell surface, we performed immunofluorescence staining of live cells (to detect CALR) and counterstained the plasma membrane with fluorescent wheat germ agglutinin (WGA), a lectin that binds to the glycocalix. Then, cells were then fixed and permeabilized with 80% ice-cold ethanol and stored overnight at −20° C. After that, cells were stained to visualize P-eIF2α by immunofluorescence and counterstained with DAPI to measure DNA content. Finally, the four different parameters (CALR, WGA, P-eIF2α, DAPI) were analyzed on a cell-per-cell basis by means of an Amnis® imaging flow cytometer which combines flow cytometry with image microscopy in a single instrument (Fig. 1). Gates were placed to solely analyze single cells for which focused and intact images were available and the fluorescence staining were non-saturated (with the exception that we allowed for CALR staining to reach a 3% maximum saturation). This procedure led to the exclusion of cells that were not viable during the first immunofluorescence procedure and hence exhibit intense intracellular staining of CALR and WGA.

Nocodazole treatment of mouse colon carcinoma CT26 cells induced an increase in ploidy, as indicated by an augmentation of nuclear area (Fig. 2a) and fluorescence intensity per cells, revealing doubling of the DNA content (Fig. 2b). Such near-to-tetraploid cells showed an increase in CALR exposure (Fig. 2c) and eIF2α phosphorylation (Fig. 2d). In previous works, we used nuclear size as an indirect measurement of DNA content [9, 17, 21]. Here, taking advantage of the combination of flow cytometry and image microscopy, we confirmed that nuclear size may be considered as an acceptable indirect measurement of DNA content. An increase in fluorescence intensity was generally accompanied by an increase in nuclear area (Fig. 3a). The simultaneous measurement of the distinct parameters in the same cellular population allowed us to correlate the measurements among each other, confirming that near-to-tetraploid cells (defined as cells with elevated DAPI fluorescence intensity values) showed an increase in CALR fluorescence intensity at the cell surface (Fig. 3b) and an augmentation of phosphorylated eIF2α (Fig. 3c). Moreover, the phosphorylation of eIF2α correlated with CALR exposure on a cell per cell basis (Fig. 3d). In summary, all the three parameters (ploidy, eIF2α phosphorylation, CALR exposure) significantly correlated among each other (Table 1).

Briefly, we provide a detailed method for immunofluorescence staining and cytofluorometric analysis of untreated and nocodazole-treated cells, allowing to analyze changes in ploidy, ER stress-associated eIF2α phosphorylation and consequent CALR exposure.

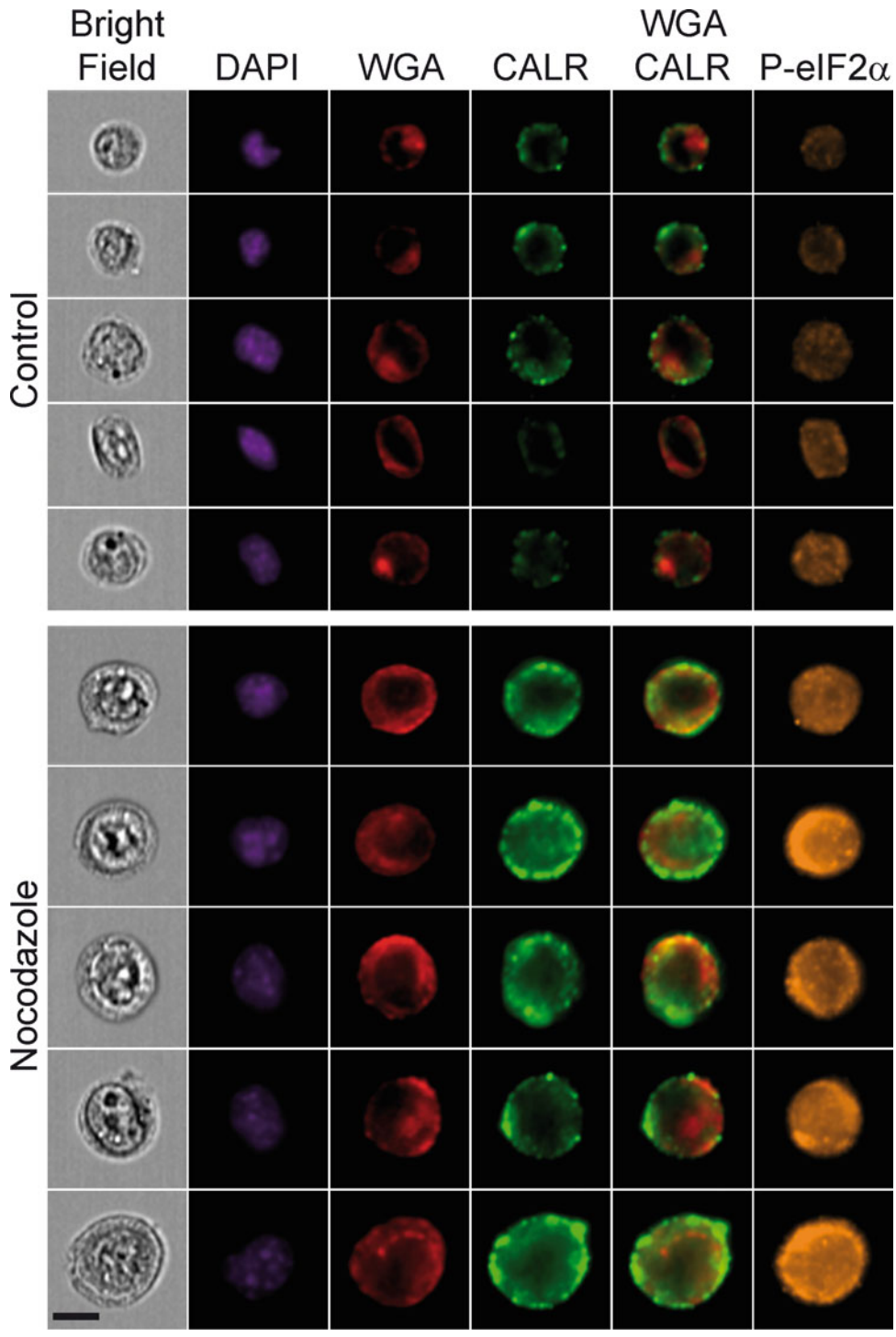

Fig. 1 Multicolor staining for the detection of ploidy and ER stress markers. Representative control and nocodazole-treated cells were stained to detect surface calreticulin (CALR) and intracellular P-eIF2α by immunofluorescence staining, counterstained with DAPI and WGA, and analyzed by means of an Amnis® imaging flow cytometer. Five representative cells from each group are depicted. CALR staining co-localizes with WGA staining. *Bright field* images are acquired as controls. Calibration bar: 10 μm. Note that nocodazole-treated cells exhibit an increase in size, as well as in CALR and P-eIF2α fluorescence intensity compared to control cells

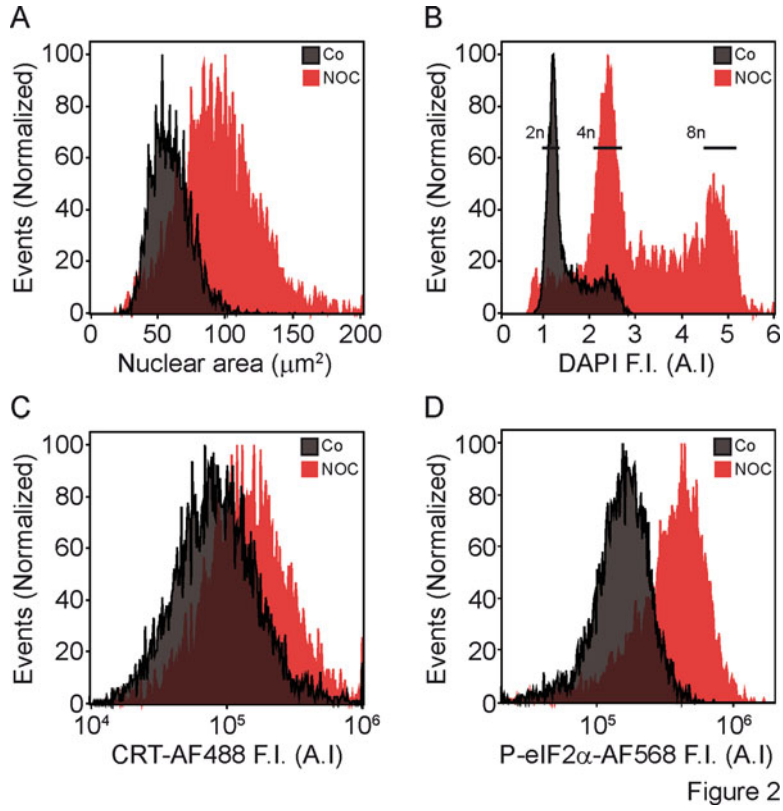

Fig. 2 ER stress analysis in near-to-diploid *versus* near-to-tetraploid cells. The control and nocodazole (NOC)-treated cells were analyzed for DNA content either as nuclear area (**a**) or as fluorescence intensity (**b**), CALR exposure (**c**) and eIF2α phosphorylation (**d**). Control (near-to-diploid) cells are shown in *black* and nocodazole-treated (near-to-tetraploid) cells in *red. F.I.* means fluorescence intensity, and *A.I.* signifies arbitrary units

2 Materials

2.1 Disposables

1. 75 or 175 cm^2 flasks for cell culture.
2. 50 ml conical centrifuge tubes.
3. 5 ml, 12×75 mm FACs tubes.
4. 1.5 ml microcentrifuge tubes.

2.2 Equipments

1. Heraeus™ Megafuge™ 40R centrifuge (The Thermo Fisher Scientific Inc., Waltham, MA, USA) provided with a CFC-free refrigeration system (from −10 °C to +40 °C) essential for the CALR staining.

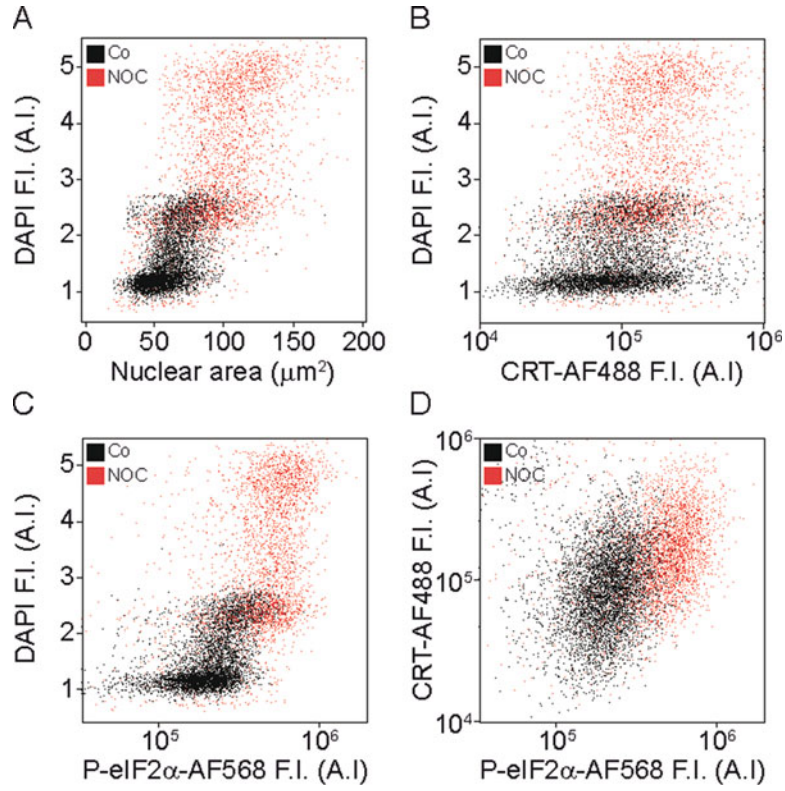

Fig. 3 Correlation between ploidy and the signs of ER stress. Values of DAPI fluorescence intensity were confronted with the nuclear area (**a**), the fluorescence intensity of CALR at the cell surface (**b**) and the phosphorylated eIF2α fluorescence intensity (**c**). The ER stress marker P-eIF2α was correlated with CALR exposure (**d**). Control (near-to-diploid) cells are shown in *black* and nocodazole (NOC)-treated (near-to-tetraploid) cells in *red. F.I.* means fluorescence intensity, and *A.I.* refers to arbitrary units

Table 1

Spearman correlations between ploidy, ER stress, and CALR exposure

	Control cells		Nocodazole-treated cells	
	rs	*p*	*rs*	*p*
DAPI vs. nuclear area	0.53	$<2.2\times10^{-16}$	0.60	$<2.2\times10^{-16}$
DAPI vs. CALR	0.28	$<2.2\times10^{-16}$	0.31	$<2.2\times10^{-16}$
DAPI vs. P-eIF2α	0.49	$<2.2\times10^{-16}$	0.49	$<2.2\times10^{-16}$
CRT vs. P-eIF2α	0.23	$<2.2\times10^{-16}$	0.34	$<2.2\times10^{-16}$

2. ImageStream X Mark II (ISX MkII, Amnis Corporation, Seattle, WA, USA, part of Millipore EMD, Darmstadt, Germany) equipped with 375, 488, 561, 642 lasers, 20×, 40× and 60× magnification lenses, an Extended Depth Field module and AutoSampler.

2.3 Reagents

2.3.1 Culture and Tetraploidization

1. Complete growth medium: RPMI medium supplemented with 1 mM sodium pyruvate, 100 mM HEPES buffer, 100 U/ml penicillin G, 100 μg/ml streptomycin sulfate, and 10% fetal bovine serum (FBS).
2. Nocodazole (Sigma-Aldrich, St. Louis, MO, USA), 1 μM stock solution in DMSO, stored at −20 °C (*see* **Notes 1** and **2**).
3. TrypLE™ Express Enzyme with EDTA without red phenol (Gibco, Gaithersburg, MD, USA), stable for 24 months stored at 4 °C (*see* **Note 3**).

2.3.2 Immunocytochemistry

1. PBS pH 7.4, stored at 4 °C.
2. Blocking buffer: 5% Bovine serum albumin (BSA) (w/v) in PBS pH 7.4, stored at 4 °C (*see* **Note 4**).
3. 80% Ice-cold ethanol (v/v) in dH_2O, stored at −20 °C (*see* **Note 5**).
4. 0.25% Tween-20 (v/v) in PBS pH 7.4, stored at room temperature (RT) (*see* **Note 6**).
5. 2-(4-Amidinophenyl)-6-indolecarbamidine dihydrochloride (DAPI; Molecular Probes, Eugene, OR, USA), stock solution at 1 mg/ml and stored at 4 °C under protection from light (*see* **Notes 7** and **8**).

2.3.3 Antibodies

1. Chicken polyclonal against calreticulin (ab2908) (Abcam, Cambridge, UK). Secondary antibody goat anti-chicken Alexa Fluor 488 (Abcam, ab1500169).
2. Rabbit monoclonal against eIF2α phosphorylated on Ser51 (Abcam, ab32157). Secondary antibody donkey anti-rabbit Alexa Fluor 568 (Abcam, ab175470).
3. Wheat germ agglutinin (WGA) conjugate Alexa Fluor 633 (Invitrogen, Carlsbad, CA, USA), stock solution at 1.5 mg/ml under protection of light (*see* **Note 9**).

All of them stored at −20 °C.

2.3.4 ISX MKII Operational Liquids

1. PBS without Ca^{2+} or Mg^{2+} pH 7.4 as sheather (ThermoFisher), stored at 4 °C.
2. Sterilized 18.2 mΩ water to rinse.
3. FlowClean Cleaning Agent (Beckman Coulter, Brea, CA, USA), stored at 4 °C.

4. Speed Beads calibration reagent (AMNIS) for alignment, stored at 4 °C.
5. 70% Isopropanol (v/v) in dH_2O as debubbler, stored at RT.
6. 0.5% Bleach (v/v) in dH_2O to sterilize, stored at RT.

3 Methods

3.1 Cell Culture

1. Upon thawing, maintain CT26 cells in complete growth medium in 75 cm^2 flasks (37 °C, 5% CO_2) (*see* **Note 10**).
2. When confluence approaches 70–80%, detach cells with TrypLE™ enzyme (*see* **Notes 11** and **12**) to constitute fresh maintenance cultures and to provide cells for experimental determinations.

3.2 Generation of Near-to-Tetraploid Cells

1. Seed 2–4 × 10^6 CT26 cells in 40 ml complete growth medium in 175 cm^2 flasks and let adapt for 24 h (*see* **Note 13**).
2. After 24 h, discard culture supernatants and add fresh complete growth medium alone (to the flask of control cells) or supplemented with nocodazole to a final concentration of 100 nM. Culture cells for 48 h before the staining (*see* **Notes 14** and **15**).

3.3 Multicolor Immunostaining

1. Remove the supernatants from the control and nocodazole-treated flask and detach adherent cells with 5 ml TrypLE™ (*see* **Notes 11** and **12**).
2. Upon detachment, add 15 ml of complete growth medium and transfer to 50 ml tubes.
3. Count cells in a classical hemocytometer and add 1 × 10^6 cells to FACs tubes. From this moment, cell staining for CALR and WGA is performed on ice (*see* **Notes 16** and **17**).
4. Centrifuge samples at 300 × *g* for 5 min at 4 °C, discard supernatants, and resuspend cell pellets in 2 ml cold PBS pH 7.4.
5. Re-centrifuge samples at 300 × *g* for 5 min at 4 °C, discard supernatants.
6. Incubate the corresponding tubes with 100 μl of CALR primary antibody (diluted 1:100 in cold blocking buffer) for 1 h on ice (*see* **Note 18**).
7. Add 2 ml cold PBS pH 7.4 and centrifuge samples at 300 × *g* for 5 min at 4 °C, discard supernatants.
8. Incubate for 30 min with 300 μl goat anti-chicken conjugated Alexa fluor 488 secondary antibody (diluted 1:500 in cold blocking buffer) and/or WGA conjugated Alexa fluor 633 (diluted 1:300 in cold blocking buffer) on ice (*see* **Note 18**).

9. Add 2 ml cold PBS pH 7.4 and centrifuge samples at 300×*g* for 5 min at 4 °C, discard supernatants.
10. Fix cells by adding 500 µl of 80% ice-cold ethanol drop by drop and vortexing at the same time (*see* **Note 19**).
11. Store cells at −20 °C overnight (ON).
12. Next day, wash the cells by adding 2 ml of cold PBS pH 7.4 and centrifuge samples at 300×*g* for 5 min (at 4 °C), discard supernatants (*see* **Note 20**).
13. Permeabilize cells with 500 µl of 0.25% Tween-20 for 15 min at 4 °C (*see* **Note 21**).
14. Neutralize the reaction using 2 ml of blocking buffer.
15. Centrifuge samples at 300×*g* for 5 min and discard supernatants.
16. Incubate the corresponding tubes with 100 µl of P-eIF2α primary antibody (diluted 1:50 in cold blocking buffer) for 1 h (*see* **Note 18**).
17. Wash cells by adding 2 ml cold PBS (pH 7.4) and centrifuge samples at 300×*g* for 5 min, discard supernatants.
18. Incubate for 30 min with 300 µl donkey anti-rabbit conjugated Alexa fluor 568 secondary antibody (diluted 1:500 in cold blocking buffer) and/or DAPI (diluted 1:1000 in cold blocking buffer) (*see* **Note 18**).
19. Add 2 ml cold PBS pH 7.4 and centrifuge samples at 300×*g* for 5 min at 4 °C, discard supernatants and transfer to 1.5 ml Eppendorf tubes for the cytofluorometric acquisition in a final volume of 50 µl (*see* **Note 22**).

3.4 Sample Acquisition and Analysis

1. Perform acquisition and analysis by first gating on events that are defined by ratio, area, shape ratio, circularity, and diameter, while applying upper and lower thresholds for DAPI and side scatter (SSC) (*see* **Note 23**).
2. Export data as .fcs files and generate graphs using FlowJo Software v10.0.8 (Tree Star, Ashland, OR, USA).
3. For correlation computation, .fcs files are loaded in R software v3.0.1 by means of the flowCore package. Pearson correlation was determined using the cor.test() function of the stats package.

4 Notes

1. Nocodazole is hazardous to health and it can be fatal if inhaled, swallowed, or absorbed through skin. Always handle nocodazole using protective eye shields, gloves, and respiratory filters.

2. Undissolved nocodazole appears as a white powder and may be stored at 4 °C under protection from light for 2–3 years.
3. TrypLE™ contains no substances that are considered to be hazardous to health. Nevertheless, it may be harmful by inhalation, swallowed, and it may cause eye and skin irritation.
4. Undissolved BSA appears as yellow powder and should be stored at 4 °C under protection from light.
5. Ethanol is a highly inflammable liquid and should be handled using protective eye shields, gloves, and respiratory filters.
6. Tween-20 contains no components considered to be persistent, bioaccumulative, or toxic. Store at RT.
7. Undissolved DAPI powder is stored at −20 °C under protection from light.
8. DAPI is not considered hazardous to health. Nevertheless, it may be harmful upon inhalation or ingestion and may cause eye and skin irritation.
9. WGA is provided as a lyophilized reagent. Once dissolved in distilled H_2O, it should be stored at −20 °C for less than 1 month, protected from light.
10. For maintenance of cell cultures, CT26 cells can be split at 1:5–1:10 ratios, according to the experimental needs.
11. While 4 ml trypsin/EDTA are sufficient for 75 cm^2 flasks, 5 ml should be used for 175 cm^2 flasks.
12. Trypsinization time is a function of cell type, viability, and culture density. For CT26 cells (and most cell lines), 5 min at 37 °C are amply sufficient to fully detach a totally confluent, healthy population. However, complete cell detachment should be checked by visual inspection or by light microscopic observation.
13. CT26 cells need 24 h of adaptation before any experimental manipulation. This adaptation period may be variable depending on the cell type.
14. To become tetraploid, CT26 need 48 h to escape from the cell cycle arrest induced by the nocodazole treatment, which occurs after approximately 24 h.
15. The percentage of near-to-tetraploid CT26 arising after 48 h of nocodazole treatment is close to 90–100%. This percentage is widely variable between different cell lines and also depends on the tetraploidization-inducing agent. Depending on the cell line, cytochalasin D may be an alternative to nocodazole.
16. Two FACs tubes at least are necessary for both control and nocodazole-treated conditions, one for the quadruple staining and the other without any dye (negative control). It is

necessary, at least for the first time, to perform single staining of each of the fluorescent parameters for the calibration of the ISX MKII equipment.

17. CALR exposure staining is carried out on live cells. To avoid the internalization of CALR during the experiment, cell staining must be performed on ice.
18. At this moment, unstained or single staining controls can be incubated in blocking buffer in the same conditions while omitting the antibody of interest.
19. Once the supernatant has been removed, mix the cells with the ethanol-containing solution while pipetting to avoid the formation of unwarranted cell clusters.
20. From this moment, the remaining steps are carried out at RT unless specified differently.
21. P-eIF2α immunostaining should be localized in the cytoplasm (and sometimes in the nuclei). For this reason, the cells must be permeabilized before the incubation with the antibody.
22. Using the ISX MKII equipment, there is possibility to use 96-well plates with a final volume of 70 μl/well. The sample acquisition is run automatically when plates are used. Depending on the number of samples, the acquisition mode may be adapted to Eppendorf tubes.
23. Only focused events were kept using gradient RMS feature on bright field images. Saturated signals in fluorescent channels and cropped images (raw centroid X) were eliminated.

Acknowledgments

GK is supported by the Ligue contre le Cancer (équipes labelisées); Agence Nationale de la Recherche (ANR); Association pour la recherche sur le cancer (ARC); Cancéropôle Ile-de-France; Institut National du Cancer (INCa); Fondation Bettencourt-Schueller; Fondation de France; Fondation pour la Recherche Médicale (FRM); the European Commission (ArtForce); the European Research Council (ERC for GK); the LabEx Immuno-Oncology; the SIRIC Stratified Oncology Cell DNA Repair and Tumor Immune Elimination (SOCRATE); the SIRIC Cancer Research and Personalized Medicine (CARPEM); and the Paris Alliance of Cancer Research Institutes (PACRI). LS is supported by the Institut national de la santé et de la recherche médicale (INSERM) and the Association pour la recherche sur le cancer (ARC). JH is supported by Fondation Philanthropia and NB by a fellowship by the French Ministry of Research and Technology.

References

1. Hanahan D, Weinberg RA (2011) Hallmarks of cancer: the next generation. Cell 144:646–674
2. Davoli T, de Lange T (2011) The causes and consequences of polyploidy in normal development and cancer. Annu Rev Cell Dev Biol 27:585–610
3. Shackney SE, Smith CA, Miller BW, Burholt DR, Murtha K, Giles HR, Ketterer DM, Pollice AA (1989) Model for the genetic evolution of human solid tumors. Cancer Res 49:3344–3354
4. Ganem NJ, Storchova Z, Pellman D (2007) Tetraploidy, aneuploidy and cancer. Curr Opin Genet Dev 17:157–162
5. Vitale I, Galluzzi L, Castedo M, Kroemer G (2011) Mitotic catastrophe: a mechanism for avoiding genomic instability. Nat Rev Mol Cell Biol 12:385–392
6. Vitale I, Galluzzi L, Senovilla L, Criollo A, Jemaa M, Castedo M et al (2011) Illicit survival of cancer cells during polyploidization and depolyploidization. Cell Death Differ 18:1403–1413
7. Fujiwara T, Bandi M, Nitta M, Ivanova EV, Bronson RT, Pellman D (2005) Cytokinesis failure generating tetraploids promotes tumorigenesis in p53-null cells. Nature 437:1043–1047
8. Andreassen PR, Lohez OD, Lacroix FB, Margolis RL (2001) Tetraploid state induces p53-dependent arrest of nontransformed mammalian cells in G1. Mol Biol Cell 12:1315–1328
9. Senovilla L, Vitale I, Martins I, Tailler M, Pailleret C, Michaud M et al (2012) An immunosurveillance mechanism controls cancer cell ploidy. Science 337:1678–1684
10. Finn OJ (2012) Immuno-oncology: understanding the function and dysfunction of the immune system in cancer. Ann Oncol 23(Suppl 8):viii6–viii9
11. Fridman WH, Pages F, Sautes-Fridman C, Galon J (2012) The immune contexture in human tumours: impact on clinical outcome. Nat Rev Cancer 12:298–306
12. Kroemer G, Galluzzi L, Kepp O, Zitvogel L (2013) Immunogenic cell death in cancer therapy. Annu Rev Immunol 31:51–72
13. Senovilla L, Vitale I, Martins I, Kepp O, Galluzzi L, Zitvogel L et al (2013) An anticancer therapy-elicited immunosurveillance system that eliminates tetraploid cells. Oncoimmunology 2:e22409
14. Senovilla L, Galluzzi L, Castedo M, Kroemer G (2013) Immunological control of cell cycle aberrations for the avoidance of oncogenesis: the case of tetraploidy. Ann N Y Acad Sci 1284:57–61
15. Zitvogel L, Galluzzi L, Smyth MJ, Kroemer G (2013) Mechanism of action of conventional and targeted anticancer therapies: reinstating immunosurveillance. Immunity 39:74–88
16. Galluzzi L, Buque A, Kepp O, Zitvogel L, Kroemer G (2015) Immunological effects of conventional chemotherapy and targeted anticancer agents. Cancer Cell 28:690–714
17. Bloy N, Sauvat A, Chaba K, Buque A, Humeau J, Bravo-San Pedro JM et al (2015) Morphometric analysis of immunoselection against hyperploid cancer cells. Oncotarget 6:41204–41215
18. Kepp O, Galluzzi L, Lipinski M, Yuan J, Kroemer G (2011) Cell death assays for drug discovery. Nat Rev Drug Discov 10:221–237
19. Michalak M, Milner RE, Burns K, Opas M (1992) Calreticulin. Biochem J 285(Pt 3):681–692
20. Obeid M, Tesniere A, Ghiringhelli F, Fimia GM, Apetoh L, Perfettini JL et al (2007) Calreticulin exposure dictates the immunogenicity of cancer cell death. Nat Med 13:54–61
21. Boileve A, Senovilla L, Vitale I, Lissa D, Martins I, Metivier D et al (2013) Immunosurveillance against tetraploidization-induced colon tumorigenesis. Cell Cycle 12:473–479

Chapter 4

Large-Scale Mitotic Cell Synchronization

Kalyan Dulla and Anna Santamaria Margalef

Abstract

Understanding cell growth and cell division involves the study of regulatory events that occur in a cell cycle phase-dependent manner. Studies analyzing cell cycle regulatory mechanisms and cell cycle progression invariably require synchronization of cell populations at specific cell cycle stages. Several methods have been established to synchronize cells, including serum deprivation, contact inhibition, centrifugal elutriation, and drug-dependent synchronization. Despite potential adverse cellular consequences of synchronizing cells by pharmacological agents, drug-dependent methods can be advantageous when studying later cell cycle events to ensure specific enrichment at selected mitotic stages. This chapter describes protocols used in our laboratory for isolating mitotic mammalian cells in a large-scale manner. In particular, we discuss the technical aspects of adherent or suspension cell isolation, the methods necessary to enrich cells at different mitotic stages and the optimized culture conditions.

Key words Mitosis, Large-scale synchronization, HeLa S3, HeLa S, Spinner cultures, Triple flasks, Prometaphase, Metaphase, Anaphase/telophase

1 Introduction

The cell cycle is the series of events that leads to genome duplication and cell division [1]. In eukaryotic cells, containing a nucleus, the cell cycle is divided into interphase and M-phase. Interphase proceeds in three stages, G1, S, and G2, in which the cell duplicates its DNA (during S phase) and grows. The result of the M-phase of the cell cycle is the generation of two daughter cells that are genetically identical to each other as well as to their parental cell. This phase comprises mitosis and cytokinesis. Mitosis is the process by which a eukaryotic cell equally segregates its chromosomes. It is immediately followed by cytokinesis, which drives the division of the cytoplasm, cell membrane, and other organelles into two cells that will contain about the same amount of these cellular compartments. During M-phase, activation of each successive stage phase is dependent on the proper progression and completion of the previous one. A large number

Gaspar Banfalvi (ed.), *Cell Cycle Synchronization: Methods and Protocols*, Methods in Molecular Biology, vol. 1524,
DOI 10.1007/978-1-4939-6603-5_4,

of regulatory protein complexes and signaling pathways are devoted to ensure normal progression through the cell cycle and deregulation of this process may lead to tumorigenesis [1].

Elucidating the events and regulatory mechanisms of the cell cycle is an active field of investigation. Advances in the sensitivity and throughput of mass spectrometry-based methods and associated bioinformatic tools, have made it feasible to perform large-scale analysis at a systems level [2, 3]. The strength of proteomic approaches for the global analysis of the cell cycle, and mitosis in particular, has been demonstrated in several recent studies, as exemplified by an atlas of mitotic phosphorylation compared to interphase phosphorylation [4], the generation of quantitative datasets of spindle protein and kinase phosphoproteomes at distinct cell cycle and mitotic stages [5–8], the assignment of phosphorylation sites to individual kinases [9, 10], the analysis of the proteome and phosphoproteome of the human cell cycle [11], or the global analysis of phosphorylation states of the anaphase promoting complex in response to antimitotic drugs [12]. All these studies required large amount of cells that are synchronized in various stages of the cell cycle, in particular in specific mitotic stages. The latter proved difficult, due to the lack of methods for obtaining mammalian cells in later stages of mitosis in sufficient amounts.

Drug-independent methods allow successful synchronization with minimal perturbation of biological systems and several of these approaches are described in other chapters of this book. However, none of them allow distinction between different mitotic phases such as prometaphase, metaphase, and the later stages anaphase and telophase. The "mitotic shake-off" method for instance, originally described by Terasima and Tolmach [13], is useful for cells synchronized in mitosis, which on plating into culture dishes move into G1 in a synchronous manner. A drawback of this method is that only a small percentage of the cells is in mitosis at any given time and therefore the yield is extremely low, and as mentioned, it does not allow distinction between different mitotic stages. On the other hand, "centrifugal elutriation" [14] allows isolation of almost all cell types, adherent or suspension, based on their size, yielding large populations of phase-specific cells. For details of centrifugal elutriation see also Chapter 2. Yet again, cells only in interphase but not in different mitotic stages could be discriminated with this method.

The methods presented here have been developed using HeLa S3 or HeLa suspension (S) (*see* Subheading 2). HeLa cells are established, immortalized cells derived from a cervical cancer. HeLa cells are a common model system for mammalian cell cycle research and they are suitable for large-scale mitotic studies as they can be easily synchronized in mitosis. Here, we describe drug-derived protocols to synchronize cells at specific mitotic stages, as well as protocols that were developed to synchronize HeLa S cells, which can be grown in a larger scale in suspension cultures (*see* **Note 1**).

2 Materials

2.1 Cell Lines

All cell lines used in this study (American Type Culture Collection, ATCC, Manassas, VA), HeLa S3 and HeLa S cells were grown at 37 °C in a humidifier incubator with a 5% CO_2 atmosphere in Dulbecco's modified Eagle's medium (DMEM), supplemented with 10% heat-inactivated fetal calf serum and penicillin–streptomycin (100 U/ml and 100 μg/ml, respectively).

2.2 Reagents, Solutions, and Media

1. Fetal calf serum (heat inactivated at 56 °C for 30 min).
2. Pluronic F-68 nonionic surfactant (Sigma).
3. FITC-labeled-α-Tubulin antibody (Sigma).
4. MG132 cell-permeable proteasome inhibitor (Calbiochem).
5. RO-3306 selective CDK1 inhibitor (Alexis Biochemicals).
6. Noscapine (also known as Narcotine, Nectodon, Nospen, and Anarcotine) benzylisoquinoline alkaloid (Sigma).
7. Cell culture media: Dulbecco's Modified Eagle's Medium (DMEM) (Gibco/BRL, Bethesda, MD), supplemented with 10% fetal calf serum (heat inactivated at 56 °C for 30 min) and penicillin–streptomycin (100 U/ml and 100 μg/ml, respectively).
8. Phosphate Saline Buffer (PBS): 8 g NaCl, 0.2 g KCl, 1.44 g Na_2HPO_4, 0.24 g KH_2PO_4, in 1 l of distilled water, pH 7.4.
9. Mounting media for immunofluorescence: 50 mM Tris pH 8.6 (2.5 ml 1 M)+2.5 ml water, 90% glycerol, 250 mg p-phenylenediamine (PPD) (5 mg/ml). Dissolve 250 mg PPD in Tris (protect from light). Add 45 ml glycerol 100% and mix vigorously.

2.3 Cell Culture Spinner and Culture Flasks

1. Triple flasks (Nunc).
2. Stirring platform (CELL SPIN).
3. Spinner flasks and other accessories (INTEGRA Bioscience).

2.4 Drug Stock Solutions

1. Thymidine stock solution: 200 mM (*see* **Note 2**). Store at room temperature or in aliquots at −20 °C.
2. Nocodazole stock: concentration 500 mg/ml in DMSO. Store in aliquots at −20 °C.
3. MG132 stock: concentration 20 mM in DMSO. Store in aliquots at −20 °C.
4. RO-3306 stock: concentration 5 mg/ml in DMSO. Store in aliquots at −20 °C, in the dark.
5. Noscapine stock: concentration 100 mM in DMSO. Store in aliquots at −20 °C.

3 Methods

3.1 Large-Scale Synchronization of Adherent HeLa S3 Cells

1. HeLa S3 cells are firstly seeded in 15 cm diameter culture dishes at a density of approximately 1×10^7 cells/dish.
2. For large-scale studies we use ten culture triple-flasks… (*see* **Note 3**),…, containing three growth layers on top of each other with a total surface of 500 cm^2. Cells are expanded to culture triple flasks in a ratio of approximately 1:3 from the 15 cm diameter culture dishes.

A schematic representation of the protocols described below is depicted in Fig. 1.

3.1.1 Synchronization of Cells in Prometaphase

Prometaphase begins when the nuclear envelope breaks down and continues until all sister chromatids are attached to the spindle microtubules in a bi-oriented fashion. To synchronize cells in prometaphase, treatment with the depolymerizing agent nocodazole is amongst the most common methods [15] (*see* **Note 4**). Use low enough concentration (40 ng/ml) to affect microtubule dynamics and induce a spindle assembly checkpoint (SAC) arrest, but allow re-polymerization later on.

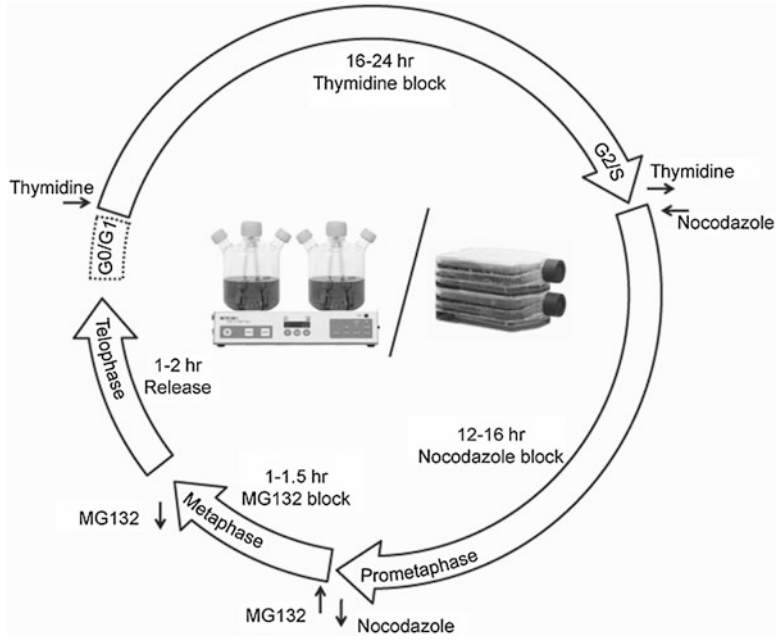

Fig. 1 Schematic representation of the synchronization protocols described in the text to isolate cells in a large-scale manner, in G1/S (Thymidine block), prometaphase (Nocodazole block), metaphase (Nocodazole release into MG132) and telophase (MG132 release into fresh medium). Protocols are optimized for growing cells in triple flasks or spinner cultures

1. Wash cells that had been previously pre-synchronized in G1/S by the addition of 2 mM thymidine (*see* **Note 5**) for 16–24 h twice with 60 ml PBS/flask and once with 60 ml/flask pre-warmed drug-free fresh medium and release into fresh medium for 12–16 h.
2. 6 h after release (cells will be then in S phase), replace medium by fresh medium containing 40 ng/ml of nocodazole (*see* **Note 6** and **7**). As cells will enter mitosis synchronously, the variability in the time that different cells are exposed to nocodazole before being harvested will be reduced.
3. Collect cells by mitotic shake-off. For this, remove the medium by decanting and add 1 ml PBS/flask.
4. Knock the flasks several times to the side-wall of the bench to detach the mitotic cells. This procedure yields about $1–2 \times 10^7$ mitotic cells per flask. Too much or not enough liquid in the flasks results in a poorer mitotic yield or requires stronger strokes that result in the co-release of interphase cells. Also, cells should not be too confluent. The best results are obtained when cells are 60–70% confluent at the time of shake-off.

3.1.2 Synchronization of Cells in Metaphase

Metaphase is the period where chromosomes await at the metaphase equator to complete alignment, thereby switching off the spindle assembly checkpoint. To enrich cells in metaphase, MG132, a reversible, cell-permeable proteasome inhibitor is used. Importantly, cells blocked by MG132 are characterized by an inactive SAC. This, combined with nocodazole-treated cells, allows the comparison between SAC-dependent and independent events.

1. Isolate prometaphase-arrested cells by shake-off as described before. Subsequently, wash the cells twice with PBS and once with fresh medium and release into fresh medium containing 20 μM MG132 for 60–90 min.
2. Harvest metaphase-arrested cells by centrifugation at $300 \times g$ for 3 min.

3.1.3 Synchronization of Cells in Anaphase/Telophase

In anaphase, sister chromatids are pulled apart to opposite poles of the mitotic spindle. Mitosis is completed in telophase when the chromosomes and other components are repackaged into the daughter nuclei. Synchronizing cells at late stages of mitosis is most difficult to achieve reproducibly due to their rather short duration (20–30 min). In addition, there are no drugs available to block cells efficiently in anaphase or telophase.

1. To isolate cells in late stages of mitosis (anaphase/telophase), wash metaphase-arrested cells (by MG132 treatment) twice with PBS and once with fresh medium and release into fresh drug-free medium for 60–90 min (*see* **Note 8**).

2. Harvest Anaphase/Telophase cells by centrifugation at 300 × *g* for 3 min. Commonly, a proportion of 25/75% anaphase to telophase cells can be observed at this time.

3.2 Large-Scale Synchronization of HeLa S Cells Growing in Suspension

Growth of cells in suspension (spinner) cultures allows synchronization of even larger amounts of cells. A disadvantage of suspension cultures compared to adherent cells is that the "shake-off" method of the rounded mitotic cells cannot be applied. As a result suspension cultures may contain higher proportion of interphase cells. To improve the purity of mitotic states, cells can be grown in medium supplemented with 20% FCS, instead of 10%. The increase in the growth stimulus helps the cells reaching prometaphase faster and more synchronously [8]. In addition, cells can be grown in the presence of 0.1% pluronic, which helps to minimize cell aggregation.

A schematic representation of the protocols described below is depicted in Fig. 1.

1. Expand cell cultures in spinner flasks which are operated at 45 rpm and kept inside the cell culture incubator at constant 37 °C temperature and 5% CO_2 atmosphere. Seed cells in spinner flasks at a minimum density of 0.3×10^6 cells/ml and allow them to grow to a maximum density of 1.8×10^6 cells/ml and the medium is changed every 2 days.
2. Prior to synchronization, transfer cells to 400 ml of fresh medium containing 20% FCS at a density of 0.6×10^6 cells/ml (*see* **Note 3**).
3. Similar to the procedure described for HeLa S3 cells, first presynchronize HeLa S cells in G1/S by addition of 4 mM thymidine for 16–24 h (more than 90% of cells reach prometaphase within the 12 h of thymidine release).
4. Subsequently, wash cells with PBS and release into fresh medium. To minimize the time that cells stay at room temperature do the following: Transfer the medium (containing the cells) to eight 50 ml falcon tubes and centrifuge at 300 × *g* for 2 min in two batches of four each. Discard the medium leaving less than 1 ml of old media and resuspend the cells in PBS (at room temperature) with a 10 ml glass pipette. Again centrifuge and remove PBS and resuspend cells in fresh medium.
5. After 6 h, add nocodazole at a concentration of 40 ng/ml to arrest cells in prometaphase.
6. Harvest part of the population of prometaphase cells by centrifugation at 300 × *g* for 3 min and wash the rest of cells as mentioned before and release into fresh medium containing 20 μM MG132 for 60–90 min.
7. Harvest part of the population of metaphase-arrested cells by centrifugation at 300 × *g* for 3 min and wash the rest of cells

once and release into fresh drug-free medium for 90–120 min. Note that the time to release cells in suspension from MG132 is longer than the one needed for adherent cells that had been shaken-off.

3.3 Immunofluorescence Staining of Cells in Suspension

1. Before harvesting the cells at different mitotic stages, transfer 500 µl of cell suspension (from the total spinner culture) to a fresh 1.5 ml tube.
2. Spin down the cells at 300 × *g* for 3 min.
3. Resuspend the cells in 500 µl fixing solution (1% paraformaldehyde and 3% sucrose) and incubate for 10 min at room temperature (*see* **Note 9**).
4. Centrifuge at 300 × *g* for 3 min, discard the supernatant and resuspend in 500 µl PBS. This cell suspension can be kept at 4 °C for few days.
5. Transfer around 50 µl of cell suspension to a fresh eppendorf tube and add Triton X-100 (0.1% final concentration) and incubate for 15 min at room temperature with constant shaking. Note that starting with a too large amount of cells may create problems in mixing and staining may not be uniform. On the other hand, the initial number of cells cannot be too low, as a considerable amount may be lost during the centrifugation steps.
6. Centrifuge again at 300 × *g* for 3 min and discard the supernatant.
7. Resuspend the cell pellet in 100 µl of PBS-Tween 20 (0.2% final concentration) with 2% BSA.
8. Add 4′-6-diamidino-2-phenylindole (DAPI) and FITC-labeled anti-α-Tubulin antibody at concentrations of 1 µg/ml and incubate for 1 h at room temperature with constant shaking.
9. Centrifuge at 300 × *g* for 3 min and wash the cell pellet once with PBS to reduce background staining.
10. Keep cells at 4 °C until analysis by immunofluorescence microscopy or examine directly. For this, mix 10 µl of stained cell suspension with 10 µl mounting solution, use 10 µl on a microscope glass slide and place a glass coverslip on top.
11. Visualize under the microscope [7, 8] (*see* **Note 10**).

4 Notes

1. The methods outlined here can be also applied to synchronize other cell types. However, when choosing a particular cell synchronization method, the cell cycle event to be studied, the doubling time of the cell type of interest, and the duration between each phase need to be considered.

2. The preparation of the thymidine stock requires extensive mixing at room temperature in a rotating wheel until the powder is completely dissolved.
3. The protocols described here have been optimized for the isolation of human mitotic spindles and for the study of dynamic phosphorylation of kinases at different mitotic stages, using HeLa S3 and HeLa S, respectively. These amounts can be scaled down or up accordingly to match the specific purpose of the experiment.
4. Generally, drug-induced mitotic states mimic normal mitotic stages but might not represent exactly unperturbed mitosis. Although both thymidine and nocodazole block/release methods are synchronization protocols commonly used that provide high proportions of synchronized cells and adequately reproduce cell cycle events, methods that induce cell cycle arrest in a particular phase of the cell cycle can potentially affect the protein of study or the biology of the cells.
5. Alternative methods to synchronize cells in G1/S phase are the DNA polymerase inhibitor aphidicolin [16] or hydroxyurea that targets the ribonucleotide reductase [17].
6. RO-3306 is an ATP-competitive inhibitor that has been proven to efficiently block cells in G2 by specifically inhibiting Cdk1/Cyclin B1 activity [18]. It has been shown that treatment of HeLa S3 with RO-3306 for 20 h led to a complete block of the cell cycle in the G2/M phase and removal of this inhibitor allowed rapid and synchronous entry into mitosis [18]. To our knowledge, this inhibitor has not been used yet for cell synchronization in large-scale experiments. Provided that the same effect is displayed when larger amount of cells (or cells in suspension) are treated, this would help minimizing the possible adverse effects of nocodazole, providing a healthier mitotic population.
7. It is possible to successfully synchronize large amounts of HeLa S3 cells in a late prometaphase stage by the use of 25 μM noscapine [7]. Noscapine is a microtubule-interacting agent that binds to tubulin and alters its conformation, thereby reducing the dynamics of microtubule turnover [19]. As consequence, cells arrest in a SAC-dependent late prometaphase stage, with a fairly normal mitotic spindle and most of the chromosomes aligned in the metaphase plate but few remaining near the spindle poles. The effect induced by noscapine treatment can be reverted by washing out the drug from the cells in culture. Approximately 30–60 min after noscapine washout, most of the cells can be found in a stage close to metaphase and late mitotic stages (i.e., anaphase and telophase), respectively. Treatments for a maximum of 9–10 h with noscapine are recommended. If the goal is to isolate mitotic spindles, this method can be advantageous, as spindle structures remain organized upon noscapine treatment.

8. The actual time it takes the cells to reach telophase may slightly differ from experiment to experiment. So after 50 min, every 10 min, 10 μl of cell suspension is pipetted onto a coverslip, mixed with quick stain (DAPI, 0.15% Triton X-100 in PBS) and observed under the microscope.
9. The protocol described here employs paraformaldehyde as fixation method. However, other cell fixation methods can be applied when staining with different antibodies is desired. We have successfully used the above-described protocol for fixation, using Methanol as fixative.
10. The samples can be further benchmarked using Western blotting analysis of specific mitotic markers [8].

Acknowledgments

We are thankful to Erich A. Nigg and Roman Körner for their support and critical reading of the original initial version chapter, and Herman H. Silljé, Albert Ries, and Elena Nigg for technical help to optimize these protocols. We apologize for any omission in references. We also acknowledge funding when this chapter was originally written by the Biozentrum of the University of Basel, the Max Planck Society and by ENFIN, funded by the European Commission within its FP6 Program. AS is currently supported by the Miguel Servet Program (CP13/00158) from the Instituto Carlos III cofunded by the European Regional Development Fund (ERDF).

References

1. Morgan DO (2007) The cell cycle: principles of control. New Science Press/Sinauer Associates, London/Sunderland, MA
2. Picotti P, Bodenmiller B, Mueller LN, Domon B, Aebersold R (2009) Full dynamic range proteome analysis of S. cerevisiae by targeted proteomics. Cell 138:795–806
3. Choudhary C, Mann M (2010) Decoding signalling networks by mass spectrometry-based proteomics. Nat Rev Mol Cell Biol 11:427–439
4. Dephoure N, Zhou C, Villen J, Beausoleil SA, Bakalarski CE, Elledge SJ, Gygi SP (2008) A quantitative atlas of mitotic phosphorylation. Proc Natl Acad Sci U S A 105:10762–10767
5. Nousiainen M, Sillje HH, Sauer G, Nigg EA, Körner R (2006) Phosphoproteome analysis of the human mitotic spindle. Proc Natl Acad Sci U S A 103:5391–5396
6. Daub H, Olsen JV, Bairlein M, Gnad F, Oppermann FS, Körner R, Greff Z, Kéri G, Stemmann O, Mann M (2008) Kinase-selective enrichment enables quantitative phosphoproteomics of the kinome across the cell cycle. Mol Cell 31:438–448
7. Malik R, Lenobel R, Santamaria A, Ries A, Nigg EA, Körner R (2009) Quantitative analysis of the human spindle phosphoproteome at distinct mitotic stages. J Proteome Res 8:4553–4563
8. Dulla K, Daub H, Hornberger R, Nigg EA, Körner R (2010) Quantitative site-specific phosphorylation dynamics of human protein kinases during mitotic progression. Mol Cell Proteomics 9:1167–1181
9. Holt LJ, Tuch BB, Villen J, Johnson AD, Gygi SP, Morgan DO (2009) Global analysis of Cdk1 substrate phosphorylation sites provides insights into evolution. Science 325:1682–1686
10. Santamaria A, Wang B, Elowe S, Malik R, Zhang F, Bauer M, Schmidt A, Silljé HH, Körner R, Nigg EA (2011) The Plk1-dependent

phosphoproteome of the early mitotic spindle. Mol Cell Proteomics 10:M110.004457

11. Olsen JV, Vermeulen M, Santamaria A, Kumar C, Miller ML, Jensen LJ, Gnad F, Cox J, Jensen TS, Nigg EA, Brunak S, Mann M (2010) Quantitative phosphoproteomics reveals widespread full phosphorylation site occupancy during mitosis. Sci Signal 3(104):ra3
12. Steen JA, Steen H, Georgi A, Parker K, Springer M, Kirchner M, Hamprecht F, Kirschner MW (2008) Different phosphorylation states of the anaphase promoting complex in response to antimitotic drugs: a quantitative proteomic analysis. Proc Natl Acad Sci U S A 105:6069–6074
13. Terasima T, Tolmach LJ (1963) Growth and nucleic acid synthesis in synchronously dividing populations of HeLa cells. Exp Cell Res 30:344–362
14. Banfalvi G (2008) Cell cycle synchronization of animal cells and nuclei by centrifugal elutriation. Nat Protoc 3:663–673
15. Zieve GW, Turnbull D, Mullins JM, McIntosh JR (1980) Production of large numbers of mitotic mammalian cells by use of the reversible microtubule inhibitor nocodazole. Nocodazole accumulated mitotic cells. Exp Cell Res 126:397–405
16. Ikegami S, Taguchi T, Ohashi M, Oguro M, Nagano H, Mano Y (1978) Aphidicolin prevents mitotic cell division by interfering with the activity of DNA polymerase-alpha. Nature 275:458–460
17. Reichard P, Ehrenberg A (1983) Ribonucleotide reductase—a radical enzyme. Science 221:514–519
18. Vassilev LT, Tovar C, Chen S, Knezevic D, Zhao X, Sun H, Heimbrook DC, Chen L (2006) Selective small-molecule inhibitor reveals critical mitotic functions of human CDK1. Proc Natl Acad Sci U S A 103:10660–10665
19. Ye K, Ke Y, Keshava N, Shanks J, Kapp JA, Tekmal RR, Petros J, Joshi HC (1998) Opium alkaloid noscapine is an antitumor agent that arrests metaphase and induces apoptosis in dividing cells. Proc Natl Acad Sci U S A 95:1601–1606

Part III

Chemical Blockade

Chapter 5

Synchronization and Desynchronization of Cells by Interventions on the Spindle Assembly Checkpoint

Mohamed Jemaà*, Gwenola Manic*, and Ilio Vitale

Abstract

Cell cycle checkpoints are surveillance mechanisms that sequentially and continuously monitor cell cycle progression thereby contributing to the preservation of genetic stability. Among them, the spindle assembly checkpoint (SAC) prevents the occurrence of abnormal divisions by halting the metaphase to anaphase transition following the detection of erroneous microtubules-kinetochore attachment(s). Most synchronization strategies are based on the activation of cell cycle checkpoints to enrich the population of cells in a specific phase of the cell cycle. Here, we develop a two-step protocol of sequential cell synchronization and desynchronization employing antimitotic SAC-inducing agents (i.e., nocodazole or paclitaxel) in combination with the depletion of the SAC kinase MPS1. We describe cytofluorometric and time-lapse videomicroscopy methods to detect cell cycle progression, including the assessment of cell cycle distribution, quantification of mitotic cell fraction, and analysis of single cell fate profile of living cells. We applied these methods to validate the synchronization-desynchronization protocol and to qualitatively and quantitatively determine the impact of SAC inactivation on the activity of antimitotic agents.

Key words Anaphase, APC/C, Cell cycle, Chromosome, Microtubules, Mitosis, Tetraploidy, Polyploidy

1 Introduction

The cell cycle is a refined and tightly regulated process through which the genetic information is faithfully transmitted across consecutive generations. This (evolutionary conserved) mechanism encompasses two main events: DNA replication and cell division [1, 2]. The sequential and coordinated execution of these two cellular processes enables the duplication of the genetic material and its correct segregation into two daughter cells [3–5]. In eukaryotes, DNA is synthesized and replicated in semi-conservative fashion during the S phase of the cell cycle by a multiprotein complex comprising the DNA polymerase [1, 6–8]. As for cell division, this

Both authors equally contributed to this chapter.

Gaspar Banfalvi (ed.), *Cell Cycle Synchronization: Methods and Protocols*, Methods in Molecular Biology, vol. 1524,
DOI 10.1007/978-1-4939-6603-5_5,

process involves mitosis, during which the duplicated DNA condenses into sister chromatids (prophase) that are captured at their kinetochore by microtubules of the assembled mitotic spindle (pro-metaphase) and then aligned into the metaphase plate (metaphase), and cytokinesis, during which sister chromatids are split toward the opposite poles (anaphase) and the two daughter cells are physically separated by the action of the actin-based contractile ring (telophase) [2, 9–11]. Along with partitioning the genetic material, cell division also provides the progeny with the indispensable set of cytoplasmic organelles, including centrioles and mitochondria. In the canonical cell cycle, two additional steps, the gap 1 and the gap 2 phase (best known as G_1 and G_2 phase), are inserted between S and M phases. G_1 and G_2 phases are crucial as they increase cell size and set the stage for the correct duplication and segregation of the genome [5, 10, 12]. The transition between the different phases is monitored by multiple cell cycle checkpoints, including the G_1, intra-S, G_2, and spindle assembly checkpoint [5, 10, 13, 14]. These surveillance mechanisms arrest cell cycle progression in the presence of potential threat(s) by modulating the activity of members of cyclin-dependent kinase (CDK) family. CDKs together with other specific kinases, such as Aurora kinases (AURKs), MPS1, and Polo-like kinases (PLKs), orchestrate the timely and sequential activation/deactivation of the machineries responsible for DNA replication and mitosis [15–17]. The G_1 checkpoint and the intra-S checkpoint are triggered by a variety of genetic lesions of exogenous or endogenous origin resulting in the arrest in G_1 or during S phase depending on the phase in which the damage is generated [1, 3, 10]. The frequency of abortive cell divisions is limited by mechanisms halting either the mitotic entry of cells presenting damaged and/or partially unreplicated DNA [18–20] or the anaphase entry of metaphases displaying misaligned chromosomes [2, 13, 17]. This is accomplished via the activation, respectively, of the G_2 checkpoint, which inhibits the activity of the mitotic initiating complex CDK1-Cyclin B1 [16, 18], or the spindle assembly checkpoint (SAC), which blocks the anaphase-promoting complex or cyclosome (APC/C)-mediated degradation of Cyclin B1 and Securin thereby maintaining sister-chromatid cohesion [13, 17]. In addition, the proliferation and survival of unscheduled tetraploid cells are restricted by a hitherto poorly characterized post-mitotic checkpoint known as tetraploidy checkpoint [21–24]. In support of their physiological relevance, checkpoint deregulation(s) is frequently found in tumors, and is believed to initiate oncogenesis, foster tumor progression/spreading and/or contribute to cancer resistance to therapy [24, 25].

Besides presenting heterogeneous proliferation rate, cells within a multicellular organism may be reversibly or irreversibly arrested in their growth by genetically programmed alteration of the canonical G_1-S-G_2-M cell cycle. Thus, in a physiological context

the fate of daughter cells generated by a round of cell division includes (but is not limited to): (1) entering a second round of cell division, which, as in the case of embryonic stem cells, may present shortened G_1 and G_2 phases [26–28]; (2) differentiating in non-proliferating, specialized and in some cases polyploid cells (e.g., cardiomyocytes [29] and megakaryocytes [25, 30]); (3) arresting the proliferation in a specific phase of the cell cycle (e.g., the meiotic prophase for human primary oocytes [31]); (4) reversibly exiting cell cycle and entering into quiescence (e.g., some mammalian adult stem cells [32, 33]); and (5) activating pathway(s) of regulated cell death as during the genesis or homeostatic regulation of some tissues or organs [34, 35]. In physiological or experimental conditions, proliferating cells are often asynchronous, i.e., their proliferation is not synchronized and coordinated in time. Cell synchronization has proven to be a fundamental tool in the research field dealing with cell cycle-related events, such as the activation of macrocomplexes involved in cellular processes as diverse as DNA transcription, DNA translation, DNA repair, autophagy and ubiquitination, or with the intracellular localization of proteins. Through cell synchronization it was also possible to elucidate the mechanisms of cell cycle progression and checkpoint regulation, and uncover unconventional activities of proteins whose functions were believed to be restricted in a specific cell cycle phase.

Several synchronization methods have been developed so far to enrich the population of viable cells in a specific cell cycle phase [36–38]. These include the depletion of selective nutrient (e.g., serum starvation or amino acid deprivation), mechanical shake-off to isolate mitotic cells, and the use of chemical agents often acting as cell cycle checkpoint inducers by perturbing DNA replication (e.g., the nucleoside thymidine [39], whose administration arrests cells in G_1 phase), mitotic entry (e.g., the CDK inhibitor roscovitine [40], which induces the accumulation of cells in G_2 phase), or mitotic progression (e.g., the anti-microtubular agents such as taxanes [41], which cause metaphase block). By these strategies, it is possible to isolate and analyze synchronous population of cells immediately or after recovering their proliferation growth in basal culture condition (i.e., desynchronization).

In this chapter, we describe a pharmacological protocol of sequential cell synchronization and desynchronization based on the treatment with the antimitotic agent paclitaxel or nocodazole, which synchronizes cells in metaphase by triggering the SAC, and the depletion of the SAC kinase MPS1 [42–45], which desynchronizes previously mitotic-arrested cells by inducing SAC bypass [46]. We first validated this method by evaluating cell cycle progression through cytofluorometry and videomicroscopy, and then applied this strategy to compare the effects of the inhibition of the SAC on the cytostaticity and cytotoxicity of spindle poisons. This procedure can be routinely employed in experiments

involving cell synchronization and desynchronization as well as for determining the impact of SAC inactivation on the activity of conventional or novel antimitotic agents.

2 Materials

2.1 Disposables

1. 75 or 175 cm^2 flasks for cell culture.
2. 6-well and 12-well plates for cell culture.
3. 15 and 50 ml conical centrifuge tubes.
4. 5 ml FACS tubes.
5. 0.5, 1.5, and 2 µl microcentrifuge tubes.
6. Cell counting chamber slides (e.g., Kova® Glasstic® Slide, Kova International, Inc., Garden Grove, CA) (*see* **Note 1**).

2.2 Equipment

1. FACSCalibur cytofluorometer (BD Biosciences, Franklin Lakes, NJ), equipped with a 488 nm-blue laser and a 70 µm nozzle, and controlled by the BD CellQuest™ Pro software (BD Biosciences, Franklin Lakes, NJ) (*see* **Note 2**).
2. Bright-field inverted microscope: Leica DM IL LED (Leica Microsystems GmbH, Wetzlar, Germany), equipped with 10×, 20×, and 60× long working distance objectives (*see* **Note 2**).
3. Automated live cell inverted microscope: Leica DM IRE2 (Leica) equipped with a 20×/0.4 LMC condenser/objective, different fluorochrome-specific filters (for DAPI/Hoechst, GFP/FITC, TRITC/Cy3, and Cy5), a Micromax YHS 1300 camera (Roper Scientific-Princeton Instruments, Acton, MA) and a temperature and CO_2 controlled incubator (*see* **Note 2**).

2.3 Software

1. CellQuest™ Pro (BD Biosciences) (*see* **Note 3**).
2. MetaMorph® Microscopy Automation & Image Analysis (Molecular Devices, Sunnyvale, CA).
3. Image J (freely available from the National Institute of Health, Bethesda, MD at the address http://rsb.info.nih.gov/ij/).

2.4 Reagents

1. Phosphate buffered saline (PBS); storage, room temperature (RT).
2. Trypan Blue solution: 0.4% w/v in PBS (Thermo Scientific Inc.); storage, RT (*see* **Note 4**).
3. Dimethyl sulfoxide (DMSO); storage, RT (*see* **Note 5**).
4. Complete growth medium for the human colon carcinoma cell line HCT 116: McCoy's 5A medium containing 4.5 g/l glucose and 4 mM L-glutamine, and supplemented with 10% (v/v) fetal bovine serum (FBS), 100 mM 4-(2-Hydroxyethyl)

piperazine-1-ethanesulfonic acid (HEPES) buffer, 100 U/ml penicillin G sodium, 100 μg/ml streptomycin sulfate and, 1 mM sodium pyruvate, storage, 4 °C. Complete growth medium for HCT 116 cell line transfected with a cDNA coding for a histone 2B-green fluorescent protein (hereafter referred as H2B-GFP HCT 116) also includes 20 μg/ml blasticidine (*see* **Notes 6** and **7**).

5. Trypsin/EDTA solution: 0.25% trypsin, 0.38 g/l (1 mM) EDTA×4 Na^+ in Hanks' buffered salt solution (HBSS); storage, −20 °C (*see* **Note 8**).
6. Sheath fluid: FACSFlow™ (BD Biosciences) and IsoFlow™ Sheath Fluid (Beckman Coulter, Brea, CA); storage, RT (*see* **Note 9**).
7. Nocodazole (Sigma-Aldrich, St. Louis, MO), MW: 301.3 g/mol; stock solution: 16 mM in DMSO; storage, −20 °C (*see* **Notes 10–12**).
8. Paclitaxel (Sigma-Aldrich), MW: 853,9 g/mol; stock solution: 52 mM in DMSO; storage, −20 °C (*see* **Notes 10–12**).
9. Control small interfering (si)RNA, i.e., a siRNA for unrelated sequence to the human genome (siUNR) (Eurogentec, Liège, Belgium): sense 5′-GCCGGUAUGCCGGUUAAGUdTdT-3′.
10. Specific siRNAs directed against MPS1 mRNAs (siMPS1) (Eurogentec): sense 5′-UGGUUGAGUUUGUUGCUCAUUdTdT-3′.
11. Lipofectamine® RNAiMAX Transfection Reagent (Invitrogen-Thermo Fisher Scientific Inc., Waltham, MA) (*see* **Note 13**).
12. Opti-MEM® medium (Gibco-Thermo Fisher Scientific).

2.5 Assessment of Cell Cycle Profiling and Histone H3 Phosphorylation

1. Fixative solution: ice-cold 75% ethanol in dH_2O; storage, −20 °C (*see* **Note 14**).
2. Permeabilization solution: 0.25% (v/v) Tween 20 in PBS; storage, RT.
3. Blocking solution: 1% (w/v) bovine serum albumin (BSA) in PBS; storage, 4 °C.
4. Propidium iodide (PI) solution: 1 mg/ml in dH_2O (Molecular Probes-Thermo Fisher Scientific); storage, 4 °C protected from light (*see* **Notes 15** and **16**).
5. RNase A solution: 20 mg/ml in 50 mM Tris–HCl (pH 8.0) and 10 mM EDTA (Invitrogen-Thermo Fisher Scientific); storage, 4 °C (*see* **Note 17**).
6. Anti-phosphorylated histone H3 (Ser28), rabbit polyclonal antibody (# 07-145, Calbiochem-Merck Millipore, Billerica, MA); storage, 4 °C (*see* **Note 18**).

7. Alexa Fluor®488 Goat Anti-rabbit IgG (H + L) (#A-11034, Molecular Probes-Thermo Fisher Scientific); storage, 4 °C under protection from light (*see* **Note 19**).

3 Methods

3.1 Cell Culture

1. Thaw frozen HCT 116 and H2B–GFP HCT 116 cells and put them in culture in complete pre-warmed growth medium within 75 cm^2 flasks (37 °C, 5 % CO_2) (*see* **Notes 20–22**).
2. Allow cells adhere, readapt and recover, and, when confluence approaches around 80 %, remove and discard culture medium.
3. Rinse the flask once with pre-warmed PBS and detach adherent cells by adding 3 ml of Trypsin/EDTA into the cell layer (*see* **Notes 8** and **23–25**).
4. Upon detachment, add complete growth medium, collect cells in a conical centrifuge tube and centrifuge sample for 5 min at 300 × *g* (RT).
5. Discard supernatants, resuspend cell pellets in complete growth medium and transfer aliquots of the cell suspension to new 75 or 175 cm^2 flasks.
6. Incubate flasks in standard culture condition (37 °C, 5 % CO_2).
7. Repeat the **steps 2–5** for the maintenance of fresh cultures (*see* **Notes 26–28**).

3.2 siRNA Transfection and Chemical Treatment

1. Detach and collect HCT 116 or H2B–GFP HCT 116 cells as reported in Subheading 3.1 (*see* also **Notes 22–25**).
2. Count cells with a counter chamber slide and seed them in 6-well or 12-well plates at density of 1×10^5 in 2 ml growth medium per well or 5×10^4 cells in 1 ml growth medium per well, respectively (*see* **Notes 1, 29** and **30**).
3. Upon 24 h, transfect adherent cells in the 12-well plates with siMPS1 or siUNR as described below (*see* **Note 31**).
4. Remove the medium and gently add 750 µl of serum-free growth medium into the cell layer (*see* **Notes 32** and **33**).
5. Prepare two solutions containing 6 pmol siMPS1 or siUNR diluted in 25 µl Opti-MEM® for each well to be transfected (siRNA solution A and B).
6. Prepare one solution containing 1 µl of Lipofectamine® RNAiMAX diluted in 24 µl Opti-MEM® for each well to be transfected (liposome solution) (*see* **Note 13**).
7. Mix siRNA solution A or B with an equal amount of the liposome solution (MIX solution A and B) and incubate for 15 min at RT (*see* **Note 34**).

8. Add 50 μl of the MIX solution A or MIX solution B to each well (final volume = 800 μl) and let them incubate for 6 h (*see* **Note 35**).
9. Remove the medium and gently add into the cell layer 1 ml of complete growth medium containing 200 nM nocodazole, 100 nM paclitaxel or equivalent volumes of the solvent used for drug reconstitution as negative control (*see* **Notes 11, 12, 32** and **36**).

3.3 Assessment of Cell Cycle Profiling and Histone H3 Phosphorylation

1. Seed, transfect, and treat HCT 116 cells as reported in Subheadings 3.1 and 3.2 (*see* also **Notes 8, 11, 12, 22–25, 30–32, 34** and **36**).
2. After 16 h from the treatment, collect culture supernatants in 5 ml FACS tubes and detach adherent cells adding ~0.5 ml trypsin/EDTA per well to the cell layers (*see* **Notes 8, 23–25** and **37**).
3. Collect detached cells into the corresponding FACS tubes and centrifuge samples for 5 min at 300 × *g* (RT) (*see* **Note 38**).
4. Remove and discard supernatants, then fix cells by adding drop by drop 1 ml of ice-cold 75 % ethanol (*see* **Notes 14** and **39**).
5. Incubate samples at −20 °C for at least 24 h after which centrifuge tubes at 300 × *g* for 5 min (4 °C) (*see* **Note 40**).
6. Remove ethanol, rinse samples twice with cold PBS and then incubate cells at 4 °C for 15 min with 1 ml 0.25 % (v/v) Tween 20 in PBS (*see* **Note 41**).
7. Rinse twice with 1 % (w/v) BSA in PBS and then add 1 ml of 3 % (w/v) BSA in PBS to each tube (*see* **Note 42**).
8. Incubate samples for 30 min at 4 °C, then centrifuge as reported in **step 5**.
9. Remove supernatants and resuspend cells with 200 μl of a solution containing the primary anti-phospho-H3 antibody diluted 1:100 in 1 % (w/v) BSA in PBS or with 200 μl of 1 % (w/v) BSA in PBS as negative staining control (*see* **Notes 18, 43** and **44**).
10. Incubate samples for 1 h at RT, then centrifuge them as reported in **step 5** (*see* **Note 45**).
11. Remove supernatants, wash samples thrice with 1 % (w/v) BSA in PBS and then add 200 μl of a solution containing secondary Alexa Fluor®488 Goat anti-rabbit antibody diluted 1:300 in 1 % (w/v) BSA in PBS (*see* **Note 19**).
12. Upon incubation for 30 min at 4 °C protected from light, centrifuge samples as reported in **step 5** (*see* **Note 46**).
13. Discard supranatants and add 300 ml of a solution containing 50 μg/ml PI, 0.1 μg/ml (w/v) RNase, and 0.1 % (w/v) D-glucose in PBS (*see* **Notes 15–17** and **47**).

14. Incubate for 30 min at 37 °C and then store at least for 3 h at 4 °C, always under protection from light (*see* **Note 48**).
15. Analyze samples by means of a cytofluorometer equipped for the acquisition of light scattering data and fluorescence in green and red channels (*see* **Notes 49–51**).

3.4 Live-Cell Videomicroscopy

1. Seed and transfect H2B–GFP HCT 116 cells as reported in Subheadings 3.1 and 3.2 (*see* also **Notes 8, 22–25** and **30–35**).
2. Switch on the microscope, pre-warm the on-stage incubator at the Leica DMIRE2 inverted microscope for live cell imaging to 37 °C and regulate CO_2 and oxygen concentration (*see* **Notes 52** and **53**).
3. After 6 h from the transfection, treat cells as reported in Subheading 3.2 (*see* also **Notes 11, 12, 32** and **36**).
4. Immediately after the treatment, place the plate on the microscope stage and supply cells of CO_2 by putting the plastic cover with an outlet for 5% CO_2 on top of the plate.
5. Focus in bright field with 20× objective until cells are visible, then manually shift the on-stage to the region of choice (*see* **Note 54**).
6. Set up the light and laser power/exposure, image acquisition parameters and duration of the experiment using the microscope software MetaMorph® Microscopy Automation & Image Analysis (*see* **Note 55**).
7. Perform the time-lapse experiment by separately acquiring pulsed transmitted light and fluorescence images every 15 min for a period up to 30 h (*see* **Notes 56** and **57**).
8. Analyze the images tracking individual cells and their progeny, and finally assemble the correspondent movie with the open source software Image J (*see* **Note 58**).

3.5 Interpretation of Results

In this Subheading, we report the analysis and interpretation of the data for the validation of the two-step synchronization–desynchronization protocol described here and we briefly report a potential application of our results in the field of anticancer therapy.

1. *Synchronization*. The administration of the antimitotic agents in condition of SAC proficiency (i.e., upon transfection with siUNR) induces an accumulation of cells presenting a $4n$ DNA content, i.e., G_2/M phase cells (Fig. 1a lower panel, Fig. 1b lower panel and Fig. 1c right panel; analysis by flow cytometry). In particular, nocodazole and paclitaxel provoke an arrest in metaphase as demonstrated by the increase in cells presenting the phosphorylation of the histone H3 (Fig. 1a top panel, Fig.1b top panel and Fig. 1c left panel; analysis by flow cytom-

etry) and in the fraction of blocked mitosis (Figs. 2 and 3; analysis and quantification by videomicroscopy).

2. *Desynchronization*. The depletion of the SAC kinase MPS1 abrogates the SAC thereby avoiding the metaphase arrest as induced by antimitotic agents (Figs. 1, 2, and 3). Thus, the fraction of cells presenting a 4*n* DNA content (Fig. 1b lower panel and Fig. 1c right panel) or arrested in metaphase (Fig. 1b

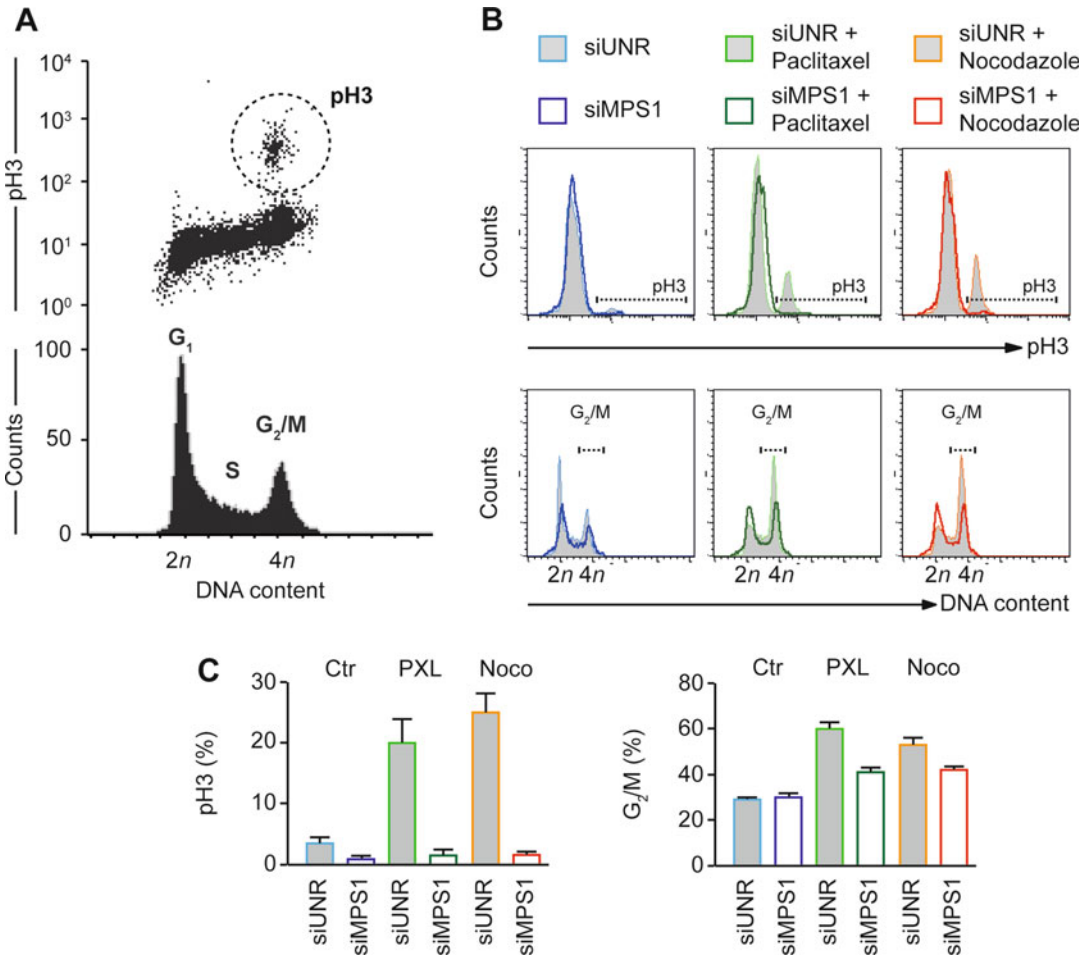

Fig. 1 Cell cycle distribution analysis after cell synchronization and desynchronization. (**a–c**) Human colon carcinoma HCT 116 cells were transfected with an unrelated small interfering (si) RNA (siUNR) or a specific siRNA directed against MPS1 (siMPS1) for 6 h and then were left untreated (Control) or treated with 200 nM nocodazole (Noco) or 100 nM paclitaxel (PXL). After 16 h cells were fixed, immunostained for the cytofluorometric detection of phosphorylated histone H3 (pH3) and finally labeled with the DNA dye propidium iodide (PI). Panel (**a**) illustrates a representative cell cycle profile reporting the canonical division in G_1, S, and G_2/M phase based on PI staining (*low part of the panel*) and the fraction of mitotic cells, i.e., those presenting the phosphorylation of histone H3 (*upper part of the panel*). Histograms in panel (**b**) depicts cell cycle profiling (*lower part of the panel*) and the phosphorylation of histone H3 (*upper part of the panel*) for each experimental condition. Quantitative data of pH3 and G_2/M phase positive cells after different treatments are reported in panel (**c**)

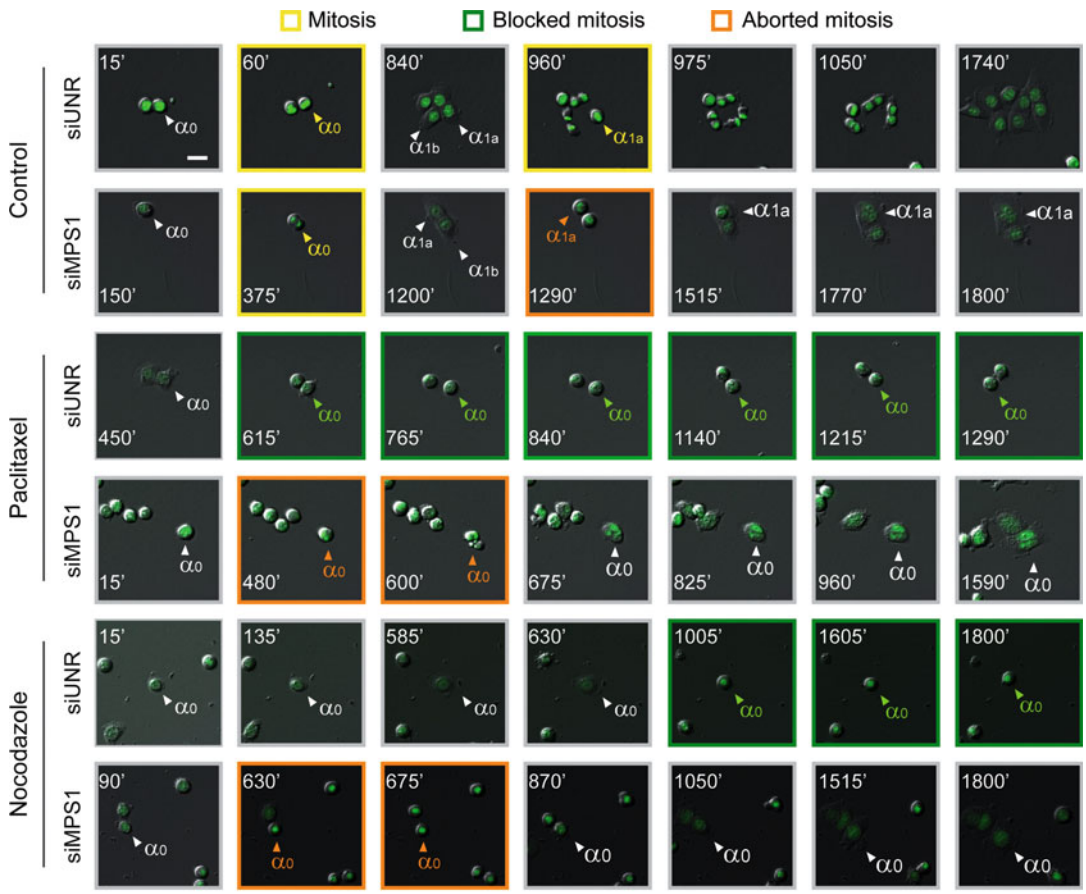

Fig. 2 Time-lapse videomicroscopy of the cell cycle progression after cell synchronization and desynchronization. Human colon carcinoma HCT 116 cells engineered to express a histone H2B-green fluorescent protein (GFP) fusion protein (H2B-GFP HCT 116) and transfected for 6 h with an unrelated small interfering (si) RNA (siUNR) or a specific siRNA directed against MPS1 (siMPS1) were left untreated (Control) or administered with 200 nM nocodazole or 100 nM paclitaxel. Cells were immediately monitored by live videomicroscopy for 1800 min. Representative snapshots are shown (scale bar = 10 μm). *Alphas* $(\alpha)_0$ indicate individual tracked cells. A successful cell division is illustrated by the sequential number increase in the subscripted numbers ($\alpha 1$ and $\alpha 2$). The two daughter cells generated by a bipolar division are depicted with "*a*" and "*b*", while the single cell derived by an abortive division by size type increase. The snapshot and letter color code depict three different mitotic events: a successful mitosis (framed in *yellow*) generating two daughter cells, blocked mitosis (framed in *green*) or abortive mitosis (framed in *orange*). Interphases are represented with *gray traits.*

Fig. 3 (continued) 1800 min. Panel (**a**) reports the single-cell fate profiles for 30 cells in each transfection/treatment condition. The following color code has been used: *yellow traits* depict successful mitoses, *orange traits* the first abortive cell division, *red traits* the second abortive cell division, *green traits* blocked mitoses, *black traits* apoptosis induction. An increase in cell ploidy due to abortive mitoses is represented with darkening *gray traits*. Representative snapshots illustrating these events are reported in Fig. 2. The histogram in panel (**b**) illustrates quantitative data on the frequency of blocked mitosis (*green columns*), aborted mitosis (*orange columns*), and cell death in mitosis or interphase (*light gray* and *dark gray columns*, respectively) in all the transfection/treatment conditions

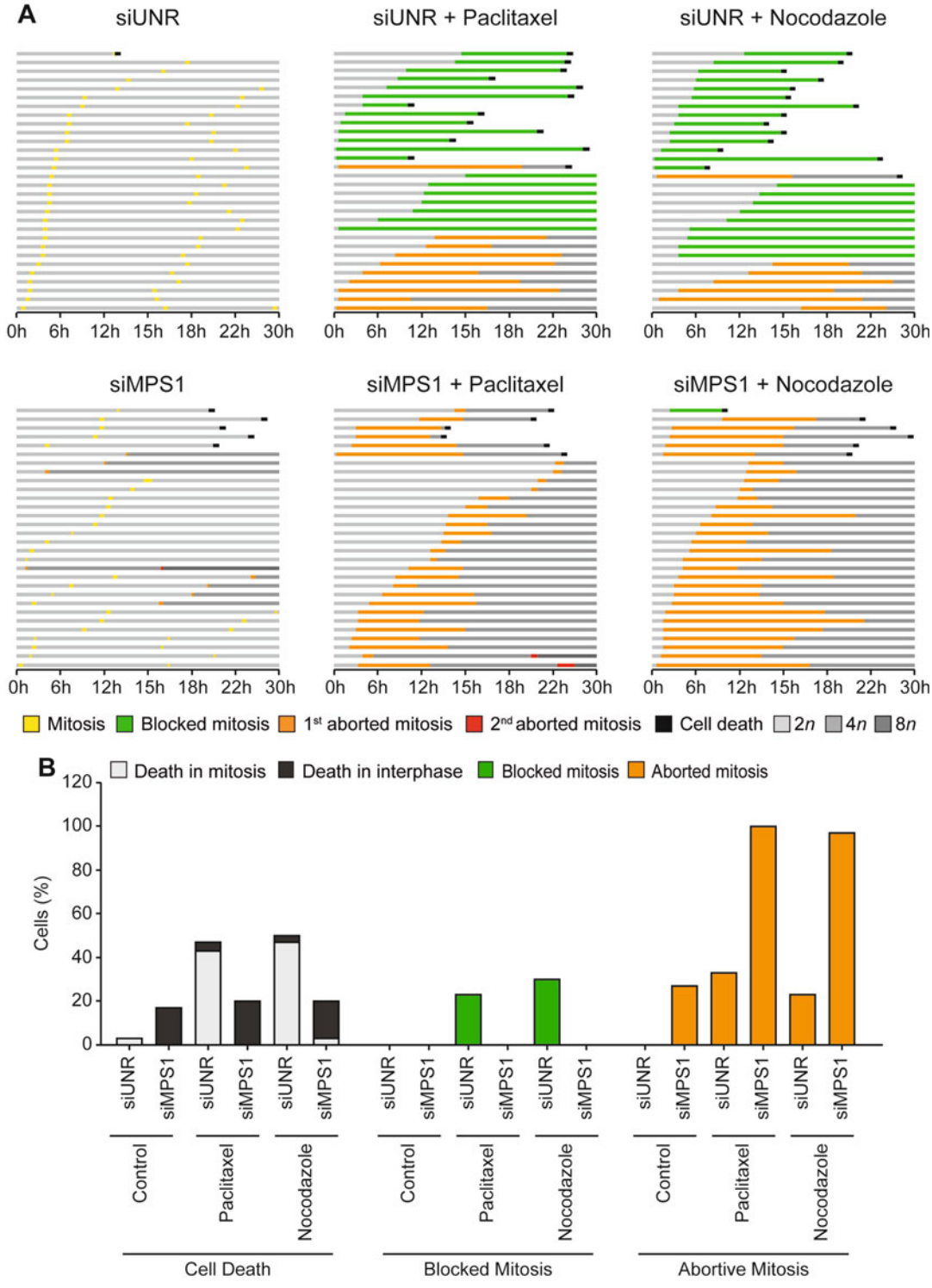

Fig. 3 Videomicroscopic analysis of the cell cycle progression after cell synchronization and desynchronization. (**a**) and (**b**) Human colon carcinoma HCT 116 cells engineered to express a histone H2B-green fluorescent protein (GFP) fusion protein (H2B-GFP HCT 116) and transfected for 6 h with an unrelated small interfering (si) RNA (siUNR) or a specific siRNA directed against MPS1 (siMPS1) were left untreated (Control) or administered with 200 nM nocodazole or 100 nM paclitaxel. Cells were immediately monitored by live videomicroscopy for

top panel, 1c left panel, Figs. 2 and 3) gets back close to that of control conditions (i.e., in absence of treatment and in condition of SAC proficiency). Concerning the mechanism of desynchronization, it involves the progression of cells in mitosis, the generation of abortive cell divisions and the resulting cell polyploidization (Figs. 2 and 3).

3. *Impact for anticancer therapy.* By videomicroscopic analysis, we put in evidence that the depletion of MPS1 decreases the killing effect of both microtubular poisons, which are well-known anticancer agents (Fig. 3b). We ascribe this effect to SAC bypass and the generation of polyploid cells in the absence of the SAC (Figs. 2 and 3). Further experiments are required to demonstrate whether the activity of the SAC is mandatory for an efficient cell killing by spindle poisons or other antimitotic agents.

4 Notes

1. When available, cell counting chamber slides may be replaced by an automated cell counter such as Countess® Automated Cell Counter (Thermo Fisher Scientific Inc.).
2. It is strongly recommended to follow the manufacturer's recommendations for the proper use of the equipment. In addition, cleaning protocols as well as fluid, optical and mechanical maintenance procedures should be performed regularly to preserve the correct functioning of the equipment over the time.
3. Alternative purchasable analysis softwares are the Kaluza Analysis Software (Beckman Coulter Inc., Brea, CA) or FlowJo Single Cell Analysis Software (FlowJo, Ashland, OR).
4. Trypan Blue is listed as a possibly carcinogenic to humans by The International Agency for Research on Cancer (IARC, http://monographs.iarc.fr/) and may cause eyes, skin and respiratory tract irritation (https://pubchem.ncbi.nlm.nih.gov/).
5. DMSO is combustible and may be harmful if absorbed by the skin or inhaled (https://pubchem.ncbi.nlm.nih.gov/). Handle DMSO always using protective equipment (gloves, clothing and eyewear) and avoid exposure to heat or flame.
6. We strongly recommend to prepare the medium following the recommendations of the American Type Culture Collection (ATCC, Manassas, VA).
7. Concerning complete cell growth medium composition: HEPES is included as a buffering agent, penicillin G and streptomycin as antibiotics, sodium pyruvate as a carbon source and

blasticidine for the maintenance of cells expressing H2B-GFP, which contain the blasticidin-resistance gene.

8. Trypsin-EDTA solution may be irritating to the eyes, respiratory system and skin as it contains EDTA (https://pubchem.ncbi.nlm.nih.gov/).
9. These fluids are not reported to cause potential hazardous health effects.
10. Before reconstituting, handling and storing any compounds, we recommend to carefully see the information reported on the labels and the Material Safety Data Sheets (MSDS) provided with the shipment. We also suggest to check the information reported at https://pubchem.ncbi.nlm.nih.gov/ for each agent. As a general rule to wear protective equipment (gloves, clothing and goggles), to work in a fume hood under protection from light and to dispense the solution into well-sealed aliquots is strongly recommended.
11. Antimitotic agents act by interfering with the machinery for cell division. In particular, spindle poisons belong to the category of antimitotic agents that act by perturbing the dynamic of the microtubules of the mitotic spindle. These include nocodazole, which is a microtubule-depolymerizing agent, and paclitaxel, which is a microtubule-hyperpolymerizing agent.
12. Nocodazole and paclitaxel are not currently listed as a carcinogen by IARC (http://monographs.iarc.fr/). The structure, chemical and physical properties, safety, hazards and toxicity of these compounds can be found at the following link https://pubchem.ncbi.nlm.nih.gov/. For more information on the solubility, storage temperature and stability of powders and solutions also refer to the MSDS or product information sheet downloadable for free at http://www.sigmaaldrich.com/.
13. This product is classified as not hazardous, yet should be handled wearing suitable protective equipment (gloves, clothing and eyewear). Under normal conditions, Lipofectamine® RNAiMAX Transfection Reagent is stable for more than 1 year.
14. Ethanol is classified as highly flammable liquid and vapor and should always be kept away from heat and flames. For more details on the structure, chemical/physical properties, safety, hazards and toxicity refer to https://pubchem.ncbi.nlm.nih.gov/.
15. PI (3-(3,8-diamino-6-phenylphenanthridin-5-ium-5-yl) propyl-diethyl-methylaza-nium; diiodide) is not currently listed as a carcinogen by IARC (http://monographs.iarc.fr/). More information on the structure, chemical/physical proper-

ties, safety, hazards, toxicity, storage conditions and stability of this compound can be found at https://pubchem.ncbi.nlm.nih.gov/. The MSDS is downloadable for free at http://www.sigmaaldrich.com/.

16. PI is a DNA dye that intercalates between double-stranded nucleic acids. PI has an absorbance peak of ~535 nm and an emission peak of ~617 nm.
17. RNase A is a bovine pancreatic ribonuclease that cleaves single-stranded RNA. It is classified as not hazardous to health.
18. This antibody is provided as a 1 mg/ml solution in buffer containing 0.1 M Tris-Glycine (pH 7.4), 150 mM NaCl and 0.05 % sodium azide (N_3Na). Sodium azide is fatal if swallowed and may cause eye and respiratory irritation (https://pubchem.ncbi.nlm.nih.gov/). Therefore, antibody should always be handled with the maximal care wearing appropriate protective equipment.
19. This antibody is provided as a 2 mg/ml PBS solution containing 5 mM sodium azide (pH 7.5) and is particularly prone to photobleaching. Handle this antibody with the maximal care, wearing appropriate protective equipment and protected from light (*see* also **Note 18**).
20. For an optimal growth recovery and to limit thawing-related stress cells should be plated rapidly and at high density.
21. Given the presence of DMSO as cryoprotectant, the cryovials should be handled with caution and wearing personal protective equipment (*see* also **Note 5**).
22. We recommend employing only early-passage cells in your studies, as prolonged cell splitting and passaging may promote genetic drift thereby selecting clonal populations.
23. To limit cell loss due to mechanical detachment, the wash in PBS should be performed gently.
24. The presence of serum or salt residual may limit the efficiency of cell detachment by inhibiting trypsin activity.
25. The time of trypsinization should be optimized for each cell lines. However, we recommend not to exceed 5 min and to place cells 37 °C avoiding to violently hit or shake the flask.
26. For the HCT 116 cell line, a subcultivation ratio of 1:3 to 1:8 every 2–3 days is appropriate.
27. For the optimal growth of the culture, we recommend to avoid seeding cells at low- or over-confluency (*see* also **Note 22**).
28. Upon recovery from thawing, freeze aliquots of cells in exponential growth phase using complete growth medium supplemented with 5 % (v/v) DMSO (*see* also **Notes 5** and **21**).

29. The number of seeded cells may vary depending on the cell lines. As a general rule, low-confluency (around 40%) is reported to favor cell transfection.
30. The experiment should be designed for having duplicata or triplicata for each experimental condition. The depletion by siRNA transfection should always be validated through parallel analyses (e.g., by Western blot).
31. The adhesion, confluence state and general appearance of cells should always be checked under a light microscopy before starting the transfection protocol.
32. Remove and add the medium very gently to prevent significant cell detachment that may dramatically influence the transfection efficiency and increase transfection toxicity.
33. For cells seeded in 6-well plates: add 1500 µl of serum-free growth medium into each transfected well (*see* also **Note 32**).
34. This incubation is performed to promote the generation of siRNA–liposome complexes. A gentle mix after combining the solutions is also suggested.
35. For cells seeded in 6-well plates: add 100 µl of the mix solutions to reach a final volume of 1600 µl.
36. Given the potential cytotoxicity of DMSO, we recommend to design the experiment for using low volume (<1%, v/v) of the solvent (*see* also **Note 5**).
37. The supernatants containing detached and presumably dead cells may be discarded should the experimental design require the analysis exclusively of the viable population of cells.
38. The serum and salt in the supernatant inhibit trypsin activity. Freshly complete medium must be added in case the supernatant has been discarded in the previous step (*see* also **Note 37**).
39. Rapid addition of ethanol or violent vortexing of the tubes should be avoided as they may disintegrate cell membrane or damage intracellular structures.
40. The incubation at −20 °C increases the quality of the fixation and cell cycle profiles. Prolonged storage can, however, have negative consequences for the sample integrity.
41. Supernatant removal should be performed gently to avoid loss of fixed cells. When working with a limited amount of cells, the number of washes can be diminished.
42. The incubation with 3% (w/v) BSA or, alternatively, with 10% (v/v) fetal bovine serum (FBS) in PBS blocks unspecific bindings thereby reducing the intensity of the background signal.
43. Primary antibodies are particularly prone to degradation especially following prolonged and/or repeated variations from the

optimal storage temperature. Therefore, handle antibodies with the maximal care and always dispense them into aliquots.

44. Resuspending cell pellets with a volume of antibody solution <100 µl is not recommendable for staining efficiency and sample integrity.
45. Alternatively, samples may be incubated overnight at 4 °C.
46. The time of incubation for the secondary antibody should never exceed 1 h.
47. RNA-degradation by RNase A is fundamental as PI also binds RNA.
48. The incubation at 4 °C for >3 h may increase the quality of cell cycle profiles. Upon staining, samples can be stored at 4 °C (sealed and protected from light) for few days.
49. We strongly recommend to control the flow rate and calibrate the cytofluorimeter before starting the staining.
50. Acquire samples setting up the cytofluorimeter to gate on events with normal light scattering parameters (forward scatter, FSC; and side scatter, SSC).
51. To increase the quality of cell cycle profiles, we recommend to vortex samples before each acquisition and acquire at least 10,000 cells per condition at low flow rates (i.e., <200 events per second) (*see* also **Note 50**).
52. The microscope should be switched on at least 30 min before beginning experiment to stabilize the on-stage.
53. To limit experimental-driven cellular stress, time-lapse should start only after the stabilization of both temperature and gas content.
54. The use of 20× objective allows for visualizing a large number of cells in a single field and tracking multiple single cells without the risk of their exiting out of the field. Lower or higher magnification objective may replace the 20× objective depending on the experiment design, duration time and aim.
55. Excessive laser intensity and scan acquisition time may induce cell phototoxicity and/or photobleaching, and should thus be avoided.
56. It is strongly suggested to check the preservation of precise focus, laser intensity and scan acquisition parameters, the general appearance of cells, and the executed saving of the data during the course of the time-lapse.
57. Including a mineral oil layer on the top of the medium may prevent medium evaporation and the resulting cellular stress.
58. The size of the movie can be reduced using open-source, free software (e.g., Virtual Dub, http://virtualdub.sourceforge.net/).

Acknowledgements

GM was funded by Associazione Italiana per la Ricerca sul Cancro (AIRC: Triennal Fellowship "Antonietta Latronico", 2014). IV was supported by the Associazione Italiana per la Ricerca sul Cancro (AIRC: MFAG 2013 cod. 14641), Ministero Italiano della Salute (RF_GR-2011-02351355), and the Programma per i Giovani Ricercatori "Rita Levi Montalcini" 2010.

References

1. Fragkos M, Ganier O, Coulombe P, Mechali M (2015) DNA replication origin activation in space and time. Nat Rev Mol Cell Biol 16:360–374
2. Lara-Gonzalez P, Westhorpe FG, Taylor SS (2012) The spindle assembly checkpoint. Curr Biol 22:R966–R980
3. Sclafani RA, Holzen TM (2007) Cell cycle regulation of DNA replication. Annu Rev Genet 41:237–280
4. Frouin I, Montecucco A, Spadari S, Maga G (2003) DNA replication: a complex matter. EMBO Rep 4:666–670
5. Nurse P (2000) A long twentieth century of the cell cycle and beyond. Cell 100:71–78
6. Mailand N, Gibbs-Seymour I, Bekker-Jensen S (2013) Regulation of PCNA-protein interactions for genome stability. Nat Rev Mol Cell Biol 14:269–282
7. Lange SS, Takata K, Wood RD (2011) DNA polymerases and cancer. Nat Rev Cancer 11:96–110
8. Branzei D, Foiani M (2010) Maintaining genome stability at the replication fork. Nat Rev Mol Cell Biol 11:208–219
9. Dominguez-Brauer C, Thu KL, Mason JM, Blaser H, Bray MR, Mak TW (2015) Targeting mitosis in cancer: emerging strategies. Mol Cell 60:524–536
10. Rhind N, Russell P (2012) Signaling pathways that regulate cell division. Cold Spring Harb Perspect Biol 4(10):pii: a005942
11. Lian ATY, Chircop M (2016) Mitosis in animal cells A2. In: Bradshaw RA, Stahl PD (eds) Encyclopedia of cell biology. Academic, Waltham, pp 478–493
12. Lew DJ (2013) Cell cycle A2. In: Maloy S, Hughes K (eds) Brenner's encyclopedia of genetics, 2nd edn. Academic, San Diego, CA, pp 456–464
13. Musacchio A (2015) The molecular biology of spindle assembly checkpoint signaling dynamics. Curr Biol 25:R1002–R1018
14. Kastan MB, Bartek J (2004) Cell-cycle checkpoints and cancer. Nature 432:316–323
15. Asghar U, Witkiewicz AK, Turner NC, Knudsen ES (2015) The history and future of targeting cyclin-dependent kinases in cancer therapy. Nat Rev Drug Discov 14:130–146
16. Malumbres M, Barbacid M (2009) Cell cycle, CDKs and cancer: a changing paradigm. Nat Rev Cancer 9:153–166
17. Musacchio A, Salmon ED (2007) The spindle-assembly checkpoint in space and time. Nat Rev Mol Cell Biol 8:379–393
18. Lindqvist A, Rodriguez-Bravo V, Medema RH (2009) The decision to enter mitosis: feedback and redundancy in the mitotic entry network. J Cell Biol 185:193–202
19. Lobrich M, Jeggo PA (2007) The impact of a negligent G2/M checkpoint on genomic instability and cancer induction. Nat Rev Cancer 7:861–869
20. Stark GR, Taylor WR (2006) Control of the G2/M transition. Mol Biotechnol 32:227–248
21. Ganem NJ, Cornils H, Chiu SY, O'Rourke KP, Arnaud J, Yimlamai D, Thery M, Camargo FD, Pellman D (2014) Cytokinesis failure triggers hippo tumor suppressor pathway activation. Cell 158:833–848
22. Castedo M, Coquelle A, Vivet S, Vitale I, Kauffmann A, Dessen P, Pequignot MO, Casares N, Valent A, Mouhamad S, Schmitt E, Modjtahedi N, Vainchenker W, Zitvogel L, Lazar V, Garrido C, Kroemer G (2006) Apoptosis regulation in tetraploid cancer cells. EMBO J 25:2584–2595
23. Vitale I, Galluzzi L, Castedo M, Kroemer G (2011) Mitotic catastrophe: a mechanism for avoiding genomic instability. Nat Rev Mol Cell Biol 12:385–392
24. Vitale I, Galluzzi L, Senovilla L, Criollo A, Jemaa M, Castedo M, Kroemer G (2011) Illicit survival of cancer cells during polyploidization and depolyploidization. Cell Death Differ 18:1403–1413

25. Vitale I, Manic G, Senovilla L, Kroemer G, Galluzzi L (2015) Karyotypic aberrations in oncogenesis and cancer therapy. Trends Cancer 1:124–135
26. Ballabeni A, Park IH, Zhao R, Wang W, Lerou PH, Daley GQ, Kirschner MW (2011) Cell cycle adaptations of embryonic stem cells. Proc Natl Acad Sci U S A 108:19252–19257
27. Stead E, White J, Faast R, Conn S, Goldstone S, Rathjen J, Dhingra U, Rathjen P, Walker D, Dalton S (2002) Pluripotent cell division cycles are driven by ectopic Cdk2, cyclin A/E and E2F activities. Oncogene 21:8320–8333
28. White J, Stead E, Faast R, Conn S, Cartwright P, Dalton S (2005) Developmental activation of the Rb-E2F pathway and establishment of cell cycle-regulated cyclin-dependent kinase activity during embryonic stem cell differentiation. Mol Biol Cell 16:2018–2027
29. Mollova M, Bersell K, Walsh S, Savla J, Das LT, Park SY, Silberstein LE, Dos Remedios CG, Graham D, Colan S, Kuhn B (2013) Cardiomyocyte proliferation contributes to heart growth in young humans. Proc Natl Acad Sci U S A 110:1446–1451
30. Pandit SK, Westendorp B, de Bruin A (2013) Physiological significance of polyploidization in mammalian cells. Trends Cell Biol 23:556–566
31. Sanchez F, Smitz J (2012) Molecular control of oogenesis. Biochim Biophys Acta 1822:1896–1912
32. Cheung TH, Rando TA (2013) Molecular regulation of stem cell quiescence. Nat Rev Mol Cell Biol 14:329–340
33. Li L, Bhatia R (2011) Stem cell quiescence. Clin Cancer Res 17:4936–4941
34. Galluzzi L, Bravo-San Pedro JM, Vitale I, Aaronson SA, Abrams JM, Adam D, Alnemri ES, Altucci L, Andrews D, Annicchiarico-Petruzzelli M, Baehrecke EH, Bazan NG, Bertrand MJ, Bianchi K, Blagosklonny MV, Blomgren K, Borner C, Bredesen DE, Brenner C, Campanella M, Candi E, Cecconi F, Chan FK, Chandel NS, Cheng EH, Chipuk JE, Cidlowski JA, Ciechanover A, Dawson TM, Dawson VL, De Laurenzi V, De Maria R, Debatin KM, Di Daniele N, Dixit VM, Dynlacht BD, El-Deiry WS, Fimia GM, Flavell RA, Fulda S, Garrido C, Gougeon ML, Green DR, Gronemeyer H, Hajnoczky G, Hardwick JM, Hengartner MO, Ichijo H, Joseph B, Jost PJ, Kaufmann T, Kepp O, Klionsky DJ, Knight RA, Kumar S, Lemasters JJ, Levine B, Linkermann A, Lipton SA, Lockshin RA, Lopez-Otin C, Lugli E, Madeo F, Malorni W, Marine JC, Martin SJ, Martinou JC, Medema JP, Meier P, Melino S, Mizushima N, Moll U, Munoz-Pinedo C, Nunez G, Oberst A, Panaretakis T, Penninger JM, Peter ME, Piacentini M, Pinton P, Prehn JH, Puthalakath H, Rabinovich GA, Ravichandran KS, Rizzuto R, Rodrigues CM, Rubinsztein DC, Rudel T, Shi Y, Simon HU, Stockwell BR, Szabadkai G, Tait SW, Tang HL, Tavernarakis N, Tsujimoto Y, Vanden Berghe T, Vandenabeele P, Villunger A, Wagner EF, Walczak H, White E, Wood WG, Yuan J, Zakeri Z, Zhivotovsky B, Melino G, Kroemer G (2015) Essential versus accessory aspects of cell death: recommendations of the NCCD. Cell Death Differ 22:58–73
35. Galluzzi L, Vitale I, Abrams JM, Alnemri ES, Baehrecke EH, Blagosklonny MV, Dawson TM, Dawson VL, El-Deiry WS, Fulda S, Gottlieb E, Green DR, Hengartner MO, Kepp O, Knight RA, Kumar S, Lipton SA, Lu X, Madeo F, Malorni W, Mehlen P, Nunez G, Peter ME, Piacentini M, Rubinsztein DC, Shi Y, Simon HU, Vandenabeele P, White E, Yuan J, Zhivotovsky B, Melino G, Kroemer G (2012) Molecular definitions of cell death subroutines: recommendations of the Nomenclature Committee on Cell Death. Cell Death Differ 19:107–120
36. Cooper S (2003) Rethinking synchronization of mammalian cells for cell cycle analysis. Cell Mol Life Sci 60:1099–1106
37. Jackman J, O'Connor PM (2001) Methods for synchronizing cells at specific stages of the cell cycle. Curr Protoc Cell Biol. Chapter 8:Unit 8.3
38. Rosner M, Schipany K, Hengstschlager M (2013) Merging high-quality biochemical fractionation with a refined flow cytometry approach to monitor nucleocytoplasmic protein expression throughout the unperturbed mammalian cell cycle. Nat Protoc 8:602–626
39. Tobey RA, Crissman HA, Kraemer PM (1972) A method for comparing effects of different synchronizing protocols on mammalian cell cycle traverse. The traverse perturbation index. J Cell Biol 54:638–645
40. Meijer L, Borgne A, Mulner O, Chong JP, Blow JJ, Inagaki N, Inagaki M, Delcros JG, Moulinoux JP (1997) Biochemical and cellular effects of roscovitine, a potent and selective inhibitor of the cyclin-dependent kinases cdc2, cdk2 and cdk5. Eur J Biochem 243:527–536
41. Jordan MA, Toso RJ, Thrower D, Wilson L (1993) Mechanism of mitotic block and inhibition of cell proliferation by taxol at low concentrations. Proc Natl Acad Sci U S A 90:9552–9556
42. Jemaa M, Galluzzi L, Kepp O, Senovilla L, Brands M, Boemer U, Koppitz M, Lienau P, Prechtl S, Schulze V, Siemeister G, Wengner

AM, Mumberg D, Ziegelbauer K, Abrieu A, Castedo M, Vitale I, Kroemer G (2013) Characterization of novel MPS1 inhibitors with preclinical anticancer activity. Cell Death Differ 20:1532–1545

43. Jemaa M, Manic G, Lledo G, Lissa D, Reynes C, Morin N, Chibon F, Sistigu A, Castedo M, Vitale I, Kroemer G, Abrieu A (2016) Whole-genome duplication increases tumor cell sensitivity to MPS1 inhibition. Oncotarget 7:885–901
44. Abrieu A, Magnaghi-Jaulin L, Kahana JA, Peter M, Castro A, Vigneron S, Lorca T, Cleveland DW, Labbe JC (2001) Mps1 is a kinetochore-associated kinase essential for the vertebrate mitotic checkpoint. Cell 106:83–93
45. Stucke VM, Sillje HH, Arnaud L, Nigg EA (2002) Human Mps1 kinase is required for the spindle assembly checkpoint but not for centrosome duplication. EMBO J 21: 1723–1732
46. Schmidt M, Budirahardja Y, Klompmaker R, Medema RH (2005) Ablation of the spindle assembly checkpoint by a compound targeting Mps1. EMBO Rep 6:866–872

Chapter 6

Synchronization of Mammalian Cell Cultures by Serum Deprivation

Thomas J. Langan, Kyla R. Rodgers, and Richard C. Chou

Abstract

Mammalian cells are amenable to the study of regulatory mechanisms dictating cell cycle progression in vitro by shifting them into the same phase of the cycle. Procedures to arrest cultured cells in specific phases of the cell cycle may be termed in vitro synchronization. The procedure described here was developed for the study of primary astrocytes and a glioma cell line, but is broadly applicable to other mammalian cells. Its application allows astrocytes to re-enter the cell cycle from a state of quiescence (G_0) under carefully defined experimental conditions to move together into subsequent phases such as the G_1 and S phases. A number of methods have been established to synchronize mammalian cell cultures, which include counterflow centrifugal elutriation, mitotic shake off, chemically induced cell cycle arrest, and newer live cell methods, such as cell permeable dyes. Yet, there are intrinsic limitations associated with these methods. In the present protocol, we describe a simple, reliable, and reversible procedure to synchronize astrocyte and glioma cultures from newborn rat brain by serum deprivation. The procedure is similar, and generally applicable, to other mammalian cells. This protocol consists essentially of two parts: (1) proliferation of astrocytes under optimal conditions in vitro until reaching desired confluence; and (2) synchronization and G_0 phase arrest of cultures by serum down-shift. This procedure has been utilized to examine cell cycle control in astroglioma cells and astrocytes from injured adult brain. It has also been employed in precursor cloning studies in developmental biology, suggesting wide applicability.

Key words G_0, Astrocytes, Cell cycle, Glioma, Synchronization, Serum deprivation

1 Introduction

Cell cycle regulation is critical to survival of mammalian species. Development of the mature organism from embryonic primordial cells is clearly a time of regulated sequences of cell division, and yet in mammals, only a minority of cells in fully mature individuals retains the capacity to re-enter the cell cycle. These include epithelial cells of the epidermis, intestinal tract and mammary gland, hepatocytes, and glial cells of the central nervous system [1, 2].

In conceptualizing cell fate in higher organisms, it has been suggested that certain cells enter a state of terminal differentiation, which can be abbreviated as G_d. Cells that can re-enter the cell

Gaspar Banfalvi (ed.), *Cell Cycle Synchronization: Methods and Protocols*, Methods in Molecular Biology, vol. 1524,
DOI 10.1007/978-1-4939-6603-5_6,

cycle are in contrast considered to be in the G_0 phase of the cell cycle. This includes the presumptively differentiated cells mentioned above [1–3]. It is absolutely necessary for this minority of cells to remain in G_0, since inhibition of cell cycle re-entry, as might for example occur in humans after massive radiation exposure, leads to death in several days [1, 2]. In contrast, un-regulated proliferation of cells in G_0 can result in various cancers [1, 2, 4]. Thus, the cell types noted above contribute to many types of cancers in humans, including melanoma, basal and squamous cell carcinoma of skin, bowel, breast and intestine, and various grades of malignant astrocytoma in brain. More recently, it has been established that disordered cell cycle regulation is part of the pathogenesis of degenerative disorders, including Alzheimer's disease [3, 5].

Using primary astrocytes derived from newborn rat brain, this laboratory has focused on control of the G_0 to cell cycle re-entry transition. In the 1970s, Arthur Pardee demonstrated that established cell lines could be rendered into a quiescent state (G_0); he argued that that this capacity represents a unique mechanism of cell cycle control in normal animal cells [6]. However, it is clear that established cell lines differ fundamentally from normal cells, which tend to undergo either senescence or into transformation with repeated culture [1, 2].

Working a decade later with Dr. Joseph Volpe, we were able to extend the approach of Pardee to primary brain cells extracted from the brains on newborn rodents [7]. In so doing, we confirmed the value of serum depletion and subsequent up-shift to investigate mechanisms of cell cycle regulation in primary cells, which are more likely to represent their counterparts in intact organisms than cell lines [1, 2, 8, 9]. This simple technique of serum depletion to establish a G_0 state, is followed by the re-addition to serum to enable re-entry into G_1 and S phases (Fig. 1, *see* also **Notes 1–3**).

2 Materials

2.1 Mammalian Astrocyte Cultures

1. Primary astrocytic cultures harvested from neonatal (not older than 48 h) Sprague Dawley rat pups (Harlan Sprague Dawley, Indianapolis, IN).
2. Glioma cell line, C6 (ATCC CCL-107), purchased from ATCC (Walkersville, MD, USA).

2.2 Solutions

1. 10× Trypsin EDTA (Sigma, St. Louis, MO).
2. Tris EDTA (pH 7.4).
3. 10% (v/v) bovine calf serum (BCS) (Hyclone, Logan, UT) in Dulbecco's Modified Eagle's Medium (DMEM) (Sigma, St. Louis, MO).

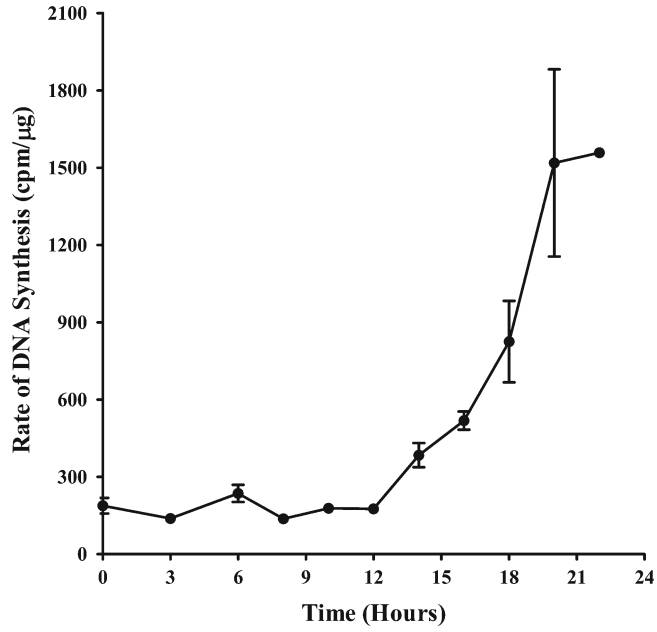

Fig. 1 Kinetics of primary astrocyte cell cycle. Primary astrocytes were plated in 6-well plates at a concentration of 10^4 cells/cm^2, and allowed to grow to confluence of 30–50% in the presence of 10% BCS/DMEM and at 37 °C and 5% CO_2/95% humidified air. After reaching the desired confluence, the cell cultures were serum down-shifted from 10% BCS/DMEM to 0.1% BCS/DMEM for 48 h. At the end of the incubation, astrocytic cultures were allowed to re-enter the cell cycle through serum upshift in 10% BCS/DMEM. At various time points after serum upshift, astrocytic cultures were pulse-labeled with ^{3}H-thymidine at a final concentration of 1 µCi/ml for 1 h prior to termination. Incorporation of ^{3}H-thymidine into DNA of astrocytic cultures was measured as expressed as mean ± S.E.M (N = 4–9.)

4. 0.1% (v/v) BCS in DMEM (pH 7.4).
5. 30% (v/v) BCS in PBS (pH 7.4).
6. Phosphate buffer saline (PBS) (pH 7.4).
7. [Methyl ^{3}H]-thymidine (Amersham, Arlington Heights, IL) at final concentration 1 µCi/ml of medium.

3 Methods

Perform the following procedure in a sterile environment:

1. Maintain neonatal rat astrocytic culture (or C6 glioma cell culture) (Figs. 1, 2 and 3, and *see* also **Notes 3–5**), or other mammalian cells in primary or secondary cultures in 9 ml of 10% BCS in DMEM in T75 flasks.

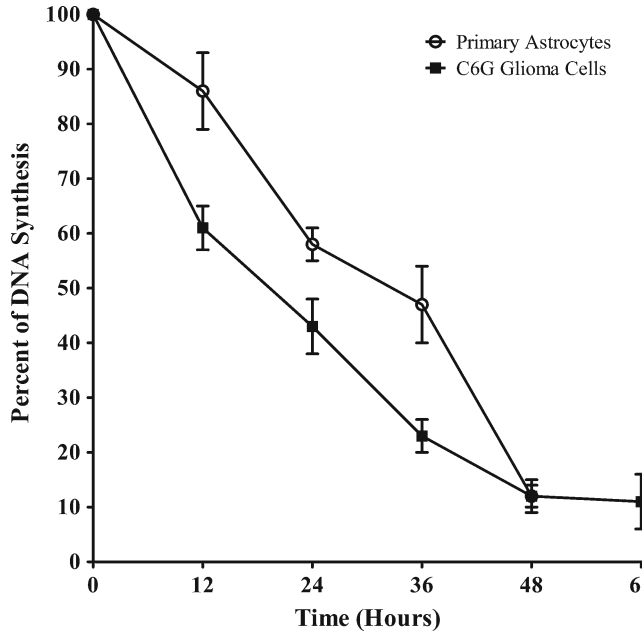

Fig. 2 Effect of serum deprivation on ^{3}H-thymidine incorporation into DNA of primary astrocytic and C6G cell cultures. Both astrocytic cultures and C6 glioma cells were plated in the 6-well plates and allowed to grow to 30–50% confluence in the presence of 10% BCS/DMEM at 37 °C and 5% CO_2/95% humidified air. At the end of the incubation, the media were removed and cultures were overlaid with 0.1% BCS/DMEM. Both cultures were incubated at 37 °C and 5% CO_2/95% humidified air for various time periods. One hour prior to termination of incubation, cell cultures were pulse-labeled with ^{3}H-thymidine at a final concentration of 1 μCi/ml. Incorporated ^{3}H-thymidine into DNA of astrocytic cultures at different time points was compared with the controls at T0. Results were expressed as means ± S. E. M (N = 4–6 for primary astrocyes and 5–6 for C6G cells.)

2. Cells are ready for experiment upon reaching confluence. At this point, aspirate media from the flasks and rinse cultures with 6 ml of Tris EDTA, followed by aspiration.
3. To detach the cells from the dishes, add 6 ml of 1× Trypsin EDTA/Tris EDTA (pH 7.4) at 37 °C to the cultures.
4. Agitate the flasks gently by hand and incubate at 37 °C and 5% CO_2/95% humidified air for 5 min.
5. Remove flasks from the incubator and rap them sharply against hood surface, causing cells to detach.
6. Triturate cells and add sufficient 30% BCS in PBS to achieve a final concentration of 10% BCS. Spin the cells in a tabletop centrifuge at 800 × g and 4 °C for 5 min.
7. Aspirate supernatants and cells then resuspend in 10% BCS in DMEM (usually about 40 ml media/flask to facilitate cell counting).
8. Triturate and filter cells through 20 μm mesh to remove debris and cell clumps, then count under a phase contrast microscope.

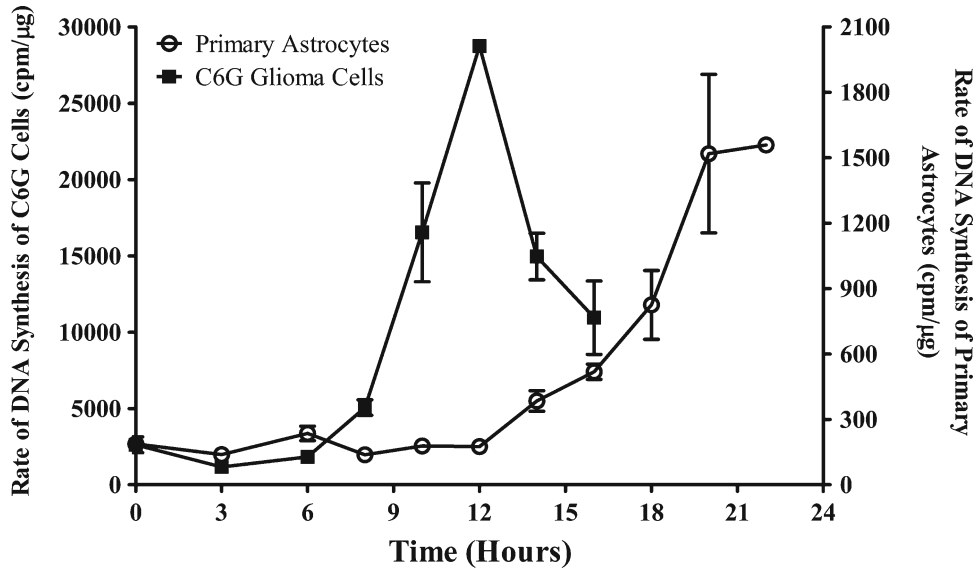

Fig. 3 Comparison of cell cycle in C6G cells and primary astrocytes. Both C6 glioma cells and primary astrocytes were plated in 6-well plates at concentrations of 10^4 and 2000 cells/cm^2, respectively, and allowed to grow to confluence of 30–50% in the presence of 10% BCS/DMEM and at 37 °C and 5% CO_2/95% humidified air. After reaching the desired confluence, the medium was removed and the cells overlaid with 0.1% BCS/DMEM for 48 h. At the end of incubation, both cultures were allowed to re-enter the cell cycle through serum shift-up in 10% BCS/DMEM. At various time points after the serum shift-up, both cultures were pulse-labeled with ^{3}H-thymidine at a final concentration of 1 μCi/ml for 1 h prior to termination. Incorporated ^{3}H-thymidine into DNA of both cultures was measured and presented as mean ± S.E.M (N = 4–9 for primary astrocytes and 5–7 for C6G cells.)

We have found that neonatal astrocytes perform optimally when re-plated at 1×10^4 cells/mm^3, and C6G cells at 2000 cells/mm^3 (Figs. 1, 2 and 3). For re-plating astrocytic cultures, 75 cm^2 flasks get a final volume of 9 ml, while 3 ml/well is satisfactory for 6-well plates (9.1 cm^2 total surface area/well).

9. Plate cells at desired densities and incubate at 37 °C, and 5% CO_2/95% humidified air until reaching a confluence of 30–50%, at which point they are ready for synchronization (*see* **Notes** 7 and **8**).
10. Aspirate media from 30 to 50% confluent cultures, and rinse cells with PBS at 37 °C. Overlay cells with 0.1% BCS in DMEM (same volume as above), and incubate at 37 °C with 5% CO_2/95% humidified air for about 48–72 h before starting the experiment (*see* **Notes** 7 and **8**).
11. At the end of the 48–72 h serum deprivation/synchronization process, aspirate media and replace with 10% BCS/DMEM. This point is called the serum up-shift, and represents the start of the experiment (*see* **Notes 1, 8** and **9**).
12. Assess rates of cell proliferation and degree of synchrony at any point of the cell cycle by pulse labeling cell cultures with 1 μCi/

ml of ^{3}H-thymidine for 1 h prior to termination of experiments. Counts of [Methyl ^{3}H]-thymidine incorporated into the trichloroacetic acid-precipitated fraction is rapid and straightforward, resulting in determination cpm per μg protein [1, 11, 13]. Alternatively, the fraction of cells in S phase can also be measured by pulse-label with bromodeoxyuridine (BrDU) for 2.5 h, followed by immunocytochemical staining for BrDU [13] (*see* **Notes 8–10**).

4 Notes

1. Serum deprivation in this procedure decreases the rate of DNA synthesis in cultured neonatal astrocytic cells by about 88% in the end of the 48-h synchronization process, as based on ^{3}H-thymidine incorporation (Fig. 2). By using immunofluorescent staining, BrDU pulse-labeling demonstrated that the fraction of cells in S phase declined from 70 ± 3% (N = 10, Total cell count = 100) to 15 ± 2% (N = 10, Total cell count = 105) under the same conditions.
2. Further serum deprivation beyond 48-h period rendered the neonatal astrocytic cells unable to re-enter the cell cycle, and caused subsequent cell death (data not shown).
3. Subsequent repletion of serum allowed neonatal astrocytic cells to re-enter G_1 and S phases of the cell cycle in an approximately first-order manner [2, 3, 10] (Figs. 1 and 3). In neonatal astrocytes, the basal level of DNA synthesis observed in G_1 phase persists until reaching the G_1/S intersection, and lasts for 12 h. In an optimal synchronization procedure, repletion of 10% BCS in DMEM caused a seven- to tenfold increase in DNA synthesis at the peak of S phase, when progressing from G_1 phase (Figs. 1 and 3).
4. We have also used this procedure had to successfully synchronize the C6G cell line. The kinetics of cell cycle re-entry in C6 glioma cells resembled those in neonatal astrocytes: an initial G_1 phase, followed by S phase. However, the G_1/S intersection shifted to an earlier time point in C6G cells as compared to primary astrocytes (Fig. 3). Despite the shortening of G_1 phase, the peak of DNA synthesis in S phase was also seven- to tenfold increase above the baseline in G_1 phase (Fig. 3). C6G cells were also able to sustain the synchronization process for a much longer period (i.e., 60 h) than neonatal astrocytes, while maintaining ability to re-enter the cell cycle (Fig. 3) following serum shift-up.
5. The present protocol arrests astrocytic cultures in G_0 phase of the cell cycle [7, 8, 11], as compared to a variety of other methods, which synchronize cell lines in other phases of the cell cycle, such as G_1 [7, 12, 13], S [12, 14], or M [15, 16] phase.

This procedure is relatively free from major problems, and satisfies the following criteria of synchronization, as set forth by Keyomarsi et al. [12]: (a) both normal and tumor cells should be arrested at the same specific cell cycle phase; (b) the synchronization must be reversible and non-cytotoxic; (c) the metabolic block should target a specific reaction and must be reversible; and (d) large quantities of synchronous cells should be obtained.

It must be acknowledged that techniques that use pharmacologic or physical methods to arrest cultured cells in specific cell cycle phases may be considered to be non-physiological and therefore limited as tools to study cycle progression [17–20]. Yet, serum deprivation remains straightforward and inexpensive, and continues to be used in a wide array of studies, including investigations at a cellular level, such as the response of tumors to treatment [4], and at an organelle level, such as centrosomal [21] and mitochondrial functions [22].

6. Astrocytic cultures undergoing synchronization are extremely sensitive to fluctuations in temperature, pH values, and CO_2 levels, all of which invariably affect molecular mechanisms involved in the progression of the cell cycle into quiescence [1, 2, 23]. Therefore, a stable environment, provided by a rapidly equilibrating incubator, is essential for the success of synchronization by this method.
7. Other factors that determine the success of synchronization include the confluence and the rate of proliferation of the cell cultures before synchronization [24]. Over-confluent, as well as rapidly growing cultures often fail to survive synchronization, or are unable to re-enter the cell cycle after synchronization.
8. The optimal time for synchronization depends on the type of cell culture under study, and it is advisable to conduct simple kinetic studies on synchronization before proceeding to actual experimentation. For example, in our kinetic studies, astrocytic cultures were synchronized for different periods of time. Based on the BrDU pulse-labeling, the present protocol arrested about 85 % of cultured astrocytes in G_0 phase (data not shown), which is well above the desired cell fraction (75 %) for a successful cell synchronization process [7].
9. At the end of the synchronization process, the rate of DNA synthesis, as well as the potential of cultured cells to re-enter cell cycle, can be measured by ^{3}H-thymidine pulsing as described above. Alternatively, the cell fractions in different phases of the cell cycle can be measured by flow cytometry in certain cell populations [25, 26]. However, our laboratory has been unable to demonstrate distinct primary astrocytic cell populations in different phases of the cell cycle following synchronization by employing flow cytometry.

10. Our results (Figs. 1 and 3) have confirmed the utility of the serum deprivation protocol in determining differences between the kinetic curves of primary astrocytic cultures and C6 glioma cells following synchronization [9]. The molecular basis of the difference between these two kinetic curves remained unidentified, but may well reflect a fundamental difference between normal and tumoral glial cells. Additionally, as noted above, the initiation of cell cycling by astrocytes in situ is considered to be critical in the pathogenesis of Alzheimer's disease and other neurodegenerative processes [3, 5]. Other laboratories have used serum deprivation to synchronize additional types of mammalian cells [2, 7, 10, 12, 23, 26, 27]. Thus, this procedure may eventually provide new insights into disease mechanisms related to oncogenesis and degenerative processes in other differentiated cells that retain the capacity to re-enter the cell cycle [1, 2, 4, 21–24].

References

1. Alberts B, Johnson A, Lewis J, Raff M, Roberts K, Walter P (2002) Molecular biology of the cell, 4th edn. Garland Science, New York, pp 983–1026
2. Ashihara T, Baserga R (1979) Cell synchronization. Methods Enzymol 58:248–262
3. Salomoni P, Callegari F (2010) Cell cycle control of mammalian neural stem cells: putting a speed limit on G 1. Trends Cell Biol 20:233–243
4. Mueller S, Schittenhelm M, Honecker F, Malenke E, Lauber K, Wesselborg S, Hartmann JT, Bokemeyer C, Mayer F (2006) Cell-cycle progression and response of germ cell tumors to cisplatin in vitro. Int J Oncol 29(2):471–479
5. Wang W, Bu B, Zhang M, Yu Z, Tao D (2009) Neural cell cycle dysregulation and central nervous system diseases. Prog Neurobiol 89:1–17
6. Pardee AB (1974) A restriction point for control of normal animal cell proliferation. Proc Natl Acad Sci U S A 71:1286–1290
7. Krek W, DeCaprio JA (1995) Cell synchronization. Methods Enzym 254:114–124
8. Langan TJ, Volpe JJ (1986) Obligatory relationship between the sterol biosynthetic pathway and DNA synthesis and cell proliferation in glial primary cultures. J Neurochem 46:1283–1291
9. Li V, Kelly K, Schrot R, Langan TJ (1996) Cell cycle kinetics and commitment in newborn, adult, and tumoral astrocytes. Brain Res 96:138–147
10. Quesney-Huneeus V, Galick HA, Siperstein MD, Erickson SK, Spencer TA, Nelson JA (1983) The dual role of mevalonate in the cell cycle. J Biol Chem 258:378–385
11. Mitchell BF, Tupper JT (1977) Synchronization of mouse 3T3 and SV40 3T3 cells by way of centrifugal elutriation. Exp Cell Res 106:351–355
12. Keyomarsi K, Sandoval L, Band V, Pardee AB (1991) Synchronization of tumor and normal cells from G_1 to multiple cell cycles by lovastatin. Cancer Res 51:3602–3609
13. Pardee AB, Keyomarsi K (1992) Modification of cell proliferation with inhibitors. Curr Opin Cell Biol 4:186–191
14. Huberman JA (1981) New views of the biochemistry of eucaryotic DNA replication revealed by aphidicolin, an unusual inhibitor of DNA polymerase alpha. Cell 23:647–648
15. Langan TJ, Slater MC (1991) Quiescent astroglia in long-term primary cultures re-enter the cell cycle and require a nonsterol isoprenoid in late G_1. Brain Res 548:9–17
16. Zieve GW, Turnbull D, Mullins JM, McIntosh JR (1980) Production of large numbers of mitotic mammalian cells by use of the reversible microtubule inhibitor nocodazole. Exp Cell Res 126:397–405
17. Henderson L, Bortone DS, Lim C, Zambon AC (2013) Classic "broken cell" techniques and newer live cell methods for cell cycle assessment. Am J Physiol Cell Physiol 304:C927–C938
18. Sanchez I, Goya L, Vallerga AK, Firestone GL (1993) Glucocorticoids reversibly arrest rat hepatoma cell growth by inducing an early G_1 block in cell cycle progression. Cell Growth Differ 4:215–225

19. Terasima T, Tolmach LJ (1963) Growth and nucleic acid synthesis in synchronously dividing populations of HELA cells. Exp Cell Res 30:344–362
20. Webber LM, Garson OM (1983) Fluorodeoxyuridine synchronization of bone marrow cultures. Cancer Genet Cytogenet 8:123–132
21. Chen TY, Syu JS, Han TY, Cheng HL, Lu FI, Wang CY (2015) Cell cycle-dependent localization of dynactin subunit p150 glued at centrosome. J Cell Biochem 116:20 49–2060
22. Lopez-Mejia IC, Fajas L (2015) Cell cycle regulation of mitochondrial function. Curr Opin Cell Biol 33:19–25 [review]
23. Bartholomew JC, Neff NT, Ross PA (1976) Stimulation of WI-38 cell cycle transit: effect of serum concentration and cell density. J Cell Physiol 89:251–258
24. Campbell A (1957) Synchronization of cell division. Bacteriol Rev 21:263–272
25. Johnston DA, White RA, Barlogie B (1978) Automatic processing and interpretation of DNA distributions: comparison of several techniques. Comput Biomed Res 11:393–404
26. Merrill GF (1998) Cell synchronization. Methods Cell Biol 57:229–249
27. Wilmut I, Schnieke AE, McWhir J, Kind AJ, Campbell KHS (1997) Viable offspring derived from fetal and adult mammalian cells. Nature 385:810–813

Chapter 7

DNA Damage Response Resulting from Replication Stress Induced by Synchronization of Cells by Inhibitors of DNA Replication: Analysis by Flow Cytometry

Dorota Halicka, Hong Zhao, Jiangwei Li, Jorge Garcia, Monika Podhorecka, and Zbigniew Darzynkiewicz

Abstract

Cell synchronization is often achieved by transient inhibition of DNA replication. When cultured in the presence of such inhibitors as hydroxyurea, aphidicolin or excess of thymidine the cells that become arrested at the entrance to S-phase upon release from the block initiate progression through S then G_2 and M. However, exposure to these inhibitors at concentrations commonly used to synchronize cells leads to activation of ATR and ATM protein kinases as well as phosphorylation of *Ser*139 of histone H2AX. This observation of DNA damage signaling implies that synchronization of cells by these inhibitors is inducing replication stress. Thus, a caution should be exercised while interpreting data obtained with use of cells synchronized this way since they do not represent unperturbed cell populations in a natural metabolic state. This chapter critically outlines virtues and vices of most cell synchronization methods. It also presents the protocol describing an assessment of phosphorylation of *Ser*139 on H2AX and activation of ATM in cells treated with aphidicolin, as a demonstrative of one of several DNA replication inhibitors that are being used for cell synchronization. Phosphorylation of *Ser139*H2AX and *Ser*1981ATM in individual cells is detected immunocytochemically with phospho-specific Abs and intensity of immunofluorescence is measured by flow cytometry. Concurrent measurement of cellular DNA content followed by multiparameter analysis allows one to correlate the extent of phosphorylation of these proteins in response to aphidicolin with the cell cycle phase.

Key words DNA repair, γH2AX, ATM phosphorylation, DNA double-strand breaks, Apoptosis, DNA fragmentation, G_1/S boundary, Aphidicolin

1 Introduction

1.1 Advantages and Limitations of Different Cell Synchronization Methods

Different methods are being used to obtain populations of cells synchronized in the cell cycle (reviews: [1–6]). Each of them offers certain advantages but also suffers limitations. One of the widely used approaches is based on isolation of mitotic cells by their selective detachment from the culture flask [7]. Its advantage stems from the fact that the synchronization process does not perturb the

Gaspar Banfalvi (ed.), *Cell Cycle Synchronization: Methods and Protocols*, Methods in Molecular Biology, vol. 1524,
DOI 10.1007/978-1-4939-6603-5_7,

cell cycle progression and therefore the metabolic status of the population of synchronized cells represents their native state. However, this approach is applicable to relatively few cell lines, such as Chinese hamster ovary (CHO) or HeLa cells that grow in an adherent fashion but detach during mitosis. Somewhat similar technique selecting cells in mitosis was designed for murine leukemic L1210 cells that grow in suspension but are being enforced to adhere to polylysine-coated membranes. During mitosis one of the daughter cells detaches from its sister and floats in culture medium whereas the non-detached cell may still remain attached to the membrane until the following mitosis [8–10]. In this way, continuous "production" of mitotic cells can be achieved. It is unknown how widely this approach can be used because cells other than L1210 lines cannot be synchronized this way [11]. Furthermore, the enforced attachment of cells to polycation-coated membranes was shown to lead to endomitosis and polyploidy [11].

Cells of certain lines can be synchronized in G_1 by inhibitors of protein farnesylation and geranyl-geranylation such as statins [12, 13], or CDK2 protein kinase inhibitors [13–16]. These techniques also are not universally applicable since other lines do not respond to statins or protein kinase inhibitors by reversible arrest in G_1. Normal, non-tumor cells can be synchronized in $G_{0/1}$ either by removal of growth factors, e.g., by "serum starvation" [17, 18], by depletion of a particular amino-acid [19], or by contact inhibition [20]. These approaches generally fail to synchronize tumor cell lines. Moreover, metabolism of such synchronized cells is often perturbed resulting that after release from the arrest their rate of progression through the cycle is being accelerated compared to the control, asynchronous cell populations [21]. It should also be noted that the cells synchronized in early G_1 or at mitosis start to lose synchrony while progressing through G_1 and thereby become less synchronous during S or G_2 phases of the cell cycle.

The approach based on separation of cells based on their size, centrifugal elutriation, is also being used to obtain relatively synchronous cell populations [22, 23]. However, while this procedure does not perturb cell cycle progression, the synchrony of uniformly sized elutriated cells is not sufficiently narrow. Furthermore, elutriation requires complex and expensive instrumentation and an experienced operator. Density gradient centrifugation appears to yield cell populations even less synchronous than elutriation [24]. Fluorescence-activated cell sorting (FACS) is also used to obtain synchronous cell populations, e.g., based on DNA content analysis after supravital staining with fluorochromes such as Hoechst 33342 [25, 26]. However, Hoechst 33342 elicits DNA damage response [27], long-term toxicity [28], and undergoes redistribution from labeled to unlabeled cells in mixed cell populations [29].

Cell synchronization at mitosis by mitotic spindle poisons such as colchicines, vinca alkaloids, or nocodazole is another common

methodology [30, 31]. Its advantage is simplicity, low cost, and high degree of synchrony when one opts to obtain mitotic or immediately post-mitotic cell populations [32]. As mentioned, cell populations synchronized this way become less synchronous after progression through G_1. Furthermore, undesirable effects such as cytotoxicity and growth imbalance are seen during arrest in mitosis [33–35].

1.2 Inhibitors of DNA Replication

Among the most common approaches to obtain populations of synchronized cells, particularly in S-phase, is cell synchronization with the use of DNA replication inhibitors such as hydroxyurea, methotrexate, aphidicolin or high concentrations of thymidine [36–39]. A combination of replication inhibitors with other synchronizing agents is also widely used [40]. The advantage of cell synchronization by DNA replication inhibitors is simplicity and low cost. However, a major drawback is the induction of growth imbalance [41]. Specifically, while cells become arrested in their progression through S, their growth in terms of an increase in RNA and protein content synthesis continues which leads to the perturbation of the metabolic functions. Furthermore, the cell cycle progression machinery of cells synchronized by DNA replication inhibitors is severely perturbed as reflected by unscheduled expression of cyclin proteins [41, 42]. When released from the block such cells traverse S and G_2 at greatly accelerated rates as compared to the non-synchronized cells [43].

Inhibition of DNA replication causes also the replication stress which manifests as a DNA damage response (DDR). The inhibitors of DNA replication such as hydroxyurea, aphidicolin, or excess of thymidine were shown to induce phosphorylation of histone H2AX on *Ser*139 [44, 45]. Phosphorylated H2AX is being termed γH2AX [46]. Phosphorylation of H2AX and activation of ataxia telangiectasia-mutated protein kinase (ATM), through its phosphorylation on *Ser*1981 (ATM-S1981^{P}), are the key markers of DDR, often reflecting DNA damage that involves formation of DNA double-strand breaks (DSBs) [46–49]. Both activation of ATM and H2AX phosphorylation can be detected immunocytochemically using phospho-specific Abs, and degree of phosphorylation of these proteins which reports on severity of DNA damage can be assessed by flow- or laser scanning-cytometry (LSC), the instruments measuring intensity of fluorescence of individual cells [50, 51]. It should be noted that during DNA replication stress H2AX is initially phosphorylated by ATM Rad3-related protein kinase (ATR) rather than by ATM [44, 45, 49, 52]. Phosphorylation of ATR can be detected either using phospho-specific ATR Ab or indirectly using Ab to ATM/ATR substrate that is phosphorylated on Ser/Thr at SQ/TQ cluster domains (sATM/ATR^{P}) [49]. The response induced by DNA replication inhibitors thus can be assessed by detecting activation of ATR and phosphorylation of H2AX (expression of γH2AX) [44, 45]. It should be noted,

however that in certain instances DNA replication stress, e.g., as caused by UV light may also induce activation of ATM and DNA-dependent protein kinase (DNA-PK*cs*) [53]. Redundancy in terms of activation of different protein kinases targeting the same substrate, as in this case is H2AX, is a characteristic feature of DNA damage response [53, 54].

1.3 Analysis of DDR Induced by DNA Replication Inhibitors

The protocol presented in this chapter is designed to assess intensity of Ser139-H2AX and ATM-1981^{P} immunofluorescence using phospho-specific Abs measured by flow cytometry. In human promyelocytic leukemia HL-60 cells, phosphorylation of H2AX and ATM was induced by the treatment with DNA polymerase-α inhibitor aphidicolin under the conditions that are being used to induce cell synchronization. It should be noted that the identical protocol can be also used to measure immunofluorescence of cells to detect phosphorylation of ATR (ATR^{P}) or the ATM/ATR substrate (sATM/ATR^{P}). The detection of γH2AX and ATM-S1981^{P} is combined with differential staining of DNA to assess cellular DNA content which reveals the cell cycle phase (*see* **Note 1**). The procedure can be based either on *indirect immunofluorescence* detection of these phosphorylated proteins using the unlabeled primary Ab and the secondary Ab conjugated with FITC or AlexaFluor 488. Alternatively, one can use direct immune-labeling with the fluorochrome-tagged primary Ab (*see* **Note 2**). DNA is counterstained with propidium iodide (PI) whose emission spectrum (red) is separated from the green color emission of either FITC or AlexaFluor 488. The cells are briefly fixed in methanol-free formaldehyde and then transferred into 70% ethanol in which they can be kept briefly (≥2 h) or stored at −20 °C for weeks or longer. Ethanol treatment makes the plasma membrane permeable to the phospho-specific Abs; further permeabilization is achieved by including the detergent Triton X-100 into the solution used to incubate cells with the Ab. After incubation with the primary γH2AX Ab, the cells are incubated with FITC or Alexa Fluor 488-labeled secondary Ab and their DNA is counterstained PI in the presence of RNase A to remove RNA, which otherwise, similar as DNA, is also being stained with PI. As an alternative to PI cellular DNA can be stained with the 4′,6-diamidino-2-phenylindole (DAPI), the fluorochrome whose fluorescence has to be excited with UV or near UV laser. Intensity of cellular green (FITC or Alexa Fluor 488) and red (PI) (or blue—DAPI) fluorescence is measured by multiparameter flow cytometry (*see* **Note 3**).

It should be noted that H2AX undergoes constitutive phosphorylation in healthy cells, untreated by radiation or genotoxic agents [54]. This constitutive expression of γH2AX, which is more pronounced in S and G_2M than in G_1 cells, is considered to be in large part a reflection of oxidative DNA damage caused by the metabolically generated oxidants [54]. Moreover, DNA fragmentation during apoptosis [55] leads to formation of large number of DSBs inducing high level of H2AX phosphorylation [56] (Fig. 1).

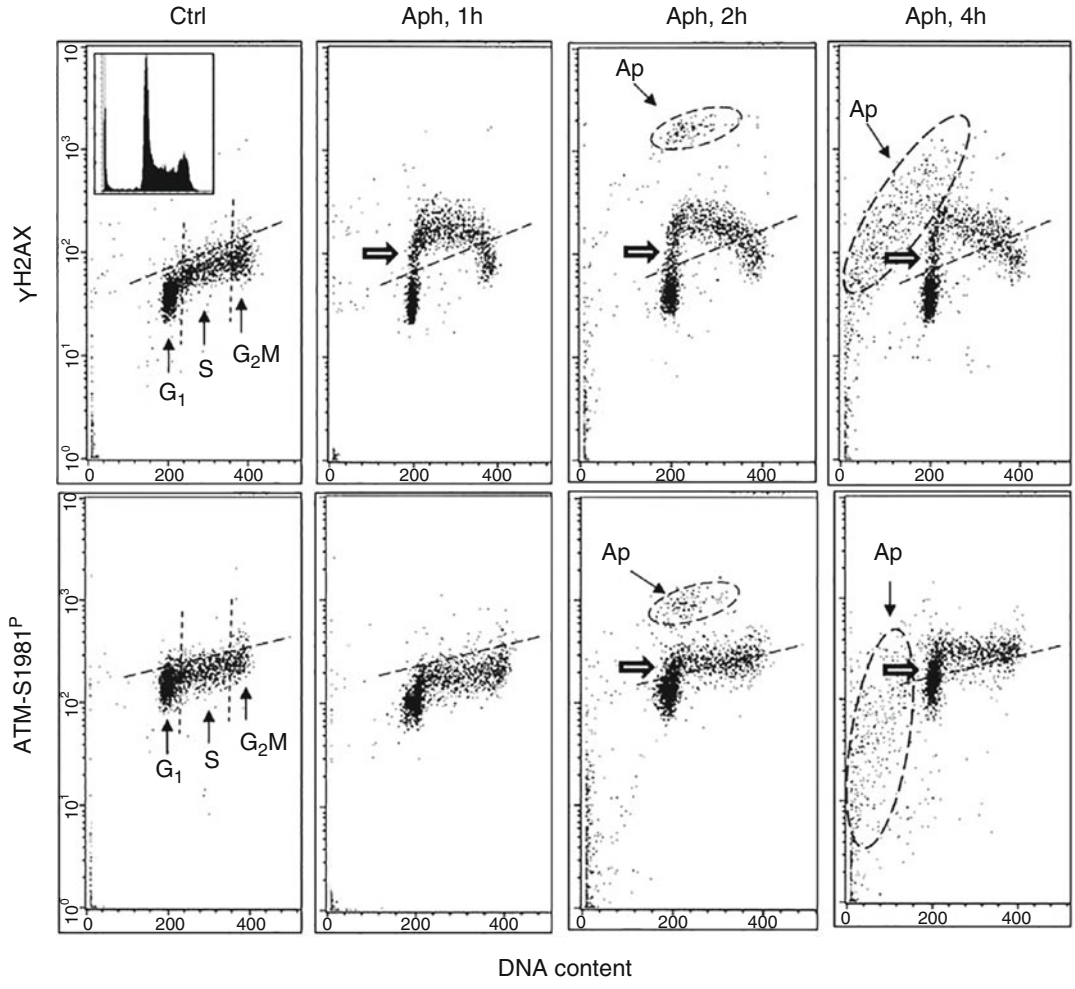

Fig. 1 Detection of histone H2AX phosphorylation and ATM activation in HL-60 cells treated with DNA polymerase-α inhibitor aphidicolin (Aph). The cells were untreated (Ctrl) or treated in culture with 4 μlM Aph for 1, 2, or 4 h and expression of γH2AX and ATM-S1981^P was measured as described in the protocol (indirect immunofluorescence). The bivariate distributions (scatterplots) of DNA content versus γH2AX or ATM-S1981^P immunofluorescence (IF) allow one to identify subpopulations of cells in G_1, S, and G_2M phases of the cell cycle as shown in left panels. The *dashed skewed lines* show the upper γH2AX IF or ATM-S1981^P threshold of IF for 95 % cells in the untreated (Ctrl) culture; the cells above this threshold in the Aph-treated cultures are considered to express these phosphoproteins above the control level. As it is evident the most pronounced increase in expression of γH2AX in cultures treated with Aph, seen already after 1 h, is at the G_1/S interphase (marked with *thick arrows*). Activation ATM occurs later (2 h) than phosphorylation of H2AX (1 h) which is the evidence that ATR (or/and DNA-PKcs) initially phosphorylate(s) H2AX. Apoptotic cells (Ap) have conspicuously higher expression of γH2AX and ATM-S1981^P after 2 h. After 4 h, due to progressive DNA fragmentation concurrent with loss of DNA and proteins [55–57] apoptotic cells show a decreased DNA content, expression of ATM-S1981^P and of γH2AX, compared to 2 h. Note that the γH2AX and ATM-S1981^P coordinates are exponential while DNA content scale is linear

Strategies are presented to distinguish the DNA damage induced by DNA replication inhibitors from the constitutive damage occurring in untreated cells (*see* **Note 4**), or from the apoptosis-associated (AA) DSBs (*see* **Note 5**).

2 Materials

2.1 Required Reagents

1. Cells to be analyzed: 10^6–5×10^6 cells, untreated (control) and treated in culture with inhibitors of DNA replication (e.g., hydroxyurea, aphidicolin or thymidine at their respective concentrations generally used to inhibit DNA synthesis and synchronize cells at the entrance to S phase) suspended in 1 ml of tissue culture medium.
2. Methanol-free formaldehyde (Polysciences, Warrington, PA).
3. 70% ethanol.
4. Phosphate-buffered saline (PBS).
5. Triton X-100 (Sigma-Aldrich).
6. Bovine serum albumin (BSA; Sigma-Aldrich).
7. Abs: There are several commercially available phospho-specific Abs mono- as well as poly-clonal, unconjugated and FITC- or Alexa Fluor 488-conjugated, applicable to cytometry, that can be used to detect γH2AX, ATM-S1981^P or ATM/ATR substrate [e.g., from BioLegend (San Diego, CA), Cell Signaling/Santa Cruz Biotechnology (Danvers, MA), ThermoFisher Scientific/Molecular Probes (Eugene, OR)]. The same companies also offer FITC- or Alexa 488-tagged secondary Abs to be used in conjunction with the non-conjugated primary Abs to these phosphorylated proteins.
8. Propidium iodide (PI; ThermoFisher Scientific/Molecular Probes).
9. DNase-free RNase A (Sigma-Aldrich).
10. 12 × 75 mm polypropylene tubes.

2.2 Reagents to be Prepared

1. Methanol-free formaldehyde fixative: Prepare 1% (v/v) solution of methanol-free formaldehyde in PBS. This solution may be stored at 4 °C for up to 2 weeks.
2. BSA-T-PBS: Dissolve BSA in PBS to obtain 1% (w/v) BSA solution. Add Triton X-100 to obtain 0.2% (v/v) of its concentration. This solution may be stored at 4 °C for up to 2 weeks.
3. PI stock solution: Dissolve PI in distilled water to obtain a 1 mg/ml solution. This solution can be stored at 4 °C in the dark (e.g., in the tube wrapped in aluminum foil) for several months.
4. PI staining solution: Dissolve RNase A (DNase-free) in PBS to obtain a 0.1% (w/v; 100 mg/ml) solution. Add an appropriate

aliquot of PI stock solution (e.g., 5 μl per 1 ml) to obtain its 5 μg/ml final concentration. Store the PI staining solution in the dark. This solution may be stored at 4 °C for up to 2 weeks.

2.3 Instrumentation

1. Flow cytometers of different types, offered by several manufacturers, can be used to measure cell fluorescence following staining according to the protocol given below. The most common flow cytometers are from Coulter Corporation (Miami, FL), Becton Dickinson Immunocytometry Systems (San Jose, CA), PARTEC (Zurich, Switzerland), Accuri Cytometers Inc. (Ann Arbor, MI), Millipore-Guava (Billerica, MA) or Applied Biosystems (Foster City, CA).
2. Centrifuge and rotor capable of 300 × *g*.

3 Methods

1. Centrifuge cells collected from tissue culture (suspended in culture medium) at 300 × *g* for 4 min at room temperature. Suspend cell pellet (1–2 × 10^6 cells) in 0.5 ml of PBS.
2. With a Pasteur pipette transfer this cell suspension into polypropylene tube (*see* **Note 6**) containing 4.5 ml of ice-cold 1% methanol-free formaldehyde solution in PBS. Keep on ice for 15 min.
3. Centrifuge at 300 × *g* for 4 min at room temperature and suspend cell pellet in 4.5 ml of PBS. Centrifuge again as above and suspend cell pellet in 0.5 ml of PBS. With a Pasteur pipette, transfer the suspension to a tube containing 4.5 ml of ice-cold 70% ethanol. The cells should be maintained in 70% ethanol for 1 h but may be stored in 70% ethanol at –20 °C for several weeks.
4. Centrifuge at 200 × *g* for 4 min at room temperature, remove the ethanol and suspend cell pellet in 2 ml of BSA-T-PBS solution.
5. Centrifuge at 300 × *g* for 4 min at room temperature and suspend the cells again in 2 ml of BSA-T-PBS. Keep at room temperature for 5 min.
6. Centrifuge at 300 × *g* for 4 min at room temperature and suspend the cells in 100 μl of BSA-T-PBS containing 1 μg of the primary γH2AX Ab (*see* **Notes 2** and **7**).
7. Cap the tubes to prevent drying and incubate them overnight at 4 °C (*see* **Note 8**).
8. Add 2 ml of BSA-T-PBS and centrifuge at 300 × *g* for 4 min at room temperature.
9. Centrifuge at 300 × *g* for 4 min at room temperature and suspend the cells in 2 ml of BSA-T-PBS.

10. Centrifuge at 300 × *g* for 4 min at room temperature and suspend the cells pellet in 100 μl of BSA-T-PBS containing the appropriate (anti-mouse or anti-rabbit, depending on the source of the primary Ab) FITC- or Alexa Fluor 488- tagged secondary Ab (*see* **Note 6**).
11. Incubate for 1 h at room temperature, occasionally gently shaking. Add 5 ml of BSA-T-PBS and after 2 min centrifuge at 300 × *g* for 4 min at room temperature.
12. Suspend the cells in 5 ml of BSA-T-PBS and after 1 min centrifuge at 300 × *g* for 4 min.
13. Suspend the cells in 1 ml of the PI staining solution. Incubate at room temperature for 30 min in the dark (*see* **Note 3**).
14. Set up and adjust the flow cytometer for excitation with light at blue wavelength (488-nm laser line or BG-12 excitation filter) filter) (*see* **Note 9**).
15. Measure intensity of green (530 ± 20 nm) and red (>600 nm) fluorescence of the cells by flow cytometry. Record the data (*see* **Note 3**).

4 Notes

1. On the bivariate distributions (scatterplots) subpopulations of cells in G_1, versus S versus G_2/M are distinguished based on differences in their DNA content (intensity of PI or DAPI fluorescence; *see* Fig. 1). To assess the mean extent of expression of γH2AX (or ATM-S1981^P) for cells at a particular phase of the cycle the mean values of γH2AX or ATM-S1981^P immunofluorescence or (IF) are calculated separately for G_1, S, and G_2/M cell sub-populations distinguished based on differences in DNA content, by the computer-interactive "gating" analysis. The gating analysis should be carried out to obtain mean values of γH2AX or ATM-S1981^P IF for G_1 (DNA Index; DI = 0.9–1.1), S (DI = 1.2–1.8) and G_2M (DI = 1.9–2.1) cell subpopulations, respectively. The mean values of the control cells, untreated with potential DNA damaging agents, are then subtracted for each cell cycle phase cells. As mentioned in the Subheading 1 the expression of ATM-S1981^P or γH2AX of the untreated control cells represents their constitutive level, to a large degree due to the DNA damage response induced by endogenous oxidants [55].
2. If primary Ab conjugated with fluorochrome (e.g., with FITC or Alexa Fluor 488) is being used replace the unconjugated Ab in **step 5** with a conjugated Ab, then move to **step 10**, omitting **steps 6–9**. Nota Bene: Often, it is preferable to use indirect immunofluorescence because of greater choices of secondary

Abs having higher intensity of fluorochrome labeling. On the other hand, using the primary fluorochrome-tagged Ab shortens the labeling procedure.

3. As an alternative to PI cellular DNA can be stained with DAPI. An advantage of DAPI is that there is no need to treat cells with RNase and resolution of cell cycle phases may be more distinct compared to PI. However, the excitation wavelength of DAPI is in the UV range, or near UV (405-nm), and not all flow cytometers have such a laser. In **step 12**, instead with PI the cells may be stained with DAPI at a concentration of 1 μg/ml in PBS, at room temperature, for 10 min. In **step 14**, instead of red, blue fluorescence emission (450–500 nm) should be measured.
4. As mentioned in the Subheading 1 the low level of expression of γH2AX or ATM-S1981^{P} IF seen in cells that have not been treated with exogenous inducers of DDR represents the constitutive ("background") H2AX phosphorylation and ATM activation [55]. To quantify the γH2AX or ATM-S1981^{P} IF induced by DNA replication inhibitors, the constitutive component of γH2AX or ATM-S1981^{P} IF has to be subtracted. Toward this end, the means of γH2AX or ATM-S1981^{P} IF of G_1, S, and G_2/M-phase of the untreated cells are subtracted from the respective means of the G_1, S, and G_2/M subpopulations of the inhibitor-treated cells, respectively (Fig. 1). After the subtraction, the extent of *increase* in intensity of γH2AX (Δ γH2AX IF) or ATM-S1981^{P} (ΔATM-S1981^{P} IF) over the untreated sample represents the *treatment-induced phosphorylation* of this protein, per each phase of the cell cycle. Alternatively, one can express the inhibitor-induced phosphorylation of H2AX or sATM/ATR as a percent (or multiplicity) of the increase of the mean IF value of the inhibitor-treated- to the mean of the untreated cells, in the respective phases of the cell cycle. The irrelevant isotype control may be used to estimate the nonspecific Ab binding component, although its use may be unnecessary when one is interested only in the assessment of the inhibitor-induced increase (Δ) in IF.
5. DNA undergoes extensive fragmentation during apoptosis which leads to the appearance of a multitude of DSBs in apoptotic cells, triggering H2AX phosphorylation and ATM activation [56, 57]. It is often desirable, therefore, to distinguish between primary DSBs induced by DNA damaging agents such as DNA replication inhibitors versus DSBs generated during apoptosis. The following attributes of γH2AF IF allow one to distinguish the cells with the inhibitor-induced H2AX phosphorylation from the cells that have phosphorylation of this histone triggered by apoptosis-associated (AA) DNA fragmentation: (a) The γH2AX IF induced by replication inhibitors is seen

rather early during the treatment (30 min–1 h) whereas AA γH2AX IF is seen later (>1 h), but there are exceptions [56]; (b) The intensity AA γH2AX IF is much higher than that of the inhibitor-induced γH2AX IF, unless the cells are at a late stage of apoptosis [57, 58] (Fig. 1); (c) The induction of AA γH2AX IF is prevented by cell treatment with the caspase inhibitor z-VAD-FMK, which precludes activation of endonuclease responsible for DNA fragmentation [56]; (d) The AA H2AX phosphorylation occurs concurrently with activation of caspase-3. Multiparameter analysis [activated (cleaved) caspase-3 versus γH2AX IF], thus allows one to distinguish cells in which DSBs were caused by inducers of DNA damage (active caspase-3 is undetectable) from those cells that have H2AX phosphorylation and ATM activation additionally triggered in response to apoptotic DNA fragmentation (active caspase-3 is present).

6. If the sample initially contains a small number of cells they may be lost during repeated centrifugations. Polypropylene or siliconized glass tubes are recommended to minimize cell loss. Since transferring cells from one tube to another causes electrostatic attachment of a large fraction of cells to the surface of each new tube, all steps of the procedure (excluding fixation) should preferentially be done in the same tube. Addition of 1% (w/v) BSA to rinsing solutions also decreases cell loss. When the sample contains very few cells, carrier cells (e.g., chick erythrocytes) may be included; they may be recognized during analysis based on differences in DNA content (intensity of PI fluorescence).
7. Quality of the primary and of secondary antibody is of utmost importance. The ability to detect γH2AX, sATM/ATR^{P} or ATM-S1981^{P} is often lost during improper transport or storage conditions of the Ab. We occasionally observed that the Abs provided by the vendor were defective. Also of importance is use of the Abs at optimal concentration. It is recommended that serial dilution tests be done before the first use of every new batch of the primary or secondary Ab (e.g., within the range between 0.2 and 2.0 μg/100 μl) to find their optimal titer for detection of these phospho-proteins. The optimal titer is recognized as giving maximal signal to noise ratio, i.e., the maximal ratio of the mean IF intensity of the drug treated to the untreated cells. As an alternative one may consider a ratio of fluorescence intensity of the cells maximally responding, such as the S-phase cells in the case of treatment with aphidicolin, to the not-responding cells–G_1 cells (Fig. 1). The titer recommended by the vendor is not always the optimal one.
8. Alternatively, incubate for 1 h at 22–24 °C. The overnight incubation at 4 °C, however, appears to yield a somewhat higher intensity of γH2AX IF, sATM/ATR^{P}, or ATM-S1981^{P} IF compared to 1 h incubation.

9. The cells have to be thoroughly dispersed, isolated from each other, with no cell clumps/aggregates that can clog the nozzle of flow cytometer. Repeated channeling through orifice of Pasteur pipette is often able to disperse larger cell aggregates. Passage (filtering) of cells through 54 μm mesh is required to remove cell aggregates. When there is a significant number of dead-, and in particular mechanically damaged-, cells in the sample, free DNA released from these cells works as a glue entrapping also live cells and forming cell aggregates. Such aggregates cannot be dispersed after fixation. To disperse cells from the aggregates, prior to fixation, the cells should be incubated with 50 μlg/ml of DNase, in PBS for 20 min at room temperature, then rinsed with PBS twice and fixed.

Acknowledgment

Supported by NCI CA RO1 28 704 and Robert A. Welke Cancer Research Foundation

References

1. Jandt U, Platas Barradas O, Pörtner R, Zeng AP (2014) Mammalian cell culture synchronization under physiological conditions and population dynamic simulation. Appl Microbiol Biotechnol 98:4311–4319
2. Henderson L, Bortone DS, Lim C, Zambon AC (2013) Classic "broken cell" techniques and newer live cell methods for cell cycle assessment. Am J Physiol Cell Physiol 304:C927–C938
3. Banfalvi G (2011) Overview of cell synchronization. Methods Mol Biol 761:1–23
4. Davis PK, Ho A, Dowdy SF (2001) Biological methods for cell-cycle synchronization of mammalian cells. Biotechniques 30:1322–1331
5. Merril GF (1998) Cell synchronization. Methods Cell Biol 57:229–249
6. Amon A (2002) Synchronization procedures. Methods Enzymol 351:457–467
7. Terasima T, Tolmach LJ (1963) Growth and nucleic acid synthesis in synchronously dividing populations of HeLa cells. Exp Cell Res 30:344–362
8. Edward KL, Van Ert MN, Thornton M, Helmstetter CE (2004) Cyclin mRNA stability does not vary during the cell cycle. Cell Cycle 3:1057–1060
9. Thornton M, Edward KL, Helmstetter CE (2002) Production of minimally disturbed synchronous cultures of hematopoetic cells. Biotechniques 32:1098–10100
10. Helmstetter CE (2015) A ten-year search for synchronous cells: obstacles, solutions, and practical applications. Front Microbiol 6:238
11. Huang X, Dai W, Darzynkiewicz Z (2005) Enforced adhesion of hematopoietic cells to culture dish induces endomitosis and polyploidy. Cell Cycle 4:801–805
12. Jakóbisiak M, Bruno S, Skierski J, Darzynkiewicz Z (1991) The cell cycle specific effects of lovastatin. Proc Natl Acad Sci U S A 88:3628–3613
13. Ma HT, Poon RY (2011) Synchronization of HeLa cells. Methods Mol Biol 761:151–161
14. Crissman HA, Gadbois DM, Tobey RA, Bradbury EM (1991) Transformed mammalian cells are deficient in kinase-mediated progression through the G_1 phase of the cell cycle. Proc Natl Acad Sci U S A 88:7580–7585
15. Bruno S, Ardelt B, Skierski JS, Traganos F, Darzynkiewicz Z (1992) Different effects of staurosporine, an inhibitor of protein kinases, on the cell cycle and chromatin structure of normal and leukemic lymphocytes. Cancer Res 52:470–476
16. Bruno S, Traganos F, Darzynkiewicz Z (1996) Cell cycle synchronizing properties of staurosporine. Methods Cell Sci 18:99–107
17. Griffin MJ (1976) Synchronization of some human cell strains by serum and calcium starvation. In Vitro 12:393–400
18. Bonnesen C, Nelander GM, Hansen BF, Jensen P, Krabbe JS, Jensen M, Hegelund

AC, Svendsen JE, Oleksiewicz MB (2010) Synchronization in G0/G1 enhances the mitogenic response of cells overexpressing the human insulin receptor A isoform to insulin. Cell Biol Toxicol 26:293–307

19. Tobey RA, Crissman HA (1972) Use of flow microfluorimetry in detailed analysis of effects of chemical agents on cell cycle progression. Cancer Res 32:2726–2731
20. Holley RW, Kiernan MA (1968) "Contact inhibition" of cell division in 3T3 cells. Proc Natl Acad Sci U S A 60:300–305
21. Pardee AB, Keyomarsi K (1992) Modification of cell proliferation with inhibitors. Curr Opin Cell Biol 4:186–191
22. Mitchell BF, Tupper JT (1977) Synchronization of mouse 3T3 and SV40 3T3 cell by way of centrifugal elutriation. Exp Cell Res 106:351–355
23. Banfalvi G (2008) Cell cycle synchronization of animal cells and nuclei by centrifugal elutriation. Nat Protoc 3:663–673
24. Cymerman U, Beer JB (1980) Some problems in using density gradient centrifugation for synchronization of L5178Y-S cells. Neoplasma 27:429–436
25. Juan G, Hernando E, Cordon-Cardo C (2002) Separation of live cells in different phases of the cell cycle for gene expression analysis. Cytometry 49:170–175
26. Vecsler M, Lazar I, Tzur A (2013) Using standard optical flow cytometry for synchronizing proliferating cells in the G1 phase. PLoS One 8:e83935
27. Zhao H, Traganos F, Dobrucki J, Wlodkowic D, Darzynkiewicz Z (2009) Induction of DNA damage response by the supravital probes of nucleic acids. Cytometry A 75A:510–519
28. Zhang X, Chen J, Davis B, Kiechle F (1999) Hoechst 33342 induces apoptosis in HL-60 cells and inhibits topoisomerase I *in vivo*. Arch Pathol Lab Med 123:921–927
29. Mohorko N, Kregar-Velikonja N, Repovs G, Gorensek M, Bresjanac M (2005) An *in vitro* study of Hoechst 33342 redistribution and its effects on cell viability. Hum Exp Toxicol 24:573–580
30. Samake S, Smith LC (1996) Synchronization of cell division in eight-cell bovine embryos produced in vitro: effects of nocodazole. Mol Reprod Dev 44:486–492
31. Harper JV (2005) Synchronization of cell populations in G_1/S and G_2/M phases of the cell cycle. Methods Mol Biol 296:157–165
32. Darzynkiewicz Z, Crissman H, Traganos F, Stainkamp J (1982) Cell heterogeneity during the cell cycle. J Cell Physiol 112:465–474
33. Urbani L, Sherwood SW, Schimke RT (1995) Dissociation of nuclear and cytoplasmic cell cycle progression by drugs employed in cell synchronization. Exp Cell Res 219:159–168
34. Chou LF, Chou WG (1999) DNA-end binding activity of Ku in synchronized cells. Cell Biol Int 23:663–670
35. Piotrowska K, Modlinski JA, Korwin-Kossakowski M, Karasiewicz J (2000) Effects of preactivation of ooplasts or synchronization of blastomere nuclei in G_1 on preimplantation development of rabbit serial nuclear transfer embryos. Biol Reprod 63:677–682
36. Tobey RA, Oishi N, Crissman HA (1990) Cell cycle synchronization: reversible induction of G2 synchrony in cultured rodent and human diploid fibroblasts. Proc Natl Acad Sci U S A 87:5104–5109
37. Vogel W, Schempp W, Sigwarth I (1978) Comparison of thymidine, fluorodeoxyuridine, hydroxyurea, and methotrexate blocking at the G_1/S phase transition of the cell cycle, studied by replication patterns. Hum Genet 45:193–198
38. Fox MH, Read RA, Bedford JS (1987) Comparison of synchronized Chinese hamster ovary cells obtained by mitotic shake-off, hydroxyurea, aphidicolin, or methotrexate. Cytometry 8:315–320
39. Matherly LH, Schuetz JD, Westin E, Goldman ID (1989) A method for the synchronization of cultured cells with aphidicolin: application to the large-scale synchronization of L1210 cells and the study of the cell cycle regulation of thymidylate synthase and dihydrofolate reductase. Anal Biochem 182:338–345
40. Kues WA, Anger M, Carnawath JW, Paul D, Motlik J, Niemann H (2000) Cell cycle synchronization of porcine fetal fibroblasts: effects of serum deprivation and reversible cell cycle inhibitors. Biol Reprod 62:412–419
41. Gong J, Traganos F, Darzynkiewicz Z (1995) Growth imbalance and altered expression of cyclins B1, A. E and D3 in MOLT-4 cells synchronized in the cell cycle by inhibitors of DNA replication. Cell Growth Differ 6:1485–1492
42. Jiang J, Liu L, Li X, Tao D, Hu J, Qin J (2013) Defining the restriction point in normal asynchronous human peripheral blood lymphocytes. Cytometry A 83(A):944–951
43. Kurose A, Tanaka T, Huang X, Traganos F, Dai W, Darzynkiewicz Z (2006) Effects of hydroxyurea and aphidicolin on phosphorylation of ATM on Ser 1981 and histone H2AX on Ser 139 in relation to cell cycle phase and induction of apoptosis. Cytometry A 69A:212–221
44. Kurose A, Tanaka T, Huang X, Traganos F, Darzynkiewicz Z (2006) Synchronization in

the cell cycle by inhibitors of DNA replication induces histone H2AX phosphorylation, an indication of DNA damage. Cell Prolif 39:231–240

45. Rogakou EP, Pilch DR, Orr AH, Ivanova VS, Bonner WM (1998) DNA double-stranded breaks induce histone H2AX phosphorylation on serine139. J Biol Chem 273:5858–5868
46. Sedelnikova OA, Rogakou EP, Panuytin IG, Bonner W (2002) Quantitive detection of ^{125}IUdr-induced DNA double-strand breaks with γ-H2AX antibody. Radiat Res 158:486–494
47. Lavin MF, Kozlov S (2007) ATM activation and DNA damage response. Cell Cycle 6:931–942
48. Darzynkiewicz Z, Zhao H, Halicka HD, Rybak P, Dobrucki J, Wlodkowic D (2012) DNA damage signaling assessed in individual cells in relation to the cell cycle phase and induction of apoptosis. Crit Rev Clin Lab Sci 49:199–217
49. Traven A, Heierhorst J (2005) SQ/TQ cluster domains: concentrated ATM/ATR kinase phosphorylation site regions in DNA-damage-response proteins. Bioessays 27:397–407
50. Darzynkiewicz Z, Bedner E, Li X, Gorczyca W, Melamed MR (1999) Laser scanning cytometry. A new instrumentation with many applications. Exp Cell Res 249:1–12
51. Pozarowski P, Holden E, Darzynkiewicz Z (2013) Laser scanning cytometry: principles and applications. An update. Methods Mol Biol 913:187–212
52. Zhao H, Traganos F, Darzynkiewicz Z (2010) Kinetics of the UV-induced DNA damage response in relation to cell cycle phase. Correlation with DNA replication. Cytometry A 77A:285–293
53. Yajima H, Lee KJ, Zhang S, Kobayashi J, Chen BP (2009) DNA double-strand break formation upon UV-induced replication stress activates ATM and DNA-PKcs kinases. J Mol Biol 385:800–810
54. Darzynkiewicz Z (2011) Redundancy in response to DNA damage: the key to protection of genome integrity. Cell Cycle 10:3425–3426
55. Tanaka T, Halicka HD, Huang X, Traganos F, Darzynkiewicz Z (2006) Constitutive histone H2AX phosphorylation and ATM activation, the reporters of DNA damage by endogenous oxidants. Cell Cycle 5:1940–1945
56. Kajstura M, Halicka HD, Pryjma J, Darzynkiewicz Z (2007) Discontinuous fragmentation of nuclear DNA during apoptosis revealed by discrete "sub-G_1" peaks on DNA content histograms. Cytometry A 71A:125–131
57. Tanaka T, Kurose A, Huang X, Dai W, Darzynkiewicz Z (2006) ATM kinase activation and histone H2AX phosphorylation as indicators of DNA damage by DNA topoisomerase I inhibitor topotecan and during apoptosis. Cell Prolif 39:49–60
58. Huang X, Traganos F, Darzynkiewicz Z (2003) DNA damage induced by DNA topoisomerase I- and topoisomerase II-inhibitors detected by histone H2AX phosphorylation in relation to the cell cycle phase and apoptosis. Cell Cycle 2:614–619

Chapter 8

Chromosome Formation During Fertilization in Eggs of the Teleost *Oryzias latipes*

Takashi Iwamatsu

Abstract

Upon fertilization, eggs shift their cell cycle from the meiotic to the mitotic pattern for embryogenesis. The information on chromosome formation has been accumulated by various experiments using inhibitors to affect formation and behavior of chromosomes in the cycle of cell proliferation. Based on experimental results on meiosis and early stages of development of the teleost *Oryzias latipes*, we discuss the roles of the activities of histone H1 kinase, microtubule-associated protein kinase, DNA polymerase, DNA topoisomerase, and other cytoplasmic factors in formation and separation of chromosomes.

Key words Teleost, Meiosis, Fertilization, DNA replication, Chromosome formation, Chromosomal separation, Aphidicolin, Camptothecin

1 Introduction

1.1 Meiosis in Non-mammalian Vertebrates

In the ovary, proliferating oogonia shift from a mitotic cell cycle to a meiotic cell cycle as they differentiate to follicle-enclosed oocytes. Then in response to junctional interactions with the surrounding follicle cells, oocytes interrupt their first meiotic cell division at prophase (Pro I arrest) while they continue to grow until substances and structures indispensable for early embryonic development are fully accumulated. This process is aided by the hormonally cooperative actions of gonadotropins and the follicle cells that are in intimate contact with the oocyte. In most animal species the oocyte in the preovulatory follicle is arrested at metaphase of the first or second meiotic division, and meiosis is completed upon fertilization followed by initiation of embryonic mitotic divisions. Thus, in life cycle transition from mitotic to meiotic cell cycle is seen at the time of differentiation of oogonia to oocytes in the ovary, while the opposite transition from meiosis to mitosis occurs at fertilization.

In non-mammalian vertebrates, meiosis of fully grown oocytes remains arrested at the germinal vesicle (GV) stage until the oocytes acquire the ability to respond to maturation-inducing

Gaspar Banfalvi (ed.), *Cell Cycle Synchronization: Methods and Protocols*, Methods in Molecular Biology, vol. 1524,
DOI 10.1007/978-1-4939-6603-5_8,

hormone (MIS) secreted by mature follicle cells. When expression of maturation-promoting factor (MPF) [1] is induced in the ooplasm upon stimulation by MIS, fully grown fish oocytes begin to undergo cytoplasmic maturation. In response to MIS, the fully grown oocytes begin to undergo cytoplasmic maturation. In response to MIS, the fully grown oocytes, which have a supply of inactive MPF (a complex of p32cdc2 and cyclin B), form active MPF through the de novo synthesis of cyclin B and then resume meiosis (germinal vesicle breakdown, GVBD) (Fig. 1) [2]. Thus, meiosis is released from Pro I arrest and then proceeds to metaphase of the second meiotic division (Meta II) (Pro I-Meta II transition), at which time meiosis stops again (Meta II arrest). During the period from GVBD to Meta II arrest, maturing preovulatory oocytes acquire fertilizability (the ability to respond to sperm penetration), and a cytostatic factor (Mos protein kinase) [3–5] is de novo synthesized from dormant maternal mRNA stored in the ooplasm. Meta II-arrested vertebrate oocytes are ovulated as eggs and complete meiosis with extrusion of the second polar body upon sperm penetration. Resumption of meiosis in the oocyte involves the activation of MPF, inactivation of which is associated with degradation of cyclic B upon fertilization. Proteasomes participate in degradation of cyclic B, the decrease in MPF activity and completion of the first meiotic division (polar body extrusion)

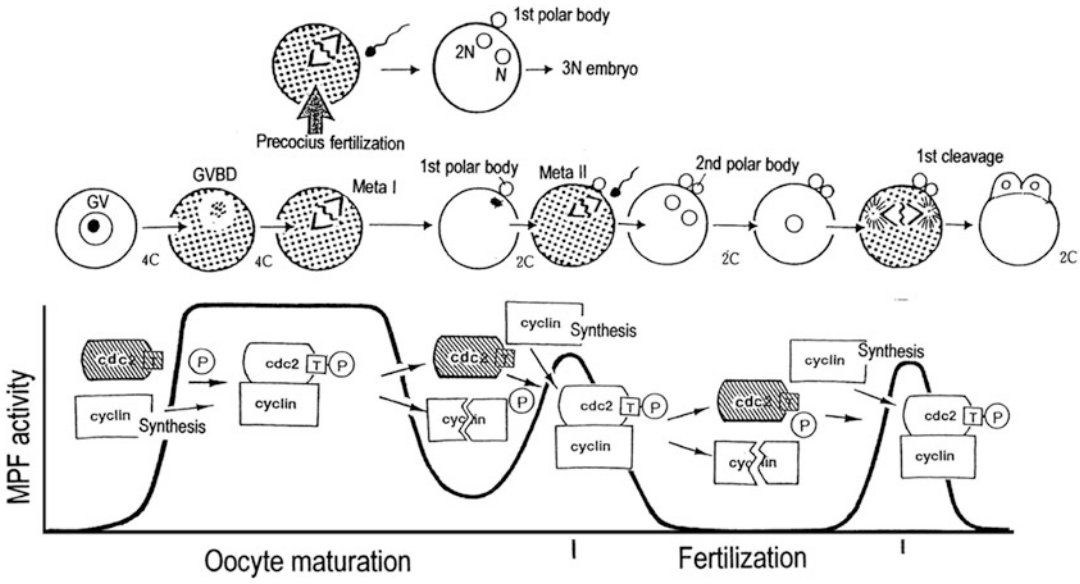

Fig. 1 Profile of maturation-promoting factor (MPF) activity in early *Oryzias* development. Maturation-inducing hormone (MIS) releases oocytes from the first arrest allowing them to proceed through the two consecutive meiotic cell divisions without DNA replication. An increase in MPF activity is required for entry into the meiotic metaphases (Meta I, Meta II). The mature oocytes (eggs) arrest again at the second meiotic metaphase (Meta II) until fertilization. Upon fertilization or precocious fertilization, the egg shifts from meiotic cell division to mitotic cell division

in goldfish [6] and rat [7] oocytes. Thus, upon fertilization, eggs shift their cell cycle from the meiotic to the mitotic pattern for embryogenesis. At the G2/M transition, MPF induces mitosis by phosphorylation of a variety of structural and regulatory proteins that control mitotic processes such as chromosome condensation, spindle assembly, and nuclear envelope breakdown [8].

It has been generally believed that at the final step of fertilization, chromosomes of the zygote nucleus are formed around the time of karyogamy. Two types of karyogamy occur in the process of fertilization in different species [9]: the male and the female pronuclei associate in the central region of the egg cytoplasm with or without pronuclear membrane fusion. In fish eggs, which have discoidal cleavage, chromosome formation begins within the fused zygote nucleus in the period from the termination of DNA replication to the pronuclear karyogamy. The condensed chromatin becomes first visible by electron microscopy at the early stage of pronuclear membrane fusion [10]. Although most of the investigations mentioned here concern fish oocytes or eggs, some new data on chromosome formation during fertilization in other organisms will be described. We expect readers to find pivotal questions for understanding the mechanisms of chromosome formation during fertilization.

To elucidate the factors involved in cytoplasmic control of chromosome formation during early development of the fish, we have examined chromosomal behavior at various developmental and experimental conditions by applying the following materials and methods.

1.2 Chromosome Behavior in the Precocious Fertilization of Prevoluntary Oocytes

Non-activated oocytes penetrated by a spermatozoon contain metaphase chromosome arrays within 20 min post-insemination. In mammalian oocytes, the cytoplasm develops the ability to transform the highly condensed chromatin of the sperm into metaphase chromosomes [11]. Similar observations on the transformation of sperm nuclei into metaphase chromosomes in non-activated immature oocytes have been reported previously for *Urechis* [12], an amphibian [13, 14], and mammals (mouse) [15, 16]. Early experiments in amphibians in which the nucleus was transplanted into non-activated oocytes with MPF and CSF activity also revealed that the nuclei were transformed to metaphase chromosomes [17–19]. Based on these findings, Masui et al. [20] proposed that the ooplasmic activity that promotes condensation of metaphase chromosomes could be sustained only at low levels of intracellular Ca^{2+}. According to data obtained in a cell-free system from the amphibian oocyte, the levels of free Ca^{2+} may play an important role in controlling nuclear behavior [21]. We also verified the role of intracellular Ca^{2+} in chromosomal condensation in *Oryzias* oocytes. Oocyte activation, probably dependent on the loss of MPF activity caused by an increase in the intracellular Ca^{2+} concentration and pH, is indispensable for the transformation of gamete nuclei into pronuclei. Both an internal calcium increase and an internal pH rise are responsible for meiosis reinitiation from prophase I (*see* [9]).

In vertebrate oocytes, MPF activity appears as a result of mixing the nucleoplasm with the cytoplasm after GVBD, and it diffuses throughout the ooplasm based on observations that chromosomal formation from incorporated sperm nuclei could be observed during the period after GVBS but not before or at the time of GVBD. This is different from the situation of marine invertebrates such as the brittle star [22], the starfish, oyster, and the surf clam [23, 24], in which maturing oocytes may have the ability to form female meiotic chromosomes only within the restricted cytoplasm containing the GV materials but not form male chromosomes from the incorporated sperm nucleus. The requirement for GV material for chromosomal formation has been demonstrated experimentally in previous studies on fish oocytes [25, 26] in which no chromosomes from the penetrated sperm nucleus could be found in blastomeres formed from inseminated oocytes that had been matured without GVBD. A similar finding, that the development of chromosomal condensation activity depends upon the release of some component(s) from the GV, has been reported by Ziegler and Masui [18] for amphibian oocytes.

During fertilization processes, dynamic responses take place in nuclei of both the egg and the spermatozoon: the resumption of meiosis, breakdown of the poreless nuclear envelope [27, 28], reduction of disulfide bonds in protamines [29, 30], decondensation of chromatin, replacement of protamines by histones [31–36], reformation of the nuclear envelope [27], DNA replication [37–41], and chromosome formation [42]. In mitosis, the formation and behavior of chromosomes involve consecutive changes such as cohesion, condensation, and separation of chromosomes following DNA replication.

1.3 DNA Synthesis in the Period from Sperm Penetration to Karyogamy

In fish eggs, chromatin condensation and transformation of the penetrated sperm nucleus to the pronucleus take place in cytoplasm lacking MPF activity between 3 and 30 min post-insemination. The sperm nucleus undergoes breakdown of the nuclear envelope and transforms to a large male pronucleus by reformation of the nuclear envelope under these cytoplasmic conditions. Judging from the result of experiments [43] with inhibitors, DNA synthesis, transcription, protein synthesis, and phosphorylation-sensitive 6-DMAP may not be required for nuclear behavior in fertilization processes from sperm penetration to karyogamy.

When fertilized during maturation, oocytes of the starfish initiate the first DNA replication shortly after the end of meiosis [44]. Why the penetrated sperm nucleus neither transforms into the male pronucleus (or meiotic chromosomes in harmony with the oocyte nucleus) nor initiates DNA replication until meiosis finishes in the oyster and the starfish is not known at present. Starfish oocytes that are naturally fertilizable at any stage of meiosis are

endowed with a built-in stability of the cell cycle driving mechanism that can be looked upon as a substitute for the metaphase arrest observed in most vertebrate eggs [130].

In zygotes of many animals, DNA synthesis occurs simultaneously in both female and male pronuclei as they migrate toward each other after fertilization and before pronuclear fusion [45–47]. The timing of DNA replication in mammals has been determined by measuring the incorporation of ^{3}H-thymidine or 5-bromodeoxyuridine (BrdU) into pronuclei. It is 7–11 h post fertilization (pf) [48] or 8–13 h pf [37] in the mouse, 5–6.5 h pf [49] in the golden hamster, and 3–5 h pf (44) or 3–6 h pf [50] in the rabbit. In the sea urchin *Arbacia*, DNA synthesis normally follows pronuclear fusion and occurs in the zygote nucleus about 16 min post-insemination at 20 °C [51]. Increases in both the intracellular Ca^{2+} concentration and the pH appear to be required for the initiation of DNA synthesis in sea urchin eggs [52]. These increases synchronize with the decline in MPF (histone H1 kinase) activity and act as regulatory signals for cell cycle control and stimulation of DNA replication [53]. In normal mitotic cell cycle, MPF is held in its inactive form by tyrosine phosphorylation of its p34cdc2 subunit until DNA replication is completed [54–56]. In this connection, calyculin A induces an increase in MPF activity and chromosome condensation [57] and specifically inhibits the protein phosphatases (pp1 and pp2) that are involved in the initiation of DNA replication in *Xenopus* egg extracts [58].

In unfertilized *Oryzias* eggs with an adequate amount of fluorescent-labeled BrdU microinjected into the cortical cytoplasm in advance of fertilization, the earliest BedU fluorescence is detected in developing pronuclei of eggs 15 min post-insemination [59]. The synchronized DNA synthesis of the migrating female and male pronuclei is observed in eggs that were microinjected with BrdU 25 min post-insemination, as previously reported for the hamster egg [38]. However, eggs no longer show labeled pronuclei when injected with BrdU after 30 min post-insemination. If fertilized eggs with BrdU microinjected into the cytoplasm are incubated in 10 μg/ml aphidicolin saline at 27 °C, no incorporation of BrdU into the pronuclei is observed at the end of a 30 min incubation. These results reveal that DNA synthesis occurs during a period between 15 and 30 min post-insemination in *Oryzias* eggs.

1.4 Chromosome Formation in the Period from Sperm Penetration to Karyogamy

In fertilized eggs, the changes in the sperm nucleus occur synchronously with the progression of meiotic from Meta II to interphase in the egg nucleus, being perhaps controlled by cytoplasmic factors such as MPF and MAP (microtubule-associated protein) kinase activities [60–63]. The interaction of increased intracellular Ca^{2+} with ooplasmic components upon fertilization brings about a loss of the MPF activity which in turn induces the formation of metaphase chromosomes [21]. The data obtained with fish eggs also

confirm the important roles of MPF activity in regulating nuclear envelope disassembly, chromosome condensation, and spindle formation for the first cleavage [43].

During the fertilization processes in an *Oryzias* hybrid between *O. latipes* and *O. javanicus*, chromosome condensation occurs more slowly in the *O. javanicus* male pronucleus than in the female *O. latipes* pronucleus in the cytoplasm of *O. latipes* eggs [64]. This time lag leads to the preferential elimination of *O. javanicus* chromosomes in the hybrid cells [65]. This may infer that the hybrid zygotes lack some cytoplasmic factors involved in DNA replication or chromosome condensation and needed to form the individual sister chromatids of *O. javanicus* in the ooplasm of *O. latipes*. The resulting probably aberrant *O. javanicus* chromosomes would be lost from blastomeres during cleavage because they missed the proper timing of normal chromosome formation. Similarly, human sperm chromosomal regions replicate later than the female regions in the golden hamster egg [40]. According to the results of genetic and cytoplasmic approaches in *Drosophila*, the correct timing of DNA replication may be essential for the assembly of chromatin that is fully competent to undergo chromosome condensation in mitosis [66].

1.5 Effects of Inhibitors on Chromosomal Behavior in the Zygote

For the faithful segregation of chromosomes with their pivotal genetic information, metaphase chromosomes consisting of two separable sister chromatids are formed during or soon after chromosome duplication. At the onset of the metaphase to anaphase transition, the cohesion between the condensed sister chromatids is dissolved, thereby allowing the chromosomes to be pulled apart toward opposite poles of the blastodisc by the spindle microtubules. Specific inhibitors of various enzymes that participate in chromosome formation are used to examine the behavior of chromosomes during cell division, since the behavior of chromosomes must reflect their structural features. The relationship between the changes in gamete nuclei and MPF activity has been analyzed using inhibitors of DNA synthesis and chromosome segregation during fertilization.

1.5.1 DNA Polymerase α Inhibitor, Aphidicolin

Eukaryotic DNA polymerase α that is located in the GV of fully grown oocytes of the toad [67], the frog [68–70], the sea urchin [71], and the starfish [72, 73] shifts to the endoplasmic reticulum or granules in the cytoplasm when the GV breaks down [67, 74]. Aphidicolin is a specific inhibitor of DNA polymerase α and is known to inhibit replicative DNA synthesis, namely DNA replication but not RNA and protein [75–78]. In aphidicolin-treated starfish *Asterina pectinifera* zygotes [79], the mitotic spindle (mitotic apparatus) develops and grows, but although the chromatin mass is free of the nuclear envelope, it does not associate with the mitotic apparatus and remains as a linear rod-like chromatin structure near the first cleavage furrow. In the advanced stages of cleavage in aphidicolin-treated embryos, observations by electron

microscopy show that the nuclear envelope is not reformed after Meta I, and the chromatin mass is dispersed in the cytoplasm, indicating that aphidicolin causes achromosomal cleavage in fertilized starfish eggs [80, 81]. In the presence of aphidicolin, the cell cycle of the egg cytoplasm progresses independently of DNA synthesis blockade and the formation of abnormal chromosomes, so that the subsequent cleavages give rise to achromosomal blastomeres. This abnormality of chromosome separation reflects the formation of incomplete chromosomes which is induced by aphidicolin treatment only during the limited period of the restricted pronuclear migration (about 10 min) from the end of DNA synthesis to the encounter of the pronuclei. Aphidicolin seems to interfere with reformation of the nuclear envelope, the resolution of intramolecular DNA folding, and the organization of kinetochores [82, 83] subsequent to the inhibition of DNA synthesis.

Aphidicolin prevents chromosomal DNA replication but does not prevent meiotic maturation divisions in oocytes of the starfish [84]. During fertilization of fish eggs, the morphological processes of the second meiotic division also occur normally in the presence of aphidicolin. On the other hand, in non-activated, fertilized eggs with high histone H1 kinase and MAP kinase activities, the compact nucleus (haploid) of a penetrated spermatozoon is also directly transformed to the same meiotic metaphase chromosomes (Meta III) as female meiotic Meta II in the presence of aphidicolin. The male chromosomes that are formed without formation of a male pronucleus and DNA synthesis are normally segregated into two anaphase chromosomal masses, when the egg is artificially activated [59]. Thus the difference between meiotic and mitotic chromosomes that are formed under conditions preventing DNA synthesis is whether or not the chromosomes are separable in the cell division. This difference infers at least a possibility that aphidicolin may intervene in short process (only about 10 min) of forming separable chromosomes while DNA synthesis is inhibited in mitosis, unlike the simple pairing of homologous chromosomes in meiosis.

As already found in simian virus 40, complete separation of parental DNA strands is not observed when the polymerization reaction is inhibited by aphidicolin, which induces supercoiling in replicative intermediate DNA [85]. From the results obtained using novobiocin and aphidicolin, Droge et al. [85] conclude that DNA synthesis and strand separation are closely linked.

1.5.2 DNA Topoisomerase Inhibitors

In fish eggs, the effects of camptothecin (inhibitors of DNA topoisomerase I (topo I)) [86–88], etoposide, and β-lapachone (inhibitors of DNA topoisomerase II (topo II)) on formation of individual sister chromosomes were examined [89]. Results of these experiments revealed that only camptothecin-treated eggs displayed an aberrant segregation of chromosomes in the first cleavage, as seen in aphidicolin-treated eggs. A similar effect has been obtained in

fertilized starfish eggs exposed to different topo I inhibitor, kalihinol F, that does not inhibit topo II and chromosomal DNA synthesis [89]. In the starfish, inseparable metaphase chromosomes are formed at the first cleavage, when fertilized eggs are exposed to kalihinol F during the second meiotic period for about 20 min after the extrusion of the first polar body and formation of the female pronucleus. This period precedes chromosomal DNA synthesis and pronuclear fusion [45–49]. These results indicate that topo I inhibition cannot affect the formation process of meiotic sister chromosomes in non-activated fish egg [59], suggesting that the enzyme topo I has a pivotal function in the formation of mitotic chromosomes in starfish and fish embryos.

What step in chromosome formation could be affected by topo I inhibitor? So far the mechanism of action of topo I inhibitors in formation of inseparable sister chromatids remains unknown. Camptothecin inhibits the relaxation of supercoiled DNA induced by topo I [90] during DNA synthesis in HeLa cells by more than 80% [91] as well as the DNA rejoining step catalyzed by eukaryotic topo I [86, 87]. A possible function of topo I in DNA replication is also suggested by its swivel-like enzymatic activity [92]. The abnormality of metaphase chromosomes may be related to (1) the formation of a camptothecin-induced cleavage complex or (2) the specific interference by camptothecin in the swivel mechanism of topo I, which possibly leads to the inhibition of both DNA and RNA syntheses [91, 93]. Topo I activity is also required for proper chromosomal segregation in a prokaryote *Escherichia coli* [94, 95]. Further experiments examining the function of topo I on formation and segregation of chromosomes will help to elucidate the mechanism of formation of chromosomes capable of normal segregation in cell division.

Although a topo II inhibitor has no inhibitory effects on the formation of individual meiotic or mitotic chromosomes in fertilized fish eggs, there have been extensive investigations on the participation of topo II in successful sister chromosomes segregation in meiosis and mitosis of the yeast [96–99], *Drosophila* [100], surf clam [101], frog [102, 103], mouse oocytes [104–108], Chinese hamster eggs [109], and kangaroo rat eggs [110]. Intertwined both positively and negatively supercoiled DNA can be relaxed by topo II which transiently breaks and rejoins double-stranded DNA in the presence of ATP [111–115]. Topo II is required in the mitotic cell division cycle for untangling intertwined sister chromosomes following the completion of DNA synthesis [116–119]. According to the two-step scaffolding model [120], topo II α is initially required for the decantation of DNA fibers to generate individual chromosomes into mature mitotic forms. In chromosomal formation, the structural maintenance of chromosome (SMC) protein complexes, condensins and cohesins, plays central roles in chromosome condensation and sister chromatin cohesion, respectively. Recently, aberrant segregation has been considered to

result from incomplete formation of mitotic chromosomes from newly replicated DNA in the absence of the activity of key components such as DNA topoisomerases and condensin [121].

Although a tremendous number of genetic and biochemical investigations have been carried out during the last 30 years [122–124], the mechanism of chromosomal formation during the fertilization processes remains to be unraveled. There is also little information on how the architecture of mitotic chromosomes might be organized following DNA replication in pronuclei during fertilization processes. During the fertilization of the surf clam, the female and male nuclei behave differently within the same ooplasmic conditions. The oocyte nucleus undergoes consecutive meiotic divisions independent of the behavior of the sperm nucleus. More biochemical information on the existence of a presumptive regulatory factor [9] or cytoplasmic compartment in the oocyte should also provide a deeper insight into the intracellular mechanism of chromosomal formation during fertilization. In particular, elucidation of the loss or non-disjunction of chromosomes in interspecific hybrid zygotes could solve a crucial question on the specific molecular mechanism for formation of complete individual chromosomes; however, we are still too early in the research to answer this mysterious question. Further investigations using gene targeting methodology to clarify chromosome formation have made it possible to test which key components are required for the processes of fertilization including the steps from DNA replication to chromosome formation in embryogenesis.

2 Materials

2.1 Reagents

1. Alkaline phosphatase-conjugated goat anti-mouse immunoglobulin G (Tago, Burlingame, CA, USA).
2. Alkaline phosphatase-conjugated rabbit anti-mouse immunoglobulin G (Amersham, Little Chalfont, Buckinghamshire, UK).
3. Aphidicolin (Wakojunyaku-kogyo, Osaka, Japan).
4. [γ-^{32}P]-ATP (NEN Research Products, Boston, MA, USA).
5. Biotinylated anti-mouse sheep IgG (Amersham).
6. Chloretone (acetone chloroform; Nakarai Chemicals, Kyoto).
7. FITC-conjugated goat antibody against mouse IgG (Amersham).
8. FITC-conjugated streptavidin (Amersham).
9. Hoechst 33258 (Hoechst AG, Melbourne, VIC, Australia).
10. Monoclonal antibody against α-tubulin YL1/2 (Sera Laboratory, Crawley Down, Sussex, England).
11. Monoclonal antibody against BrdU (Becton Dickinson) Immunocytometry stems, CA, USA).

12. Monoclonal mouse antibody against single-stranded DNA (Chemicon International, EL Segundo, CA, USA).
13. MS222 (meta-aminobenzoic acid ethyl ester methane sulfonate; Sandoz Ltd., Switzerland).
14. Ploy vinylidene difluoride membrane (Immobilon; Millipore, Bedford, MA, USA).
15. RX-H X-ray film (Fuji, Tokyo, Japan).
16. All other chemicals are commercial chemical substances and personal gifts.

2.2 Gametes

1. Mature medaka fish *Oryzias latipes* (Local fish farmer, Yamato-Kouriyama, Nara Prefecture, Japan). Keep fish under artificial reproductive conditions (26–28 °C, 14 h illumination) for at least 2 weeks before use.
2. Isolate oocytes into saline (123) from ovaries of females that had spawned every day. Under these reproductive conditions, oocytes are at the GVBD stage 5–6 h before the onset of light [125].
3. Prepare sperm suspension ($2–3 \times 10^7$ cells/ml) for insemination by removing testes from mature males and releasing spermatozoa into saline or a test solution contained in a depression glass slide.

3 Methods

3.1 Experimental Procedures in Oocytes

1. Transfer female fish that had spawned every day into a dark, cold (water temperature, 10 °C) chamber 10 h before onset of light.
2. Return them 10 h later to an aquarium at 27 °C (R27).
3. Fix aliquots of oocytes obtained from the ovaries at various times after R27 immediately with 2% glutaraldehyde-1.5% paraformaldehyde (0.1 M phosphate buffer, pH 7.4) for cytological observation.
4. Inseminate the remaining oocytes at given time intervals after R27.
5. Calculate the rates of egg activation and sperm penetration on the basis of the numbers of activated oocytes and the percentage of oocytes with sperm nucleus in the cortical cytoplasm at the end of 30 min immersion in sperm suspension.

3.2 Treatment of Eggs with Drugs

1. Pretreat unfertilized eggs with 10 μg/ml actinomycin D (RNA synthesis inhibitor), 10 μg/ml aphidicolin (inhibitor of DNA polymerase α), 25 μg/ml cycloheximide (protein synthesis inhibitor), or 5 mM 6-dimethyl-aminopurine (6-DMAP; protein phosphorylation inhibitor) for 30 min (27 °C) prior to insemination, as mature eggs became overripe during the long treatment.

2. Just before each experiment, dilute stock solutions of 1 mg/ml actinomycin D and 10 mg/ml aphidicolin in dimethyl sulfoxide (DMSO) with saline. Dissolve the other drugs directly in saline just before each experiment.
3. Inseminate and incubate the pretreated eggs in saline containing each drug at the same concentration as during pretreatment (*see* **Note 1**). Present values as mean ± SE μm.
4. Prepare a stock solution of each inhibitor (aphidicolin, camptothecin, etoposide, and β-lapachone) by dissolving it in DMSO.
5. For testing, dilute each stock solution in saline to yield a concentration of 10 μg/ml of inhibitor and 0.1% DMSO. This concentration of DMSO has no effect on the morphological events of fertilization, including formation of spindle and chromosomes for the first cleavage.
6. Preincubate eggs for 30 min at 27 °C by immersion in the test solutions.
7. Inseminate the pretreated eggs by spermatozoa suspended in the same solution.
8. In other experiment, pretreat unfertilized eggs by immersing in saline containing 10 μg/ml of inhibitor and 0.25% anesthetic MS222 for 30 min and then inseminate by spermatozoa suspended in the same saline: 0.25% MS222 saline (10 ml) supplemented with 0.08 ml of 1 N NaOH and buffered pH 7 with 10 mM HEPES buffer.
9. To ascertain the time during fertilization that eggs were sensitive to aphidicolin, expose eggs to 10 μg/ml aphidicolin saline for given times post-insemination at 27 °C.

3.3 Cytological Assessment of Oocytes Before and After Activation

1. Examine the nuclear states of the oocytes by staining them with Hoechst 33258 dye (0.1–0.2 μg/ml of 50% glycerol) after gametes were fixed in 4% glutaraldehyde in 0.1 M phosphate buffer (pH 7) for at least 30 min at room temperature.
2. For examination of the cortical cytoplasm, use a pair of scalpels under a binocular dissecting microscope (×20) to isolate the cortex at the animal pole region from the yolk mass of fixed eggs in distilled water.
3. Mount the cortical cytoplasm with a small amount of distilled water on a clean glass slide [126].
4. Measure the distribution (diameter) of chromosomes and the diameter of interphase nuclei with nuclear envelopes by micrometer under a fluorescence microscope (Olympus BH-2, ×400).
5. To prepare cells for observation of chromosomes, place morulae in a depression glass slide coated with Sigma-coat and containing L15 culture medium with 0.4% bovine serum albumin and 0.0003% colchicine.

6. Cut the chorions deeply at the vegetal pole region with a pair of scalpels, and separate cells by carefully vibrating the chorions with forceps before the cells are pushed out of the opening cut in each chorion.
7. After removal of empty chorions, incubate the cell suspension for 60–90 min at 27 °C.
8. Wash cells five times for 15–20 min at room temperature in 3 ml of 0.7% Na-citrate.
9. Collect swollen cells in a small pipette.
10. Mount the cell suspension on a cold Carnoy's fixative and spread cells by gently blowing on the glass slide.
11. Then dry the slide immediately over a flame on alcohol lamp.
12. After the slide is completely dried, stain the chromosomes with Hoechst dye and observe under fluorescence microscope.
13. For examination of the aster and spindle, fix eggs in 0.25% glutaraldehyde, 4% paraformaldehyde, 3% Triton X-100, 3 μM taxol, 5 mM ethyleneglycol-bis-(amino-ethylether)-*N*,*N*,*N*′,*N*′-tetraacetic acid (EDTA), 1 mM $MgCl_2$, 80 mM piperazine-*N*,*N*-bis[2-ethanesulfonic acid] (PIPES), pH 6.8 (MTSB), for 6 h at room temperature and store in methanol (−20 °C) for approximately 12 h.
14. Rinse the fixed eggs in PBS (136 mM NaCl, 2.5 mM KCl, 8 mM Na_2HPO_4, 1.5 mM KH_2PO_4, pH 7.4).
15. Stain their microtubules immunologically by incubating the eggs in PBS containing 0.1% Tween 20, a monoclonal antibody against α-tubulin YL1/2 (1:100), and a fluorescein isothiocyanate (FITC)-conjugated goat antibody against mouse IgG for 12 h at 4 °C.
16. Following five rinses in PBS for 5 min each, incubate the eggs in PBS containing 50% glycerol and 0.1 μg/ml Hoechst 33582 for 20 min at room temperature.
17. Isolate the slightly thickened cortex of the animal pole region from the spherical yolk mass of the eggs by dissecting with a pair of scalpels.
18. Mount samples on a clean glass slide and cover with a coverslip.
19. Observe the samples by fluorescence microscopy.

3.4 Anesthetization of Eggs

1. In order to anesthetize mature eggs, dissolve 5 mM chloretone or 0.25% MS222 in saline.
2. Adjust the 5 mM chloretone saline to pH 4.4 with 50 mM acetate buffer and supplement 10 mM of 0.25% MS222 saline with 0.1 ml of 1 N NaOH buffered to pH 7 with 20 mM HEPES-Na HEPES buffer.

3. Pretreat unfertilized eggs with anesthetic saline for 30 min (27 °C) and then inseminate for 1 min with sperm (2×10^7 spermatozoa/ml) suspended in anesthetic saline.
4. Rinse eggs for 4 min in anesthetic saline.
5. Incubate eggs in regular saline or saline containing a test drug.

3.5 Microinjection into the Egg

1. For microinjection into the egg, treat spermatozoa with 0.001% dodecylsulfate saline to damage the plasma membrane by sucking repeatedly in a small pore pipette for about 3 min on ice and rinse three times in saline by centrifugation ($1000 \times g$, 5 min).
2. Rinse unfertilized eggs three times in calcium- and magnesium-free (CMF) saline (128.3 mM NaCl, 27 mM KCl, 6.0 mM $NaHCO_3$, 0.2 mM EDTA, 4 mM HEPES-NaOH, pH 7).
3. Microinject about 1 nl of aequorin solution into the cortical cytoplasm by pressure (126).
4. Prepare aequorin solution by mixing 0.64% recombinant hcp-aequorin solution containing 50 mM KCl, 0.1 mM EDTA, and 10 mM MOPS, pH 7.3 (gift of Dr. O. Shimomura), with 1/4–1/5 vol of 20 mM $MgCl_2$ solution to remove free EDTA from the solution just before use.
5. Place the microinjected eggs in Mg-free physiological saline containing 0.2 mM $CaCl_2$ for 1 h to allow the injected aequorin to diffuse uniformly throughout the cortical cytoplasm.
6. Keep eggs in CMF saline in complete darkness.
7. In order to induce Ca^{2+} release and exocytosis (CABD) in the aequorin-loaded cytoplasm of unfertilized eggs, micro-inject about 0.3 nl of 0.5 mM $CaCl_2$ into the cortical cytoplasm at the animal pole of an egg held in CMF saline. Observe the easily visible CABD carefully and the disappearance of the cortical alveoli in translucent eggs with a binocular dissecting microscope.

3.6 DNA Synthesis

Measure the initiation time of DNA synthesis by detecting the fluorescently labeled nucleus of fertilized eggs from the time of sperm penetration.

1. In this experiment, microinject approximately 60 nl of saline containing 10 mM 5-bromo-2-deoxyuridine (BrdU) into the cortical cytoplasm at the animal pole region, as soon as exocytosis of cortical alveoli starts upon insemination.
2. Then fix eggs with 4% paraformaldehyde, 10% methanol, and 100 mM phosphate buffer, pH 7.0 (PMP fixative), for 6 h at room temperature.
3. To determine the duration of DNA synthesis, also microinject approximately 60 nl of 10 mM BrdU into the cortical cytoplasm at the animal pole region of dechorionated eggs, 20, 25, 30, and 40 min post-insemination. DNA synthesis is the period from sperm penetration to karyogamy.

4. Prepare dechorionated eggs according to a simplified procedure [127], by cutting off the chorion at the vegetal pole side with small scissors during exocytosis upon insemination.
5. Then, transfer BrdU-injected eggs into PMP fixative at the stage of karyogamy for 40 min post-insemination and fix for 6 h at room temperature.
6. Stain the BrdU-injected eggs with an anti-BrdU monoclonal mouse antibody.
7. Then counterstain the entire DNA with 0.1 μg/ml Hoechst 33582 [128].
8. After rinsing away the fixative, dissect out the cortical cytoplasm at the animal pole region from the egg yolk mass.
9. Subsequently incubate in a few drops of 4 N HCl for 2 h in a moist chamber to denature the DNA.
10. Following acid denaturation, rinse the slides three times with PBS.
11. Successively incubate the cortical cytoplasms on the slide in the moist chamber at 25–27 °C with the reagents listed below:
    (a) Monoclonal mouse antibody against BrdU (1:6 in PBS) for 2 h.
    (b) Biotinylated anti-mouse sheep IgG (1:50) for 1 h.
    (c) FITC-conjugated streptavidin (1:100) for 30 min.
    (d) Monoclonal mouse antibody against single-stranded DNA (1:10) for 1 h.
    (e) Hoechst 33582 containing 50% glycerol for 20 min at room temperature.
12. Rinse each incubation three tomes with PBS.

3.7 P13suc1 Precipitation

1. Rinse 30 eggs quickly three times in cold (0–4 °C) extraction buffer (100 mM β-sodium glycerophosphate, 40 mM Mes, pH 6.8, 30 mM EGTA, 65 mM $MgCl_2$, 3 μg/ml leupeptin, 100 μM phenylmethylsulfonyl fluoride (PMSF), and 1 mM DTT) in an Eppendorf tube (*see* **Note 2**).
2. Then add 60 μl of fresh extraction buffer.
3. Homogenize samples for 5 s (0–4 °C) and immediately place in liquid nitrogen.
4. Thaw samples and centrifuge at 15,000 × *g* for 15 min at 4 °C.
5. Supplement 60 μl of each supernatant with 6 μl of 1 M HEPES (pH 7.5) and mix with 10 μl of a 50% (v/v) suspension of p13suc1 beads, equilibrated previously with extraction buffer.
6. Following incubation overnight at 4 °C, wash the beads three times in cold washing buffer (modified extraction buffer supplemented with 0.2% Tween-20, 100 mM HEPES, pH 7.5), with an exchange of Eppendorf tube at the second wash.

7. Boil the washed beads for 3 min.
8. Analyze the beads by polyacrylamide gel electrophoresis (PAGE) in the presence of SDS (SDS-PAGE 12.5% gel) [129].
9. Following electrophoresis immunoblot with anti-cyclin B antibody, anti-cdc2 antibody, or anti-cdk antibody [130].

3.8 Histone H1 Kinase and MBP Kinase Assay

Histone H1 kinase assays were performed according to a modified procedure described elsewhere [131] and detailed below:

1. To detect histone kinase activity, transfer each group of 20 eggs into an Eppendorf tube.
2. Wash eggs rapidly three times within 10 s in an excess of extraction buffer (100 mM β-glycerophosphate, 40 mM Mes-Mes Na, 5 mM $MgCl_2$, 30 mM EGTA, 100 μM PMSF, 3 μg/ml leupeptin, and 1 mM DDT at 0–4 °C) in the Eppendorf tube.
3. Place eggs in 50 μl of extraction buffer (two eggs in 5 μl), homogenate for 5 s (0–4 °C), and freeze immediately in liquid nitrogen.
4. Immediately after thawing, spin down 10 μl of sample at 15,000 × *g* for 15 min at 4 °C.
5. Mix sample with 40 μl of a reaction medium containing 1.25 μM [γ-^{32}P]-ATP (1.36 mCi/μmol), 5.6 mM 2-mercaptoethanol, 25 mM Tris–HCl, pH 7.4, 5.6 mM adenosine triphosphate (ATP), 0.6 μM cAMP-dependent protein kinase inhibitor, 0.1 mM histone type III-S or 2 mg/ml lysine-rich histone H1, and 1.5 μCi/50 μl [γ-^{32}P]-ATP.
6. After various incubation times at 30 °C, stop the kinase reaction by the addition of 5 μl of 3 M phosphoric acid.
7. Absorb aliquots of samples onto P81 phosphocellulose paper (Whatman).
8. After extensive washing with 0.1 M phosphoric acid, measure the radioactivity remaining on the paper by liquid scintillation counting.
9. Measure MAP kinase activity by incubation of a final volume of 40 μl with 40 μg of myelin basic (MBP), 50 μM [γ-^{32}P]-ATP (2.5 mCi/μmol), and 5 μM protein kinase A inhibitor peptide for 15 min at room temperature.
10. Boil an aliquot of samples for 3 min, then separate the protein by SDS-PAGE.
11. Visualize phosphorylation of histone H1 by autoradiography, which is performed on dried gels with RX-H X-ray film.

3.9 Immunoblotting

1. Analyze samples of 30 eggs in each group. Following SDS/PAGE (12.5% separation gel) after precipitation with p13suc beads and electrotransfer to Immobilon, rinse the blots in

150 mM NaCl and 20 mM Tris–HCl (pH 7.5) and block for 1 h with 5% non-fat dry milk dissolved in TTBS (150 mM NaCl, 0.1% Tween-20, 0.01% NaN_3, and 20 mM Tris–HCl, pH 7.5).

2. After rinsing in TTBS for 10 min, incubate the membranes with an anticyclin B (1:1000 dilution of *Xenopus* cyclin B1 antibody; X1-158) or a 1:1000 cdk2 antibody (α-gold-fish cdk2C1-42) overnight at room temperature.
3. After three rinses in TTBS, incubate with 1:1000 or 2000 dilution of alkaline phosphatase-conjugated rabbit or goat anti-mouse immunoglobulin G (IgG) for 2 h.
4. Finally, wash three times by treating the membranes with 0.2 mM 5-bromo-4-chloro-3-indolylphosphate *p*-toluidine salt and nitroblue tetrazolium in 100 mM Tris–HCl buffer (pH 9.8) containing 1.0 mM $MgCl_2$ for visualization of phosphatase activity (AP-kit; Bio-Rad, Tokyo, Japan).

3.10 Chromosome Formation in Meiosis

To understand the formation and segregation of chromosomes in meiosis and mitosis, a number of cytological approaches have been developed using fertilized oocytes in which chromosomal formation is inhibited by chemical agents. The meiotic cell cycle that produces haploid gametes consists of two consecutive divisions in the absence of DNA synthesis.

1. The fully grown oocytes of a teleost, *Oryzias latipes*, gradually enlarge with the progression of meiotic divisions from the germinal vesicle (GV) stage (meiotic prophase I) to Meta II (meiotic metaphase II) for about 7 h (27 °C) after MIS stimulation.
2. Two hours before GV breakdown (GVBD), thread-like lampbrush chromosomes are scattered throughout the nucleoplasm of the GV as illustrated in Fig. 2 (*see* **Note 3**).
3. One hour later, the thread-like chromosomes condense to diminutive chromosomes that are shortened but remained in situ scattered within the GV. In oocytes just at the time of GVBD, divalent chromosomes aggregate at the central region of the GV. The aggregation of condensed chromosomes begins concurrently with nuclear envelope breakdown and the disappearance of the nucleoli.
4. One to two hours after GVBD, chromosomes at prometaphase (pro-Meta I) or metaphase (Meta I) of the first meiotic division are distributed on the spindle or arranged on the equatorial plate or the fist meiotic spindle, respectively.
5. Most oocytes 3–4 h after GVBD are at Meta I or anaphase (Ana I) of the first meiotic stage (*see* **Notes 4** and **5**).

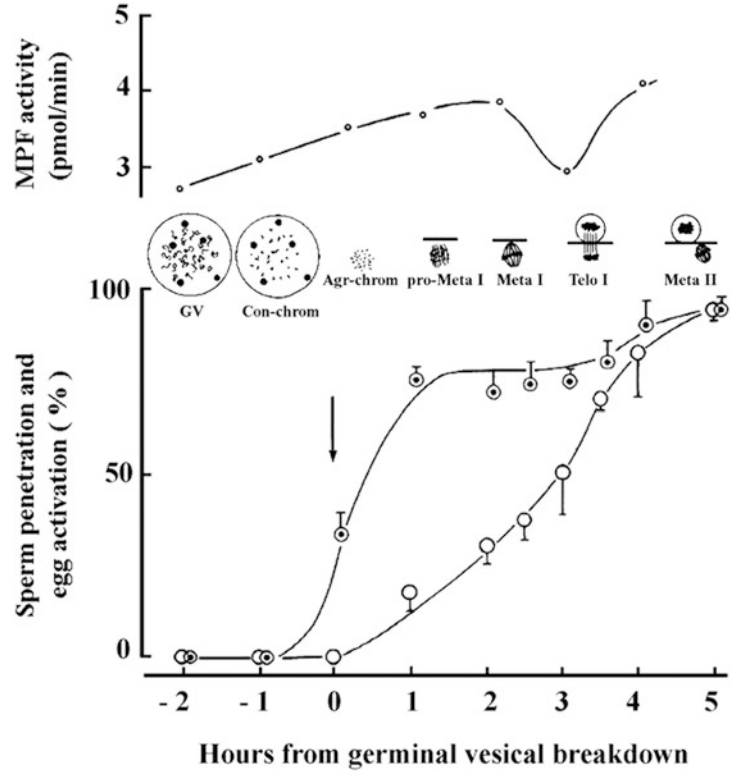

Fig. 2 Sperm penetration and oocyte response in the precocious fertilization of *Oryzias latipes*. The state of meiotic divisions from germinal vesicle (GV) breakdown (GVBD) to metaphase of the second meiotic division (Meta II), including condensation (con-chrom) and aggregation (agr-chrom) of chromosomes. Sperm penetration (*double circles*) is first seen at GVBD, and oocyte activation follows (*open circles*) 1 h later

6. About 5 h after GVBD, the oocytes ovulate. Following the extrusion of the first polar body, Meta II chromosomes of the egg align on the equatorial plate of the second meiotic apparatus, which occurs without intervening telophase and prophase stages (*see* **Notes 6** and 7).

3.11 Susceptibility of Metaphase Chromosomes to Aphidicolin in Fertilized Eggs

The treatment of fish eggs with aphidicolin that prevents both DNA replication and the cyclic change in MPF activity during fertilization also inhibits the formation of individual sister chromosomes that are normally separated into blastomeres at the time of the subsequent first cleavage [59].

1. To examine the time at which aphidicolin is effective in causing formation of aberrant chromosomes, treat un-fertilized eggs with aphidicolin for 30 min (27 °C).

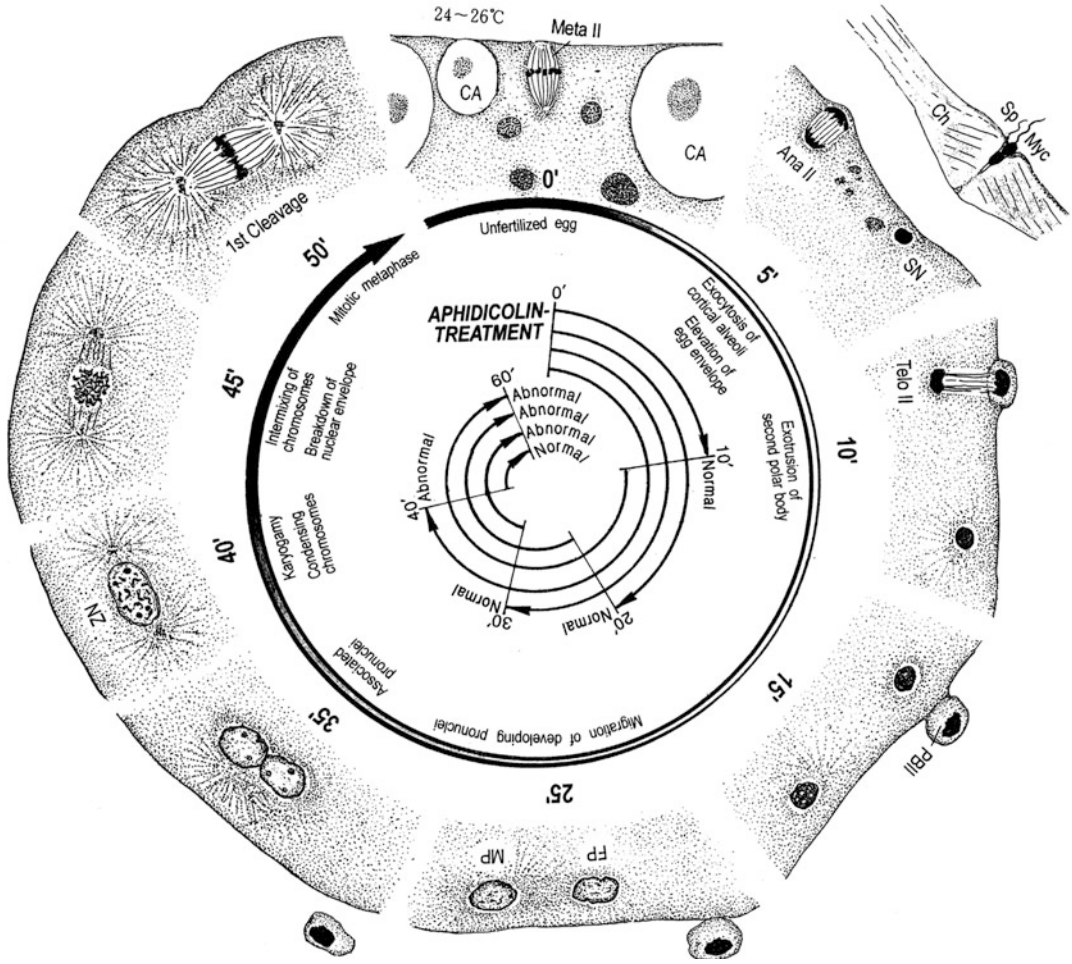

Fig. 3 Schematic illustration of nuclear behavior during fertilization of fish eggs. Numbers indicate the time (minutes) from insemination (0′) to the first cleavage (50′). The *large encircling arrow* indicates MPF activity (*shade of black*). In the central part of the illustration, the experimental procedure and the results of aphidicolin treatment are represented by the length of the *small arrows* indicating the time intervals of treatment. The effects of respective aphidicolin treatments are represented at the end of each *arrow* as "normal" or "abnormal" segregation of chromosomes (From ref. [77] (*see* **Note 8**))

2. Then inseminate in a sperm suspension containing aphidicolin (Fig. 3).
3. At the end of incubation with aphidicolin for a given time post insemination, rinse fertilized eggs and further incubate in regular saline until 70 min post-insemination, the time of the first cleavage.
4. Transfer eggs from aphidicolin containing saline to regular saline within 30 min post-insemination, to form normal interphase nuclei in each blastomere (*see* **Notes 8** and **11**).
5. In another experiment, immerse dechorionated eggs into saline containing aphidicolin at given times post-insemination.

6. Transfer from regular saline to saline containing the inhibitor within 30 min post-insemination and incubate until 70 min post-insemination (*see* **Note 10**).

In the fertilization of the fish *Oryzias* (Fig. 3), the nucleus of the spermatozoon (Sp) penetrates into the egg cytoplasm beneath the micropyle (Myc) in the chorion (Ch) 5 s post-insemination, and then meiotic chromosomes following Ana II aggregate compactly as the second polar body is extruded in the perivitelline space (Ps) 15 min post-insemination. Between 10 and 20 min post-insemination, the female pronucleus begins to migrate away from the second polar body toward the swollen male pronucleus. The female pronucleus encounters the male pronucleus at the center of blastodisc about 35 min post-insemination. The female and male pronuclei containing several nucleoli-like bodies fuse at adjacent region of their nuclear envelopes 40 min post-insemination. In the initial stage of nuclear fusion, chromatin condensation is not yet distinct. In the oval-shaped zygote nucleus of the most advanced stage, condensing chromatin mass is first detected throughout the nucleoplasm [10]. Forty-three minutes post-insemination, the irregularly shaped zygote nucleus, which starts to shrink, still contains the condensed chromosomes and nucleolus-like bodies. Forty-five minutes post-insemination, the zygote nucleus has a highly convoluted and collapsed nuclear envelope but no nucleolus-like bodies. In eggs at a more advanced stage, metaphase chromosomes are arranged on the equatorial plate of the first cleavage, and the sister chromatids are disentangled and then pulled to opposite poles of the zygote. Cytokinesis occurs about 60 min post-insemination.

These results show that in fertilized eggs the normal formation of individual metaphase chromosomes was susceptible to disruption by aphidicolin in a critical period between 30 and 40 min post-insemination (Fig. 3) (*see* **Note 11**). This is the limited period from the termination of DNA synthesis to the appearance of condensed chromatids in the zygote nucleus, corresponding to the period in which MPF has high activity to phosphorylate topo II α [82] or topo I. In the blastomeres of *Xenopus* embryos that are treated with aphidicolin, non-replicated chromatids are also frequently stretched out during the separation of chromatids at anaphase and telophase [83]. Thus, the effect of aphidicolin on sister chromosome formation during fertilization does not seem to be species-specific.

4 Notes

1. When ovarian intrafollicular oocytes of *O. latipes* are inseminated after mechanical removal of follicular cell layers including the micropylar cell, by use of a pair of fine forceps, the spermatozoon can penetrate into the egg cytoplasm through the

opened micropyle. Morphology and behavior of nuclei did not change in the period from sperm penetration to karyogamy.

2. The concentrations of EGTA and $MgCl_2$ in the buffer were modified to inhibit egg activation, as medaka eggs contain calcium and magnesium at high concentrations, probably in the yolk mass.
3. If oocytes are penetrated by a spermatozoon before or at the stage of GVBD, they fail to activate. The penetrated sperm nucleus is only slightly swelled in the cytoplasm of the non-activated oocytes.
4. Upon sperm penetration 1 h after GVBD, most oocytes in pro-Meta I undergo no or only partial activation with restricted exocytosis of cortical alveoli at a restricted region of the animal hemisphere. In these oocytes normal pronuclei are not formed. The partial activation may be due to an incomplete increase in the intracellular Ca^{2+} which partially inactivates MPF.
5. In contract, Meta I oocytes normally undergo full activation upon insemination. Meiotic Meta II chromosomes and the incorporated sperm nucleus transform into a diploid female pronucleus and a haploid male pronucleus by decondensation of the sperm chromatin immediately after the extrusion of the first polar body. Therefore, the ability to undergo normal exocytosis of cortical alveoli is intimately related to the loss of MPF activity which allows the cytoplasm to form pronuclei (Figs. 1 and 2).
6. The association of these abilities of the oocyte may be mediated by common cytoplasmic factors, such as intracellular Ca^{2+}, inositol 1,4,5-triphosphate (IP_3), pH, and/or the sensitivity of these oocytes. In mouse oocytes, the increase in intracellular calcium can differ depending on the stage of maturation, and the oocytes appear to develop an increased sensitivity to IP_3 during the course of maturation [132].
7. When a fertilizable fish oocyte is activated upon insemination, an incorporated sperm nucleus rapidly transforms into a pronucleus. A diploid female pronucleus (2n) is formed after the extrusion of the first polar body. The diploid female and the haploid male pronuclei undergo karyogamy to form a triploid zygote nucleus [133, 134] (Fig. 1). In a study on the mouse [135], intrafollicular oocytes precociously fertilized before completion of Meta I also skip the second meiotic division and develop to polyploid embryos. Thus, after Meta I, intrafollicular oocytes that have not completed the first meiotic division acquire the competence essential for the formation of female and male pronuclei or condensed chromosomes and can skip the second meiotic division upon activation by sperm penetration [134].
8. When inseminated at pro-Meta I 2 h after GVBD, 25% of fish oocytes exhibit normal activation by sperm penetration, followed

by the extrusion of the first polar body, formation of female and male pronuclei, and karyogamy within 60 min post-insemination [136].

9. Unlike oyster [23, 137] and the surf clam [24, 137] oocytes, which do not allow the incorporated sperm nucleus to undergo pronucleus formation until completion of meiotic division, these preovulatory fish and mouse oocytes do not possess the negative regulatory system within the ooplasm to insure the completion of meiosis. Therefore, these vertebrate oocytes must be protected from extracellular factors until at least Meta II (the time of ovulation) by their follicular cell layers. The extracellular factors include sperm entry and the mechanical stimulations that induce a rise in intracellular Ca^{2+} and pH which would disturb the meiotic process. Thus the oocytes normally ovulate in a safe condition in which the final meiotic division is completed upon external stimulation.
10. During the transfer of eggs from aphidicolin-containing saline to regular saline a mass of elongated thread-like chromatids or a condensed, compact chromatin mass was observed near the furrow between blastomeres in the eggs that were treated with aphidicolin until 40 min post-insemination or later.
11. Most of these aphidicolin-treated eggs showed aberrant thread-like chromatids elongated near the cleavage furrow, while all eggs that were exposed to the inhibitor 40 min post-insemination or were cleaved later showed normal chromosome segregation [59].

Acknowledgments

The author is grateful to the collaborators Drs. T. Haraguchi, S. Ikegami, T. Kishimoto, H. Kobayashi, S. Oda, H. Ohta, Y. Shibata, and M. Yamashita for their help in preparing the manuscript.

References

1. Masui Y, Clarke HJ (1979) Oocyte maturation. Int Rev Cytol 57:185–282
2. Yamashita M (2000) Toward modeling of a general mechanism of MPF formation during oocyte maturation in vertebrates. Zoolog Sci 17:841–851
3. Sagata N, Oscarsson M, Copeland T, Brumbaugh J, Woude GFV (1988) Function of c-mos protooncogene product in meiotic maturation in *Xenopus* oocytes. Nature 335:519–525
4. Freeman RS, Kanki JP, Ballantyne SM, Pickham KM, Donophue DJ (1989) Effects of the v-mos on Xenopus development: meiotic induction in oocytes and mitotic arrest in cleaving embryos. J Cell Biol 111:533–541
5. Sheets MD, Wu M, Wickens M (1995) Polyadenylation of c-mos mRNA as a control point in Xenopus meiotic maturation. Nature 274:511–546
6. Tokumoto T, Yamashita M, Tokumoto M, Tanaka H, Katsu Y, Horiguchi R, Kajiura H, Nagahama Y (1997) Initiation of cyclin B degeneration by the 26S proteasome upon egg activation. J Cell Biol 138:1313–1322

7. Josefsberg LB, Galiani D, Dantes A, Amsterdam A, Dekel N (2000) The proteasome is involved in the first metaphase-to-anaphase transition of meiosis in rat oocytes. Biol Reprod 62:1270–1277
8. Mueller PR, Coleman TR, Dunphy WG (1995) Cell cycle regulation of a *Xenopus* Wee 1-like kinase. Mol Biol Cell 6:119–134
9. Longo FJ (1997) Fertilization. Chapman & Hall, New York
10. Iwamatsu T, Kobayashi H (2002) Electron microscopic observations of karyogamy in the fish egg. Dev Growth Differ 44:357–363
11. Clarke HJ, Masui Y (1986) Transformation of sperm nuclei to metaphase chromosomes in the cytoplasm of maturing oocytes of the mouse. J Cell Biol 102:1039–1046
12. Das NK, Baker C (1976) Mitotic chromosome condensation in the sperm nucleus during postfertilization maturation division in *Urechis* eggs. J Cell Biol 68:155–159
13. Tchou S, Chen CH (1942) Fertilization of artificially ovulated pre mature eggs of *Bufo*. Sci Rec China (K'e Hsuch Chi u) 1:203–208
14. Elinson RP (1977) Fertilization of immature frog eggs: cleavage and development following subsequent activation. J Embryol Exp Morphol 37:187–201
15. Iwamatsu T, Chang MC (1972) Sperm penetration *in vitro* of mouse oocytes at various times during maturation. J Reprod Fertil 31:237–247
16. Abeydeera LR, Niwa K, Okuda K (1993) Maturation promoting factor (MPF) is responsible for the transformation of sperm nuclei to metaphase chromosomes in maturing bovine oocytes *in vitro*. J Reprod Fertil 98:409–414
17. Gurdon JB (1968) Changes in somatic cell nuclei inserted into growing and maturing amphibian oocytes. J Embryol Exp Morphol 20:401–414
18. Ziegler D, Masui Y (1973) Control of chromosome behavior in amphibian oocytes. II. The effect of inhibitors of RNA and protein synthesis on the induction of chromosome condensation. J Cell Biol 68:620–628
19. Moriya M, Katagiri C (1976) Microinjection of toad sperm into oocytes undergoing maturation division. Dev Growth Differ 18:349–356
20. Masui Y, Lohka MJ, Shibuya EK (1984) Roles of Ca ions and ooplasmic factors in the resumption of metaphase-arrested meiosis in *Rana pipiens* oocytes. Symp Soc Exp Biol 38:45–66
21. Lohka MJ, Masui Y (1984) Effects of Ca^{2+} ions on the formation of metaphase chromosomes and sperm pronuclei in free preparations from unactivated *Rana pipiens* eggs. Dev Biol 103:434–442
22. Yamashita M (1983) Electron microscopic observations during monospermic fertilization process of the brittle-star *Amphipholis kochii* Lutken. J Exp Zool 2289:109–120
23. Longo FJ, Mathews L, Hedgecock D (1993) Morphogenesis of maternal and paternal genomes in fertilized oyster eggs (*Crassostrea gigas*): effects of cytocharasin B at different periods during meiotic maturation. Biol Bull 185:197–214
24. Longo FJ, Anderson E (1970) An ultrastructural analysis of fertilization in the surf clam, *Spisula solidissima*. I. Polar body formation and development of the female pro-nucleus. J Ultrastruct Res 33:495–514
25. Iwamatsu T (1966) Role of the germinal vesicle materials on the acquisition of developmental capacity of the fish oocyte. Embryologia 9:205–221
26. Iwamatsu T, Ohta T (1980) The changes in sperm nuclei after penetrating fish oocytes matured without germinal vesicle material in their cytoplasm. Gamete Res 3:56–67
27. Longo FJ (1973) The unset of DNA synthesis and its relation to morphogenetic events of the pronuclei in activated eggs of the sea urchin, *Arbacia ounctulata*. Dev Biol 30:56–67
28. Longo FJ, Kuncle M (1978) Transformation of sperm nuclei upon insemination. Curr Top Dev Biol 12:149–184
29. Wolgemuth DJ (1983) Synthetic activities of the mammalian early embryo: molecular and genetic alterations following fertilization. In: Hartmann JF (ed) Mechanisms and control of animal fertilization. Academic Press, New York, pp 415–452
30. Ohsumi K, Katagiri C, Yanagimachi R (1996) Development of pronuclei from human spermatozoa injected microsurgically into frog (*Xenopus*) eggs. J Exp Zool 237:319–325
31. Kopecny V, Pavlok A (1975) Autoradiographic study of mouse spermatozoan arginine-rich nuclear protein in fertilization. J Exp Zool 191:85–96
32. Poccia D, Salik J, Krystal G (1981) Transitions in histone variants of the male pronucleus following fertilization and evidence for a material store of cleavage stage histones in the sea urchin egg. Dev Biol 82:287–296

33. Rodman TC, Pruslin FH, Hoffmann HP, Allfrey VG (1981) Turnover of basic chromosomal proteins in fertilized eggs. A cytoimmunochemical study of events *in vitro*. J Cell Biol 90:351–361
34. Zirkin BR, Soucek DA, Chang TSK, Perreault SD (1985) *In vitro* and *in vivo* studies of mammalian sperm nuclear decondensation. Gamete Res 11:349–365
35. Ohsumi K, Katagiri C (1991) Occurrence of H1 subtypes specific to pronuclei and cleavage stage cell nuclei of anuran amphibians. Dev Biol 147:110–120
36. Philpott A, Leno GH (1992) Nucleoplasmin remodels sperm chromatin in *Xenopus* egg extracts. Cell 69:759–767
37. Luthardt FW, Donohue RP (1973) Pronuclear DNA synthesis in mouse eggs: an autographic study. Exp Cell Res 82:143–151
38. Naish SJ, Perreault SD, Foehner L, Zirkin BR (1993) DNA synthesis in the fertilizing hamster sperm nucleus: sperm temperate availability and egg cytoplasmic control. Biol Reprod 36:245–253
39. Barns FL, Callos P, Powell R, Westhusin WA, Shepherd D (1993) Influence of recipient oocyte cell cycle stage on DNA synthesis, nuclear envelope breakdown, chromosome constitution, and development in nuclear transplant bovine embryos. Mol Reprod Dev 36:33–41
40. Campbell KHS, Loi P, Cappai P, Wilmut I (1994) Improved development to blastocyst of ovine nuclear transfer embryos reconstructed during the presumptive S phase of enucleated activated oocytes. Biol Reprod 50:1385–1393
41. Laurincik J, Kopecny V, Hyttel P (1994) Pronucleus development and DNA synthesis in bovine zygotes *in vitro*. Theriogenology 42:1285–1293
42. Hirano T (2000) Chromosome cohesion, condensation, and separation. Annu Rev Biochem 69:115–144
43. Iwamatsu T, Shibata Y, Yamashita M (1999) Studies on fertilization of the teleost. II. Nuclear behavior and changes in histone H1 kinase. Dev Growth Differ 41:473–482
44. Nomura A, Maruyama YK, Yoneda M (1991) Initiation of DNA replication cycle in fertilized eggs of the starfish, *Asterina pectinifera*. Dev Biol 143:289–296
45. Simmel EB, Karnofsky DA (1961) Observation on the uptake of tritiated thymidine in the pronuclei of fertilized sand dollar embryos. J Biophys Biochem Cytol 10:59–65
46. Oprecue S, Thibault C (1965) Duplication de l'AND dans les oeufs de lapine apres la fecundation. Ann Biol Anim Biochim Biophys 5:151–156
47. Howlett SK, Bolton VN (1985) Sequence and regulation of morphological and molecular events during the first cell cycle of mouse embryo-genesis. J Embryol Exp Morphol 67:175–206
48. Abramczuk J, Sawicki W (1975) Pro-nuclear synthesis of DNA in fertilized and parthenogenetically activated mouse eggs: a cytophotometric study. Exp Cell Res 92:361–372
49. Balkan W, Martin RH (1982) Timing of human sperm chromosome replication following fertilization of hamster eggs *in vitro*. Gamete Res 6:115–119
50. Szollosi D (1966) Time and duration of DNA synthesis in rabbit eggs after sperm penetration. Anat Rec 154:209–212
51. Longo FJ, Plunkett W (1973) The onset of DNA synthesis and its relation to morphogenetic events of the pronuclei in activated eggs of the sea urchin, *Arbacia punctulata*. Dev Biol 30:56–67
52. Whitaker MJ, Steinhardt RA (1981) The relation between the increase in reduced nicotinamide nucleotides and the initiation of DNA synthesis in the sea urchin eggs. Cell 25:95–103
53. Collas P, Chang T, Long C, Robl JM (1995) Inactivation of histone H1 kinase by Ca^{2+} in rabbit oocytes. Mol Reprod Dev 40:253–258
54. Gould KL, Nurse P (1989) Tyrosine phosphorylation of the fission yeast $cdc2^{+}$ protein kinase regulates entry into mitosis. Nature 342:39–45
55. Enoch T, Nurse P (1990) Mutation of fission yeast cell cycle control genes abolishes dependence of mitosis on DNA replication. Cell 60:665–673
56. Pagano M, Pepperkok R, Verde F, Ansorge W, Graetta G (1992) Cyclin A is required at two points in the human cell cycle. EMBO J 11:961–971
57. Tosuji H, Mabuchi I, Fusetani N, Nakazawa H (1992) Calyculin A induces contractile ring-like apparatus formation and condensation of chromosomes in unfertilized sea urchin eggs. Proc Natl Acad Sci U S A 89:10613–10617
58. Someya A, Tanaka N, Okuyama A (1993) Inhibition of initiation of DNA replication in *Xenopus* egg extracts by a phosphatase inhibitor, Calyculin A. Biochem Biophys Res Commun 196:85–91

59. Iwamatsu T, Shibata Y, Hara O, Yamashita M, Ikegami S (2002) Studies on fertilization in the teleost. IV. Effects of aphidicolin and Camptothecin on chromosome formation in fertilized medaka eggs. Dev Growth Differ 44:293–302
60. Doree M, Peaucellier G, Picard A (1983) Activity of the maturation-promoting factor and the extent of protein phosphorylation oscillate simultaneously during meiotic mat- uration of starfish oocytes. Dev Biol 99:489–501
61. Gerhart JC, Wu M, Kirschner MW (1984) Cell cycle dynamics of an M phase-specific cytoplasmic factor in *Xenopus laevis* oocytes and eggs. J Cell Biol 98:1247–1255
62. Newport JW, Kirshner MW (1984) Regulation of the cell cycle during early *Xenopus* development. Cell 37:731–742
63. Picard A, Labbé JC, Peaucellier G, Le Bouffant F, Le Peuch C, Doree M (1987) Changes in the activity of the maturation-promoting factor are correlated with those of a major cAMP- and calcium independent protein kinase during the first mitotic cell cycles in the starfish embryo. Dev Growth Differ 29:93–103
64. Iwamatsu T, Kobayashi H, Yamashita M, Shibata Y, Yusa A (2003) Experimental hybridization among *Oryzias* species. II. Karyogamy and abnormality of chromosome separation in the cleavage of interspecific hybrids between *Oryzias latipes* and *O. javanicus*. Zoolog Sci 20:1381–1387
65. Sakai C, Konno F, Nakano O, Iwai T, Yokota T, Lee J, Nishida-Umehara C, Kuroiwa A, Matsuda Y, Yamashita M (2007) Chromosome elimination in the interspecific hybrid medaka between *Oryias latipes* and *O. hubbsi*. Chromosome Res 15:697–709
66. Loupart ML, Krause SA, Heck MMS (2000) Aberrant replication timing induces chromosome condensation in *Drosophila* ORC2 mutants. Curr Biol 10:1547–1556
67. Nagano H, Okano K, Ikegami S, Katagiri C (1982) Changes in intracellular location of DNA polymerase-alpha during oocyte maturation of the toad, *Bufo bufo japonicas*. Biochem Biophys Res Commun 106:683–690
68. Fox AM, Breaux CB, Benbow RM (1980) Intracellular localization of DNA polymerase activities within large oocytes of the frog, *Xenopus laevis*. Dev Biol 80:79–95
69. Grippo PC, Taddei C, Locorotondo G, Gambino-Giuffrida A (1977) Cellular localization of DNA polymerase activities in full-grown oocytes and embryos of *Xenopus laevis*. Exp Cell Res 190:247–252
70. Martini G, Tato F, Attardi DG, Tocchini-Valentini GP (1976) Nuclear localization of DNA polymerase alpha in *Xenopus laevis*. Biochem Biophys Res Commun 72:875–879
71. Shioda M, Nagano H, Mano Y (1977) Cytoplasmic location of DNA polymerase-α and -β of sea urchin eggs. Biochem Biophys Res Commun 78:1362–1368
72. Haraguchi T, Nagano H (1983) Isolation and characterization of DNA polymerases from mature oocytes of the starfish, *Asterina pectinifera*. J Biochem 93:87–97
73. Oishi N, Shimada H (1983) Intracellular localization of DNA polymerases in the oocyte of starfish, *Asterina pectinifera*. Dev Growth Differ 25:547–551
74. Iwamatsu T, Haraguchi T, Nagano H (2010) Cytoplasmic location of DNA polymerase in oocytes of the teleost fish, *Oryzias latipes*. Aichi Univ Educat (Nat Sci) 59:1–8
75. Ikegami S, Taguchi T, Ohashi M, Oguro M, Nagano H, Mano Y (1978) Aphidicolin prevents mitotic cell division by interfering with the activity of DNA polymerase-α. Nature 275:458–460
76. Ikegami S, Amemiya S, Oguro M, Nagano H, Mano Y (1979) Inhibition by aphidicolin of cell cycle progression and DNA replication in sea urchin embryos. J Cell Physiol 100:439–444
77. Oguro M, Suzuki-Hori C, Nagano H, Mano Y, Ikegami S (1979) The mode of inhibitory action by aphidicolin on eukaryotic DNA polymerase-α. Eur J Biochem 97:603–607
78. Brachet J, De Ptrocellis B (1981) The effects of aphidicolin, an inhibitor of DNA replication, on sea urchin development. Exp Cell Res 135:179–189
79. Yamada H, Hirai S, Ikegami S, Kawarada Y, Okuhara E, Nagano H (1985) The fate of DNA originally existing in the zygote nucleus during a chromosomal cleavage of fertilized echinoderm eggs in the presence of aphidicolin: microscopic studies with anti-DNA antibody. J Cell Physiol 124:9–12
80. Nagano H, Hirai S, Okano K, Ikegami S (1981) Achromosomal cleavage of fertilized starfish eggs in the presence of aphidicolin. Dev Biol 85:409–415
81. Saiki T, Kyozuka K, Osanai K, Hamaguchi Y (1991) Chromosomal behavior in starfish (*Asterina pectinifera*) zygotes under the effect of aphidicolin, an inhibitor of DNA polymerase. Exp Cell Res 192:380–388

82. Wells NJ, Hickson ID (1995) Human topoisomerase II alpha is phosphorylated in a cell-cycle phase-dependent manner by a proline-diected kinase. Eur J Biochem 23:491–497
83. Clute P, Masui Y (1997) Microtubule dependence of chromosome cycles in *Xenopus laevis* blastomeres under the influence of a DNA synthesis inhibitor, aphidicolin. Dev Biol 185:1–13
84. Taguchi T, Ohashi M, Oguro M, Nagano H, Mano Y (1978) Aphidicolin prevents mitotic cell division by interfering with the activity of DNA polymerase-α. Nature 275:458–460
85. Droge P, Sogo JM, Stahl H (1985) Inhibition of DNA synthesis by aphidicolin induces supercoiling in simian virus 40 replicative intermediates. EMBO J 4:3241–3246
86. Wang JC (1985) DNA topoisomerases. Annu Rev Biochem 54:665–697
87. Drlica K, Franco A (1988) Inhibitors of DNA topoisomerases. Biochemistry 27:2253–2259
88. Gupta M, Fujimori A, Pommier Y (1995) Eukaryotic DNA topoisomerases I. Biochem Biophys Acta 1262:1–14
89. Ohta E, Ohta S, Hongo T, Hamaguchi Y, Ando T, Shioda M, Ikegami S (2003) Inhibition of chromosome separation in fertilized starfish eggs by kalihinol F, a topoisomerase I inhibitor obtained from a marine sponge. Biosci Biotechnol Biochem 67:2365–2372
90. Horowitz MS, Horowits SB (1971) Intracellular degeneration of HeLa and adenovirus type 2 DNA induced by camptothecin. Biochem Biophys Res Commun 45:723–727
91. Annunziato TA (1989) Inhibitors of topoisomerases I and II arrest DNA replication, but do not prevent nucleosome assembly *in vivo*. J Cell Sci 93:593–603
92. Gellert M (1981) DNA topoisomerases. Annu Rev Biochem 50:879–910
93. Hsian YH, Hertzberg R, Hecht S, Liu LF (1985) Camptothecin induces protein-linked DNA breaks *via* mammalian DNA topoisomerase I. J Biol Chem 260:14873–14878
94. Zhu Q, Pongpech P, DiGate RJ (2001) Type I topoisomerase activity is required for proper chromosomal segregation in *Escherichia coli*. Proc Natl Acad Sci U S A 98:9766–9771
95. Usongo V, Nolent F, Sanscartier P, Tanguay C, Broccoli S, Baaklini I, Drlica K, Drolet M (2008) Depletion of RNase H1 activity in *Escherichia coli* lacking DNA topoisomerase I leads to defects in DNA supercoiling and segregation. Mol Microbiol 69:968–981
96. Uemura T, Ohkura H, Adachi Y, Morino K, Shiozaki K, Yanagida M (1987) DNA topoisomerase II is required for condensation and separation of mitotic chromosomes in *S. pombe*. Cell 50:917–925
97. Holm C, Goto T, Wang JC, Botstein D (1985) DNA topoisomerase I is required at the time of mitosis in yeast. Cell 41:553–563
98. Holm C, Stearns T, Botstein D (1989) DNA topoisomerase II must act at mitosis to prevent nondisjunction and chromosome breakage. Mol Cell Biol 9:159–168
99. Rose D, Thomas W, Holm C (1990) Segregation of recombined chromosomes in meiosis I requires DNA topoisomerase II. Cell 60:1009–1017
100. Bhar MA, Philp AV, Glover DM, Bellen HJ (1996) Chromatid segregation at anaphase required the barren product, a novel chromosome-associated protein that interacts with topoisomerase II. Cell 87:1103–1114
101. Wright SJ, Schatten G (1990) Teniposide, a topoisomerase II inhibitor, prevents chromosome condensation and separation but not decondensation in fertilized surf clam (*Spisula solidissima*) oocytes. Dev Biol 142:224–232
102. Shamu CE, Murray AW (1992) Sister chromatic separation in frog egg extracts requires DNA topoisomerase II activity during anaphase. J Cell Biol 117:921–934
103. Buchenau P, Saumweber H, Arndt-Jovin DL (1993) Consequences of TOPO II inhibition in early embryo-genesis of *Drosophila* revealed by *in vivo* confocal laser scanning micro-scopy. J Cell Biol 104:1175–1185
104. Kallio M, Lahdtie J (1996) Fragmentation of centromeric DNA and prevention of homologous chromosome separation in male meiosis *in vivo* by the topoisomerase II inhibitor etoposide. Mutagenesis 11:435–443
105. Kallio M, Lähdetie J (1997) Effects of the DNA topoisomerase II inhibitor merbarone in male mouse meiotic divisions *in vivo*: cell cycle arrest and induction of aneuploidy. Environ Mol Mutagen 29:16–27
106. Mailhes JB, Marchetti F, Young D, London SN (1996) Numerical and structural chromosome aberrations induced by etoposide (VP 16) during oocyte maturation of mice: transmission to 1-cell zygotes and damage to dictyate oocytes. Mutagenesis 11:357–361
107. Marchetti F, Bishop JB, Lowe X, Generoso WM, Hozier J, Wyrobek AJ (2001) Etoposide induces heritable chromosomal aberrations and aneuploidy during male meiosis in the mouse. Proc Natl Acad Sci U S A 98:3952–3957

108. Tateno H, Kamiguchi Y (2001) Abnormal chromosome migration and chromosome aberrations in mouse oocytes during meiosis II in the presence of topoisomerase II inhibitor ICRF-193. Mutat Res 502:1–9
109. Charron M, Hancock R (1990) DNA topoisomerase II is required for formation of mitotic chromosomes in Chinese hamster ovary cells: studies using the inhibitor 4-demethylepi-podophyllotoxin9-(4,6-*O*-thenylidene-β-D-gluco-pyranoside). Biochemistry 29:9531–9537
110. Downes CDS, Mullinge AM, Johnson RT (1991) Inhibitors of topoiso merase II prevent chromatid separation in mammalian cells but do not prevent exit from mitosis. Proc Natl Acad Sci U S A 88:8895–8899
111. Baldi MI, Benedetti P, Mattoccia E, Tocchi-Valentini GP (1980) *In vitro* catenation and decatenation of DNA and a novel eukaryotic ATP-dependent topoisomerase. Cell 20:461–467
112. Hsieh T-S (1983) Knotting of the circular duplex DNA by type II DNA topoisomerase from *Drosophila melanogaster*. J Biol Chem 258:8413–8420
113. Hsieh T-S, Brutlag D (1980) ATP-dependent DNA topoisomerase from *D. melanogaster* reversibly catenates duplex DNA rings. Cell 27:115–254
114. Kreuzer KN, Cozzarelli NR (1980) Formation and resolution of DNA catenates by DNA gyrase. Cell 20:245–254
115. Liu LF, Davis JI, Calendar R (1981) Novel topologically knotted DNA from bacteriophage P4 capsids: studies with DNA topoisomerases. Nucleic Acids Res 9:3979–3989
116. Sundin O, Varshavsky A (1980) Terminal stages of SV40 replication proceed *via* multiply intercatenated dimers. Cell 21:103–114
117. Sundin O, Varshavsky A (1981) Arrest of segregation leads to accumulation of highly intertwined catenated dimers: dissection of the final stage of SV40 DNA replication. Cell 25:659–669
118. DiNardo S, Voelkel K, Sternglanz R (1984) DNA topoisomerase II mutant of Saccharomyces cerevisiae: topoisomerase II is required for segregation of daughter molecules at the termination of DNA replication. Proc Natl Acad Sci U S A 81:2616–2620
119. Weaver DT, Fields-Berry SC, DePamphilis ML (1985) The termination region for SV40 DNA replication directs the mode of segregation for the two sibling molecules. Cell 41:565–575
120. Maeshima K, Laemmli UK (2003) A two-step scaffolding for mitotic chromosome assembly. Dev Cell 4:467–480
121. Xu Y-X, Manley JL (2007) New insights into mitotic chromosome condensation. A role for the prolyl isomerase Pin 1. Cell Cycle 6:2896–2901
122. Kelly TJ, Brown GW (2000) Regulation of chromosome replication. Annu Rev Biochem 69:829–880
123. Hirano T (2005) SMC proteins and chromosome mechanics: from bacteria to humans. Philos Trans R Soc Lond B Biol Sci 36:507–514
124. Yanagida M (2005) Basic mechanism of eukaryotic chromosome segregation. Philos Trans R Soc Lond B Biol Sci 36:609–1615
125. Iwamatsu T (1978) Studies on oocyte maturation of the medaka, *Oryzias latipes*. VI. Relationship between the circadian cycle of oocyte maturation and activity of the pituitary gland. J Exp Zool 206:355–363
126. Iwamatsu T, Onitake K, Nakashima S (1992) Polarity of responsiveness in sperm and artificial stimuli in medaka eggs. J Exp Zool 264:351–358
127. Iwamatsu T, Fluck RA, Mori T (1993) Mechanical dechorionation of fertilized eggs for experimental embryology in the medaka. Zoolog Sci 10:945–951
128. Nomura A, Yoneda M, Tanaka S (1993) DNA replication in fertilized eggs of the starfish *Asterina pectinifera*. Dev Biol 159:288–297
129. Laemmli UK (1970) Cleavage of structural proteins during the assembly of the head of bacteriophjage T4. Nature 277:680–685
130. Yamashita M, Yoshikuni M, Hirai T, Fukuda S, Nagahama Y (1991) A monoclonal antibody against the PSTAIR sequence of p34cdc2, catalytic subunit of maturation-promoting factor and key regulator of the cell cycle. Dev Growth Differ 33:617–624
131. Yamashita M, Jiang J, Onozato H, Nakanishi T, Nagahama Y (1992) M phase-specific histone H1 kinase in fish oocytes: purification, components and biochemical properties. Eur J Biochem 205:537–543
132. Mehlman LM, Kline D (1994) Regulation of intracellular calcium in the mouse egg: calcium release in response to sperm or inositol triphosphate is enhanced after meiotic maturation. Biol Reprod 51:1088–1198
133. Iwamatsu T (1965) On fertilizability of preovulatory eggs of the medaka, *Oryzias latipes*. Embryologia 8:327–336

134. Iwamatsu T (1997) Abbreviation of the second meiotic division by precocious fertilization in fish oocytes. J Exp Zool 277:450–459
135. Eppig JJ, Schultz MR, O'Brien M, Chenel F (1994) Relationship between the developmental programs controlling nuclear and cytoplasmic maturation of mouse oocytes. Dev Biol 164:1–9
136. Iwamatsu T (2000) Fertilization in fishes. In: Tarin JJ, Cana A (eds) Fertilization in protozoa and metazoan animals–Cellular and molecular aspects. Springer, Berlin, pp 89–145
137. Kuraishi R, Osanai K (1988) Behavior of sperm nuclei in meiotic eggs of the oyster, *Crassostrea gigas*. Bull Mar Biol Stn Asamushi 18:57–65

Chapter 9

Flow Cytometry Analysis of Cell Cycle and Specific Cell Synchronization with Butyrate

Cong-Jun Li

Abstract

Synchronized cells have been invaluable in many kinds of cell cycle and cell proliferation studies. Butyrate induces cell cycle arrest and apoptosis in MDBK cells. We explore the possibility of using butyrate-blocked cells to obtain synchronized cells and we characterize the properties of butyrate-induced cell cycle arrest. The site of growth inhibition and cell cycle arrest was analyzed using 5-bromo-2′-deoxyuridine (BrdU) incorporation and flow cytometry analyses. Exposure of MDBK cells to 10 mM butyrate caused growth inhibition and cell cycle arrest in a reversible manner. Butyrate affected the cell cycle at a specific point both immediately after mitosis and at a very early stage of the G1 phase. After release from butyrate arrest, MDBK cells underwent synchronous cycles of DNA synthesis and transited through the S phase. It takes at least 8 h for butyrate-induced G1-synchronized cells to begin the progression into the S phase. One cycle of cell division for MDBK cells is about 20 h. By combining BrdU incorporation and DNA content analysis, not only can the overlapping of different cell populations be eliminated, but the frequency and nature of individual cells that have synthesized DNA can be determined.

Key words Bovine kidney epithelial cell, BrdU incorporation, Butyrate, Cell cycle synchronization, Flow cytometry

1 Introduction

An optimal cell cycle synchronization protocol is required in order to study the proliferative biomarkers of the cell cycle. Highly synchronized cell populations greatly facilitate cell cycle analysis [1, 2]. A number of agents and protocols have been described to block cell cycle progression reversibly. These protocols and agents can be used to either arrest actively dividing cells in chemotherapeutic protocols or devise synchronizing regimens for cultured cells [3]. Most of these agents have an extensive history as chemotherapeutic agents, and their mechanisms of action are well understood. Among the most widely used protocols are the use of nutritional or serum deprivation to arrest cells in G0/G1, the use of DNA synthesis inhibitors to block the cell cycle at the early S phase, and the

Gaspar Banfalvi (ed.), *Cell Cycle Synchronization: Methods and Protocols*, Methods in Molecular Biology, vol. 1524,
DOI 10.1007/978-1-4939-6603-5_9,

use of nocodazole—a mitotic inhibitor—to synchronize cells at the M/G2 phases. However, not all agents that produce cell cycle blocks are suitable for different kinds of block-and-release experiments or different kind of cell types. We have recently reported that butyrate can arrest MDBK cells specifically at the early G1 phase [4]. However, the properties of butyrate-induced cell cycle arrest and cell cycle progression after release have not been characterized. To obtain cell populations at specific cell cycle stages and to develop a model for studies of cell growth regulation, we examined synchronization protocol of butyrate-induced cell cycle arrest and demonstrated that butyrate blocks the cell cycle at the very early G1 phase and that butyrate-induced cell cycle block is reversible. Using butyrate-synchronized cells, we also determined that the cell division cycle of MDBK cells is about 20 h. The use of flow cytometry allows us to monitor the progression of the cell cycle and to characterize the cell cycle arrest induced by butyrate.

2 Materials

1. Madin-Darby bovine kidney epithelial cells (MDBK, American Type Culture Collection, Manassas, VA).
2. Dulbecco's Modified Eagle's Medium (DMEM) supplemented with 5% fetal bovine serum.
3. Solution of trypsin (0.25%).
4. Sodium Butyrate is dissolved in Molecular Grade Water at 1 M and stored in single use aliquots at −20 °C.
5. BrdU Flow kits (BD Pharmingen, San Diego, CA).
6. 25 cm^2 T-flask with 0.2 μm vent cap.

3 Methods

3.1 Cell Culture and Cell Treatment

1. Madin-Darby bovine kidney epithelial cells were cultured in a 25 cm^2 flask, and the medium was renewed twice per week. Cell cultures were maintained in a water-jacked incubator with 5% CO_2 at 37 °C. The cells were used for treatment testing at approximately 50% confluence during the exponential phase of growth.
2. Sodium butyrate was prepared as 1 M stock. Adding up to 10 mM sodium butyrate into the cell culture medium did not cause a measurable pH change. Duplicated flasks of cells were used for treatment (*see* **Note 1**).

3.2 Flow Cytometric Analysis with Measurement of DNA Content

1. Flow cytometry analysis can be done with the measurements of increased DNA content in proliferating cells going through cell cycle phases and with the combined measurements of

increased DNA content in proliferating cells going through cell cycle phases and immunostaining on the newly synthesized DNA containing BrdU, which reflects the cell cycle progression status. Cellular DNA content increases from the original amount of the two copies (2C) in the G1 phase to twice the amount of four copies (4C) in the M/G2 phases, with intermediate DNA content in the S phase cells. To measure the DNA content, cells were stained with a fluorescent dye (propidium iodide) that directly binds to the DNA in the nucleus. Measuring the fluorescence by flow cytometry provided a measure of the amount of dye taken up by the cells and, indirectly, the amount of DNA content. The cells collected by trypsinization were washed with an ice-cold PBS (pH 7.4) buffer. The cells were then resuspended in the PBS buffer and two volumes of ice-cold 100% ethanol were added dropwise into tubes and mixed with cells in suspension by slow vortexing. After ethanol fixation, the cells were centrifuged (400 g, 5 min) and washed in the PBS buffer once. The cells were then resuspended at 10^6/ml. Fifty μg/ml of RNase A (Sigma Chemical Co., St. Louis, MO) was then added to each sample and the samples were incubated at 37 °C for 30 min. After incubation, 20 μg of propidium iodide was added to each tube for at least 30 min to provide the nuclear signal for fluorescence-activated cell sorting (flow cytometry). After staining the cells with propidium iodide, the tubes were transferred to ice or stored at 4 °C and PROTECTED FROM LIGHT. The stained cells can be analyzed within 48 h or stored for up to 2 weeks. However, in this case, the stained cells require nylon mesh filtration (Filcons, BD Cat. NO. 340627) to remove cell clumps or syringing (25 G) to break up cell clumps. Flow cytometric data are acquired using a flow cytometer equipped with a 488 nm argon laser. In our laboratory, we used the FC500 from Beckman Coulter (Beckman Coulter Inc. Palatine, IL). This laser permits the excitation of the fluorescent dye, propidium iodide (FL2). In the mean time, forward angle (FS) and side-scattered (SSC) are also generated from illuminated cells.

2. Cell cycle analysis of DNA histograms: A pragmatic approach: The problem with deconvoluting the DNA content of cells into their component parts is the overlapping of the cell populations. There are a variety of computer programs available for the analysis of DNA histograms. We are using Cylchred software (University of Wales College of Medicine) for this purpose, which is a freeware that can be downloaded from several websites. The package accepts histograms in an FCS single parameter binary format with up to 1024 channels. Cylchred has been available in a DOS environment since 1996 and also works with Windows operation systems. The measure function

of this program invokes the main cell cycle algorithm and displays the derived components on the histogram with the associated data in the result window. Figure 1 shows the deconvoluted DNA histograms with the associated data.

3.3 5-Bromo-2′-deoxyuridine (BrdU) Incorporation Pulse-labeling and Flow Cytometric Analysis of Cells

1. The most accurate method of measuring the relative number of cells in the different cell cycle stages is to pulse-label the cells with BrdU and to use an antibody to BrdU. BrdU is a thymidine (TdR) analog and is incorporated into cellular DNA through the same pathway. DNA synthesis can be visualized in situ by direct immunofluorescence using an antibody against BrdU [5]. By combining the immunofluorescent staining of the incorporated BrdU and DNA content stained by the DNA

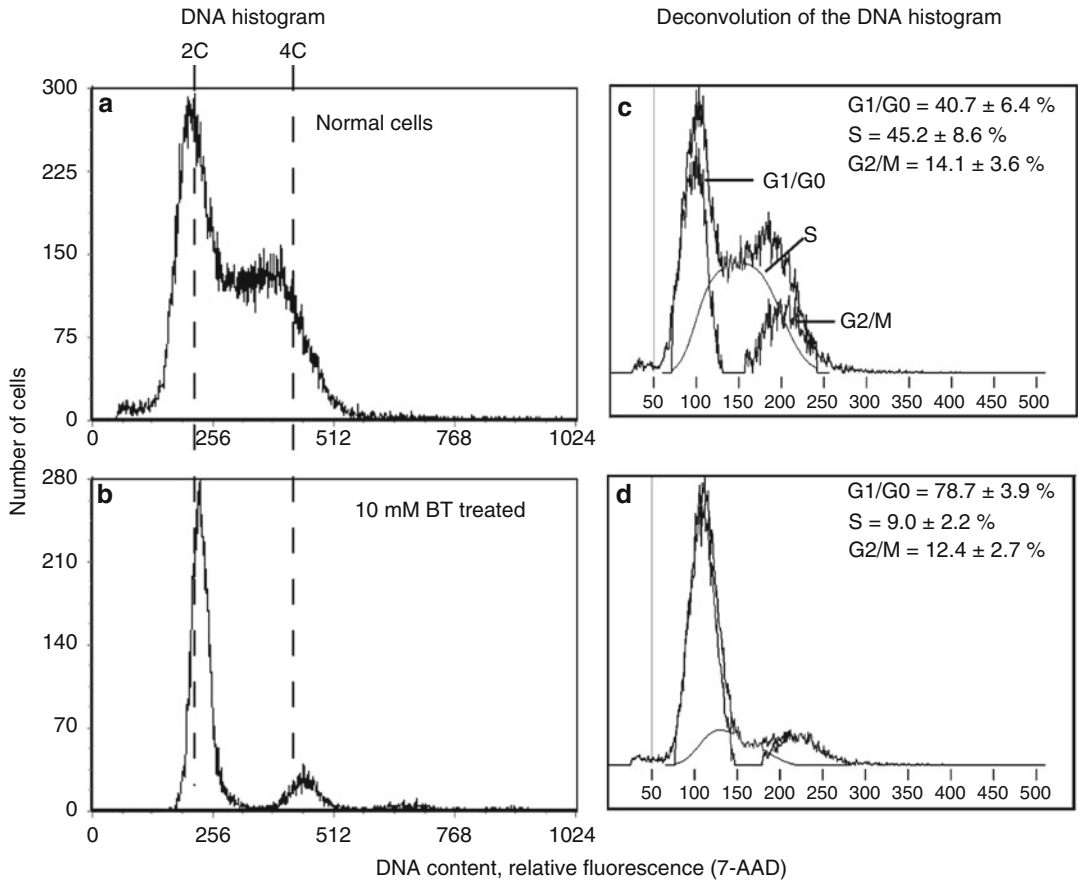

Fig. 1 Deconvolution of the DNA histogram using Cylchred software (University of Wales College of Medicine). One set of representative histogram plots of the flow cytometry analysis (DNA content) of MDBK cells: (**a**) and (**c**): Histogram and its deconvolution of the flow cytometric analysis of the exponential growing cells. (**b**) and (**d**): Histogram plot and the deconvolution of flow cytometry analysis of MDBK cells treated with 10 mM sodium butyrate

marker, we can not only analyze cell cycle synchrony with high resolution, but we can also monitor the cell cycle progression after the cells are released from the treatments.

2. Asynchronously growing MDBK cells were treated with butyrate for 24 h. Cells were washed with a fresh medium to eliminate the dead cells and then replaced with a fresh medium with 5% feral bovine serum. Cells were pulse-labeled with BrdU using BrdU Flow kits (BD Pharmingen, San Diego, CA) by following the manufacturer's instructions. In summary, to pulse-label the cells, 10 μl of BrdU solution (1 mM BrdU in PBS) was carefully added directly to each ml of culture media and cultured for 40 min. To stain cells with fluorescence-labeled antibody, cells were collected with trypsinization, fixed, and permeabilized with a BD Cytofix/Cytoperm buffer supplied with the kits. The cells were then treated with DNase to expose the incorporated BrdU (30 μg of DNase to each sample, incubated at 37 °C for 1 h). After washing with 1 ml of 1 X BD Perm/wash buffer, the cells were resuspended with 50 μl of BD Perm/Wash buffer containing diluted fluorescent (Fluorescent isothiocyanate, FITC) anti-BrdU antibody and incubated for 20 min at room temperature. After washing with the BD Perm/Wash buffer, the cells were resuspended in 20 μl of 7-AAD solution (supplied with kits) to stain the cellular DNA content.
3. Cell DNA content and BrdU labeling were acquired using flow cytometry (FC500, Beckman Coulter Inc.). The 488 nM argon laser permits the excitation of the fluorescent isothiocyanate (FITC) (FL1), and DNA-content marker 7-ADD (FL3). Fluorescent signals from the 7-ADD are normally acquired in the linear signal amplification mode, and fluorescent signals generated by other fluorochromes such as FITC are typically acquired in a logarithmic mode. Collected data were analyzed using Cytomic RXP (Beckman Coulter Inc.). Figure 2 shows the representative data from the normal growing cell population to show that a second fluorescence parameter (BrdU) provides more flexibility for the quantitative cell cycle analysis of populations. The fluorescent signal generated by FITC was acquired in a logarithmic mode and the fluorescent signal from the DNA-content marker 7-ADD was acquired in the linear signal amplification mode. Using double color staining (immunofluorescent staining of the BrdU incorporation and fluorescents staining of the total DNA), cells can be separated into three major clusters. The first is a cell population with two copies of DNA and without any DNA synthesis activity, e.g., the cells in the G1/G0 phases (cluster a). The second is the cell population (G2/M phases) that has four copies of DNA and is without any synthesis activity (cluster c). The last is a cell population (cluster b) that has the DNA content between cluster a and c, but has a strong

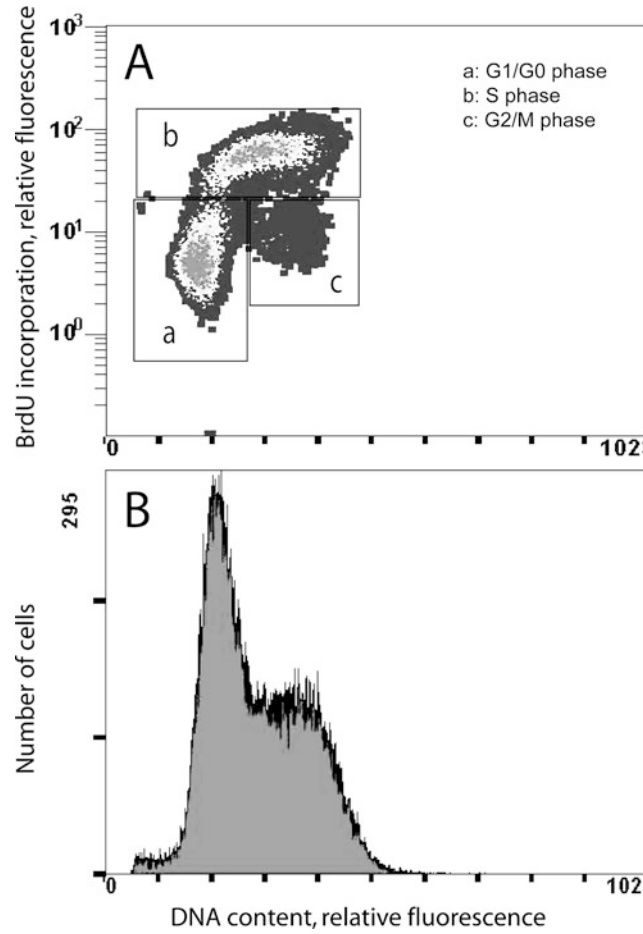

Fig. 2 Density and histogram plots of the flow cytometry analysis of normal proliferating cell population. (**a**): Pulse-label with BrdU and using an antibody to BrdU accurately measure the relative number of cells in different stages of the cell cycle. For flow cytometric analysis, the cells were first pulse-labeled with BrdU for 30 min. The collected cells were first stained with diluted fluorescent (fluorescent isothiocyanate, FITC) anti-BrdU antibody and then stained with a DNA marker (7-ADD). The fluorescent signal generated by FITC was acquired in a logarithmic mode, and the fluorescent signal from the DNA-content marker 7-ADD was normally acquired in the linear signal amplification mode. Cells were separated into three clusters by double staining analysis. (*a*) G1/G0 cells, with 2C DNA content and without any DNA synthesis activity; (*b*) S phase cells, with DNA content between 2C and 4C (two and four copies of DNA content, respectively), and high BrdU incorporation (DNA synthesis) activity; (*c*) G2/M cells, with 4C DNA content and also without DNA synthesis activity. (**b**): Histogram, the flow cytometric analysis of the cell cycle by DNA content for the same cell preparation (*see* **Note 2**)

shift of immunofluorescent staining of the newly synthesized DNA. Those cells are in the S phase. All data are displayed in density plots. In comparison with the profiles from the DNA content analysis, the immunofluorescent staining of incorpo-

rated BrdU and flow cytometric analysis provides a high-resolution technique to eliminate the overlap between different cell populations and to determine the frequency and nature of individual cells that have synthesized DNA.

4. Synchrony/release MDBK cells from butyrate treatment: Asynchronously growing MDBK cells were incubated 24 h in the presence of 10 mM butyrate; the cells were washed with a fresh medium to eliminate the dead cells and then were replaced in a fresh medium with 5% fetal bovine serum. The cells were pulse-labeled with BrdU at indicated time points and were collected for flow cytometric analysis. Figure 2a, b are the flow cytometric data representing the 1 h and 6 h time points after release from butyrate. The average flow cytometric cell cycle distribution from four experiments showed an arrest of the cells in the G1 phase with the majority of the cells in the G0/G1 phases (81.0 ± 2.9%), while 8.9 ± 1% and 10.1 ± 2.4% of the cells were in the S and G2/M phases, respectively. However, during the first 8 h post-release, the G1 synchronized cells progressed very little into the succeeding stage. Only 18.5 ± 3.7% of the cells at 6 h post-release and 38.1 ± 5.5% of the cells at 8 h post-release progressed into the S phase (data not shown). These data indicated that butyrate blocks the cell cycle at a very early G1 phase and may induce some of the cells into the G0 phase.

Figure 3 shows the flow cytometric data representing data acquired from normal cells (without butyrate treatment), and cells treated for 24 h with 5 mM and 10 mM butyrate. These data confirmed that cells respond to butyrate treatment in a dose-dependent manner. Data are displayed in contour plots.

One cycle of cell division for MDBK cells takes about 20 h. Using butyrate-induced synchronized cells, we determined the length of the cell division cycle of MDBK cells (Fig. 4). After release from the butyrate treatment, the cells were collected at various times post-release and processed for cycle analysis by flow cytometry. Monitoring the cell cycle progression for 24 h after the removal of butyrate showed that the synchronized G1 cells underwent synchronous cycles of DNA synthesis and transited through the S phase (Fig. 5).

Synchronized G1 cells remained in the G1 phase for at least 8 h, with a weak increase in the S phase and a weak decrease in the G1 phase between 6 and 8 h. At 10 h post-release, almost all of the cells progressed into the S phase. Between 16 and 18 h post-release, the majority of the cells were in the G2/M phase. At 20 h post-release, the G1 cell population becomes dominant population of the cells again. These results demonstrated that butyrate blocks the cells at an early stage in G1 and prevents their cell cycle progression. Once released from butyrate, the cell cycle block was

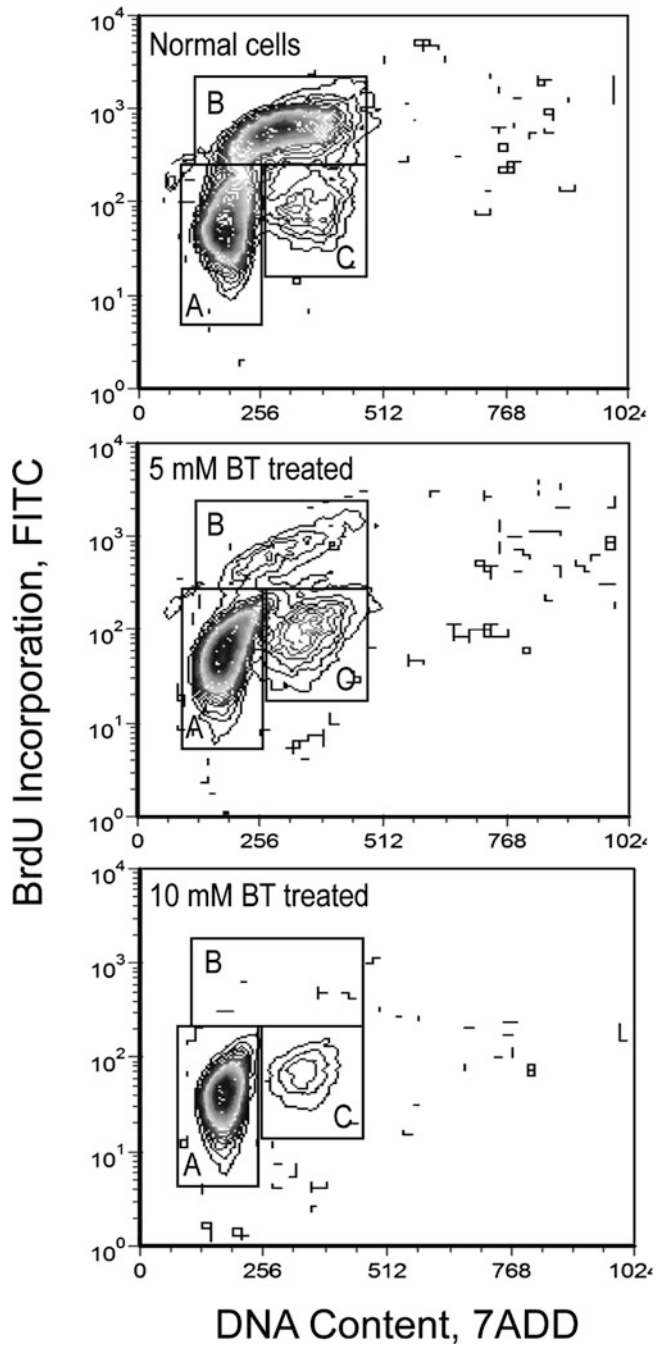

Fig. 3 MDBK cells response to different concentration of butyrate treatments. Cells were treated with butyrate at 0, 5, and 10 mM for 24 h and then pulse-labeled with BrdU. The collected cells were first stained with a diluted fluorescent (fluorescent isothiocyanate, FITC) anti-BrdU antibody and then stained with a DNA marker (7-ADD). Cell DNA content and BrdU pulse-labeling were analyzed using flow cytometry (FC500, Beckman Coulter Inc., Palatine, IL) and collected data were analyzed using Cytomics RXP (Beckman Coulter Inc.). The fluorescent signal generated by FITC was acquired in a logarithmic mode, and the fluorescent signal from the DNA-content marker 7-ADD was normally acquired in the linear signal amplification mode. Data are displayed in contour plots

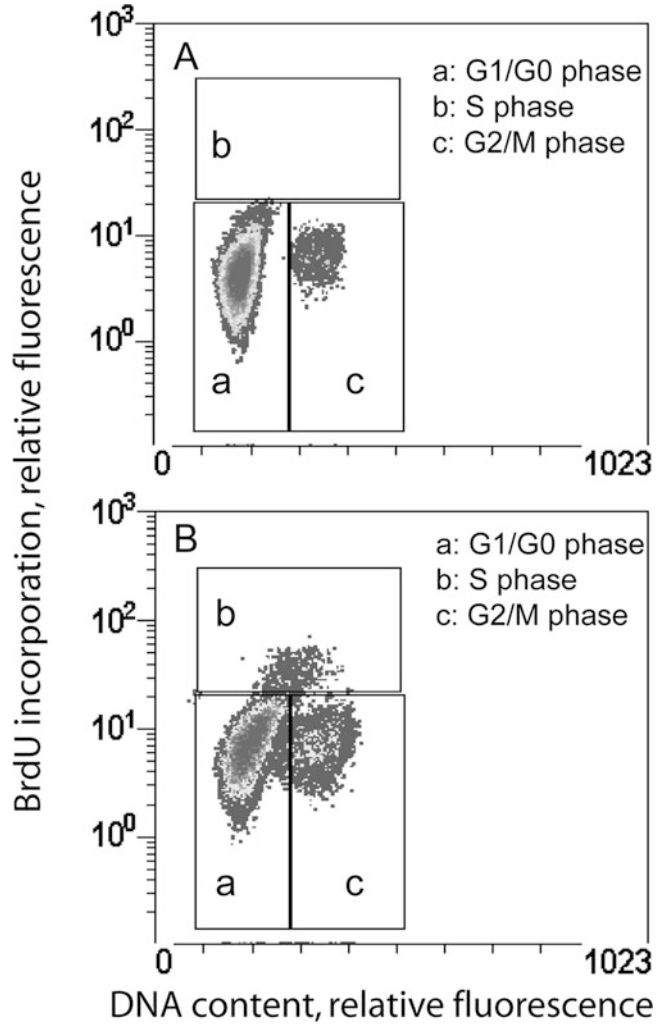

Fig. 4 The cell cycle progression after release from aphidicolin treatment. The cells were first incubated in a serum-depraved medium for 48 h and replaced with a fresh medium with 5% fetal bovine serum and 10 μg/ml aphidicolin for another 24 h. The cells were released into fresh medium containing 5% fetal bovine serum. At the indicated time point, cells were pulse-labeled with BrdU. Collected cells were first stained with a diluted fluorescent (fluorescent isothiocyanate, FITC) anti-BrdU antibody and then stained with a DNA marker (7-ADD). **A**: A representative flow cytometric analysis of the cells 1 h after released from butyrate. **B**: A representative flow cytometric analysis of cells 6 h after released from butyrate. Data are from two individual experiments and are presented as mean ± SEM

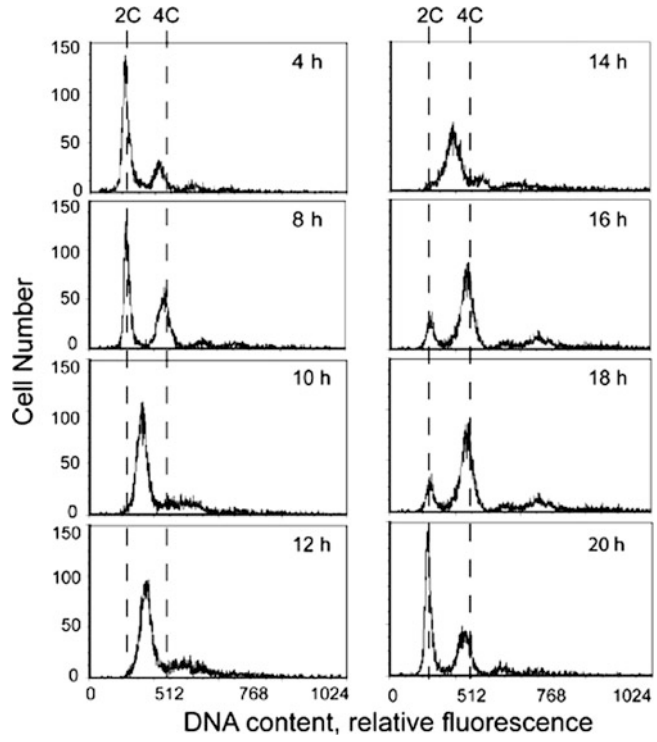

Fig. 5 The cell cycle determination using butyrate synchronized MDBK cells. After released from the butyrate treatment, the cells were collected at indicated times post-release and processed for cycle analysis by flow cytometry. 2C and 4C: two and four copies of DNA content, respectively

reversed and the cells progressed in synchrony into next cell cycle phases. It took about 8 h to complete the S phase and about 20 h for one cycle of cell division in MDBK cells (*see* **Note 3**).

4 Notes

1. This study was undertaken in order to examine the cell cycle characteristics of the Madin Darby Bovine Kidney (MDBK) cell line after culture in the presence of 10 mM butyrate. This study demonstrated that the Madin Darby Bovine Kidney (MDBK) cells, a commonly used cell line in veterinary research, can be effectively synchronized at the G1 phase using butyrate. However, since different cells may respond to butyrate differently, a titration must be performed to optimize the condition and dosage of butyrate.
2. There are also significant (from 10 to 15% of total cell population) M/G2 cell populations accumulated after the butyrate treatment. However, by vigorously tapping the flasks 10 times

to remove any loosely attached mitotic cells before collecting the cells by trypsinization, one can easily eliminate the M/G2 population.

3. Among the most common experimental approaches to cell cycle study is to arrest cell growth using incubation in a low-serum medium or a cell cycle inhibitor such as aphidicolin. It is generally accepted that serum deprivation produces cells arrest at a point in the G1 phase [6]. Aphidicolin is a DNA synthesis inhibitor that blocks the cell cycle at the very early S phase (not at the G1/S boundary) by inhibiting the activity of the DNA polymerase α complex in eukaryotic cells [7, 8]. Nocodazole, an inhibitor of microtubule formation, has been extensively used for cell synchronization for many different cell types [9, 10]. Nocodazole-treated cells gradually progress into mitosis, but without cell division. After a short treatment of 3–4 h, accumulated M phase cells can be collected by shake-off. With these time points for comparison, we have also clearly shown that the major population of butyrate-treated cells is arrested at the very early G1 phase, possibly immediately after mitosis, and some cells may be in G0. Because G1 is a decisive stage for the capacity of cells to progress in the cell cycle, butyrate can be an invaluable tool to study cell cycle regulatory events.

References

1. Futcher B (1999) Cell cycle synchronization. Methods Cell Sci 21:79–86
2. Uzbekov R, Chartrain I, Philippe M, Arlot-Bonnemains Y (1998) Cell cycle analysis and synchronization of the *Xenopus* cell line XL2. Exp Cell Res 242:60–68
3. Levenson V, Hamlin JL (1993) A general protocol for evaluating the specific effects of DNA replication inhibitors. Nucleic Acids Res 21:3997–4004
4. Li CJ, Elsasser TH (2005) Butyrate-induced apoptosis and cell cycle arrest in bovine kidney epithelial cells: involvement of caspase and proteasome pathways. J Anim Sci 83:89–97
5. Sun WH, DePamphilis ML (2004) Methods for detecting cells in S phase. Methods Mol Biol 241:37–53
6. Cooper S, Shedden K (2003) Microarray analysis of gene expression during the cell cycle. Cell Chromosome 2:1
7. Kobayashi T, Rein T, DePamphilis ML (1998) Identification of primary initiation sites for DNA replication in the hamster dihydrofolate reductase gene initiation zone. Mol Cell Biol 18:3266–3277
8. Li CJ, Bogan JA, Natale DA, DePamphilis ML (2000) Selective activation of pre-replication complexes in vitro at specific sites in mammalian nuclei. J Cell Sci 113:887–898
9. Li CJ, DePamphilis ML (2002) Mammalian Orc1 protein is selectively released from chromatin and ubiquitinated during the S-to-M transition in the cell division cycle. Mol Cell Biol 22:105–116
10. Mendez J, Zou-Yang XH, Kim SY, Hidaka M, Tansey WP, Stillman B (2002) Human origin recognition complex large subunit is degraded by ubiquitin-mediated proteolysis after initiation of DNA replication. Mol Cell 9:481–491

Chapter 10

Chemically Induced Cell Cycle Arrest in Perfusion Cell Culture

Gabor Nagy, Bence Tanczos, Eszter Fidrus, Laszlo Talas, and Gaspar Banfalvi

Abstract

In contrast to most present methods, continuous imaging of live cells would require full automation in each processing step. As an integrated system that would meet all requirements does not exist, we have established a long-term scanning-perfusion platform that: (a) replaces old medium with fresh one, (b) bypasses physical contact with the cell culture during continuous cell growth, (c) provides uninterrupted photomicrography of single cells, and (d) secures near physiological conditions and sterility up to several weeks. The system was validated by synchronizing cells using serum starvation and butyrate-induced cell cycle arrest of HaCaT cells.

Key words Time-lapse imaging microscopy, Mammalian cell culture, Perfusion system, Cell cycle synchronization, Serum starvation, Sodium-butyrate synchronization

1 Introduction

Perfusion operations in cell culture have been widely used to improve the cell productivity of bioreactors. Perfusion bioreactors feed solutions and media constantly to reduce the waste of nutrients, remove by-products under relatively high flow rate without washing out cells from the bioreactor. Cells can be retained by filtration, sedimentation, or centrifugation. Filtration techniques require the replacement of filters or keeping filters free of clogging by tangential crossflow. Sedimentation has gained only limited commercial use, due to the adjustment to the specific settling requirements. Centrifugal devices face the difficulty of keeping them under commonly used sterile conditions required for cell cultures. Most of the perfusion systems pump the cells through the separation chamber and back to the bioreactor. Beside the difficulties of maintaining sterility, cells are damaged by shearing forces, oxygen depletion, declining productivity, and quality. Benchtop

Gaspar Banfalvi (ed.), *Cell Cycle Synchronization: Methods and Protocols*, Methods in Molecular Biology, vol. 1524,
DOI 10.1007/978-1-4939-6603-5_10,

bioreactors have been used for fermentation to provide optimal growth conditions for different types of cell cultures [1]. Bioreactors in combination with innovative process technologies contributed to the advancement of antibody industry [2]. Perfusion systems improved the productivity achieved by high cell number in industrial, benchtop, and disposable bioreactors (*see* **Note 1**).

Perfusion chambers with live-cell imaging fulfill two important requirements by maintaining cells in healthy conditions and observing them under high resolution. Open chambers are easily accessed, approach equilibrium with the surrounding atmosphere, but exhibit restricted control. Closed chambers avoid the evaporation of medium, allow the control of temperature, pH and CO_2 concentration. The addition of fresh medium or drugs is favored in long-term experiments focusing on the design of microfluidic chips in 2D and 3D cell cultures. To obtain high optical quality the depth of the perfusion chamber is to be minimized. Large coverslip surface area is prone to leaks and physical damages. Unbalanced perfusion may cause hydrodynamic pulsation of liquid, cellular damages and produce pressure under the coverslip.

The continuous long-term operation of bioreactors could be exploited especially during time-lapse microscopy and image analysis of single cells grown in a cell population. Earlier studies have combined time-lapse fluorescence microscopy and automated image analysis to investigate the dynamic events at the single-cell level [3]. This was followed by the automated analysis of fluorescent foci in single cells [4]. Computer-automated platform combined time-lapse image analysis with a cell tracking software has assisted studies of early embryonal development and helped to improve embryo selection [5].

Time-lapse scanning (TLS) microscopy is an integral and critical branch of live-cell imaging that provides a wide spectrum of design during the microscopic observations of individual cells. Long-term scanning video-microscopy offers excellent optical conditions while allowing specimens to be maintained for varying amounts of time. The essence of LTS is that digital photos are taken every minute and the light microscopic observation of cells lasts during the whole period of examination. The digital pictures are converted to videos and/or analyzed along quantitative parameters. TLS allows the long-term observation of individual cells and cell cultures at population level.

Our computer-automated platform combines time-lapse image analysis that is tracking individual cells, with a perfusion system aided by a control system and software (Fig. 1). The perfusion subsystem is controlled and protected against contamination, mechanical manipulation and disturbance of growth and by avoiding any physical contact with the cell culture during the experiment. Perfusion contributes to the extended observation of specific effects that would be interrupted by the removal of tissue flasks from the incubator, and by the addition of fresh medium or chemicals. The in vitro

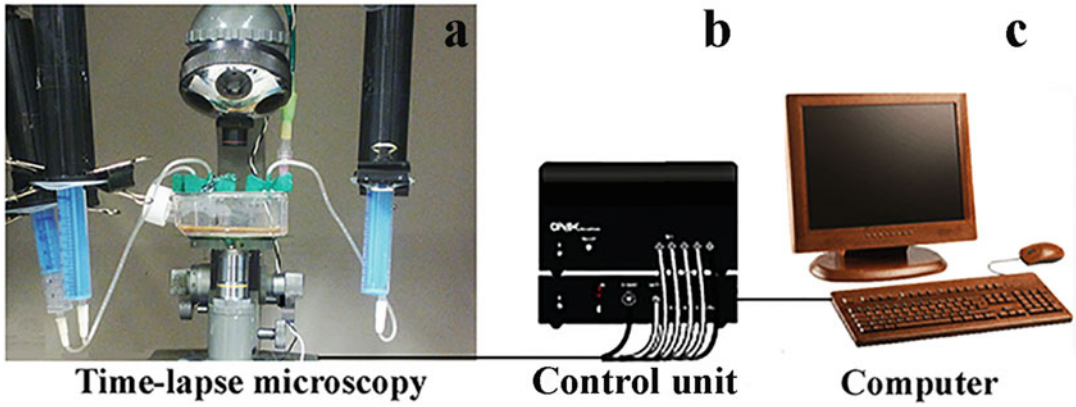

Fig. 1 Time-lapse scanning—perfusion platform. The system combines time-lapse microscopy with perfusion and control units. (**a**) Cell growth is taking place in the perfusion unit sitting in the carbon dioxide incubator. The perfusion unit serves the administration of fresh RPMI 1640 medium containing 10 % fetal bovine serum (FBS) and addition of substances to the cell culture while the old medium is being removed. Parts of the perfusion unit are: (1) pneumatic cylinders, (2) sterile syringes, (3) tissue culture flask (T-flask), (4) charge coupled device (CCD camera), (5) inverse microscope. (**b**) Control panel responsible for the electronic steering and contains the main switch for the activation of the system and other switches responsible for the direction of four working cylinders and the vacuum. (**c**) Software

evolutionary perspective of the LTS-perfusion system (LTS-PS) lies in the observation of individual cells for several generations.

2 Materials

2.1 Disposables

1. T-25 flasks for cell culture.
2. 20 ml syringes.
3. 0.09 mm injection needles for outlet.
4. Butterfly infusion needles for inlet.

2.2 Media and Solutions

1. RPMI 1640 growth medium.
2. Fetal bovine serum (FBS).
3. Phosphate-buffered saline (PBS): 2.7 mM KCl, 4.3 mM sodium phosphate dibasic (Na_2HPO4), 1.8 mM potassium phosphate monobasic (KH_2PO_4), 137 mM NaCl, pH 7.2. Sterilize in an autoclave.
4. Sodium-butyrate solution for synchronization.

3 Methods

3.1 The TLS-PS System

The TLS-PS system consists of the time-lapse video microscopy (TLS), electric steering, and computer subsystems (Fig. 1).

The perfusion subsystem was designed to run the time-lapse imaging system (TLS) under physiological conditions and provide a simple and reliable means to test the effect of serum deprivation and sodium butyrate on individual cells without being in physical contact with the cell culture (*see* **Note 2**).

Time-lapse microscopy subsystem consists of:

1. *Inverse m\icroscope* sitting in CO_2 incubator (Fig. 1a).
2. High-sensitivity digital camera.
3. Illumination under minimized heat- and photo toxicity, operated in the near-infrared range (940 nm), with light emitting diodes synchronized by image-acquisition periods.
4. *Cell culture*. The growth of HaCaT cells in a 25 ml TL-flask starts at low (10–20%) confluency. Cell confluence is measured by the adaptation of the Image J program based on the occupation of the empty space by the cells in the visual field not in the entire growth chamber. The culture is placed under the inverse microscope and subjected to time-lapse videomicroscopy. Frames are recorded every minute and the video sequence converted to database form. The time of exposure is indicated in the filename of each frame. Exposures are converted to video films by speeding up the projection to 30 exposures/s. Proliferation of cells is measured by (a) the observation of cells undergoing cell division expressed on graphs as number of cells/frame and (b) as the surface area covered by cells (confluency) in square pixels [6–9].
5. *Control unit*. Electronic steering takes place through the control unit (Fig. 1b). This unit is located outside the CO_2 incubator and contains the activating contact stud, the activating buttons of the working chambers, and the vacuum/pressure switch. The control panel is working parallel with the relay-driven computer interface to provide full manual control during the experiment.
6. *Image acquisition computer system* (Fig. 1c). Open-source software Fiji is used for quantitative image analysis. Image sequences are converted to 8-bit grey scale. Resulting image stacks are deflickered to eliminate transient brightness changes. Background is homogenized by fast Fourier transformation and bandpass-filtering. Covered area (confluency) is determined by the dynamic thresholding of the image J progam of the National Institute of Healthy after background removal. This plugin is corrected for uneven illuminated background by using a rolling-ball algorithm. The number of dividing cells is determined by dynamic under/over thresholding and particle size analysis and circularity calculations of the segmented binary images frame by frame. Due to the large frame number providing fast results, operations are optimized for calculated speed.

3.2 Subsystems of TLS-PS

3.2.1 Perfusion Subsystem

The vacuum and the pneumatic pressure are measured by the vacuum gauge (VG) and manometer (MM), respectively. The vacuum is built up by the pneumatic pump and is directed toward the vacuum reservoir (VR). Leaky vacuum hoses and tubes could cause poor pump performance and in severe cases cylinder failures to function properly. To avoid such malfunction the vacuum reservoir was inserted to buffer and to protect the air vacuum pump that generates full vacuum within a minute after connecting it to the air line. The vacuum spreads from the vacuum reservoir through the three-way plastic valve (PV) to the distribution box that directs the low pressure either to the perfusion system or to the vacuum flask (VF). During the assembly the perfusion unit, including the vacuum flask is placed inside the laminar flow hood under sterile conditions. To secure sterility all instruments and materials placed under the hood are sprayed with 70% ethanol, the sterile air flow is turned on for at least 30 min to avoid the danger of setting on fire. The vacuum-side cleaner runs from the pump to the tissue culture (TC) and forces the debris into the vacuum flask. The overflow of the vacuum flask containing old medium, washing buffer, detached dividing or damaged cells can be disconnected from the system if necessary. The vacuum-side ends in the distribution box (DB) (Fig. 2a).

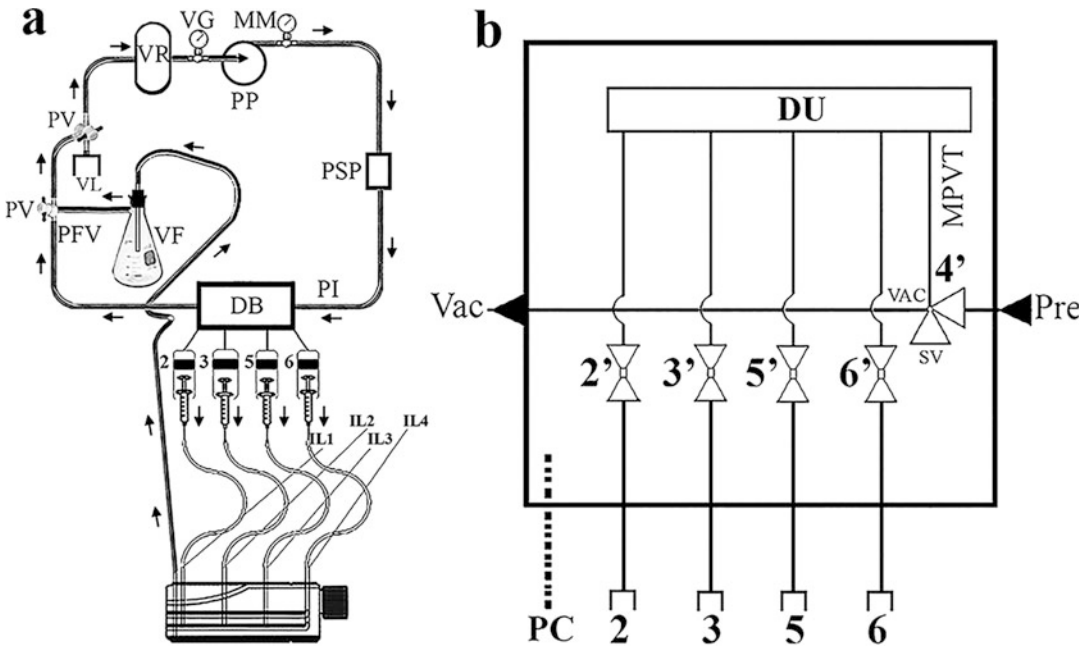

Fig. 2 Schematic representation of perfusion unit. (**a**) Parts of the perfusion circuits: *VR* vacuum reservoir, *VG* vacuum gauge, *PP* pneumatic pump, *MM* manometer, *PSP* pressure side port, *PI* pressure inlet, *DB* distribution box, *VF* vacuum flask, *PFV* perfusion vacuum, *PV* plastic valve, *VL* vacuum toward the laminar box. (**b**) Schematic view of the distribution box (DB) of perfusion system. *Vac* vacuum, *MPVT* major pressure-vacuum tube, *Pre* pressure, *DU* distributing unit, *PC* personal computer

3.2.2 Attachment of Liquid-Containing Syringes to the Perfusion Subsystem

All liquids to be added to the cell culture during the experiment are stored in syringes and incorporated in the perfusion system before starting the experiment. Each syringe is filled with the appropriate liquid under the sterile hood and two more ml-s of sterile air secure that the input tubing runs empty at the end of the injection steps. The piston is placed on the plunger and the syringe is fitted to the working chamber. By pressing the button belonging to one of the pistons of the control panel and at the same time pressing the vacuum knob, the plastic pads and the syringes are clamped to the pistons in standby position.

3.2.3 Vacuum-Side of Perfusion Unit

Safety considerations dictate the application of a pneumatic rather than a hydraulic perfusion unit. The hydraulic pressure could not only disrupt the plastic tubing system that is transporting the liquid, but the fluid could also cause short circuit.

The perfusion circuit is maintained by the pump that is compressing air at one end and generating vacuum at the other end. The vacuum-side of the system generates low pressure circuit through the inlet of the pump in the closed tubing system. The outlet-side of the pump, called the pressure circuit, works in compression mode.

The pressure-side of the perfusion unit is connected to the distribution box (Fig. 2a), starting at the outlet of the pump and containing a security pressure-side port. The function of the port is to prevent the sudden increase of pressure that can go up to 80–100 hPa during the installation of the system. The sudden pressure elevation may disrupt the tubing system at the connections. This is to be prevented at the pressure-side port by releasing the excess pressure. The circuit can be closed again and the normal working pressure restored.

The main function of the distribution box is to spread the pressure and vacuum evenly and in a regulated manner among the working chambers and to provide the uniform motion of the liquid contained in the syringes (lower part of Fig. 2a). The distribution box (DB) contains five electronic safety valves (2′, 3′, 5′, 6′, and 4′ in Fig. 2b). Four of them are connected to the working chambers (2, 3, 5, and 6 in Fig. 2b). The fifth three-way safety valve provides connection between the pressure and vacuum circuit branches, and is responsible for the electronic steering of the distribution box (valve 4′ in Fig. 2b). The principal function of this valve is to place the system under pressure or vacuum. Under electric current the valve introduces vacuum to the distribution box. The other four valves are turned off in the absence of electric signals. Upon activation the valves open toward the working chambers building up the vacuum/pressure in the cylinders.

3.3 Running the TLS-PS System

1. Activate the perfusion system by turning on the units in the following order:

- Pump.
- Interface electric power.
- Steering control panel.

2. After activating the system, let each working chamber work independently directed by its own valve.

3.3.1 Cell Growth in the TLS-Perfusion System

1. Perform all sterile operations under the laminar flow hood. Alcoholic disinfection at this point is not allowed due to the danger of inflammation while inserting the hot perfusion needles.
2. Heat the butterfly blood collection needle gradually to red-hot temperature and insert it into the T-flask (*see* **Note 3**).
3. Remove the first plug of the butterfly blood collection needle before the syringe is attached to it. This needle serves to introduce solutions to the flask.
4. Fix the needle to the flask with hot (200 °C) glue. The number of further needles inserted depends on the number of planned additions of solutions.
5. Add each solution through a separate sterile needle and syringe.
6. Cut the outlet needle blunt-ended, then heat, insert, and place near the bottom of the culture flask, then fix with hot glue (*see* **Note 4**).

3.3.2 Connecting the Cell Culture Flask to the TLS Unit

1. After the inserted needles cooled down to room temperature, but before starting the TLS experiment in the CO_2 incubator, spray and disinfect the outer surface of perfusion system with 70% ethanol.
2. Transfer the perfusion subsystem to the nearby CO_2 incubator and combine with the TLS subsystem. Place and fix the cells in the T flask supplied with the inlet and outlet needles, containing medium and cells to the object table of the inverted microscope sitting in the carbon dioxide incubator.
3. After fixing the flask to the object holder, focus the microscope to give sharp images of cells and start the TLS-PS experiment.

3.3.3 Running the TLS-PS Experiments

Replacement of the culture medium and other solutions during the TLS-perfusion experiments takes place in the closed sterile system without opening the carbon dioxide incubator. Carry out the experiments as follows:

1. Turn ON the TLS-perfusion system and the power unit by separate switches and by the “ON” button of the control panel.
2. To develop vacuum and pressure turn on the vacuum pump. Allow to develop proper vacuum pressure (45–50 hPa) and manometric overpressure (40 hPa) to run the perfusion system.

3. Make corrections by screw valves to run the system under optimal working conditions.
4. Add solution from the corresponding syringe to the culture flask by pressing the button of the control panel as long as needed. By pressing one of the 2′, 3′, 5′, or 6′ buttons the pressure increases in the corresponding 2, 3, 5, or 6 working camber and the pneumatic pressure forces the liquid out of the syringe into the T-flask (Fig. 2b).
5. By pressing simultaneously the VACUUM knob and one of the buttons (2′, 3′, 5′, 6′, Fig. 2b) of the control panel the opposite process takes place, namely the generated vacuum pulls back the liquid to the syringe. This operation is used when the suspended cells that were not attached to the monolayer were withdrawn without being discarded. The removal of the excess material from the T-flask takes place through the unit with its own switches directing the liquid through the outlet needle from the cell culture to the vacuum flask (*see* **Note 5**).

3.4 Cell Cycle Synchronization

To prove the applicability and reproducibility as well as to demonstrate the advantage of the LTS-perfusion system, two validation studies have been performed by synchronizing HaCaT cells. With respect to the most frequently used synchronization methods, bulk synchronization by physical separation, flow cytometry, cytofluorometric purification, and dielectrophoresis was not applicable to the LTS-perfusion system. The synchronization of cells by the LTS-perfusion system was limited to chemical blockade. Metabolic reactions of cells are most often blocked by nutritional deprivation and inhibition of DNA synthesis. Of the known classes of synchronization [10], nutrient deprivation and butyrate treatment belonging to the classes of chemical synchronization [11, 12] were used to test the TLS-PS system (*see* **Note 6**).

3.4.1 Synchronization by Serum Starvation

Nutritional serum starvation has been widely used for synchronization by arresting cells in the G_0/G_1 phase of the cell cycle, but it often reduced cell survival and increased DNA fragmentation [13–15]. In transformed cells, the proliferation turned out to be relatively independent of serum and growth factors, thus neoplastic cells do not necessarily cease proliferation immediately upon serum deprivation and subjection to stringent G_0 arrest [16]. HaCaT-transformed cells served to prove that serum deprivation could be used for their synchronization. Follow the protocol given below:

1. In the control experiment grow HaCaT cells and visualize growth by time-lapse microphotography in RPMI 1640 medium containing 10% FBS using the perfusion attachment as described.
2. After 24 h growth add fresh medium containing 10% FBS by the perfusion unit to maintain the logarithmic growth of cells.

Cell growth (Fig. 3a) and increase in confluency (Fig. 3b) show the continuous growth and 100% confluency attained after 66 h incubation.

3. Visualize cell growth by time-lapse microscopy with dividing cells being in the foreground, and monolayer cells in the background (Fig. 3c). Black numbers at the bottom of each panel

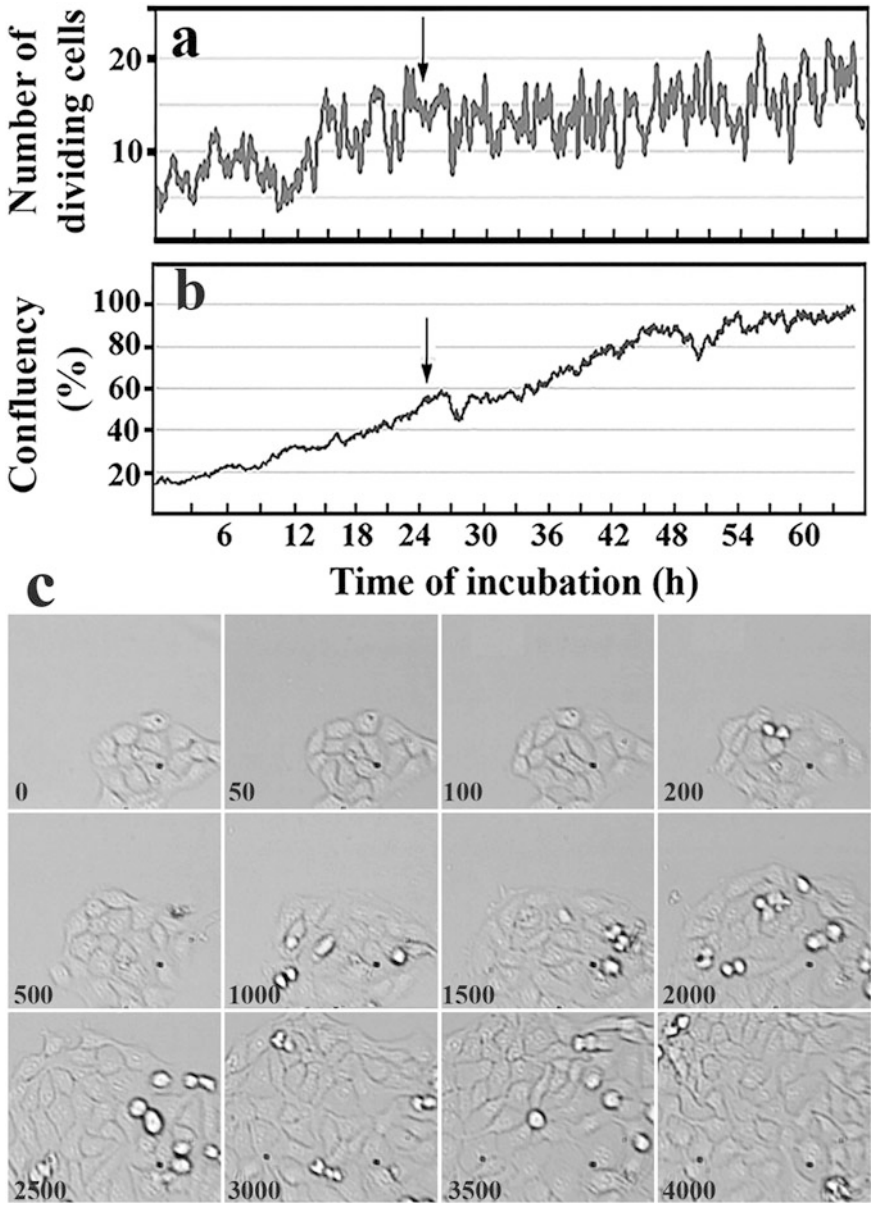

Fig. 3 The growth of control cells started in 10% serum containing RPMI medium. After 24 h additional 10% FBS was added and grown to 66 h. (**a**) Number of dividing cells and (**b**) increase in confluency were measured by time-lapse scanning microscopy. (**c**) Cell growth of a group of cells was revealed in the visual field of the microscope minute-by-minute

show the time in minutes passed from the recording. Images are to be brightness and contrast balanced, freed of interlacing and flickering, and gradient equalized, then subjected to histogram equation [6].

4. Start serum deprivation in RPMI 1640 medium in the absence of FBS causing a stagnation, then a drop, followed by a short increase in the mitotic cell number (Fig. 4a). Serum starvation increases temporarily the confluency as a consequence of expansion of cells binding to the attachment surface representing

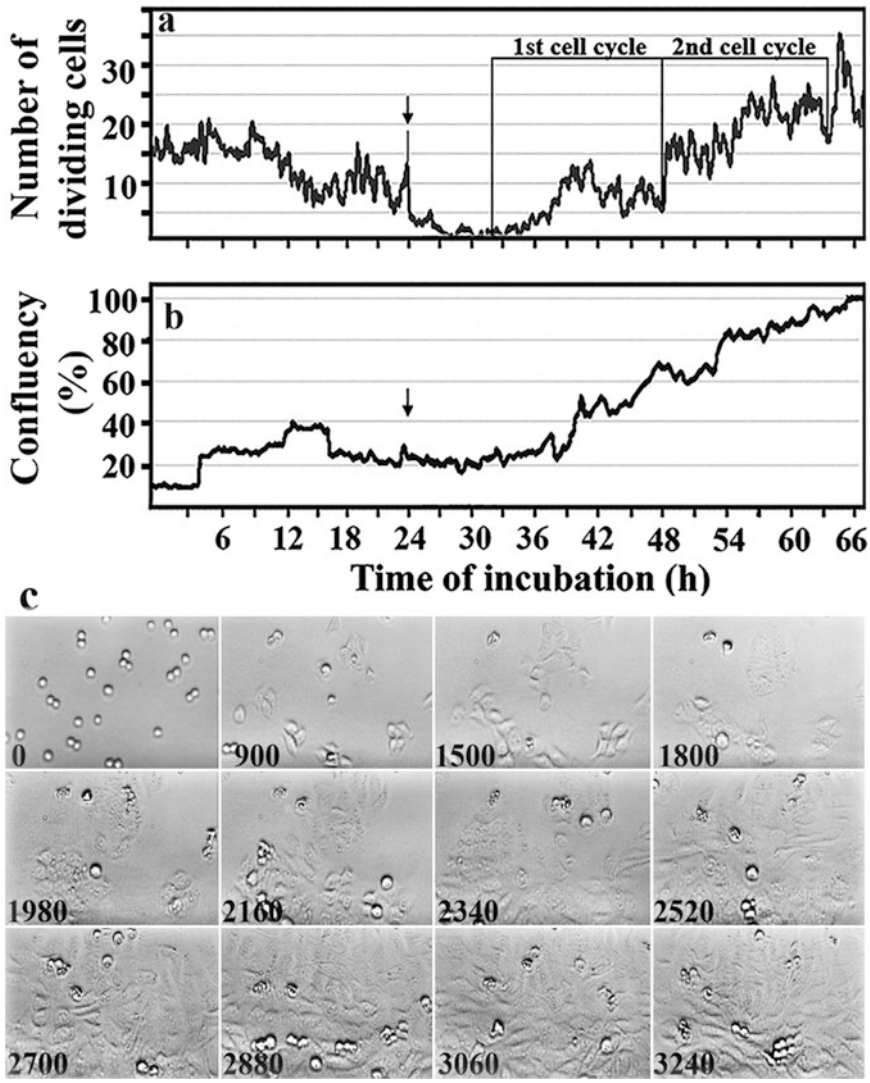

Fig. 4 Growth of HaCaT cells in serum-free RPMI medium. After 24 h serum deprivation was terminated and growth was continued in the presence of 10% FBS. (**a**) Number of dividing cells and (**b**) confluency changes were measured by time-lapse scanning microscopy. *Black arrow* indicates the time of serum addition. (**c**) Cell growth of a group of cells was revealed in the visual field of the microscope minute-by-minute

larger cell surface than rounded up mitotic cells that are not attached to the surface (Fig. 4b). The temporary increase of mitotic cell number after serum deprivation could be explained by the observation of others that HaCaT cell cultures could extend their proliferation in serum-free medium in contrast to normal human keratinocytes whose growth in vitro requires a feeder layer and/or the supplementation with hormones and growth factors [17]. The extension of the proliferation of HaCaT cells can be accounted for by the delayed attachment of cells to the monolayer that could be observed even after 10 h of incubation (Fig. 4c). In conformity with the autocrine activation of the epidermal growth factor (EGF) receptor on keratinocytes, extended proliferation has been recognized as an important growth regulatory mechanism involved in epithelial homeostasis [18]. These observations underline the importance of using cell cultures rather than individual cells in cell cycle studies.

5. After 24 h serum starvation, remove old medium and add fresh medium containing 10% FBS to the cell culture through the perfusion unit. The cell cycle from the lowest mitotic activity (32 h 50 min) to the next mitotic minimum (48 h 05 min) lasted for 15 h 15 min, corresponding to the length of the first synchronized cell cycle. In the next synchronized cell cycle with an initial logarithmic growth and mitotic drop after 63 h 25 min incubation, the length of the cell cycle corresponds to 15 h 20 min (Fig. 4a).

3.4.2 Synchronization with Butyrate

DNA synthesis can be blocked by butyrate as an inhibitor of DNA replication [19–21]. The major population of butyrate-treated cells is arrested at the very early G_1 phase, possibly immediately after mitosis, with some cells resting in G_0 [12].

1. Grow HaCaT cells in RPMI 1640 medium, 10% FBS and 10 mM sodium butyrate for 24 h.
2. Wash cells with PBS and replace by regular RPMI 1640 containing 10% FBS. After the removal of the cell cycle inhibitor fast growth and differentiation takes place that is manifested as expansion and motility changes of separate groups of morphological changes of clumping cells as well as individual round cells being in metaphase.
3. Take micrographs every minute during the differentiation process and collect data for image analysis showing changes in the cell number of dividing cells and confluency in the cell culture (Fig. 5). The cells treated with butyrate retain their initial growth characteristics, without significant changes in growth dynamics (Fig. 5a) and confluency increase (Fig. 5b) relative to the growth without butyrate. In the presence of butyrate the confluency level reach its maximum at ~12 h, followed by a

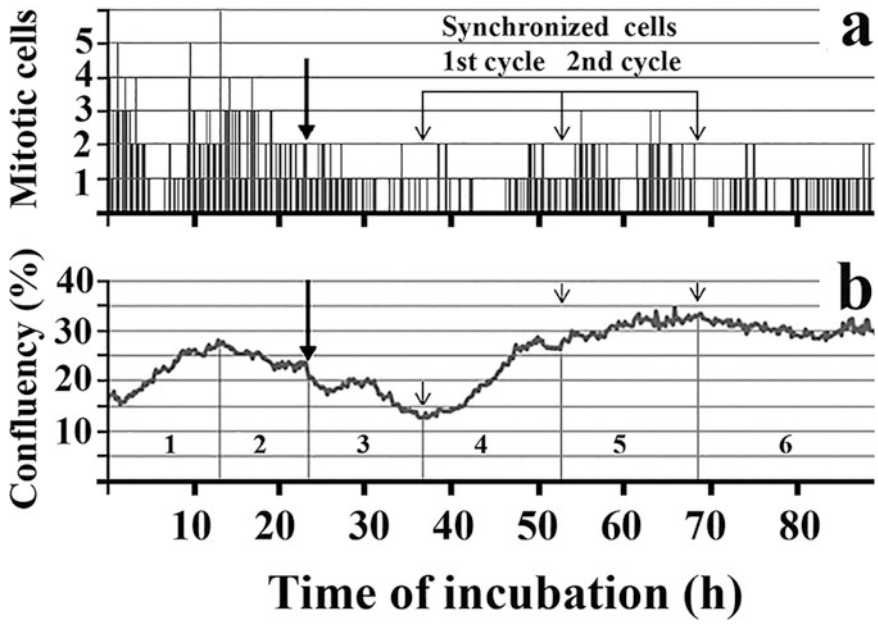

Fig. 5 Synchronization of HaCaT cells with sodium butyrate. HaCaT cells were grown in RPMI 1640 medium containing 10 % FBS and 10 mM sodium butyrate for 24 h. Then the medium was removed by the perfusion system and the cells were washed with PBS and fresh RPMI 1640 medium containing 10 % PBS culture was added. (**a**) Number of mitotic cells in the TLS-perfusion experiment. *Large black arrow* indicates the time of butyrate removal. *Small arrows* indicate the boundaries of the two synchronized cell cycles. (**b**) Confluency changes during synchronization with butyrate. Subphases of cell growth: (1) Residual growth in the presence of butyrate. (2) Reduction of mitotic cells and confluency. (3) Further reduction of mitotic cells and confluency changes after removal of butyrate. (4) First cell cycle of synchronized cells. (5) Second cell cycle after synchronization. (6) Loss of synchrony

gradual decrease, before the mitotic cell number culminates at ~14 h. This discrepancy could be explained by those dividing cells that detached from the monolayer, rounded up and caused a temporary confluency decrease. Further reduction in mitotic cell number and confluency points to apoptotic cell death. Butyrate treatment causes the clustering of apoptotic cells that could be distinguished and subtracted from the number of round metaphase cells (not shown).

4. After the removal of butyrate and replacement of medium, a significant reduction of confluency level became visible by TLS microscopy as a result of cellular shrinkage. The maximal value of shrinkage and minimal value of mitosis become detectable 38.3 h (2300 min) after the removal of butyrate. The regeneration of synchronized population could be divided into two consecutive cell cycles, the first one lasting for 15 h 34 min and the second cell cycle for 15 h 50 min indicated by the small arrows in Fig. 5a, b. These values of cell cycle length are somewhat higher, nevertheless comparable to those obtained by the synchronization of serum deprivation (15 h 15 min and 15 h 20 min).

One of the differences relative to the synchronization with serum deprivation was that 96 h after butyrate treatment the control population did not reach its initial confluency also pointing to the damaging effect of butyrate on the proliferative activity of cells and its toxicity causing death of some of the cells in the HaCaT population. In spite of these differences one can conclude that synchronization with serum deprivation and butyrate treatment can be performed by the TLS-perfusion system. The reproducibility is indicated by two consecutive cell cycles with the two different methods used for synchronization resulting in measurements with similar lengths of cell cycles:

Serum starvation:	15 h 15 min and 15 h 20 min (Fig. 4a)
Butyrate treatment:	15 h 34 min and 15 h 50 min (Fig. 5a)

The confluency during the second cell cycle was somewhat higher (Fig. 4b and Fig. 5b, respectively), while the cell cycle length was moderately extended in the second cell cycle, reflecting that confluency did not impact severely growth dynamics (*see* **Note 7**).

4 Notes

1. A wide range of commercially available perfusion and imaging systems are available, offering designs such as glass bottom dishes, multiwell chambers on microscope slides, heating stages with perfusion adapters, specialized chambers with conductive coatings for tight control of temperature. Typical packages include: chamber, temperature control, stage adapter, and accessories but no carbon dioxide incubator. The long-term use of these systems is limited due to the small volume that is another limiting factor to get a large and homogeneous monolayer. Cells in our system are growing in a 25 ml T-flask providing sufficient growth capacity against temporary fluctuations other systems are likely to be subjected.
2. Originally we started to add solutions manually to the cell culture through butterfly blood collection needles. Incandescent hot needles were used to penetrate the T-flask and fix them with hot (200 °C) glue. The inlet needle was directed toward and touching the wall of the T-flask to avoid the turbulence of the cell culture medium. The end of the outlet needle was cut blunt before its insertion, then placed as close to the bottom of the flask as possible. The T-flask was slightly tilted (3%) toward the outlet needle to secure complete removal of the old medium. Initially, the culture medium was removed manually through the outlet needle with another needle and syringe. Although the T-flask was fixed to the stage of the inverted

microscope, it occasionally changed slightly its position during the manipulation. Due to these technical hindrances, it was mandatory to improve and automate the perfusion system. As a result we have developed a pneumatic-driven force transduction method, to keep the system as simple and fail-safe as possible. In this setup during the experiment the working chambers push or pull the plunger of the syringe without touching the T-flask or the syringe.

3. Use another incandescent hot needle of 3 mm diameter to penetrate the T-flask before inserting the inlet and outlet needles. This way, the molten plastic in the inlet and outlet needles will not caulk the flow of solutions.
4. In the course of working, you could get some non-sterile tools in the laminar flow hood (e.g., the glue gun for fixing the needles)—be very careful not to contaminate the cell culture while using them.
5. Cleaning of the perfusion system: Parts of the perfusion system were autoclaved then connected under the laminar flow hood and rinsed with 70% ethanol. The ethanol was removed by pumping and drying the passages with sterile-filtered compressed air. The vacuum flask containing the discarded solution was removed and sterilized separately.
6. HaCaT cell synchronization in the perfusion system is based on the visibility of dividing cells. The number of dividing cells corresponded to the number of mitotic cells counted every minute by time-lapse photomicroscopy. Before division detached cells were rounded up and after division the two daughter cells separated and reattached to the monolayer. Detached cells through a thin plasma bridge did not lose contact with the monolayer [7]. The detachment of mitotic cells and their division was visualized by time-lapse photomicroscopy that turned out to be a reliable measure to follow synchronization without necessitating markers for synchronized and non-synchronized cells.
7. We confirm the existence of a significant lag period, before butyrate-induced G_1-synchronized cells entered S phase in agreement with the observation of others [12]. The length of the two consecutive cell cycles after serum starvation was 15 h 15 min and 15 h 20 min *versus* 15 h 34 min and 15 h 50 min measured after synchronization by butyrate treatment. Due to the undisturbed growth conditions in the TLS-perfusion system, the length of the cell cycle of HaCaT cells was significantly shorter and uniform relative to the consecutive cell cycles measured in single cells by the TLS system without perfusion [22]. TLS visualizes not only the cell growth of a group of cells in the visual field of the microscope, but also the fate of

individual cells can be followed minute-by-minute. Synchronization did not measurably affect growth. 100% confluency in control population was attained after 66 h. Similarly, after serum starvation 100% cell confluence was obtained after 66 h growth and after butyrate treatment at around 68 h.

Acknowledgements

This work was supported by the National Science Research Foundation of the Hungarian Academy of Sciences OTKA grant T42762 to G.B. and by TAMOP 4.2.4. A/2-11-1-2012-0001 National Excellence Program to G.N. The project was subsidized by the European Union and co-financed by the European Social Fund.

References

1. Obom KM, Magno A, Cummings PJ (2013) Operation of a benchtop bioreactor. J Vis Exp 79:e50582
2. Alahari A (2009) Implementation of cost-reduction strategies for HuMAb manufacturing Processes. BioProcess Int 7:48–54
3. Muzzey D, van Oudenaarden A (2009) Quantitative time-lapse fluorescence microscopy in single cells. Annu Rev Cell Dev Biol 25:301–327
4. Dzyubachyk O, Essers J, van Cappellen WA, Baldeyron C, Inagaki A, Niessen WJ et al (2010) Automated analysis of time-lapse fluorescence microscopy images: from live cell images to intracellular foci. Bioinformatics 26:2424–2430
5. Conaghan J, Chen AA, Willman SP, Ivani K, Chenette PE, Boostanfar R et al (2013) Improving embryo selection using a computer-automated time-lapse image analysis test plus day 3 morphology: results from a prospective multicenter trial. Fertil Steril 100:412–419
6. Farkas E, Ujvarosi K, Nagy G, Posta J, Banfalvi G (2010) Apoptogenic and necrogenic effects of mercuric acetate on the chromatin structure of K562 human erythroleukemia cells. Toxicol In Vitro 24:267–275
7. Nagy G, Pinter G, Kohut G, Adam AL, Trencsenyi G, Hornok L et al (2010) Time-lapse analysis of cell death in mammalian and fungal cells. DNA Cell Biol 29:249–259
8. Nagy G, Hennig GW, Petrenyi K, Kovacs L, Pocsi I, Dombradi V et al (2014) Time-lapse video microscopy and image analysis of adherence and growth patterns of Candida albicans strains. Appl Microbiol Biotechnol 98:5185–5194
9. Horvath E, Nagy G, Turani M, Balogh E, Papp G, Pollak E et al (2012) Effect of the fungal mycotoxin patulin on the chromatin structure of fission yeast Schizosaccharomyces pombe. J Basic Microbiol 52:1–11
10. Banfalvi G (2008) Cell cycle synchronization of animal cells and nuclei by centrifugal elutriation. Nat Protoc 3:663–673
11. Banfalvi G (2011) Overview of cell synchronization. Methods Mol Biol 761:1–23
12. Li C (2011) Specific cell cycle synchronization with butyrate and cell cycle analysis. Methods Mol Biol 761:125–136
13. Kues WA, Anger M, Carnwarth JW, Motlik J, Nieman H (2000) Cell cycle synchronization of porcine fibroblasts: effects of serum deprivation and reversible cell cycle inhibitors. Biol Reprod 62:412–419
14. Langan TJ, Chou RC (2011) Synchronization of mammalian cell culture by serum deprivation. Methods Mol Biol 761:75–83
15. Basnakian A, Banfalvi G, Sarkar N (1989) Contribution of DNA polymerase δ to DNA replication in permeable CHO cells synchronized in S phase. Nucleic Acids Res 17:4757–4767
16. Scher CD, Stone ME, Stiles CD (1979) Platelet-derived growth factor prevents Go growth arrest. Nature 281:390–392
17. Pozzi G, Guidi M, Laudicina F, Marazzi M, Falcone L, Betti R et al (2004) IGF-I stimulates proliferation of spontaneously immortalized human keratinocytes (HACAT) by autocrine/paracrine mechanisms. J Endocrinol Invest 27:142–149
18. Vardy DA, Kari C, Lazarus GS, Jensen PJ, Zilberstein A, Plowman GD et al (1995)

Induction of autocrine epidermal growth factor receptor ligands in human keratinocytes by insulin/insulin-like growth factor-1. J Cell Physiol 163:257–265

19. Li CJ, Elasser TH (2006) Specific cell cycle synchronization with butyrate and cell cycle analysis by flow cytometry for Madin Darby Bovine Kidney (MDBK) cell line. J Anim Vet Adv 5:916–923
20. Wright JA (1973) Morphology and growth rate changes in Chinese hamster cells cultured in presence of sodium butyrate. Exp Cell Res 78:456–460
21. Kruh J, Defer N, Tichonicky L (1992) Molecular and cellular action of butyrate. C R Seances Soc Biol Fil 186:12–25
22. Nagy G, Kiraly G, Banfalvi G (2012) Ch. 7. In: Conn, PM (ed) Laboratory methods in cell biology. Elsevier. pp 143–161

Chapter 11

Analysis of Nuclear Uracil DNA–Glycosylase (nUDG) Turnover During the Cell Cycle

Jennifer A. Fischer and Salvatore J. Caradonna

Abstract

Uracil-DNA glycosylases (UDG/UNG) are enzymes that remove uracil from DNA and initiate base-excision repair. These enzymes play a key role in maintaining genomic integrity by reducing the mutagenic events caused by G:C to A:T transition mutations. The recent finding that a family of RNA editing enzymes (AID/APOBECs) can deaminate cytosine in DNA has raised the interest in these base-excision repair enzymes. The methodology presented here focuses on determining the regulation of the nuclear isoform of uracil-DNA glycosylase (nUDG), a 36,000 Da protein. In synchronized HeLa cells, nUDG protein levels decrease to barely detectable levels during the S phase of the cell cycle. Immunoblot analysis of immunoprecipitated or affinity-isolated nUDG reveals ubiquitin-conjugated nUDG when proteolysis is inhibited by agents that block proteasomal-dependent protein degradation.

Key words Uracil-DNA glycosylase, Cell cycle, Ubiquitin conjugation, Immunoprecipitation, Cell transfection

1 Introduction

Research concerning the removal of uracil moieties from DNA and the subsequent repair has been an area of interest to a number of investigators. Uracil misincorporation and cytosine deamination are potentially mutagenic events that can occur with significant frequency under various cellular conditions. Thus to preserve genomic integrity, it is critical that the cell contains enzymes to recognize and repair this damage [1]. Uracil-DNA glycosylases catalyze the first step in the base excision repair pathway to remove uracil from DNA. In mammalian cells there are at least three structurally distinct families of UDGs [2]. These enzymes hydrolyze the *N*-glycosyl bond between the uracil base and the deoxyribose moiety. The resulting apyrimidinic site is then repaired by the sequential actions of an AP endonuclease, phosphodiesterase, DNA polymerase, and DNA ligase [3].

Gaspar Banfalvi (ed.), *Cell Cycle Synchronization: Methods and Protocols*, Methods in Molecular Biology, vol. 1524,
DOI 10.1007/978-1-4939-6603-5_11,

The discovery that regulated generation of uracil in DNA is part of certain cellular processes has raised awareness of this base-excision repair pathway. B lymphocytes require the generation of G:U mismatches in selected regions of immunoglobulin genes to promote both somatic hypermutation and class-switch recombination [4, 5]. Activation-induced cytidine deaminase (AID), which is specific for B cells, is required for both processes in maturing lymphocytes.

Cytosine deamination to uracil in DNA appears to be a form of innate immunity to HIV infection. Using a murine leukemia virus model system, Harris and co-workers show that the CEM15/APOBEC3G DNA deaminase can be packaged into virions during virus production [6]. The presence of this APOBEC family member triggers deamination of cytosine to uracil within the virus minus-strand cDNA after infection and during retroviral replication. This was shown to lead to HIV genome destruction, possibly due to uracil-DNA glycosylase action on the overabundance of uracil moieties. Research in our laboratory has focused on the post-translational mechanisms that alter the stability of the nuclear isoform of UDG (nUDG, UNG2). We have shown that nUDG turnover is a function of cell cycle phase and in certain cell lines a function of drug-induced stress during DNA replication [7, 8].

2 Materials

2.1 Cell Culture

1. Dulbecco's Modified Eagle's Medium (DMEM) containing 10% fetal bovine serum (FBS). Sodium pyruvate is added to 1 mM Dulbecco's Phosphate Buffered Saline (PBS), Trypsin/EDTA (0.25%/1 mM).
2. HeLa S3 cell line (CCL2.2) (American Type Culture Collection).
3. Human Embryonic Kidney cells (293H) (11631-017, Invitrogen Corp.).
4. Mycoplasma PCR Detection Kit.

2.2 Cell Synchronization

1. Nocodazole is dissolved in dimethyl sulfoxide (DMSO) to a final concentration of 1 mg/ml. The solution is stored at −20 °C in aliquots and used within 1 year.
2. Aphidicolin is dissolved in DMSO to a final concentration of 1 mg/ml. Aliquots are stored at −20 °C and used within 2 months.
3. *N*-acetyl-leu-leu-Norleu-al (LLnL) is dissolved in DMSO at a final concentration of 10 mM. Aliquots are stored at −20 °C and used within 1 month.

4. Carbobenzoxy-l-leucyl-l-leucyl-l-leucinal (Z-LLL-CHO, MG132) is dissolved in DMSO at a final concentration of 10 mM. Aliquots are stored at −20 °C and used within 1 month.
5. [Methyl-^{3}H]-thymidine (81.5 Ci/mmol, 1uCi/ul). Stocks are stored at +4 °C in airtight containers.
6. Trichloroacetic acid (TCA) is dissolved in H_2O to make a 100% solution (i.e., 500 g TCA plus 227 ml H_2O). Solution is stored at +4 °C and diluted as needed.
7. GF/C filters (Whatman glass microfiber filters, 2.5 cm) were used.

2.3 Protein Extraction, SDS-PAGE, and Western Blotting

1. NP40 extraction buffer; 50 mM Tris–Cl, pH 7.5, 250 mM NaCl, 0.1% NP40, 5 mM EDTA, 50 mM sodium fluoride. Protease Inhibitor Cocktail Set III (Calbiochem), EDTA-Free, and Phosphatase Inhibitor Cocktail Set III (Calbiochem) were added. BioRad protein assay dye reagent concentrate and Bovine serum albumin (BSA) were used for standard curve in protein determinations.
2. Polyacrylamide gel solutions; 40% ProtoGel, 37.5 : 1 acrylamide : bisacrylamide (National Diagnostics), 4× Resolving Buffer for the separating gel (National Diagnostics), ProtoGel Stacking Buffer for the stacking gel (National Diagnostics). *N*-,*N*-,*N*′-,*N*′-tetramethylethylenediamine (TEMED), Molecular Biology Grade. 10% Ammonium Persulfate made up fresh on a weekly basis. SDS-PAGE sample loading buffer (3× stock concentrations); 240 mM Tris–Cl pH 6.8, 6% SDS, 30% glycerol, 0.6 mg/ml bromophenol blue. 2-Mercaptoethanol (BME). Running buffer (5× stock diluted to 1× the day of use). 5× stock (4 l, stored at room temperature); 60 g Tris base, 288 g glycine, 20 g SDS (all reagents electrophoresis grade). Prestained protein molecular weight markers were used.
3. Protein transfer and immunostaining. Blotting membrane: InVitrolon PVDF and Whatman 3MM chromatography paper were used for the transfer. Transfer (Electroblot) buffer; 1× (for 5 l); 15.15 g Tris base, 72 g Glycine, 1 l methanol. Transfer buffer is made up and stored at 4° C in a carboy. 10× TBS (tris-buffered saline, for 1 l); 100 ml of 1 M Tris–Cl, pH 8.0, 87.66 g NaCl, volume brought to 1 l and stored at 4 °C. TBST (Tris-buffered saline plus Tween-20). Make up 4 l and store at 4 °C (use within a month). 400 ml 10× TBS, 2 ml Tween-20. We cut the tips off a 1 ml pipet tip, slowly pipet the Tween-20 into the stirring solution and let the tips swirl in the solution to remove remaining detergent. Bring the volume up to 4 l.
4. TBST-5% skim milk block. 5 g of non-fat skim milk in 100 ml of TBST. Make this up fresh daily. There is a high degree of variability in background levels due to non-fat skim milk from

different commercial vendors. We use Carnation packets or Nonfat dry milk (Cell Signaling Technology Corp.). Polyclonal AU1 antibody (Covance Corp.). Ab225 antibody against the amino-terminal end of nUDG is prepared for us by Covance Corp using our bacterially expressed protein. Detection of immunostaining is done using ECL Western Blotting Detection Reagents (Amersham).

2.4 Ubiquitination of nUDG

1. pCINeo vector (Promega Corp.) was transfected using Lipofectamine 2000 (Invitrogen).
2. NiNTA-agarose (Qiagen Corp.) used with Buffer A; 6 M guanidine–HCl, 0.1 M sodium phosphate and 10 mM imidazole, pH 8.0. Buffer TI; 25 mM Tris-Cl, 20 mM Imidazole, pH 6.8.

3 Methods

3.1 Maintenance of Cell Cultures

1. HeLa S3 cells are maintained in DMEM media supplemented with 10% calf serum. Cells are cultured in a humidified atmosphere of 5% CO_2 at 37 °C. 293H cells and HT-29 cells are maintained in DMEM media supplemented with 10% fetal calf serum. We routinely passage cells at 3–4 day intervals, reseeding flasks at a 1–10 dilution. Cells are not carried for more than 10–15 passages and are not allowed to become totally confluent. We do not use antibiotics (*see* **Note 1**).
2. The day before the experiment, cells are seeded into dishes. For experiments requiring 6 cm dishes, cells are seeded at between 1 and 2×10^6 per dish. For 10 cm dishes cells are seeded at between 5 and 6×10^6 per dish. Experiments are carried out using the growth conditions described above.

3.2 Synchronization of Cells at Different Points in the Cell Cycle

1. To arrest cells at the G_2/M border, HeLa S3 cells are treated with 100 ng/ml of nocodazole for times ranging from 12 to 20 h (*see* **Note 2**).
2. Cells are released from nocodazole block by washing twice in media free of the drug. Cells will tend to float off the surface at this point so it is essential to wash the cells off the surface using a sterile pipet and spinning the cells down, washing again and pelleting the cells. Cells are replated and immediately placed in the incubator (*see* **Note 3**).
3. Individual plates are harvested at the appropriate times. Since at the early time points cells have not adhered they are harvested in the media, spun down and washed once in ice-cold PBS. Cells are pelleted by centrifugation, the wash is aspirated and the pellets are frozen at –80 °C until extraction (*see* **Note 3**).

4. To synchronize cells at the G_1/S border, HeLa S3 cells are treated with aphidicolin at a final concentration of 5 μg/ml for 20 h.
5. After this time period, cells are washed three times with complete media minus the drug. Media is added and cells allowed to incubate for the appropriate time intervals before harvesting. Since aphidicolin does not disrupt adherence to the plates, washing of cells is done on the plates without the need for centrifugation.
6. To examine the post-translational fate of nUDG prior to proteolysis, cells are treated with inhibitors to prevent proteosomal degradation. Cells are treated with 100 ng/ml of nocodazole for 6 h and then treated with either LLnL at 50 μM or MG132 at 25 μM for an additional 6 h. At the appropriate time the cells are harvested as described above (*see* **Note 4**).
7. A convenient method to monitor progression through S phase is by pulse-labeling individual cultures with [^{3}H]-thymidine at time intervals that correspond to the experimental time points (*see* **Note 5**). Plates are seeded and treated as appropriate, outlined above. At individual time points 10 μCi of [^{3}H]-thymidine is added to the cell culture and incubated for 30 min. After this time the cells are washed once with ice-cold PBS, scraped and pelleted by centrifugation. The cell pellet is resuspended in 400 μl of PBS and 100 μl of 10% TCA. The mixture is incubated on ice for 15 min and then filtered through a pre-wet (10% TCA) GF/C filter on an appropriate filtration apparatus. The filter is washed with 10 ml of 10% ice-cold TCA and finally with 1–2 ml of 100% acetone. Filters are dried and counted.

3.3 Protein Analysis by SDS-PAGE and Western Blot

1. Cell extracts are prepared in NP40 buffer containing Calbiochem protease inhibitor cocktail set III (1–200 dilution) and 1 mM PMSF as well as Calbiochem phosphatase inhibitor cocktail set II (1–200 dilution). The −80 °C stored pellets are resuspended directly in prepared NP40 buffer and sonicated using a Branson sonifier and cup horn, 90% pulse and mid-range intensity setting. The extract is pulsed 8–10 times and incubated on ice for 30 min.
2. After this period the extract is centrifuged in a microfuge, top-speed for 5 min. The supernatant is reserved for further use and the pellet is stored at −80 °C (*see* **Note 6**). Total protein concentration per sample is determined using the BioRad Bradford protein assay reagent and BSA for the standard curve.
3. The BioRad SDS-PAGE Mini-PROTEAN Electrophoresis Cell is routinely used. Glass plates are washed with glass detergent dried and cleaned with 100% ethanol and dried. The apparatus is put together and a mark is made to indicate the height of the separating gel (usually 1.75 cm from the shorter glass plate).

4. Formulation for 12% separating gel utilizes per 10 ml; 3 ml of 40% Protogel (37.5:1 acrylamide : bisacrylamide), 2.5 ml of 4× resolving buffer and 4.4 ml of H_2O. The solution is degassed for 5 min by using a rubber stopper with a cut plastic pipet through the hole. House vacuum is applied to the stopped 50 ml flask. Polymerization is initiated with the addition of 0.10 ml of 10% (w/v) ammonium persulfate (made fresh weekly) and 0.01 ml of TEMED. Working quickly at this point, the solution is poured between the glass plates with a plastic pipet up to the mark. This solution is overlayed with water-saturated butanol to a depth of 1–2 mm. You should begin to see polymerization within 15 min.
5. After 30 min the (4%) stacking gel is prepared using per 10 ml; 1.0 ml of 40% ProtoGel, 2.8 ml of ProtoGel Stacking Buffer, and 6.1 ml of H_2O. The solution is degassed as described above and polymerization initiated by the addition of 0.05 ml fresh ammonium persulfate and 0.01 ml of TEMED. The overlay is removed, stacking gel is poured in using a plastic pipet and a comb is slowly inserted at an angle, to avoid trapping of bubbles (*see* **Note** 7). Gels are allowed to set for a minimum of 1 h before placing in the buffer tank apparatus. Gels can be stored overnight wrapped in parafilm with the comb still in the stacking gel.
6. Appropriate volumes of extract, based on total protein, are mixed with either 2× or 3× SDS-PAGE buffer and 1% BME. The samples are heated to 80 °C for 5 min and briefly centrifuged. During this time the polyacrylamide gel is assembled into the buffer tank assembly with the comb still in place. Running buffer is added and the comb is gently removed allowing the running buffer to enter the wells. The wells are washed out using a plastic pipet, slowly pipeting up and down.
7. Samples are loaded and appropriate protein markers are used. We routinely use prestained markers which makes it easy to monitor progress of electrophoresis, and orientation of the gel and the blot throughout the procedure. Electrophoresis is conducted at 150–200 V, until the dye is at the bottom or just run off (usually around an hour to an hour and a half).
8. Subsequent to SDS-PAGE fractionation, proteins are transferred to a solid support is accomplished using a Mini Trans-Blot Cell from BioRad. The electrophoretic apparatus is taken apart and the gel carefully removed from the plates. Stacking gel is removed with a single-edged razor and the gel is soaked in cold transfer buffer for 5 min at room temperature with gentle rocking (*see* **Note 8**). During this time a piece of PVDF (*see* **Note 9**) membrane is removed, wetted in methanol and soaked in a tray of transfer buffer (insure that the membrane is

submerged by rocking the tray). A second tray is set up containing the gel holder cassette (black side down). A 1 l beaker of cold transfer buffer is placed near the tray and used to wet the sponges and the 3MM paper.

9. In this order; lay down a wetted sponge, three pieces of wetted 3MM paper (two come with the PVDF). Using a cut plastic 10 ml pipet (size should be a little longer than the cassette, lengthwise) roll over the paper and insure that all bubbles are out. Place the soaked polyacrylamide gel on the 3MM paper (top side toward you). Roll the gel out gently to remove all air bubbles. Carefully place the wet PVDF membrane on the gel. Again gently roll all air bubbles out (*see* **Note 10**). Place 1 piece of wet 3 MM paper on the PVDF, gently roll over the surface again, turn the gel 90° and roll out the air bubbles from this direction. Carefully place the second wetted sponge on top. Close and lock the cassette.
10. Place the frozen ice-block container (stored at –80 °C containing H_2O to three-quarters full) in the tank, add a small stir bar and add transfer buffer to about 75% full (it helps to have a third tray under the transfer tank to collect any spill-over and avoid electrical issues once on the stir plate). Carefully place the cassette in the tank (black to black, black to back). Connect the lid making sure the red electrode is on the red side and the black electrode is on the black side. Run the transfer at 100 V for one hour with stirring. A power supply that maintains about 200 mA is required (i.e., BioRad PowerPac HC High-Current Power Supply, 250 V, 3.0 A, 300 W). Insure that the amperage is registering. If it is not the connections are faulty. Under these conditions the temperature of the transfer is between 10 and 15 °C for the whole run.
11. After the run the PVDF membrane is submerged in TBS and transferred to 5% skim milk in TBST. The membrane is blocked for 30 min at room temperature with rocking.
12. The blocking solution is discarded and new block is added to the tray containing the membrane. Primary antibody is added at a dilution that is dependent on the antibody. Appropriate dilutions should be determined empirically for the particular protein species being examined. Incubation is done overnight at room temperature with rocking. 0.01% thimerosal is included in the overnight incubation to prevent growth of any bacterial contamination.
13. After the incubation period the membrane is washed in TBST twice and then incubated in TBST for 5 min with rocking. This is repeated twice more.
14. The membrane is again blocked in 5% skim milk/TBST for 15–20 min, the block is discarded and secondary antibody is

added with new blocking solution. The membrane is incubated for 1 h at room temperature with rocking.

15. The washing steps are repeated exactly as above. The membrane is place in TBS and rocked while the ECL developing solution is prepared. The membrane and the tray are emptied of TBS and shaken to remove as much liquid as possible.
16. The membrane is then incubated with 4 ml of ECL solution for 1 min. The membrane is gently shaken and laid on a piece of saran wrap transfer side down (the side that touched the polyacrylamide gel). The membrane is wrapped in the saran wrap, taped (transfer side up) in an appropriate x-ray cassette or holder such as technal proof-printer (*see* **Note 11**). Tape the wrapped membrane, transfer side up on the inside glass of the proof-printer along with a fluorescent ruler (used to align the gel and the film).
17. Expose to film in an appropriate dark room by placing the film on the membrane and closing the proof-printer and applying even pressure. Make sure the correct film side is in contact with the membrane.
18. Develop the film in an x-ray processor. Use the imprint of the ruler on the film to correctly align the colored markers on the membrane. Examples of these procedures are illustrated in Figs. 1 and 2.

3.4 Determination of nUDG Ubiquitination in Cells as a Function of the Cell Cycle

1. For ectopic expression of nUDG, a eukaryotic expression vector is constructed to contain the open reading frame of nUDG. The DNA containing the open reading frame is cloned into the pCINeo vector.
2. The protein is designed to contain an in-frame epitope tag at the C-terminus of the protein. PCR and appropriate primers are used to incorporate the epitope tag (DTYRYI) at the 3' end of the sequence. This epitope is recognized by the antibody, AU1 (*see* **Note 12**).
3. A eukaryotic expression vector, that contains a His-tagged ubiquitin construct, was generously provided by Dr. Dirk Bohmann (*see* **Note 13**). The vector consists of a CMV promoter/enhancer region driving the transcription of an mRNA encoding a multimeric precursor protein composed of eight ubiquitin units with an amino-terminally added pHis tag (six histidine residues, pMT107) to each ubiquitin unit 9.
4. The constructs are transiently co-transfected into 293H cells using lipofectAMINE 2000. Twenty-four hours prior to transfection, 293H cells are plated in 6 cm dishes at 2×10^6 cells/dish. Cells are transfected with 3 μg of nUDG construct (vector alone or AU-tagged nUDG) and 5 μg of pMT107. Cells are allowed to incubate with the DNA complexes for 24 h. The

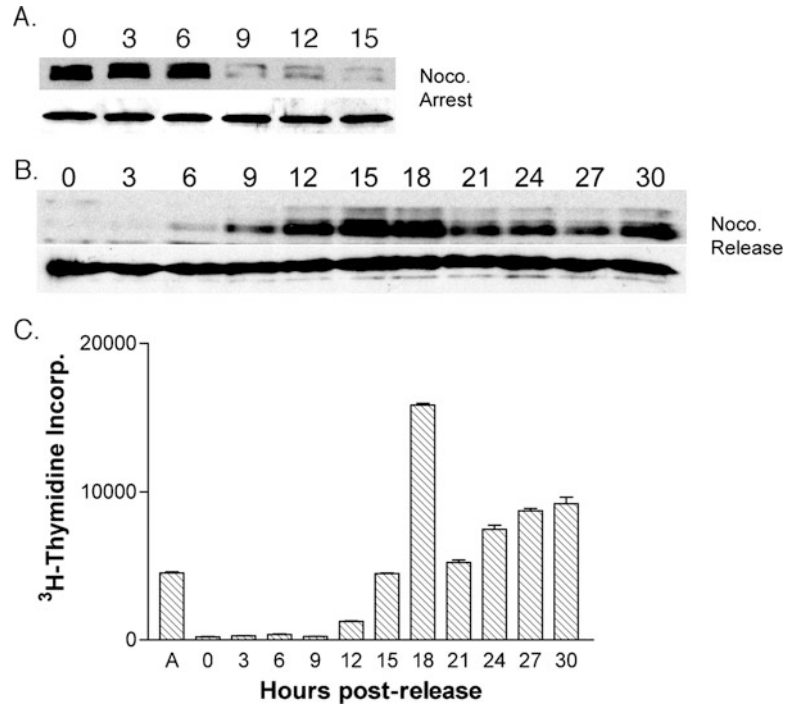

Fig. 1 Analysis of the steady-state levels of nUDG during nocodazole block and release. A. HeLa cells were incubated with nocodazole and harvested at 3 h intervals post-arrest (indicated by *numbers* above each lane). Immunoblot analysis was performed using equivalent amounts of cell extract to detect nUDG protein levels at the indicated times. As a control to insure that equivalent amounts of protein were applied to each lane, the nitrocellulose was stripped of antibody and reprobed with antisera against glyceraldehyde-3-phosphate dehydrogenase (GAPDH). As seen in the *lower panel* of (**a**), equivalent amounts of total protein was applied per lane. (**b**) HeLa cells were treated with nocodazole for 12 h. The drug was then removed and the cells were released from G_2/M phase arrest. Extracts from cells harvested at 3 h intervals post-release were analyzed by Western blot. The numbers above each lane indicate hours post-release. *Lower panel*: GAPDH immunostain loading control. (**c**) To verify that release from nocodazole block occurred when the drug was removed, parallel cultures (2×10^{-5} cells per 6 cm dish) were pulse-labeled with ^{3}H-thymidine and the DNA extracted and analyzed for ^{3}H-dTMP incorporation. Cells were treated for 12 h with nocodazole. The cells were then washed twice with media free of nocodazole and at the indicated times (in hours), cells were harvested and incorporation (reported as cpm $\times 10^{-3}$) was determined. "*A*" indicates a 20 min labeling of an asynchronous population of HeLa cells. 0 h indicates a 20 min pulse immediately after nocodazole release. Values indicate the means averaged from triplicate pulse-labeled cultures

media is then changed and in selected plates the proteosome inhibitor, MG132 is added to a final concentration of 25 μM. Cells are incubated for an additional 12 h before harvesting. Cells are scraped into cold PBS and pelleted.

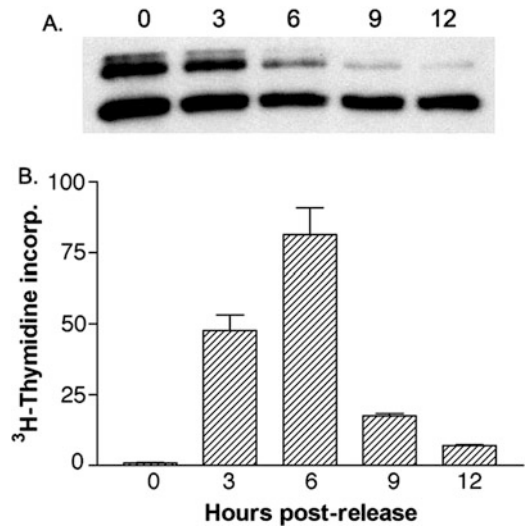

Fig. 2 Analysis of steady-state levels of nUDG during release from an aphidicolin block. (**a**). HeLa cells were treated with aphidicolin for 18 h. Cells were then washed three times with DMEM minus serum. Complete media was added and cells were harvested at the indicated times in hours. Western blot analysis was then performed on cell extracts using antisera (C8) that recognizes both forms of UDG (nuclear and mitochondrial). As seen in the figure, the upper bands (nUDG) significantly diminish by 6 h post-release from aphidicolin block. In contrast the lower band (mitochondrial UDG) maintains a relatively constant level up to 12 h post-release. (**b**) Parallel cultures (1×10^6 cells per 10 cm dish) were pulse-labeled with ^{3}H-thymidine at the indicated hours post-release from the aphidicolin block. The cells were harvested and the DNA was extracted and analyzed for ^{3}H-dTMP incorporation (reported as cpm $\times 10^{-3}$). Values indicate the means averaged from triplicate pulse-labeled cultures

5. To detect pHis-Ub conjugated UDG1A, the procedures as outlined by the Tansey laboratory are followed 10. Cell pellets are resuspended in buffer A, sonicated and allowed to bind to Ni–NTA agarose for 3 h at room temperature. The agarose is washed with buffer A, buffer A/buffer TI and buffer TI. The protein–agarose complex is resuspended in SDS-PAGE buffer and proteins analyzed by Western blot using AU1 antibody. Typical results from this procedure are presented in Fig. 3.

4 Notes

1. Stocks of cells used in the lab are routinely banked at an early passage after being tested for mycoplasma contamination using PCR methods.
2. Insure that chemical inhibitors are used before the expiration date as stated by the company for the particular solution or dry form.

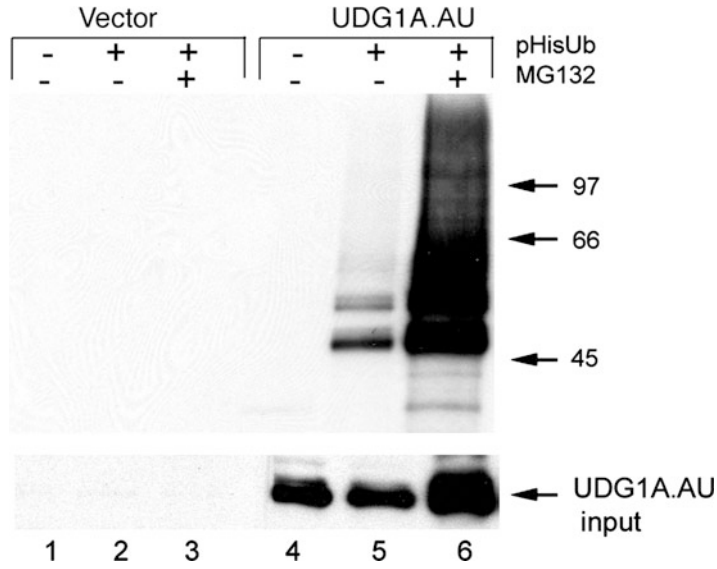

Fig. 3 In vivo ubiquitination of epitope-tagged nUDG. (**a**) AU-tagged nUDG containing plasmid constructs were co-transfected with pHis-tagged ubiquitin plasmid constructs as described in experimental procedures. Extracts derived from transfected cells were subjected to Ni-NTA agarose affinity fractionation under denaturing conditions. Fractionated protein was analyzed by Western blot using AU1 antibody as probe. *Lower panel*—Total cell extracts, prior to Ni–NTA fractionation, were analyzed for AU-tagged nUDG expression by Western blot analysis. 10 % of the extracts used as input for fractionation are represented here

3. Be consistent throughout the protocol. If you wash the cell monolayer on the plate do this throughout the time course. If cells come off the plate and have to be washed in suspension, do this for all the points in the time course.
4. These inhibitors produce a significant percentage of cell death. Drugs should be titered for the particular cell line to minimize cell killing and still produce the desired response (i.e., inhibition of proteolysis).
5. The down side to these experiments is the need to use radioactivity. All appropriate protection and approvals must be in place before using even low energy radioactivity. Cell cytometry can be a replacement protocol. Most Universities have central facilities for cell cycle analysis.
6. Initial experiments need to establish correct fractionation of the protein of interest under every condition tested. The bulk of nUDG is readily extracted into the supernatant under these procedures at all the time points. However, a small consistent fraction does remain in the pellet.
7. Acrylamide is a neurotoxin and should be treated as such. Adjust volumes as appropriate for the particular apparatus being used.

8. Besides the toxicity of acrylamide, finger prints leave proteins behind that can obscure results, particularly when using sensitive systems such as ECL, wear gloves for all gel and membrane handling.
9. Nitrocellulose can also be used. PVDF appears more stable for stripping and reprobing. It is also more useful when proteins are further analyzed (i.e., mass spectrometry).
10. Take great care to remove bubbles because transfer is interrupted if air is trapped between the gel and the membrane. This usually occurs right at the spot of your protein of interest.
11. Technal proof-printer; http://www.terapeak.com/worth/technal-made-in-the-u-s-a-8-x-10-proof-printer-photo-darkroom-proof-printer/331638999629/.
12. When reverse translating from amino acid sequence to nucleotide sequence (i.e., codons for DTYRYI) make sure to check with codon usage charts for the particular species that will be expressing this protein. Choose the codon with the highest percentage used by that species.
13. Expression vectors obtained from other labs should be checked either by restriction mapping, sequence analysis or transient transfection and Western blot analysis before being used in further experiments.

References

1. Lindahl T, Wood RD (1999) Quality control by DNA repair. Science 286:1897–1905
2. Pearl LH (2000) Structure and function in the uracil-DNA glycosylase superfamily. Mutat Res 460:165–181
3. Krokan HE, Standal R, Slupphaug G (1997) DNA glycosylases in the base excision repair of DNA. Biochem J 325:1–16
4. Rada C, Williams GT, Nilsen H, Barnes DE, Lindahl T, Neuberger MS (2002) Immunoglobulin isotype switching is inhibited and somatic hypermutation perturbed in UNG-deficient mice. Curr Biol 12:1748–1755
5. Di Noia J, Neuberger MS (2002) Altering the pathway of immunoglobulin hypermutation by inhibiting uracil-DNA glycosylase. Nature 419:43–48
6. Harris RS, Bishop KN, Sheehy AM, Craig HM, Petersen-Mahrt SK, Watt IN, Neuberger MS, Malim MH (2003) DNA deamination mediates innate immunity to retroviral infection. Cell 113:803–809
7. Fischer JA, Muller-Weeks S, Caradonna S (2004) Proteolytic degradation of the nuclear isoform of uracil-DNA glycosylase occurs during the S phase of the cell cycle. DNA Repair (Amst) 3:505–513
8. Fischer JA, Muller-Weeks S, Caradonna SJ (2006) Fluorodeoxyuridine modulates cellular expression of the DNA base excision repair enzyme uracil-DNA glycosylase. Cancer Res 66:8829–8837
9. Treier M, Staszewski LM, Bohmann D (1994) Ubiquitin-dependent c-Jun degradation in vivo is mediated by the delta domain. Cell 78:787–798
10. Salghetti SE, Kim SY, Tansey WP (1999) Destruction of Myc by ubiquitin-mediated proteolysis: cancer-associated and transforming mutations stabilize Myc. EMBO J 18:717–726

Chapter 12

Synchronization of HeLa Cells

Hoi Tang Ma and Randy Y.C. Poon

Abstract

HeLa is one of the oldest and most commonly used cell lines in biomedical research. Owing to the ease of which they can be effectively synchronized by various methods, HeLa cells have been used extensively for studying the cell cycle. Here, we describe several protocols for synchronizing HeLa cells from different phases of the cell cycle, including G_1 phase using the HMG-CoA reductase inhibitor lovastatin, S phase with a double thymidine block procedure, and G_2 phase with the CDK1 inhibitor RO-3306. Cells can also be enriched in mitosis using nocodazole and mechanical shake-off. Releasing the cells from these blocks enables researchers to follow gene expression and other events through the cell cycle. We also describe several protocols, including flow cytometry, BrdU labeling, immunoblotting, and time-lapse microscopy, for validating the synchrony of the cells and monitoring the progression of the cell cycle.

Key words Cell cycle, Cyclin, Cyclin-dependent kinases, Flow cytometry, Synchronization

1 Introduction

HeLa is one of the oldest and most commonly used cell lines in biomedical research. The cell line was originally derived from human cervical carcinoma taken from an individual named Henrietta Lacks [1]. Due to the presence of the human papillomavirus E6 and E7 proteins, which inactivates p53 and pRb respectively, both cell cycle checkpoints and apoptosis are dysregulated [2]. HeLa cells are therefore relatively easy to be synchronized by many methods, making them good model systems for studying cell cycle-regulated events.

Synchronization can be used to enrich specific cell populations for different types of analyses, including gene expression, biochemical analysis, and protein localization. In additional to analyzing individual gene products, whole genome approaches have been performed using synchronized HeLa cells, including microarray analysis of gene expression [3], miRNA expression patterns [4], translational regulation [5], as well as proteomic analysis of protein modifications [6]. Synchronization can also be used to study the

Gaspar Banfalvi (ed.), *Cell Cycle Synchronization: Methods and Protocols*, Methods in Molecular Biology, vol. 1524,
DOI 10.1007/978-1-4939-6603-5_12,

effects of gene expression or chemicals on cell cycle progression. Thus it is possible to design synchronization experiments that incorporate overexpression or loss-of-function studies of gene products.

Synchronization generally involves the isolation of cells in specific cell cycle phases based on either physical properties or perturbation of cell cycle progression with biochemical constraints. Methods based on physical characteristics have the advantage that cells are not exposed to pharmacological agents. For example, centrifugal elutriation can be used to separate cells in different points of the cell cycle based on cell size [7, 8]. A major limitation of this method is that specially designated equipments are required.

Several chemicals are effective for synchronizing HeLa cells because they are able to reversibly block unique steps of the cell cycle (Fig. 1). Releasing the blockade allows the cells to progress synchronously into the cell cycle. Although these synchronization methods are relatively easy to perform, a caveat is that the chemicals may alter normal gene expression and post-translational modifications. Another limitation of synchronization using chemicals is that while synchrony is generally good immediately after the release, it deteriorates progressively at later time points. Therefore, experiments should ideally be designed to use more than one synchronization methods from different parts of the cell cycle.

We describe below protocols for blocking HeLa cells in G_1 phase, S phase, G_2 phase, or mitosis, and for releasing them synchronously into the cell cycle. Unlike cells such as normal fibroblasts, HeLa cells cannot be synchronized at G_0 with methods based on serum starvation or contact inhibition.

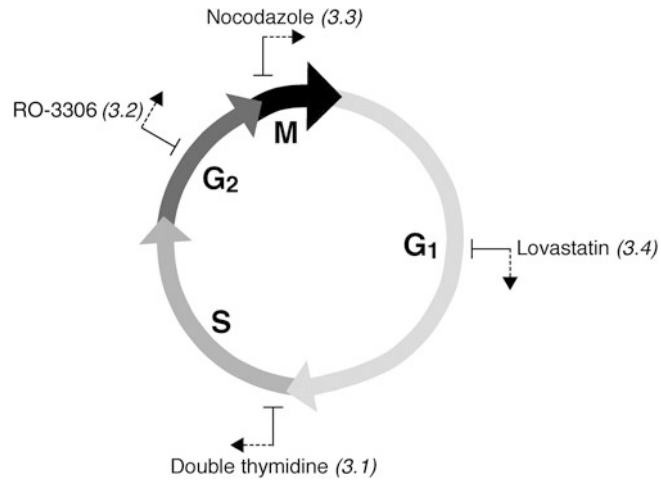

Fig. 1 Synchronization of HeLa cells at different phases of the cell cycle. HeLa cells can be synchronized at different phases of the cell cycle and released. See the indicated sections for detailed protocols

Inhibitors of DNA synthesis including thymidine, aphidicolin, and hydroxyurea are frequently used for blocking HeLa cells in S phase. High concentration of thymidine interrupts the deoxynucleotide metabolism pathway, thereby halting DNA replication. As treatment with thymidine arrests cells throughout S phase, a double thymidine block procedure, which involves releasing cells from a first thymidine block before trapping them with a second thymidine block, is generally used to induce a more synchronized early S phase block.

Cyclin-dependent kinase 1 (CDK1) is the main protein kinase driving cells from G_2 phase into mitosis. Accordingly, inhibition of CDK1 activity with a specific inhibitor called RO-3306 blocks cells in G_2 phase [9]. As RO-3306 is a reversible inhibitor, the cells can then be released synchronously into mitosis after the drug is washed out.

In HeLa cells, mitosis typically last for 40–60 min. But cells can be trapped in mitosis by the continuous activation of the spindle-assembly checkpoint. The checkpoint is activated by unattached kinetochores or the absence of tension between the paired kinetochores. Hence spindle poisons such as nocodazole (which prevents microtubule assembly) can activate the checkpoint and trap cells in a prometaphase-like state. Several factors should be considered when using nocodazole to synchronize HeLa cells. As nocodazole displays a relatively high cytotoxicity, it is used in combination with other synchronization methods (such as the double thymidine block described here) to minimize the exposure time. Furthermore, as nocodazole-blocked cells can return to interphase precociously by a process known as mitotic slippage, the synchronization protocol also involves the isolation of mitotic cells based on their physical properties (by using mechanical shake-off). In fact, mechanical shake-off is one of the oldest synchronization procedure developed for mammalian cells [10].

Finally, the method described here for synchronizing HeLa cells in G_1 phase is based on using lovastatin. Lovastatin is an inhibitor of HMG-CoA reductase [11], an enzyme catalyzing the conversion of HMG-CoA to mevalonate. Cells are released from the lovastatin-mediated blockade by the removal of lovastatin and addition of mevalonic acid (mevalonate).

An important aspect of synchronization experiments is to validate the degree of synchronization and to monitor the progression of the cell cycle. Here, we describe protocols for analyzing the cell cycle by flow cytometry after propidium iodide staining, which provides basic information about the DNA content of the cell population after synchronization. A more accurate method of cell cycle analysis based on BrdU labeling and flow cytometry is also detailed. Biochemically, the periodic fluctuation of specific cell cycle markers can be analyzed with immunoblotting. Finally, the progression through the cell cycle of individual cells can also be monitored using time-lapse microscopy and the FUCCI cell cycle reporter system.

2 Materials

2.1 Stock Solutions and Reagents

1. BrdU: 10 mM BrdU (Sigma, St. Louis, MO, USA) in H_2O (*see* **Note 1**).
2. BrdU antibody (DAKO, Glostrup, Denmark).
3. Cell lysis buffer: 50 mM Tris–HCl (pH 7.5), 250 mM NaCl, 5 mM EDTA, and 50 mM NaF, and 0.2% NP40. Add fresh: 1 mM PMSF, 1 μg/ml leupeptin, 2 μg/ml aprotinin, 10 μg/ml soybean trypsin inhibitor, 15 μg/ml benzamidine, 10 μg/ml chymostatin, and 10 μg/ml pepstatin.
4. Deoxycytidine: 240 mM deoxycytidine (Sigma) in H_2O.
5. FITC-conjugated rabbit anti-mouse immunoglobulins (DAKO).
6. Lovastatin (Mevinolin): 10 mM lovastatin (Sigma). Inactive lactone form of mevinolin is activated by dissolving 52 mg in 1.04 ml EtOH. Add 813 μl of 1 M NaOH and then neutralize with 1 M HCl to pH 7.2. Bring the solution to 13 ml with H_2O to make a 10 mM stock solution. Store at –20 °C. It has been reported that in vitro activation of mevinolin lactone may not be necessary [12, 13]. In that case, simply dissolve 52 mg of mevinolin in 13 ml of 70% EtOH.
7. Mevalonic acid: 0.5 M mevalonic acid. Dissolve 1 g of mevanlonic acid lactone in 3.5 ml of EtOH. Add 4.2 ml of 1 M NaOH. Bring the solution to 15.4 ml with H_2O to make a 0.5 M stock solution.
8. Nocodazole: 5 mg/ml nocodazole in DMSO (*see* **Note 1**).
9. PBS (phosphate buffered saline): 137 mM NaCl, 2.7 mM KCl, 10 mM sodium phosphate dibasic, and 2 mM potassium phosphate monobasic, pH 7.4.
10. PBST: PBS with 0.5% Tween 20 and 0.05% w/v BSA.
11. PI/RNase A solution: 40 μg/ml propidium iodide and 40 μg/ml RNase A in TE (make fresh).
12. Propidium iodide: 4 mg/ml propidium iodide in H_2O (*see* **Note 1**).
13. RNase A: 10 mg/ml RNase A (Sigma) in 0.01 M NaOAc (pH 5.2); heat to 100 °C for 15 min to remove DNase; then add 0.1 volume of 1 M Tris–HCl (pH 7.4).
14. RO-3306: 10 mM RO-3306 (Santa Cruz Biotechnology, Santa Cruz, CA, USA) in DMSO (*see* **Note 2**).
15. SDS sample buffer: 10% w/v SDS, 1 M Tris–HCl (pH 6.8), 50% v/v glycerol, and bromophenol blue (to taste). Add 2-mercaptoethanol (50 μl/ml) before use.
16. TE: 10 mM Tris–HCl (pH 7.5) and 0.1 mM EDTA.
17. Thymidine: 100 mM Thymidine (Sigma) in DMEM (*see* **Note 3**).

2.2 Cell Culture

All solutions and equipment coming into contact with the cells must be sterile. Proper sterile technique should be used accordingly.

1. HeLa cells (American Type Culture Collection, Manassas, VA, USA). Cells are grown in a humidified incubator at 37 °C in 5% CO_2.
2. HeLa cells stably expressing histone H2B-GFP for live-cell imaging.
3. Growth medium: Dulbecco's Modified Eagle Medium (DMEM) containing 10% heat-inactivated calf serum (Life Technologies, Carlsbad, CA, USA) and 30 U/ml penicillin-streptomycin (*see* **Note 4**).
4. Trypsin: 0.25% trypsin containing 1 mM EDTA (Life Technologies).
5. Tissue culture plates and standard tissue culture consumables.

2.3 Equipments

1. Standard tissue culture facility.
2. Centrifuge that can accommodate 15 and 50 ml centrifuge tubes.
3. Microcentrifuge that can reach 16,000 × *g* at 4 °C.
4. Flow cytometer equipped with 488 nm (for GFP and FUCCI) and 561 nm (for FUCCI) lasers.
5. Inverted fluorescence wide-field microscope equipped controlled environment chamber and camera for time-lapse analysis.

3 Methods

3.1 Synchronization from Early S: Double Thymidine Block

1. Grow HeLa cells in 100-mm plates with 10 ml of growth medium to ~40% confluence (*see* **Note 5**).
2. Add 200 µl of 100 mM thymidine (2 mM final concentration).
3. Incubate for 14 h.
4. Aspirate the medium and wash the cells twice with 10 ml of PBS.
5. Add 10 ml of growth medium containing 24 µM deoxycytidine.
6. Incubate for 9 h.
7. Add 200 µl of 100 mM thymidine.
8. Incubate for 14 h.
9. Aspirate the medium and wash the cells twice with 10 ml of PBS.

10. Add 10 ml of growth medium containing 24 μM deoxycytidine and return the cells to the incubator.
11. Harvest the cells at different time points for analysis.

Typically, cells are harvested every 2 or 3 h for up to 24 h. This should cover at least one cell cycle. As significant loss of synchrony occurs after one cell cycle, it is not very meaningful to follow the cells with longer time points (*see* **Note 6**).

3.2 Synchronization from G_2: RO-3306

Here, we describe a method that involves first blocking the cells with a double thymidine block procedure before releasing them into a RO-3306 block. Alternatively, asynchronously growing cells can be treated directly with RO-3306 for 16–20 h. The main challenge is that cells can escape the G_2 arrest and undergo genome reduplication if they are exposed to RO-3306 for a long period of time [14].

1. Synchronize cells at early S phase with the double thymidine block procedure (Subheading 3.1).
2. After release from the second thymidine block, incubate the cells for 2 h.
3. Add RO-3306 to 10 μM final concentration (*see* **Note 7**).
4. Incubate for 10 h.
5. Aspirate the medium and wash the cells twice with 10 ml of PBS.
6. Add 10 ml of growth medium.
7. Harvest the cells at different time points for analysis.

Cells treated with RO-3306 are trapped in late G_2 phase. As cells rapidly enter mitosis after release from the block, this synchronization procedure is best suited for studying entry and exit of mitosis. After release from the block, the cells can be harvested every 15 min for up to 4 h. Progression through mitosis can also be tracked with time-lapse microscopy (Subheading 3.8).

3.3 Synchronization from Mitosis: Nocodazole

While it is possible to treat asynchronously growing HeLa cells with nocodazole directly, the yield of the mitotic population is rather low. On the one hand, many cells remain in interphase if the nocodazole treatment is too short. On the other hand, cells may undergo mitotic slippage and apoptosis following a long nocodazole treatment. In the method described here, cells are first synchronized with a double thymidine block procedure before releasing into the nocodazole block.

1. Synchronize cells at early S phase with the double thymidine block procedure (Subheading 3.1).
2. After release from the second thymidine block, allow the cells to grow for 2 h.

3. Add nocodazole to a final concentration of 0.1 μg/ml.
4. Incubate for 10 h.
5. Collect the mitotic cells by mechanical shake-off and transfer the medium to a centrifuge tube (*see* **Note 8**).
6. Add 10 ml of PBS to the plate and repeat the shake-off procedure.
7. Combine the PBS with the medium and pellet the cells by centrifugation.
8. Wash the cell pellet twice with 10 ml of growth medium by resuspension and centrifugation.
9. Resuspend the cell pellet with 10 ml of growth medium and put onto a plate.
10. Harvest the cells at different time points for analysis.

3.4 Synchronization from G_1: Lovastatin

1. Grow HeLa cells in 100-mm plates in 10 ml of growth medium to ~50% confluency.
2. Add lovastatin to a final concentration of 20 μM.
3. Allow the cells to grow for 24 h.
4. Aspirate the medium and wash the cells twice with 10 ml of PBS.
5. Add 10 ml of fresh growth medium containing 6 mM mevalonic acid.
6. Harvest the cells at different time points for analysis.

3.5 Assessment of Synchronization: Flow Cytometry (Propidium Iodide)

The DNA content of the cells reflects their position in the cell cycle. While G_1 cells contain one copy of the genome (2N), cells in G_2 and mitosis contain two copies (4N). After staining with propidium iodide, the amount of DNA in cells can be quantified with flow cytometry. Note that this method cannot distinguish between G_1 and early S phase or between late S phase, G_2, and mitosis (*see* Subheading 3.6).

1. Collect medium to a 15-ml centrifugation tube.
2. Wash the plates with 2 ml of PBS and combine with the medium.
3. Add 2 ml of trypsin and incubate for 1 min.
4. Add back the medium to the plate. Dislodge cells by pipetting up and down.
5. Collect the cells by centrifugation at 1500 rpm (524 × *g*) for 5 min.
6. Wash the cells twice with 10 ml of ice-cold PBS by resuspension and centrifugation.
7. Resuspend the cell pellet with the residue buffer (~0.1 ml) (*see* **Note 9**).

8. Add 1 ml of cold 80% EtOH dropwise with continuous vortexing.
9. Keep the cells on ice for 15 min (fixed cells can then be stored indefinitely at 4 °C).
10. Centrifuge the cells at 1500 rpm for 5 min. Drain the pellet thoroughly.
11. Resuspend the pellet in 0.5 ml of PI/RNase A solution.
12. Incubate at 37 °C for 30 min.
13. Analyze with flow cytometry (*see* **Note 10**).

3.6 Assessment of Synchronization: Flow Cytometry (BrdU)

The DNA content of G_1 cells (2N) can readily be distinguished from those in G_2/M (4N) using propidium iodide staining and flow cytometry. However, the DNA content of G_1 and G_2/M cells overlap with a significant portion of S phase cells. The DNA content of cells in early S phase is indistinguishable to that in G_1 cells. Likewise, cells in late S phase contain similar amount of DNA as G_2/M cells. Although several computer algorithms are available to estimate the S phase population from the DNA distribution profile, they at best provide a good approximation and are particularly limiting for synchronized cells. The BrdU labeling method described here provides more precise information on the percentage of cells in G_1, S, and G_2/M. BrdU (5-bromo-2-deoxyuridine) is a thymidine analog that can be incorporated into newly synthesized DNA. Hence only S phase cells are labeled with a brief pulse of BrdU. The BrdU-positive cells are then detected using antibodies against BrdU.

1. At 30 min before harvesting cells at each time point, add BrdU to a concentration of 10 μM.
2. Harvest and fix cells as described in Subheading 3.5, **steps 1–9**.
3. Collect the cells by centrifugation at 1500 rpm for 5 min.
4. Wash the cells twice with 10 ml of PBS by resuspension and centrifugation. Remove all supernatant.
5. Add 500 μl of freshly diluted 2 M HCl.
6. Incubate at 25 °C for 20 min.
7. Wash the cells twice with 10 ml of PBS and once with 10 ml of PBST by resuspension and centrifugation.
8. Resuspend the cell pellet with the residue buffer (~0.1 ml).
9. Add 2 μl of anti-BrdU antibody.
10. Incubate at 25 °C for 30 min.
11. Wash twice with 10 ml of PBST by resuspension and centrifugation.
12. Resuspend the cell pellet in the residue buffer (~0.1 ml).

13. Add 2.5 μl of FITC-conjugated rabbit anti-mouse immunoglobulins.
14. Incubate at 25 °C for 30 min.
15. Wash the cells once with 10 ml of PBST by resuspension and centrifugation.
16. Stain the cells with propidium iodide as described in Subheading 3.5, **steps 10–12**.
17. Analyze with bivariate flow cytometry.

3.7 Assessment of Synchronization: Cyclins

Another way to evaluate the synchrony of cells is through the detection of proteins that vary periodically during the cell cycle. Given that cyclins are components of the engine that drives the cell cycle, we are using this as an example. Cyclin E1 accumulates during G_1 and decreases during S phase. In contrast, cyclin A2 increases during S phase and is destroyed during mitosis. The accumulation and destruction of cyclin B1 are slightly later than cyclin A2 in HeLa cells.

1. Harvest cells as described in Subheading 3.5, **steps 1–6**.
2. Resuspend the cells with 1 ml of PBS and transfer to a microfuge tube.
3. Centrifuge at 16,000 × *g* for 1 min.
4. Aspirate the PBS and store the microfuge tube at −80 °C until all the samples are ready.
5. Add ~2 pellet volume of cell lysis buffer into the microfuge tube. Vortex to mix.
6. Incubate on ice for 30 min.
7. Centrifuge at 16,000 × *g* at 4 °C for 30 min.
8. Transfer the supernatant to a new tube.
9. Measure the protein concentration of the lysates. Dilute to 1 mg/ml with SDS sample buffer (*see* **Note 11**).
10. Run the samples on SDS-PAGE and analyze by immunoblotting with specific antibodies against cyclin A2, cyclin B1, and cyclin E1 (*see* **Note 12**).

3.8 Assessment of Synchronization: Time-Lapse Microscopy of Histone H2B–GFP-Expressing Cells

As they have the same DNA content, cells in G_2 and mitosis cannot be distinguished by flow cytometry after propidium iodide staining. To differentiate these two populations, mitotic markers such as phosphorylated histone $H3^{Ser10}$ can be analyzed. Antibodies that specifically recognize phosphorylated form histone $H3^{Ser10}$ are commercially available and can be used in conjunction with either immunoblotting or flow cytometry.

Another method for monitoring mitosis is based on microscopic analysis of the chromosomes. Here we describe a method using time-lapse microscopy, thereby allowing the tracking individual cells into and out of mitosis after RO-3306 synchronization.

For this purpose, HeLa cells expressing GFP (green fluorescent protein)-tagged histone H2B are used in the following method. The duration of the entire cell cycle can also be analyzed by tracking individual cells from one mitosis to the next (either one or both of the daughter cells can be tracked).

1. Synchronize cells in G_2 with RO-3306 as described in Subheading 3.2. An extra plate is needed to set aside for the time-lapse microscopy.
2. Setup the fluorescence microscope and equilibrate the growth chamber with 5% CO_2 at 37 °C (*see* **Note 13**).
3. After release from the RO-3306 block, place the plate immediately into the growth chamber.
4. Focus the microscope at the optical plane of the chromatin. As the cells are going to round up during mitosis, it is not a good idea to focus the images based on the bright field.
5. Images are taken every 3 min for 2–4 h (*see* **Notes 14** and **15**).

3.9 Assessment of Synchronization: FUCCI Cell Cycle Reporters

HeLa cells expressing the FUCCI (Fluorescent Ubiquitin-based Cell Cycle Indicators) cell cycle reporter system [15] can be used to analyze the cell cycle after synchronization. The system consists of a fragment of Geminin (an APC/C target, present from early S phase to the end of mitosis) labeled with mVenus and a fragment of CDT1 (a SCF complex target, present from early G_1 phase to the beginning of S phase) labeled with mCherry (note that other pairs of fluorescent proteins are also used in different FUCCI systems). A characteristic of the system is that both reporters are present during early S phase and absent immediately after mitosis. Either flow cytometry or microscopy can be used to detect the FUCCI system (both are described below). A limitation of the FUCCI system is that cells in S phase, G_2, and mitosis are not distinguishable.

1. Synchronize cells with different procedures as described in Subheadings 3.1–3.4.
2. At different time points after release from the block, harvest the cells by using trypsin (Subheading 3.5, **steps 1–6**). The cells are then analyzed with flow cytometry using 488 and 561 nm lasers for excitation. Alternatively, the cells can be examined with fluorescence microscope and live-cell imaging (Subheading 3.8).

4 Notes

1. Mutagen. Handle with care.
2. RO-3306 is sensitive to light and freeze–thaw cycles. We keep the stock solution in small aliquots wrapped with aluminum foils at −80 °C.

3. Dissolve thymidine and filter sterile to make the 100 mM stock solution. Incubation at 37 °C may help to solubilize the thymidine.
4. HeLa cells are often recommended to be grown in medium containing 10% fetal bovine serum. If calf serum is to be used, it is important to ensure that the cells are adapted in this growing condition before the synchronization experiments.
5. The synchronization procedures described in these protocols are for using 100-mm plates. Cells obtained from one 100-mm plate at each time point should be sufficient for both flow cytometry analysis and immunoblotting. The procedures can be scaled up proportionally.
6. It is possible to break up a 24 h experiment into two independent sessions. Alternatively, it is possible for two researchers to work in shifts to harvest the cells at different time points. However, we found that the best results are obtained when all the cells are harvested by the same researcher.
7. For HeLa cells, CDK1 but not other CDKs is inhibited with 10 μM of RO-3306 [9, 14]. The exact concentration of RO-3306 used should be determined for each stock.
8. The basis of this method is that mitotic cells are rounded and attach less well to the plate than cells in interphase. It is possible to collect the mitotic cells by blasting them off with the medium using the a pipette. Alternatively, shakers that hold plates and flasks securely can be used. It is also possible to hold the plates on a vortex and shake for 20 s with the highest setting. In any case, the cells should be examined under a light microscope before and after the mechanical shake-off to ensure that most of the mitotic cells are detached.
9. It is crucial to resuspend the cells very well before adding EtOH to avoid crumbing.
10. As cells from some phases of the cell cycle may be missing in the synchronized population, it is a good idea to first use asynchronously growing cells to setup the DNA profile.
11. Many reagents are available for measuring the concentration of the lysates. We use BCA protein assay reagent from Pierce (Rockford, IL, USA) using BSA as standards.
12. Cyclins are readily detectable in HeLa cells using commercially available monoclonal antibodies: cyclin A2 (E23), cyclin B1 (V152), and cyclin E2 (HE12).
13. We use a Ti-E-PFS inverted fluorescence microscope (Nikon, Tokyo, Japan) equipped with an ultra-low noise sCMOS camera (Andor Technology, Belfast, UK) and a Chamlide TC temperature, humidity, and CO_2 control system (Chamlide, Live Cell Instrument, Seoul, Korea). A GFP filter cube (480 nm

excitation; 535 nm emission) is used to acquire the signals from histone H2B–GFP-expressing cells. Filters for mCherry (565 nm excitation; 630 nm emission) and mVenus (500 nm excitation; 535 nm emission) filters are used to acquire the signals from FUCCI reporters. Data acquisition and analysis are carried out using the Metamorph software (Molecular Devices, Downingtown, PA, USA).

14. A critical parameter in every time-lapse microscopy experiment is photobleaching and phototoxicity. The exposure time should be minimized.
15. Although not unique to HeLa cells, a drawback of time-lapse imaging of HeLa cells is the relatively high cell mobility. It can be challenging to follow individual cells accurately at relatively high cell density. A solution is to image areas with relatively low cell density.

Acknowledgements

Related works in our laboratory were supported in part by the Research Grants Council grants 662213 and T13-607/12R to R.Y.C.P.

References

1. Skloot R (2010) The immortal life of Henrietta Lacks. Random House, New York
2. McLaughlin-Drubin ME, Munger K (2009) Oncogenic activities of human papillomaviruses. Virus Res 143:195–208
3. Chaudhry MA, Chodosh LA, McKenna WG, Muschel RJ (2002) Gene expression profiling of HeLa cells in G1 or G2 phases. Oncogene 21:1934–1942
4. Zhou JY, Ma WL, Liang S, Zeng Y, Shi R, Yu HL, Xiao WW, Zheng WL (2009) Analysis of microRNA expression profiles during the cell cycle in synchronized HeLa cells. BMB Rep 42:593–598
5. Stumpf CR, Moreno MV, Olshen AB, Taylor BS, Ruggero D (2013) The translational landscape of the mammalian cell cycle. Mol Cell 52:574–582
6. Chen X, Simon ES, Xiang Y, Kachman M, Andrews PC, Wang Y (2010) Quantitative proteomics analysis of cell cycle-regulated Golgi disassembly and reassembly. J Biol Chem 285:7197–7207
7. Wahl AF, Donaldson KL (2001) Centrifugal elutriation to obtain synchronous populations of cells. Curr Protoc Cell Biol Chapter 8:Unit 8.5
8. Banfalvi G (2008) Cell cycle synchronization of animal cells and nuclei by centrifugal elutriation. Nat Protoc 3:663–673
9. Vassilev LT, Tovar C, Chen S, Knezevic D, Zhao X, Sun H, Heimbrook DC, Chen L (2006) Selective small-molecule inhibitor reveals critical mitotic functions of human CDK1. Proc Natl Acad Sci U S A 103: 10660–10665
10. Terasima T, Tolmach LJ (1963) Growth and nucleic acid synthesis in synchronously dividing populations of HeLa cells. Exp Cell Res 30: 344–362
11. Keyomarsi K, Sandoval L, Band V, Pardee AB (1991) Synchronization of tumor and normal cells from G1 to multiple cell cycles by lovastatin. Cancer Res 51:3602–3609
12. Mikulski SM, Viera A, Darzynkiewicz Z, Shogen K (1992) Synergism between a novel amphibian oocyte ribonuclease and lovastatin in inducing cytostatic and cytotoxic effects in human lung and pancreatic carcinoma cell lines. Br J Cancer 66:304–310

13. Javanmoghadam-Kamrani S, Keyomarsi K (2008) Synchronization of the cell cycle using lovastatin. Cell Cycle 7:2434–2440
14. Ma HT, Tsang YH, Marxer M, Poon RYC (2009) Cyclin A2-cyclin-dependent kinase 2 cooperates with the PLK1-SCFbeta-TrCP1-EMI1-anaphase-promoting complex/cyclosome axis to promote genome reduplication in the absence of mitosis. Mol Cell Biol 29: 6500–6514
15. Sakaue-Sawano A, Kurokawa H, Morimura T, Hanyu A, Hama H, Osawa H, Kashiwagi S, Fukami K, Miyata T, Miyoshi H et al (2008) Visualizing spatiotemporal dynamics of multicellular cell-cycle progression. Cell 132: 487–498

Part IV

Synchronization of Unicellular Organisms

Chapter 13

Synchronization of *Bacillus subtilis* Cells by Spore Germination and Outgrowth

Gaspar Banfalvi

Abstract

This protocol defines conditions under which the germination of spores can be used to synchronize *Bacillus subtilis* cells, utilizing the time-ordered sequence of events taking place during the transition from spore to vegetative cells. The transition stages involve: phase change, swelling, emergence, initial division, and elongation. By using this method we have obtained two distinctive synchronized cell cycles, while the synchrony faded away in the third cycle. The advantage of using spore outgrowth and germination is that a highly synchronized population of bacterial cells can be obtained. Non-dividing spores stay synchronized, while synchrony rapidly decays during a few divisions. The limitations of this method are that it can be applied only for sporulating bacteria and synchrony lasts for only a limited period of time exceeding not more than two cycles.

Key words Endospore formation, Spore outgrowth, Transition stage, Vegetative cells, Permeabilization, DNA synthesis, Spectrophotometry

1 Introduction

The process of vegetative bacterial cells converted into a dormant structure is called sporogenesis and the return to the vegetative stage is known as spore germination. Contrary to endospores, vegetative cells are capable to active growth. Endospore formation is typical to three genera of Gram-positive bacteria: Bacillus (*B. anthracis*, *B. subtilis*), *Clostridium* (*C. botulinum*, *C. perfingens*, *C. tetani*), and Sporosarcina. *Bacillus subtilis* is a sporulating model organism for differentiation, gene/protein regulation, and cell cycle events [1]. That sporulation and spore germination can be used as a model system to study the transition between different cell forms has been described four decades ago [2–4]. In spore-forming bacteria, "de novo" nucleotide synthesis is not operative in the early stage of transition from spore to vegetative stage known as germination [5]. After the germination stage, the nucleoside triphosphate levels increase rapidly by the utilization of the nucleoside and

Gaspar Banfalvi (ed.), *Cell Cycle Synchronization: Methods and Protocols*, Methods in Molecular Biology, vol. 1524,
DOI 10.1007/978-1-4939-6603-5_13,

nucleoside monophosphate pools of the dormant spores [6]. Consequently, DNA synthesis takes place only after the formation of these substrates. The processes of germination and spore outgrowth take place in a time-ordered sequence allowing to follow closely the transition between spore and vegetative stages [7–13].

The process of germination of the bacterial spore is known as a change from the heat-resistant to a heat-labile stage which does not represent the true vegetative cell. The transition has been divided into two distinct stages. The term germination is known as the first stage and the transformation of germinated spores into vegetative cells is called outgrowth [14], or post-germinative development [15]. One of the most important reactions in this chain is the initiation of germination also referred to as trigger reaction. The germination process can be triggered by heavy metals, heat, hydrostatic pressure, a variety of chemicals of nutrient, and non-nutrient origin [16]. Although little is known about the mechanism of activation, it is believed that molecular rearrangements taking place inside the spores develop into the germination process. The triggering is operationally similar to the opposite process of sporulation representing a stage of no return. One of the best triggering agent is L-alanine when present in high concentration in the germination medium. It was demonstrated that a short exposure to L-alanine caused a subsequent germination in spores of *Bacillus cereus* [17]. The quintessential germination receptor in *B. subtilis* is GerA that is activated by a single germinant, L-alanine and inhibited by its stereoisomer, D-alanine [18]. Most of what is known about Ger receptor function has been derived from studies in the gerA operon [19]. A homologous gerA operon of *B. subtilis* was isolated from *Bacillus thuringiensis* [20].

The germination process involves loss of resistance to injuring agents such as heat or heavy metals, loss of refractibility, decrease in the optical density of the spore suspension, increase in stainability [21, 22], decrease in dry weight due to the loss of picolinic acid, calcium and mucopeptides [23], the initiation of respiration [24], as well as imbibition of water [25]. These changes point to initial biochemical steps preceding visual signs of germination. Outgrowth includes four stages occurring in the following order: swelling, emergence from the spore coat, elongation of the emergent organism, and finally division of the elongated organism.

As the bacterial endospore metabolism, structure and composition differ from that of the vegetative cell, sporulation and spore germination can be applied as a simple model system to study biochemical mechanism regulating these transitions. The differentiation is cyclic and can serve the purpose of synchronizing those bacteria that undergo sporulation. This chapter describes how germination and outgrowth of *Bacillus subtilis* ATCC23857(strain 68, indole$^-$) can be adapted for cell cycle synchronization. Studies have shown that in cells of *B. subtilis* 168 rendered permeable to

small molecules by treatment with toluene, the incorporation of [^{3}H]dTTP incorporation depended on the presence of ATP and was sensitive to the inhibitor of DNA replication (6-((*p*-hydroxyphenyl)azo))uracil (HP-Ura) and to the gyrase inhibitor novobiocin [26].

2 Materials

2.1 Chemicals

1. Indole.
2. Trichloroacetic acid.
3. Casamino acids (Bacto), Becton, Dickinson and Company (Sparks, MD).
4. 60 Ci/mmol ^{3}H-dTTP, 100 Ci/mmol ^{3}H-thymidine (Amersham Pharmacia Biotech AB, Uppsala, Sweden).
5. K_2HPO_4, KH_2PO_4, $(NH_4)_2SO_4$, trisodium citrate.
6. $MgSO_4$ 7 H_2O, $FeCl_3$.6 H_2O.
7. Amino acids: L-alanine, L-arginine, L-asparagine, sodium glutamate, L-histidine, L-methionine, L-phenylalanine, L-serine, L-threonine, L-tryptophane.
8. Nucleotides: ATP, dATP, dGTP, dCTP.
9. Inhibitors of DNA synthesis: 1-β-D-arabinofuranosyl-cytosine--5′-triphosphate (ara-dCTP) (6-((*p*-hydroxyphenyl)azo))uracil (HP-Ura).

2.2 Disposables, Instruments

1. 1.5 ml microcentrifuge tubes (Eppendorf, Hamburg, Germany).
2. 5, 15, and 50 ml conical centrifuge tubes (BD Falcon, San José, USA).
3. Glass culture tubes and flasks.
4. Whatman GF/C glass microfilters diameter 2.4 cm, Sigma-Aldrich (St. Louis, MO).
5. Rotating incubator.
6. Microcentrifuge tubes.
7. Spectrophotometer and cuvettes.

2.3 Buffers, Solutions

1. KPO_4 buffer (K_2HPO_4/KH_2PO_4), 0.5 M, pH 7.5, 2 M $MgSO_4$, 15 mM ATP, 0.4 mM dNTP (dATP, dGTP, dCTP, each), 2 mM HP-Ura, 2 mM 1-β-D-arabinofuranosylcytosine-5′-triphosphate (ara-dCTP) (*see* **Notes 1–3**).
2. Betafluor, pre-mixed scintillation solution, National Diagnostics, Atlanta, GA.

2.4 Lyophylized Spores

1. Spores of *B. subtilis* 168 in 1.5 ml microcentrifuge tubes were kept in 50% glycerol (*see* **Note 4**).
2. Lyophylized spores: 10 mg spores plus 1 ml 50% glycerol (10 mg/ml).

2.5 Germination of Spores

1. Sterile germination medium, pH 7.4 contained 14 g K_2HPO_4, 6 g KH_2PO_4, 2 g $(NH_4)_2SO_4$, 1 g trisodium citrate, 0.5 g $MgSO_4$ 7 H_2O, 8 mg $FeCl_3$.6 H_2O, 0.5 g L-alanine, 50 mg L-arginine, 50 mg L-asparagine, 100 mg sodium glutamate, 50 mg L-histidine, 5 mg L-methionine, 50 mg L-phenylalanine, 5 mg L-serine, 100 mg L-threonine, 50 mg L-tryptophane in 1 l.
2. For germination: To 30 ml germination medium 0.3 ml 50% glucose and 1.5 ml 10 mg/ml spores were added (*see* **Note 5**).

2.6 Monitoring of Germination

1. Germination was monitored by the decrease in optical density at 525 nm on a Beckman spectrophotometer (*see* **Note 6**).

2.7 Cell Culture Medium

1. Antibiotic medium 3 (Penassay broth) (DIFCO—Becton Dickinson and Company, Franklin Lakes, NJ): 5 g/l Tryptone, 1.5 g/l yeast extract, 1.5 g/l beef extract, 3.5 g/l sodium chloride, 1 g/l dextrose, 3.68 g/l potassium phosphate dibasic, 1.32 g/l potassium phosphate monobasic. pH adjusted to 6.9.
2. Medium C, pH 7.4 contained in 1 l: 14.0 g K_2HPO_4, 6.0 g KH_2PO_4, 2 g $(NH_4)_2SO_4$, 1 g trisodium citrate, 0.2 g $MgSO_4$ 7 H_2O, 5 g glucose, 0.5 g casamino acids and 50 mg indole.

3 Methods

3.1 Cell Growth

1. To 50 ml Penassay broth, 10 µl spores in 50% glycerol were added and grown overnight in a 250 ml Erlenmeyer flask at 37 °C in a Becton Dickinson orbital incubator shaker (General Scientific Instrument Services Inc., London, UK) at 100 rpm. From the overnight culture 4 ml was added to 200 ml medium C in a 1 l flask and grown at 37 °C in the orbital shaker at 100 rpm.

3.2 Preparation of Toluene-Treated Cells

1. At 3×10^7 cells/ml density take 25 ml cells each in six 50 ml conical tubes and harvest them in a Beckmann J21 centrifuge at room temperature ($5000 \times g$, 5 min). Decant the supernatant and resuspend the pellet of each tube in 2 ml of 0.1 M KPO_4 buffer, pH 7.4. Pool the suspension in one 15 ml tube and spin down cells. Resuspend cells in 3 ml 0.1 M KPO_4 buffer, pH 7.4, add 30 µl toluene. Shake the mixture for 10 min at room temperature then chill it in ice. Add 10 ml cold 0.1 M KPO_4 buffer, pH 7.4, spin in centrifuge and resuspend cells in 1.5 ml of the phosphate buffer. The density of cells

(1.5 ml/4.5×10^9) corresponds to 3×10^9 cells/ml. Distribute toluene-treated cells in 100 µl aliquotes, freeze them in liquid nitrogen (*see* **Note 7**).

3.3 Spore Germination and Outgrowth

1. Homogenized lyophylized spores (20 mg + 2 ml H_2O) in a 5 ml test tube were subjected to a Bronson sonicator, model B-12, with a microtip and setting 4 for 5 min at 1 min intervals while immersed in ice-water bath.
2. Sonicated spores were prewarm to 37 °C for 5 min and heat-activated at 80 °C for 20 min.
3. Heat-activated spores were centrifuged at $5000 \times g$ for 10 min at +4 °C in a Sorwall RC2-B centrifuge (Ivan Sorwall, Inc., Norwalk, Co., USA).
4. The pellet of spores was resuspended in sterile 2 ml H_2O (10 mg/ml).
5. Germination was initiated in a 250 ml Erlenmeyer flask by adding to 30 ml germination medium 0.3 ml 50% glucose and 1.5 ml 10 mg/ml heat activated spores. Germination mixture was placed in a rotary shaker with the temperature set at 37 °C and a rotary speed of 100 rpm.
6. Germination was monitored by measuring the optical density at 525 nm in a spectrophotometer.

3.4 DNA Polymerase Assay in Permeable Cells of B. Subtilis

To assure that in outgrowing spores of *B. subtilis* 168 replicative DNA synthesis is dealt with, the inhibition of DNA replication can be measured in the presence and absence of both ATP and HP-Ura. Table 1 demonstrates that in toluene-treated permeable *B. subtilis* cells DNA synthesis is an ATP-dependent process and this process can be blocked by inhibitors of semiconservative replication.

3.5 DNA Synthesis in Outgrowing Spores

1. ^{3}H-thymidine incorporation is advised to be measured from zero level absorption every 10 min by adding 5 µl ^{3}H-thymidine to 0.3 ml germination medium and 0.2 ml germination mixture incubated at 37 °C for 10 min.
2. Terminate DNA synthesis by adding 5 ml 0.3 M ice-cold trichloroacetic acid (TCA).
3. Collect precipitate on Whatman GF/C glass fiber filter, wash three times with 5 ml portions of 0.3 M TCA and then with absolute alcohol.
4. Dry filters under an infrared lamp and the radioactivity determined with a toluene-based scintillation fluid.

A typical spore germination and outgrowth curve as well as the DNA synthesis profile are shown in Fig. 1. A lag period can be seen between the addition of the germination-inducing medium and the first sign of germination manifested as a decrease of absorption corresponding to the observation of Woese and Morowitz [27].

Table 1
DNA polymerase assay to prove semiconservative replication in *B. subtilis* 168 toluene-treated cells

Number of sample	^{3}H-dTTP (μl)	H_2O (μl)	KPO_4 (μl)	$MgSO_4$ (μl)	ATP (μl)	dNTP (μl)	HP-Ura (μl)	+ara-dCTP-dCTP (μl)	*B. subtilis* (μl)	Counts (cpm)
1	5	55	14	6	10	–	–	–	10	54 ± 21
2	5	55	14	6	–	10	–	–	10	36 ± 16
3	5	45	14	6	10	10	–	–	10	1180 ± 38
4	5	35	14	6	10	10	10	–	10	337 ± 29
5	5	35	14	6	10	10	–	10	10	78 ± 26

The final volume of each reaction mixture was 100 μl. Incubation lasted for 30 min at 37 °C. Termination took place by the addition of ice-cold 0.3 M trichloroacetic acid (TCA). Precipitate was collected on Whatman GF/C glass fiber filters washed with three 5 ml portions of 0.3 M TCA and then with 3 × 5 ml ethanol. Filters were dried under an infrared lamp and the radioactivity was determined in a toluene-based scintillation fluid

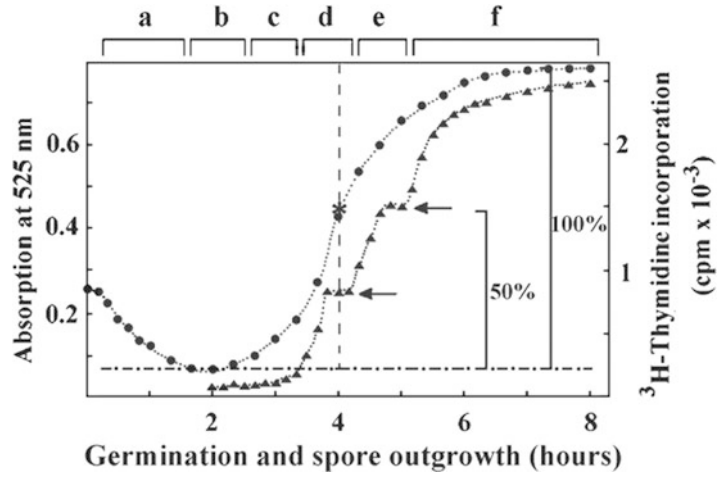

Fig. 1 Synchronization of *B. subtilis* 168 cells by spore outgrowth and germination. Lyophylized spores were homogenized, heat-activated and germinated as described in the Subheading 2. Germination is given as decrease in optical density vs. time. The germination and outgrowth curve consists of (*a*) phase change (germination), (*b*) swelling stage (zero level), (*c*) emergence, (*d*) 1st cell cycle, (*e*) 2nd cell cycle, (*f*) stationary phase (●…●). DNA synthesis showing (*b*) the lack of ^{3}H-thymidine incorporation in the swelling stage, (*c*) emergence, (*d*) initiation of DNA synthesis and the 1st cell cycle, (*e*) elongation and 2nd cell cycle, (*f*) stationary phase (▲…▲). The swelling stage is regarded as the zero level of absorption (-●-). For the best synchrony stop outgrowth of spores after the swelling stage when the optical density at 525 starts to increase and does not exceed twice the value of its original absorption before germination. The upper limit of synchrony corresponding to the inflexion point of DNA synthesis (~50 % of maximal outgrowth) is indicated by the *asterisk* (*). The two *arrows* (←) indicate the end of the first and second round of the cell cycle

The germination phase (Fig. 1a) continues till the absorption reaches its minimum referred to as zero level (Fig. 1b). The zero level of absorption is followed by spore outgrowth involving RNA and protein synthesis and finally DNA synthesis. The outgrowth consists of several subphases (Fig. 1c–f) including swelling and emergence from spore coat (Fig. 1c), elongation of the emerging vegetative cells from the spore coats proceeding to the early phase of logarithmic growth and cell division (Fig. 1d), to mid logarithmic phase and cell growth (Fig. 1e) and to late log and the stationary phase (Fig. 1f). Synchrony is indicated by the biphasic curve of ^{3}H-thymidine incorporation, involving back-to-back division cycles such that the population doubles in number every generation time (Fig. 1d and e). Synchrony is lost in late logarithmic and stationary phase (Fig. 1f) (*see* **Note 8**).

However, this does not mean that the stationary phase could not be selected for the synchronization of bacteria. Cultures of *Escherichia coli* and *Proteus vulgaris* have been synchronized by the stationary-phase method. This method consists of growing the bacteria to an early stationary phase, harvesting them quickly under minimal conditions of stress, and inoculating them into fresh medium at a dilution of about sevenfold. By repeating this procedure on partially synchronized cultures up to four-generation cycles of high percentage of phasing were obtained [28]. Other early methods used filtration to synchronize bacteria [29–31], the principle of binding bacteria to various surfaces and elute unbound sister cells from the surface [32, 33], by means of temperature shift [34], or by amino acid starvation [35].

4 Notes

1. Unless otherwise stated, all solutions should be prepared with distilled water that has an electric conductance of <0.055 mS and an organic content of less than five parts per billion. The solvent is mentioned as “distilled water” in the text.
2. KPO_4 buffer is best stored at 4 °C and can be used for up to 2 months.
3. dNTP solutions (dATP, dGTP, dCTP) have been prepared with distilled water and neutralized with 0.1 M NaOH to pH 7.5.
4. Freshly harvested spores germinate more reproducibly, but spores kept in glycerol also gave reproducible results. For long-term storage, spores were stored in 50% glycerol at –20 °C.
5. To start germination, initial absorbance values at 525 nm should be between 0.25 and 0.3 optical density.
6. To obtain best synchrony stop outgrowing spores after the swelling stage. The best choice regarding synchrony is to take

outgrowing spores after zero level absorption when the OD 525 nm value starts to increase and reaches the initial optical density of spores before germination.

7. After toluene treatment work as quickly as possible, toluene-treated cells are vulnerable. For short-term storage (1 day) keep toluene-treated cells in dry ice–ethanol mixture; for long-term store permeable *B. subtilis* cells at −80 °C or in liquid nitrogen.
8. Do not use outgrowing spores after the inflexion point of the growth curve as the vegetative culture will be already in stationary phase.

References

1. Graumann P (ed) (2007) Bacillus: cellular and molecular biology, 1st edn. Caister Academic Press, Haverhill, UK, http://www.horizonpress.com/bac
2. Hansen JN, Spiegelman G, Halvorson HO (1970) Bacterial spore outgrowth: its regulation. Science 168:1291–1298
3. Keynan A (1973) The transformation of bacterial endospores into vegetative cells. Symp Soc Gen Microbiol 23:85–123
4. Mandelstam J (1976) Bacterial sporulation: a problem in the biochemistry and genetics of a primitive developmental system. Proc R Soc B 193:89–106
5. Nelson DL, Kornberg A (1970) Biochemical studies of bacterial sporulation and germination. XVIII. Free amino acids in spores. J Biol Chem 245:1128–1136
6. Setlow P, Kornberg A (1970) Biochemical studies of bacterial sporulation and germination. XXIII. Nucleotide metabolism during spore germination. J Biol Chem 245:3645–3652
7. Balassa G (1965) Synthesis macromoleculaires au cours de la germination des spores de B. Subtilis. I. Cinctique. Ann De I'lnstitut Pasteur 109:13–35
8. Balassa G (1969) Biochemical genetics of bacterial sporulation. I. Unidirectional pleiotropic interactions among genes controlling sporulation in Bacillus subtilis. Mol Gen Genet 104:73–103
9. Kobayashi I, Steinberg W, Higa A, Halvorson HO, Levinthal C (1965) Sequential synthesis of macromolecules during outgrowth of bacterial spores. In: Campbell LL, Halvorson HO (eds) Spores IZZ. American Society for Microbiology, Washington, DC, pp 200–212
10. Torriani A, Levinthal C (1967) Ordered synthesis of proteins during outgrowth of spores of B. cereus. J Bacteriol 94:176–183
11. Armstrong RL, Sueoka N (1968) Phase transition in ribonucleic acid synthesis during germination of B. Subtilis spores. Proc Natl Acad Sci U S A 59:153–160
12. Steinberg W, Halvorson HO (1968) Timing of enzyme synthesis during outgrowth of Bacillus cereus. I. Ordered enzyme synthesis. J Bacteriol 95:469–478
13. Kennett RN, Sueoka N (1971) Gene expression during outgrowth of B. subtilis spores. The relationship between order on the chromosome and temporal sequence of enzyme synthesis. J Mol Biol 60:31–44
14. Campbell LL Jr (1957) Bacterial spore germination. Definitions and methods of study. In Spores. HO Halvorson (ed.). American Institute of Biological Sciences, Washington, DC, pp. 33–38
15. Levinson HS, Hyatt MT (1956) Correlation of respiratory activity with phases of spore germination and growth in Bacillus megaterium as influenced by manganese and L-alanine. J Bacteriol 72:176–183
16. Halvorson HO (1959) Symposium on initiation of bacterial growth. Bacteriol Rev 23:267–272
17. Harrell WK, Halvorson H (1955) Studies on the role of L-alanine in the germination of spores of Bacillus terminalis. J Bacteriol 69:275–279
18. Yasuda Y, Tochikubo K (1984) Relation between D-glucose and L- and D-alanine in the initiation of germination of Bacillus subtilis spores. Microbiol Immunol 28:197–207
19. McCann KP, Robinson C, Sammons RL, Smith DA, Corfe BM (1996) Alanine germination receptors of Bacillus subtilis. Letts Appl Microbiol 23:290–294
20. Liang L, Gai Y, Hu K, Liu G (2008) Te gerA operon is required for spore germination in

Bacillus thuringiensis. Wei Sheng Wu Xue Bao 48:281–286 (article in Chinese)

21. Powell JF (1950) Factors affecting the germination of thick suspensions of Bacillus subtilis spores in L-alanine solution. J Gen Microbiol 4:330–338
22. Pulvertaft RJV, Haynes JA (1951) Adenosine and spore germination; phasecontrast studies. J Gen Microbiol 5:657–663
23. Powell JF, Strange RE (1953) Biochemical changes occurring during the germination of bacterial spores. Biochem J 54:205–209
24. Murrell WG, Scott WJ (1958) The permeability of bacterial spores to water. In: Proceedings of the 7th international congress of microbiology, Stockholm, p. 26
25. Powell JF (1957) Biochemical changes occurring during spore germination in bacillus species. J Appl Bacteriol 20:349–358
26. Bhattacharya S, Sarkar N (1981) Study of deoxyribonucleic acid replication in permeable cells of Bacillus subtilis using mercurated nucleotide substrates. Biochemistry 20:3029–3034
27. Woese C, Morowitz HJ (1958) Kinetics of the release of dipicolinic acid from spores of Bacillus subtilis. J Bacteriol 76:81–83
28. Cutler RG, Evans JE (1966) Synchronization of bacteria by a stationary-phase method. J Bacteriol 91:469–476
29. Maruyama Y, Yanagita T (1956) Physical methods for obtaining synchronous culture of *Escherichia coli*. J Bacteriol 71:542–546
30. Abbo FE, Pardee AB (1960) Synthesis of macromolecules in synchronously dividing bacteria. Biochim Biophys Acta 39:473–485
31. Lark KG, Lark C (1960) Changes during the division cycle in bacterial cell wall synthesis, volume, and ability to concentrate free amino acids. Biochim Biophys Acta 43:520–530
32. Helmstetter CE, Uretz RB (1963) X-ray and ultraviolet sensitivity of synchronously dividing *Escherichia coli*. Biophys J 3:35–47
33. Helmstetter CE, Cummings DJ (1963) Bacterial synchronization by selection of cells at division. Proc Natl Acad Sci U S A 50:767–774
34. Lark KG, Maaloe O (1954) The induction of cellular and nuclear division in *Salmonella typhimurium* by means of temperature shift. Biochem Biophys Acta 15:345–356
35. Ron EZ, Rozenhak S, Grossman N (1975) Synchronization of cell division in *Escherichia coli* by amino acid starvation: strain specificity. J Bacteriol 123:374–376

Chapter 14

Synchronization of Yeast

Jessica Smith, Arkadi Manukyan, Hui Hua, Huzefa Dungrawala, and Brandt L. Schneider

Abstract

The budding yeast *Saccharomyces cerevisiae* and fission yeast *Schizosaccharomyces pombe* are amongst the simplest and most powerful model systems for studying the genetics of cell cycle control. Because yeast grows very rapidly in a simple and economical media, large numbers of cells can easily be obtained for genetic, molecular, and biochemical studies of the cell cycle. The use of synchronized cultures greatly aids in the ease and interpretation of cell cycle studies. In principle, there are two general methods for obtaining synchronized yeast populations. Block-and-release methods can be used to *induce* cell cycle synchrony. Alternatively, centrifugal elutriation can be used to *select* synchronous populations. Because each method has innate advantages and disadvantages, the use of multiple approaches helps in generalizing results. An overview of the most commonly used methods to generate synchronized yeast cultures is presented along with working *Notes*: a section that includes practical comments, experimental considerations and observations, and hints regarding the pros and cons innate to each approach.

Key words Yeast, Cell cycle, Synchronization, Block-and-release, Centrifugal elutriation

1 Introduction

The budding yeast, *Saccharomyces cerevisiae*, and the fission yeast, *Schizosaccharomyces pombe*, are the two most frequently studied yeasts [1–7]. While they share a number of basic characteristics, the *S. cerevisiae* and *S. pombe* genomes evolutionarily diverged more than a billion years ago. Both yeasts have relatively small and compact genomes, on the order of only 3–4 times larger than the *E. coli* genome [1–6]. The fission yeast genome is slightly smaller and more unique because unlike budding yeast, it lacks large segmental genome duplications. Nonetheless, despite a small genome, the genetic, biochemical, and molecular mechanisms of many common cellular processes (e.g., cell cycle control) are highly conserved between yeasts and higher eukaryotes. Moreover, like bacteria, the culturing of yeast is simple and inexpensive. Extremely rapid growth and short cell cycle times (1.5–2 h) are easily achieved

Gaspar Banfalvi (ed.), *Cell Cycle Synchronization: Methods and Protocols*, Methods in Molecular Biology, vol. 1524,
DOI 10.1007/978-1-4939-6603-5_14,

in rich medium allowing for the production of enormously large numbers of cells in very short periods of time. Given adequate nutrients, both yeasts can be mitotically propagated ad infinitum, but deprivation of key nutrients (e.g., nitrogen and glucose) induces meiosis. Moreover, unlike most microorganisms, yeasts can be easily propagated as haploids. This improves the ease with which recessive mutations can be isolated and studied. These characteristics coupled with protocols that allow for highly efficient transformation of DNA molecules make yeast an amazingly powerful genetic system and one of the best and most tractable experimental model organisms.

Both budding and fission yeast grow and divide rapidly in rich medium containing glucose. However, excellent growth can be obtained in a wide range of minimal synthetic media allowing for the selection and propagation of strains with specific auxotrophies. Haploid fission yeast has a cylindrical shape that averages 3–4 μm in diameter and 7–15 μm long while diploids range from 4 to 5 μm in diameter and 15–25 μm long at division. In contrast, haploid budding yeast is ovoid with an average diameter of 3–8 μm. Diploid budding yeast has a size range from 4 to 12 μm in diameter depending upon the strain. However, cell size is not a static phenotype [8, 9]. Rather, size is strongly modulated by environmental factors and nutrient quality [8, 9]. In general, rapidly proliferating cells tend to be large while slowly dividing cells are considerably smaller. While the cell cycle times of both yeasts are highly sensitive to incubation temperatures, they can be successfully propagated over a very wide range of temperatures (e.g., from 12 to 38°C for *S. cerevisiae*). In contrast to the fission yeast, the budding yeast can also be cultured in the presence of a wide range of carbon sources (e.g., glucose, galactose, ethanol, and glycerol) [6, 10, 11]. Thus, cell cycle times, growth rates, and cell size can be easily manipulated by altering the amount or quality of the carbon provided in the growth medium. These properties are often useful in synchronization protocols.

Like higher eukaryotes, the cell cycle of yeast is divided into four independent phases: G1, S, G2, and M. In the budding yeast, cell cycle position can be easily determined microscopically (Fig. 1). G1-phase cells are unbudded and often smaller than average (Fig. 1a). Consequently, cell cycle progression and commitment past the yeast equivalent of the restriction point (START) is dependent upon growth to a critical cell size (Fig. 1b, c) [8, 9]. The emergence of a small bud signals entry into S-phase (Fig. 1c). Buds grow dramatically with cell cycle progression. Subsequently, cell cycle position can be inferred by comparing the size of the bud to the mother cell (Fig. 1d, e). Thus, analysis of the budding profile of a culture (*see* **Protocol 10**) is a good means of assessing cell synchrony.

In contrast to the budding yeast, in the fission yeast there are no obvious morphological features that can be used to microscopically determine cell cycle position. However, like the

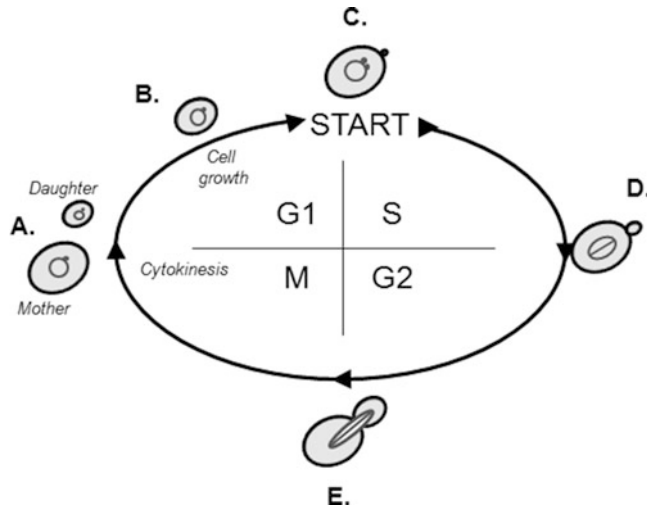

Fig. 1 *S. cerevisiae* cell cycle. In the budding yeast, cell cycle position can be determined microscopically. Yeast cells are shown in *light gray*, with nuclei (*circles*) and spindles (*ellipses with lines* through the center) in *dark gray*. Nuclei and spindles can only be visualized by fluorescence or electron microscopy. (**a**) Following cytokinesis, separated mother and daughter cells are in G1-phase with a round nucleus and a single spindle pole body. Because budding yeast divides asymmetrically, mother cells are nearly always larger than daughter cells. (**b**) However, both cells must grow in size in order to progress past START. Typically, this growth requirement is smaller in mother cells. (**c**) The emergence of a small bud signals progression past START. (**d**) Subsequently, the bud enlarges in S-phase and a short spindle is formed. (**e**) In G2/M-phase, buds are even larger. Nuclei and spindles become elongated. In *Sz. pombe*, cell cycle progression is less distinct. However, since fission yeast grow steadily in length with cell cycle progression, cell cycle position can be inferred from cell size measurements

budding yeast, cell cycle progression is size dependent. Thus, small cells tend to be in G1-phase. Moreover, because fission yeast only grows in length during the cell cycle, size measurements can be used to estimate cell cycle position. Most of the protocols and techniques described herein are specifically relevant to the synchronization of budding yeast, however, where possible relevant approaches for the synchronization of fission yeast are noted [12, 13]. Detailed below are 13 specific protocols complete with a detailed *Notes* section for the growth (**Protocol 1**) and synchronization of yeast. The synchronization section is subdivided into methods for monitoring cell synchrony (Protocols 2–4), methods for inducing synchrony (Protocols 5–10), and methods for selecting synchronous cells (Protocols 11–13). New for this edition is an Emerging Technologies section which briefly describes methods for applying microfluidics and digital photomicroscopy protocols to study cell cycle progression.

2 Materials

1. Rich medium (*see* **Note 1**).
2. Synthetic medium (*see* **Note 2**).
3. Dropout medium (*see* **Note 3**).
4. Rotating incubator.
5. Glass culture tubes and flasks.
6. Microcentrifuge tubes.
7. Spectrophotometer and cuvettes.
8. Sonicator.
9. Handheld counters.
10. 95 % ethanol (*see* **Note 8**).
11. 20 mg/ml Proteinase K (*see* **Note 9**).
12. PI Solution: 16 mg/ml propidium iodide (*see* **Note 10**).
13. 10 mg/ml RNase A (DNase free) (*see* **Note 11**).
14. 50 mM sodium citrate pH 7.0.
15. Cytometer.
16. Formaldehyde solution.
17. DAPI mounting medium (*see* **Note 12**).
18. Teflon-coated slides.
19. Poly-L-lysine solution (*see* **Note 12**).
20. Alpha factor (*see* **Note 13**).
21. Hydroxyurea (*see* **Note 14**).
22. Nocodazole (*see* **Note 15**).
23. Centrifugal Elutriator (*see* **Note 16**).

3 Methods

3.1 Growth and Propagation of Yeast

Liquid log-phase cultures are used for most synchronization protocols (*see* **Note 17**). Because yeast grows best when highly aerated, the use of baffled Erlenmeyer flasks is recommended (*see* **Note 18**). Log phase is frequently subdivided into early log ($<1\times10^7$ cells/ml), mid-log ($1–4\times10^7$ cells/ml), and late log phase ($>4\times10^7$ cells/ml) based predominantly on cell number. As cell density increases and cultures become saturated; yeast cells collect in G1-phase and tend to be more round and refractile. Depending on the protocol used, either log phase or saturated cultures might be needed. Therefore, the determination of cell density (Protocol 1) is frequently a prerequisite to beginning a synchronization protocol.

3.1.1 Protocol 1: Determination of Cell Density

1. Starting with ~1×10^6 cells/ml in the appropriate medium propagate cells until the approximate cell density is achieved (*see* **Note 19**). Determining the optical density (OD) of a yeast culture is the easiest method for estimating cell density (*see* **Note 20**).
2. Place 1 ml of culture medium in spectrophotometer cuvette and read OD_{600}. Zero the absorbance and use this sample as a blank control. Remove 1 ml of culture and place in a cuvette. Read OD_{600} absorbance. If necessary for better accuracy, dilute initial culture such that OD_{600} readings are <1.
3. In this range, an OD_{600} reading of 0.1 is equivalent to ~3×10^6 cells/ml (*see* **Note 21**).

3.2 Monitoring Cell Cycle Synchrony

Before beginning any cell cycle synchronization experiment, it is vital to determine both the cell cycle position of individual cells as well as monitor the rate of cell cycle progression. These observations are essential in order to accurately assess the degree of synchronization. The simplest method of monitoring cell cycle position in *S. cerevisiae* involves observing the number and size of buds (Fig. 1). G1-phase cells are unbudded and have a 1N DNA content (Fig. 2a). S-phase cells have small buds (Fig. 2b). In G2/M-phase cells, buds are larger and nearly approach the size of the mother cell (Fig. 2c). Thus, by counting the number of the cells that are budded (aka the budding index), the percentage of cells in G1-phase or S/

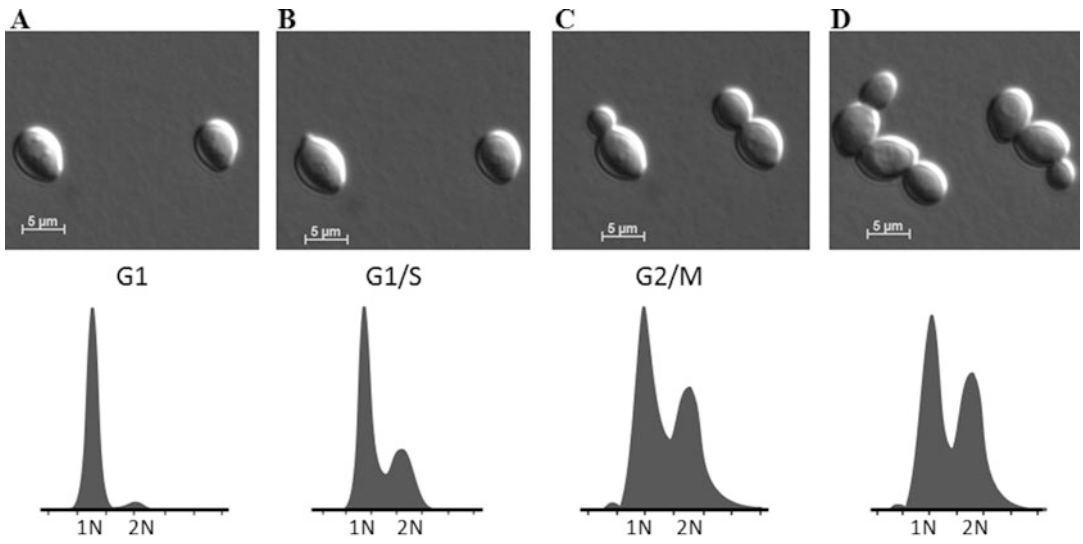

Fig. 2 Differential interference contrast microscopy of budding yeast and corresponding flow cytometry analyses. (**a**) In a culture of synchronized unbudded G1-phase cells, a single peak of cells with 1N DNA content is observed. (**b**) As cells progress past START, larger cells with small buds become apparent. A second peak of cells with 2N DNA content is observed, and cells in the "saddle" between the 1N and 2N peaks are in S-phase. (**c**). In G2/M-phase cells, buds are larger and the 2N DNA peak higher. (**d**) An asynchronous culture is shown for reference

G2/M-phases can be easily determined (**Protocol 2**). In addition, flow cytometry can also be readily used for determining cell cycle position (Fig. 2) by measuring the DNA content of individual cells stained with propidium iodide (**Protocol 3**). Immunofluorescent staining of DNA (**Protocol 4**) and/or microtubules are the best methods for microscopically determining cell cycle position in single cells [4, 6, 10, 11, 14–18]. Finally, excellent microarray studies have identified stage-specific gene transcripts that are very useful in confirming mitotic or meiotic cell cycle position (*see* **Note 22**) [19, 20].

3.2.1 Protocol 2: Determining the Percentage of Budded Cells

1. Add 500 µl of the culture into a labeled ice-cold microcentrifuge tube (*see* **Note 23**).
2. Sonicate each tube to disperse cells that have completed cytokinesis (*see* **Note 24**).
3. To ensure precise and accurate measurements, count the number of budded cells amongst a total of at least 200 cells.
4. Determine the percentage of budded and unbudded cells by dividing by the total number of cells counted (*see* **Note 25**).

3.2.2 Protocol 3: Analyses of Cell Cycle Distributions by Flow Cytometry (See Note 26)

1. Place 0.5 ml of log phase culture in a 2 ml microcentrifuge tube (*see* **Note 27**).
2. Fix cells by adding 1.5 ml 95% ethanol.
3. Sonicate briefly..
4. Centrifuge in microcentrifuge for 5 min at max speed.
5. Pour off supernatant and resuspend pellet in 2 ml of 50 mM sodium citrate. Repeat.
6. Add 25 µl of 10 mg/ml RNAse A and incubate at 50° C for 1 h.
7. Add 25 µl of 20 mg/ml Proteinase K and incubate at 50° C for 1 h.
8. Add 1 ml of PI solution.
9. Analyze samples with cytometer or save tubes in light protected box at 4° C.

3.2.3 Protocol 4: Analyses of Cell Cycle Position by DAPI Staining of Nuclear DNA (See Note 28)

1. Place 0.5 ml of log phase culture in a 2 ml microcentrifuge tube (*see* **Note 27**).
2. Fix cells by adding 1.5 ml 95% ethanol or formaldehyde (*see* **Note 29**).
3. Sonicate briefly.
4. Centrifuge in microcentrifuge for 5 min at max speed.
5. Resuspend cells in 50 µl DAPI mounting medium.
6. Coat Teflon slide wells with Poly-L-lysine solution.
7. Place 3–5 µl of cells on a slide, cover and observe with UV fluorescence (*see* **Note 30**).

3.3 Synchronization of Yeast

There are two methods that are commonly used for yeast cell synchronization. In the first case, an agent or a condition is used that blocks cell cycle progression. By removing the block, synchrony is induced. There are several advantages to block-and-release methods. First, block-and-release protocols can be carried out quicker and yield a large number of synchronized cells. In addition, these protocols can be used successfully with small cultures. Finally, block-and-release protocols do not require special and expensive equipment. However, inducing synchrony using blocking agents has several distinct disadvantages. A major disadvantage is the disruption of the normal coordination between cell growth and cell division. For example, extended cell cycle blocks will produce very large cells that may exhibit altered gene expression or cell cycle progression profiles. Drug-induced cell cycle arrests are unnatural and can have potentially toxic effects on the cells. Using temperature-sensitive mutants to block the cell can cause heat shock effects. In addition, the induction of cell stress responses may complicate results obtained. Below, common protocols for block-and-release synchronization are provided.

3.4 Induced Synchronization: Block-and-Release Methods

Block-and-release protocols block cell cycle progression but not cell growth. Cells can be blocked at various points in the cell cycle using pheromones, different drugs, or temperature-sensitive mutants. The basic protocol involves blocking cell cycle progression for a short time. Synchrony is achieved by releasing cells into fresh medium. Numerous block-and-release protocols can be used to obtain a synchronized cell culture. For example, alpha factor (**Protocol 5**), nutrient starvation (**Protocol 6**), depletion of essential cell cycle regulators (**Protocol 7**), or temperature-sensitive mutants (e.g., *cdc28*) (**Protocol 10**) can be used to arrest the cells in G1-phase. Hydroxyurea can be used to arrest the cells in S-phase (**Protocol 8**). Finally, cells can be arrested in G2/M-phase by nocodazole (**Protocol 9**) or using a variety of temperature-sensitive *cdc* mutants (e.g., *cdc15*) (**Protocol 10**).

3.4.1 Protocol 5: Synchronization of S. cerevisiae in G1-phase with Alpha Factor (See Note 31)

Alpha factor is a mating pheromone that is produced by MATα cells and arrests MATα cells at the G1/S transition point (Fig. 1) with 1N DNA content by inhibiting Cdc28 kinase activity. Arrested cells become enlarged and display a distinct comma-shaped "schmoo" morphology (Fig. 3a). Pheromone-mediated arrests are very useful because cells recover rapidly after release due to the Bar1p protease (*see* **Note 32**) and progress very synchronously through two or three cell cycles. While the alpha factor arrest protocol is more traditional, α-factor, the "opposite" mating pheromone produced by MATα cells, is also available to arrest MATα cells (*see* **Note 13**).

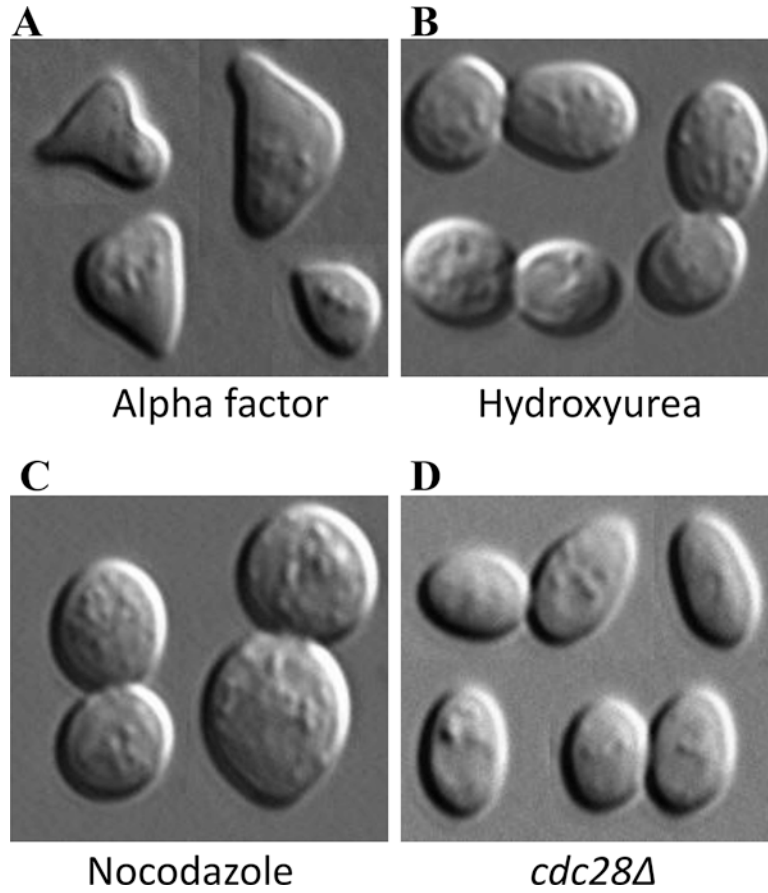

Fig. 3 Synchronized cultures of *S. cerevisiae*. (**a**) Cells treated with alpha factor arrest as enlarged unbudded cells. The "schmoo" morphology shown here is typical of arrested cells. (**b**) Hydroxyurea arrests cells in S-phase as large budded doublets. (**c**) Nocodazole arrests cells in G2/M-phase also as large budded doublets that frequently resemble "dumbbells." (**d**) A *cdc28* mutant arrested at the restricted temperature collects as large unbudded cells. Note other *cdc* mutants have terminal phenotypes like that seen in hydroxyurea or nocodazole arrests

Step by step:

1. Grow yeast cultures in YPD at 30°C to early log phase (0.2–0.5×10^7 cells/ml) (*see* **Note 33**).
2. Centrifuge cells and wash 2× in sterile YPD pH 3.5 (*see* **Note 34**).
3. Resuspend cells at a density of 1×10^6 cells/ml and add alpha factor to 5–10 μg/ml.
4. To arrest cells in G1-phase, incubate cultures at 30°C for 3 h (*see* **Note 35**).
5. Centrifuge cultures ($4000 \times g$ for 3–5 min) and wash twice by resuspending cell pellets in large volumes of pre-warmed YPD.

6. Resuspend cultures (1×10^7 cells/ml) in pre-warmed YPD to release from arrest (*see* **Note 36**).
7. Remove a time-zero aliquot (*see* **Note 37**).
8. Collect samples every 15 min to monitor cell cycle progression (*see* **Note 38**).

3.4.2 Protocol 6: Synchronization by Nutrient Depletion (See Note 39)

When yeast exhaust nutrients in the culture medium or grow to saturating densities, they arrest as highly retractile unbudded G1-phase cells.

1. Grow yeast cultures in YPD or YEP Raffinose at 30°C to saturation (*see* **Note 40**).
2. Centrifuge 1–2 min at 1800–2000 × *g* in swing-out rotor.
3. Discard the supernatant containing debris and small cells. Repeat (*see* **Note 41**).
4. Resuspend the pellet in sterile YEP and incubate at 30°C for 6 h (*see* **Note 42**).
5. Centrifuge 1–2 min at 1800–2000 × *g* in swing-out rotor.
6. Discard the supernatant containing debris and small cells. Repeat.
7. Resuspend (1×10^7 cells/ml) in pre-warmed YPD to initiate a synchronously dividing culture.
8. Remove a time-zero aliquot (*see* **Note 37**).
9. Collect samples every 15 min to monitor cell cycle progression (*see* **Note 38**).

3.4.3 Protocol 7: Synchronization of Cultures by G1-phase Cyclin Depletion (See Note 43)

1. Grow yeast cultures (*see* **Note 44**) in YEP Raffinose Galactose at 30°C to early log phase (*see* **Note 45**).
2. Centrifuge cells and wash twice in sterile YEP 2 % Raffinose (*see* **Note 46**).
3. Resuspend cells (1×10^7 cells/ml) in sterile YEP 2 % Raffinose.
4. Incubate at 30°C for 3 h (*see* **Note 47**).
5. Add galactose to 1 % to initiate a synchronously dividing culture.
6. Remove a time-zero aliquot (*see* **Note 37**).
7. Collect samples every 15 min to monitor cell cycle progression (*see* **Note 38**).

3.4.4 Protocol 8: Synchronization in S-phase with Hydroxyurea (See Note 48)

Hydroxyurea blocks cells in S-phase by inhibiting ribonucleotide reductase. Subsequently, cells accumulate with medium-sized buds (Fig. 3b) and DNA content between 1N and 2N.

1. Grow yeast cultures in YPD at 30°C to early log phase (0.2–0.5×10^7 cells/ml).

2. To arrest cells, add hydroxyurea as a powder to final concentration of 0.2 M.
3. Incubate cultures at 30°C for 3 h (*see* **Note 49**).
4. Centrifuge cultures (4000 × *g* for 3–5 min) and wash twice by resuspending cell pellets in large volumes of pre-warmed YPD.
5. Resuspend cultures (1×10^7 cells/ml) in pre-warmed YPD to release from arrest.
6. Remove a time-zero aliquot (*see* **Note 37**).
7. Collect samples every 15 min to monitor cell cycle progression (*see* **Note 38**).

3.4.5 Protocol 9: Synchronization in G2/M-phase with Nocodazole (See Note 48)

Nocodazole inhibits microtubule polymerization and blocks cells in G2/M phase. Subsequently, cells accumulate as large budded cells (Fig. 3c) with and 2 N DNA content.

1. Grow yeast cultures in YPD at 30°C to early log phase (0.2–0.5×10^7 cells/ml).
2. Add nocodazole to a final concentration of 15 μg/ml.
3. Incubate cultures at 30°C for 3 h (*see* **Note 50**).
4. Centrifuge cultures (4000 × *g* for 3–5 min) and wash twice by re-suspending cell pellets in large volumes of pre-warmed YPD.
5. Resuspend cultures (1×10^7 cells/ml) in pre-warmed YPD to release from arrest.
6. Remove a time-zero aliquot (*see* **Note 37**).
7. Collect samples every 15 min to monitor cell cycle progression (*see* **Note 38**).

3.4.6 Protocol 10: Synchronization of Cultures Using cdc^{ts} Mutants

Temperature-sensitive cell division cycle (*cdc*) mutants are widely used to synchronize cell cultures. With these mutations, specific and essential cell cycle control proteins are rapidly inactivated at elevated temperature. The result is a stage-specific cell cycle arrest. Subsequently, by lowering the culture temperature, synchronous cell cycle progression is initiated. In *S. cerevisiae*, *cdc28* (arrests in G1-phase), *cdc7* (arrests in S-phase), *cdc14*, *cdc15*, and *cdc20* mutants (arrest in G2/M-phase) are most commonly used (*see* **Note 51**).

1. Grow the appropriate strain (e.g., *cdc15*) in YPD at 23°C to early log phase ($0.2–0.5 \times 10^7$ cells/ml).
2. Transfer the culture to a 37°C incubator.
3. Incubate cultures at 37°C for 3.0–3.5 h to arrest the cells (*see* **Note 52**).
4. Transfer cultures to a 23°C incubator to release from arrest.
5. Remove a time-zero aliquot (*see* **Note 37**).
6. Collect samples every 15 min to monitor cell cycle progression (*see* **Note 38**).

3.5 Synchronization Through Cell Selection

The use of centrifugal elutriation is another method for yeast cell synchronization [10, 11, 20–25]. Unlike block-and-release protocols, this method does not induce synchrony but rather directly selects for synchronized cells. Specifically, centrifugal elutriation separates cells on the basis of size, mass, and shape. Centrifugal elutriation uses a counter flow to oppose centrifugal force (Fig. 4). In so doing, this creates two opposing forces that act on cells (Fig. 5). The centrifugal force sediments cells toward the bottom of the chamber, while the fluid flow washes cells toward the top of the chamber (Fig. 5a). The balance of the two forces causes large budded or irregularly shaped cells to move slower than small unbudded cells. Consequently, large cells collect at the bottom of the rotor (Fig. 5b, c). In contrast, the large surface-area-to-volume ratio typical of small cells causes little cells to be pushed toward the top of the elutriation chamber (Fig. 5b, c). Subsequently, by increasing the fluid flow rate through the elutriation chamber while maintaining the centrifuge at a constant speed, cells are forced out of the rotor in a size-dependent manner. In this way, a log phase culture can be easily size-fractionated. Since progression past START is size dependent (Fig. 1), the selection of similarly sized cells allows for the synchronous outgrowth of yeast cultures.

Centrifugal elutriation is probably the best method for obtaining a pure population of synchronously dividing cells. Compared to block-and-release methods, this technique has three main advantages. First, it generates synchrony in the most physiologically relevant manner. Since this is a size selection technique, it does not

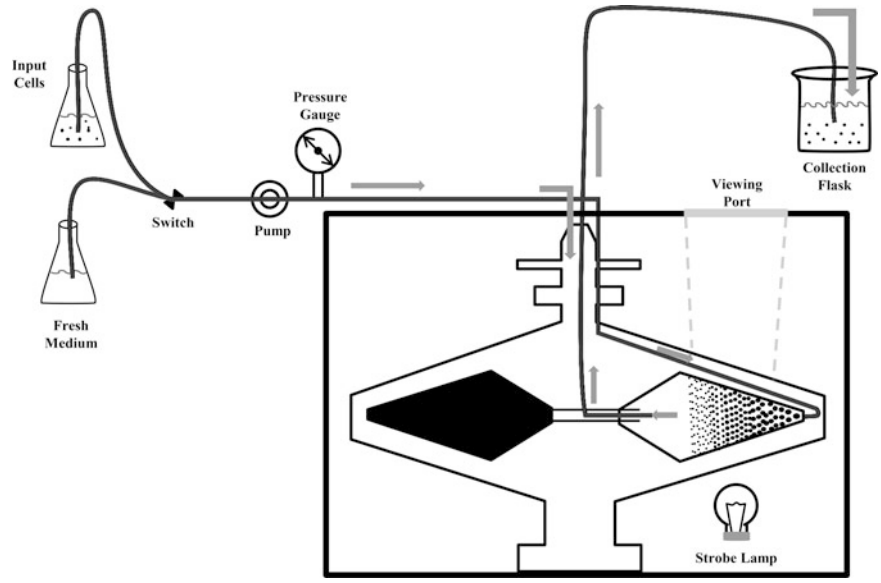

Fig. 4 Basic centrifugal elutriation setup. *Arrows* indicate direction of cell movement. Larger cells collect at the outer edge of the rotor (Fig. 5) while smaller cells can easily be elutriated and enriched in a collection flask

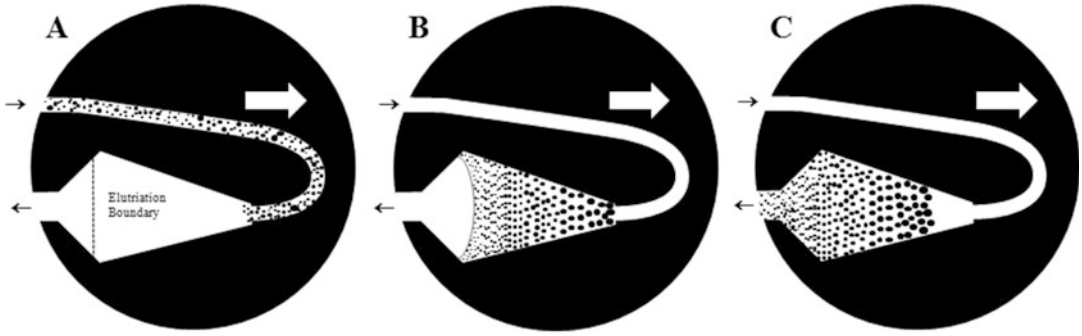

Fig. 5 Elutriation rotor. Using a strobe lamp and a viewing port (Fig. 4), the elutriation process can be visualized throughout the experiment. *Small arrows* indicate the direction of fluid flow, and the large *white arrow* indicates the direction of centrifugal force. (**a**) The appearance of cloudy and opaque medium at the outer edge of the rotor signifies the entrance of small and large cells into the elutriation chamber. Note the *dotted line* indicates the elutriation boundary. The chamber should not be filled past this point or poor size separation will occur. (**b**) Centrifugal elutriation generates a size gradient with smaller cells toward the top and larger cells toward the bottom of the elutriation chamber. Note when the chamber is filled to capacity, the elutriation boundary (*grey line*) will appear as concave opaque line. (**c**) After the chamber is filled to capacity, gradually increasing pump speed results in a higher rate of counter flow which in turn begins to elute the smallest cells out of the elutriation chamber and into a collection flask

perturb the normal coordination between cell growth and cell division. Second, it is a widely used, adaptable protocol and virtually any yeast strain can be used for this technique. Finally, elutriation is the only method which provides the opportunity of studying the earliest events in cell cycle regulation. The major disadvantage to elutriation is the requirement for large and expensive centrifugation equipment. Moreover, the manipulation and centrifugation has the potential to induce stress responses in the yeast cells. Therefore, it is suggested to compare the results from the elutriation protocols with other cell synchronization protocols. Two different methods of elutriation are detailed here: synchronized outgrowth of size-fractionated cells and chilled incremental fractionation. In addition, some investigators have further optimized protocols [26], as well as protocols specifically optimized for fission yeast [12, 13].

3.5.1 Protocol 11: Centrifugal Elutriation I: Synchronized Outgrowth of Size-Fractioned Cells

In the first protocol, log phase cultures are loaded onto the rotor at 30°C and elutriated off in warm clarified medium. If done properly, this allows for the rapid and synchronous outgrowth of size-selected cells (*see* **Note 53**).

1. Grow 2–4 l of the appropriate strain to mid-log phase ($2–3 \times 10^7$ cells/ml).
2. Assemble the elutriator, and set the centrifuge to the corresponding culture temperature. Ensure that a pressure gauge or bubble trap is installed in the input line as large air bubbles can disrupt the sensitivity of separation (Fig. 4) (*see* **Note 16**).

3. To help reduce the risk of contamination, flush all tubing and the rotor with 70% ethanol. Subsequently, rinse the elutriator with sterile water.
4. Measure cell density and pellet the cells by centrifugation at the proper growth temperature. Pour off supernatant and resuspend the pellet in 100–200 ml of fresh medium. Best results can be achieved by minimizing the time that cells spend in **steps 5–12** as timely efficiency increases synchrony and decreases artifacts.
5. Sonicate the cells at a medium setting twice for 30 s. Continuously swirl cells for even sonication and dispersion of heat (*see* **Note 54**).
6. Fill the elutriator chamber, tubing, and pressure gauge with clarified medium. Invert the pressure gauge to ensure it is filled completely. Tap the pressure gauge to remove any bubbles. Make sure that there are no air bubbles in the tubing or elutriation chamber and begin collecting the flow through in a sterile flask (Fig. 4).
7. Set the centrifuge to 2400 rpm (average approximately 820 × *g*, max approximately 1100 × *g*) (*see* **Note 55**), place the centrifuge timer on "hold" and start the centrifuge. Begin pumping the cells into the centrifuge at a rate of approx 20 ml/min. Cells can be visualized while being loaded into the chamber using the strobe lamp and observation port (Fig. 5a). At first the cell front will appear cloudy and turbulent, but as the remainder of cells load into the elutriation chamber, they will appear as a compact, sharp crescent front (Fig. 5b).
8. After cells have been loaded into the elutriation chamber, begin pumping in a clarified medium (Fig. 5c) (*see* **Note 56**). Gradually increase pump speed every 1–2 min until the cell front reaches the top of the elutriation chamber. Depending on the number and size of cells, this should take between 10 and 20 min at a pump rate of approx 30–40 ml/min (*see* **Note 57**).
9. As the cell front reaches the top of the elutriation chamber, the smallest cells, debris, and cell ghosts (cells broken by sonication) will begin to elute off the centrifuge (Fig. 5c).
10. When cells begin to elute, the flow through medium will become slightly cloudy. At this point examine 3 μl of flow with a phase-contrast microscope with a 40× objective. Begin collecting 200–300 ml fractions. Increase the pump speed in small increments between fractions. Check 3 μl of the flow through after every 100 ml with a phase-contrast microscope to determine the morphology and density of the cells that are eluting in each fraction. Roughly assess the number of budded cells. The goal is to collect a high-density fraction of cells that are <5% budded. It is very useful at this time to measure the cell number and size with a Z2 Coulter Counter/Channelyzer (*see* **Note 58**). Continue collecting fractions until the percentage of budded cells approaches 10%.

11. Depending on the experimental design and the number of cells needed, choose either the best fraction (e.g., the highest concentration of cells with a budding percentage (<5%)) or pool fractions. The final cell concentration should be ~1×10^7 cells/ml (*see* **Note 59**).
12. Remove time-zero samples as a control to assess synchrony. Return the synchronized population to the original incubator. Begin taking time points every 15–30 min. Monitor synchrony and cell cycle progression (*see* **Note 60**).

3.5.2 Protocol 12: Synchronization by Centrifugal Elutriation: Chilled Incremental Fractionation

Outgrowth of a size-selected log phase culture is an excellent method for initiating synchronous yeast cultures. Alternatively, centrifugal elutriation can be used to size fractionate a chilled log phase culture. In this case, each elutriation fraction represents a single "synchronized snapshot" of the entire yeast cell cycle. Using this approach, early small unbudded fractions will be enriched for G1-phase cells (Fig. 6). Subsequent fractions will contain larger cells, with a higher budding index as cells are enriched in S-phase, and G2/M-phase (Fig. 6). While the synchrony achieved using this approach is not as high as the previous approach (*see* **Note 61**), it is technically much easier (*see* **Note 62**), and considerably larger numbers of cells can be obtained. Alternatively, centrifugal elutriation of saturated cultures can be used to age-fractionate cells (*see* **Note 63**) or to induce meiotic synchrony (*see* **Note 64**).

1. Grow 2–4 l of the appropriate strain to mid-log phase ($2–3 \times 10^7$ cells/ml) (*see* **Note 65**).
2. Assemble the elutriator, and set the centrifuge to the corresponding culture temperature (*see* **Note 16**). Ensure that a pressure gauge or bubble trap is installed in the input line as large air bubbles can disrupt the sensitivity of separation (Fig. 4).
3. Set the elutriator centrifuge to 4°C and chill a mid-speed centrifuge and centrifuge bottles to 4°C.
4. Mid-log-phase grown culture (e.g., $2–3 \times 10^7$ cells/ml) should be immediately chilled by placing the flask on ice and adding equal volume of ice into it. Once chilled at 0–4°C, centrifuge the cells.
5. Pour off supernatant and resuspend pellet in 100–200 ml of ice-cold water.
6. Sonicate cells (setting 7) twice for 30s while swirling cells continuously on ice.
7. Set the centrifuge to 2400 rpm (*see* **Note 55**), place the centrifuge timer on "hold" and start the centrifuge. Begin pumping the cells into the centrifuge at a rate of approx. 20 ml/min. Cells can be visualized loading into the chamber using the strobe lamp and observation port (Fig. 5a). At first the cell

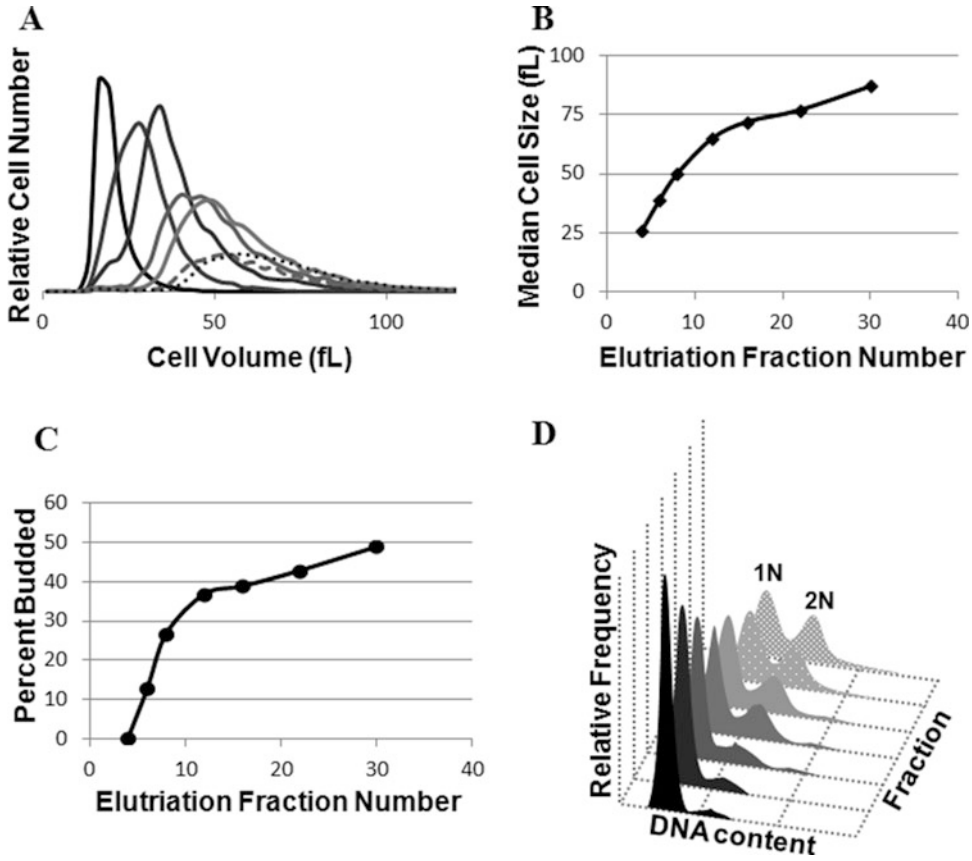

Fig. 6 Typical centrifugal elutriation results. (**a**) Z2 Coulter counter channelyzer analyses of seven elutriation fractions reveals a homogenous and sharp initial peak (*darkest line*) which enlarges and gradually flattens out in subsequent fractions. The first peak is typically used in an outgrowth experiment, and other fractions typify results obtained in an incremental elutriation. (**b**) Plotting of median cell size as a function of fraction number indicates that size increases rapidly in the first ~15 fractions and then more slowly. (**c**) Plotting of the budding index of cells as function of fraction number demonstrates cell cycle progression. The appearance of >50 % budded cells is suggestive of progression past START. Note the initial fraction has <5 % budded cells suggestive of a high degree of homogeneity. (**d**) Flow cytometry analyses of individual fractions can be used to assign cell cycle position. Note the initial fraction (front darkest peak) consists of >95 % G1-phase cells, whereas the last fraction has >50 % S/G2/M-phase cells

front will appear cloudy and turbulent, but as the remainder of cells load into the elutriation chamber, they will appear as a compact, sharp crescent front (Fig. 5b).

8. After cells have been loaded into the elutriation chamber, begin pumping in a clarified medium (Fig. 5c) (*see* **Note 56**). Gradually increase pump speed every 1–2 min until the cell front reaches the top of the elutriation chamber. Depending on the number and size of cells, this should take between 10 and 20 min at a pump rate of approx. 30–40 ml/min (*see* **Note 57**).

9. As the cell front reaches the top of the elutriation chamber, the smallest cells, debris, and cell ghosts (cells broken by sonication) will begin to elute off the centrifuge (Fig. 5c).
10. When cells begin to elute, the flow through medium will become slightly cloudy. At this point examine 3 μl of flow with a phase-contrast microscope with a 40× objective. Begin collecting 200–300 ml fractions. Increase the pump speed in small increments between fractions. Check 3 μl of the flow through after every 100 ml with a phase-contrast microscope to determine the morphology and density of the cells that are eluting in each fraction. Roughly assess the number of budded cells. The goal is to collect high-density fractions of cells that range from 0 to 95 % budded.
11. Making sure to keep cells chilled, remove samples for cell cycle analyses (*see* **Note 66**).
12. Centrifuge the remaining fractions and pellet cells. Pour off supernatant and resuspend cells in 1 ml of ice-cold water. Transfer cells to pre-chilled 1.5–2.0 ml microcentrifuge tubes. Centrifuge for 30 s to pellet cells. Pour off the supernatant and freeze cells at −80°C for future studies (*see* **Note 67**).

3.5.3 Protocol 13: Centrifugal Elutriation of Nutrient Depleted Cultures (See Note 39)

When yeast exhaust nutrients in the culture medium or grow to saturating densities, they arrest as highly retractile unbudded G1-phase cells. Depending upon growth conditions, arrested G1-phase cells will be found in a wide range of sizes. This protocol is very useful for collecting large quantities of G1-phase cells. Centrifugal elutriation can be used to collect different sized fractions which, in turn, will have distinct cell cycle kinetics (*see* **Note 68**).

1. Grow yeast cultures in YPD or YEP Raffinose at 30°C to saturation (*see* **Note 40**).
2. Centrifuge 1–2 min at 1800–2000 × *g* in swing-out rotor.
3. Discard the supernatant containing debris and small cells. Repeat (*see* **Note 41**).
4. Resuspend the pellet in sterile YEP and incubate at 30°C for 6 h (*see* **Note 42**).
5. Centrifuge 1–2 min at 1800–2000 × *g* in swing-out rotor.
6. Assemble and load elutriator as in **Protocol 11** (*see* **Note 16**).
7. When cells begin to elute, the flow through medium will become slightly cloudy. At this point examine 3 μl of flow with a phase-contrast microscope with a 40× objective. Begin collecting 200–300 ml fractions. Increase the pump speed in small increments between fractions. Check 3 μl of the flow through after every 100 ml with a phase-contrast microscope to determine the morphology and density of the cells that are eluting in each fraction. Roughly assess the number of budded cells. The goal is to collect

a high-density fraction of cells that are <5% budded. It is very useful at this time to measure the cell number and size with a Z2 Coulter Counter/Channelyzer (*see* **Note 58**).

8. Depending on the experimental design and the number of cells needed, collect either small, medium, or large cells. For best synchrony, ensure that the budding percentage is <5%. For best results, the final cell concentration should be ~1×10^7 cells/ml (*see* **Note 59**).
9. Remove time-zero samples as a control to assess synchrony. Return the synchronized population to the original incubator. Begin taking time points every 15–30 min. Monitor synchrony and cell cycle progression (*see* **Note 60**).

3.6 Emerging Technologies

Several laboratories have adapted the science of microfluidics to develop microminiaturized devices (e.g., chips) with built-in chambers and tunnels which use fluids to control the migration of cells based predominately on cell size [27–29]. This technology provides investigators with the ability to precisely manipulate environmental conditions at the cellular level. Specifically, several laboratories have developed protocols for the simple and efficient isolation of G1-phase cells (~62%) from asynchronous populations based on cell size [29]. However, enrichments for G1-phase approaches 80% when periodic nutrient modulation is used to alternate between rich and poor growth mediums [28]. In this case, these technologies are approaching the efficiency of the standard techniques described earlier. However, the necessity for unique and expensive equipment is currently limiting the wide applicability of these techniques.

Real-time photomicroscopy of living yeast in microscope-based incubators is another emerging technology for the studying cell cycle regulation in yeast. As an example, cell cycle progression can be observed, documented, and studied unobtrusively by propagating cells on thin strips of agar at 30°C in an incubation chamber on a Zeiss Axiovert 200 microscope [30]. Cell cycle transitions (e.g., birth size, size at START, or the length of G1-phase) can easily be recorded and measured (Fig. 7). In so doing, researchers can directly observe cell cycle synchrony in situ without impacting physiological conditions or perturbing the dynamics of cell cycle progression [30–33]. With this approach, extremely accurate and reproducible cell cycle measurements can be achieved. This method is likely subject to the least number of artifacts since individual cells are tracked in physiological environments. However, as discussed above, it requires expensive equipment, a considerable degree of expertise and training, and is highly time-consuming. Nonetheless, these emerging technologies are immediate useful in specialized laboratories while providing the future foundation for new widely applicable synchronization protocols.

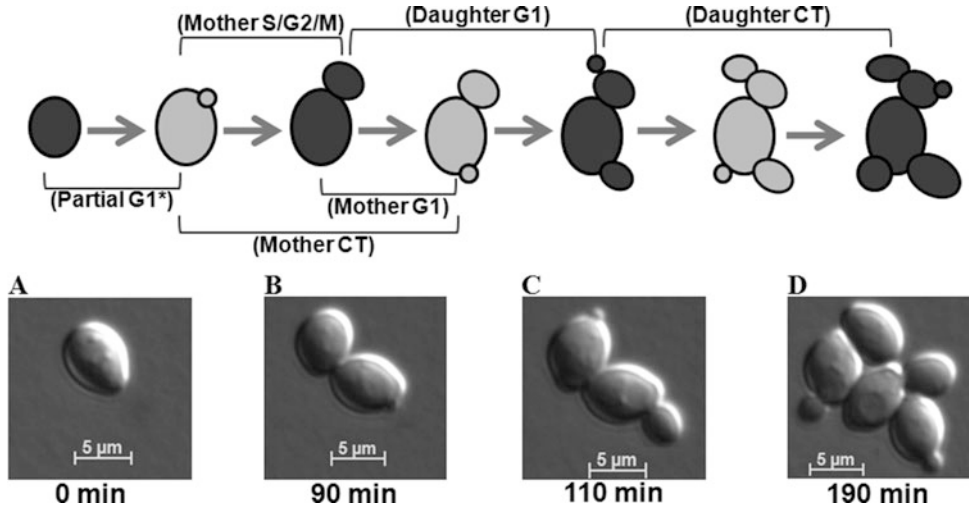

Fig. 7 Photomicroscopy of yeast cell cycle progression in situ. The *upper panel* provides the diagrammatic details of a typical time course movie. *Dark gray* diagrams correspond to labeled pictures with time taken at the bottom. (**a**) Virgin cell. The appearance of a bud (next *light gray* diagram) marks the end of the first (*partial) G1-phase. (**b**) The mother cell has completed S/G2/M-phase, and the first daughter has separated. Appearance of another bud from the mother (next *light gray* diagram) marks the end of the mother's complete G1 phase. The mother's complete cycle time (CT) is visualized from the complete production of one bud to the appearance of another (first *light grey* diagram to second *light gray* diagram). (**c**) The daughter has completed G1-phase and has begun to produce a bud. The daughter's S/G2/M-phase will be completed when the bud separates (next *light gray* diagram). (**d**) The appearance of another bud from the daughter marks the daughter's complete CT. Imaging software can be used to measure cell diameters in images such that size can be correlated with any number of cell cycle parameters

3.7 Conclusions

Synchronization of yeast cultures is essential for many different types of studies. There are two general methods for obtaining synchronized yeast populations: Block-and-release methods and centrifugal elutriation. Several variations of each type of protocol are detailed here. In addition, basic approaches for yeast monitoring yeast cell cycle are provided. Finally, an extensive *Notes* section is appended. Herein basic materials are listed and brief discussion of appropriate steps is available including practical comments, experimental considerations and observations, and hints regarding the pros and cons innate to each approach. In summary, this chapter provides a place to start for beginners and detailed specifics for investigators ready to synchronize yeast.

4 Notes

1. Yeast Extract Peptone (YEP) is a rich, complex medium without a carbon source. YEP is made by 1% yeast extract, 2% peptone in 1 l distilled water, sterilize by autoclaving. YPD is YEP supplemented with 2% filter-sterilized D-glucose

(U.S. Biological cat. no. G1030). Because autoclaving can break down complex carbon sources into simple sugars like glucose, it is highly recommended that all carbon sources be filter-sterilized and added after autoclaved media has cooled. Detailed alternative recipes for yeast rich and synthetic media are also available [6, 34].

2. Synthetic Dextrose Medium (SD) is a synthetic minimal medium containing yeast nitrogen base (YNB), vitamins, trace elements, salts, and glucose. SD is made by adding 1.7 g YNB (without amino acids and without ammonium sulfate), 5 g ammonium sulfate, 20 g glucose in 1 l distilled water. Synthetic Complete Medium (SC) is made by supplementing SD with 0.65 g primary amino acids mix (*see* **Note 4**), 0.35 g secondary amino acids mix (*see* **Note 5**), 0.2 g "drop-out" amino acid mix (**Note 6**), 0.45 g Na_2HPO_4 (Fisher cat. no. BP 332–1), 20 g glucose in 1 l distilled water.
3. "Drop-Out" medium is basic (SC) medium where one or more supplemented amino acids have been omitted ("dropped-out"). Most frequently these are histidine, leucine, tryptophan, or uracil but could include any amino acid in the primary or secondary mixes. For the sake of simplicity, individual "drop-out" powders can be made for each medium (*see* **Note 7**).
4. Primary amino acids mix contains 6 g each of the following amino acids: alanine, aspartic acid, asparagine, cysteine, glutamic acid, glutamine, isoleucine, valine, phenylalanine, proline, serine, threonine, and glycine and 0.6 g of PABA.
5. Secondary Amino Acids Mix: This mix contains 6 g each of the following amino acids: arginine, lysine, methionine, tyrosine, and adenine.
6. "Drop-Out" Amino Acid Mix: This mix contains 1 g each of the following amino acids: histidine, leucine, tryptophan, and uracil.
7. As an example, the recipe for -URA "drop-out" medium is given. It contains 1.7 g YNB without amino acids and without ammonium sulfate, 5 g ammonium sulfate, 0.65 g primary amino acids mix, 0.35 g secondary amino acids mix, 0.05 g leucine 0.05 g histidine, 0.05 g tryptophan, 0.45 g Na_2HPO_4, 20 g glucose in 1 l distilled water.
8. Ethanol can be industrial grade.
9. Proteinase K (Fisher) is made up by adding 5 ml of sterile water to one 100 mg bottle.
10. Propidium iodide (PI) solution is stored as a 100× stock (1.6 mg/ml) in 50 mM sodium citrate in a light protected bottle at 4°C.
11. To prepare DNAse-free RNase A, add 2.5 ml of water to one 5 mg bottle. Boil for 30 min. Aliquot into 1 ml tubes and store at –20°C.

12. DAPI (4′,6-diamidino-2-phenylindole dihydrochloride, Sigma) is made up by adding 5 ml of sterile water to one 5 mg bottle. DAPI mounting medium is prepared by adding DAPI (final concentration 0.05 μg/ml) in mounting medium: add 10 ml PBS pH 8.0 to 100 mg *p*-phenylenediamine (Sigma). Store at −20° C and discard if it turns brown. Adding 0.1% Triton X-100 can improve staining. Poly-L-lysine solution is from Sigma. Alternative protocols are also available [4, 35].
13. Alpha factor is a 13 amino acid peptide (TRP-HIS-TRP-LEU-GLN-LEU-LYS-PRO-GLY-GLN-PRO-MET-TYR, MW 1684). Stocks are made up at 1–50 mg/ml in ethanol and stored at −20°C. Alpha factor is available from a variety of sources, but it is much more economical to have it synthesized and purified (Zymo Research). For the mating arrest of MATα cells, α-factor is also available (Zymo Research).
14. Hydroxyurea is from Sigma.
15. Nocodazole (Sigma) stock solutions (1.5 mg/ml) are made by adding 6.7 ml of dimethyl sulfoxide (DMSO Sigma) directly to a 10 mg bottle. Aliquots are stored at −20°C. The addition of DMSO (final concentration of 1%) to the culture medium prevents the nocodazole from precipitating and improves the kinetics of arrest.
16. Complete elutriation systems are available from Beckman Instruments (2500 Harbor Blvd., Fullerton) (Fig. 4). The JE-5.0 rotor is recommended and can be used in Beckman J6 series or Avanti J-20 series centrifuges. Three sizes of elutriation chambers are available: a large 40-ml chamber, a standard 4 ml chamber, and a Sanderson 5.5 ml chamber. Researchers are encouraged to examine the Beckman manual for detailed equipment specifications, references, and instructions on use. The complete elutriator system includes a midspeed centrifuge, rotor, one or two elutriation chambers, pressure gauge, stroboscope, control unit, tubing, injection ports, and spare parts. In addition, a variable-speed peristaltic pump (Cole-Parmer Masterflex drive and pump head) and appropriate tubing are required. Recently, Tormos-Pérez et al. provided an illustration and description of assembling an elutriator centrifuge [13]. Earlier protocols of centrifugal elutriation were published by Banfalvi [36, 37] and Manukyan et al. [38].
17. Standard yeast culture requires prior knowledge of general yeast manipulation techniques. In addition, access to the following typical yeast culture equipment and supplies are necessary [3, 5, 7]: variable temperature incubators, shaking water baths, standard culture flasks, tubes, glassware, microcentrifuges, mid-speed centrifuges, spectrophotometer, centrifuge tubes and bottles, filter apparatus, standard and fluorescent

microscopes. Although not required, access to a Z2 Coulter Counter/Channelyzer (for monitoring cell size and cell number) and a bench top flow cytometer are highly recommended. All other equipment and/or reagents are specifically stated. It is highly recommended that beginning researchers read Methods in Yeast Genetics [34], Guide to Yeast and Molecular Biology [6], and Getting Started with Yeast [3]. Other excellent resources are also available [1, 2, 4, 5, 11, 39] and the Saccharomyces Genome Database website (http://www.yeastgenome.org/) is an invaluable resource. Additional excellent protocols can also be found online at CSHL protocols (http://cshprotocols.cshlp.org/).

18. The use of flasks with narrow necks (O.D. 38 mm) and foam stoppers (Fisher) helps limit bacterial contamination. In general, the possibility of contamination can be easily assessed microscopically, and a visual examination of all working cultures is always highly recommended prior to beginning synchronization experiments. This also helps ensure that the yeast culture is growing and proliferating with a normal and healthy morphology. Because rapidly proliferating yeast cultures seem to preclude bacterial growth, contamination should rarely be an issue except in cultures that propagate very slowly. In such cases, the addition of standard antibiotics (e.g., ampicillin) at bacteriostatic levels can be useful, but is not recommended under standard culture conditions.
19. In rich medium (e.g., YPD), cell number doubles every ~1.5 h. Given 1–2 h to exit lag phase, a starting culture is expected to reach early log phase in 5–8 h. For cells propagated in synthetic media (e.g., SC, SD, or "dropouts") or with poorer carbon sources (e.g., raffinose, ethanol, or glycerol) this time increases due to longer cell cycle times. Empirically determining cell cycle times is essential in accurately predicting the time it will take any given culture to reach log phase. An excellent example for mathematically determining cell cycle times and preparing cultures for log phase growth can be found online at CSHL protocols (http://cshprotocols.cshlp.org/).
20. Alternatively, the use of a Z2 Coulter Counter Channelyzer, while considerably more expensive is a more precise method for determining cell number. Count 100 μl diluted in 10 ml of sheath fluid for cultures $<2 \times 10^7$ and 10 μl for more concentrated cultures. Additionally, this method also allows for cell size measurements and distributions.
21. OD readings are dependent upon both cell number and cell size. Therefore, it is advisable to calibrate the spectrophotometer using either a hemacytometer or through plating cells and counting the number of colonies. Keep in mind that the latter method measures the number of viable cells.

22. The expression of specific genes can be used for staging cells in both the mitotic and meiotic cell cycles. For the mitotic cell cycle, *CLN2*, *H2A*, *CLB4*, *CLB2*, and *EGT2* can be used to stage cells in G1/S-, S-, G2-, M-, and M/G1-phases respectively [19, 40]. For the meiotic cell cycle, *DMC1*, *SPS1*, *DIT1*, and *SPS100* are useful for staging cells in early, middle, late middle, and late sporulation [41, 42]. However, meiotic gene expression patterns are more strain-specific than are mitotic gene expression patterns [41, 42].
23. Coding the tubes or having two lab members independently count buds helps eliminate investigator bias. Cells can be stored on ice for 4–6 h or fixed with formaldehyde (3% final concentration) and stored at 4°C indefinitely.
24. Place sonicator (Fisher) on a low setting for only 1–3 s. Wipe sonicator tip between tubes to avoid cross-contamination.
25. It is easiest to use two handheld counters using one to count the number of budded and the other the number of unbudded cells observed.
26. Excellent alternative protocols also exist [10, 23, 41, 43–45].
27. Because too many cells distort the results, use 50 μl for stationary or late log phase cultures.
28. Microscopic immunofluorescent analysis of the mitotic spindle by staining for tubulin is also an excellent method for ascertaining cell cycle position [4, 6, 10, 11, 14–17, 34, 45]. G1-phase cells have a small number of microtubules associated with the spindle pole body (Fig. 1a–c) which expands to become a short spindle spanning the nucleus in S-phase (Fig. 1d). Later in the cycle, the nucleus and the spindle become elongated and thinner (Fig. 1e).
29. Cells may also be fixed by adding 37% formaldehyde to a final concentration of 3%.
30. DAPI excitation wavelengths are 340–365 nm and emission wavelengths are 450–488 nm.
31. Synchronization of *S. cerevisiae* with alpha factor is very straightforward and easy [10, 20, 23, 25, 46]. In addition, large cultures can be arrested. Release from arrest is rapid and very synchronous. Moreover, partial synchrony can last for several cycles. However, the fact that alpha-factor arrest produces abnormally large cells can lead to significant artifacts. For example, the absence of a G1-phase leads to cell cycle times that are shorter than normal. Moreover, alpha-factor arrest disrupts the normal coordination between growth and cell division and since some molecular pathways are size-dependent, they are likely to be disrupted. In addition, MATa cells, diploid cells, and some mutants cannot be arrested with alpha-factor. Finally,

some mutant strains (e.g., *swi4Δ*) will not synchronously release from alpha-factor arrests [10, 21, 22]. In general, alpha-factor arrests the cell more completely in rich mediums.

32. MATα cells produce the Bar1p protease that degrades alpha factor [10, 20, 23, 25, 46]. For this reason, some investigators use *bar1-* strains because they can be efficiently arrested with 100–1000-fold less alpha factor. However, while these strains arrest at lower concentrations of alpha factor, they release less synchronously. The effects of the Bar1p protease can be counteracted by thoroughly washing cells prior to the addition of alpha factor. In addition, low cell densities and low medium pH improve the kinetics of arrest.
33. Cultures grown in YPD arrest better than any other medium.
34. YPD buffered to pH 3.5 with 50 mM sodium succinate helps inactivates the Bar1p protease.
35. Examine 3 μl of the culture under the microscope. In addition, count and size 100 μl with a Z2 Coulter Counter channelyzer. Cells will arrest at the G1/S-phase boundary, adopt "schmoo" morphology and continue to get larger. Cell number should not increase after 2 h. Cultures are fully arrested when less 5% cells are budded.
36. The addition of the filter-sterilized pronase E (Sigma P-6911) final concentration of 0.1 mg/ml increases the rate at which cells recover from the alpha factor arrests.
37. Time zero samples are an essential control. At this point, cultures should display the highest degree of cell cycle synchrony.
38. When monitoring cell cycle progression, small aliquots (1–2 ml) can be stored on ice for 4–6 h before processing. Immediately chilling samples, stops cell cycle progression and prevents inappropriate degradation of unstable RNAs and proteins. Subsequently, these samples can be fixed or stored a 4°C. However, if the purpose of the experiment is to collect large aliquots for RNA or protein extraction, it is most effective to collect samples in pre-chilled 50 ml centrifuge tubes. For these experiments, add 25 ml of culture to a chilled 50 ml tube already containing ~25 ml of ice. Centrifuge and transfer pelleted cells to a pre-chilled microcentrifuge tube by resuspending the pellet with ice-cold water. Microcentrifuge, remove supernatant, and store cell pellets at −80°C before extracting RNA or proteins. Yeast cell pellets kept at −80°C are stable for years, and RNA and protein can easily and efficiently isolated from frozen cell pellets.
39. Limitless numbers of cells can be synchronized using this method. However, because starved cells are less metabolically active, release from starvation arrests is slow and less synchronous than with other protocols. Moreover, nutrient starvation reduces cell size and induces stress response pathways which may adversely affect cell cycle synchrony and progression.

40. Cultures should be grown in large baffled flasks with constant aeration in a rotary shaker at 300 rpm. Culture volumes should not exceed 25% of the flask volume. Cultures should be incubated for 1–3 days or until the budding index is less than 5%. Cultures grown in poorer mediums reach saturation later.
41. Because small cells must grow in order to bud, they disrupt culture synchrony. However, because they sediment less well, they are easily washed out.
42. Incubating cultures in YEP without a carbon source primes cultures for cell cycle release. However, this step can be skipped.
43. G1-phase cyclins (Clns) are required for progression past START [47]. Because these cyclins are extremely unstable with a half-life less than 10 min [48], Cln depletion leads to a rapid G1-phase arrest. Because growth is not blocked, arrested cells rapidly become large, unbudded refractile cells. Unlike alpha factor arrested cells, Cln depletion results in round cells. Strains lacking both *CLN2* and *CLN3* and kept viable by a *CLN1* gene under the control of the *GAL*-promoter are the best for this approach [9]. This approach suffers from the same disadvantages that result from the generation of abnormally large cells due to extensive unbalanced growth.
44. While strains engineered for Cln-depletion are the most commonly used, in principle the depletion of any unstable *CDC* gene should also induce cell cycle arrest [25].
45. In YEP Raffinose/Galactose, each carbon source is added to a final concentration of 1% from sterile-filtered 20% stocks.
46. In order to ensure a rapid G1-phase cell cycle arrest, it is important to remove all galactose. Alternatively, glucose can be added to a final concentration of 2%. However, in this case, cultures must be washed 2× in YEP after **step 4**, before resuspending in fresh pre-warmed YEP Raffinose/Galactose in **step 5**.
47. Cultures should arrest as large unbudded spherical cells. When culture is >95% unbudded, the G1-phase arrest is complete.
48. The use of drugs (e.g., hydroxyurea or nocodazole) or *cdc* mutations to induce cell cycle arrests is simple and large cultures can be arrested. Release from arrest is rapid and very synchronous. Partial synchrony can last for several cycles. However, like all block-and-release protocols, they produce abnormally large cells that can lead to significant artifacts due to a disruption of the normal coordination between cell growth and proliferation. Thus, care must be taken in interpreting results.
49. Examine 3 μl of the culture under the microscope. In addition, count and size 100 μl with a Z2 Coulter Counter channelyzer. Cells will arrest as budded cells in S-phase boundary, and the buds will continue to get larger (Fig. 3b). Cell number should not increase after 2 h. Cultures are fully arrested when greater than 95% cells are budded.

50. Examine 3 μl of the culture under the microscope. In addition, count and size 100 μl with Z2 Coulter Counter channelyzer. Cells will arrest as budded cells in G2/M-phase. Most cells should be doublets with buds similar in size to mother cells (Fig. 3c). Cell number should not increase after 2 h. Cultures are fully arrested when greater than 95 % cells are budded.
51. Similar protocols are also available for *Sz. pombe* that routinely use alleles of *cdc2* and *cdc25* [4, 10, 11, 14, 18, 25, 45]. Note that the genetic nomenclature is not consistent between *S. pombe* and *S. cerevisiae* such that *cdc25* represents a different gene in each organism [7].
52. While 37° is used to arrest most *cdc* mutants, consult the literature or empirically determine the best temperature to use for individual experiments. Examine 3 μl of the arrested culture under the microscope. In addition, count and size 100 μL with Z2 Coulter Counter channelyzer. Cell number should not increase after 2 h. Cultures are fully arrested when greater than 95 % cells are budded. Figures 2 and 3 illustrate the phenotypes of appropriate arrests.
53. Centrifugal elutriation is a challenging technique that demands practice and patience to become adept [10, 11, 20–25]. Because a number of tasks need to be performed in rapid succession, it is suggested that investigators work in pairs. The first consideration is the determination of the appropriate growth conditions. Culture conditions that support rapid cell division (e.g., YPD) generate buds that are close in size to mother cells, particularly in haploid cells. In this case G1-phase is so short that it is nearly impossible to isolate a homogenous population of small unbudded cells (>95 % unbudded). As a result, synchrony is poor. Thus, the use of YPD cultures for haploid elutriations is not recommended. Substitution of raffinose for glucose or the use of synthetic medium alleviates these difficulties. In contrast, it is much easier to successfully elutriate diploid YPD cultures. Care must also be taken to ensure that cultures are in mid-log phase. Cultures in early log phase yield too few cells, and cultures in late log phase proliferate less synchronously upon release. A single 40 ml elutriation chamber can hold $4–6 \times 10^{10}$ cells. Too many cells reduce the resolution of size-fractionation, and too few reduces yield and lengthens elutriation time.
54. Sonication helps ensure the separation of daughters from the mother cells and disperses clumps that are caused by centrifugation.
55. Observe and listen to the centrifuge carefully. An unbalanced rotor can be easily visualized through the viewing port (Fig. 4) (unstable image), heard (unusual rattles or sounds), or felt (strong vibrations). Any loose tubing or leaking fittings can lead to an unbalanced rotor, and this condition usually presents

itself early in the experiment. If the rotor becomes seriously unbalanced, it is necessary to stop the centrifuge *immediately* to avoid damage to the elutriation equipment.

56. This is achieved by switching the stopcock from input cells to clarified medium (Fig. 4). Ensure that no air bubbles enter the tubing and that the clarified medium flask is not allowed to run dry.
57. Because the length of the tubing, pump strength, cell number, cell size, and the density of the medium all affect the rate of elutriation, the time and pump rate necessary to elute cells must be empirically determined.
58. Uniformity of cell size is an excellent measure of the homogeneity of a given elutriation fraction (Fig. 6a). Fractions that display sharp cell size peaks tend to display a high degree of synchrony upon release.
59. While cells can be released in clarified medium, best results are obtained by centrifuging fractions and resuspending pelleted cells in pre-warmed fresh medium.
60. Save at least four different aliquots for each time point. For example, a 100 μl sample for determining cell number and size, a 200 μl sample for determining the percentage of budded cells, a 500 μl for flow cytometry, and the remainder 25–50 ml for protein and/or RNA isolation. In addition, samples from the log phase culture prior to elutriation should be kept and analyzed as controls.
61. The types of data that can be obtained using this approach are illustrated in Fig. 6. Using an *S. cerevisiae* log phase culture, fractions can be obtained that range from a median size of 25 to 85 fl (Fig. 6a, b). Analysis of budding (Fig. 6c) or flow cytometry data (Fig. 6d) demonstrate cell cycle progression from G1-phase to G2/M-phase. However, because later elutriation fractions also contain large G1-phase cells, synchrony is not as good as when a single homogenous G1-phase fraction is released into fresh medium.
62. Elutriations of chilled cultures are much simpler because speed is not of essence. As long as cells are kept cold, the procedure may be completed slowly and methodically.
63. As older cells tend be larger than younger cells, a number of protocols have been developed to use elutriation to age-fractionate cells [49, 50].
64. Like mitosis, meiotic cell cycle progression is also size dependent. Therefore, size fractionation by elutriation helps initiate synchronous entry into meiosis [51, 52].
65. Centrifugal elutriation can also be used in combination with a nutrient starvation (*see* Protocol 13) because size selection

improves synchrony. Thus, when using saturated cultures (~1×10^8 cells/ml) smaller input cultures (0.5–1 l) can be used. This is also applicable when synchronizing meiotic cell cultures. In both cases, selection of large unbudded fractions for subsequent release work best.

66. Save at least three different aliquots for each time point. For example, a 100 µl sample for determining cell number and size, and a 200 µl sample for determining the percentage of budded cells, a 500 µl for flow cytometry. In addition, samples from the log phase culture prior to elutriation should be kept and analyzed as controls.
67. Yeast cell pellets kept at −80°C are stable for years, and RNA and protein can easily and efficiently isolated from frozen cell pellets.
68. Since small cells have a larger growth requirement in order to progress past START, small cells will spend a considerably longer amount of time in G1-phase as compared to larger cells. As a result, cell cycle times are significantly longer. In addition, cells isolated in this manner have to exit a saturation-induced lag phase which will alter the normal kinetics of G1-phase exit.

References

1. Forsburg SL (2003) Overview of Schizosaccharomyces pombe. Curr Protoc Mol Biol Chapter 13:Unit 13.14
2. Forsburg SL (2005) The yeasts *Saccharomyces cerevisiae* and *Schizosaccharomyces pombe*: models for cell biology research. Gravit Space Biol Bull 18(2):3–9
3. Sherman F (2002) Getting started with yeast. Methods Enzymol 350:3–41
4. Forsburg SL, Rhind N (2006) Basic methods for fission yeast. Yeast 23(3):173–183
5. Broach JR, Pringle JR, Jones EW (1991) The Molecular and cellular biology of the yeast Saccharomyces. Cold Spring Harbor monograph series, vol 21. Cold Spring Harbor Laboratory Press, Cold Spring Harbor, NY
6. Guthrie C, Fink GR (1991) Guide to yeast genetics and molecular biology, vol 194. Methods Enzymol Academic Press, Inc, Pasadena, CA
7. Murray AW, Hunt T (1993) The cell cycle: an introduction. W.H. Freeman, New York
8. Jorgensen P, Tyers M (2004) How cells coordinate growth and division. Curr Biol 14:R1014–R1027
9. Schneider BL, Zhang J, Markwardt J, Tokiwa G, Volpe T, Honey S, Futcher B (2004) Growth rate and cell size modulate the synthesis of, and requirement for, G1-phase cyclins at start. Mol Cell Biol 24:10802–10813
10. Fantes P, Brooks R (1993) The cell cycle: a practical approach. The practical approach series. IRL Press at Oxford University Press, Oxford, New York
11. Johnston JR (1994) Molecular genetics of yeast: a practical approach. The practical approach series, vol 141. IRL Press at Oxford University Press, Oxford, New York
12. Kume K (2016) Elutriation for cell cycle synchronization in fission yeast. Methods Mol Biol 1342:149–155
13. Tormos-Perez M, Perez-Hidalgo L, Moreno S (2016) Fission yeast cell cycle synchronization methods. Methods Mol Biol 1369:293–308
14. Gomez EB, Forsburg SL (2004) Analysis of the fission yeast Schizosaccharomyces pombe cell cycle. Methods Mol Biol 241:93–111
15. Green MD, Sabatinos SA, Forsburg SL (2009) Microscopy techniques to examine DNA replication in fission yeast. Methods Mol Biol 521:463–482
16. Humphrey T, Brooks G (2005) Cell cycle control: mechanisms and protocols. Methods in molecular biology, vol 296. Humana Press, Totowa, NJ, p 402
17. Day A, Schneider C, Schneider BL (2004) Yeast Cell Synchronization. Cell Cycle Checkpoint Control Protocols 241:55–76

18. Luche DD, Forsburg SL (2009) Cell-cycle synchrony for analysis of *S. pombe* DNA replication. Methods Mol Biol 521:437–448
19. Spellman PT, Sherlock G, Zhang MQ, Iyer VR, Anders K, Eisen MB, Brown PO, Botstein D, Futcher B (1998) Comprehensive identification of cell cycle-regulated genes of the yeast Saccharomyces cerevisiae by microarray hybridization. Mol Biol Cell 9:3273–3297
20. Futcher B (1999) Cell cycle synchronization. Methods Cell Sci 21:79–86
21. Walker GM (1999) Synchronization of yeast cell populations. Methods Cell Sci 21:87–93
22. Johnston LH, Johnson AL (1997) Elutriation of budding yeast. Methods Enzymol 283:342–350
23. Day A, Schneider C, Schneider BL (2004) Yeast cell synchronization. Methods Mol Biol 241:55–76
24. Sonoda E (2006) Synchronization of cells. Subcel Biochem 40:415–418
25. Amon A (2002) Synchronization procedures. Methods Enzymol 351:457–467
26. Marbouty M, Ermont C, Dujon B, Richard GF, Koszul R (2014) Purification of G1 daughter cells from different Saccharomycetes species through an optimized centrifugal elutriation procedure. Yeast 31:159–166
27. Wang S, Luo C (2016) Cell cycle synchronization using a microfluidic synchronizer for fission yeast cells. Methods Mol Biol 1342:259–268
28. Tian Y, Luo C, Lu Y, Tang C, Ouyang Q (2012) Cell cycle synchronization by nutrient modulation. Integr Biol (Camb) 4:328–334
29. Hur JY, Park MC, Suh KY, Park SH (2011) Synchronization of cell cycle of *Saccharomyces cerevisiae* by using a cell chip platform. Mol Cells 32:483–488
30. Yang J, Dungrawala H, Hua H, Manukyan A, Abraham L, Lane W, Mead H, Wright J, Schneider BL (2011) Cell size and growth rate are major determinants of replicative lifespan. Cell Cycle 10:144–155
31. Bean JM, Siggia ED, Cross FR (2006) Coherence and timing of cell cycle start examined at single-cell resolution. Mol Cell 21:3–14
32. Di Talia S, Skotheim JM, Bean JM, Siggia ED, Cross FR (2007) The effects of molecular noise and size control on variability in the budding yeast cell cycle. Nature 448:947–951
33. Schmoller KM, Turner JJ, Koivomagi M, Skotheim JM (2015) Dilution of the cell cycle inhibitor Whi5 controls budding-yeast cell size. Nature 526:268–272
34. Amberg DC, Burke D, Strathern JN (2005) Methods in yeast genetics : a Cold Spring Harbor Laboratory course manual, 2005th edn. Cold Spring Harbor Laboratory Press, Cold Spring Harbor, NY
35. Hasek J (2006) Yeast fluorescence microscopy. Methods Mol Biol 313:85–96
36. Banfalvi G (2008) Cell cycle synchronization of animal cells and nuclei by centrifugal elutriation. Nat Protoc 3:663–673
37. Banfalvi G (2011) Synchronization of mammalian cells and nuclei by centrifugal elutriation. Methods Mol Biol 761:25–45
38. Manukyan A, Abraham L, Dungrawala H, Schneider BL (2011) Methods Mol Biol 761:173–199
39. Ausubel FM (1987) Current protocols in molecular biology. Greene Publishing Associates, Brooklyn, N. Y & Media, Pa
40. Futcher B (2002) Transcriptional regulatory networks and the yeast cell cycle. Curr Opin Cell Biol 14:676–683
41. Chu S, DeRisi J, Eisen M, Mulholland J, Botstein D, Brown PO, Herskowitz I (1998) The transcriptional program of sporulation in budding yeast. Science 282:699–705
42. Primig M, Williams RM, Winzeler EA, Tevzadze GG, Conway AR, Hwang SY, Davis RW, Esposito RE (2000) The core meiotic transcriptome in budding yeasts. Nat Genet 26:415–423
43. Haase SB, Reed SI (2002) Improved flow cytometric analysis of the budding yeast cell cycle. Cell Cycle 1:132–136
44. Sabatinos SA, Forsburg SL (2009) Measuring DNA content by flow cytometry in fission yeast. Methods Mol Biol 521:449–461
45. Zhang H, Siede W (2004) Analysis of the budding yeast Saccharomyces cerevisiae cell cycle by morphological criteria and flow cytometry. Methods Mol Biol 241:77–91
46. Breeden LL (1997) Alpha-factor synchronization of budding yeast. Methods Enzymol 283:332–341
47. Richardson HE, Wittenberg C, Cross F, Reed SI (1989) An essential G1 function for cyclin-like proteins in yeast. Cell 59:1127–1133
48. Schneider BL, Patton EE, Lanker S, Mendenhall MD, Wittenberg C, Futcher B, Tyers M (1998) Yeast G1 cyclins are unstable in G1 phase. Nature 395:86–89
49. Woldringh CL, Fluiter K, Huls PG (1995) Production of senescent cells of Saccharomyces cerevisiae by centrifugal elutriation. Yeast 11:361–369
50. Egilmez NK, Chen JB, Jazwinski SM (1990) Preparation and partial characterization of old yeast cells. J Gerontol 45:B9–B17
51. Day A, Markwardt J, Delaguila R, Zhang J, Purnapatre K, Honigberg SM, Schneider BL (2004) Cell size and Cln-Cdc28 complexes mediate entry into meiosis by modulating cell growth. Cell Cycle 3:1433–1439
52. Nachman I, Regev A, Ramanathan S (2007) Dissecting timing variability in yeast meiosis. Cell 131:544–556

Chapter 15

Synchronization of Pathogenic Protozoans

Staffan Svärd and Karin Troell

Abstract

Protozoans are single-celled eukaryotes and many of the best-studied protozoans are parasitic to humans (e.g., *Plasmodium falciparum* causing malaria and *Trypanosoma brucei* causing sleeping sickness). These organisms are distantly related to humans but with retained eukaryotic type of cellular processes, making them good model systems for studies of the evolution of basic processes like the cell cycle. *Giardia intestinalis* causes 250 million cases of diarrhea yearly and is one of the earliest diverging protozoans. It is possible to synchronize its cell cycle using compounds that inhibit different steps of the cell cycle and the detailed protocol is described here.

Key words Cell cycle, Malaria, Parasite, Aphidicolin, *Giardia*

1 Introduction

Pathogenesis of infectious diseases is often the result of uncontrolled expansion of the infectious microbes, resulting in tissue destruction and inflammation. Protozoan parasites are not an exception to this but surprisingly little is known about the regulation of cell growth and the cell cycle in these organisms. Protozoans are single-celled eukaryotic microbes and most are free-living. However, several are parasitic to humans and other mammals and they cause significant morbidity and mortality worldwide. Our understanding of cell cycle regulation in protozoans has been lagging behind, mainly due to the lack of good synchronization protocols. Genomic analyses performed during the last 15 years have shown that parasitic protozoans have typical eukaryotic set-ups for cell cycle regulation [1, 2]. The number of regulatory components (e.g., cyclins and cyclin-dependent kinases, are reduced and this make these organisms interesting model systems to understand the evolution of cell cycle regulation in higher eukaryotes. Here, we will first summarize what is currently known about synchronization of medically important human protozoan parasites and then we will focus on protocols for synchronization of the most diverged protozoan parasite, *Giardia intestinalis*.

Gaspar Banfalvi (ed.), *Cell Cycle Synchronization: Methods and Protocols*, Methods in Molecular Biology, vol. 1524,
DOI 10.1007/978-1-4939-6603-5_15,

Malaria, one of the most important infectious diseases, is caused by *Plasmodium* parasites. Patients with severe disease show higher parasite burdens (high parasitemia) and virulent strains isolated from these patients have a more rapid multiplication rate in vitro [3]. The erythrocytic cycle of *P. falciparum* has been well-studied due to its relevance to disease and treatment. The merozoite, a haploid invasive form of the parasite, invades an erythrocyte and after approximately 48 h up to 32 new merozoites leave the erythrocyte. This process is called schizogony and the first recognizable cell cycle event is initiation of DNA replication 30 h after invasion of the erythrocyte [4]. This DNA replication continues for at least 8–10 h and the first M-phase occurs 36 h after invasion. However, the understanding of the regulation of these processes is still very fragmented. Several protocols for synchronization of the erythrocytic cycle of *P. falciparum* have been developed using density gradients [5], temperature shifts [6], osmotic lysis [7], magnets [8], and inhibitors of the cell cycle [9]. The main problem with these methods is that the synchrony and yield is not good enough for detailed molecular studies of the cell cycle. One publication describes a method for preparing cultures with very high parasitemia, synchronized at any erythrocytic stage [10]. A recent publication used density centrifugation in combination with a SyBr green-based method for synchrony confirmation [11]. An alternative method, counterstreaming centrifugation to purify protozoan parasites including *Plasmodium* sp. was applied by others [12]. The advantage of centrifugal elutriation is that it is rapid and a large number of cells can by synchronized [13]. These types of protocols generating tightly synchronized cells with higher yields will in the future allow more detailed cell cycle studies in *P. falciparum*.

Toxoplasma gondii is a relative to the *Plasmodium* parasite in the Apicomplexa group and it is a leading cause of death due to food-borne disease [14]. Rates of proliferation play a critical role in the disease pathogenesis and certain types of the parasite with high multiplication rate are much more virulent in mice [15]. Two main protocols have been developed for synchronization of the cell cycle. Parasites have been engineered to express the herpes simplex virus thymidine kinase [16]. Treatment of these recombinant parasites with exogenous thymidine arrests parasites in late G1/early S phase and this can be released by addition of fresh medium, resulting in synchronized cultures [16]. A novel method uses the antioxidant and metal chelating compound pyrrolidine dithiocarbamate (PDTC, [17]. This can be used on all types of *T. gondii* parasites and it synchronizes parasites in the G1 stage.

Leishmania and *Trypanosma* parasites belong to the order Kinteoplastida. *Leishmania* parasites are transmitted by sandflies and depending on species they cause cutaneous, mucocutaneous, and systemic (visceral) infections. *Trypanosma cruzi* is transmitted by bugs and cause Chaga's disease in South America. *Trypanosma brucei* is

transmitted by the tse-tse fly and it causes Sleeping sickness in Africa. Hydroxyurea has been used to synchronize *L. tarentolae* and *T. cruzi* parasites [18, 19] and partial synchronization of *T. brucei* can be obtained by re-feeding stationary phase cells [20]. Re-feeding of stationary phase cells has also been used to get semi-synchronized cultures of *Acanthamoeba castellani* [21]. *Acanthamoeba* can cause keratitis and it is also known to transmit pathogenic bacteria like *Legionella* and *Campylobacter*. *Acanthamoeba* is transmitted as resistant cysts and cyst-formation is optimal in the end of the G2 stage of the cell cycle, close to the stationary phase exit point [21].

Another cyst-forming parasitic protozoan is *Giardia intestinalis*. *Giardia* is a eukaryotic microbe that forms one of the earliest diverging lineages within the eukaryotic part of the universal tree of life. The basal position in the phylogenetic tree makes *Giardia* an excellent model system for identification and investigation of fundamental eukaryotic processes like cell cycle regulation [22]. The organism is unusual in containing two, apparently identical, diploid nuclei. Moreover, it is able to leave the vegetative cell cycle and enter into a differentiation pathway (encystation), triggered by intestinal stimuli (bile stress or cholesterol starvation). During encystation, a trophozoite undergoes two rounds of DNA replication with a single karyokinesis, to form a quadrinucleate 16N cyst [22]. Although presumed to be asexual, *Giardia* has low levels of allelic heterozygosity [1], indicating that the two nuclear genomes may exchange genetic material. Recent data demonstrate fusion between nuclei during encystations [23]. When a cyst awakens from dormancy, in response to signals from the host, it undergoes two rounds of cytokinesis, with a single round of nuclear division, to form four binucleate trophozoites, which only then re-enter the cell cycle. Thus, the giardial cell cycle displays unusual features and DNA replication is tightly coupled to vegetative growth and differentiation of the parasite. Furthermore, *Giardia* is also a medically important diarrhea-causing parasite and an effective replication of trophozoites is essential for the induction of symptoms [24]. We have for the first time been able to synchronize *Giardia* cultures by arresting the cells at the G1/S transition point with aphidicolin [25] and cell cycle-regulated genes were identified. The cell cycle can also be synchronized using aphidicolin in combination with nocodazole treatment [26, 27]. Nocodazole affects the microtubuli system, which results in arrest in the junction between G2 and M but the use of nocodazole treatment in synchronization has been questioned [28].

2 Materials

2.1 Cell Culture

1. Diamond's TYI-S-33 (Tryptone-Yeast extract-Iron-Serum): 30 g/L BBL Biosate peptone (tryptone and yeast extract mixture) (BD Biosciences), 55.6 mM glucose, 34.2 mM NaCl,

1.14 mM l-ascorbic acid, 5.74 mM $K_2HPO_4 \cdot 3H_2O$, 4.41 mM KH_2PO_4, 11.4 mM l-cysteine, and 0.038 mM ferric ammonium citrate. The pH is set to 7.0. Sterile filter through a 0.45 μm filter. Add sterile-filtered bovine bile (Sigma) to a final concentration of 0.5 mg/ml and 10% v/v heat-inactivated bovine serum (Gibco).

2. 10 ml Nunclon delta flat side tubes.

2.2 Whole Culture Synchronization

1. Diamond's TYI-S-33 medium.
2. 50 ml Falcon tubes (*see* **Note 1**).
3. Aphidicolin (Fluka-Sigma Aldrich) is dissolved in dimethyl sulfoxide (DMSO) to a final concentration of 10 mg/ml and is stored at −20 °C.
4. Cell scrapers (NUNC).
5. Phosphate buffered saline (PBS): 137 mM NaCl, 2.7 mM KCl, 10 mM Na_2HPO_4, 1.76 mM KH_2PO_4 (adjust to pH 7.4 with HCl if necessary).

2.3 Flow Cytometry

2.3.1 Fixing Cells

1. Cell fixative: 1% Triton X-100, 40 mM citric acid, 20 mM dibasic sodium phosphate, 0.2 M sucrose, adjust pH to 3.0.
2. Diluent buffer: 125 mM $MgCl_2$ in PBS.
3. Phosphate buffered saline (PBS): as above.

2.4 Wash and DNA Labeling

1. Phosphate buffered saline (PBS): as above.
2. Dissolve RNase A in ddH_2O to a concentration of 10 mg/ml.
3. FLOW buffer: 10 mM Tris (pH 7.5), 10 mM $MgCl_2$. Filter through 0.2 μm pore size filter to remove particles to avoid light scatter background noise. Store at 4 °C.
4. Dissolve Ethidium bromide (Sigma-Aldrich) in ddH_2O to a concentration of 4 mg/ml.
5. Dissolve Mithramycin A (Sigma-Aldrich) in ddH_2O to a concentration of 2.5 mg/ml.
6. DNA staining solution: Prepare fresh each time a staining solution for the number of samples you have. For each sample use 0.75 μl Ethidium bromide (4 mg/ml), 6 μl Mithramycin A (2.5 mg/ml) and 68.25 μl Flow buffer.

3 Methods

3.1 Cell Culture

1. Trophozoites from *Giardia* is axenically maintained in 10 ml flat side tubes in TYI-S-33 medium at 37 °C.
2. The cells are sub-cultured twice per week. Before re-inoculation the cells are kept on ice for 10 min to let cells detach from

the tube surface. The sample is homogenized and 5–10 μl of confluent trophozoite culture is transferred to a new tube with prewarmed TYI-S-33 medium.

3.2 Measuring Generation Time

Since the generation time for *Giardia* isolates all differ depending on the isolate, this protocol is based on number of generation cycles rather than hours. Below is described a simple way to determine the generation time of your cells. The knowledge of generation time together with FLOW data can also be used to estimate the length of the different stages during the cell cycle.

1. The generation time of exponentially growing trophozoites is determined by continuous counting of a culture.
2. Fresh cultures with 5×10^4 cells per ml is set up into three separate 10 ml tubes in 37 °C TYI-S-33 medium.
3. Every 90 min, for up to 12 h, the cells are detached by chilling the tube on ice for 10 min and then swirled to obtain a homogenized culture.
4. The total cell count is determined in a Bürker chamber. 10 μl from each tube is administered to the chamber and the averages of counts from the three tubes per time point is used to determine the generation time.

3.3 Whole Culture Synchronization

1. TYI-S-33 enough for all cultures for both aphidicolin treatment and re-feeding to release the cells from the drug is prepared and filtered. The medium is kept refrigerated. However, appropriate amount should be pre-warmed to 37 °C at all steps to avoid cold stress on the cells.
2. Grow cells to ~80% confluence.
3. Chill cells on ice for 10 min and dilute cells 1:10 with fresh medium (*see* **Note 2**). Make sure to swirl the bottle regularly and keep it on ice while preparing your cultures for synchronization. This is important to make sure all cultures are equal from the start.
4. For synchronization with release from the drug the number of samples plus two DMSO controls is set up. Use one tube or flask per time point as *Giardia* trophozoites attach to the surface and need to be kept on ice or scraped to detach. This will influence the cells too much in case cells would be harvested from the same sample.
5. Let the cultures grow for three-generation cycles or to approximately 70% before adding the drug.
6. Add aphidicolin, 0.5 μl/ml culture to each tube (except the controls) and 0.5 μl/ml culture DMSO to the controls.
7. Let the cultures grow for one generation cycle before release to allow all cells to reach the synchronization point in the cell cycle.

8. To release the cells from aphidicolin arrest pour of the drug containing medium and add fresh pre-warmed medium. The release is instant so to allow a sample with all cells arrested in G1 that sample should not be released but collect cells with aphidicolin containing medium.
9. Use a small cell scraper to harvest the cells (*see* **Note 3**). If the cells are to be analyzed with flow cytometry as well make sure to save approximately 7 ml of culture for that analysis (see fixing cells). Spin cells at 900 g for 5 min at 4 °C and snap freeze in liquid nitrogen and then move to freezer to preserve the sample for further analysis of RNA, DNA, or proteins.

3.4 Flow Cytometry

In flow cytometry, cells are individually analyzed. In this case, when cells are stained with DNA-specific dye the strength of fluorescence signal is proportional to the intracellular DNA content in each cell. The method is one way to visualize the success of the cell cycle synchronization as the flowgrams illustrate the number of cells with the different number of genome copies (in the case of *Giardia* 4N for GI cells and 8N for G2 cells). *See* Figs. 1 and 2.

3.5 Fixing Cells

1. The scraped cell culture is spun at 900 × *g* for 5 min at 4 °C.
2. As much of the medium as possible is removed. Some liquid (~50 μl) needs to be kept to avoid to destroy the often time loose pellet.

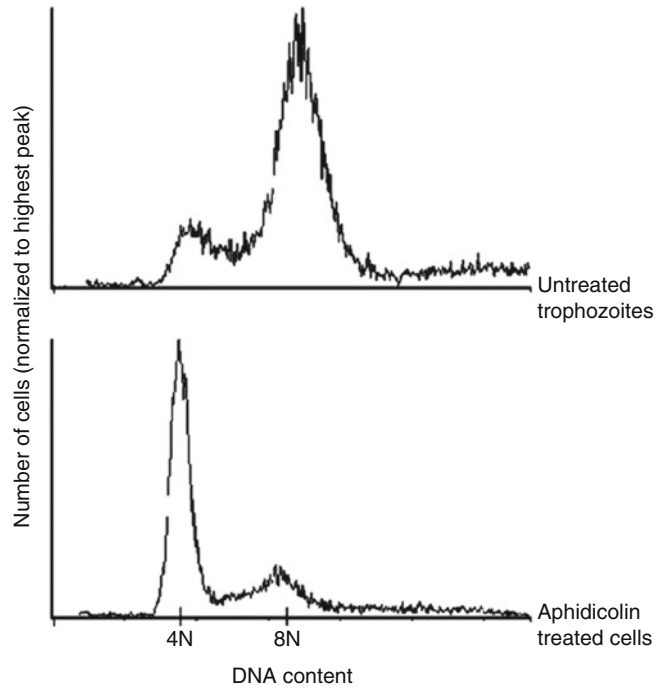

Fig. 1 Flow cytometry analysis of treated and untreated *Giardia* trophozoites. Cells were treated with aphidicolin according to the protocol described here

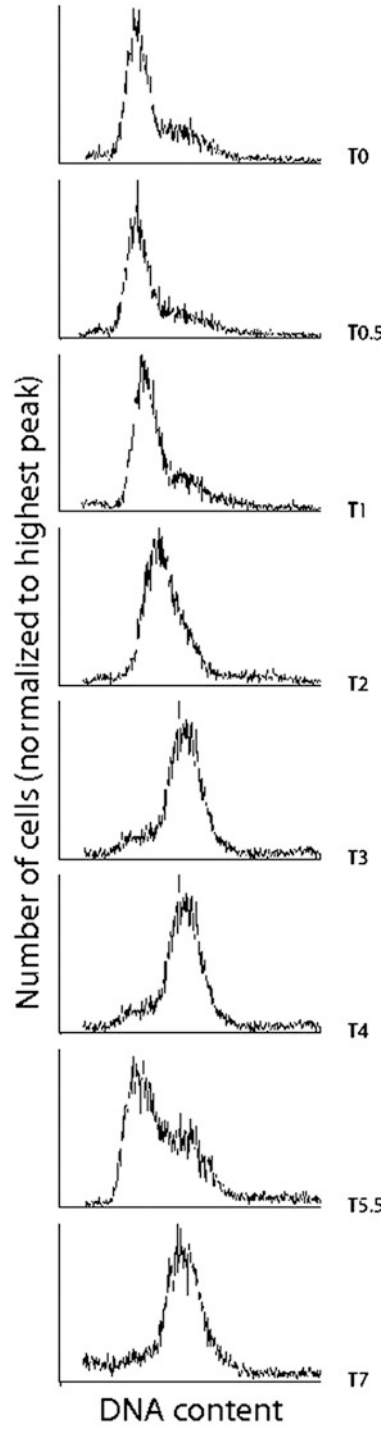

Fig. 2 Flow cytometry analysis of synchronized *Giardia* trophozoites. The cells were arrested in GI/S with aphidicolin and released from the drug after 6 h (i.e., one generation cycle. The WB strain C6 has a generation time of 6 h)

3. Immediately add 150 µl cell fixative. Mix carefully by pipetting the sample twice. Incubate for 5 min in room temperature.
4. After incubation 350 µl Diluent Buffer is added to the sample. Mix by pipetting carefully. Do not vortex the sample (*see* **Note 4**).
5. The cells could either be kept in 4 °C until the day after or continue the protocol immediately.

3.6 Wash and DNA Labeling

1. Transfer the sample to a 1.5 ml tube. Spin for 3 min at 900 × *g*.
2. Remove the supernatant carefully to avoid losing cells and add 100 µl PBS. Mix sample very gently until pellet is dissolved. Spin again for 3 min at 900 × *g*.
3. Remove the supernatant carefully and add 500 µl PBS and 2.5 µl RNase A (10 mg/ml). Mix sample very gently until pellet is dissolved.
4. Incubate samples for 30 min at 37 °C.
5. Spin sample for 3 min at 900 × *g*. Remove supernatant and add 75 µl of DNA staining solution. Mix carefully not to destroy the cells. When the cell pellet is dissolved add 75 µl FLOW buffer and mix carefully. Incubate samples on ice for 20 min and keep covered from light until analysis.
6. Read samples at 405 nm in a flow cytometry analyzer (*see* **Note 5**).

4 Notes

1. Depending on the further analysis of the synchronized cells, less or more cells might be needed. However, synchronizing cells in tubes instead of flasks results in more cells per volume and therefore saves aphidicolin. If it is important to easily view the cells during the progression through the cell cycle flask or flat side tubes should be used.
2. Depending on what the cultures are grown in (10 ml tube, 50 ml tube or flask), the number of cells/ml needed for 100% confluence differs. This is important to take into consideration if cells are the type of container is changed (tube for flask or vice versa) for synchronization. If using different containers there is a great risk of having too many or too few cells in the final culture, which will affect the result of the synchronization.
3. Cells could also be put on ice to de-attach from the tube. However, to minimize the time from harvest to fixation use of cell scraper is recommended.
4. The cells are very fragile after the acid cell fixative and it is crucial to be careful when mixing the sample with diluents buffer. If the cells are handled to rough they break and the FLOW will not look good.

5. The cells are fixed in acid but the diluents buffer should neutralize the pH to protect the cells and the DNA. However, best results are reached if the flow analysis is performed within the next 2 days.

References

1. Morrison HG, McArthur AG, Gillin FD, Aley SB, Adam RD, Olsen GJ et al (2007) Genomic minimalism in the early diverging intestinal parasite Giardia lamblia. Science 317:1921–1926
2. Gardner MJ, Hall N, Fung E, White O, Berriman M, Hyman RW et al (2002) Genome sequence of the human malaria parasite plasmodium falciparum. Nature 419:498–511
3. Reilly HB, Wang H, Steuter JA, Marx AM, Ferdig MT (2007) Quantitative dissection of clone-specific growth rates in cultured malaria parasites. Int J Parasitol 37:1599–1607
4. Inselburg J, Banyal HS (1984) Synthesis of DNA during the asexual cycle of Plasmodium falciparum in culture. Mol Biochem Parasitol 10:79–87
5. Kutner S, Breuer WV, Ginsburg H, Aley SB, Cabantchik ZI (1985) Characterization of permeation pathways in the plasma membrane of human erythrocytes infected with early stages of Plasmodium falciparum: association with parasite development. J Cell Physiol 125:521–527
6. Rojas MO, Wasserman M (1993) Effect of low temperature on the in vitro growth of Plasmodium falciparum. J Eukaryot Microbiol 40:149–152
7. Lambros C, Vanderberg JP (1979) Synchronization of Plasmodium falciparum erythrocytic stages in culture. J Parasitol 65:418–420
8. Bhakdi SC, Ottinger A, Somsri S, Sratongno P, Pannadaporn P, Chimma P et al (2010) Optimized high gradient magnetic separation for isolation of Plasmodium-infected red blood cells. Malar J 9:38
9. Naughton JA, Bell A (2007) Studies on cell-cycle synchronization in the asexual erythrocytic stages of Plasmodium falciparum. Parasitology 134:331–337
10. Radfar A, Mendez D, Moneriz C, Linares M, Marin-Garcia P, Puyet A et al (2009) Synchronous culture of Plasmodium falciparum at high parasitemia levels. Nat Protoc 4:1828–1844
11. Childs RA, Miao J, Gowda C, Cui L (2013) An alternative protocol for Plasmodium falciparum culture synchronization and a new method for synchrony confirmation. Malar J 12:386
12. Rüssmann L, Jung A, Heidrich HG (1982) The use of percoll gradients, elutriator rotor elution, and mithramycin staining for the isolation and identification of intraerythrocytic stages of *Plasmodium berghei*. Z Parasitenkd 66:273–280
13. Banfalvi G (2008) Cell cycle synchronization of animal cells and nuclei by centrifugal elutriation. Nat Protoc 3:663–673
14. Guo M, Dubey JP, Hill D, Buchanan RL, Gamble HR, Jones JL et al (2015) Prevalence and risk factors for Toxoplasma gondii infection in meat animals and meat products destined for human consumption. J Food Prot 78:457–476
15. Taylor S, Barragan A, Su C, Fux B, Fentress SJ, Tang K et al (2006) A secreted serine-threonine kinase determines virulence in the eukaryotic pathogen Toxoplasma gondii. Science 314:1776–1780
16. Radke JR, White MW (1998) A cell cycle model for the tachyzoite of Toxoplasma gondii using the Herpes simplex virus thymidine kinase. Mol Biochem Parasitol 94:237–247
17. Conde de Felipe MM, Lehmann MM, Jerome ME, White MW (2008) Inhibition of Toxoplasma gondii growth by pyrrolidine dithiocarbamate is cell cycle specific and leads to population synchronization. Mol Biochem Parasitol 157:22–31
18. Simpson L, Braly P (1970) Synchronization of Leishmania tarentolae by hydroxyurea. J Protozool 17:511–517
19. Galanti N, Dvorak JA, Grenet J, McDaniel JP (1994) Hydroxyurea-induced synchrony of DNA replication in the Kinetoplastida. Exp Cell Res 214:225–230
20. Gale M Jr, Carter V, Parsons M (1994) Cell cycle-specific induction of an 89 kDa serine/threonine protein kinase activity in Trypanosoma brucei. J Cell Sci 107:1825–1832
21. Jantzen H, Schulze I, Stohr M (1988) Relationship between the timing of DNA replication and the developmental competence in Acanthamoeba castellanii. J Cell Sci 91:389–399
22. Svärd SG, Hagblom P, Palm JE (2003) Giardia lamblia -- a model organism for eukaryotic cell differentiation. FEMS Microbiol Lett 218:3–7

23. Poxleitner MK, Carpenter ML, Mancuso JJ, Wang CJ, Dawson SC, Cande WZ (2008) Evidence for karyogamy and exchange of genetic material in the binucleate intestinal parasite Giardia intestinalis. Science 319:1530–1533
24. Roxstrom-Lindquist K, Palm D, Reiner D, Ringqvist E, Svärd SG (2006) Giardia immunity--an update. Trends Parasitol 22:26–31
25. Reiner DS, Ankarklev J, Troell K, Palm D, Bernander R, Gillin FD et al (2008) Synchronisation of Giardia lamblia: identification of cell cycle stage-specific genes and a differentiation restriction point. Int J Parasitol 38:935–944
26. Poxleitner MK, Dawson SC, Cande WZ (2008) Cell cycle synchrony in Giardia intestinalis cultures achieved by using nocodazole and aphidicolin. Eukaryot Cell 7:569–574
27. Reaume C, Moore B, Hernandez P, Ruzzini A, Chlebus M, Wasserman M et al (2013) Evaluation of drugs and stationary growth on the cell cycle of Giardia intestinalis. Mol Biochem Parasitol 187:72–76
28. Cooper S, Iyer G, Tarquini M, Bissett P (2006) Nocodazole does not synchronize cells: implications for cell-cycle control and whole-culture synchronization. Cell Tissue Res 324:237–242

Part V

Synchronizing Mammalian and Transfected Cells

Chapter 16

Synchronization of In Vitro Maturation in Porcine Oocytes

Tamás Somfai and Yuji Hirao

Abstract

When removed from the follicles, during the 44 h process of in vitro maturation (IVM) fully grown porcine oocytes resume meiosis spontaneously from the late diplotene stage of the first meiotic prophase and proceed to the metaphase-II (MII) stage at which they remain arrested until fertilization. However, the spontaneous resumption may start at various times causing heterogeneity in the nuclear stage and also in cytoplasmic characteristics within a population. Those oocytes that reach the MII stage earlier than others undergo an aging process which is detrimental for further embryo development. The synchronization of nuclear progression of porcine oocytes can be achieved by a transient inhibition of meiotic resumption during the first 20–22 h of IVM by the elevation of intracellular levels of cyclic adenosine monophosphate (cAMP) using the cellular membrane-permeable analog of cAMP, dibutyryl cyclic AMP. A simple and efficient protocol for such treatment is described below.

Key words Porcine, Oocyte, In vitro maturation, Synchronization, cAMP

1 Introduction

Recent progress in the in vitro embryo production (IVP) technology in farm animals allows us to produce embryos in large numbers at relatively low costs. The IVP technology includes three major consecutive steps: in vitro maturation (IVM) of immature oocytes, in vitro fertilization (IVF), and in vitro culture (IVC) of the fertilized oocytes. The first step, IVM, mostly determines the scale of embryo production (i.e., the number of embryos produced), as it provides the base material (i.e., matured oocytes) for further steps of IVP, or for other applications such as nuclear transfer [1].

In porcine IVP systems, fully grown immature oocytes are usually obtained from 3 to 6 mm antral follicles of ovaries collected at commercial slaughterhouses. Within the follicle, such oocytes are arrested at the late diplotene stage of the first meiotic prophase (aka, germinal vesicle or GV-stage) [2]. When removed from the follicle and cultured, immature mammalian oocytes resume meiosis spontaneously [3]. Under in vitro conditions, immature porcine

Gaspar Banfalvi (ed.), *Cell Cycle Synchronization: Methods and Protocols*, Methods in Molecular Biology, vol. 1524,
DOI 10.1007/978-1-4939-6603-5_16,

oocytes undergo germinal vesicle breakdown (GVBD) in 16–20 h and reach the metaphase-II (MII) stage by 40 h, at which stage meiosis is arrested again until the oocyte is activated by a penetrating sperm [2, 4]. Although in 3–6 mm antral follicles all oocytes are at the GV-stage, they appear to be at various sub-stages toward the end of diplotene [3]. Therefore, the population of fully grown porcine oocytes from 3 to 6 mm follicles are still somewhat "heterogeneous," in terms of in nuclear morphology and the timing of meiotic resumption during culture [5, 6]. Previous studies have shown that when porcine oocytes allowed to mature "freely" under in vitro conditions they reached the MII stage at various time points of culture [7, 8]. Oocytes performing precocious nuclear resumption during IVM culture reach the MII stage earlier than others. When matured oocytes are not fertilized for an excessive duration, they undergo a time-dependent aging process which greatly reduces their competence for normal monospermic fertilization and further embryo development [9]. Accordingly, oocytes undergoing precocious nuclear maturation during IVM have high affinity to polyspermic fertilization [8, 10] which is still the main problem of IVF systems in pigs [11]. To prevent this phenomenon, synchronization of the meiotic progress is necessary. Synchronization of oocyte maturation during IVM has further advantages; it enables the precise control and manipulation of the timing of oocyte maturation which makes the planning of experiments flexible in time [12], and also it improves the competence of oocytes to develop to embryos (*see* **Note 1**). In pigs, synchronization of the meiotic progress can be effectively achieved by a transient inhibition of GVBD (*see* **Note 2**) during the first 20–24 h of IVM, using dibutyryl cyclic AMP (dbcAMP), a membrane permeable cAMP analog (*see* **Note 3**) [7]. Alternatively, for synchronization an enzymatic procedure for the isolation of ovarian follicles and oocytes at early stages of development from the ovaries of newborn piglets was applied. The isolated oocytes were then separated by centrifugal elutriation from the overwhelming majority of the ovarian cells [13]. Elutriation is a rapid technique and subpopulations represent different stages of the cell cycle [14].

2 Materials

2.1 Basic Reagents and Consumables

1. PXM-Hepes medium [15] (for oocyte collection): 108.00 mM NaCl, 10.00 mM KCl, 0.35 mM KH_2PO_4, 0.40 mM $MgSO_4 \cdot 7H_2O$, 5.00 mM$NaHCO_3$, 25 mM Hepes, 0.20 mM Na-pyruvate, 2.00 mM Ca-$(lactate)_2 \cdot 5H_2O$, 0.01 μM gentamicin, and 3.00 mg/ml polyvinyl alcohol.
2. POM medium [15] (for in vitro maturation): 108.00 mM NaCl, 10.00 mM KCl, 0.35 mM KH_2PO_4, 0.40 mM $MgSO_4 \cdot 7H_2O$, 25.00 mM $NaHCO_3$, 4.00 mM glucose, 0.20 mM Na-pyruvate, 2.00 mM Ca-$(lactate)_2 \cdot 5H_2O$,

2.00 mM L-glutamine, 5.00 mM hypotaurine, 20.00 ml/l BME amino acids, 10.00 ml/l MEM non-essential amino acids, 600 μM L-cysteine, 0.01 μM gentamicin, and 3.00 mg/ml polyvinyl alcohol.

2.2 Stock Solutions

1. Hormone mixture stock (100×): Equine chorinonic gonadotrophin (eCG) and human chorionic gonadotropin (hCG) are dissolved together at a concentration of 1000 IU/ml each in POM medium. The stock is stored at –20 °C in 85–200 μl aliquots.
2. Epidermal growth factor (EGF) stock (1000×): EGF is dissolved in Dulbecco's Phosphate Buffered Saline supplemented with 10 mg/ml bovine serum albumin at a concentration of 10 μg/ml. The stock is stored at –20 °C in 20 μl aliquots.
3. dbcAMP stock (100×): dbcAMP is dissolved in POM at 100 mM concentration. The solution is stored in 85–200 μl aliquots at –20 °C until use.

2.3 Media

1. IVM medium: POM is supplemented with EGF stock at 1000×dilution rate to achieve a final concentration of EGF at 10 ng/ml (*see* **Note 4**). Then the medium is filtered through a 0.22 μm filter. The medium should be prepared freshly before use. This medium is the basis of the IVM-Arrest medium (described below). For the culture of 100 oocytes, approximately (a minimum of) 16 ml base medium should be prepared in total.
2. IVM-Arrest medium: IVM medium is supplemented with hormone mixture stock and dbcAMP stock both at 100×dilution rate to achieve a final concentrations of eCG, hCG, and dbcAMP at 10 IU/ml, 10 IU/ml, and 1 mM, respectively. Then the medium is filtered through a 0.22 μm filter. The medium should be prepared freshly before use. For the culture of 100 oocytes, a minimum of 8 ml base medium should be prepared.

3 Methods

The outline of the treatment regimen for meiosis synchronization of porcine oocytes is depicted in Fig. 1.

3.1 Oocyte Collection

In porcine IVP systems, immature oocytes are usually obtained rom the antral follicles of ovaries collected at commercial slaughterhouses. Among the antral follicles, those of 3–6 mm in diameter are optimal, since they contain a fully grown oocyte with an adequate developmental competence [16, 17]. The entire collection procedure should be finished within 2 h.

1. Five to six porcine ovaries are placed in Petri dishes (60 × 15 mm) on a 37.0 °C warm plate and the follicles are dissected with a lance allowing the follicular fluid and the

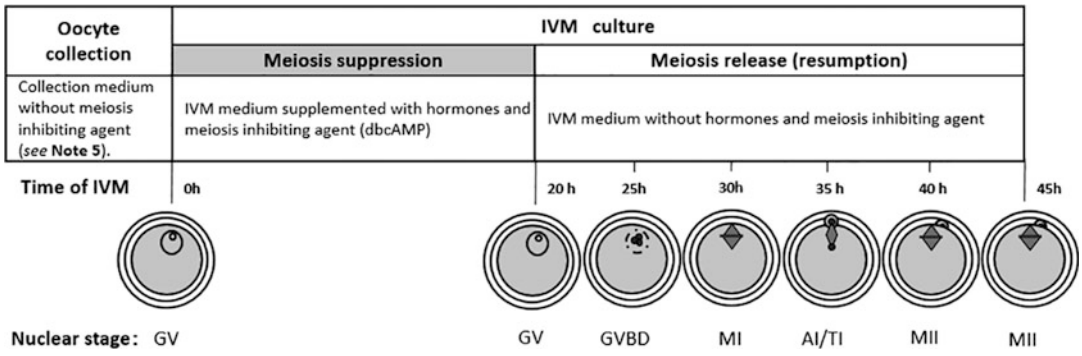

Fig. 1 The outline of treatment regimen for meiosis synchronization of porcine oocytes and the approximate timing of nuclear events during IVM. *GV* germinal vesicle stage (prophase, late diplotene), *GVBD* germinal vesicle breakdown, *MI* metaphase-I, *AI* anaphase-I, *TI* telophase-I, *MII* metaphase-II

oocytes to flow out into the petri dish. Alternatively, the oocytes can also be aspirated from the follicles using a syringe and needle (gauge size 19–20).

2. After either method the follicular fluid containing the oocytes and other cell types is placed in 15 ml centrifuge tubes kept vertically at 37.0 °C for 3–5 min.
3. Approximately 0.3–0.5 ml sediment is picked up by a pipette and placed as several (15–20) separate droplets in a Petri dish (60 × 15 mm) containing 5 ml of the collection medium (*see* **Note 5**) which is PXM-Hepes (*see* **Note 6**). The oocytes are then selected under a stereo microscope equipped with a warm stage at 37.0 °C. Only fully grown oocytes with a homogenous cytoplasm and at least two layers of surrounding cumulus cells are collected (*see* **Note 7**).
4. The selected oocytes are consecutively washed three times in 2 ml aliquots of the collection medium in 35 mm petri dishes before IVM.

3.2 IVM1: Meiosis Suppression

1. The oocytes are washed three times in 2 ml aliquots of the IVM-Arrest medium in 35 mm petri dishes covered by paraffin oil.
2. After washing, the oocytes are placed in 500 µl aliquots of IVM-Arrest medium in groups of 30–50 per well in four-well dishes without oil covering (*see* **Note 8**).
3. The COCs are cultured in the humidified atmosphere of 5% CO_2, 20% O_2 and 75% N_2, at 39 °C in a water-jacketed incubator (*see* **Note 9**).
4. The oocytes are cultured in IVM arrest medium for approximately 20–24 h (*see* **Note 10**). After culture in IVM-Arrest medium for 20 h, all oocytes remain at the GV stage whereas over 40% of the oocytes cultured without a meiosis blocking agent resume meiosis and undergo GVBD (Fig. 1a).

3.3 IVM2: Meiosis Release

During this phase, the COCs are transferred to the *IVM medium* that allows the nuclear progression of oocytes.

1. The oocytes are washed three times in 2 ml aliquots of the IVM medium in 35 mm petri dishes covered by paraffin oil.
2. The oocytes are cultured in 500 µl aliquots of the IVM medium in four-well dishes under the same conditions used in the previous step of the arrest for an additional 24 h (*see* **Note** 7).
3. At 44–48 h the total IVM period (IVM1+IVM2), the oocytes can be used for embryo production either by IVF or parthenogenetic activation [15, 18, 19].

3.4 Meiotic Resumption and Nuclear Progression During IVM

One millimolar dbcAMP effectively blocks the meiotic resumption during IVM1, whereas without the drug over 40% of them undergoes GVBD by 20 h of IVM (Fig. 2a). When the first 20 h of IVM is conducted in the presence of 1 mM dbcAMP, the breakdown of the germinal vesicle starts approximately 5 h and finishes within 15 h after the medium exchange in the entire oocyte population (Fig. 2a). The percentage of oocytes at the metaphase-I (MI) stage reaches the maximum approximately 10 h after the medium change (at 30 h after of the entire IVM culture) (Fig. 2b) and the percentage of oocytes showing the signs of homologue chromosome segregation (being at either anaphase-I (AI) or telophase-I (TI) of the meiotic transition) reaches its maximum level 15 h after the release from meiotic blockade (i.e., at 35 h of the entire IVM culture) (Fig. 2c). Irrespective of meiotic suppression for the first 20 h of IVM by dbcAMP, the percentage of oocytes at the MII stage (i.e., those which successfully finished nuclear maturation) reaches its maximum level around 20–25 h after the medium change (i.e., at 40–45 h of the total IVM period) (Fig. 2d). There is no significant difference in the percentages of oocytes at the MII stage with or without the application of 1 mM dbcAMP during the first 20 h of IVM (Fig. 2d). Nevertheless, after meiotic blockade with dbcAMP, oocytes reach each meiotic stage in a more synchronized manner compared with those cultured without dbcAMP treatment which is indicated by higher maximum levels (peaks) for oocytes at transient stages between the GVBD and MII (such as MI, AI, and TI) and the shortened time duration between the minimum levels of each stage by approximately 5 h after the use of dbcAMP (Fig. 2b, c). Furthermore, the duration during which the percentage of matured oocytes reaches the maximum level from none becomes approximately 10 h shorter after the conduction of the meiosis suppression by dbcAMP (Fig. 2d). Figure 3 demonstrates clear differences in nuclear heterogeneity during IVM2 (release) period (especially at 20, 25, and 30 h of the total IVM period) between the oocyte populations which had been matured without or after a pre-culture with or 1 mM dbcAMP, which confirms the synchronized manner of nuclear progression after the temporary meiotic arrest with dbcAMP.

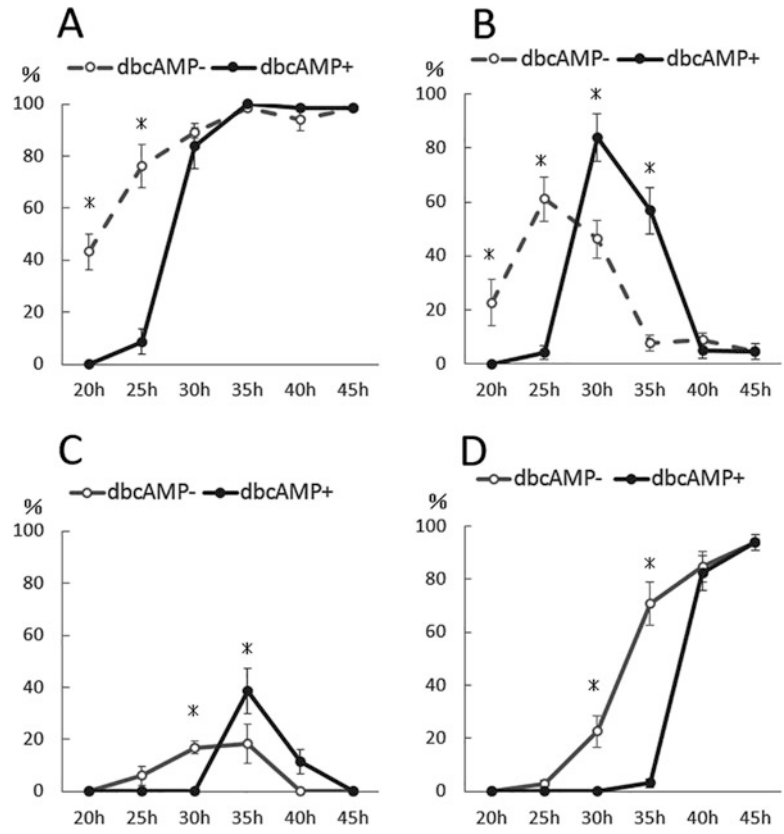

Fig. 2 Nuclear progression of cumulus-enclosed porcine oocytes during IVM, after 20 h culture in the absence (dbcAMP–) or presence (dbcAMP+) of 1 mM dbcAMP. (**a**) Percentage of oocytes showing germinal vesicle breakdown (i.e., meiotic resumption); (**b**) percentage of oocytes at the MI stage; (**c**) percentage of oocytes at AI or TI stage; (**d**) percentage of oocytes at the MII stage (i.e., matured oocytes). Data are expressed as mean ± SEM. Three replications were performed. Asters denote significant differences at specific time points between dbcAMP– and dbcAMP+ groups (paired *t*-test). Nuclear status of oocytes was determined by phase-contrast microscopy after staining with 1 % acetic-orcein according to the method of Nagai et al. (*6*). *GV* germinal vesicle, *DIA* diakinesis, *MI* metaphase-I, *AI/TI* anaphase-I or telophase-I, *MII* metaphase-II

4 Notes

1. A transient blocking of meiosis resumption in porcine oocytes during the first 20–22 h of IVM by 1 mM dbcAMP reduced the frequency of polyspermic fertilization during IVF and improved embryo development during subsequent culture [20, 21]. Furthermore, nuclear synchronization by dbcAMP seems to exert other positive effects on the competence of porcine oocytes in addition to the avoidance of polyspermy [7]. cAMP

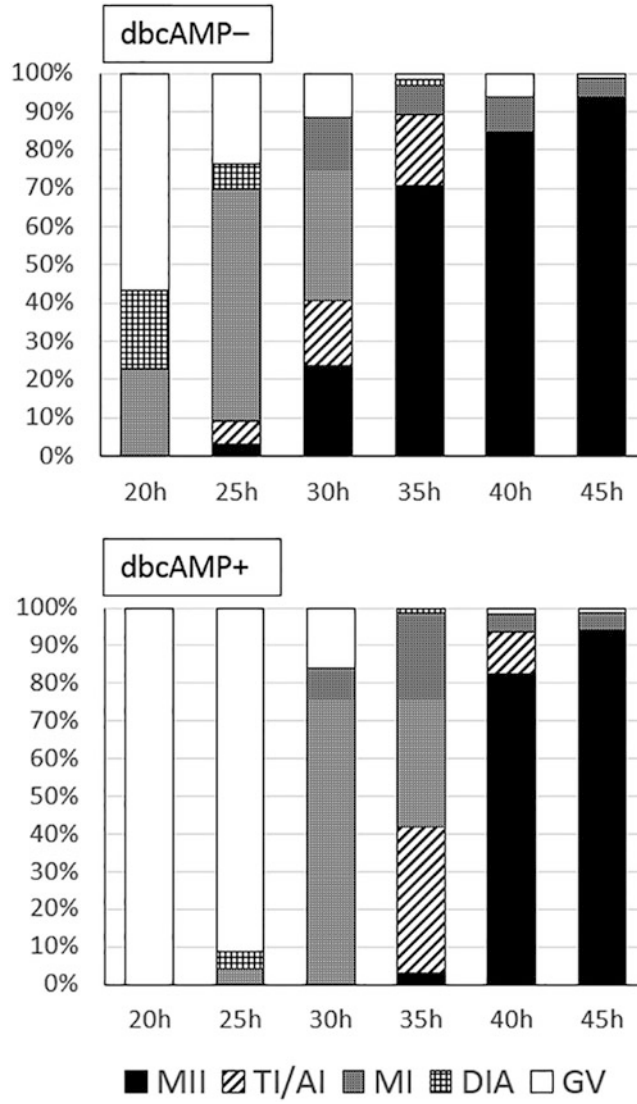

Fig. 3 Heterogeneity of nuclear status in populations of porcine oocytes at different time points of the total IVM period after 20 h culture in the absence (dbcAMP–) or in the presence (dbcAMP+) of 1 mM

promotes maintenance of the gap junctional communications between the cumulus cells and the oocyte in pigs, which positively affects cytoplasmic maturation of oocytes [22].

2. In pigs, a transient inhibition of GVBD can be achieved either by the elevation of intracellular levels of cyclic adenosine monophosphate (cAMP) or by the suppression of activity of metaphase (or maturation) promoting factor (MPF) using chemical supplements in medium. Intracellular cAMP levels can be elevated by dibutyryl cyclic AMP (dbcAMP), a membrane permeable cAMP

analog which effectively and reversibly blocks GVBD without any negative side effects [7, 23], Forskolin, a natural diterpene, activates adenylate cyclase in oocytes [24] or 3-isobutylmethylxanthine (IBMX), a phosphodiesterase inhibitor which prevents the degradation of cAMP in oocytes [25]. MPF activity can be effectively suppressed by butyrolactone-I (BL-I) or roscovitine (ROS), specific reversible inhibitors of $p34^{cdc2}$ protein kinase, the catalytic subunit of MPF [26, 27].

3. Although nuclear synchronization of porcine oocytes has also been achieved, enhanced development was not reported by the use of MPF-modulating agents [26, 28, 29]. Therefore, cAMP-modulating agents (dbcAMP) are recommended for the nuclear synchronization of porcine oocytes.
4. Supplementation of base medium with EGF is not a prerequisite for the success of IVM when using POM medium [15]. However, its use is recommended as it enhances cytoplasmic maturation in a synergic pathway with dbcAMP [30].
5. The process of oocyte collection itself does not trigger precocious oocyte maturation, therefore supplementation of collection medium with meiosis suppressing agent is not necessary [20].
6. Optionally, non-defined media can also be used as base media for oocyte collection and IVM such as Hepes-buffered TCM199 supplemented with serum and modified NCSU 37 supplemented with follicular fluid, respectively [31].
7. Use of follicles smaller than 1–2 mm in diameter for oocyte collection should be avoided, because the oocytes within are still at the growing stage showing low abilities to undergo the MI to MII transition and to develop to normal embryos [6, 7, 32]. The presence of an intact, morphologically normal cumulus compartment is crucial since the cumulus cells play a basic role in the regulation of both nuclear [22, 33] and cytoplasmic processes [34] in maturing porcine oocytes. The presence or absence of granulosa cell mass attached to the COCs is irrelevant for the production of MII-stage oocytes [8].
8. The washing and culture dishes should be prepared and preincubated under culture conditions for at least 2 h before use.
9. Optionally, maturation culture can be performed under 5 % CO_2, 5 % O_2, and 90 % N_2 tensions; although reducing O_2 tension during IVM does not affect embryo development to the blastocyst stage, it seems to have some advantages for subsequent embryo development by promoting the activation process in oocytes and improving cell numbers in blastocysts [18].
10. One millimolar dbcAMP effectively blocks the meiotic resumption of porcine oocytes for up to 48 h; however, such a long treatment exerts negative effects on developmental competence [19].

References

1. Betthauser J, Forsberg E, Augenstein M, Childs L, Eilertsen K, Enos J et al (2000) Production of cloned pigs from in vitro systems. Nat Biotech 18:1055–1059
2. Motlik J, Fulka J (1976) Breakdown of the germinal vesicle in pig oocytes in vivo and in vitro. J Exp Zool 198:155–162
3. Pincus G, Enzmann EV (1935) The comparative behavior of mammalian eggs in vivo and in vitro. I. The activation of ovarian eggs. J Exp Med 62:665–675
4. Wehrend A, Meinecke B (2001) Kinetics of meiotic progression, M-phase promoting factor (MPF) and mitogen-activated protein kinase (MAP kinase) activities during in vitro maturation of porcine and bovine oocytes: species specific differences in the length of the meiotic stages. Anim Reprod Sci 66:175–184
5. Funahashi H, Cantley TC, Day BN (1997) Preincubation of cumulus–oocyte complexes before exposure to gonadotropins improves the developmental competence of porcine embryos matured and fertilized in vitro. Theriogenology 47:679–686
6. Nagai T, Ebihara M, Onishi A, Kubo M (1997) Germinal vesicle stages in pig follicular oocytes collected by different methods. J Reprod Dev 43:339–343
7. Funahashi H, Cantley TC, Day BN (1997) Synchronization of meiosis in porcine oocytes by exposure to dibutyryl cyclic adenosine monophosphate improves developmental competence following in vitro fertilization. Biol Reprod 57:49–53
8. Somfai T, Kikuchi K, Onishi A, Iwamoto M, Fuchimoto D, Papp AB et al (2004) Relationship between the morphological changes of somatic compartment and the kinetics of nuclear and cytoplasmic maturation of oocytes during in vitro maturation of porcine follicular oocytes. Mol Reprod Dev 68:484–491
9. Miao YL, Kikuchi K, Sun QY, Schatten H (2009) Oocyte aging: cellular and molecular changes, developmental potential and reversal possibility. Hum Reprod Update 15:573–585
10. Grupen CG, Nagashima H, Nottle MB (1997) Asynchronous meiotic progression in porcine oocytes matured in vitro: a cause of polyspermic fertilization? Reprod Fertil Dev 9:187–191
11. Grupen CG (2014) The evolution of porcine embryo in vitro production. Theriogenology 81:24–37
12. Alfonso J, García-Rosello E, García-Mengual E, Salvador I, Silvestre MA (2009) The use of R-roscovitine to fit the "time frame" on in vitro porcine embryo production by intracytoplasmic sperm injection. Zygote 17:63–70
13. Lazzari G, Galli C, Moor RM (1992) Centrifugal elutriation of porcine oocytes isolated from the ovaries of newborn piglets. Anal Biochem 200:31–35
14. Banfalvi G (2008) Cell cycle synchronization of animal cells and nuclei by centrifugal elutriation. Nat Protoc 3:663–673
15. Yoshioka K, Suzuki C, Onishi A (2008) Defined system for in vitro production of porcine embryos using a single basic medium. J Reprod Dev 54:208–213
16. Mcgaughey RW, Montgomery DH, Richter JD (1979) Germinal vesicle configurations and patterns of polypeptide synthesis of porcine oocytes from antral follicles of different size as related to their competency for spontaneous maturation. J Exp Zool 209:239–254
17. Marchal R, Vigneron C, Perreau C, Bali-Papp Á, Mermillod P (2002) Effect of follicular size on meiotic and developmental competence of porcine oocytes. Theriogenology 57:1523–1532
18. Iwamoto M, Onishi A, Fuchimoto D, Somfai T, Takeda K, Tagami T et al (2005) Low oxygen tension during in vitro maturation of porcine follicular oocytes improves parthenogenetic activation and subsequent development to the blastocyst stage. Theriogenology 63:1277–1289
19. Fuchimoto D, Senbon S, Suzuki S, Onishi A (2011) Effects of preservation of porcine oocytes by dibutyryl cyclic AMP on in vitro maturation, fertilization and development. Jpn Agr Res Q 45:295–300
20. Somfai T, Kikuchi K, Onishi A, Iwamoto M, Fuchimoto D, Papp AB et al (2003) Meiotic arrest maintained by cAMP during the initiation of maturation enhances meiotic potential and developmental competence and reduces polyspermy of IVM/IVF porcine oocytes. Zygote 11:199–206
21. Kim JS, Cho YS, Song BS, Weec G, Park JS, Choo YK et al (2008) Exogenous dibutyryl cAMP affects meiotic maturation *via* protein kinase A activation; it stimulates further embryonic development including blastocyst quality in pigs. Theriogenology 69:290–301
22. Ozawa M, Nagai T, Somfai T, Nakai M, Maedomari N, Fahrudin M et al (2008) Comparison between effects of 3-isobutyl-1-methylxanthine and FSH on gap junctional communication, LH-receptor expression, and meiotic maturation of cumulus-oocyte complexes in pigs. Mol Reprod Dev 75:857–866

23. Bagg MA, Nottle MB, Grupen CG, Armstrong DT (2006) Effect of dibutyryl cAMP on the cAMP content, meiotic progression, and developmental potential of in vitro matured prepubertal and adult pig oocytes. Mol Reprod Dev 73:1326–1332
24. Racowsky C (1985) Effect of forskolin on maintenance of meiotic arrest and stimulation of cumulus expansion, progesterone and cyclic AMP production by pig oocyte-cumulus complexes. J Reprod Fertil 74:9–21
25. Shimada M, Nishibori M, Isobe N, Kawano N, Terada T (2003) Luteinizing hormone receptor formation in cumulus cells surrounding porcine oocytes, and its role during meiotic maturation of porcine oocytes. Biol Reprod 68:1149–1159
26. Wu GM, Sun QY, Mao J, Lai L, McCauley TC, Park KW et al (2002) High developmental competence of pig oocytes after meiotic inhibition with a specific M-phase promoting factor kinase inhibitor, butyrolactone I. Biol Reprod 67:170–177
27. Marchal R, Tomanek M, Terqui M, Mermillod P (2001) Effects of cell cycle dependent kinases inhibitor on nuclear and cytoplasmic maturation of porcine oocytes. Mol Reprod Dev 60:65–73
28. Schoevers EJ, Bevers MM, Roelen BA, Colenbrander B (2005) Nuclear and cytoplasmic maturation of sow oocytes are not synchronized by specific meiotic inhibition with roscovitine during in vitro maturation. Theriogenology 63:1111–1130
29. Coy P, Romar R, Ruiz S, Cánovas S, Gadea J, García Vázquez F et al (2005) Birth of piglets after transferring of in vitro-produced embryos pre-matured with R-roscovitine. Reproduction 129:747–755
30. Sugimura S, Ritter LJ, Rose RD, Thompson JG, Smitz J, Mottershead DG et al (2015) Promotion of EGF receptor signaling improves the quality of low developmental competence oocytes. Dev Biol 403:139–149
31. Kikuchi K, Onishi A, Kashiwazaki N, Iwamoto M, Noguchi J, Kaneko H et al (2002) Successful piglet production after transfer of blastocysts produced by a modified in vitro system. Biol Reprod 66:1033–1041
32. Hirao Y, Tsuji Y, Miyano T, Okano A, Miyake M, Kato S et al (1995) Association between p34cdc2 levels and meiotic arrest in pig oocytes during early growth. Zygote 3:325–332
33. Shimada M, Ito J, Yamashita Y, Okazaki T, Isobe N (2003) Phosphatidylinositol 3-kinase in cumulus cells is responsible for both suppression of spontaneous maturation and induction of gonadotropin-stimulated maturation of porcine oocytes. J Endocrinol 179:25–34
34. Maedomari N, Kikuchi K, Ozawa M, Noguchi J, Kaneko H, Ohnuma K et al (2007) Cytoplasmic glutathione regulated by cumulus cells during porcine oocyte maturation affects fertilization and embryonic development in vitro. Theriogenology 67:983–993

Part VI

Synchronization of Plant Cells

Chapter 17

Detection of Changes in the *Medicago sativa* Retinoblastoma-Related Protein (MsRBR1) Phosphorylation During Cell Cycle Progression in Synchronized Cell Suspension Culture

Ferhan Ayaydin, Edit Kotogány, Edit Ábrahám, and Gábor V. Horváth

Abstract

Deepening our knowledge on the regulation of the plant cell division cycle depends on techniques that allow for the enrichment of cell populations in defined cell cycle phases. Synchronization of cell division can be achieved using different plant tissues; however, well-established cell suspension cultures provide large amount of biological sample for further analyses. Here, we describe the methodology of the establishment, propagation, and analysis of a *Medicago sativa* suspension culture that can be used for efficient synchronization of the cell division. A novel 5-ethynyl-2′-deoxyuridine (EdU)-based method is used for the estimation of cell fraction that enters DNA synthesis phase of the cell cycle and we also demonstrate the changes in the phosphorylation level of *Medicago sativa* retinoblastoma-related protein (MsRBR1) during cell cycle progression.

Key words *Medicago sativa* suspension culture, Cell cycle synchronization, Hydroxyurea, Retinoblastoma-related protein phosphorylation, 5-Ethynyl-2′-deoxyuridine staining, Fluorescence microscopy

1 Introduction

Understanding the changes in the metabolic processes and in the structure of plant cells during cell division requires a detailed analysis of the cell cycle. This can be complicated, because the cell cycle progression in most somatic tissues is asynchronous and only a minor fraction of the cells are cycling. Therefore, to synchronize cells artificially, different methods had to be developed for the enrichment of cells in a single stage of the cell cycle. Different plant tissues and cell cultures can be used to obtain synchronously dividing cell populations.

Leaf mesophyll protoplasts from *Petunia hybrida* were shown to re-enter the mitotic cell cycle from G1 phase after incubation in a medium supplemented with growth regulators [1]. This system

Gaspar Banfalvi (ed.), *Cell Cycle Synchronization: Methods and Protocols*, Methods in Molecular Biology, vol. 1524,
DOI 10.1007/978-1-4939-6603-5_17,

has been used for other species [2, 3]; however, lack of protoplast isolation methods and optimized culturing procedures for a given species may limit widespread application of protoplastation-based methods.

Root meristems can be a material of choice for a variety of studies, since root tips are very rich in rapidly cycling cells. In *Vicia faba*, more than 90% of the cells in the root meristems are cycling [4]. Seedlings with actively growing roots can be obtained from most plant species and it is easy to expose the root tips to a great variety of nutritional, hormonal, and other chemical treatments. Reliable root meristem synchronization protocol is available [5] and this can be modified for different species.

Rapidly growing suspension cultures are a suitable system to follow cell cycle-associated changes in most biochemical or cytological parameters; because large number of cells is grown in an aqueous environment under well-defined conditions and they can be uniformly exposed to synchronizing treatments. High degree of synchrony could be achieved in cultured cells of *Arabidopsis* [6], carrot [7], tomato [8], and wheat [9]. One of the most popular systems is the tobacco BY-2 cell line which has an improved, efficient synchronization protocol [10].

Chemical methods of the synchronization of suspension cultures are reproducible and effective. These are based either on the deprivation of an essential growth compound [6], or on the action of chemical agents that blocks cell cycle progression. Hydroxyurea is frequently used for root meristem and suspension culture synchronization. This compound reversibly inhibits the ribonucleotide reductase enzyme and hence the production of deoxyribonucleotides [11]. A treatment of suspension cells for 24–36 h at a concentration of 10–20 mM leads accumulation of cells in G1 and early S phase. Aphidicolin, a fungal toxin derived from *Cephalosporium aphidicola*, is a specific inhibitor of the eukaryotic DNA polymerase and the plant α-like DNA polymerase, arrests cycling cells also in G1/S phase, giving similar or slightly better results on suspension cultures than hydroxyurea [7]. Besides hydroxyurea and aphidicolin, a plant amino acid mimosine can be used to block cell cycle traverse near the G1/S phase boundary by suppressing the formation of the rare amino acid hypusine in the eukaryotic translation factor 4D [12]. This compound can also be efficiently used in plant suspension cultures. In carrot cells, it was found to be superior to aphidicolin or to hydroxyurea [7].

The detailed analysis of mitotic events may require a highly synchronous population of the cells during mitotic division. In such a case, a two-step protocol can be followed [10], in which the cells released from aphidicolin are subsequently treated with propyzamide, a microtubule assembly inhibitor. However, the two-step protocol in this setup would not be appropriate for analyzing prophase or metaphase-specific changes.

In the present protocol, we give a detailed description for the establishment of *Medicago sativa* cell suspension culture and the synchronization procedure using hydroxyurea. A novel method for the determination of the fraction of cells entering S-phase using 5-ethynyl-2′-deoxyuridine (EdU)-based fluorescent staining [14] is described in details, as well. We also demonstrate the efficacy of the synchronization by showing the changes of the phosphorylation status and intracellular localization of the *Medicago sativa* retinoblastoma-related protein (MsRBR1) using Western blotting and immunolocalization [13]. Plant RBR proteins are considered as key regulators of G1/S phase transition, with functions in cell differentiation and organ development. Dicot plants (e.g., *Medicago sativa*) have a single *RBR* gene, whereas monocots carry at least two distinct genes. We reported previously that both the MedsaCDKA1;1/1;2 and the mitotic MedsaCDKB2;1 cyclin-dependent kinase-cyclin complexes could phosphorylate the C-terminal fragment of MsRBR1 of alfalfa. Using immunolocalization, here we also demonstrate that a significant decrease of phospho-MsRBR1 level can be observed at different stages of the mitosis.

2 Materials

2.1 Cell Culturing

1. Murashige and Skoog Basal Salt Mixture (MS)—Plant tissue culture tested.
2. Sucrose.
3. Myoinositol: Prepare a 10 g/l stock solution (100× stock, final concentration 100 mg/l) and store at 4 °C.
4. Thiamine hydrochloride: Prepare a 1 g/l stock solution (100× stock, final 10 mg/l), store at 4 °C.
5. Nicotinic acid (Free Acid): Prepare a 100 mg/l stock solution (100× stock, final 1 mg/l), store at 4 °C.
6. Pyridoxine-HCl: Prepare a 100 mg/l stock solution (100× stock, final 1 mg/l), store at 4 °C.
7. 2,4-Dichlorophenoxyacetic acid (2,4-D): Prepare 1 g/l stock solution (1000× stock, final 1 mg/l), store at 4 °C.
8. Kinetin (N^6-furfuryladenine): Prepare 0.2 g/l stock solution (1000× stock, final 0.2 mg/l), store at 4 °C.
9. Plant Agar (Duchefa Biochemie).
10. Sterile tissue culture equipment.
11. Glass pipettes.
12. Erlenmeyer flasks.
13. Gyratory shaker and laminar flow hood.

2.2 Synchronization

1. Hydroxyurea: Prepare 1 M stock solution (100× stock, final 10 mM), store at 4 °C (*see* **Note 1**).
2. Miracloth (or glass filter funnel with G3 pore size).

2.3 Flow Cytometry

1. 5-Ethynyl-2′-deoxyuridine (EdU) stock solution: 10 mM EdU is prepared in dimethyl sulfoxide (DMSO) as a 1000× concentrated stock solution.
2. Nuclei isolation buffer: 45 mM $MgCl_2$, 20 mM MOPS, 30 mM sodium citrate, 0.1 % Triton X-100, pH: 7.0.
3. Sharp razor blades.
4. Plastic dishes (6 cm in diameter).
5. Nylon sieve (20 μm).
6. Desktop centrifuge with swing-out rotor.
7. Formaldehyde stock solution: Prepare 8 % (w/v) stock solution by dissolving 8 g paraformaldehyde powder in 100 ml water by heating to 60–70 °C in a fume hood (*see* **Note 2**). Add a drop of 5 M KOH to the solution to depolymerize paraformaldeyde by heating at alkaline pH. After cooling to room temperature, adjust pH between 6.5 and 7.5 with 5 % (v/v) H_2SO_4. Aliquots of this stock solution can be stored at −20 °C for 6 months.
8. EdU detection cocktail: For each sample, prepare 0.5 ml detection cocktail freshly (*see* Subheading 2.4).
9. Propidium iodide (PI) solution: Prepare 10 mg/ml PI stock solution in water (*see* **Note 3**).
10. FACSCalibur flow cytometer (Becton, Dickinson and Company, NJ, USA) with the standard 488 nm laser for detection of PI and Alexa Fluor 488.
11. CellQuest software.

2.4 In Vivo EdU Staining, Mitotic Index Determination, and Fluorescence Microscopy

1. Formaldehyde stock solution (8 % w/v): *see* Subheading 2.3.
2. Fixation solution (4 % formaldehyde in PBS with Triton X-100): Mix 8 % formaldehyde stock solution with equal volume of 2× PBS (2× PBS: 5.4 mM KCl, 2.94 mM NaH_2PO_4, 274 mM NaCl, 16 mM Na_2HPO_4, pH: 7.4), add Triton X-100 to a final concentration of 0.1 % (*see* **Note 4**).
3. DNA staining (DAPI) solution: Prepare 1 mg/ml DAPI (4′,6-diamidino-2-phenylindole) solution in DMSO (10,000× stock) and dilute to 100 ng/ml in 1× PBS (2.7 mM KCl, 1.47 mM NaH_2PO_4, 137 mM NaCl, 8 mM Na_2HPO_4, pH: 7.4) for staining nuclei (*see* **Note 5**).
4. EdU detection cocktail: 4 mM $CuSO_4$, 40 mM sodium ascorbate, 2.5–10 μM Alexa Fluor 488 azide (Invitrogen) in 1× PBS (for intact cells) or in nuclei isolation buffer (for nuclei).

To prevent oxidation of the formed Cu (I) to non-catalytic Cu (II) species, prepare the detection cocktail freshly and use within an hour.

5. Mounting solution: For short-term mounting of samples use 1× PBS which prevents cell shrinkage. For long-term preservation or prolonged microscopy observation of samples, use an anti-fade mounting solution (e.g., Fluoromount-G, Southern Biotech).
6. Fluorescence microscope or confocal laser scanning fluorescence microscope with appropriate filter sets.

2.5 Immunolocalization of Phospho-MsRBR1 Protein in M. Sativa Suspension Cells

1. Formaldehyde stock solution (8% w/v): *see* Subheading 2.3.
2. Fixation solution, DNA staining (DAPI) solution and mounting solution: *see* Subheading 2.4.
3. MES buffer: 0.5% (w/v) 2-(*N*-morpholino)ethanesulfonic acid (MES) in water, pH: 5.8.
4. Cell wall digestion solution: 1% cellulase and 0.5% pectinase (Chromatographically purified enzymes from Worthington Biochemical Corporation, Lakewood, NJ, USA) in MES buffer.
5. Permeabilization buffer: 0.1% Triton X-100 in 1× PBS.
6. Blocking buffer: Fish gelatin (5% v/v) in 1× PBS or bovine serum albumin (1% w/v) in 1× PBS.
7. Primary antibody solution: Rabbit polyclonal α-Phospho-Rb (Ser807/811) antibody (#9308, Cell Signaling Technology) diluted 1:200 in blocking buffer.
8. Secondary antibody solution: Anti-rabbit fluorochrome-conjugated (e.g., Alexa Fluor 488) secondary antibody diluted 1:400 in blocking buffer.
9. Coverslip coating solution: 0.1% (w/v) poly-l-lysine in water, filter sterilized and kept at 4 °C.
10. Fluorescence microscope or confocal laser scanning fluorescence microscope with appropriate filter sets. Microscope slides and 12 mm diameter round coverslips.

2.6 Protein Extraction, SDS-PAGE, and Western Blotting

1. F1 protein extraction buffer: 25 mM Tris–HCl, 75 mM NaCl, 60 mM β-glycerophosphate, 15 mM $MgCl_2$, 15 mM EGTA, 1 mM NaF, 0.1 mM Na_3VO_4, 0.1% NP-40, 1× protease inhibitor cocktail (Complete, Roche), 1× PhosSTOP phosphatase inhibitor cocktail (Roche). Final pH of the extraction buffer is adjusted to 7.6. 50× protease inhibitor cocktail and 10× phosphatase inhibitor cocktail is prepared by dissolving 1 tablet in 1 ml sterile MilliQ water. Stock solutions are stored at –20 °C and used within 1 month. 1, 4-Dithiotreitol (DTT) and and phenylmethylsulfonyl fluoride (PMSF) are added to the extraction buffer just before use at 1 mM concentration each. Quartz

sand (Sigma-Aldrich), conical-shaped glass homogenizer fitting to 1.5 ml Eppendorf tube or mortar (6 cm in diameter) and pestle for cell disruption. Bio-Rad Protein Assay reagent for the determination of protein concentration, bovine serum albumin (BSA) for calibration curve determination.

2. SDS-PAGE solutions: 29.2:0.8 acrylamide:bisacrylamide solution in MilliQ water, *N*-,*N*-,*N*′-,*N*′-tetramethylethylenediamine (TEMED) (molecular biology grade), 10% ammonium persulfate (electrophoresis grade) in water (aliquots stored at −20 °C). SDS-PAGE sample loading buffer (5× stock): 250 mM Tris–Cl (pH 6.8), 30% glycerol, 10% SDS (sodium dodecyl sulfate), 5% β-mercaptoethanol, 0.02% Bromophenol blue, running buffer (5× stock): 25 mM Tris-base, 192 mM glycine, 0.1% SDS, pH 8.3. Protein molecular weight markers: ThermoFisher PageRuler Plus Prestained Protein Ladder, PageRuler Unstained Protein Ladder.
3. Protein transfer and immunoblotting: Immobilon-P PVDF transfer membrane from EMD Millipore, Whatman 3MM chromatography paper. Protein transfer buffer (for 2 l): 2.9 g Tris-base, 14.4 g glycine and 200 ml methanol in MilliQ water, freshly prepared. 1× TBS (1 l): 10 mM Tris–HCl, pH 7.5, 8.77 g NaCl. TBST: 1× TBS plus 0.1% or 0.5% TWEEN-20 (from 20% stock solution), store at 4 °C and use within a week. Ponceau S staining solution: 0.1% Ponceau S dye in 5% acetic acid. TBST-5% BSA: 1× TBS with 0.1% TWEEN-20 and 5% bovine serum albumin. TBST-5% non-fat milk powder: 1× TBS with 0.1% TWEEN-20 and 5% non-fat milk powder. Dissolve BSA or milk powder entirely with stirring, prepare this solution daily. Detection: Immobilon Western Chemiluminescent HRP Substrate from EMD Millipore.

3 Methods

3.1 Establishment and Maintenance of *M. Sativa* Cell Suspension Culture for Synchronization

1. Initiate *Medicago sativa* ssp. varia (genotype A2) callus cultures from the hypocotyl explants of 7-day-old seedlings on medium containing 4.3 g/l MS basal salt, 3% (w/v) sucrose, 100 mg/l myoinositol, 10 mg/l thiamine hydrochloride, 1 mg/l nicotinic acid, 1 mg/l pyridoxine-HCl with 1 mg/l 2,4-D. Adjust the pH of the solution to 5.8 with 1 M KOH and for plates the medium is solidified with 0.8% Plant Agar.
2. Subculture proliferative friable calli to 20 ml of the above-mentioned medium lacking Plant Agar and supplemented with 0.2 mg/l kinetin.
3. After 2 and 4 weeks, add 10 ml each of fresh medium to the culture.

4. After 4 weeks, pour off 20 ml of the supernatant culture medium and replace with 20 ml fresh medium weekly (no cells should be wasted!).
5. Following four rounds of such subculturing regime, increase the culture volume stepwise: first dilute 25 ml of non-sedimented culture to 50 ml with fresh culture medium in a 100 ml Erlenmeyer flask.
6. Finally (after 3 months of culture initiation) establish 100 and 200 ml cultures by weekly subculturing: dilute 50 ml non-sedimented culture to 100 ml (2× dilution) or 200 ml (4× dilution) by adding 50 ml or 150 ml fresh culture medium in a 300 or 500 ml Erlenmeyer flask, respectively (*see* **Note 6**). Only well-established, rapidly dividing suspension culture can be used for a reproducible, efficient synchronization.
7. Monitor the status of the suspension culture continuously as follows: pour 50 ml non-sedimented culture into a sterile graduated tube (e.g., 50 ml CELLSTAR tube from Greiner Bio-One) and measure sedimented cell volume. Mark the position of the settled cells (12–15 ml for 4× diluted and 18–22 ml for 2× diluted culture) on the flask. This way the variation in the sedimented volume of the culture (that should not exceed ±10%) can be followed regularly (*see* **Note 6**).

Different dilution ratios will result suspension cultures of distinct proliferative activity. Rapid cycling can be assayed by the detection of the levels of cell cycle regulators in the protein extracts of the cultures. The proteins examined can be cyclin-dependent kinases (particularly CDKB2;1-type plant specific kinases that show G2/M phase-specific accumulation) [15], cyclins, or other cell division regulators. Plant retinoblastoma-related proteins are also good choice for this purpose, since for example *A. thaliana* RBR1 protein shows proliferative activity-dependent accumulation in sucrose-starved suspension cultures [16]. We used the α-AtRBR1 C-terminal polyclonal antibody to detect changes in the level of MsRBR1 protein in alfalfa cell suspension cultures [13]. Such approach can help to optimize not only the subculturing regime of the cell suspension but also the correct timing of blocking agent treatment. G1/early S phase blockers like hydroxyurea should be added to the culture that is determined to undergo cell division but does not contain high portion of cells in S phase, since hydroxyurea has an irreversible toxic effect on these cells [17]. According to our results, the 4× diluted culture should be blocked after 3 days of subculturing (*see* **Note 6**).

3.2 Synchronization of M. sativa Cell Culture with Hydroxyurea Treatment

1. Add 2 ml 1 M hydroxyurea solution to 200 ml of an early exponential phase *Medicago sativa* ssp. varia (genotype A2) suspension culture (4× dilution regime, 3 days after subcultur-

ing) under sterile conditions. Efficient blocking of the cells needs 36 h long treatment (26 °C, 130 rpm shaking on a rotary shaker in the dark).

2. Remove the blocking agent from the culture by excessive washing. Use preconditioned medium for this purpose (*see* **Note 7**). Filter the suspension culture on Miracloth placed in a glass funnel of appropriate size or on glass filter. Use only gravitational flow of the culture medium and never allow the suspension cells to dry completely. After the first filtration, resuspend the cells gently but thoroughly (no clumps should remain in the suspension) in 200 ml preconditioned culture medium and filter them again. Repeat this washing step two more times. Finally, resuspend the cells in the original (200 ml) volume of the preconditioned medium.
3. Take samples for flow cytometry (Subheading 3.3), for in vivo EdU staining, mitotic index determination, fluorescence microscopy (Subheadings 3.4 and 3.5) and for RNA and protein analysis (Subheading 3.5). For the last two purpose take 10 ml of the suspension, filter the cells on Miracloth, dry them by pressing the cells wrapped in Miracloth gently to two–three layers of filter paper. Divide the cells into microfuge tubes in 2:1 ratio, the bigger samples are for RNA isolation (gives several hundred micrograms of total RNA) the smaller ones for protein analysis (at least one hundred micrograms of protein can be isolated from such samples).

   A typical flow cytometric histogram of the cell cycle progression of hydroxyurea-blocked alfalfa cell suspension is presented in Fig. 1a. The data demonstrate that most of the cells enter G2/M phase between 12 and 14 h after the removal of the blocking agent and after 24–26 h the cells are ready to start a new round of cell division. A sharp increase in EdU-stained cells following hydroxyurea removal (Figs. 1b and 2) clearly shows that the chemical block is reversible and the cells start DNA synthesis simultaneously (*see* **Note 8**). The efficient staining and the sharp change in the number of the fluorescent cells during cell cycle progression also demonstrate the usability of the presented method for the calculation of cells entering S phase.

3.3 Analysis of Cell Cycle Parameters with Flow Cytometry

1. Incubate 5 ml alfalfa culture with 10 μM EdU for 1 h in 6 cm Petri dishes by gentle rotation at 25 °C at dark.
2. Centrifuge (5 min, 400×*g*) EdU-labeled and 0.1% DMSO-treated control cultures.
3. Chop the pellet with a sharp razor blade in 2 ml nuclei isolation buffer in 6 cm Petri dishes on ice.
4. Filter nuclei into 15 ml conical bottom tubes through 20 μm nylon sieves and fix on ice for 30 min by the addition of 8% formaldehyde solution to a final concentration of 1% (*see* **Note 2**).

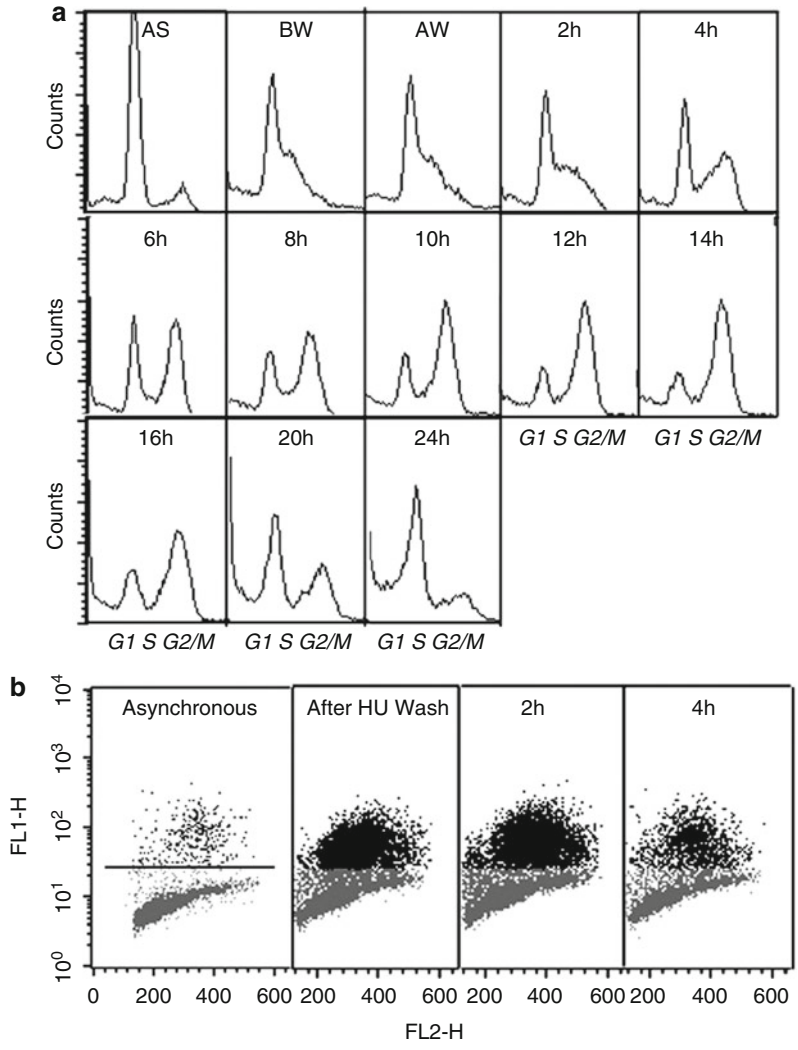

Fig. 1 (**a**) Flow cytometric histogram analysis of the cell cycle progression of cells synchronized at the G1/S boundary. *AS* asynchronous culture, *BW* before wash, *AW* after wash. (**b**) Flow cytometric dual parameter analysis of the in vivo EdU-labeled cells (cells in S phase) synchronized at the G1/S boundary. *Horizontal line* at the leftmost panel indicates the EdU labeling threshold

5. Wash the fixed nuclei twice with 2 ml 1× PBS containing 0.01% Triton X-100 (resuspension and centrifugation at 4 °C, 10 min, 400×*g*) using a desktop centrifuge with swing-out rotor.
6. Incubate nuclei in 500 μl EdU-detection cocktail for 30 min at room temperature at dark.
7. Wash nuclei (4 °C, 10 min, 400×*g*) with 1× PBS containing 0.01% Triton X-100, and counterstain either with 100 ng/ml (final concentration) DAPI (for microscopy check) or with 5 μg/ml (final concentration) PI.

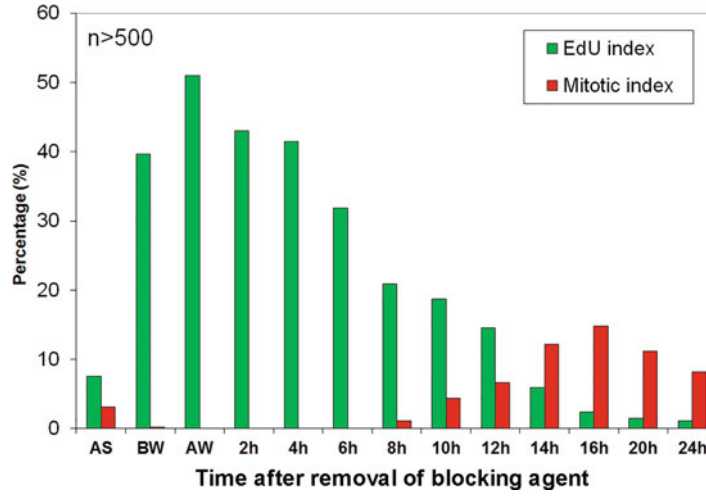

Fig. 2 The EdU index (cells in S-phase) and mitotic index of hydroxyurea-synchronized alfalfa cultures (*see* **Note 3**)

8. Analyze on a FACSCalibur flow cytometer with CellQuest software. Use two fluorescence detectors with the standard 488 nm laser. For Alexa Fluor 488-EdU intensity, use 515–545 nm emission range (FL1 channel). For detection of PI intensity (DNA content), use 564–606 nm emission range (FL2 channel). Locate and gate nuclear populations by particle size using side scatter versus forward scatter diagrams. To exclude particles which are not fluorescent with PI staining, use dot-plot diagram of "total PI fluorescence of a particle at FL2 channel" (FL2-A) versus "transit time of a particle at FL2 channel" (FL2-W) as secondary gating. To locate the boundary of EdU-Alexa Fluor 488-labeled nuclei in biparametric plots (EdU threshold value), use counts versus FL1-H (EdU-Alexa Fluor 488 channel, log scale) histograms. The left (major) peak of this histogram (with low green channel intensity) represents EdU unlabeled G1 and G2 populations while the higher green intensity second peak represents EdU-labeled nuclei. To determine the EdU threshold value, use the right border of the leftmost major peak (where the unlabeled G1/G2 counts reach zero value).

3.4 EdU Staining, Mitotic Index Determination, and Fluorescence Microscopy

1. Incubate 1 ml of alfalfa culture in a 2 ml microfuge tube on a roller with 10 μM final concentration of EdU for 1 h in its own culture medium.
2. Settle cells by centrifugation (5 min, 400 × *g*) and resuspend the pellet in 2 ml 1× PBS and re-centrifuge. Discard the supernatant.
3. Fix the cell pellet 15 min in 2 ml fixation solution on a roller. Replace the fixer with the same volume of 1× PBS by centrifu-

gation. At this stage, the cells can be kept at the fridge for several days until further processing (*see* **Note 2**).

4. Following 3× 5 min 1× PBS (2 ml each) washes, incubate 20–30 µl packed cell volume of cells in 150 µl EdU detection cocktail by rotating for 30 min at room temperature in a 0.2 ml microfuge tube (*see* **Note 9**).
5. After 2× 5 min washes with 1× PBS (2 ml each) containing 100 ng/ml (final concentration) DAPI, mount 20 µl aliquot of cells onto microscope slide with a coverslip and gently press with a tissue paper to flatten the clusters. The rest of the labeled cells can be kept at 0–4 °C in a dark container for several weeks (*see* **Note 10**).
6. Set the confocal microscope configuration as follows: objective lenses: UPLSAPO 20× (dry, NA:0.75) and UPLFLN 40× (oil, NA:1.3); sampling speed: 4 µs/pixel; line averaging: 2×; scanning mode: sequential unidirectional; excitation: 405 nm (DAPI) and 488 nm (Alexa Fluor 488); laser transmissivity: less than 1% for DAPI and 5% for Alexa Fluor 488, respectively; main dichroic beamsplitter: DM405/488; intermediate dichroic beamsplitter: SDM 490; DAPI fluorescence detection: 425–475 nm; Alexa Fluor 488 detection: 500–600 nm. For transmitted light imaging (Fig. 3) differential interference contrast (DIC) mode can be used. Count more than 500 cells for mitotic index and EdU labeling index determinations.

3.5 Immunodetection of the Phosphorylation of M. sativa Retinoblastoma-Related Protein (MsRBR1)

3.5.1 Protein Extraction

1. Collect approximately 250 mg (pressed wet weight) samples of synchronized *M. sativa* cell suspension in an 1.5 ml Eppendorf tube as described in Subheading 3.2, **step 3**, add 100–120 mg quartz sand to each sample and freeze in liquid N_2.
2. Disrupt the cells with a conical-shape glass homogenizer or (preferably) using pre-cooled (liquid N_2) mortar and pestle, do not allow the samples to thaw.

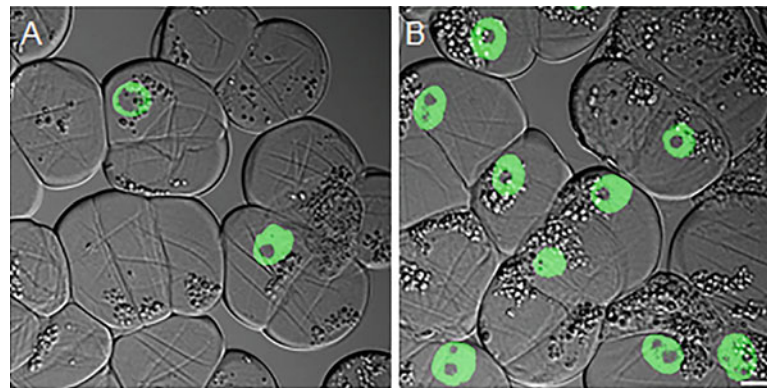

Fig. 3 EdU-based replication assay on (**a**) asynchronous, (**b**) hydroxyurea-synchronized (after wash sample) alfalfa cells. Transmission images (grayscale) are overlaid onto Alexa Fluor 488-labeled (*green*) nuclei. Bar 10 µm

3. Add 0.5 ml F1 extraction buffer to each sample, thaw them on ice and vortex for 30 s.
4. Centrifuge the homogenate in a refrigerated microfuge for 15 min (17,000×*g*, 4 °C).
5. Place the samples on ice, carefully collect the supernatants and centrifuge them for 5 min (17,000×*g*, 4 °C) to remove all insoluble material.
6. Collect the supernatants in Eppendorf tubes placed on ice, take 2 µl aliquots of the samples and mix with 800 µl MilliQ water, add 200 µl Bio-Rad Protein Assay reagent to each sample. Expected protein concentration is 3–4 µg/µl.
7. Briefly (2 s) vortex samples, wait 5 min at RT and measure absorbance at 595 nm against a blank control (800 µl MilliQ water, 200 µl Bio-Rad Protein Assay reagent, 2 µl F1 extraction buffer).
8. Calculate protein concentration using BSA as standard. Take out 100 µg protein sample and mix it with the appropriate volume of 5× SDS-PAGE sample loading buffer.
9. Heat the samples to 95 °C for 5 min, briefly centrifuge and store at −20 °C for further analysis.

3.5.2 SDS-PAGE and Protein Transfer

High molecular weight (>100 kDa) proteins can be separated on low concentration (6%) medium-sized polyacrylamide gels. For such purpose, use electrophoresis units similar to Bio-Rad Criterion™ Vertical Electrophoresis Cell.

1. Wash glass plates with detergent, MilliQ water and ethanol, let them dry. Assemble glass plates and comb, label the maximal height of separation gel (16–18 mm beneath the comb) with permanent marker.
2. Prepare 6% separation gel (for 10 ml mix: 5.3 ml MilliQ water, 2 ml 30% acrylamide mix, 2.5 ml 1.5 M Tris–HCl pH: 8.8, 0.1 ml 10% SDS, 8 µl TEMED) and 4% stacking gel (for 5 ml mix: 3.4 ml MilliQ water, 0.83 ml 30% acrylamide mix, 0.63 ml 1 M Tris–HCl pH: 6.8, 50 µl 10% SDS, 5 µl TEMED) (*see* **Note 11**). For faster polymerization the mixes can be degassed, however this is not absolutely necessary.
3. Remove the comb from the assembled glass plates, prepare pipette for gel pouring and thaw 10% APS solution if it was not freshly prepared.
4. Add APS solution to the separation gel mix (100 µl to 10 ml), mix it briefly and immediately pipette it between the assembled glass plates to the marked height. Overlay the gel with 100 µl water saturated n-butanol.

5. Allow the polymerization of the separation gel (15–30 min), pour off the n-butanol and dry the surface carefully with a strip of filter paper.
6. Add APS solution to the stacking gel mix (50 μl to 5 ml), mix it briefly and quickly pipette it onto the top of the separation gel. Insert the comb between the glass plates, avoid trapping bubbles.
7. After stacking gel polymerization (although it is faster than the polymerization of the separation gel, but let stand the gel for at least 30 min), assemble the vertical gel electrophoresis unit, fill up the chamber with running buffer, and slowly remove the comb. Wash the wells with running buffer pipetting it slowly into the wells. Be sure that no traces of polyacrylamide film remained inside. Remove trapped air bubbles from underneath the gel by pipetting running buffer quickly with a 10 ml syringe equipped with a bent needle.
8. Thaw the denatured protein samples at RT (or at 37 °C) completely dissolving SDS, briefly centrifuge and load the samples into the wells. For the monitoring of gel electrophoresis progression and to ease the subsequent orientation of the blot, load prestained protein marker onto the gel along with the samples (*see* **Note 12**).
9. Electrophoresis is carried out at constant electric potential. Run protein samples through the stacking gel at 50 V, increase it to 100–150 V when the samples enter the separation gel. In order to avoid overheating do not exceed 50 mA electric current, this will ensure good resolution and minimal distortion of the bands.
10. Meanwhile prepare a blotting tray (25 cm × 30 cm) which can accommodate 1 l transfer buffer, blotting cassette, and the polyacrylamide gel. Cut four pieces of Whatman 3MM paper and PVDF membrane of the appropriate size. Soak the membrane in methanol, the Whatman papers and transfer sponges in transfer buffer.
11. Stop electrophoresis when the bromophenol blue dye left the gel. Disassemble the vertical electrophoresis unit, remove one glass plate from the gel and cut off the stacking gel with a sharp razor blade. Since it is difficult to handle low concentration polyacrylamide gels, do not remove it from the second glass plate; submerge both of them together into the transfer buffer.
12. Take out the PVDF membrane from the methanol and soak it in the transfer buffer. Assemble the transfer cassette: put two pieces of presoaked Whatman 3MM paper on the sponge that sits on the bottom half of the cassette, gently float the gel from the glass plate onto the top of the blotting papers and put the presoaked PVDF membrane on the top of the gel. Cover the membrane with two pieces of presoaked Whatman 3MM paper

and with the second sponge. Carefully remove all bubbles from the assembled blotting sandwich by a glass rod or a glass test tube, rolling it slowly several times on the surface of the sandwich. Finally close the blotting sandwich with the top of the cassette, fill the transfer apparatus with transfer buffer and quickly insert the assembled sandwich into the transfer chamber.

13. Transfer the proteins onto the PVDF membrane applying constant electric current fluxes: approximately 4 mA/cm² for 2 h and 0.2–0.3 mA/cm² for overnight transfer.
14. Disassemble the sandwich, mark the protein-covered surface with a soft pencil and soak the membrane in TBST containing 0.1% TWEEN-20.

3.5.3 Immunoblotting of Phospho-MsRBR1

1. Stain membrane with Ponceau S solution briefly to check correct protein transfer, remove stain with several washes of TBST (0.1% TWEEN-20).
2. Incubate blot in TBST-5% BSA for 1 h at RT with gentle shaking.
3. Wash membrane with TBST (0.1% TWEEN-20) for 5 min.
4. Incubate the membrane with rabbit polyclonal α-Phospho-Rb (Ser807/811) Antibody (#9308, Cell Signaling Technology) diluted in 1:2000 ratio in TBST-5% BSA for 16 h at 4 °C with gentle shaking. Details of the antibody specificity is described in [13].
5. Wash the membrane as follows: once with TBST (0.1% TWEEN-20), 5 min; five times with MilliQ water, 1 min; once with TBST (0.5% TWEEN-20). This procedure helps to reduce background with high efficiency.
6. Incubate membrane with 1:20,000 diluted goat-α-rabbit IgG-horseradish peroxidase conjugate (in TBST-5% non fat milk powder) for 1 h at RT with gentle shaking.
7. Wash the blot according to step 5.
8. Incubate blot with MilliQ water diluted Immobilon Western Chemiluminescent HRP Substrate (1:1 dilution) for 5 min at RT, use 0.1 ml diluted substrate per cm² of the membrane.
9. Seal the blot into a transparent plastic bag, expose an X-ray film to the chemiluminescent signal for 2 min. Result can be seen in Fig. 4.

3.5.4 Immunolocalization of Phospho-MsRBR1

1. Settle 0.1 ml packed cell volume of alfalfa cells by centrifugation (5 min, 400×*g*) and resuspend the pellet in 2 ml fixation solution. Roll for 30 min in a tube roller (*see* **Note 2**).
2. Replace fixer with 2 ml 1× PBS by centrifugation. At this stage the cells can be kept at the fridge for several days until further processing.

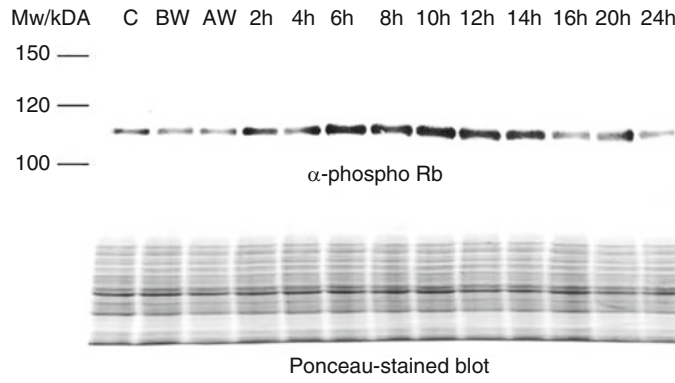

Fig. 4 Immunoblot detection of the phospho-MsRBR1 protein in synchronized *Medicago sativa* suspension cells during cell cycle progression after synchronization with 10 mM hydroxyurea (HU) treatment. Equal protein loading is demonstrated with Ponceau S-stained filter (*lower panel*). *C* control, non-synchronized culture, *BW* before washing out HU, *AW* after washing out HU

3. Following 3× 5 min 1× PBS (2 ml each) washes, incubate 20 µl packed cell volume of cells in 2 ml cell wall digestion solution for 30 min.
4. Place 12 mm diameter, clean, ethanol-wiped round coverslips onto a piece of parafilm (forms a hydrophobic barrier) and load 80 µl coverslip coating solution to allow the positively charged poly-l-lysine polymer to coat the negatively charged glass coverslip. After incubating for 15 min, remove all coating solution using vacuum suction and airdry the coverslip completely.
5. Following (2× 5 min) 1× PBS washes of cells, load 5–10 µl packed cell volume of cells (in 30–50 µl 1× PBS) onto coated coverslip and settle for 10 min.
6. Carefully remove and discard the supernatant of settled cells as well as unattached, floating cells. Allow coverslip-attached cells to partially—but not completely—airdry.
7. Slowly and carefully load 50 µl permeabilization solution to permeabilize plasma membranes and to allow antibody penetration. Incubate for 15 min.
8. Replace permeabilization solution with 80 µl 1× PBS while taking care not to dislodge the cells. Incubate for 5 min and repeat this washing step three more times.
9. Incubate cells with 80 µl blocking solution for 20 min.
10. Remove blocking solution and incubate cells with 80 µl primary antibody solution in a humid chamber (4 °C overnight or 24 °C 2–3 h or 37 °C 1 h) (*see* **Note 13**).

11. Wash primary antibody solution with four changes of blocking buffer (5 min each).
12. Incubate with fluorescent-conjugated secondary antibody solution for 1 h at 24 °C in a humid chamber (*see* **Note 9**).
13. Wash primary antibody solution with three changes of 1× PBS (5 min each).
14. Incubate 5 min with DNA staining (DAPI) solution to counterstain the chromatin (*see* **Note 5**).
15. Remove DAPI solution and add a drop of anti-fade mounting solution (e.g., Fluoromount-G) and mount the coverslip face down onto a clean, ethanol-wiped glass microscope slide. Gently press the coverslip with a tissue paper to flatten large cell clusters.
16. Observe with a fluorescence microscope (*see* Subheading 3.4).

Typical immunolocalization results are shown in Fig. 5 where cell cycle-related changes in the localization and distribution of phospho-MsRBR1 epitopes are detected using confocal laser scanning microscopy.

4 Notes

1. Caution: Hydroxyurea is toxic and carcinogenic; use appropriate precautions.
2. Paraformaldehyde powder and formaldehyde-containing fixers are hazardous in case of skin contact, eye contact or inhalation (irritant/corrosive). Work in a fume hood and wear protective equipment.
3. Caution: Propidium iodide is a known mutagen; use appropriate precautions.
4. The addition of Triton X-100 to the fixation solution provides uniform fixation with reduced cell shrinkage.
5. Caution: DAPI is a known mutagen; use appropriate precautions.
6. Careful propagation of the cell culture is an absolute prerequisite of efficient synchronization. Since the establishment of a culture may take a long time, it should be started well before the planned synchronization. For scientific purposes, established cultures of *Medicago sativa* ssp. varia (genotype A2) can be obtained (G.V. Horváth, Institute of Plant Biology, Biological Research Center HAS, Szeged).
7. Use of preconditioned medium in the washing steps and for the final resuspension will greatly increase the success of synchronization. To obtain this, the same *Medicago sativa* suspen-

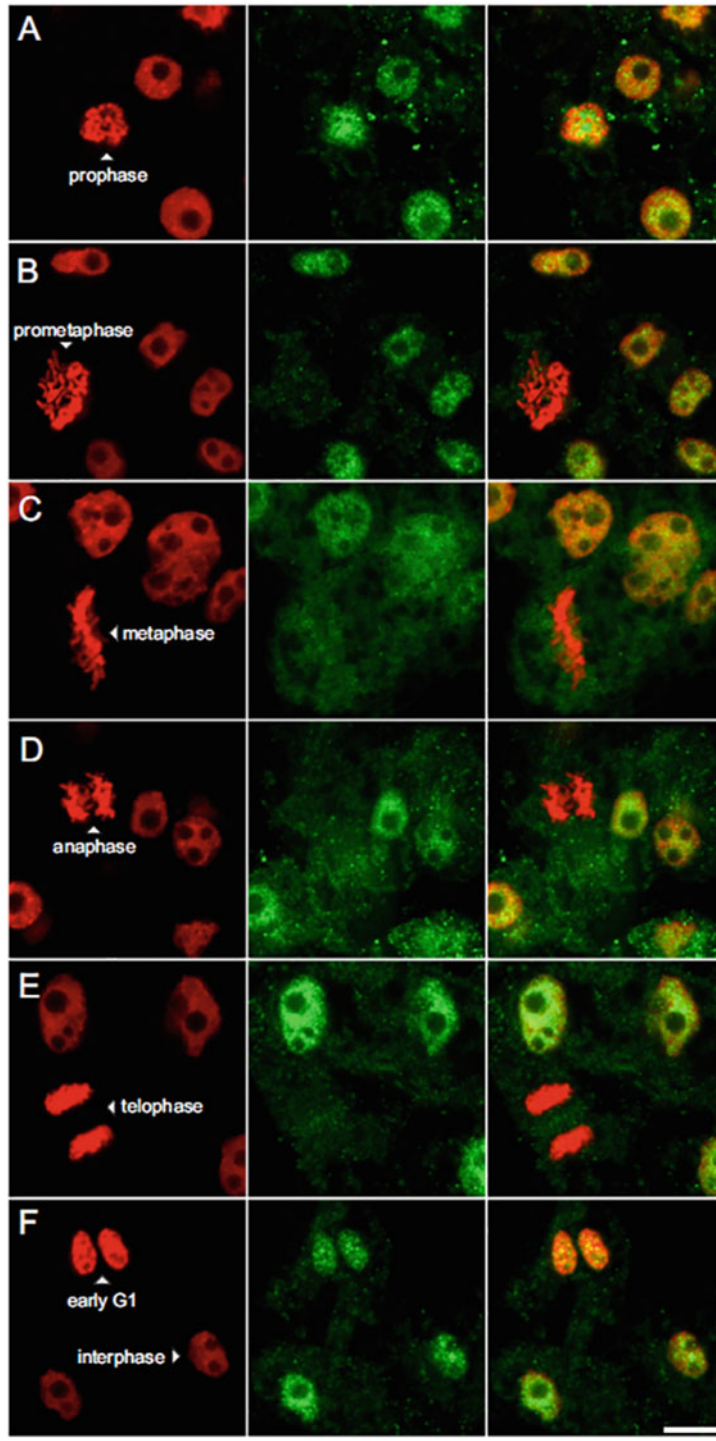

Fig. 5 Immunolocalization of phospho-MsRBR1 during mitotic cell division of alfalfa (*M. sativa*) suspension cells. Nuclei and chromosomes are labeled with DAPI (pseudocolored *red*). Cell cycle phases are as indicated. Alexa Fluor 488-conjugated antibody (*green*) was used for protein detection. Merged images are shown at the last column. Note that phospho-MsRBR1 epitopes disappear after prometaphase stage of mitosis (B) and then reappear at the end of cell division (F). Scale bar 10 μm

sion culture should be grown under the same subculturing regime, and just prior to the beginning of hydroxyurea removal, four times 200 ml of this culture should be filtered through sterile glass filter. Cells can be collected and used as unblocked control; the resulted preconditioned medium is used to remove hydroxyurea from blocked suspension.

8. Relatively high labeling efficiency can be detected in "Before Wash" samples, although the labeling intensity is very low compared to the other samples. Since EdU is a thymidine analog, cells with depleted nucleotide pools (due to the action of hydroxyurea) starts to incorporate EdU; however, the DNA synthesis can not proceed due to the lack of other nucleotides.
9. Fluorochrome-containing solutions should not be exposed to strong light; therefore, labeling reaction should be performed at dark or under dim light. The simplest solution is to wrap the centrifuge tubes in aluminum foil for the time of the labeling.
10. Glycerol-based (or high osmolarity) mounting media may cause cell shrinkage but they better suit imaging with oil immersion objectives. Mounting the samples in PBS prevents cell shrinkage, however care must be taken not to dry out the sample. Occasional PBS loading may be necessary for prolonged observations to prevent sample drying.
11. Unpolymerized acrylamide is neurotoxic, wear gloves for solution and gel handling.
12. Prestained protein marker allows only rough estimation of protein size. For more correct molecular weight estimation use unstained protein marker in parallel.
13. To prevent sample dry out during long or warm incubations, samples must be kept in a humid environment. A wet tissue paper sealed in a large petri dish can be used for this purpose.

Acknowledgement

The authors are grateful to Katalin Török for excellent technical assistance. This work was funded by OTKA grant no. NK 69227 (G.V.H.) and National Research, Development and Innovation Office, NKFIH grant no. K116318 (F.A.). Edit Ábrahám was supported by the János Bolyai Fellowship of the Hungarian Academy of Sciences.

References

1. Bergounioux C, Perennes C, Brown SC, Gadal P (1988) Cytometric analysis of growth regulator-dependent transcription and cell cycle progression in *P. hybrida* protoplast cultures. Planta 175:500–505
2. Kapros T, Bögre L, Németh K, Bakó L, Györgyey J, Wu SC, Dudits D (1992) Differential expression of histone H3 gene variants during cell cycle and somatic embryogenesis in alfalfa. Plant Physiol 98:621–625
3. Carle SA, Bates GW, Shannon TA (1998) Hormonal control of gene expression during reactivation of the cell cycle in tobacco mesophyll protoplasts. J Plant Growth Regul 17:221–230
4. Doležel J, Číhalíková J, Lucretti S (1992) A high yield procedure for isolation of metaphase chromosomes from root tips of *Vicia faba*. Planta 188:93–98
5. Doležel J, Číhalíková J, Weiserová J, Lucretti S (1999) Cell cycle synchronization in plant root meristems. Methods Cell Sci 21:95–107
6. Menges M, Murray JAH (2002) Synchronous *Arabidopsis* suspension cultures for analysis of cell-cycle gene activity. Plant J 30:203–212
7. Ghosh S, Sen J, Kalia S, Guha-Mukherjee S (1999) Establishment of synchronization in carrot cell suspension culture and studies on stage specific activation of glyoxalase I. Methods Cell Sci 21:141–148
8. Arumuganathan K, Slattery JP, Tanksley SD, Earle ED (1991) Preparation and flow cytometric analysis of metaphase chromosomes of tomato. Theor Appl Genet 82:101–111
9. Wang ML, Leitch AR, Schwarzacher T, Heslop-Harrison JS, Moore G (1992) Construction of a chromosome-enriched *HpaII* library from flow-sorted wheat chromosomes. Nucleic Acids Res 20:1897–1901
10. Kumagai-Sano F, Hayashi T, Sano T, Hasezawa S (2006) Cell cycle synchronization of tobacco BY-2 cells. Nat Protocols 1:2621–2627
11. Young CW, Hodas S (1964) Hydroxyurea: inhibitory effect on DNA metabolism. Science 146:1172
12. Watson PA, Hanauske-Abel HH, Flint A, Lalande M (1991) Mimosine reversibly arrests cell cycle progression at the G_1-S phase border. Cytometry 12:242–246
13. Ábrahám E, Miskolczi P, Ayaydin F, Yu P, Kotogány E, Bakó L, Ötvös K, Horváth VG, Dudits D (2011) Immunodetection of retinoblastoma-related protein and its phosphorylated form in interphase and mitotic alfalfa cells. J Exp Bot 62:2155–2168
14. Kotogány E, Dudits D, Horváth VG, Ayaydin F (2010) A rapid and robust assay for detection of S-phase cell cycle progression in plant cells and tissues by using ethynyl deoxyuridine. Plant Methods 6:1–15
15. Mészáros T, Miskolczi P, Ayaydin F, Pettkó-Szandtner A, Peres A, Magyar Z, Horváth VG, Bakó L, Fehér A, Dudits D (2000) Multiple cyclin-dependent kinase complexes and phosphatases control G2/M progression in alfalfa cells. Plant Mol Biol 43:595–605
16. Hirano H, Harashima H, Shinmyo A, Sekine M (2008) *Arabidopsis* retinoblastoma-related protein 1 is involved in G1 phase cell cycle arrest caused by sucrose starvation. Plant Mol Biol 66:259–275
17. Nias AHW, Fox M (1971) Synchronization of mammalian cells with respect to the mitotic cycle. Cell Tissue Kinet 4:375–398

Part VII

Synchronization of Embryonic Cells

Chapter 18

Nuclear Treatment and Cell Cycle Synchronization for the Purpose of Mammalian and Primate Somatic Cell Nuclear Transfer (SCNT)

Yoel Shufaro and Benjamin E. Reubinoff

Abstract

Mammalian somatic cell nuclear transfer (SCNT) is a technically and biologically challenging procedure inducing rapid reprogramming of the nucleus from the differentiated into the totipotent state in a few hours. This procedure was initially successfully accomplished in farm animals, then in rodents, and more recently in primates and in humans. Though ethical concerns regarding SCNT still exist, this procedure can be utilized to generate patient and disease-specific pluripotent embryonic stem cell lines, which carry a great promise in improving our understanding of major disease conditions and a hope for better therapies and regenerative medicine. In this section, we will survey the existing literature and describe how mouse SCNT is performed and the importance of donor cell treatment and cycle synchronization prior to SCNT.

Key words Somatic cell nuclear transfer, Reprogramming, Cell cycle synchronization

1 Introduction

Mammalian terminally differentiated somatic cells' nuclei can be reprogrammed into pluripotency and even to absolute totipotency, via somatic cell nuclear transfer (SCNT) [1, 2] or by hyper-expression of transcription factors [3]. Both technologies can be used to generate pluripotent stem cell lines which are frankly embryonic in the case of SCNT (embryonic stem cells—SCNT ESCs), or embryonic-like in the case of transcription factor-mediated reprogramming (induced pluropotent stem cells—iPSCs). SCNT can be used to create cloned embryos which can implant and develop into mature animals. Mature normal and fertile offspring can be generated from SCNT ESCs and iPCSs using tetraploid complementation, providing a definite proof of these cells' pluripotency [4, 5].

SCNT is technically challenging and requires the use of mammalian oocytes, which are quite difficult to obtain for primate and

Gaspar Banfalvi (ed.), *Cell Cycle Synchronization: Methods and Protocols*, Methods in Molecular Biology, vol. 1524,
DOI 10.1007/978-1-4939-6603-5_18,

human studies. The emergence of transcription factor-based reprogramming in the last decade, bypassing these difficulties, has made SCNT a less popular research platform for studying reprogramming and development.

SCNT is performed by injection or fusion of a somatic nucleus into an enucleated oocyte. The injected ova are activated into a zygote-like state and allowed to further develop into embryos. Development to the blastocyst stage is considered a confirmation of reprogramming of the somatic differentiated nucleus into the embryonic state and activation of the early embryonic genes [6]. Once this was achieved, SCNT ESCs autologous to the nuclei donor cells can be potentially derived. This conceptual idea was initially based on experiments in amphibians in which cell differentiation was fully reversed after injection of somatic nuclei into growing oocytes. Reprogramming was demonstrated by changes in nuclear gene expression but not in gene content [7]. The next major advance in this field came with the emergence of mammalian SCNT. The first normal adult animal generated by SCNT was the sheep Dolly, which originated from reprogrammed cultured mammary gland cells [8]. In the years afterward, SCNT was successfully performed in a variety of animal models including mice, cattle, goat, pigs, dog, and primates [9, 10]. Human SCNT was initially performed with very limited success resulting in poor quality in vitro cultured embryos [11]. The principle barrier to successful human SCNT was early embryonic arrest at the eight-cell stage, presumably due to an inability to activate critical embryonic genes from the somatic donor cell nuclei [12]. These obstacles were overcome mainly by modifications in the management and conditions of the reprogramming human ooplast and not those of the somatic donor cells [13].

SCNT for reproductive purposes is ethically accepted only in animals. This procedure is not efficient, with many of the resulting embryos showing an increased rate of miscarriages, malformations, and perinatal deaths [6]. However, SCNT is efficient enough to create in vitro cultured blastocysts, from which ESCs lines can be derived. Contrary to reproduction, the employment of human SCNT for this purpose is ethically acceptable [13]. Human autologous SCNT ESCs can be potentially used for valuable benefits such as regenerative medicine or disease modeling, and their derivation does not involve the destruction of native embryos, the products of "natural" gamete fertilization, which harbor the potential to become human beings. ESCs derived from reprogrammed somatic cells are phenotypically and functionally identical to native ESCs [14]. SCNT-derived ESC lines are genetically identical to the donor of the nucleus. Once transplanted into the donor, the SCNT ES cells and all their differentiated progeny are expected not to be rejected by the immune system of the (nuclei) donor, even without immune suppression [15]. The mitochondrial DNA of the

enucleated oocyte, which is not replaced during SCNT, probably does not contribute immunogenicity. In animal models, progenitors derived from SCNT ESC lines were not rejected following transplantation into the immune intact donor of the nucleus [15]. In humans, such cells might substantially improve the treatment of neurodegenerative diseases, blood disorders, or diabetes. Since therapy for these diseases is currently limited to replacement and palliation, SCNT ESCs provide a renewable source of cells, allowing regenerative therapy to be repeated whenever needed.

An additional equally important application of SCNT ESCs lines is the generation of highly reliable in vitro human disease models. Currently, native ESC lines were derived from embryos diagnosed by pre-implantation genetic diagnosis (PGD) as affected by severe genetic disorders [16], and successfully serve to model these disorders in vitro. However, this approach is limited to disorders for which PGD is ethically accepted and practically feasible. On the other hand, using SCNT nuclei from an endless variety of diseased patients can be reprogrammed into blastocysts, followed by the derivation of SCNT ESC lines which may be authentic disease models. Although transcription factor-based reprogramming into iPSCs is also an appealing alternative for disease modeling, reprogramming in the oocytic environment is presently still the gold standard despite its difficulties and disadvantages. SCNT ESCs were proven to be epigenetically identical to native ESCs, but iPSCs were shown to vary from ESCs (and SCNT ESCs) and to partly preserve the transcriptome profile and DNA methylation patterns of the somatic cells from which they originated [17].

There are two contributors to successful reprogramming: (1) the ooplasic environment and (2) the injected nucleus. In most mammalian species, optimal reprogramming occurs in the mature (metaphase II) oocyte. The cytoplasmic activity termed maturation/meiosis/mitosis-promoting factor (MPF) is a key factor in this process [18]. Metaphase II oocytes have high MPF activity which declines rapidly after fertilization and are therefore the best reprogramming vehicle. High oocytic quality and viability ensure its survival after enucleation and are a mandatory requirement for successful reprogramming by SCNT. In human SCNT, even the type of stimulation protocol and the ovarian response of the young otherwise fertile donors had a significant impact on the oocytes' reprogramming capacity [13].

The success rate of nuclear reprogramming decreases as donor cells become more differentiated. Less differentiated cells bear a greater epigenetic resemblance to the totipotent state, and are therefore more readily reprogrammed. However, such undifferentiated cells are epigenetically less stable than cells with a committed fate. Therefore, when terminally differentiated (contrary to undifferentiated) nuclei are used for SCNT, the primary success rate is lower, but the cloned embryos bear a greater resemblance to their native parallels.

As donor nuclei progress in the cell cycle, the extent of the development of reconstituted embryos is reduced [19]. All nuclei transferred when MPF activity is high undergo nuclear envelope breakdown, which is followed by premature chromosome condensation [18]. The nuclear envelope is then reformed and DNA synthesis starts. Therefore, unless the nucleus is in the G_0/G_1 phase at the time of transfer, re-replication of previously replicated DNA will occur, resulting in incorrect DNA content and possible chromosomal damage. As a result, mammalian somatic nuclei are reprogrammed without altering their DNA content only if injected when they are at the G_0 or G_1 stages. In addition, the chromatin is stable at G_0/G_1 and its exposure to the oocytic environment is steady for the hours needed to induce its reprogramming. This process is less successful once the chromatin is open for DNA replication or packed in chromosomes for mitosis. In naturally fertilized oocytes, the S phase starts only after the organization of two pronuclei [18]. In SCNT reconstructed oocytes, two pseudopronuclei appear only after completion of oocyte activation, well after the injection of the somatic nucleus [20]. It is therefore necessary for the transplanted nucleus to be at G_0 or G_1 in order to be molecularly and morphologically "in phase" with the ooplasm it was transplanted into.

In most published mammalian SCNT systems, the injected nuclei are from quiescent differentiated cells which do not require special treatment to be maintained in this state. However, it is possible to inject and reprogram nuclei isolated from cells growing in culture if treated properly prior to their injection. We will describe the method that we used for mouse SCNT, and a survey of the published methods for cell cycle synchronization of the donor nuclei.

2 Materials

1. Pregnant Mare Serum Gonadotropin (PMSG), human Chorionic Gonadotropin (hCG).
2. Self-prepared HEPES CZB medium [21] containing the following ingredients dissolved in embryo tested water:

$CaCl_2 \cdot 2H_2O$	0.25 g/l
Sodium EDTA	0.04 g/l
Glucose	1.0 g/l
HEPES acid free	4.76 g/l
KH_2PO_4	0.16 g/l
KCl	0.36 g/l
$MgSO_4 \cdot 7H_2O$	0.29 g/l

NaCl	4.76 g/l
$NaHCO_3$	0.42 g/l
Sodium lactate (60% solution)	5.3 ml/l
Sodium pyruvate	0.03 g/l
l-Glutamine	0.146 g/l
Penicillin-G	0.05 g/l
Streptomycin	0.07 g/l
Bovine serum albumin	4 g/l

CZB is prepared daily to twice-weekly from X10 stocks (prepared biweekly and stored at 4 °C), equilibrated to pH 7.2–7.4 at room conditions. Bovine serum albumin (BSA) is added as a powder to the final preparation (w/v).

3. Polyvinylpyrrolidone (PVP MW 40000) is added from a 10% stock.
4. Self prepared modified Calcium free M16 medium containing the following ingredients dissolved in embryo tested water:

EDTA	0.037 g/l
Glucose	1.0 g/l
HEPES acid free	4.76 g/l
KH_2PO_4	0.16 g/l
KCl	0.356 g/l
$MgSO_4 \cdot 7H_2O$	0.29 g/l
NaCl	5.68 g/l
$NaHCO_3$	2.101 g/l
Sodium lactate (60% solution)	5.5 ml/l
Bovine serum albumin	4 g/l

The calcium free M16 medium is self-prepared daily from biweekly prepared stocks, equilibrated to pH 7.6–7.8 at room conditions. BSA is added as a powder to the final preparation (w/v).

5. $SrCl_2$ powder is to be weighed and dissolved daily in water prior to its addition. Cytochalasin B (CB) is stored as frozen aliquots dissolved in DMSO 1 mg/ml. The vitamins solution is stored as is in frozen aliquots. These ingredients are added to calcium free M16 a short time before its use.
6. All self-prepared media are filtered on a 0.22 μm cellulose acetate membrane.

7. Bovine testicular Hyaluronidase.
8. Protease inhibitor (PI).
9. Quinn's Advantage Cleavage Medium (Origio, Denmark, previously Sage, CT, USA, formulation patented).
10. Embryo-tested mineral oil for incubator culture. DMPSV silicon oil for micromanipulation stages.
11. Holding pipette (small 25°) and Piezodrill enucleation (12 μm 25°) and injection (6 μm 25°) pipettes (Origio, Denmark, previously Humagen, VA, USA.)
12. Electronics grade Mercury (>99% purity).
13. Nunclon 35 and 100 mm culture dishes.
14. Handling pipettes. Pasteur pipettes heated and pulled. Broken edge diameter is approx. 150–200 μm.
15. Mercury disposal container.
16. 8- to 12-Week-old $B_6C_3F_1$ or $B_6D_2F_1$ female mice.

3 Methods

3.1 Somatic Cell Nuclear Transfer

1. Ovarian stimulation and oocyte maturation is achieved with an intraperitoneal (i.p.) injection of PMSG (10 i.u.) followed by an i.p. hCG injection (10 i.u.) 48 h afterward (*see* **Note 1**). Oocytes are retrieved 13 h after hCG administration. Following scarification, the oviducts are excised by laparotomy opened and incubated in HEPES CZB PVP 0.1% containing Hyaluronidase (50 IU/ml) and PI (0.2%) at 28 °C for 10–12 min (100 μl drop on a 35 mm dish). At the end of this period, the mature oocytes are self-denuded from the surrounding cumulus cells, and are transferred for incubator culture in Quinn's Advantage Cleavage Medium (seven 30 μl drops on a 35 mm dish covered with oil) at 37 °C 5% CO_2 (*see* **Note 2**).
2. The cumulus cells are left inside the HEPES -CZB PVP 0.1% Hyaluronidase PI drop. An equal volume of Quinn's Advantage Cleavage Medium is added and the entire drop is gently pipetted. It is afterward covered with mineral oil and maintained at 4 °C until nuclear injection. The purpose of this step is to maintain cellular quiescence and prevent surface adhesion.
3. Micromanipulation is performed on the stage of an inverted microscope equipped with either a Nomarsky (DIC) or Hoffman (HMC) optical system. A temperature-controlled heated stage is beneficial but not mandatory. Top quality micromanipulators and microinjectors of a leading brand (Narashige, Eppendorf, Leica, etc.) are used on each side. It is especially important that the micro-injector controlling enucleation and injection of the transferred nucleus is very

sensitive. A piezo-micromanipulator (PMM 150 FU, PrimeTech, Japan) is essential for mouse SCNT, but is not mandatory in other species. If this device is used, its pulses are conducted via mercury which is introduced inside the enucleation and injection micropipettes. Each such micromanipulation system is individually calibrated for its users.

4. Enucleation is performed in HEPES-CZB PVP 0.1% supplemented with 2 μg/ml CB at room temperature (or 27 °C if a temperature-controlled stage is available). A 100 mm plate is used. A central 30 μl drop in which the PVP concentration is raised to 1% is placed first (*see* **Note 3**). Additional 2–3 enucleation drops are placed equally across the diameter line from each side prior to covering the entire plate with silicone oil. The meiotic spindle is visible to the naked, but skilled, eye as a lucent ball which is aspirated gently from the oocyte after the *Zona Pellucida* (ZP) is penetrated with the PMM. The presence of CB permits the aspiration of the spindle without tearing the oocyte. The volume of the ooplasm accompanying the spindle should be minimal.
5. After the rapid (<10 min) completion of the enucleation, the ooplasts are returned for recovery in the incubator in Quinn's Advantage Cleavage Medium (different dish of the same type) at 37 °C 5% CO_2 for at least 1 h.
6. The (nuclei donor) cumulus cells are then taken out of refrigeration and placed on a new 100 mm stage plate, inside drops containing injection medium. This medium is hypertonic (110%) CZB HEPES medium with 1% PVP. The plate contains a central 50 μl clean drop for maintenance of the piezo-driven injection micropipette and injection drops along the diameter line (*see* **Note 3**). The oocytes are placed and injected with the assistance of the PMM in the same drop containing the somatic cells. Prior to injection, the nuclei are stripped from the cell membrane and cytoplasm by repeated trituration through the injection micro-pipette with the PMM emitting pulses. Care should be taken to prevent stickiness inside the pipette and not to destroy the nucleus during this process.
7. After the injection, the reconstructed oocytes are allowed to recover for 1 h at room temperature in a 1:1 mixture of HEPES-CZB 0.1% PVP and Quinn's Advantage Cleavage Medium. In the next step, they are transferred for incubator culture in Quinn's Advantage Cleavage Medium for an additional 1–2 h (same type of drops and dish).
8. The reconstructed oocytes are then activated for 6 h in calcium-free M16 supplemented with 10 mM $SrCl_2$ CB (5 μg/ml) and vitamins, and then transferred to Quinn's Advantage Cleavage Medium at 37 °C 5% CO_2. At the end of this activation stage,

two pronuclei-like structures can be identified in almost all SCNT reconstructed oocytes. This point parallels the 2 pronuclei zygote stage observed after normal fertilization. Embryonic development occurs in vitro up to the blastocyst stage.

3.2 Donor Nuclei Cell Cycle Synchronization

1. The somatic nuclei are successfully reprogrammed by the ooplasm only when in the diploid G_0 or G_1 states [22]. If DNA synthesis ensues or completes in the donor nucleus prior to its injection, aneuploidy and chromosome damage will occur.
2. In most published SCNT experiments, the injected nuclei are from quiescent differentiated cells which do not require special treatment to be maintained in this state. However, it is possible to inject and reprogram nuclei isolated from cells growing in culture. The principle approaches for cellular arrest are serum starvation, culture confluence, and G_1 arrest by inhibition of DNA synthesis.
3. The most prevalent method to arrest growing cells in the G_0 stage is serum starvation. For example, Baguisi et al. [23], pioneers in goat SCNT, used nuclei from a fetal cell line cultured in a very low (0.5%) FBS concentration for 1 week prior to SCNT. Kues et al. [24] quantified the impact of serum deprivation on porcine fibroblasts and found that 48 h of such serum starvation were sufficient to halt the growth of 98% of the cells, without causing DNA damage and nuclear fragmentation (which appeared 24 h later under these conditions). The confluency and serum starvation (0.5%) approach was also successfully used for treatment of human in vitro cultured fibroblasts used as nuclei donors for SCNT [13, 25].
4. Dalman et al. demonstrated that full culture confluence was as good as serum starvation for preventing entry into the S phase with a lower rate of apoptosis than the latter [26] (*See* **Note 4**). Serum starvation and culture confluence are simple to perform, but require familiarity with the specific conditions that the cultured cells require in order to avoid DNA damage or apoptosis.
5. G_1 arrest was reported by Collas et al. [19]. The purpose of this earlier work was to investigate the impact of cell cycle stage on nuclear morphology and chromosome constitution in blastomeres. According to the methodology in this publication, mitotic arrest was accomplished by adding colcemid 0.5 μg/ml for 10 h, washing with PBS, followed by the addition of aphidicolin 0.1 μg/ml in order to inhibit DNA synthesis. Using this method, the cells were arrested very accurately at the end of G_1.
6. Kues et al. [24] have shown that cell culture with aphidicolin (6 μM for 14 h) or butyrolactone (118 μM for 5 h) are efficient in preventing DNA synthesis and cell division in the presence of standard (10% FBS) conditions. Both drugs were used to maintain cell cycle synchronization once FBS was returned to

the depleted cultures after 48 h (in order to prevent DNA fragmentation).

7. Kurosaka et al. [27] have compared serum starvation (FBS 0.2% 20 h) (G_0 arrest) to DNA synthesis inhibition by aphidicolin (2 μg/ml 20 h, 10% FBS) (G_1 arrest). Both methods were efficient in achieving cell cycle arrest. However, when G_1 arrested nuclei were used, the first round of DNA synthesis occurred earlier and SCNT was more efficient.
   Serum starvation, culture in confluence, and G_1 chemical arrest are all suitable for donor cell cycle synchronization prior to SCNT. However, it seems that the chemical arrest methods at the transition G_1–S are slightly superior. This approach was never attempted in primate or human SCNT. The explanations of this advantage might be (a) a greater homogeneity of the cell population when chemical methods are used; (b) the G_1–S transition point is more suitable for reprogramming and initiation of DNA synthesis in synchrony with the ooplasmic program.

4 Notes

1. PMSG is dissolved in NS and aliquots for injection are stored at −20 °C. hCG is dissolved in DDW, divided to aliquots for injection, and then dried in a vacuum centrifuge. Each dried aliquot is resuspended in NS prior to injection.
2. It is important to confirm at this stage that all the collected oocytes are actually at metaphase II and contain a polar body. Undenuded immature oocytes should be discarded.
3. This central drop is used for the clean maintenance of the piezo-driven enucleation pipette. Cautious spillage of mercury micro-drops inside this drop is acceptable as long as they do not contaminate the other drops.
4. Goat fibroblasts were grown on 60 mm plates in DMEM supplemented with 15% FBS. They were arrested once the culture was confluent, and did not lose this property even after several transfers.

References

1. Jaenisch R, Hochedlinger K, Blelloch R, Yamada Y, Baldwin K, Eggan K (2004) Nuclear cloning, epigenetic reprogramming, and cellular differentiation. Cold Spring Harb Symp Quant Biol 69:19–27
2. Markoulaki S, Meissner A, Jaenisch R (2008) Somatic cell nuclear transfer and derivation of embryonic stem cells in the mouse. Methods 45:101–114
3. Okita K, Ichisaka T, Yamanaka S (2007) Generation of germline-competent induced pluripotent stem cells. Nature 448:313–317
4. Wernig M, Meissner A, Foreman R, Brambrink T, Ku M, Hochedlinger K, Bernstein BE, Jaenisch R (2007) In vitro reprogramming of fibroblasts into a pluripotent ES-cell-like state. Nature 448:318–324

5. Rideout WM III, Eggan K, Jaenisch R (2001) Nuclear cloning and epigenetic reprogramming of the genome. Science 293:1093–1098
6. Solter D (2000) Mammalian cloning: advances and limitations. Nat Rev Genet 1:199–207
7. Shufaro Y, Lacham-Kaplan O, Tzuberi BZ, McLaughlin J, Trounson A, Cedar H, Reubinoff BE (2010) Reprogramming of DNA replication timing. Stem Cells 28:443–449
8. Wilmut I, Schnieke AE, McWhir J, Kind AJ, Campbell KH (1997) Viable offspring derived from fetal and adult mammalian cells. Nature 385:810–813
9. Wilmut I, Paterson L (2003) Somatic cell nuclear transfer. Oncol Res 13:303–307
10. Mitalipov SM, Zhou Q, Byrne JA, Ji WZ, Norgren RB, Wolf DP (2007) Reprogramming following somatic cell nuclear transfer in primates is dependent upon nuclear remodeling. Hum Reprod 22:2232–2242
11. Cibelli JB, Lanza RP, West MD, Ezzell C (2002) The first human cloned embryo. Sci Am 286:44–51
12. Egli D, Chen AE, Saphier G, Ichida J, Fitzgerald C, Go KJ, Acevedo N, Patel J, Baetscher M, Kearns WG, Goland R, Leibel RL, Melton DA, Eggan K (2011) Reprogramming within hours following nuclear transfer into mouse but not human zygotes. Nat Commun 2:488
13. Tachibana M, Amato P, Sparman M, Gutierrez NM, Tippner-Hedges R, Ma H, Kang E, Fulati A, Lee HS, Sritanaudomchai H, Masterson K, Larson J, Eaton D, Sadler-Fredd K, Battaglia D, Lee D, Wu D, Jensen J, Patton P, Gokhale S, Stouffer RL, Wolf D, Mitalipov S (2013) Human embryonic stem cells derived by somatic cell nuclear transfer. Cell 153:1228–1238
14. Brambrink T, Hochedlinger K, Bell G, Jaenisch R (2006) ES cells derived from cloned and fertilized blastocysts are transcriptionally and functionally indistinguishable. Proc Natl Acad Sci U S A 103:933–938
15. Shufaro Y, Reubinoff BE (2004) Therapeutic applications of embryonic stem cells. Best Pract Res Clin Obstet Gynaecol 18:909–927
16. Turetsky T, Aizenman E, Gil Y, Weinberg N, Shufaro Y, Revel A, Laufer N, Simon A, Abeliovich D, Reubinoff BE (2008) Laser-assisted derivation of human embryonic stem cell lines from IVF embryos after preimplantation genetic diagnosis. Hum Reprod 23:46–53
17. Ma H, Morey R, O'Neil RC, He Y, Daughtry B, Schultz MD, Hariharan M, Nery JR, Castanon R, Sabatini K, Thiagarajan RD, Tachibana M, Kang E, Tippner-Hedges R, Ahmed R, Gutierrez NM, Van Dyken C, Polat A, Sugawara A, Sparman M, Gokhale S, Amato P, Wolf DP, Ecker JR, Laurent LC, Mitalipov S (2014) Abnormalities in human pluripotent cells due to reprogramming mechanisms. Nature 511:177–183
18. Campbell KH, Loi P, Otaegui PJ, Wilmut I (1996) Cell cycle co-ordination in embryo cloning by nuclear transfer. Rev Reprod 1:40–46
19. Collas P, Pinto-Correia C, Ponce de Leon FA, Robl JM (1992) Effect of donor cell cycle stage on chromatin and spindle morphology in nuclear transplant rabbit embryos. Biol Reprod 46:501–511
20. Wakayama T, Perry AC, Zuccotti M, Johnson KR, Yanagimachi R (1998) Full-term development of mice from enucleated oocytes injected with cumulus cell nuclei. Nature 394:369–374
21. Chatot CL, Ziomek CA, Bavister BD, Lewis JL, Torres I (1989) An improved culture medium supports development of random-bred 1-cell mouse embryos in vitro. J Reprod Fertil 86:679–688
22. Wells DN, Laible G, Tucker FC, Miller AL, Oliver JE, Xiang T, Forsyth JT, Berg MC, Cockrem K, L'Huillier PJ, Tervit HR, Oback B (2003) Coordination between donor cell type and cell cycle stage improves nuclear cloning efficiency in cattle. Theriogenology 59:45–59
23. Baguisi A, Behboodi E, Melican DT, Pollock JS, Destrempes MM, Cammuso C, Williams JL, Nims SD, Porter CA, Midura P, Palacios MJ, Ayres SL, Denniston RS, Hayes ML, Ziomek CA, Meade HM, Godke RA, Gavin WG, Overström EW, Echelard Y (1999) Production of goats by somatic cell nuclear transfer. Nat Biotechnol 17:456–4561
24. Kues WA, Anger M, Carnwath JW, Paul D, Motlik J, Niemann H (2000) Cell cycle synchronization of porcine fetal fibroblasts: effects of serum deprivation and reversible cell cycle inhibitors. Biol Reprod 62:412–419
25. Noggle S, Fung HL, Gore A, Martinez H, Satriani KC, Prosser R, Oum K, Paull D, Druckenmiller S, Freeby M, Greenberg E, Zhang K, Goland R, Sauer MV, Leibel RL, Egli D (2011) Human oocytes reprogram somatic cells to a pluripotent state. Nature 478:70–75
26. Dalman A, Eftekhari-Yazdi P, Valojerdi MR, Shahverdi A, Gourabi H, Janzamin E, Fakheri R, Sadeghian F, Hasani F (2009) Synchronizing cell cycle of goat fibroblasts by serum starvation causes apoptosis. Reprod Domest Anim 45:e46–e53
27. Kurosaka S, Nagao Y, Minami N, Yamada M, Imai H (2002) Dependence of DNA synthesis and in vitro development of bovine nuclear transfer embryos on the stage of the cell cycle of donor cells and recipient cytoplasts. Biol Reprod 67:643–647

Part VIII

Hematopoietic Stem Cells

Chapter 19

Ex Vivo Expansion of Hematopoietic Stem Cells to Improve Engraftment in Stem Cell Transplantation

Kap-Hyoun Ko, Robert Nordon, Tracey A. O'Brien, Geoff Symonds, and Alla Dolnikov

Abstract

The efficient use of hematopoietic stem cells (HSC) for transplantation is often limited by the relatively low numbers of HSC collected. The ex vivo expansion of HSC for clinical use is a potentially valuable and safe approach to increase HSC numbers thereby increasing engraftment and reducing the risk of morbidity from infection. Here, we describe a protocol for the robust ex vivo expansion of human CD34(+) HSC isolated from umbilical cord blood. The protocol described can efficiently generate large numbers of HSC. We also describe a flow cytometry-based method using high-resolution division tracking to characterize the kinetics of HSC growth and differentiation. Utilizing the guidelines discussed, it is possible for investigators to use this protocol as presented or to modify it for their specific needs.

Key words Hematopoietic stem cell, Expansion, Cell division

1 Introduction

The use of hematopoietic stem cells (HSC) for effective transplantation can be limited by the relatively low numbers of HSC collected from the patient [1–5]. A potential solution to this is to develop a strategy to expand HSC prior to transplantation [5, 6]. Fast hematopoietic recovery after transplantation of HSC has been demonstrated in clinical trials performed with ex vivo expanded HSC and there has been evidence of improved engraftment [5–7].

Once considered a biological waste, UCB has emerged as a viable source of stem cells for transplantation. Because cord units are pre-tested for HLA (human leukocyte antigens) compatibility and then cryogenically stored, UCB is a stem cell source readily on hand that can reduce the delay in transplantation for patients with high-risk malignancies. The major drawback of cord blood as an alternate source of HSC is the slower hematopoietic recovery and higher incidence of graft failure. This finding has been repeatedly

Gaspar Banfalvi (ed.), *Cell Cycle Synchronization: Methods and Protocols*, Methods in Molecular Biology, vol. 1524,
DOI 10.1007/978-1-4939-6603-5_19,

demonstrated to relate to the infused cell dose with higher cell doses resulting in improved engraftment. The minimum accepted cell dose to achieve engraftment is variably reported to range between 2 and 3×10^7/kg total nucleated cells per recipient weight. The average cell yield in a single cord unit collection provides therefore sufficient cells for recipients less than 40 kg (Personal communication, Prof Marcus Vowels, Director Australian Cord Blood Bank, Sydney Children's Hospital) and is the major reason for limitation of this stem cell source in adult patients. Thus, the strategy of providing sufficient increased numbers of cord blood stem cells may shorten time to engraftment and improve survival in adult UCB recipients.

Two main methods to expand HSC have been explored to date: static liquid and stromal co-culture systems [8–11]. The majority of static liquid and some stromal co-culture expansion systems require the isolation of CD34(+) cells from fresh or frozen hematopoietic tissue [11, 12]. Stem cell transplantation studies indicate that a CD34(+) subpopulation in UCB can provide durable long-term donor-derived lymphohematopoietic reconstitution. Therefore, the CD34 antigen has been routinely used to identify and purify HSC. CD34(+) cells contain both primitive HSC with long-term regenerative ability and more mature hematopoietic progenitor cells (HPC) shown to mediate short-term hematopoiesis.

Positively selected CD34(+) cells enriched with HSC can be incubated in culture medium supplemented with different combinations of cytokines [13]. Cytokines promote quiescent HSC to enter the cell cycle. Different cytokine combinations and varying doses of the cytokines have previously been shown to drive HSC expansion [14]. Although, this strategy is effective in increasing total cell numbers, it is generally the case that these procedures drive HSC differentiation to progeny cells at the expense of HSC self-renewal [15]. The ex vivo expansion of short-term reconstituting HPC at the expense of long-term reconstituting higher-quality HSC has been shown to negatively impact on hematopoietic reconstitution [15, 16].

Here we describe (1) a protocol for the efficient ex vivo expansion of human CD34(+) HSC isolated from UCB and (2) a flow cytometry-based method using high-resolution division tracking to characterize the kinetics of HSC expansion [17]. The stem cell expansion protocol describes the robust ex vivo proliferation of human CD34(+) cells isolated from umbilical cord blood using a combination of cytokines previously optimized by our group [17]. The division tracking method identifies consecutive cell generations by monitoring the serial halving of carboxyfluoresceindiacetate succinidyl ester (CFDA-SE) fluorescence with each cell division and thus provides a powerful tool to monitor and quantify cell division [17]. The protocol outlines the steps used to analyze CFDA-SE-labeled cells and its utility has been demonstrated by our group in a number of CD34+ cell culture systems [17]. This method is highly useful for the analysis of

the specific parameters of, and critical modulating conditions for, HSC expansion. By combining CFDA-SE staining with the analysis of CD34 antigen, division tracking analysis provides insight into how the fundamental processes of cell division, differentiation, and apoptosis contribute to hematopoietic growth dynamics.

2 Materials

2.1 Cell Sources

1. UCB was collected by the Sydney Cord Blood Bank (Sydney Children's Hospital, Sydney, Australia). Informed consent was obtained from mothers, and both University of New South Wales and Eastern Sydney Area Health Service Human Ethics Committees approved the use of UCB for this research project (*see* **Note 1**).
2. The acute myelogenous leukemia cell line, KG1a [18], was used to optimize CFDA-SE staining.

2.2 Cell Culture Reagents

1. Serum-free medium, Stemline II Hematopoietic stem cell expansion medium (Sigma-Aldrich), was used for expansion of UCB-derived CD34(+) cells. Iscove's Modified Dulbecco's Media (IMDM) was used for KG1a cells (Gibco, Invitrogen).
2. Stem cell factor (SCF), granulocyte colony stimulation factor (G-CSF), thrombopoietin (TPO), and flt-3 ligand (FL) are obtained from R&D systems. Growth factors were dissolved in Dulbecco's Phosphate Buffered Saline (DPBS; Sigma-Aldrich) containing 1 % Bovine Serum Albumin (BSA) (Sigma-Aldrich) to concentration of 100 μg/ml. Dissolved growth factors were aliquoted into microtubes and stored at −20 °C.
3. 9.55 g of DPBS was dissolved in 1000 ml of water for irrigation (Baxter) and a pH was adjusted to 7.2 using sodium hydroxide (NaOH) or hydrochloric acid (HCl) since pH may rise during filtration. Media was sterilized by membrane filtration (0.22 μm). The solution was stored for up to 3 months at 4 °C.
4. BSA was made as a stock solution at concentration of 200 mg/ml. 20 g of BSA was dissolved in 100 ml of DPBS and pH was adjusted to 7.2 using NaOH or HCl. BSA concentrate was sterilized by membrane filtration (0.22 μm). BSA was stored for up to 6 months at 4 °C.

2.3 CD34(+) Cell Isolation

The following materials were used for CD34(+) cell isolation:

1. Histopaque (Sigma-Aldrich) was used for density gradient isolation of mononuclear cells from UCB.
2. Magnetic activated cell sorting (MACS) FCR blocking reagent (Miltenyi Biotech) and CD34 multisort microbeads (Miltenyi Biotech) were added to the mononuclear cells (100 μl per 10^8 cells).

3. Cells were separated using MACS columns (Miltenyi Biotech) according to the manufacturer's recommendations. A pre-separation filter (Miltenyi Biotech) was used to prevent blockage of columns by cell aggregates.
4. A ten times stock solution of ammonium chloride (NH_4Cl, BDH Analar, USA) was made to lyse red blood cells. 80.2 g of NH_4Cl, 8.4 g of $NaHCO_3$, and 3.7 g of disodium ethylenediaminetetraacetic acid (EDTA) were dissolved in 900 ml of water (Baxter). A pH was adjusted to 7.2 using NaOH or HCl and water (Baxter) was added to a final volume of 1000 ml. The solution was sterilized by membrane filtration (0.22 μm) and stored for up to 6 months at 4 °C. The ten times stock of NH_4Cl was diluted in cold water (Baxter) before use.

2.4 Cell Labeling and Staining

1. CFDA-SE (Bioscientific) was dissolved in dimethylsulfoxide (DMSO) at 2.8 mg/ml. 50 μl of CFDA-SE stock was stored in a sterile microtube at −20 °C overnight and then transferred to −70 °C. CFDA-SE working stock was made up just before staining cells.
2. CD34 PE antibody (Becton Dickinson Bioscience; BD) was used for CD34(+) cell expression.

2.5 Cell Counting Using Flow Cytometry

Beads for calibration representing non-fluorescent polystyrene uniform microspheres (9.62 μm diameter, Bangs Laboratories, Fishers, IN) were added into cultures or into flow cytometry tubes (BD) before analysis. The bead count was determined by gating on their distinctive low forward versus high side-light-scatter (FSC vs. SSC) properties (Fig. 1).

3 Methods

3.1 Ex Vivo HSC Expansion

3.1.1 Isolation of CD34(+) Cells from UCB

1. Transfer 10 ml of blood from the collection bag into 50 ml Falcon tubes, add 20 ml of DPBS and underlay with 15 ml of Histopaque.
2. Centrifuge at 1300 rpm 18 × *g* for 35 min.
3. Collect the buffy coat layer consisting of mononuclear cells. Red cells contaminating buffy coat layer should be lysed by addition of 50 ml of NH_4Cl followed by 15 min incubation in the dark at 4 °C.
4. Wash the cells twice with 50 ml of MACS washing buffer (DPBS containing 2 mM EDTA). Resuspend washed cells in 300 μl of MACS buffer (PBS containing 2 mM EDTA and 0.5 % BSA) at a concentration of 10^8 mononuclear cells.
5. Label cells using MACS CD34 multisort microbeads and FCR blocking reagent with 100 μl per 10^8 cells. Incubate labeled cells for 30 min at 4 °C followed by two washes with MACS buffer.

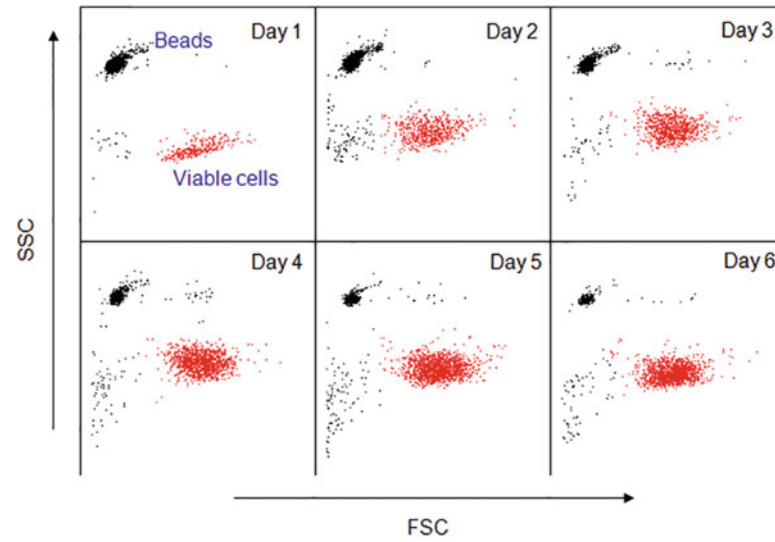

Fig. 1 Cell number measurement using flow cytometry. CFDA-SE stained and sorted CD34(+) cells were grown for 6 days in serum-free media containing SCF, TPO, G-CSF, and FL, each at 100 ng/ml. Cell counting was performed on each consecutive day. Cell number is calculated as the ratio of live cells to beads events multiplied by the number of beads added to the sample

6. Separate CD34(+) and CD34(−) cells using MACS column according to manufacturer's instructions. CD34(+) cell yield depends on the volume of UCB collection and may comprise 0.01–0.05 % of total nucleated cells (our unpublished data).

3.1.2 Analysis of CD34(+) Cell Purity

1. Transfer cells (up to 10^6 cells) to flow cytometry tube and centrifuge at 1000 rpm for 5 min.
2. Remove the supernatant with care not to disturb the cell pellet. Add 5–20 µl of anti-CD34 antibody into the tube (20 µl per 10^6 cells).
3. Incubate cells on ice for a 30 min after mixing the suspension by gentle vortexing.
4. Wash the cell suspension with DPBS containing 10 % FBS and analyze by flow cytometry (Fig. 2).

3.1.3 Freezing and Thawing Cells

Freshly isolated CD34(+) cells can be cultured immediately after isolation. Alternatively, CD34(+) cells can be frozen and then thawed prior to expansion. The procedure for cryopreservation and thawing of cells is as follows:

1. Wash cells with DPBS containing 10 % FBS.
2. Resuspend cells in 700 µl of cold media, transfer to a cryovial followed by addition of 200 µl cold FBS and 100 µl DMSO.

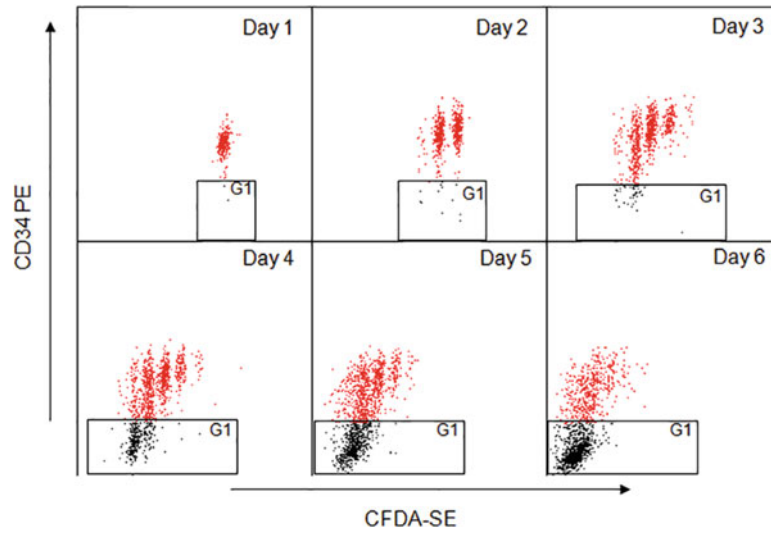

Fig. 2 The bivariate histograms of CFDA-SE/CD34/ expression in ex vivo expanded UCB CD34(+) cells. CFDA-SE stained and sorted CD34(+) cells were grown for 6 days in serum-free media containing SCF, TPO, G-CSF, and FL, each at 100 ng/ml. CFDA-SE/CD34 staining was performed daily. Isotype control (G1 gate) was used to define the CD34(+) cell region

3. Keep cells in a −70 °C freezer overnight and then transfer into liquid nitrogen.
4. Thaw cells in a 37 °C water bath before expansion. Transfer cells into a sterile centrifuge tube. Add appropriate media containing 50% FBS slowly up to 10 ml to dilute DMSO from the cells without lysing the cell pellet.
5. Wash cells by centrifugation at 1000 rpm and resuspend in appropriate media for culture.

3.1.4 CD34(+) Cell Expansion

1. Resuspend CD34(+) cells at concentration of 2×10^4 cells/ml in serum-free medium, containing SCF, G-CSF, TPO, and FL at 100 ng/ml (*see* **Note 2**).
2. Cells should be always maintained at cell density lower than 10^6cells/ml. Fresh media containing cytokines should be added when cells reach higher cell density.
3. Harvest cells on day 5–7 and count using hemocytometer. Cells can be expanded in serum-free medium for 5–7 days with some loss of CD34 expression associated with cell differentiation occurs [17].
4. Perform CD34 staining as described above.
5. Quantitate the expansion of total nucleated and CD34(+) viable cells by multiplying the proportion of viable CD34(+) cells by total cell numbers.

3.2 Cell Division Tracking

Here, we present the detailed protocol for the combined analysis of CFDA-SE and CD34 expression to quantify cell division and phenotype of ex vivo expanded CD34(+) cells.

3.2.1 CFDA-SE Staining and Sorting

1. To monitor cell divisions CFDA-SE staining of CD34(+) cells should be performed prior to cell culture.
2. Resuspend cells in 1 ml of DPBS containing 0.1% BSA after and incubate at 37 °C in a water bath for 10 min (*see* **Note 3**).
3. Add 5 μM CFDA-SE solution to an equal volume of cells to give final concentration of 2.5 μM CFDA-SE (*see* **Notes 3** and **4**). Vortex and then incubate at 37 °C for 10 min in a water bath.
4. Quench staining by adding cold FBS at three times of the original volume of the cell suspension. Centrifuge cells at 1000 rpm, 5 min followed by two further washes with PBS containing 10% FBS.
5. Resuspend cells in serum-free medium containing cytokines. Incubate cells at 37 °C overnight to remove residual CFDA-SE.
6. Centrifuge cells at 1000 rpm, 5 min, and resuspend in culture medium. Pass cells through a 40 μm cell mesh strainer (BD) to remove cell aggregates. Cells must be kept on ice until sorting is performed.
7. Prepare sterilized flow cytometry tubes (BD) for collecting cells by adding 1 ml of culture media with 1% of penicillin-streptomycin and keep them on ice. Our group routinely uses a FACSVantage (BD) for cell sorting.
8. Establish a viable sort gate using FSC vs. SSC bivariate histogram. Establish gates for CFDA-SE fluorescence by bisecting the CFDA-SE peak at the mode. Uniform labeling with CFDA-SE is essential to obtain clearly defined peaks following division. Therefore, it is useful to sort for CFSE-labeling in narrow gate [19].
9. Resuspend sorted cells in culture medium. Culture cells in serum-free medium containing SCF, G-CSF, TPO, and FL at 100 ng/ml in 37 °C incubator for 6 days.

3.2.2 CFDA-SE and CD34 Expression Analysis

Combined CFDA-SE /CD34 analysis should be performed on the day of sorting (day 1) and for the next five consecutive days in culture (*see* **Notes 5** and **6**).

1. Harvest cells and wash once in 3 ml DPBS. Centrifuge cells at 1000 rpm for 5 min.
2. Perform CD34 antibody staining.
3. Analyze CFDA-SE/CD34 by multi-parameter flow cytometry. Compensate the spectral overlap between CFDA-SE (FL1) and anti-CD34 conjugated monoclonal antibody (HPCA2-PE) (FL2) using the hardware. It is important to have appropriate

unstained and single-stained cell controls to apply the appropriate compensation. Use the same instrument settings for all of the analyses.

(a) Perform cell counts by adding known number beads to the culture or to the sample prior to collection on the flow cytometer to allow subsequent enumeration of cells in individual CFDA-SE peaks.

(b) When analyzing the data, apply appropriate electronic gates to individually view live cells, apoptotic cells, and counting beads. The ratio of bead number to cell number gives the actual cell concentration in the sample (Fig. 1). For acquisition on the flow cytometer, the logarithmic mode for the side-scatter (granularity) parameter must be used with counting beads. Collect all events so that the dataset includes beads, apoptotic cells, and live cells. Collect a sufficient number of events so that the proportion of cells in each peak can be accurately determined.

(c) The proportion of cells in the individual CFDA-SE peaks can be determined on histogram.

(d) Obtain the bivariate histograms showing CFDA-SE versus CD34 antigen expression. The typical bivariate histogram series obtained on each consecutive day following sort were obtained are shown (Fig. 2).

(e) Use corresponding isotype controls to define the CD34(+) cell region (Fig. 2)

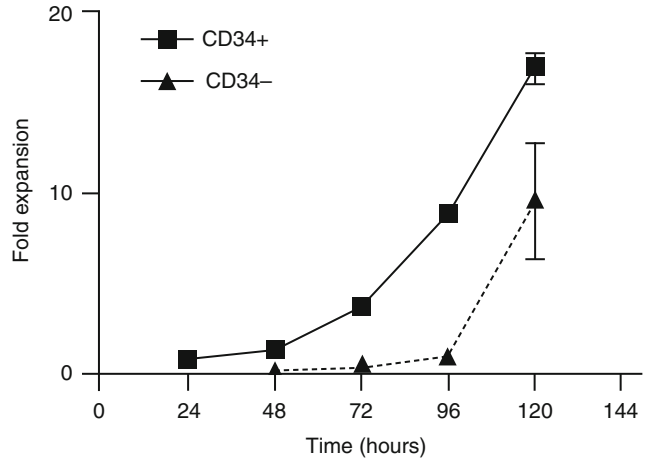

Fig. 3 Growth kinetics of UCB-derived CD34(+) and CD34(–) cells. Cells were grown for 5 days with a cytokine cocktail containing SCF, TPO, FL, and G-CSF 100 ng/ml. Cells were counted and analyzed for CD34 expression daily. Fold increase in cell number (*y*-axis) is the number of CD34(+) or CD34(–) cells divided by the input cell number at the start of culture. The *x*-axis is time in hours

(f) Calculate the cell expansion at time *t* by dividing the cell number at time *t* by the number of cells that were inoculated (Figs. 1 and 3).

4 Notes

1. UCB can only be kept for 24 h at room temperature before use following blood collection.
2. There are no ideal phenotypic markers that allow in vitro isolation of a pure and homogenous human HSC population, and there is no ultimate cytokine cocktail that allows expansion of HSC in prolonged ex vivo liquid culture. Here, we used a combination of four cytokines (SCF, FLT3L, TPO, and G-CSF) at relatively high concentration (100 ng/ml) to cultivate CD34(+) cells for up to 6 days. Ex vivo expansion of UCB-derived CD34(+) cells using this cytokine combination can be prolonged for as long as 2 weeks (group's unpublished data).
3. The cell number is one of major considerations for CFDA-SE staining protocols; at low cell numbers, the adsorption of dye per cell is higher. Commercial protocols suggest that 1×10^7 cells/ml should be used for CFDA-SE staining. However, when working with rare cells such as CD34(+) HSC, cell number is a significant consideration. Figure 4a shows that CFDA-SE and cell concentration at the time of CFDA-SE staining affects KG1a cell expansion. Higher cell numbers at the time of staining were less influenced by increase in CFDA-SE concentration compared to low cell numbers. BSA appears to act to "buffer" CFDA-SE cell adsorption, making cell number at the time of staining less of a critical parameter. When cells were stained with CFDA-SE in the absence of BSA, there were significant variations in CFDA-SE mean fluorescence. 1 mg/ml BSA was used to perform CD34(+) cell staining with CFDASE (Fig. 4b, c).

   The number of successive divisions that can be tracked depends on the CFDA-SE fluorescence intensity. Fluorescent tracking dyes produce cytotoxicity and thus delay cell growth. The titration of the CFDA-SE is required to optimize the dose of the dye. When CD34(+) cells were stained with 2.5 μM of CFDA-SE their level of expansion was close to that seen in unstained cells (data not shown). Therefore, 2.5 μM of CFDA-SE was further used for CD34(+) cell staining.
4. Labeling with CFDA-SE occurs rapidly, and it is essential that CFDA-SE be dispersed as evenly and quickly as possible so that cells are uniformly labeled.

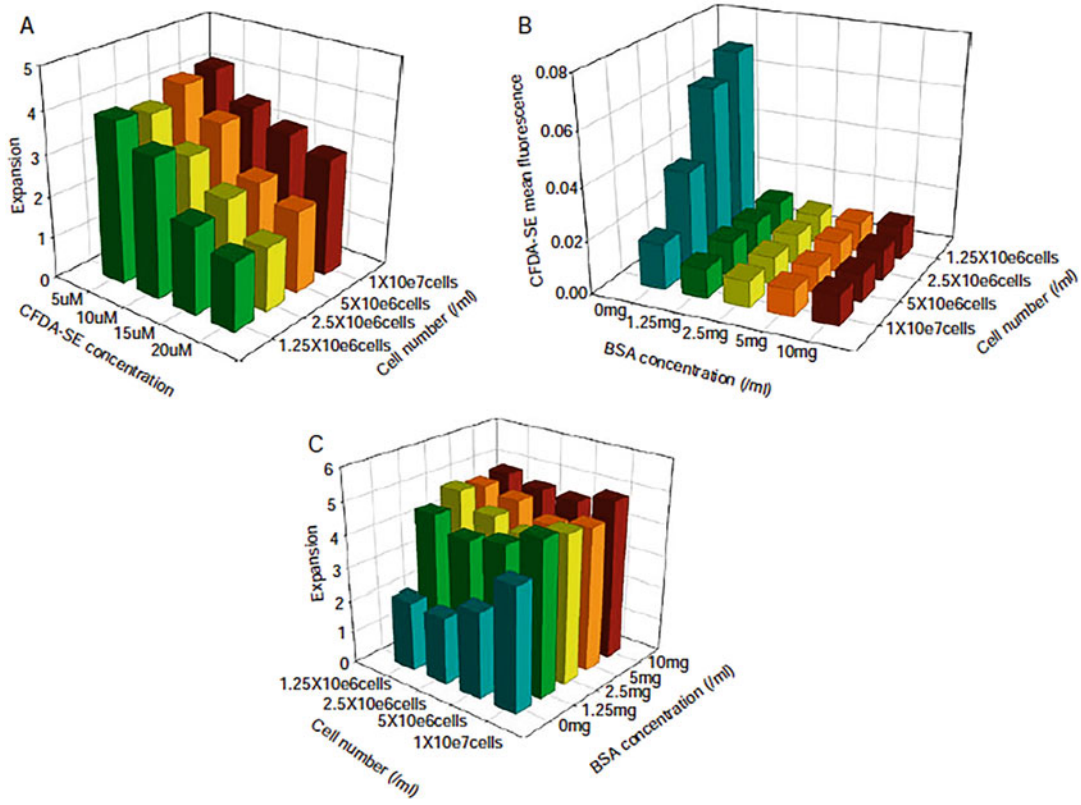

Fig. 4 Optimization of CFDA-SE and cell dose. (**a**) CFDA-SE-stained KG1a cells were cultured in IMDM with 10 % FBS. Cell numbers were counted at day 3. CFDA-SE dose vs. cell number vs. expansion is shown in three-dimensional bar graph. (**b**) Addition of BSA minimizes variations in mean CFDA-SE fluorescence in KG1a cells cultured at low cell density. Cells were stained with 5 μM of CFDA-SE on day 0. Mean CFDA-SE fluorescence is the ratio of mean fluorescence intensity measured on day 1 to day 3 in KG1a cells. (**c**) Addition of BSA protects KG1a cells cultured at low cell density from CFDA-SE-mediated cytotoxicity. 3-day expansion is shown on *y*-axis

5. Interpretation of data from time series division tracking is important to estimate specific parameters of cell growth and differentiation. Time series division tacking analysis provides accurate measurement of the distribution of cells across all generations in a relatively short time.
6. Although the assay is easy to perform, the flow cytometry read-out requires acquisition and analysis of multiple samples at regular time intervals. This makes it laborious compared with some other cell proliferation assays such as DNA analysis and BrdU incorporation. Therefore, application of division tracking should be reserved for applications where a high level of sensitivity and specificity is required to detect subtle effects on cell cycle and differentiation.

Acknowledgements

The authors thank the Australian Cord Blood Bank for providing cord blood.

References

1. Copelan EA (2006) Hematopoietic stem-cell transplantation. N Engl J Med 354:1813–1826
2. Gluckman E, Rocha V, Chastang CL (1999) Umbilical cord blood hematopoietic stem cell transplantation. Cancer Treat Res 101:79–96
3. Scheding S, Meister B, Bühring HJ, Baum CM, Mc Kearn JP, Bock T, Kanz L, Brugger W (2000) Effective ex vivo generation of granulopoietic postprogenitor cells from mobilized peripheral blood CD34(+) cells. Exp Hematol 28:460–470
4. Wingard JR, Vogelsang GB, Deeg HJ (2002) Stem cell transplantation: supportive care and long-term complications. Hematol Am Soc Hematol Educ Progr 2002:422–444
5. Haylock DN, Nilsson SK (2007) Expansion of umbilical cord blood for clinical transplantation. Curr Stem Cell Res Ther 2:324–335
6. Brunstein CG, Laughlin MJ (2010) Extending cord blood transplant to adults: dealing with problems and results overall. Semin Hematol 47:86–96
7. McNiece I, Jones R, Cagnoni P, Bearman S, Nieto Y, Shpall EJ (1999) Ex-vivo expansion of hematopoietic progenitor cells: preliminary results in breast cancer. Hematol Cell Ther 41:82–86
8. Takagi M (2005) Cell processing engineering for ex-vivo expansion of hematopoietic cells. J Biosci Bioeng 99:189–196
9. Madkaikar M, Ghosh K, Gupta M, Swaminathan S, Mohanty D (2007) *Ex vivo* expansion of umbilical cord blood stem cells using different combinations of cytokines and stromal cells. Acta Haematol 118:153–159
10. Kelly SS, Sola CB, de Lima M, Shpall E (2009) Ex vivo expansion of cord blood. Bone Marrow Transplant 44:673–681
11. Yao CL, Feng YH, Lin XZ, Chu IM, Hsieh TB, Hwang SM (2006) Characterization of serum-free ex vivo-expanded hematopoietic stem cells derived from human umbilical cord blood CD133(+) cells. Stem Cells Dev 15:70–78
12. Mobest D, Mertelsmann R, Henschler R (1998) Serum-free ex vivo expansion of CD34(+) hematopoietic progenitor cells. Biotechnol Bioeng 60:341–347
13. Heike T, Nakahata T (2002) Ex vivo expansion of hematopoietic stem cells by cytokines. Biochim Biophys Acta 1592:313–321
14. Rose-John S (2006) Designer cytokines for human hematopoietic progenitor cell expansion: impact for tissue regeneration. Handb Exp Pharmacol 174:229–247
15. McNiece IK, Almeida-Porada G, Shpall EJ, Zanjani E (2002) Ex vivo expanded cord blood cells provide rapid engraftment in fetal sheep but lack long-term engrafting potential. Exp Hematol 30:612–616
16. Peters SO, Kittler EL, Ramshaw HS, Quesenberry PJ (1995) Murine marrow cells expanded in culture with IL-3, IL-6, IL-11, and SCF acquire an engraftment defect in normal hosts. Exp Hematol 23:461–469
17. Ko KH, Odell R, Nordon RE (2007) Analysis of cell differentiation by division tracking cytometry. Cytometry A 71:773–782
18. Koeffler HP, Billing R, Lusis AJ, Sparkes R, Golde DW (1980) An undifferentiated variant derived from the human acute myelogenous leukemia cell line (KG-1). Blood 56:265–273
19. Nordon RE, Nakamura M, Ramirez C, Odell R (1999) Analysis of growth kinetics by division tracking. Immunol Cell Biol 77:523–529

Part IX

Clinical Study

Chapter 20

Intracellular Flow Cytometry Improvements in Clinical Studies

Julie Demaret, Morgane Gossez, Fabienne Venet, and Guillaume Monneret

Abstract

Flow cytometry has become a basic of biological research and clinical diagnostics, and its application has been crucial to numerous advances in immunology and cell biology. However, several issues remain when considering intracellular stainings, especially in the context of a daily routine use and in multicenter clinical research protocols including large cohorts of patients. The requirements for multiple protocol steps are not only time-consuming but also frequently associated with high cell loss and nonspecific binding or reduced fluorescence. These drawbacks make standardized intracellular flow cytometry use in multicenter studies struggling. As a consequence, intracellular flow cytometry has mostly remained a tool for experimental and clinical research. In the current chapter, we will complete flow cytometry protocols described in the previous edition by presenting novel intracellular protocols usable in clinic. These present with many advantages including shorter time-to-results, one-step whole blood procedures, lyse-no-wash-no-centrifuge protocols, improved staining quality, and lyophilized coated reagents in ready-to-use tubes. This opens novel perspectives for standardization and feasibility in clinical studies, for drug efficacy monitoring and for patients' stratification within a context of personalized medicine. Here, we present illustrative examples taken from septic patients' immunomonitoring. We consider the evaluation of myeloperoxidase and lactoferrin expressions in neutrophils, FOXP3 lymphocyte expression, and STAT5 phosphorylation in lymphocyte subsets.

Key words Intracellular flow cytometry, Sepsis, Neutrophil, Myeloperoxidase, Lactoferrin, FOXP3, Regulatory T cells, STAT5

1 Introduction

1.1 Flow Cytometry for Clinics

Flow cytometry represents one inevitable method for cell study and identification through cell analyses and sorting according to their distinguishing characteristics. Such single cell technique has helped to reveal much about cells function and position in the immune system [1]. It has evolved over the past 50 years from a niche laboratory technique to a routine tool used by clinical pathologists and immunologists for diagnosis and monitoring of patients notably with cancer and immune deficiencies [2]. However,

Gaspar Banfalvi (ed.), *Cell Cycle Synchronization: Methods and Protocols*, Methods in Molecular Biology, vol. 1524,
DOI 10.1007/978-1-4939-6603-5_20,

several issues exist when considering flow cytometric intracellular stainings (ICS), especially in the context of a daily routine use and in clinical research protocols including large cohorts of patients for whom samples need to be processed immediately [3]. More specifically, this technique is time-consuming due to permeabilization and multiple washing steps. In addition, results are usually poorly reproducible and hardly standardizable. This rendered intracellular flow cytometry barely usable on a routine basis. Novel protocols have been recently developed to perform faster and more convenient ICS protocols in order to meet criteria of improved standardization. In particular, a promising domain of application for ICS is functional testing which remains, immunologically speaking, a gold standard approach.

Here, we extend our previous report on standardized flow cytometry cell surface markers for critically ill patients monitoring (HLA-DR on circulating monocytes, percentage of CD4+CD25+ regulatory T cells and CD64 expression on neutrophils in ICU patients [4]). In the current chapter, we will describe novel ICS protocols (including functional testing) and will provide clinical examples in septic patients illustrating their potential as stratification tools in immunostimulating clinical trials.

1.2 Sepsis Pathophysiology

Septic syndromes are still associated with a high risk of death in ICU. Indeed, a recent epidemiological study including more than 25,000 patients in the USA and in Europe showed that overall hospital mortality from severe sepsis or septic shock is still over 30% [5]. In particular, over the past 30 years, the prognosis for septic patients has improved substantially, due to advances in the supportive care delivered to critically ill patients. Immune response after septic shock associates a major inflammatory response leading to organ dysfunction and shock and the development of immune dysfunctions affecting both innate and adaptive immune responses. Sepsis directly or indirectly impairs the function of almost all types of immune cells. Importantly, the intensity and duration of sepsis-induced immune alterations have been associated with increased risk of deleterious events in patients [6, 7].

There is a recognized need for markers that can rapidly (1) identify the immunological status of the patient and (2) the immune response to therapy [8]. As an example, many studies have described altered monocyte phenotype and functions in sepsis. In particular, decreased expression of HLA-DR (mHLA-DR) on circulating monocytes has been proposed as a surrogate marker of immune failure [8, 9] and is now used for patient stratification in clinical trial (NCT02361528) [10]. Likewise, T lymphocyte anergy has been shown to be a hallmark of sepsis-induced immune dysfunctions and leads the way for future IL-7 trials to rejuvenate T cells [11, 12].

This new chapter will focus on biomarkers measurable by intracellular flow cytometry: the expressions of myeloperoxidase and lactoferrin in neutrophils' granules, FOXP3 lymphocyte expression, and STAT5 phosphorylation in various lymphocyte subsets.

1.3 Marked Neutrophil Alterations in Sepsis

Neutrophils (PNN) are crucial components of the innate immune response and the first line of defense against infection. They also play a central role in initiation of adaptive immune responses by secreting cytokines [13]. Interestingly, an immunosuppressive neutrophil subset has recently been reported in the blood of volunteers challenged with LPS [14]. Furthermore, Guérin et al. described a $CD10^{-}CD16^{-}$ subset of immature neutrophils associated with mortality in septic patients, and presenting some immunosuppressive properties [15]. In agreement, we recently observed that circulating neutrophils present with phenotypic, functional, and morphologic alterations a few days after sepsis onset [16]. Indeed, activation capacities (in response to fMLP, IL-8, and GM-CSF), chemotaxis (functional test and chemokine receptor expressions), phagocytosis, and oxidative burst were found to be altered. In addition, we reported a decrease in myeloperoxidase and lactoferrin intracellular expressions a few days after sepsis onset. Most importantly, of these parameters, we observed that a diminished myeloperoxidase (MPO) expression appeared as the best predictor to identify a group of patients at higher risk of death [16].

Myeloperoxidase and lactoferrin, both contained respectively in azurophilic and secondary neutrophil granules, are essential components of PNN function. Lactoferrin possesses antimicrobial properties with the potential to prevent infections in young children. Several clinical trials involving lactoferrin for prevention of neonatal sepsis have been carried out [17]. MPO is a major player in oxidant metabolism as it reacts with hydrogen peroxide and chloride ions to generate hypochlorous acid, the most potent antimicrobial oxidant [18]. MPO activity is also a plausible mechanism for neutrophil extracellular traps (NETs)—a fibrous network released from neutrophils that can trap microorganisms [19]—antimicrobial activity and could be detrimental by generating reactive oxidants in severe inflammatory conditions, where NETs are produced [20]. Myeloperoxidase measurement is usually performed using activity assay kits, assessing peroxidase activity in a sample, or ELISA kits, in order to measure MPO expression in plasma and tissue samples. Another approach relies on ICS and flow cytometry and novel protocols have been developed to perform ICS in whole blood and in one step (including permeabilization, intra and surface stainings).

1.4 Regulatory T Cells: FOXP3 Expression

Regulatory T cells are an important $CD4^{+}$ T-cell subset involved in immune regulation. Treg percentages have been shown to differ in numerous disease states. Indeed, accumulated evidence

suggests the essential functions of Treg in the pathophysiology of many clinical conditions such as autoimmune diseases [21], transplantations [22], severe septic shock [23], cancer [24], HIV infection [25], and in the development and maintenance of immunologic tolerance [26]. More specifically, regulatory T lymphocytes may play a role in the control of immune responses and are affected by injury and sepsis [27]. This may be related to their capacity to interact with components of the innate and adaptive immune systems. The analysis of regulatory T cells is also becoming an increasingly important consideration in the development of novel immunotherapeutic strategies. Accurate quantification of Treg during treatment protocols is crucial, particularly where the therapeutic strategy is targeting Treg. However, very few studies have been conducted in large prospective clinical cohorts. This could be partly explained as Treg can only be precisely identified by ICS flow cytometry using forkhead box protein 3 (FOXP3) staining, the key transcriptional factor for Treg [28]. The requirement for permeabilization is not only time-consuming; it is also highly susceptible to cell loss, reduced fluorescence of antibody conjugates included in the staining mix, and therefore inaccurate quantification. Even if other phenotypes (such as $CD4^+CD25^+$ or $CD4^+CD25^+CD127^-$) are known to be good surrogate identification strategies for Treg [29], FOXP3 remains to date the only marker to appropriately identify those cells. We recently assessed the robustness of a new protocol allowing permeabilization and staining in one-step in daily routine conditions in clinical samples with FOXP3 [30]. By comparing a one-step ICS procedure with a reference protocol, we obtained a strong correlation between percentages of $FOXP3^+$ Treg according to difference phenotypic identification strategies. Moreover, with a better staining quality, a shorter realization time and no isotype control requirement, this one-step procedure appears adequate for a daily routine use and in whole blood prospective clinical studies.

1.5 STAT5 Phosphorylation

Signal Transducer and Activator of Transcription (STAT) family is composed of seven related proteins. STATs are latent transcription factors that mainly reside in the cytoplasm in an inactive state. STATs become activated by phosphorylation on a critical tyrosine residue. Many upstream kinases can activate STATs, though the most common is the Jak family of kinases. Additional receptor and non-receptor tyrosine kinases also have the ability to phosphorylate STATs. Tyrosine phosphorylation allows for STATs to form active dimers [31], which can be homodimers or heterodimers with another STAT family member [32]. This dimer conformation triggers translocation to the nucleus. STATs then recruit additional cofactors to modulate expression of key target genes involved in growth, survival, and differentiation. Assaying these

phosphorylation networks within the cellular context could therefore contribute to the mechanistic understanding of kinase activities in normal and disease states as well as assessing the efficacy of targeted agents. But the expansion of phospho-specific intracellular detection requires the improvement of reagents and tailored protocols. The development of phospho-specific antibodies against unique epitopes of individual proteins has been a key step that enabled intracellular phosphorylation analysis by flow cytometry to become useful for functional studies. Multiparametric staining, using both surface and intracellular stains, allows for the study of discrete biochemical events in readily discernible subsets [33]. However, again, the need of permeabilization is time-consuming and results are usually poorly reproducible and hardly standardizable. By using a novel flow cytometry procedure of intracellular signaling pathway staining, we were able to detect STAT5 phosphorylation with a one-step whole blood method (simultaneous permeabilization and staining) [34]. As an example, we combined intracellular FOXP3 staining [30] to specifically measure STAT5 phosphorylation in Treg ($CD4^+FOXP3^+$) and $CD4^+FOXP3^-$ cells in response to cytokines. Interleukin (IL)-2 and IL-7 are two cytokines indispensable for growth, proliferation, and differentiation of CD4+ T cells [35]. Recombinant (r) IL-2 is particularly assessed in autoimmune diseases [36]. In this context, low doses of IL-2 are administered so as to increase the number of Treg. In contrast, IL-7 is currently assessed in various clinical conditions with the objective of stimulating/rejuvenating $CD4^+FOXP3^-$ lymphocytes [11]. We used increasing doses of human (h)IL-2 versus recombinant human (rh)IL-7 to investigate STAT5 phosphorylation. This novel functional testing in fresh whole blood was completed in about 70 min [34]. To our knowledge, we confirm for the first time, in human whole blood, that low dose of hIL-2 preferentially activated Treg whereas low dose of rhIL-7 preferentially induced CD4+FOXP3- activation (Fig. 1). This work also illustrated the interest of this flow cytometry approach for monitoring pharmacological responses to drugs in daily clinical practice. In another study, we then assessed the ex vivo responses of septic shock patients' T-cell subsets to increasing doses of rhIL-7 by measuring intracellular pSTAT5 by flow cytometry [37]. We have reported a differential rhIL-7-induced response of T cells between surviving and non-surviving patients. In lieu of validation in a larger cohort of patients, this report indicated that such results, obtained in 70 min, may serve to stratify and monitor rhIL-7 therapy efficacy in future clinical studies.

1.6 Using Intracellular Flow Cytometry in Larger Clinical Studies

Based on these new protocols for ICS, standardization of intracellular flow cytometry seems already well underway. By shortening the realization time (<90 min) and guaranteeing staining quality, these one-step procedures available on fresh whole

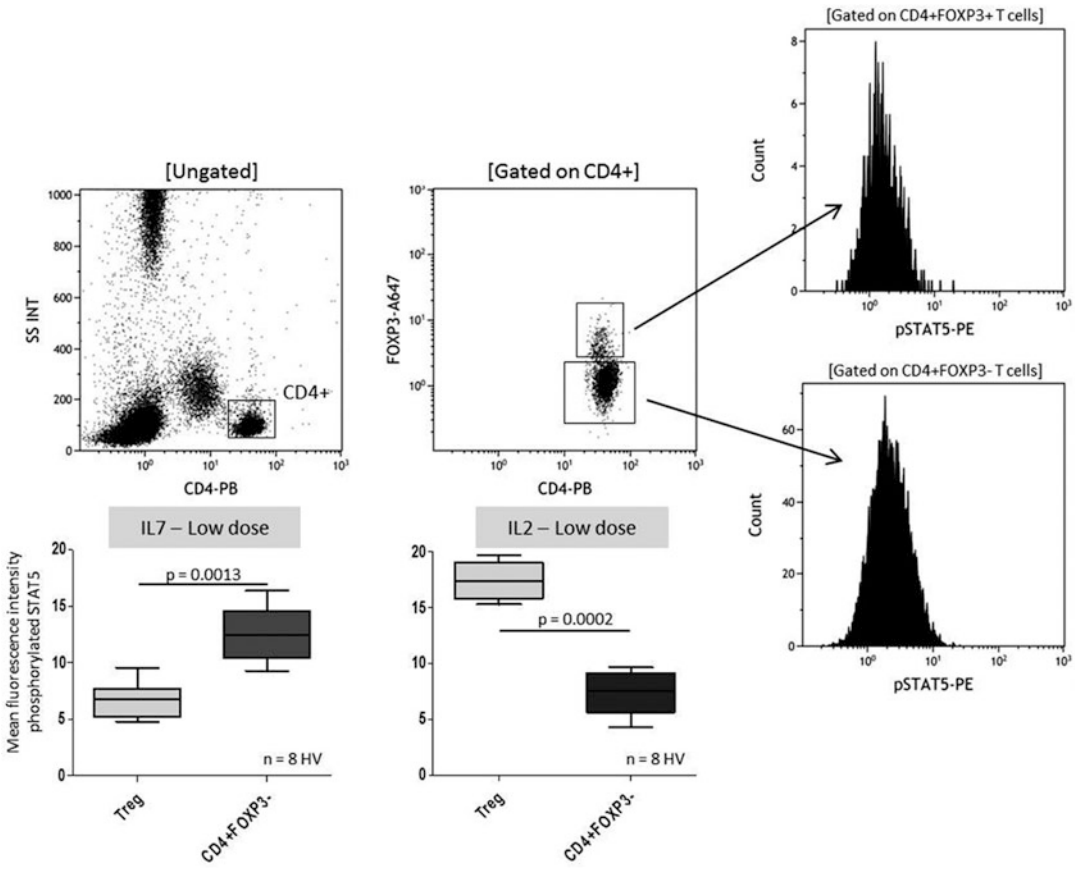

Fig. 1 Gating strategy for STAT5 phosphorylation on different T-cell subsets and response to low dose of cytokines. CD4+ were first gated based on SSC versus CD4 expression on a biparametric histogram (**a**). Regulatory T cells (Treg) and $CD4^+FOXP3^-$ were then identified among selected CD4+ cells depending on FOXP3 expression (**b**). The mean fluorescence intensity (MFI) of phosphorylated STAT5 (pSTAT5) was reported for each population (**c**, **d**). Box plots representing MFI of pSTAT5 after stimulation with low dose of IL-7 (**e**) and low dose of IL-2 (**f**) for Treg (*light grey*) and $CD4^+FOXP3^-$ lymphocytes (*dark grey*) for eight healthy controls. As expected, low dose of IL-7 preferentially activates effector T lymphocytes whereas low dose of IL-2 preferentially activates Treg. The nonparametric Mann–Whitney *U* test was used to compare the results between subsets

blood may represent, upon validation in large cohort of patients, a major improvement in study of intracellular molecules by flow cytometry in clinical studies. Furthermore, these improved protocols open various perspectives. Functional tests with phospho-epitopes have demonstrated an undeniable interest. They pave the way to other fields, in particular, intracellular cytokine staining. More generally, beyond ICU patients, various clinical contexts such as cancer therapy or immunotherapy should benefit from these new protocols for stratifying and monitoring patients.

2 Materials

2.1 Solutions

1. PerFix-nc (no centrifuge assay kit—Beckman Coulter, Brea, CA) is composed of three reagents: Buffer 1 (fixative reagent containing formaldehyde), Buffer 2 (permeabilizing reagent containing proclin 300), and Buffer 3 (final 10× solution, to be diluted to 1× solution in distilled water, containing formaldehyde) (**Note 1**).
2. PerFix EXPOSE (Phospho-Epitopes Exposure kit—Beckman Coulter) is composed of four reagents: Buffer 1 (fixative reagent containing formaldehyde), Buffer 2 (permeabilizing reagent containing proclin 300, sodium perchlorate, and detergent), Buffer 3 (staining reagent containing proclin 300, sodium perchlorate, and sodium azide), and Buffer 4 (final 20× solution, to be diluted to 1× solution in distilled water, containing formaldehyde and detergent).
3. PBS: dissolve 8.0 g of NaCl, 0.2 g of KCl, 1.15 g of Na_2HPO_4, and 0.2 g of KH_2PO_4 in 1 l of distilled water (with adjusted pH at 7.4). This solution may be stored at 4 °C up to a month.

2.2 Cytokines

1. Human IL-2 (hIL-2—Roche Diagnostics, Indianapolis, IN) from 0.01 to 100 U/ml.
2. Recombinant human IL-7 (rhIL-7—R&D systems, Minneapolis, MN) from 0.001 to 10 ng/ml.

2.3 Antibodies

1. Fluorescein isothiocyanate (FITC)-Phycoerythrin (PE)-labeled anti-myeloperoxidase (MPO—clone CLB-MPO-1) and anti-lactoferrin (clone CLB 13.17) (Beckman Coulter).
2. PE-Texas Red (ECD)-labeled anti-CD62L (clone DREG56) (Beckman Coulter).
3. PE-Cyanine 7 (PC7)-labeled anti-CD10 (clone ALB1) (Beckman Coulter).
4. Allophycocyanin-Alexa fluor 750 (AA750)-labeled anti-CD11b (clone Bearl) (Beckman Coulter).
5. Pacific Blue (PB)-labeled anti-CD16 (clone 3G8) (Beckman Coulter).
6. Krome Orange (KrO)-labeled anti-CD14 (clone RMO52) (Beckman Coulter).
7. PE-labeled anti-CD25 (clone B1.49.9) (Beckman Coulter).
8. PC7-labeled anti-CD127 (clone R34.34) (Beckman Coulter).
9. Alexa Fluor 647 (AF647)-labeled anti-FOXP3 (clone 259D) (BioLegend, San Diego, CA).
10. PB-labeled anti-CD4 (clone 13B8.2) (Beckman Coulter).
11. PE-labeled anti-phosphorylated STAT5 (Beckman Coulter).

3 Methods

3.1 Neutrophils: MPO and Lactoferrin Expressions

1. Collect samples of peripheral blood in EDTA anticoagulant tubes.
2. Mix 50 µl of whole blood with 5 µl of ECD-labeled anti CD62L, vortex and incubate 2 min at room temperature.
3. Add 20 µl of PerFix-nc Buffer 1 (fixative reagent).
4. Vortex immediately and incubate at room temperature for 15 min in the dark.
5. During these 15 min, mix in a new tube 300 µl of PerFix-nc Buffer 2 (permeabilizing reagent) with 10 µl of FITC-PE-labeled anti-myeloperoxidase and lactoferrin, 2.5 µl of PC7-labeled anti-CD10, 2.5 µl of AA750-labeled anti-CD11b, 5 µl of PB-labeled anti-CD16, and 5 µl of KrO-labeled anti-CD14. Vortex and keep it at room temperature, in the dark.
6. At the end of the 15 min, mix 325 µl of the second tube with the tube containing the blood.
7. Vortex and incubate at room temperature for 35 min in the dark.
8. Add 3 ml of PerFix-nc Buffer 3 1× (previously dilute PerFix-nc Buffer 3 10× to 1× in distilled water), vortex.
9. Flow cytometry gating strategy: Neutrophils are identified on a FSC/SSC histogram and a CD14/SSC dot-plot is used to exclude monocytes (Fig. 2). MPO, lactoferrin, CD62L, CD11b, CD10, and CD16 are then measured on the surface of neutrophils. Results are expressed as mean fluorescence intensity (MFI) related to the entire neutrophil population. Percentages of cells' subsets are also reported regarding CD10 and CD16 expressions (*see* **Note 2**).

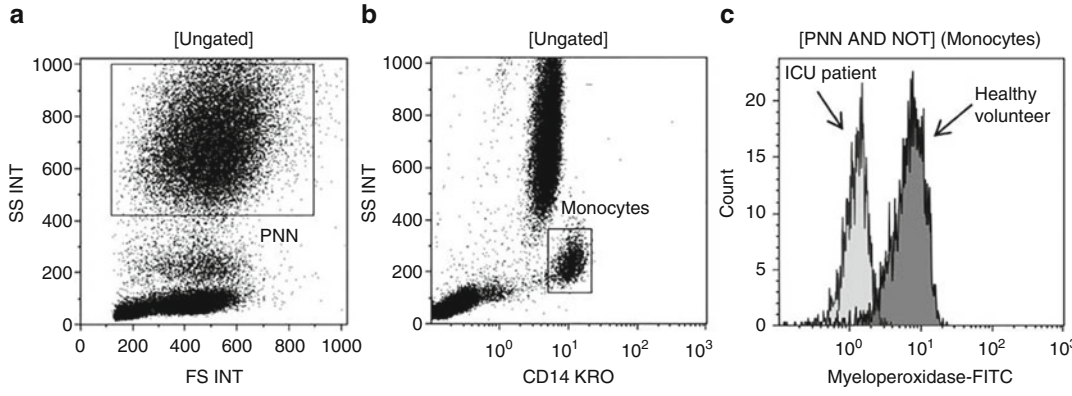

Fig. 2 Gating strategy for neutrophils. Neutrophils (PNN) are first identified on a FSC/SSC histogram (**a**) and a CD14/SSC dot-plot is used to exclude monocytes (**b**). (**c**) represents an overlay of myeloperoxidase expression for an Intensive Care Unit (ICU) patient and a healthy control gated on [PNN AND NOT (Monocytes)]

3.2 Regulatory T Cells: FOXP3 Expression

1. Collect samples of peripheral blood in EDTA anticoagulant tubes.
2. Mix 50 µl of whole blood with 5 µl of PerFix-nc Buffer 1 (fixative reagent) (*see* **Note 3**).
3. Vortex immediately and incubate at room temperature for 15 min in the dark.
4. During these 15 min, mix in a new tube 300 µl of PerFix-nc Buffer 2 (permeabilizing reagent) with 10 µl of PE-labeled anti-CD25, 10 µl of PC7-labeled anti-CD127, 10 µl of AF647-labeled anti-FOXP3, and 5 µl of PB-labeled anti-CD4. Vortex and keep it at room temperature, in the dark.
5. At the end of the 15 min, mix 335 µl of the second tube with the tube containing the blood.
6. Vortex and incubate at room temperature for 60 min in the dark.
7. Add 3 ml of PBS. Vortex and incubate at room temperature for 5 min in the dark.
8. Centrifuge for 5 min at 500 × *g* at 10 °C.
9. Discard the supernatant and resuspend the pellet in 3 ml of PerFix-nc Buffer 3 1× (previously dilute PerFix-nc Buffer 3 10× to 1× in distilled water), vortex, and centrifuge for 5 min at 500 × *g* at 10 °C.
10. Discard the supernatant and resuspend the pellet in 500 µl of PerFix-nc Buffer 3 1×.
11. Flow cytometry gating strategy: $CD4^+$ T cells are first gated on a SSC/CD4 bi-parametric dot-plot. The $CD25^+CD127^{low}$ gate is then set in order to encompass an obviously distinct population among $CD4^+$. $CD4^+FOXP3^+$ lymphocytes are also selected on a FOXP3/CD4 histogram (Fig. 3). Results are expressed as percentages of $CD25^+CD127^{low}$ and $CD4^+FOXP3^+$ cells among $CD4^+$.

3.3 Lymphocytes: STAT5 Phosphorylation

1. Collect samples of peripheral blood in EDTA anticoagulant tubes.
2. First, stimulate blood samples (100 µl of whole blood) with increasing hIL-2 or rhIL-7 concentrations (vortex immediately after adding the cytokine) at 37 °C in a water bath for 10 min. Incubate an unstimulated blood sample at the same time.
3. Add 5 µl of PB-labeled anti-CD4, vortex and incubate at 37 °C in a water bath for 5 min.
4. Mix 50 µl of PerFix EXPOSE Buffer 1 (fixative reagent) in each tube, vortex and incubate at room temperature for 10 min in the dark.
5. Add 1 ml of PerFix EXPOSE Buffer 2 (permeabilizing reagent), vortex and incubate at 37 °C in a water bath for 5 min.
6. Centrifuge for 5 min at 300 × *g* at 10 °C and discard carefully the supernatant.

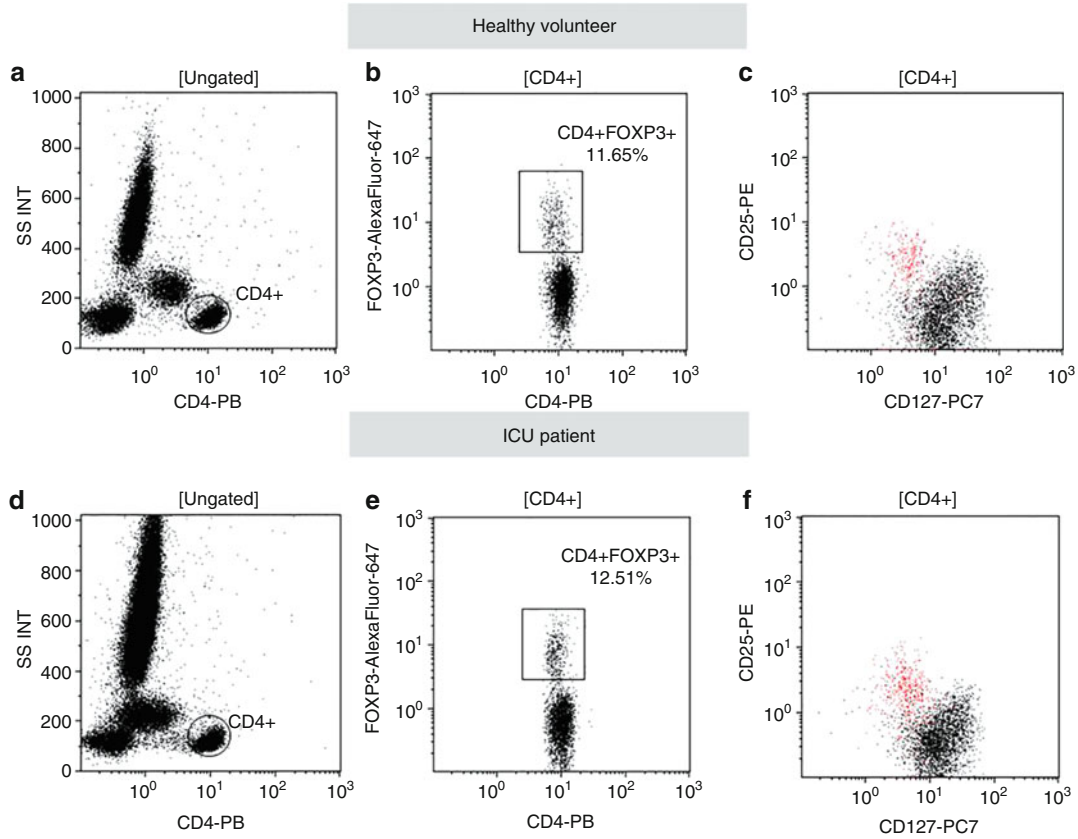

Fig. 3 Treg measurement by flow cytometry**.** SSC versus CD4 dot plots allow the gating of CD4+ lymphocytes for representative examples of healthy volunteer and ICU patient (**a**, **d**). Gated on CD4+ lymphocytes, regulatory T cells are measured as $CD4^+FOXP3^+$ cells (**b**, **e**). On (**c**) and (**f**) (gated on CD4+), *red* colored cells represent $CD4^+FOXP3^+$ cells among $CD25^+CD127^-$ lymphocytes

7. Resuspend the pellet in a mix of 100 µl of PerFix EXPOSE Buffer 2 (staining reagent), 5 µl of PE-labeled anti-STAT5 and 5 µl of AF647-labeled anti-FOXP3 that can be previously reconstituted (*see* **Notes 3** and **4**).
8. Vortex and incubate at room temperature for 30 min in the dark.
9. Add 3 ml of PerFix-nc Buffer 4 1× (previously dilute PerFix-nc Buffer 4 20× to 1× in distilled water), vortex.
10. Centrifuge for 5 min at 300×*g* at 10 °C and discard the supernatant. Resuspend the pellet in 500 µl of PerFix-nc Buffer 4 1× (*see* **Notes 5** and **6**).
11. Flow cytometry gating strategy: CD4+ lymphocytes are first gated based on SSC/CD4 biparametric histogram. Regulatory T lymphocytes (Treg) and $CD4^+FOXP3^-$ T cells are then identified among selected $CD4^+$ cells depending on FOXP3 expression. The mean fluorescence intensity of phosphorylated STAT5 is reported for each population (Fig. 1).

4 Notes

1. There is a whole-blood protocol given by the manufacturer with PerFix-nc reagents, as follows:
   - Mix 50 µl of whole blood with 5 µl of PerFix-nc Buffer 1 (fixative reagent).
   - Vortex immediately and incubate at room temperature for 15 min in the dark.
   - Vortex again the fixed blood and add 300 µl of PerFix-nc Buffer 2 (permeabilizing reagent) to each tube. Vortex immediately.
   - Add immediately to each tube the fluorochromes-conjugated antibodies against intracellular epitopes and surface molecules (alternatively, the antibodies can be pre-mixed into the PerFix-nc Buffer 2 and added altogether at the end of the fixation step).
   - Vortex immediately and incubate at room temperature for 15–30 min in the dark.
   - Add 3 ml of PerFix-nc Buffer 3 1× (prepared from the 10× concentrated PerFix-nc Buffer 3 in distilled water) to each tube, vortex immediately.
   - The sample is now ready for analysis on a flow cytometer.

   This protocol should be optimized according to the type of cells analyzed and the antibodies used (extracellular and intracellular staining). That is what we have performed for MPO and lactoferrin expressions in neutrophils and FOXP3 in Treg. Feel free to adapt at your convenience times of incubation or volumes of reagents to optimize your experiment.
2. Be careful about the different volumes of PerFix-nc Buffer 1 (fixative reagent) between the procedure for measuring MPO and lactoferrin expression in neutrophils, which is 20 µl, and the protocol for intracellular staining of FOXP3 (i.e., 5 µl).
3. Red blood cell lysis can be problematic with PerFix-nc reagents. Therefore, the usual discriminant threshold used for the analyses, based on Forward Scatter Characteristics, might not exclude all these cells. Thus, in such cases, it can be settled on a fluorochrome channel.
4. Surprisingly, to study STAT5 phosphorylation with PerFix EXPOSE method and reagents, peripheral blood can be collected in sampling tubes containing EDTA.
5. In PerFix EXPOSE protocol to explore STAT5 phosphorylation in T lymphocytes subsets, in order to obtain a better staining quality, it is preferable to add CD4-PB antibody before the one-step of intracellular/extracellular staining and

permeabilization. We chose to split the stimulation with hIL-2 and rhIL-7 and add this antibody 5 min before the end of the stimulation.

6. In PerFix EXPOSE protocol, it is very important to discard carefully the supernatant after incubation with PerFix EXPOSE Buffer 2 in order to stop red blood cell lysis that can continue insidiously otherwise.

References

1. Maecker HT, McCoy JP, Nussenblatt R (2012) Standardizing immunophenotyping for the human immunology project. Nat Rev Immunol 12:191–200
2. Robinson JP, Roederer M (2015) History of science. Flow cytometry strikes gold. Science 350:739–740
3. Perez OD, Mitchell D, Campos R, Gao GJ, Li L, Nolan GP (2005) Multiparameter analysis of intracellular phosphoepitopes in immunophenotyped cell populations by flow cytometry. Curr Protoc Cytom Chapter 6:Unit 6 20
4. Venet F, Guignant C, Monneret G (2011) Flow cytometry developments and perspectives in clinical studies: examples in ICU patients. Methods Mol Biol 761:261–275
5. Levy MM, Artigas A, Phillips GS, Rhodes A, Beale R, Osborn T, Vincent JL, Townsend S, Lemeshow S, Dellinger RP (2012) Outcomes of the surviving sepsis campaign in intensive care units in the USA and Europe: a prospective cohort study. Lancet Infect Dis 12:919–924
6. Hotchkiss RS, Monneret G, Payen D (2013) Immunosuppression in sepsis: a novel understanding of the disorder and a new therapeutic approach. Lancet Infect Dis 13:260–268
7. Hotchkiss RS, Monneret G, Payen D (2013) Sepsis-induced immunosuppression: from cellular dysfunctions to immunotherapy. Nat Rev Immunol 13:862–874
8. Venet F, Lukaszewicz AC, Payen D, Hotchkiss R, Monneret G (2013) Monitoring the immune response in sepsis: a rational approach to administration of immunoadjuvant therapies. Curr Opin Immunol 25:477–483
9. Monneret G, Venet F, Pachot A, Lepape A (2008) Monitoring immune dysfunctions in the septic patient: a new skin for the old ceremony. Mol Med 14:64–78
10. Meisel C, Schefold JC, Pschowski R, Baumann T, Hetzger K, Gregor J, Weber-Carstens S, Hasper D, Keh D, Zuckermann H, Reinke P, Volk HD (2009) Granulocyte-macrophage colony-stimulating factor to reverse sepsis -associated immunosuppression: a double-blind, randomized, placebo-controlled multicenter trial. Am J Respir Crit Care Med 180:640–648
11. Mackall CL, Fry TJ, Gress RE (2011) Harnessing the biology of IL-7 for therapeutic application. Nat Rev Immunol 11:330–342
12. Venet F, Foray AP, Villars-Mechin A, Malcus C, Poitevin-Later F, Lepape A, Monneret G (2012) IL-7 restores lymphocyte functions in septic patients. J Immunol 189:5073–5081
13. Amulic B, Cazalet C, Hayes GL, Metzler KD, Zychlinsky A (2012) Neutrophil function: from mechanisms to disease. Annu Rev Immunol 30:459–489
14. Pillay J, Kamp VM, van Hoffen E, Visser T, Tak T, Lammers JW, Ulfman LH, Leenen LP, Pickkers P, Koenderman L (2012) A subset of neutrophils in human systemic inflammation inhibits T cell responses through Mac-1. J Clin Invest 122:327–336
15. Guerin E, Orabona M, Raquil MA, Giraudeau B, Bellier R, Gibot S, Bene MC, Lacombe F, Droin N, Solary E, Vignon P, Feuillard J, Francois B (2014) Circulating immature granulocytes with T-cell killing functions predict sepsis deterioration*. Crit Care Med 42:2007–2018
16. Demaret J, Venet F, Friggeri A, Cazalis MA, Plassais J, Jallades L, Malcus C, Poitevin-Later F, Textoris J, Lepape A, Monneret G (2015) Marked alterations of neutrophil functions during sepsis-induced immunosuppression. J Leukoc Biol 98(6):1081–1090
17. Turin CG, Zea-Vera A, Pezo A, Cruz K, Zegarra J, Bellomo S, Cam L, Llanos R, Castaneda A, Tucto L, Ochoa TJ (2014) Lactoferrin for prevention of neonatal sepsis. Biometals 27:1007–1016
18. Klebanoff SJ (2005) Myeloperoxidase: friend and foe. J Leukoc Biol 77:598–625
19. Brinkmann V, Reichard U, Goosmann C, Fauler B, Uhlemann Y, Weiss DS, Weinrauch Y, Zychlinsky A (2004) Neutrophil extracellular traps kill bacteria. Science 303:1532–1535

20. Parker H, Albrett AM, Kettle AJ, Winterbourn CC (2013) Myeloperoxidase associated with neutrophil extracellular traps is active and mediates bacterial killing in the presence of hydrogen peroxide. J Leukoc Biol 91:369–376
21. Baecher-Allan C, Hafler DA (2006) Human regulatory T cells and their role in autoimmune disease. Immunol Rev 212:203–216
22. Wood KJ, Bushell A, Hester J (2012) Regulatory immune cells in transplantation. Nat Rev Immunol 12:417–430
23. Monneret G, Venet F (2010) Additional bad news from regulatory T cells in sepsis. Crit Care 14:453
24. Erfani N, Mehrabadi SM, Ghayumi MA, Haghshenas MR, Mojtahedi Z, Ghaderi A, Amani D (2012) Increase of regulatory T cells in metastatic stage and CTLA-4 over expression in lymphocytes of patients with non-small cell lung cancer (NSCLC). Lung Cancer 77:306–311
25. Elahi S, Dinges WL, Lejarcegui N, Laing KJ, Collier AC, Koelle DM, McElrath MJ, Horton H (2011) Protective HIV-specific CD8+ T cells evade Treg cell suppression. Nat Med 17:989–995
26. Fukaya T, Takagi H, Sato Y, Sato K, Eizumi K, Taya H, Shin T, Chen L, Dong C, Azuma M, Yagita H, Malissen B (2010) Crucial roles of B7-H1 and B7-DC expressed on mesenteric lymph node dendritic cells in the generation of antigen-specific CD4+Foxp3+ regulatory T cells in the establishment of oral tolerance. Blood 116:2266–2276
27. Venet F, Chung CS, Kherouf H, Geeraert A, Malcus C, Poitevin F, Bohe J, Lepape A, Ayala A, Monneret G (2009) Increased circulating regulatory T cells (CD4(+)CD25 (+)CD127 (-)) contribute to lymphocyte anergy in septic shock patients. Intensive Care Med 35:678–686
28. Sakaguchi S, Miyara M, Costantino CM, Hafler DA (2010) FOXP3+ regulatory T cells in the human immune system. Nat Rev Immunol 10:490–500
29. Saison J, Demaret J, Venet F, Chidiac C, Malcus C, Poitevin-Later F, Tardy JC, Ferry T, Monneret G (2013) CD4+CD25+CD127-assessment as a surrogate phenotype for FOXP3+ regulatory T cells in HIV-1 infected viremic and aviremic subjects. Cytometry B Clin Cytom 84:50–54
30. Demaret J, Saison J, Venet F, Malcus C, Poitevin-Later F, Lepape A, Ferry T, Monneret G (2013) Assessment of a novel flow cytometry technique of one-step intracellular staining: example of FOXP3 in clinical samples. Cytometry B Clin Cytom 84:187–193
31. Kretzschmar AK, Dinger MC, Henze C, Brocke-Heidrich K, Horn F (2004) Analysis of Stat3 (signal transducer and activator of transcription 3) dimerization by fluorescence resonance energy transfer in living cells. Biochem J 377:289–297
32. Cella N, Groner B, Hynes NE (1998) Characterization of Stat5a and Stat5b homodimers and heterodimers and their association with the glucocortiocoid receptor in mammary cells. Mol Cell Biol 18:1783–1792
33. Perez OD, Nolan GP (2006) Phosphoproteomic immune analysis by flow cytometry: from mechanism to translational medicine at the single-cell level. Immunol Rev 210:208–228
34. Dupont G, Demaret J, Venet F, Malergue F, Malcus C, Poitevin-Later F, Morel J, Monneret G (2014) Comparative dose-responses of recombinant human IL-2 and IL-7 on STAT5 phosphorylation in CD4+FOXP3- cells versus regulatory T cells: a whole blood perspective. Cytokine 69:146–149
35. Rochman Y, Spolski R, Leonard WJ (2009) New insights into the regulation of T cells by gamma(c) family cytokines. Nat Rev Immunol 9:480–490
36. Atkins MB (2002) Interleukin-2: clinical applications. Semin Oncol 29:12–17
37. Demaret J, Dupont G, Venet F, Friggeri A, Lepape A, Rimmele T, Morel J, Monneret G (2015) STAT5 phosphorylation in T cell subsets from septic patients in response to recombinant human interleukin-7: a pilot study. J Leukoc Biol 97:791–796

Part X

Cell Cycle Control

Chapter 21

Molecular Network Dynamics of Cell Cycle Control: Periodicity of *Start* and *Finish*

Alida Palmisano, Judit Zámborszky, Cihan Oguz, and Attila Csikász-Nagy

Abstract

The cell division cycle is controlled by a complex regulatory network which ensures that the phases of the cell cycle are executed in the right order. This regulatory network receives signals from the environment, monitors the state of the DNA, and decides timings of cell cycle events. The underlying transcriptional and post-translational regulatory interactions lead to complex dynamical responses, such as the oscillations in the levels of cell cycle proteins driven by intertwined biochemical reactions. A cell moves between different phases of its cycle similar to a dynamical system switching between its steady states. The complex molecular network driving these phases has been investigated in previous computational systems biology studies. Here, we review the critical physiological and molecular transitions that occur in the cell cycle and discuss the role of mathematical modeling in elucidating these transitions and understand cell cycle synchronization.

Key words Systems biology, Bistability, Oscillation, Mathematical and computational models, Checkpoints, Budding yeast, Hysteresis, Synchronization, Periodic forcing

1 Introduction

Cell theory [1] states that the cell is the functional unit of life as it is able to perform self-reproduction. Cells are the building blocks of living organisms organized in a systematic manner. All cells arise from pre-existing cells through their division. During a coordinated sequence of phases, collectively referred to as the cell cycle, a cell replicates all of its internal components (e.g., DNA, ribosomes, RNAs, phospholipid bilayers, carbohydrates, metabolic machinery, and proteins) and separates them into two nearly identical daughter cells. This important biological process is governed by a complex molecular machinery of macromolecules which act in synchrony to avoid any potential error that could lead to cellular malfunction or death. In addition to the controlled alternation between DNA replication and cell division, cells need to grow to an appropriate size. In order to ensure that, each step of cell cycle

Gaspar Banfalvi (ed.), *Cell Cycle Synchronization: Methods and Protocols*, Methods in Molecular Biology, vol. 1524,
DOI 10.1007/978-1-4939-6603-5_21,

has to occur with the right timing. A sophisticated and highly interconnected interaction network of regulatory elements gives rise to some fundamental properties of the cell cycle, such as oscillations, bistability, and hysteresis [2].

Previous research has shown that to understand biology at the systems level, researchers need to step over the boundaries between disciplines. Biology is far too complex to comprehend it piece by piece. Despite the enormous amount of available biological data, we are still far from a detailed understanding of how cells function. Mathematical and computational models help biologists to understand the organizations and dynamics of biological systems. A multidisciplinary field called "systems biology" emerged from molecular biology and genetics in the early 2000s [3–5]. Systems biology has its roots in the use of modeling and simulation, combined with experiments, to explore the dynamic features of biological systems. In systems biology practice, the interactions between the components of a system are typically described by a computational model that generates testable quantitative predictions despite system complexity.

Cell cycle regulation has always been of particular interest in mathematical biology and it led to several success stories in the field. Mathematical modeling of the cell cycle goes back to the middle of the last century, when scientists were generating hypotheses about the underlying mechanisms of this process without any knowledge of the molecules that control cell division. From 1960s, there have been fascinating discoveries regarding the rules that determine the observed physiology of cells [6]. Research on chemical oscillations by theoretical physical chemists led to several methods and tools that were later used for investigating biological oscillators, such as the cell cycle. With time, other computational frameworks were born to serve systems biology research and help us understand more about cell cycle regulation [7].

In this chapter, we introduce to readers the basic principles of the physiology of cell cycle control and its underlying molecular mechanisms. We focus our attention on the classical model organism budding yeast, *Saccharomyces cerevisae*, since the regulatory network and most of its dynamical features are very well conserved among all eukaryotes [8, 9]. We present a historical overview of mathematical and computational models of cell cycle, together with the recent advances, including recently developed complex models elucidating interesting features of cell cycle control in relationship to synchronization.

2 Physiology of the Cell Cycle

Cells run cycles of coordinated events resulting in self-reproduction and all eukaryotic cells share the major processes of the cell cycle. The underlying steps of the cell division cycle have to occur in the

correct order [10]. As the first step of the process, a cell must replicate its DNA in the S-phase. This is followed by the separation of the two copies of the DNA into two daughter nuclei in mitosis (M-phase) and the division of the daughter cells (cytokinesis). DNA replication and chromosome segregation alternates to ensure that all cells have the same DNA content. If a cell commits a run of mitosis before finishing the previous DNA replication, the daughter cells would inherit incomplete chromosomes resulting in cell death. In multicellular systems, such mistakes can potentially be fatal for the whole organism if they remain unrecognized [11].

Keeping the homeostasis of a population of cells is crucial for both single celled and multicellular organisms. Temporal gaps (called G1 and G2 phases) are inserted into the process to keep the growth balanced [12]. G1 and G2 phases provide sufficient time for cells to double all of their components. However, there are exceptions to this rule. For example, sometimes cells grow to a very large size (e.g., huge eggs) or early embryos go over several rapid divisions without growth [10]. The typical cyclic alternation between the four phases in normal somatic cells is depicted in Fig. 1.

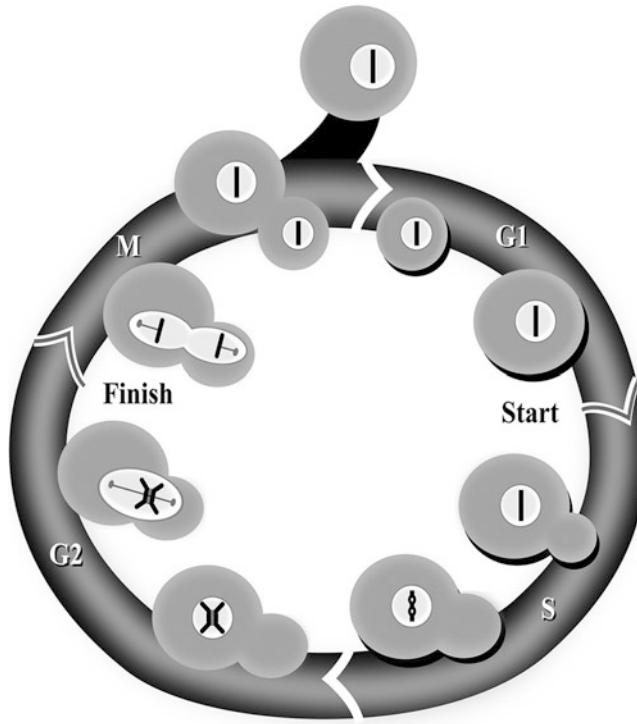

Fig. 1 Phases and transitions of the cell cycle. In G1-phase, a newborn cell has a single copy of its DNA. At the *Start* transition, the cell commits itself toward the initiation of the cycle and starts budding and DNA replication (S-phase). In budding yeast cells, S, G2, and M-phases overlap, since the chromosomes do not need to be fully condensed for mitosis. When the chromosomes are aligned at the middle of the nucleus, the *Finish* transition induces the separation of the chromosomes eventually leading to asymmetric division of the bud

Newborn cells start the cell cycle in G1 phase where they have one copy of unreplicated chromosomes. They commit to start the cell cycle only if both the internal and the external conditions are suitable for cell proliferation. This transition is called *Start* in lower eukaryotes and *restriction point* in mammals [13, 14]. The decision is irreversible: once the cell starts the cycle, it eventually takes it to completion even if the internal or external conditions become worse. These cells will stop at the *Start* transition of the subsequent G1-phase.

In the S-phase, each DNA molecule is replicated. Accuracy of this replication process is critical for producing healthy and viable daughter cells, thus the checkpoint mechanisms monitor for replication errors or DNA damage during this process. In case of a recognized problem, the cell cycle process stops and repair mechanisms are initiated to correct the defective DNA. Once the repair is done, cells can continue their cycle. Budding yeast cells also start budding after the *Start* transition: throughout the rest of the cycle, only the bud continues to grow (Fig. 1). Generally, the G2-phase is used to ensure the proper completion of DNA replication before mitosis is initiated. In budding yeast, the few chromosomes do not need to be tightly packed for mitosis, thus, S, G2, and M-phases somewhat overlap [15, 16]. The process of mitosis has several subphases. First, replicated chromosomes condense into compact structures (prophase). Then, they are aligned at the center of the cell with the help of mitotic spindles (metaphase). By the time the metaphase to anaphase transition occurs, chromosomes need to be properly replicated and their kinetochores need to be captured by the mitotic spindles. If there is a problem with the replication or the separation machinery, cell cycle is stopped before it can be finished [17]. With proper mitotic chromosomes, cells can pass the *Finish* transition: the proteins (cohesins) that "glue" the two sister chromatids together are destroyed allowing the chromosomes to be pulled to the opposite poles of the cell (anaphase). After distributing the DNA content in telophase, the daughter nuclei are formed and eventually the two daughter cells separate during cytokinesis [18].

3 Checkpoints of the Cell Cycle

The major events of the cell cycle described above are tightly regulated, checked and corrected for errors. If problems arise during the cycle, "checkpoint" mechanisms block progression of the cycle until the problems are solved [19]. Cells monitor the status of the DNA as well as the environmental conditions, and surveillance mechanisms are present in every phase of the cell cycle. Spindle poles, anaphase progression, and the size of the cell are checked at specific time points during the cycle while potential DNA damage

is monitored continuously. Checkpoint mechanisms arrest cell cycle progression either at the *Start* transition, anytime during S-phase, or at the entry or *Finish* of mitosis. If DNA damage occurs, a signaling pathway is switched on triggering several molecular events (repair mechanisms, cell cycle block, or apoptosis). Sophisticated feedback regulations induce immediate stops in case of a failure [20, 21]. As we described previously, cells go over transitions that are triggered by transient signals that emerge when the checkpoint conditions are all satisfied. The regulation of these state changes is critical for checkpoint mechanisms as it provides an opportunity to generate immediate responses upon problems that arise during the cycle [22, 23].

If a checkpoint is held active for a longer time than the mass doubling time of the cell population, then all cells will end up at the transition point which is blocked by this checkpoint. Release of this checkpoint can induce population level synchronization of cells that could last for a few cycles. In case of higher organisms, cell cycle synchronization may also emerge naturally (e.g., through the circadian rhythms that orchestrate cell cycle progression) [24, 25], but in the asynchronous budding yeast population, some sophisticated experimental techniques are needed to keep synchronized divisions for several cycles [26, 27]. Cells are experimentally blocked during DNA synthesis by inhibitory drugs that alter the structure of DNA (e.g., thymidine analogs and crosslinking agents) or by specific enzyme inhibitors (e.g., aminopterin and hydroxyurea). Other methods collect cells at *Start* by nutrition or growth factor deprivation. Sexual hormones can also induce blocks at the *Start* transition leading to mating of budding yeast cells [28]. At the *Finish* transition cells are halted by the inhibition of the chromosome segregation machinery (e.g., using paclitaxel or nocodazole to block the normal polymerization of microtubules). Temperature-sensitive mutants in the regulatory genes of *Start* and *Finish* regulation can be also used to block the cells at these checkpoints [29]. These block-and-release synchronization techniques are also applied in higher organisms as these methods are fast and do not require expensive tools. On the other hand, the blocking agents disrupt normal cell division and are often toxic to cells.

Another recent approach used to synchronize budding yeast colonies involves external perturbations to the budding yeast cell cycle control system to synchronize the activity of key cell cycle proteins among cells in colonies. Since the levels of specific proteins (e.g., cyclins) are highly correlated to specific phases of the cell cycle, it is natural to think of experiments that control the syntheses of such proteins by promoters whose expression can be induced by external stimulus like growth medium [30] (find more details about this approach in following sections).

4 Molecular Mechanism of Cell Cycle Control

The proper order of cell cycle events is maintained by a complex network of interacting macromolecules that control the cell cycle transitions. Systematic analysis of cell cycle mutants in the 1970s by Lee Hartwell [29], Paul Nurse [31], and others led to the discovery of the key regulator of the cell cycle (CDK—cyclin-dependent kinase) that works in a complex with a cyclically appearing molecule (named cyclin) that was discovered by Tim Hunt [32]. These three researchers received the Nobel Prize in 2001 for their breakthrough results in understanding the cell cycle regulation [33]. Lee Hartwell identified cell division cycle (Cdc) genes from the budding yeast *Saccharomyces cerevisiae* through a genetic screen of temperature-sensitive mutants (i.e., viable at 23 °C but inviable at 36 °C). He suggested that these mutants at the higher temperature are stopped at various checkpoints of their cycle. Furthermore, he proposed that Cdc28 might encode the key regulator of the cell cycle. Paul Nurse isolated temperature-sensitive mutants of fission yeast (*Schizosaccharomyces pombe*) cells. He found that cell cycle was blocked in long cells and also noticed small cells that seemed to be able to proliferate normally. He named this mutant Wee (small in Scottish) and suggested that the related genes must have an important role in cell cycle control. Nurse also found out that one of the genes with the Wee phenotype can have another mutation that produces cell cycle blocked elongated cells. Soon he discovered that this gene (Cdc2) is a homolog of Hartwell's Cdc28 in budding yeast and later found the human version of the gene as well. Tim Hunt studied the control of mRNA translation and found proteins with oscillating levels. He gave the name "cyclins" to these molecules. Later discoveries showed that the complex of cyclin and Cdc2 (generally called Cyclin-Dependent Kinase, CDK) is responsible for the initiation of mitosis in eukaryotic cells. Several cell cycle regulators and their functions have been identified since these discoveries, helping us understand the critical regulatory steps of the cell cycle [7, 10]. The basic mechanisms behind the steps of cell cycle are well conserved among eukaryotes, thus we can use the key regulatory loops of the budding yeast system to study cell cycle in higher eukaryotes without losing much generality. For a table that converts the budding yeast nomenclature into other organisms we refer the readers to earlier studies [8].

4.1 Cell Cycle Control in Budding Yeast

Based on several decades of genetics and molecular biology research, we know that CDK proteins work as effective kinases only if they are bound by a regulatory cyclin partner that helps substrate recognition. The budding yeast cell cycle is controlled by only one CDK (Cdc28) and its nine cyclin partners (Cln1-3, Clb1-6). Cdc28/Cln1-3 complexes control the *Start* transition and bud

initiation, Cdc28/Clb5,6 complexes initiate DNA replication by phosphorylating proteins bound to chromosomes at the "origins of replication" (specific nucleotide sequences at which DNA replication can start), Cdc28/Clb3-4 plays a role in early mitotis, and Cdc28/Clb1-2 complexes are very critical at different steps of mitosis [34]. The separation of chromosomes at the *Finish* transition happens together with the destruction of cyclins and the resulting drop in CDK activity induces cell division.

The activity of the Cdc28/cyclin complexes can be regulated in several ways, one of which is the controlled degradation of the cyclin subunits. The Anaphase Promoting Complex (APC), with the help of the regulatory protein Cdc20, labels Clb1-6 for degradation. APC can also work with another regulator (Cdh1) that recognizes only Clb1,2 molecules and induces their degradation at the end of the cell cycle [35]. Interestingly, the Cdc28/Clb2 complex can phosphorylate and inactivate Cdh1 protein molecules leading to an antagonistic interaction between Cdc28/Clb2 and Cdh1/APC. This antagonism creates two alternative stable steady states of the control system: (1) a G1 state with high Cdh1/APC activity and low Cdc28/Clb2 activity, and (2) an S-G2-M state with high Cdc28/Clb2 activity and low Cdh1/APC activity. The transition between the G1 and S-G2-M phases is facilitated by Cdc28/Cln1-3 molecules that cannot be destroyed by Cdh1/APC, while the opposite phase change is initiated by the Cdc14 phosphatase that reverses the Cdc28-induced phosphorylation on target molecules. Cdh1/APC is also helped by the CDK inhibitor Sic1 that binds to Cdc28/Clb complexes inhibiting their activity. Importantly, Sic1 is also in an antagonistic relationship with Cdc28/Clb complexes that induce Sic1 degradation through phosphorylation. Thus, the G1-phase is stabilized by the concerted action of Cdh1/APC and Sic1, and at the *Start* transition, the Cdc28/Clb complexes take over and stay active until the *Finish* transition when the system reverts back to its initial state [16, 20, 22].

In order to better explain how the progression between the different phases of the cell cycle is driven by these antagonistic relationships, let us consider a simple mechanical metaphor like the seesaw in Fig. 2. The lever represents the strong connection between the two antagonistic partners. The height of the left part of the lever represents the activity of the Cdh1/APC complex and the abundance of the stoichiometric inhibitor Sic1. The height of the right part of the lever illustrates the amount of Cdc28/Clb complexes (Clbs, for short in Fig. 2). The two buckets represent the helper molecules (Cln1-3 and Cdc14) that induce the two transitions.

After cell division, the newborn cells are in G1-phase, with high Sic1 and Cdh1 activity, and no Cdc28/Clb complexes are present. As the cells grow (the "Growth" signal in Fig. 2), they start producing Cln1,2,3 cyclins that bind to Cdc28 and these

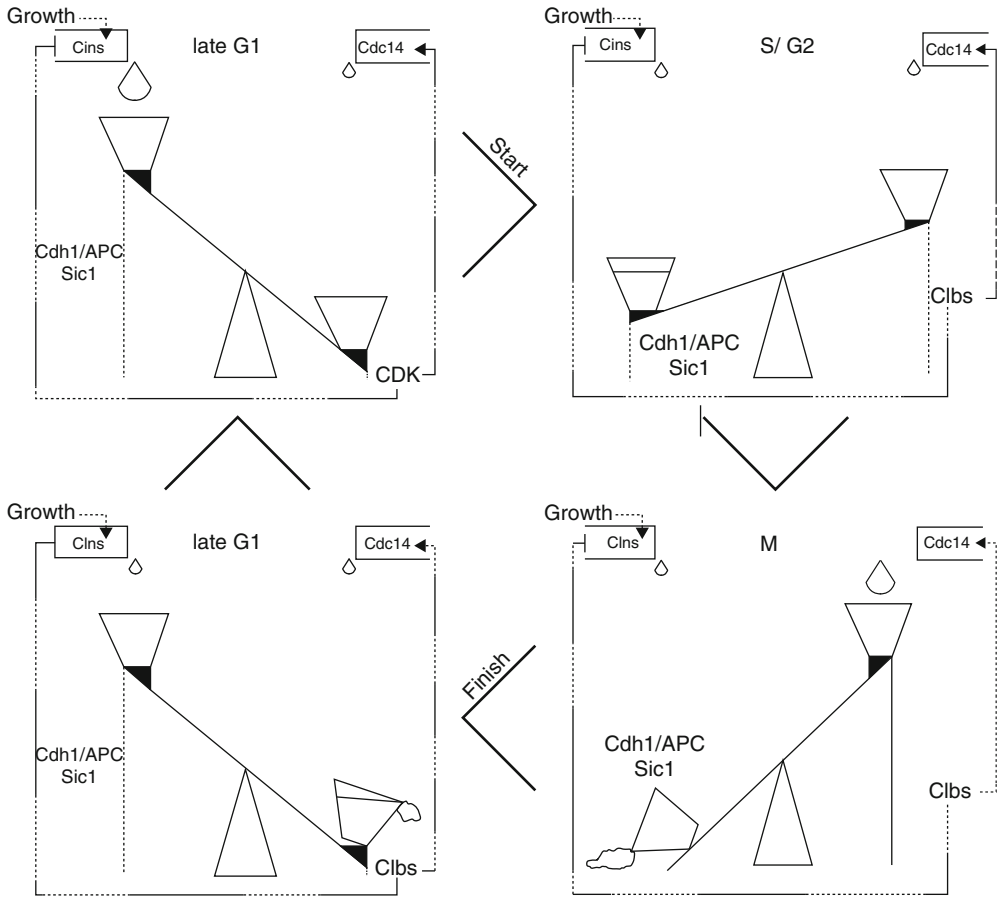

Fig. 2 A seesaw metaphor for the antagonism between Cdc28/Clb2 and its G1 enemies (Cdh1/APC and Sic1). See text for description

complexes phosphorylate—thus inactivate—Cdh1 and Sic1. As the lever turns, Cdk/Clb level increases further helping Cdh1 and Sic1 inactivation. When the lever is turned high, Cdc28 activity induces bud emergence, DNA replication, and spindle pole body duplication. Further cellular events of the *Start* transition include the activation of SBF/MBF as well as the activation of the transcription factors of the G1 cyclins (Cln1 and Cln2). SBF is kept inactive by the Whi5 inhibitor that is phosphorylated and exported from the nucleus by the Cdc28/Cln3 complexes. Upon their activation by transcription factors, Cln1,2 and Clb5,6 bind to Cdc28 and phosphorylate Cdh1 and Sic1 to flip the lever in Fig. 2. Later, the high level of Cdc28/Clb activity induces the inactivation of the transcription factors of the starter kinases Cln1,2,3 (see dashed line on Fig. 2), thus turning off the Cln synthesis emptying the left side bucket after the *Start* transition.

The *Finish* transition is facilitated by Cdc20 and Cdc14. Cdc20, in complex with the APC, degrades the Clb-kinases and

separates the sister chromatids [17, 35]. Cdc20, together with Cdc28/Clb2, also helps the activation of the Cdc14 phosphatase (see the dashed arrow on Fig. 2). Active Cdc14 reactivates Cdh1 and Sic1 helping these proteins to flip the lever back to the G1 state completing the cell cycle. When conditions are favorable, the whole process starts again.

This antagonism (or double negative feedback) is responsible for the irreversibility of the transitions we just described, as cells do not run around as free oscillators: they rather execute jumps between stable steady states at critical cell cycle transitions, closing a hysteresis loop [20]. Still, the result of the hysteretic interaction of Cdc28/Clbs and Cdh1/APC-Sic1 pair together with the regulatory proteins of the transitions show relaxation oscillations with long phases in near steady states, while also showing quick jumps between these states (Fig. 3).

4.2 Models of Cell Cycle Regulation

As some data on the key cell cycle regulator (CDK) were generated by Nurse and others (see previous sections), theoreticians started to create models in order to understand how CDK regulates cell cycle events [36, 37]. Some of these studies laid down important details and basic properties of cell cycle regulation. Further experiments on yeasts and frog eggs shed more light on the molecular mechanisms of the protein interactions in these systems and inspired studies based on mathematical analysis. This success story created a great interest in modelers to study research problems in cell biology with the help of the interdisciplinary work of mathematicians, physicists, and other scientists [7].

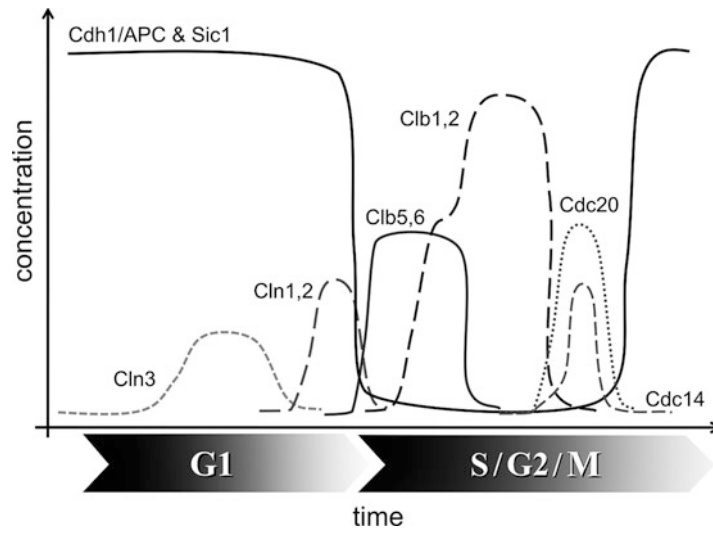

Fig. 3 Fluctuations in the activities of key regulators during cell cycle. Idealized time course of protein activity waves during the cell cycle. Cdc28 is always present in excess. Hence, only the levels of cyclin partners are noted

The dynamical properties of a cell are implicit in the topology of the protein networks that underlies cell physiology. A detailed characterization of such a complex system can be achieved by mathematical and computational approaches through modeling its temporal and spatial evolution [38]. In general, to determine whether a hypothetical regulatory network like the one in Fig. 4 is correct, the classical approach starts with the conversion of the mechanism informally described by a wiring diagram into a formal mathematical model, and then proceeds with the comparison of the model's behavior to the observed behavior of the cells. Classically, most of the physiological observations can be incorporated into a model (e.g., inviability of deletion mutants, cell size differences, and the lengths of the different cell cycle phases) but recent experiments also provide data on molecular level fluctuations to be integrated into models. If a model is found to be appropriate for most of the collected observations, but inconsistent with a few of them, it might highlight the aspects of the mechanism that require revision and further testing [22]. Insightful predictions can also be deduced from computational models and these may guide experiments to verify the predictions and generate new data to use for the next generation of more detailed computational models.

An example of this synergistic interaction between computational models and experiments are the two landmark papers from the early 2000s by Katherine C. Chen and colleagues from the Tyson lab, which stand as the most comprehensive mathematical models of the budding yeast cell cycle regulation [15, 22]. These models are based on an extensive literature data collection on more than 100 budding yeast cell cycle mutants and the final model can simulate the experimental findings from almost all of these mutants. In their first paper [15], Chen et al. focused on the molecular events regulating the *Start* transition of the cell cycle. The model accounts for many details of cell physiology (viability, inviability, cell size, and the lengths of different cell cycle phases) in wild-type and several mutant cells. In this work, the authors proposed the idea, mentioned earlier in this chapter, that the G1 and the S/G2/M phases are alternative states and cells switch between them during the *Start* transition when the CDK activity rapidly increases. The bistability of the system results from the antagonism between Cdc28/Clbs complexes and their inhibitors Sic1 and Cdh1. The authors also proposed an experiment to verify the existence of this bistability. In 2002, Fredrick R. Cross and his group performed measurements following these suggestions and confirmed the hysteresis prediction [39]. In this groundbreaking paper, Cross went further and experimentally tested various properties of the model and generated some additional experimental data to help further model development. This milestone paper was the first one that was fully devoted to test a mathematical model and one of the earliest steps toward systems biology [5, 7]. Two years later, the

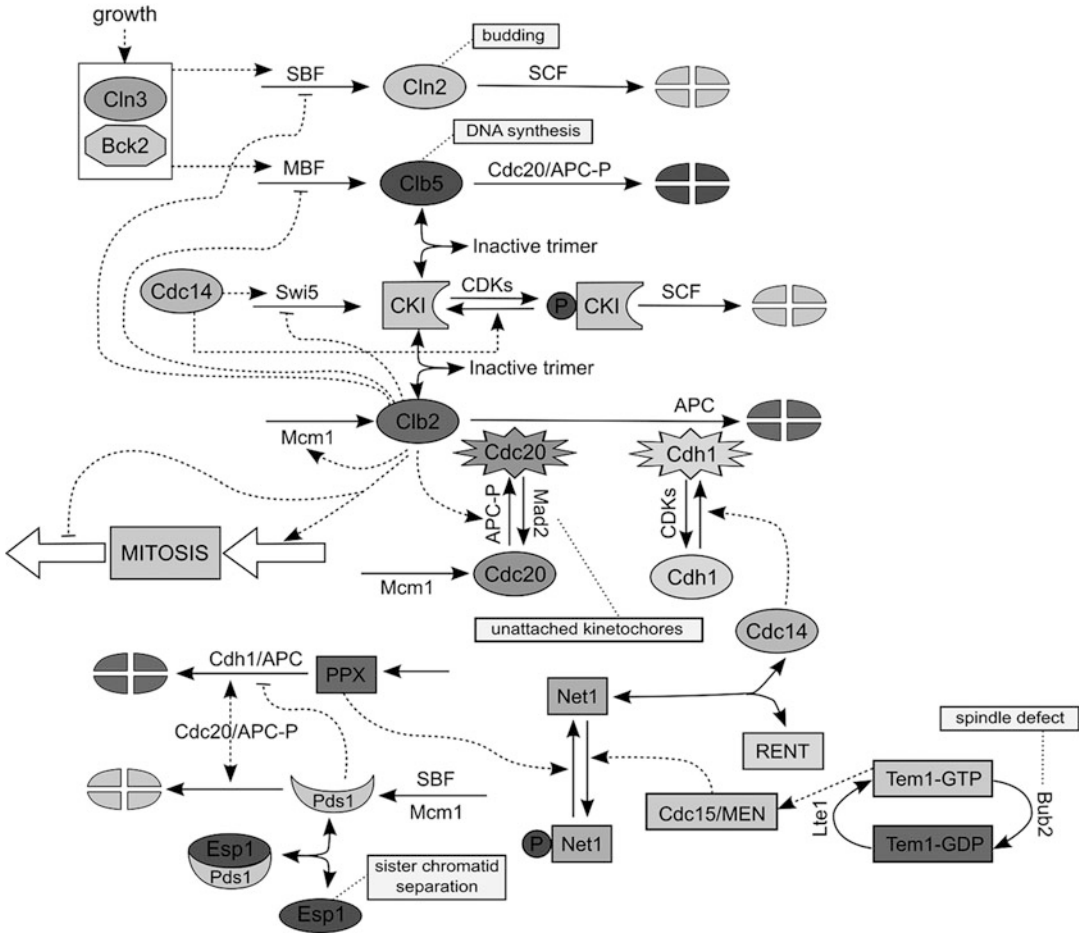

Fig. 4 Regulatory network of the budding yeast cell cycle. Adapted from Chen et al. [22]. In the diagram, Cln2 stands for Cln1 and 2, Clb5 for Clb5 and 6, and Clb2 for Clb1 and 2. Moreover, the protein kinase Cdc28 is not shown explicitly because it is present in excess and it combines rapidly with the different cyclin partners as soon as they are synthesized. Newborn daughter cells must grow to a critical size to have enough Cln3 and Bck2 to activate the transcription factors SBF and MBF, which induce the syntheses of Cln2 and Clb5, respectively. Cln2 is primarily responsible for bud emergence, whereas Clb5 is responsible for initiating DNA synthesis. Clb5-dependent kinase activity is not immediately evident since cyclin-dependent kinase inhibitors (CKI; namely, Sic1 and Cdc6) are prevalent in the G1-phase. After the CKIs are phosphorylated by Cln2 and by other active cyclin-dependent kinase complexes (collectively denoted by CDKs), CKIs are rapidly degraded by SCF, releasing Clb5 to do its job. A fourth class of cyclins, denoted Clb2, is not involved directly in the regulation of the G1-phase because its transcription factor Mcm1 is inactive during G1 and its degradation pathway guarded by Cdh1/APC is also active, and additionally, the stoichiometric inhibitors Cdc28/Clb2 complex's (CKIs) are abundant. During the cell cycle, the active CDK complexes remove the CKIs from the Cdc28/Clb2 and inactivate Cdh1, allowing Clb2 to accumulate. After some delay, Cdc28/Clb2 activates its own transcription factor, Mcm1 amplifying its activation. Furthermore, Clb2 turns off SBF and MBF. As Clb2 drives the cell into mitosis, it also stimulates the synthesis of Cdc20 and phosphorylates components of the APC, thus prepares the cells to exit from mitosis. Meanwhile, Cdc20/APC is kept inactive by the Mad2-dependent checkpoint signal responsive to unattached chromosomes. When the replicated chromosomes are attached, active Cdc20/APC initiates mitotic exit. First, it degrades Pds1, releasing Esp1, a protease involved in sister chromatid separation. It also degrades Clb5 and partially Clb2, reducing their strength on Cdh1 inactivation. In this model, Cdc20/APC promotes degradation of a phosphatase (PPX) that has been keeping Net1 in its unphosphorylated form that binds with Cdc14. As the attached chromosomes are properly aligned on the metaphase spindle, Tem1 is activated, which in turn activates Cdc15—the endpoint of the MEN signal-transduction pathway in the model). When Net1 becomes phosphorylated by Cdc15, it releases its hold on Cdc14. The Cdc14 phosphatase then works against the cyclin-dependent kinases: activating Cdh1, stabilizing CKIs, and activating Swi5 (the transcription factor for CKIs). In this manner, Cdc14 returns the cell to the G1-phase (no cyclins, abundant CKIs, and active Cdh1)

experimental measurements and findings of Cross were incorporated into a new version of the Chen model [22] that was also extended with the detailed regulation of the *Finish* transition. The resulting model was tested against the phenotypes of 131 mutants and failed only in 11 of them. These failures highlighted the parts of the network that needed more experimental observations and model development. This model also predicted the existence of a phosphatase that removes phosphates from Net1 (PPX in Fig. 4). The presence of this hypothetical phosphatase was experimentally verified in 2006 [40].

As the knowledge regarding the cell cycle regulatory network and its interactions with other cellular pathways increases, the complexity of mathematical models grows with it. Detailed analysis and parameterization of such large systems can be difficult due to large numbers of ordinary differential equations. Moreover, recent advances in experimental techniques give researchers access to single cell data and to information from biological processes involving small number of molecules. Such scenarios are better handled by computational approaches that explicitly take into account the effect of noise on the system [30, 41].

The type of approach to be used for modeling depends on the biological question of interest. Deterministic models like the ones mentioned above (and more recent ones [42, 43]) can help elucidate the average behaviors of regulatory protein networks to understand the basic mechanisms behind cell cycle progression. Different approaches are required to elucidate more in-depth questions.

Simplification by logical modeling has a long tradition in biology [44] and some applications of it in cell cycle research have been previously published [45, 46]. On small systems, formal analysis methods can be used to study interesting properties of the model. For example, model checking can be used to test if a model matches some specific conditions [47, 48]. This approach uses temporal logic formulae and allows verifying if a system can reach a given state. In [49], for example, authors used model checking on a model of cell cycle to understand the strength of the irreversible commitment to *Start* and *Finish* transitions.

Cellular noise notably affects biological systems. As a result, stochastic modeling approaches are becoming more and more popular since they provide opportunities to simulate cellular dynamics at the single cell level and also to help the identification of novel mechanisms in concert with experimental methods, such as quantitative flow cytometry [50] and fluorescence microscopy [41]. Following these experimental studies in cell cycle, detailed stochastic models of cell cycle regulation have been developed to account for biological variables including single cell levels and half-lives of mRNAs and proteins. For example, authors in [51, 52] studied the effects of stochastic fluctuations on mutant phenotypes

that show partial viability: these mutants cannot be accurately simulated and studied by deterministic models that represent dynamics at the population level. Some simulation results from [52] are plotted in Fig. 5. We note that the noise is affecting the protein levels in both plots but the effect of the noise is more evident in *sic1Δ* mutant (mutant which is missing one of the G1 regulators of Cdc28/Clb complexes). In this mutant, cycles become irregular, some of the cells might be inviable, but the whole population can still grow as previously observed in the experiments [53].

Another example where stochasticity plays an essential role is shown by [54] where alternative model setups have been studied to understand the robustness of the feedback loops across different checkpoints of the cell cycle.

Variability is observed not just in protein abundances, but also in macroscopic characteristics such as the sizes of budding yeast cells. Cell size is a critical property that requires tight control, especially in organisms that need to react to external conditions to ensure population homeostasis. It is generally accepted that budding yeast cells must reach a critical size before entering the cell cycle [55, 56]. However, experimental evidence shows that individual cells have a variable size at the *Start* transition, even under constant external and nutritional conditions [41, 57]. This observation challenges the existence of a mechanism setting the critical size in a deterministic manner.

An intrinsic control system that sets the critical size as a function of growth rate also provides a broad solution for adaptation, thus making unnecessary the existence of a plethora of sensing mechanisms transmitting different external cues to the cell cycle machinery. In [58], authors provide experimental evidence and a computational model showing that the cell size at *Start* is robustly set at a single-cell level by the volume growth rate in G1. With their computational analysis, the authors also show that the proposed mechanism provides homeostasis and an immediate solution for size adaptation to changes in the external conditions at a population level.

A final example of the synergistic interaction between experiments and computational modeling is a recently published study [59]. The authors use single cell data from cell cycle synchronization experiments [30] to test and validate a stochastic model of the budding yeast cell cycle. This complex model with nearly 200 parameters was first calibrated with the phenotypes of 110 mutant phenotypes and the single cell statistics of mother and daughter cells under *CLN3* deletion (*cln3*) strain by implementing an automated parameter estimation algorithm previously published in [60]. Then, for model validation purposes, the model's predictive ability was tested by comparing its predictions with the experimental data generated in [30] under periodic expression of *CLN2* (driven by *MET3* promoter in *cln3* background). In [30], due to

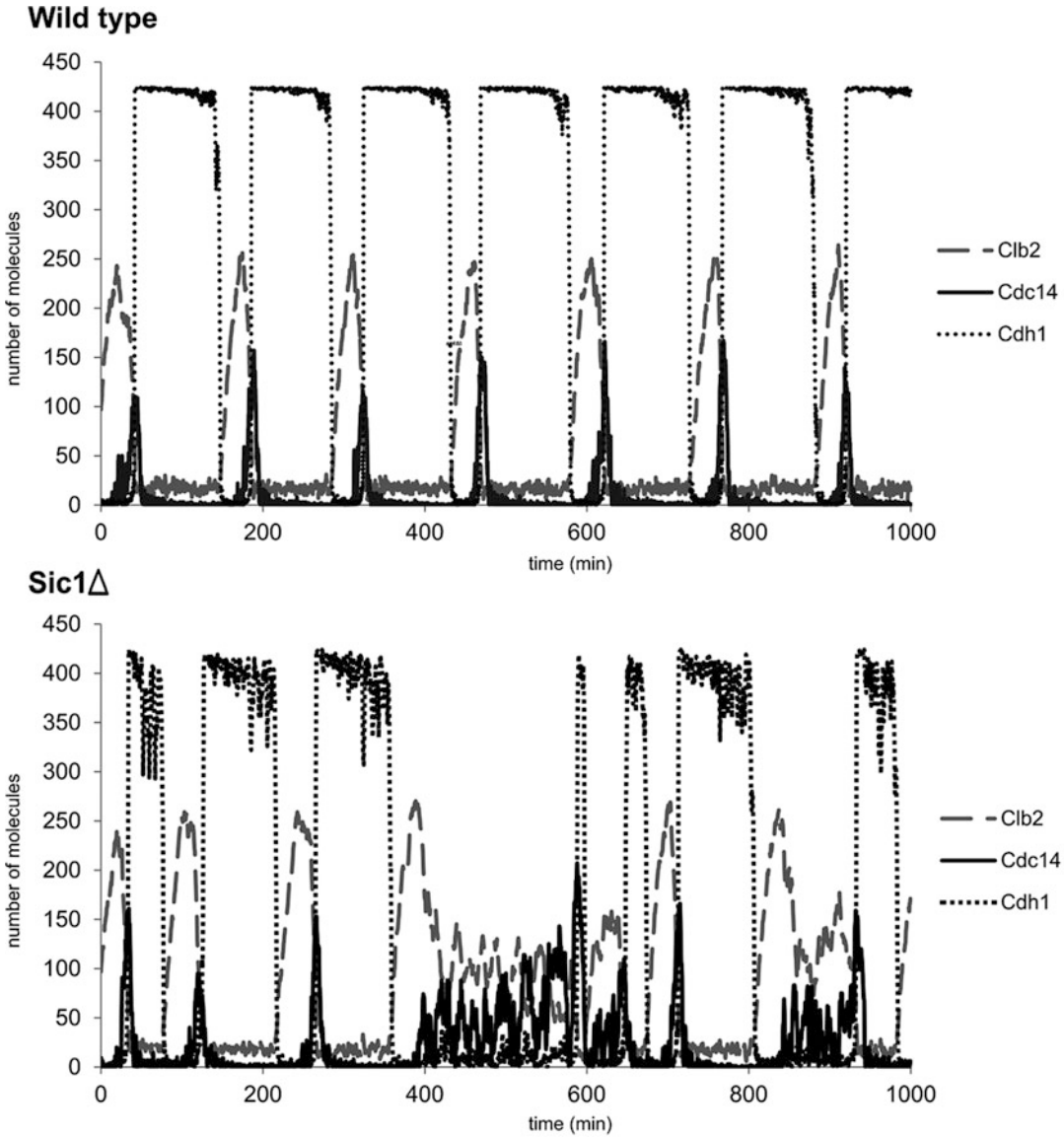

Fig. 5 Time series data from the simulations of a stochastic budding yeast cell cycle model. Stochastic fluctuations in the key regulatory components of the budding yeast cell cycle in the wild type strain (*upper*) and the *sic1Δ* mutant (*lower*). The plots are generated by following the daughter cells after each cell division. (*X*-axis: time in minutes, *Y*-axis: number of molecules)

the critical role of *CLN2* in bud formation, its periodic expression was shown to force mother and daughter cells to synchronize by reducing the dependence of the length of G1 (i.e., time spent between cell birth and budding) on the cell size at birth.

Results in [59] showed that the model correctly predicts the experimentally observed synchronization levels and cell cycle statistics of mother and daughter cells under various experimental

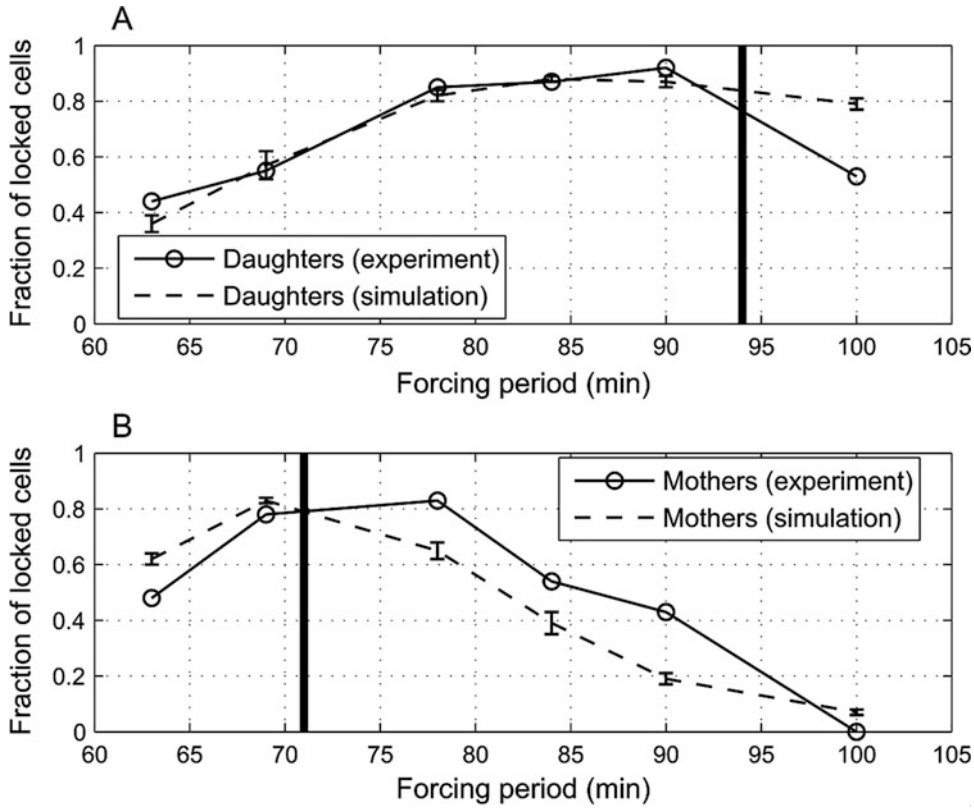

Fig. 6 Synchronization levels of daughter and mother cells with *CLN2* expression pulses. Forced CLN2 expression with six forcing periods: experimental [30] and simulation values for daughters in (**a**) and mothers in (**b**). Thick vertical lines represent the natural (cln3, no forced CLN2 expression) mother and daughter cycle times (94 and 71 min). The range of each locked (synchronized) fraction in the simulations (mean ± standard deviation) is depicted by the vertical error bars. The circles correspond to experimental values. Each range from the simulations is computed from 15 independent realizations. Each realization contains eight independently generated pedigrees of cells generated over the course of 700 min starting from a single daughter or mother cell

conditions, in addition to correctly predicting the qualitative changes in size control due to periodic *CLN2* expression. Figure 6 shows the overall agreement between the experimental and simulation-based synchronization levels (quantified as "locked cells" as defined in [59]) of daughter and mother cells with six different periods of *CLN2* expression pulses. Finally, following the model validation step, authors also generated an experimentally testable prediction that illustrated the interplay between cell cycle dynamics in synchronized cells and the size control mechanism in budding yeast. Based on this prediction, frequent *CLN2* expression pulses cause some small-born daughter cells to have extended budded periods (due to budded period size control) that results in an extended G1 period in the subsequent cycle among some of the cells (due to size control in G1) leading to bimodality of the G1 duration among small-born cells.

The model also predicted that increasing the duration of each CLN2 expression pulse from 20 to 40 min led to a 36% increase in the level of synchronization, whereas increasing the strength of the promoter driving expression pulses by threefold (i.e., from 1 to 4) resulted in an 84% increase. However, the latter improvement in the synchronization level was predicted to come at the expense of cycle failures (4% of the cycles failed due to incorrect order of cell cycle events). These predictions, which have not been verified experimentally, are examples that demonstrate the potential use of modeling to guide experimental research in identifying optimal synchronization conditions for budding yeast cells.

5 Conclusions

The molecular network dynamics of cell cycle is a complex system that can only be understood by integrating approaches from different fields while using experimental evidence to create hypotheses-generating mathematical models. Systems biology studies typically involve such hypothesis-driven research in order to shed light into specific mechanisms and bring up interesting research questions for the subsequent rounds of modeling and experimental work.

Systems biology field has emerged in 2000s with the aim of investigating cells and organisms across different levels of abstractions using approaches from multiple scientific disciplines (biology, chemistry, computer science, and mathematics just to name a few). An exciting aspect of this multidisciplinary approach of systems biology is the synergy between seemingly different fields. For example, on one hand, researchers use parameter estimation tools to study the behaviors of biological systems [60, 61]; on the other hand, the ways biological systems work have inspired the development of parameter estimation algorithms in the past (e.g., particle swarm [62], and differential evolution [63]). Another example is the fruitful interaction between the tools and languages used for analyzing biological systems [45, 46, 51, 52, 54, 61] and the distinctive needs of biological models that inspire the creation of new and different tools [64–67].

Along these lines, results in [59] demonstrate that a complex stochastic model calibrated with extensive population-level phenotype data and coarse single cell statistics (e.g., average cycle times of mother and daughter cells) from different mutants can predict higher level details of budding yeast cell cycle dynamics including shifts in size control and levels of synchronization under periodic external perturbations (i.e., pulses of cyclin expression). The achieved prediction accuracy despite model complexity and the heterogeneity of the experimental data used for model calibration in [59] exemplifies the predictive power of computational modeling for studying complex cellular dynamics. Furthermore,

experimentally testable predictions generated in this study illustrate the potential of computational models to guide further experimental research in cell synchronization.

Systems biology research in cell cycle aims at combining computational tools and experimental knowledge to gain a complete understanding of the regulation of cell cycle not only in yeast, but also in higher eukaryotes. Once achieved, this level of understanding has the potential to support biomedical research by improving treatments for human diseases. For instance, understanding how disruptions in the regulation of cell cycle can translate into a better understanding of initiation and progression of different types of cancer.

Disclaimer

This article was prepared while Alida Palmisano and Cihan Oguz were employed at Virginia Tech. The opinions expressed in this article are the authors' own and do not reflect the view of the National Institutes of Health, the Department of Health and Human Services, or the United States government.

References

1. Mazzarello P (1999) A unifying concept: the history of cell theory. Nat Cell Biol 1:E13–E15
2. Tyson JJ, Chen KC, Novak B (2003) Sniffers, buzzers, toggles and blinkers: dynamics of regulatory and signaling pathways in the cell. Curr Opin Cell Biol 15:221–231
3. Alon U (ed) (2006) An introduction to systems biology: design principles of biological circuits. CRC press, Boca Raton, FL
4. Kirschner MW (2005) The meaning of systems biology. Cell 121:503
5. Kitano H (2002) Systems biology: a brief overview. Science 295:1662–1664
6. Koch AL, Schaechter M (1962) A model for statistics of the cell division process. J Gen Microbiol 29:435–454
7. Csikasz-Nagy A (2009) Computational systems biology of the cell cycle. Brief Bioinform 10:424–434
8. Csikasz-Nagy A, Battogtokh D, Chen KC et al (2006) Analysis of a generic model of eukaryotic cell-cycle regulation. Biophys J 90:4361–4379
9. Nurse P (1990) Universal control mechanism regulating onset of M-phase. Nature 344:503–508
10. Morgan DO (ed) (2006) The cell cycle: principles of control. New Science Press, London
11. Kastan MB, Bartek J (2004) Cell-cycle checkpoints and cancer. Nature 432:316–323
12. Sveiczer A, Novak B, Mitchison JM (2004) Size control in growing yeast and mammalian cells. Theor Biol Med Model 1:12
13. Bartek J, Bartkova J, Lukas J (1996) The retinoblastoma protein pathway and the restriction point. Curr Opin Cell Biol 8:805–814
14. Nasmyth K (1996) Viewpoint: putting the cell cycle in order. Science 274:1643–1645
15. Chen KC, Csikasz-Nagy A, Gyorffy B et al (2000) Kinetic analysis of a molecular model of the budding yeast cell cycle. Mol Biol Cell 11:369–391
16. Nasmyth K (1996) At the heart of the budding yeast cell cycle. Trends Genet 12:405–412
17. Ciliberto A, Shah JV (2009) A quantitative systems view of the spindle assembly checkpoint. EMBO J 28:2162–2173
18. Guertin DA, Trautmann S, McCollum D (2002) Cytokinesis in eukaryotes. Microbiol Mol Biol Rev 66:155
19. Hartwell LH, Weinert TA (1989) Checkpoints: controls that ensure the order of cell cycle events. Science 246:629–634
20. Novak B, Tyson JJ, Gyorffy B et al (2007) Irreversible cell-cycle transitions are due to systems-level feedback. Nat Cell Biol 9:724–728
21. Tyson JJ, Csikasz-Nagy A, Novak B (2002) The dynamics of cell cycle regulation. Bioessays 24:1095–1109

22. Chen KC, Calzone L, Csikasz-Nagy A et al (2004) Integrative analysis of cell cycle control in budding yeast. Mol Biol Cell 15:3841–3862
23. Cross FR (2003) Two redundant oscillatory mechanisms in the yeast cell cycle. Dev Cell 4:741–752
24. Hong CI, Zámborszky J, Baek M et al (2014) Circadian rhythms synchronize mitosis in Neurospora crassa. Proc Natl Acad Sci 111:1397–1402
25. Masri S, Cervantes M, Sassone-Corsi P (2013) The circadian clock and cell cycle: interconnected biological circuits. Curr Opin Cell Biol 25:730–734
26. Bánfalvi G (ed) (2011) Cell cycle synchronization: methods and protocols, 1st edn, Methods in molecular biology. Humana Press, Totowa, NJ
27. Jackman J, O'Connor PM (2001) Methods for synchronizing cells at specific stages of the cell cycle. Curr Protoc Cell Biol 8.3.1–8.3.20
28. Marsh L, Neiman AM, Herskowitz I (1991) Signal transduction during pheromone response in yeast. Annu Rev Cell Biol 7:699–728
29. Hartwell LH, Mortimer RK, Culotti J et al (1973) Genetic control of the cell division cycle in yeast: V. Genetic analysis of cdc mutants. Genetics 74:267–286
30. Charvin G, Cross F, Siggia E (2009) Forced periodic expression of G1 cyclins phase-locks the budding yeast cell cycle. Proc Natl Acad Sci 106:6632–6637
31. Nurse P (1975) Genetic control of cell size at cell division in yeast. Nature 256:547–551
32. Evans T, Rosenthal ET, Youngblom J et al (1983) Cyclin: a protein specified by maternal mRNA in sea urchin eggs that is destroyed at each cleavage division. Cell 33:389–396
33. Nasmyth K (2001) A prize for proliferation. Cell 107:689–701
34. Bloom J, Cross FR (2007) Multiple levels of cyclin specificity in cell-cycle control. Nat Rev Mol Cell Biol 8:149–160
35. Zachariae W, Nasmyth K (1999) Whose end is destruction: cell division and the anaphase-promoting complex. Genes Dev 13:2039–2058
36. Goldbeter A (1991) A minimal cascade model for the mitotic oscillator involving cyclin and cdc2 kinase. Proc Natl Acad Sci U S A 88:9107–9111
37. Tyson JJ (1991) Modeling the cell division cycle: cdc2 and cyclin interactions. Proc Natl Acad Sci U S A 88:7328–7332
38. Tyson JJ (2007) Bringing cartoons to life. Nature 445:823
39. Cross FR, Archambault V, Miller M et al (2002) Testing a mathematical model for the yeast cell cycle. Mol Biol Cell 13:52–70
40. Queralt E, Lehane C, Novak B et al (2006) Downregulation of PP2A(Cdc55) phosphatase by separase initiates mitotic exit in budding yeast. Cell 125:719–732
41. Di Talia S, Skotheim JM, Bean JM et al (2007) The effects of molecular noise and size control on variability in the budding yeast cell cycle. Nature 448:947–951
42. Barik D, Baumann WT, Paul MR et al (2010) A model of yeast cell-cycle regulation based on multisite phosphorylation. Mol Syst Biol 6:405
43. Laomettachit T (2011) Mathematical modeling approaches for dynamical analysis of protein regulatory networks with applications to the budding yeast cell cycle and the circadian rhythm in cyanobacteria. Dissertation, Virginia Polytechnic Institute and State University
44. Thomas R (1973) Boolean formalization of genetic control circuits. J Theor Biol 42:563–585
45. Davidich MI, Bornholdt S (2008) Boolean network model predicts cell cycle sequence of fission yeast. PLoS One 3, e1672
46. Faure A, Thieffry D (2009) Logical modelling of cell cycle control in eukaryotes: a comparative study. Mol Biosyst 5:1569–1581
47. Heath J, Kwiatkowska M, Norman G et al (2008) Probabilistic model checking of complex biological pathways. Theor Comput Sci 391:239–257
48. Monteiro PT, Ropers D, Mateescu R et al (2008) Temporal logic patterns for querying dynamic models of cellular interaction networks. Bioinformatics 24:i227–i233
49. Ballarini P, Mazza T, Palmisano A et al (2009) Studying irreversible transitions in a model of cell cycle regulation. Electron Notes Theor Comput Sci 232:39–53
50. Pozarowski P, Darzynkiewicz, Z. (2004). Analysis of cell cycle by flow cytometry. In: Checkpoint Controls and Cancer: Volume 2: Activation and Regulation Protocols, Springer, pp 301–311.
51. Mura I, Csikasz-Nagy A (2008) Stochastic Petri Net extension of a yeast cell cycle model. J Theor Biol 254:850–860
52. Palmisano A (2010) Coding biological systems in a stochastic framework: the case study of budding yeast cell cycle. Proceedings of 1st international conference on bioinformatics
53. Nugroho TT, Mendenhall MD (1994) An inhibitor of yeast cyclin-dependent protein kinase plays an important role in ensuring the

genomic integrity of daughter cells. Mol Cell Biol 14:3320–3328

54. Romanel A, Jensen LJ, Cardelli L et al (2012) Transcriptional regulation is a major controller of cell cycle transition dynamics. PLoS One 7, e29716
55. Hartwell LH, Unger MW (1977) Unequal division in Saccharomyces cerevisiae and its implications for the control of cell division. J Cell Biol 75:422–435
56. Johnston GC, Pringle JR, Hartwell LH (1977) Coordination of growth with cell division in the yeast Saccharomyces cerevisiae. Exp Cell Res 105:79–98
57. Lord PG, Wheals AE (1981) Variability in individual cell cycles of Saccharomyces cerevisiae. J Cell Sci 50:361–376
58. Ferrezuelo F, Colomina N, Palmisano A et al (2012) The critical size is set at a single-cell level by growth rate to attain homeostasis and adaptation. Nat Commun 3:1012
59. Oguz C, Palmisano A, Laomettachit T et al (2014) A stochastic model correctly predicts changes in budding yeast cell cycle dynamics upon periodic expression of CLN2. PLoS One 9:e96726
60. Oguz C, Laomettachit T, Chen KC et al (2013) Optimization and model reduction in the high dimensional parameter space of a budding yeast cell cycle model. BMC Syst Biol 7:53
61. Schaber J, Klipp E (2011) Model-based inference of biochemical parameters and dynamic properties of microbial signal transduction networks. Curr Opin Biotechnol 22:109–116
62. Kennedy J (2011) Particle swarm optimization. In: Encyclopedia of machine learning, Springer, pp. 760–766
63. Price K, Storn RM, Lampinen JA (eds) (2006) Differential evolution: a practical approach to global optimization. Springer Science & Business Media, New York, NY
64. Chaouiya C, Bérenguier D, Keating SM et al (2013) SBML qualitative models: a model representation format and infrastructure to foster interactions between qualitative modelling formalisms and tools. BMC Syst Biol 7:135
65. Hucka M, Finney A (2005) Escalating model sizes and complexities call for standardized forms of representation. Mol Syst Biol 1(2005):0011
66. Hucka M, Finney A, Sauro HM et al (2003) The systems biology markup language (SBML): a medium for representation and exchange of biochemical network models. Bioinformatics 19:524–531
67. Palmisano A, Hoops S, Watson L et al (2014) Multistate model builder (MSMB): a flexible editor for compact biochemical models. BMC Syst Biol 8:42

INDEX

Gaspar Banfalvi (ed.), *Cell Cycle Synchronization: Methods and Protocols*, Methods in Molecular Biology, vol. 1524,
DOI 10.1007/978-1-4939-6603-5, © Springer Science+Business Media New York 2017

E

F

G

H

I

L

M

N

O

P

R

S

T

U

V

W

Z